Charles University in Prague
Faculty of Science

Developmental and Cell Biology

Mgr. Zuzana Rubíková

REGULATORY MECHANISMS OF MICROTUBULE REORGANIZATION IN ACTIVATED MAST CELLS

Ph.D. Thesis

Supervisor: Assoc. Prof. RNDr. Pavel Dráber, Ph.D.

Laboratory of Biology of Cytoskeleton
Institute of Molecular Genetics of the AS CR, v.v.i.

Prague, 2017

Prohlášení:

Prohlašuji, že jsem závěrečnou práci zpracovala samostatně, a že jsem uvedla všechny použité informační zdroje a literaturu. Tato práce ani její podstatná část nebyla předložena k získání jiného nebo stejného akademického titulu.

V Praze, 4. 9. 2017

Mgr. Zuzana Rubíková

Prohlášení:

Jménem ostatních spoluautorů publikací, které tvoří základ disertační práce Mgr. Zuzany Rubíkové, potvrzuji, že podíl autorky na jejich přípravě je popsaný v komentářích k jednotlivým publikacím pravdivě.

V Praze, 4. 9. 2017

Doc. RNDr. Pavel Dráber, CSc.

Poděkování:

Ráda bych poděkovala zejména svému školiteli Pavlu Dráberovi za trpělivé vedení, podnětné diskuze a podporu v průběhu celého mého vysokoškolského studia. Děkuji také všem současným i bývalým členům Laboratoře biologie cytoskeletu za ochotnou pomoc a podporu v profesním i osobním životě.

Velmi děkuji celé mé rodině a přátelům za naslouchání a podporu během šťastnějších i náročnějších chvil mého studia. Nejvíce pak děkuji svému muži Pavlovi za trpělivost, každodenní sdílení studijních a vědeckých radostí i strastí, a za ochotné podání pomocné ruky kdykoliv bylo během mého doktorského studia třeba.

TABLE OF CONTENTS

ABBREVIATIONS

Ag	Antigen
ATP	Adenosine 5'-triphosphate
BMMCs	Bone marrow-derived mast cells
CAMSAP	Calmodulin-regulated spectrin-associated protein
CLASP	Cytoplasmic linker-associated protein
CLIP-170	Cytoplasmic linker protein 170
CRAC	Ca^{2+} release-activated Ca^{2+} channel
EB	End-binding protein
ER	Endoplasmic reticulum
FcεRI	High-affinity IgE receptor
GCP	Gamma-tubulin complex protein
GDP	Guanosine diphosphate
GFP	Green fluorescent protein
GIT	G protein-coupled receptor kinase-interacting protein
GPCR	G protein-coupled receptor
GSK3β	Glycogen synthase kinase 3β
GTP	Guanosine 5'-triphosphate
IF	Intermediate filament
IgE	Immunoglobulin E
ITAM	Immunoreceptor tyrosine-based activation motif
ITIM	Immunoreceptor tyrosine-based inhibitory motif
MAP	Microtubule associated protein
MCAK	Mitotic centromere-associated kinesin
MF	Microfilament
MT	Microtubule
MTOC	Microtubule organizing centre
PAK1	p21 protein [Cdc42/Rac]-activated kinase 1
PCM	Pericentriolar matrix
PI3K	Phosphatidylinositol-3-kinase
βPIX	p21-activated kinase interacting exchange factor β
PKC	Protein kinase C

PTM	Post-translational modification
SOCE	Store-operated Ca^{2+} entry
TBA	Tubulin binding agent
TOG	Tumour overexpressed gene
γTuRC	γ-Tubulin ring complex
γTuSC	γ-Tubulin small complex
+TIP	Microtubule plus-end tracking protein
U2OS	Human osteosarcoma cell line

ABSTRACT

Microtubules (MTs) are highly dynamic structures essential for the spatio-temporal intracellular organization and transport, signal propagation, cell differentiation, motility and division. To perform these roles, MTs create arrangements capable of fast and precise adaptation to various signals. MTs are under the control of many factors regulating MT nucleation, stability and dynamics. Bone marrow-derived mast cells (BMMCs) are important immune system cells, which can cause serious diseases if their functions are deregulated. Although MT reorganization during BMMC activation is well established, the molecular mechanisms that control their remodelling are largely unknown. In the presented thesis we functionally characterised GIT1/βPIX signalling proteins, PAK1 kinase, and Ca^{2+} signalling in the regulation of MT nucleation in BMMCs and other cell types. We also elucidated the function of miltefosine (hexadecylphosphocholine), a promising candidate for the treatment of mast cell-driven diseases.

We found that GIT1/βPIX signalling proteins are γ-tubulin-interacting proteins associating with centrosomes in BMMCs. MT nucleation is positively regulated by GIT1 and Ca^{2+}, whereas βPIX is a negative regulator of MT nucleation in BMMCs. Cytosolic Ca^{2+} affects γ-tubulin properties and stimulates the interaction of γ-tubulin with GIT1 and γ-tubulin complex proteins. Moreover, γ-tubulin forms complexes with tyrosine-phosphorylated GIT1 in activated BMMCs. Our data suggest a novel mechanism for the concerted action of tyrosine kinases, GIT1/βPIX proteins and Ca^{2+} in the regulation of MT nucleation in activated BMMCs.

We showed that GIT1/βPIX signalling proteins, together with PAK1 kinase regulate MT nucleation from interphase centrosomes in different cell types. GIT1 and PAK1 represent positive, and βPIX negative regulators of this process. The level of MT nucleation correlates with the amount of γ-tubulin at centrosomes. We proved that GIT1 and βPIX are phosphorylated by PAK1 kinase and determined their binding domains for the interaction with γ-tubulin. Based on obtained results, we propose that GIT1/βPIX and PAK1 represent a novel regulatory mechanism of MT nucleation in interphase cells.

We showed for the first time that miltefosine modulates BMMCs both at the plasma membrane and in the cytosol. It inhibits the degranulation, MT reorganization and antigen-induced chemotaxis. While the aggregation and tyrosine phosphorylation of high-affinity IgE receptors is suppressed in activated BMMCs treated with miltefosine, Ca^{2+} influx is not inhibited. Besides that, miltefosine modulates intracellular movement of granules, MT dynamics in Ca^{2+}-dependent manner and attenuates the phosphorylation of proteins interacting with MT plus-end binding protein EB1. Miltefosine's action at multiple sites in BMMCs could explain its effectivity in the treatment of mast cell diseases.

SOUHRN

Mikrotubuly (MTs) jsou dynamické struktury nezbytné pro vnitřní buněčnou organizaci a transport, propagaci signálu, buněčnou diferenciaci, pohyb a dělení. Pro vykonávání těchto funkcí vytvářejí složitá uspořádání, schopná rychle a přesně reagovat na různé signály. MTs jsou regulovány mnoha faktory, které mají vliv na jejich nukleaci, stabilitu a dynamiku. Žírné buňky z kostní dřeně (BMMCs) jsou důležitou součástí imunitního systému. Narušení jejich funkcí však může vést ke vzniku závažných nemocí. V průběhu aktivace BMMCs dochází k podstatné reorganizaci MTs. Molekulární mechanismy, které regulují tyto změny, jsou ale často neznámé. V této práci jsme charakterizovali funkci signálních proteinů GIT1/βPIX, kinázy PAK1 a Ca^{2+} signalizace v regulaci nukleace MTs u BMMCs a v dalších buněčných typech. Rovněž jsme popsali funkci působení miltefosinu (hexadecylphosphocholinu), nové slibné látky pro léčbu onemocnění způsobených žírnými buňkami.

Zjistili jsme, že GIT1/βPIX proteiny interagují s γ-tubulinem, a že jsou lokalizovány v centrozomech žírných buněk. Nukleace MTs je pozitivně ovlivňována GIT1 proteinem a Ca^{2+}, zatímco βPIX reguluje nukleaci MTs negativně. Cytosolický Ca^{2+} ovlivňuje vlastnosti γ-tubulinu a stimuluje jeho interakci s GIT1 a proteiny γ-tubulinového komplexu. Kromě toho vytváří γ-tubulin v aktivovaných BMMCs komplexy s GIT1 proteiny fosforylovanými na tyrozinech. Naše data dokumentují nový mechanismus regulace MTs v aktivovaných BMMCs pomocí tyrozinových kináz, GIT1/βPIX proteinů a Ca^{2+} signalizace.

Ukázali jsme, že signální proteiny GIT1/βPIX společně s PAK1 kinázou ovlivňují nukleaci MTs z interfázních centrozomů v různých buněčných liniích. GIT1 a PAK1 představují pozitivní a βPIX negativní regulátory tohoto procesu. Úroveň nukleace MTs koreluje s množstvím γ-tubulinu na centrozomech. Prokázali jsme, že PAK1 fosforyluje GIT1 i βPIX proteiny a určili jsme jejich vazebné domény pro interakci s γ-tubulinem. Na základě těchto výsledků jsme navrhli nový mechanismus, kterým GIT1/βPIX signální proteiny a PAK1 kináza regulují nukleaci MTs v interfázních buňkách.

Poprvé jsme ukázali, že miltefosin ovlivňuje BMMCs jak na plazmatické membráně, tak i v cytosolu. Miltefosin inhibuje degranulaci, reorganizaci MTs a chemotaxi za antigenem. Zatímco prokřížení a tyrozinová fosforylace IgE receptorů je v aktivovaných BMMCs působením miltefosinu potlačena, vtok Ca^{2+} do buňky inhibován není. Miltefosin dále ovlivňuje pohyb granul, dynamiku MTs v závislosti na Ca^{2+} a inhibuje fosforylaci proteinů interagujících s EB1 proteinem vázajícím se na rostoucí konec MTs. Působením miltefosinu na různých místech v BMMCs lze vysvětlit jeho efektivitu při léčbě nemocí způsobených žírnými buňkami.

I. INTRODUCTION

The cellular cytoskeleton is a complex network of tubules and filaments that is found in eukaryotes as well as in archaea or bacteria. It is comprised of three main components: microfilaments (MFs), intermediate filaments (IFs), and microtubules (MTs). Whereas basic building components of MFs and MTs are globular actins and tubulins, IFs are formed by fibrillary proteins.

MFs represent with their diameter of about 7 nm the thinnest fibres of the cytoskeleton. MFs are formed by two parallel helical strands of filamentous actin (F-actin) generated by the polymerization of monomeric, globular actin (G-actin). MFs are polar structures with fast-growing barbed ends and slow-growing pointed ends. The actin filament network is highly dynamic enabling its involvement in various cellular processes. Actin filaments participate in the maintenance of the cell shape, mechanical stability, cell contractility, cell motility and cytokinesis. They are also important for signal transduction. A plethora of actin-binding proteins organise MFs into complexes, bundles and networks, and regulate their stability and functions. Between actin targeting and regulatory proteins belong sequestering, nucleating, elongating, branching, capping, bundling, cross-linking, stabilizing, severing and motor proteins [1].

IFs have typically diameter about 10 nm and are composed of one or more IF proteins. IF proteins are encoded by over 70 genes and their expression is cell- and tissue-specific. IFs are classified into six major types based on the similarities in amino acid sequences and protein structures. They are mostly localized in the cytosol (type I-IV, and VI) or in the nucleus (type V). Acidic and basic keratins belong to types I and II, respectively. Type III is represented by desmin, peripherin, vimentin, and glial fibrillary acidic protein (GFAP). Neurofilament proteins (NF-L, NF-M, NF-H, and α-internexin) are expressed in neurons and belong to type IV. Nuclear lamins A, B and C are classified as type V and nestin as type VI. Filensin and phakinin are non-classified IFs due to deviations in the structure of consensus domains. The basic structure of IF protein monomer is the central α-helical rod domain composed of three sub-helices connected by linker regions, and non-α-helical N-terminal (“head”) and C-terminal (“tail”) domains. Both ends vary in the length and sequence across the IF types. Monomers form dimers that line up to antiparallel tetramers. Tetramers associate head-to-tail into IFs that lack the polarity. IFs participate in keeping cell shape, mechanical stability,

organelle distribution, signal transduction, and motility. The importance of IFs in the cell physiology is supported by human diseases linked to mutations in IF genes [2].

I.1 Microtubules

MTs belong to the key cytoskeletal filaments of eukaryotic cells. The MT cytoskeleton critically mediates the spatio-temporal organization inside the eukaryotic cell and is responsible for essential cellular processes. MT functions rely on its specific architecture which must actively respond to environmental changes during cell growth and differentiation. Precise MT arrangement is achieved by the coordinated action of tubulin isotypes, tubulin posttranslational modifications (PTMs) and MT-associated proteins (MAPs) [3, 4].

I.1.1 Microtubule organization and functions

The organization of MT network, together with precisely regulated MT stability and dynamics are fundamental assumptions for proper MT functioning. As MTs are involved in many essential cellular functions, they have to quickly react to cellular and environmental signals. MTs participate in keeping cell shape, organizing organelle positions, providing platforms for the intracellular transport, establishing cell polarity and signal transduction. In interphase cells, MTs are essential for cell motility, whereas in mitotic cells they form mitotic spindle to segregate chromosomes [3]. The majority of MTs are nucleated from MT organizing centres (MTOCs) as centrosomes and form radial MT arrays. Nevertheless, MTs also form specialised networks and specific assemblies such as centrioles, basal bodies, axonemes of cilia and flagella, and meiotic and mitotic spindles.

Specific MT arrangements are mostly found in differentiated cells. For instance, in neurons MTs serve as tracks for axonal transport, in muscle cells they modulate sarcomere assembly and nuclei positioning, and in polarized epithelia MTs participate in transcytosis and cell polarization [5]. The non-radial organization can be also found in some types of fungi and plant cells that do not have centrosomes [6]. In plants, the significant part of MTs form sheet-like arrays associated with the cell cortex [7]. The specific geometry of MT arrays is mostly organized into parallel or antiparallel arrays, and strongly depends on the localization of MT-nucleation sites. In several types of differentiated cell types, centrosomes are switched

off and so-called acentrosomal MTs are nucleated by non-centrosomal sites [8]. The acentrosomal MTs might be also generated by a loss of MT anchorage to the centrosome [5].

Centrioles are polarized cylindrical structures that form the core of the centrosome, promote formation of spindle poles in mitosis, and serve as basal bodies of cilia and flagella [8, 9]. Their cores are composed from nine radially symmetrically arranged sets of MTs that vary in proximal and distal regions. The proximal region contains nine MT triplets that are composed from A-, B-, and C-tubules within each triplet. A-tubule is composed from 13 protofilaments (MT subunits), whereas B- and C-tubules contain only 10 protofilaments. Two latter tubules share 3 protofilaments with A- and B-tubule, respectively. Triplets are connected by an A-C linker. The centriolar distal region does not have C-tubule, and is therefore composed only from MT doublets [10]. The centre of the centriole is formed by a cartwheel which establishes the centriole's nine-fold symmetry [11]. The cartwheel is composed from a central hub from which nine radially arranged spokes emanate and extend toward outer MT triplets. The carthweel structure is then connected to MTs with a pinhead region [12]. Mature centrioles further contain subdistal and distal appendages [13]. The subdistal appendages mediate anchoring of MTs, and the distal appendages are critical for docking of basal bodies to the plasma membrane to form the axoneme of cilia or flagella [9].

Cilia are composed from the axoneme and the outward membrane. In motile cilia, the central pair of MTs is surrounded by nine MT doublets (9 + 2 structure), whereas in nonmotile primary cilia the central pair is absent (9 + 0 structure) [14]. Similarly as in centrioles, MT doublets are composed from A- and B-tubules. Inside the MT doublet is an inner sheath composed from different types of MT proteins. Its function is to stabilize the structure of MT doublet, especially the building of B-tubule [15]. Cilia are nucleated by basal bodies that are generated by the conversion from the mother centriole. Thus, the basal body contains MT triplets, while the axoneme is composed from MT doublets. The intermediate region between the basal body and the axoneme is called the transition zone [9].

The mitotic spindle is a special MT array, which has a crucial role in precise segregation of chromosomes during cell division in somatic animal cells. It is a bipolar dynamic structure composed from MTs, MT associated proteins and motor proteins. Generally, three types of MTs are recognized in the mitotic spindle. The kinetochore MTs attach the chromosomal kinetochores, the astral MTs interact with the cell cortex and position the spindle, and the non-kinetochore MTs help to separate the poles and stabilize the spindle [16]. Main organizators of the mitotic spindle are centrosomes that are embedded into the opposite poles

of the mitotic spindle. Centrosomes are important for rapid and accurate segregation of chromosomes [17].

I.1.2 Microtubule structure and dynamics instability

MTs are hollow cylindrical tubes with an outer diameter of 25 nm. They are composed from the evolutionary highly conserved αβ-tubulin heterodimers that were discovered 50 years ago [18]. The αβ-tubulin dimers associate longitudinally to form protofilaments. The most often, 13 protofilaments interact laterally to generate MTs. [19]. Tubulins represent 3-4 % of the total protein content in the mammalian cells. In the brain, their amount reaches up to 20 % [20]. While the amino acid sequence similarity between α- and β-tubulin is only 45 %, their secondary and tertiary structures are essentially identical [21]. They both contain a core formed by two β-sheets surrounded by α-helices. The tubulin monomer has a compact structure, in which three functionally distinct domains can be recognized. The N-terminal domain with a nucleotide-binding site, middle domain and C-terminal domain, which is an unstructured region exposed on the tubulin surface that extends from MTs [22].

Globular α- and β-tubulins form stable dimers with naturally curved conformation [23], but might also stay in a monomeric form for several hours. The association between α- and β-tubulin is tighter than is the association of dimers in the MT lattice [24]. This is influenced by differently regulated guanosine 5'-triphosphate (GTP) hydrolysis in α- and β-tubulins. In α-tubulin, GTP binds to a “non-exchangeable site” or N-site, and is not hydrolysed [21]. As this GTP is trapped between two monomers of the αβ-heterodimer, it tightly binds both monomers together when the heterodimer is in soluble form [25]. GTP binding to β-tubulin is at the interface between two heterodimers within the protofilament. β-Tubulin binds GTP at an “exchangeable site” or E-site. This GTP hydrolyses to guanosine diphosphate (GDP) after the heterodimer associates into the protofilament, and thus the interaction weakens [21].

Tubulins have binding sites for divalent cations as well as for low molecular weight tubulin binding agents (TBAs) that are also called “antimitotic drugs” [20]. MT-destabilizing drugs prevent MT polymerization, and include compounds such as the Vinca alkaloids (e.g. vincristine, vinblastine, vinorelbine) and colchicines. These drugs are already clinically used or are under the clinical investigation for the treatment of cancer [26]. MT-stabilizing drugs such as taxanes, epothilones and laulimalide stimulate the assembly of purified tubulin and increase the density of cellular MTs. These TBAs also play an important role in the cancer chemotherapy [27]. Most of the TBAs bind one of four main sites within the MT:

the colchicine site, vinca alkaloid site, taxane/epithilone site or laulimalide site [28]. The TBAs effects vary according to the drug concentration. While high concentrations alter overall MT mass, low concentrations of the drug disrupt MT dynamics and protein interactions [26].

Head-to-tail polymerization of the αβ-tubulin heterodimers leads to the creation of intrinsically polar structures. MTs possess α-tubulin at the minus-end, and β-tubulin at the plus-end [29]. Protofilaments could be in MTs organized in the A-type or B-type lattice. In the A-type lattice, the dimers in adjacent protofilaments form staggered arrangement (α-β lateral bond), whereas in the B-type lattice, the neighbouring dimers are lined up obliquely and form lateral bonds between the same tubulin monomers (α-α, β-β) [30]. The B-type lattice forms the left-handed helix with a helical discontinuity or a seam between the first and thirteen protofilament (α-β) [19]. Only B-type lattices were identified *in vivo* [31].

Tubulins dynamically assemble *in vitro* in the presence of GTP and only when the "critical tubulin concentration" is achieved [32]. The critical concentration of tubulin is *in vivo* lowered by associated proteins, and the highly regulated equilibrium between the MT-bound tubulin dimers and their soluble forms is generated. When the αβ-tubulin subunits polymerize into protofilaments, GTP bound to β-tubulin hydrolyses to GDP [21]. It is not clear how soon the hydrolysis occurs, but the dimers still containing GTPs at β-tubulin subunits form the GTP cap on the growing MT [25].

MTs are highly dynamic structures that can have phases of fast growing and shortening by adding and removing the αβ-tubulin heterodimers at their ends. Tubulin subunits are added and removed with different kinetics at each of the MT end, creating a fast growing plus-end and a slow growing minus-end [29]. While minus-ends are in cells mostly anchored in the nucleation centres, plus-ends are dynamic, and lengthen and shorten in response to the cellular signals. This phenomenon is called "dynamics instability" (Fig. 1) and is crucial to many MT functions [33]. The growing plus-end is usually slightly curved, flattened and resembles the sheet-like structure, whereas the shrinking plus-end is denoted by peeling protofilaments that are heavily curved [34].

Dynamic instability might be explained by the GTP cap model. In the presence of the GTP cap, MTs are stabilized and grow. Loss of the cap generates unstable MT lattice composed of GDP-tubulin, which leads to the rapid MT shrinkage [34]. The alterations between the growth and the shrinkage are supplemented by transition phases. A catastrophe is a switch from the growth to the shrinkage and a rescue is the transition from the shrinkage to

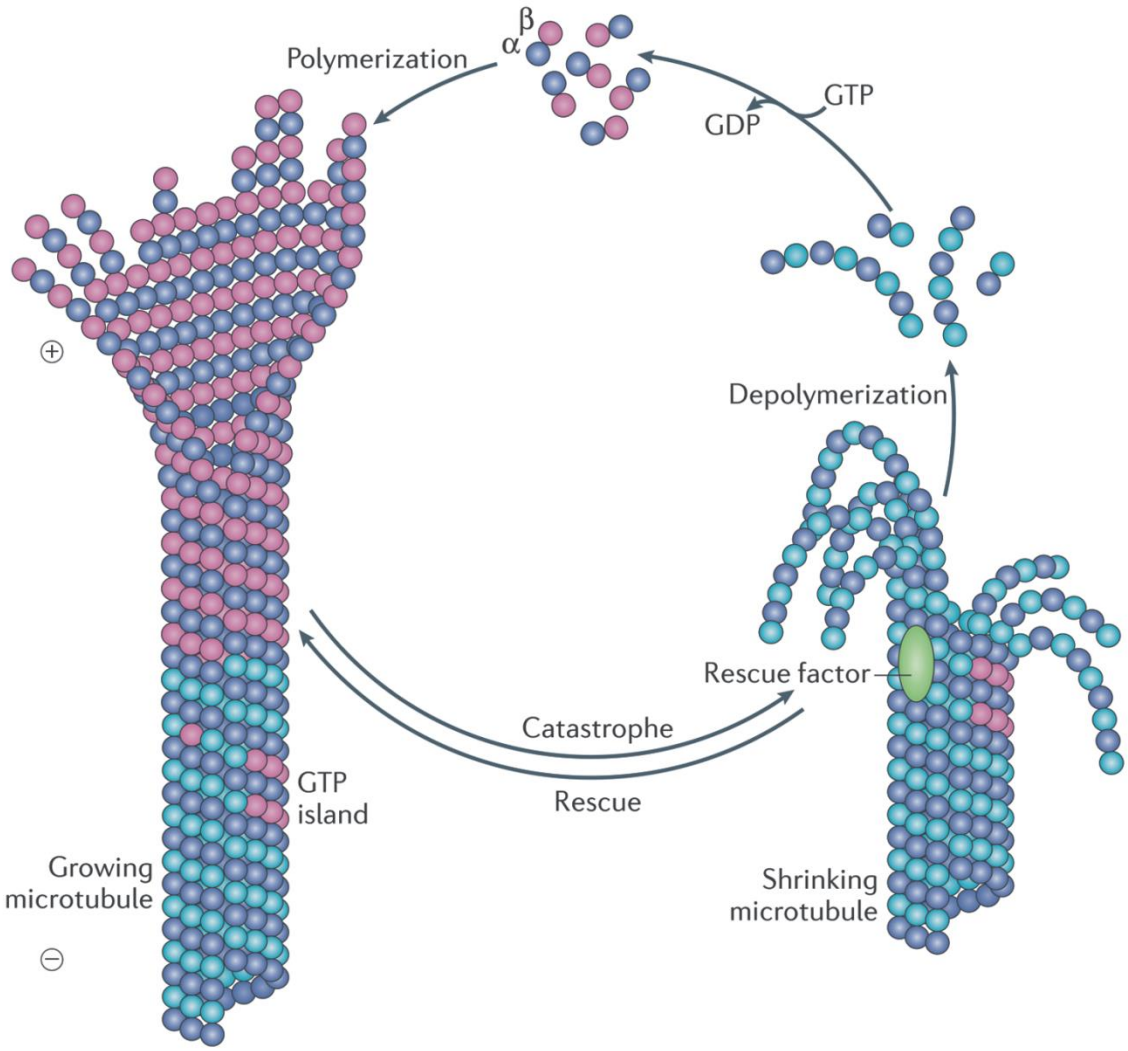

Figure 1. Dynamics instability of microtubules. The assembly of MT is driven by binding of the αβ-tubulin heterodimers into the sheet-like structure at the plus-end of MT. The growing MT is cycled with the shrinking MT. Because the GTP hydrolysis on β-tubulin occurs with a delay, a GTP cap is generated to stabilize the MT tip. When the GTP cap is disrupted or free GTP-tubulin concentration decreases, MT starts to depolymerise. The transition phase between the polymerization and the depolymerization is called a catastrophe and the reverse transition phase is called a rescue. The rescue might be induced by GTP islands or rescue factors presented at the MT. β-Tubulin with GTP is in purple and β-tubulin with GDP is in cyan. Adapted from [34].

the growth [3]. Regulation of MT dynamics is discussed in detail in chapter I.2.

Both, α- and β-tubulin belong to a large tubulin superfamily which also includes γ, δ, ε, η, ζ, θ, ι, and κ-tubulin [19]. First three members (α-, β- and γ-tubulin) are more abundant in the cell, are expressed in all eukaryotes and are highly conserved across species [35]. Only α- and β-tubulin are capable to polymerize into MTs. γ-Tubulin is, on the other hand, a well-known nucleator of MTs and is described independently in the chapter I.3.1. The remaining tubulins

are not so abundant and ubiquitous. δ-Tubulin and ε-tubulin were identified in various organisms including humans and they play important roles in the development of basal bodies and centrioles. η-Tubulin was identified in protists and animals [19, 36] and is required for proper basal body biogenesis [37]. ζ-, θ-, ι-, and κ-tubulins are less studied members of the tubulin superfamily, and their functions are largely unknown [19].

I.1.3 Tubulin code

The tubulin code (Fig. 2) of MTs is formed by different combinations of α- and β-tubulin isotypes, together with tubulin PTMs. The surface of each MT is thus variable and interacts with a specific set of regulatory proteins. The tubulin code is unique for each MT and indicates its function and specialization [4]. The expression of certain tubulin isotypes and tubulin PTMs alter during oncological diseases [20, 38].

I.1.3.1 α- and β-tubulin isotypes

The α-tubulin and β-tubulin subunits exist in numerous isotypes, which have different amino acid sequences and are encoded by multiple genes (Fig. 2A). This provides cells with highly conserved, but still different tubulin heterodimers to create MTs [19]. Nine α-tubulin and nine β-tubulin genes have been identified in mammals. The majority of α- and β-tubulin amino acid sequences are highly conserved to generate essential tertiary structures of the tubulin core. The most common alterations between tubulin isotypes occur in their unstructured flexible C-terminal tails. As C-terminal tails decorate the surface of MTs, their variability enables specific interactions with MAPs [4].

The precise impact of specific isotypes on MT properties and functions has not been clarified yet [4]. Nevertheless, various αβ-tubulin heterodimers differ in the binding of MT-associated proteins [19] and their isotype ratio and concentration also modulate MT dynamics. For example, the MT from βI-tubulins has increased switching frequency between the growth and the shrinkage in comparison to the βII-composed MT [39], the MT from βIIB has much lower catastrophe frequencies than the MT with βIII isotype [40] and the abundance of a minor isotype βV-tubulin leads to constant MT shortening and the detachment of minus-end from centrosomes [41]. Besides that, the mutation in α-tubulin gene TubA1A straightens the natively curved dimer structure, which then reduces the dynamics of MTs and generates straighter MTs [42].

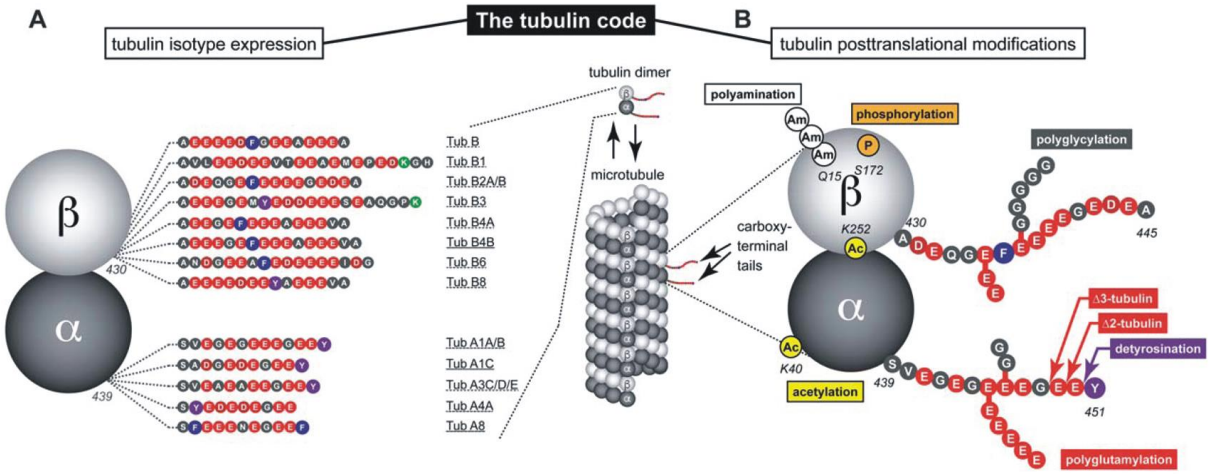

Figure 2. The tubulin code. The tubulin code reflects the heterogeneity between MTs and affects their functions and specializations. It is generated by two different processes. (**A**) The expression of tubulin isotypes. Isotypes mostly vary within their C-terminal tail regions. (**B**) The generation of PTMs. PTMs can occur at the tubulin core or within the C-terminal tail region. Examples of PTMs are depicted in various colours. Adapted from [43].

Recently, disease-related mutations of specific tubulin isotypes were identified and allowed the insight into molecular mechanisms regulated by various tubulin isotypes [43]. Mutations in the platelet-specific β-tubulin gene TubB1 cause bleeding disorders [44], mutations in TubB3 gene, an isotype specifically expressed in neurons, lead to neuronal disorders [45], and mutations in TubB8 gene cause impaired oocyte maturation [46]. Many other mutations have been identified in broadly expressed tubulin isotypes. Interestingly, mutations at different amino acid residues in a single tubulin isotype can have distinct pathological outcomes [43].

I.1.3.2 Tubulin post-translational modifications

Tubulin PTMs represent the second part of the tubulin code (Fig. 2B). They are mostly generated on the MT polymer at the tubulin core or at variable C-terminal tails. PTMs thus create local marks on the tubulin/MT and are mostly enriched on stable long-lived MTs. Well characterised are tyrosination and detyrosination, (poly)glutamylation, (poly)glycylation and acetylation [4, 47]. Detyrosination of α-tubulin generates Glu-tubulin [48] and further hydrolysis of glutamate residues from Glu-tubulin forms αΔ2- and αΔ3-tubulin [49, 50]. Recently, βΔ4-tubulin lacking four C-terminal residues, was identified [50].

Besides the above PTMs, phosphorylation, methylation, polyamination, palmitoylation, arginylation, glycosylation, nitration, ubiquitylation, and sumoylation have been described [19]. Such a large number of tubulin PTMs, together with their combinations, points to the possibility of the occurrence of many unique MTs.

I.1.4 Microtubule regulatory proteins

The MT cytoskeleton organizes into discrete three-dimensional patterns by the activity of plenty regulatory proteins. These proteins are found all along the MT lattice or interact with MT-ends. The nucleation, assembly, stability and dynamics of MTs are regulated by MT nucleation proteins, stabilizing and destabilizing MAPs, MT cross-linking proteins, molecular motors, and proteins regulating MT dynamics at the plus- and minus-ends [3, 34]. Proteins involved in the regulation of MT dynamics and MT nucleation are described in detail in chapters I.2 and I.3.

I.1.4.1 Microtubule stabilizing proteins

Proteins specialized to stabilize MTs are called structural MAPs and are localized along MTs. Their structure usually contains repeating conserved MT-binding domains. One MAP might therefore interact with more tubulin dimers, cross-link them, and promote the stable MT. MAP projection domains are also capable of cross-linking with other MTs. Structural MAPs include MAP1, MAP2, MAP4 and tau proteins [25]. MAP1, MAP2 and tau are neuronal proteins, while MAP4 is a high molecular weight protein expressed in non-neuronal cells. MAP1A and MAP1B are less described unstructured MAPs. Their repetitive sequences in MT-binding domains contain an abundance of positively charged amino acids and thus bind to the negatively charged MT surface. MAP1A was described to stimulate the nucleation and the MT growth. MAP2, MAP4 and tau proteins are thermostabile. MAP2 is an effective MT stabilizer in dendrites, whereas tau preferentially promotes the assembly and the stabilization in axonal MTs [25]. Tau was also described as a co-organizator of MT and actin networks [51]. Tau binds to the interface between the αβ-tubulin heterodimers by small groups of evolutionary conserved tau residues, whereas the rest of the protein remains flexible [52].

There are several other MT-stabilizing proteins such as stable tubule only polypeptides (STOPs) and doublecortin. STOPs stabilize MTs and provide them with the resistance

to cold [53]. Doublecortin stabilizes MTs, promotes the polymerization and might bundle MTs [25].

I.1.4.2 Microtubule destabilizing proteins

Regulatory proteins use different modes of action to destabilize MTs. Basically, they can be classified as sequestering proteins, severing proteins, and MT depolymerases.

The tubulin-sequestring protein stathmin (oncoprotein 18) recognizes curved structure of free αβ tubulin dimer [23]. Stathmin binds a pair of αβ-tubulin heterodimers to prevent their further interactions [54]. Katanin, spastin and fidgetin belong to MT severing proteins that disrupt contacts between the αβ-tubulin heterodimers in the MT wall. This leads to the breakup of MTs into short pieces, generation of new ends, and rapid depolymerization [21]. Katanin forms hexamers in two conformations forming either an open spiral or a closed ring. Cycling of these two conformations consumes the energy from adenosine 5'-triphosphate (ATP) and provides a power stroke for MT severing. The hexamer in the open spiral interacts with the MT lattice and the tubulin C-terminal tail. Following closure of the ring extracts the tubulin dimer. A similar mechanism of action was proposed to other MT-severing proteins as they possess high sequence homology [55].

MT stability is further affected by MT depolymerases that promote the catastrophe to regulate the MT length. Mitotic centromere-associated kinesin (MCAK) from kinesin-13 family of molecular motors plays an essential role during mitosis by regulating chromosome segregation at kinetochores and chromatid movement during anaphase [3]. Using the energy from ATP hydrolysis, MCAK removes terminal subunits from MT ends. Kinesin-8, on the other hand, moves along the MT lattice to the MT plus-end. At the growing end, kinesin-8 destabilizes the GTP cap by removing tubulin subunits from the MT tip [34].

I.1.4.3 Microtubule cross-linking proteins and molecular motors

MT cross-linking and bundling proteins connect MTs into networks to form effective interactions between cytoskeletal filaments, and they can also generate forces. MT-actin cross-linking factor 1 (MACF1) is a well described integrator and modulator of numerous cellular processes as it bridges MTs and MFs to co-organize both networks. It regulates cell migration, axonal growth and trafficking [56]. Structural MAPs are other examples of cross-linking proteins. Besides functioning as MT-stabilizing protein, tau also works as the molecular linker. Tau binds simultaneously to MTs and MFs *in vitro*. Interestingly, tau induces the polymerization of MT or actin filament along pre-existing filaments and thus

co-organizes the cytoskeletal network [51]. Doublecortin is another structural MAP that can cross-link MTs. It interacts with two tubulin subunits in one MT or bundle two MTs together. Kinesins are molecular motors that might have separate MT-binding sites enabling cross-bridging of MTs [25].

Molecular motors are group of MT-targeting proteins that use MT lattices as tracks for the cargo transport. MT plus-end directed molecular motors are kinesins [57]. Some of them function as MT depolymerazes at MT plus-ends [34]. Minus-end directed transport is mediated by cytoplasmic dynein 1, usually found in the complex with dynactin. The specific transport of organelles (Golgi apparatus, nucleus), viruses, and mRNAs is regulated by multiple adaptor proteins [57]. An unusual function of cytoplasmic dynein is the tethering of the MT plus-end. Dynein attached to a barrier binds MT tips, inhibits growth, and promotes catastrophes. Depolymerizing MT ends stay attached to cortical dynein which generates pulling forces and positions MT asters [58].

I.2 Regulation of microtubule dynamics

MT functioning is based on rapid reorganization of the MT arrangement in response to various signalling molecules. Therefore, the dynamics of MTs has to be precisely regulated by a plethora of MT-targeting proteins that bind either to the MT plus- or minus-end.

I.2.1 Microtubule plus-ends tracking proteins

MT plus-end tracking proteins (+TIPs) (Fig. 3) are a large group of MAPs that predominantly accumulates at MT growing ends to regulate their assembly and disassembly. While the growth and the shrinkage are relatively well known, the mechanisms how catastrophes and rescues are regulated are poorly understood [34].

+TIPs can be divided into “autonomous tip trackers” that recognize MT ends without other factors, and “hitchhikers” that primarily bind to the autonomous tip trackers for their concentration at the MT tip [59]. +TIPs form a network based on a limited set of interactions mediated by small domains, linear motifs and/or basic regions. The +TIP network regulates MT dynamics at specific cellular sites and signalling pathways. It guides MT growth, mediates the attachment of growing ends to cellular structures and concentrates signalling and transport proteins [60].

I.2.1.1 End-binding proteins

End-binding (EB) proteins, among which belong EB1, EB2 and EB3, is the most studied +TIP family. EBs autonomously recognize growing MT ends and even recruit a range of other different factors [59]. *In vitro*, EBs can bind also to the GDP-bound MT lattice, but with ~10-fold lower affinity than to the growing end [61]. Normally, EBs bind preferentially to GTP-β-tubulin subunits at the MT plus-end by its calponin-homology (CH) domain at their N-terminal region. The C-terminal region serves for the dimerization of EB proteins and for the binding of the other +TIPs [62]. EBs thus represent core +TIPs and master regulators of the +TIP interaction network. A few hundred EB molecules localize to growing MT ends to form the comet-like accumulations [63]. The binding of EB1 promotes MT maturation by accelerating the transition of GTP- to GDP-tubulin at the MT plus-end and by promoting lateral protofilament interactions [64].

I.2.1.2 Microtubule polymerases

MT polymerases rescue shrinking MTs and promote their growth. Cytoskeleton-associated protein 5 (CKAP5/ch-TOG; XMAP215 in *Xenopus*) belongs to the group of autonomously tip tracking +TIPs [3]. ch-TOG interacts with the extreme MT end [64] and enhances MT growth rates 5-fold using its tubulin-binding tumour overexpressed gene (TOG) domains [65]. TOG1 domain binds to the curved conformation of unpolymerized αβ-tubulin heterodimer and TOG2 domain recognizes the non-straight MT-end-specific conformation of αβ-tubulin. TOG domains can thus add repeatedly tubulin dimers to the MT growing end [66]. Another domain, a MT lattice-binding domain, enables ch-TOG to diffuse along MTs to reach their plus-ends [65].

I.2.1.3 Other +TIPs

Between members of +TIPs that are directly recruited to MT plus-end by EB1, are cytoplasmic linker protein 170 (CLIP-170), $p150^{Glued}$ (subunit of dynactin complex), CLIP-associated proteins (CLASPs) and adenomatous polyposis coli protein (APC). CLIP-170 and $p150^{Glued}$ use their cytoskeleton-associated protein Gly-rich (CAP-Gly) domains for binding to EB1 [59]. CLIP-170 promotes rescues, whereas $p150^{Glued}$ suppresses catastrophes [34]. Other +TIPs contain the small amino acid motif SxIP (x is any amino acid), which recognizes a specific domain of EBs and targets +TIPs to the growing MT end. SxIP is

a major “MT tip-localization signal” [67]. CLASPs can bind to MTs directly or through the interaction with EBs by SxIP motif. CLASPs promote MT rescues and suppress MT catastrophes by delivering the αβ-tubulin dimers into the growing MT [68]. APC uses its SxIP motif for binding to EB1, and for the increase of MT stability [67, 69]. Recently, third EB-binding motif enabling +TIPs to interact with EBs was identified in several +TIPs. LxxPTPh (h is a hydrophobic amino acid) motif binds to EBs and tracks the MT plus-end [70]. SLAIN2 is a special +TIP which expresses multiple binding motifs such as SxIP and LxxPTPh. Therefore, it functions as an “adhesive” factor. SLAIN2 enhances +TIP interactions and localizes several +TIPs to the growing MT end [70, 71].

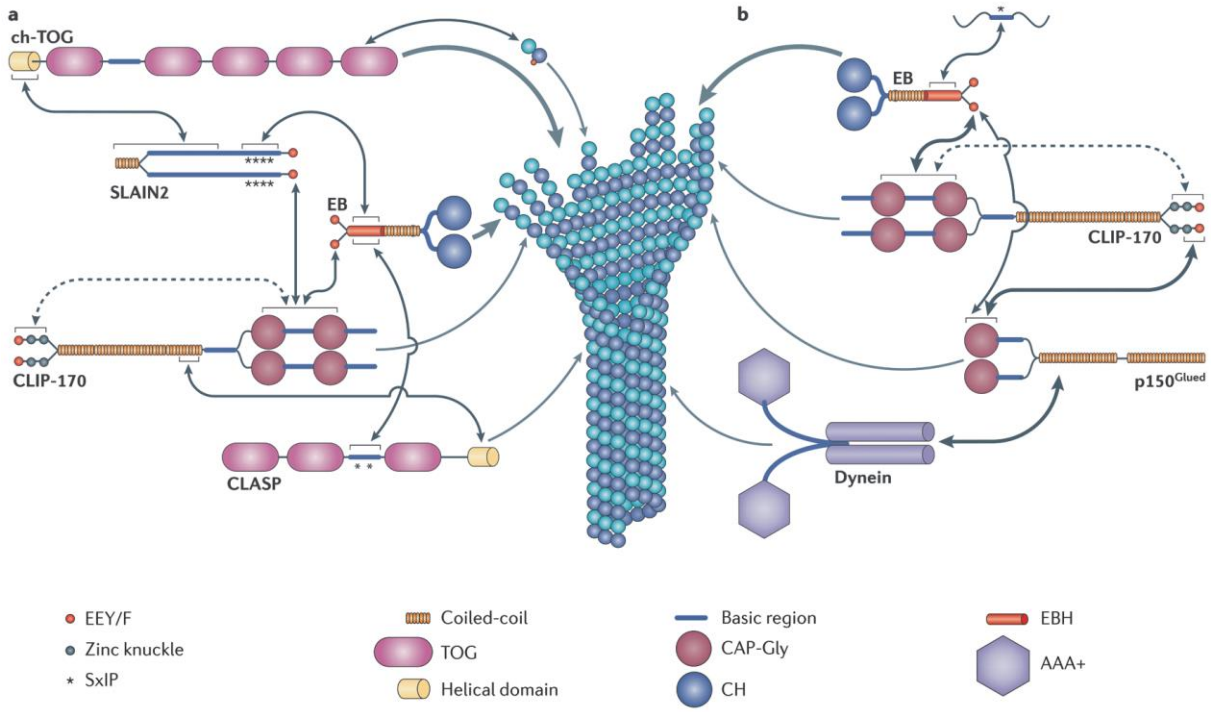

Figure 3. Network of +TIPs. Localization of various +TIPs at the MT lattice and to the plus-end are shown, together with a complex network that is formed by interactions between +TIPs. **a)** EB and ch-TOG bind directly to the MT growing end. SLAIN2 is an „adhesive” +TIP which associates simultaneously with ch-TOG and CLIP-170, and through binding to EB localizes these proteins to the MT tip. CLASP interacts with the MT directly or localize to the growing end by interaction with EB or CLIP-170. **b)** Various domains and motifs enable +TIPs to create a complex network. EB binds to CLIP-170 and $p150^{Glued}$, while the two latter interact together. $p150^{Glued}$ binds to dynein, which recruits this protein to the MT plus-end. Various interacting domains, motifs and regions are depicted. Adapted from [34].

I.2.2 Regulation of +TIPs

MT dynamics is controlled by the coordinated accumulation of different +TIPs to MT plus-ends. Since many +TIPs associate with EBs to accumulate at MT growing ends, the competitive binding between +TIPs is the main regulation of MT dynamics. Modifications of MTs (PTMs and binding of MAPs) or +TIPs provide an additional control [72]. Both, positive and negative effects of the phosphorylation on MT growth were reported. The phosphorylation of EB1 at the linker region connecting N- and C-terminal regions modulates its association with MTs. While the phosphorylation at Ser155 is critical for enhanced EB1 accumulation at MT growing ends, the phosphorylation of Thr166 has the opposite effect [73]. EB1 phosphorylation also promotes its interaction with CLIP-170 and $p150^{Glued}$, and thus enhances their accumulation at the plus-end of astral MTs [74].

At the +TIP level, the phosphorylation often occurs close to SxIP motifs on +TIPs that can interact with EB1. The accumulation of negative charge abrogates +TIP binding to the negatively charged EB1 C-terminal end. Therefore, phosphorylated +TIPs dissociate from the MT growing end by the reduction of their affinity for EB1 [67]. Glycogen synthase kinase 3β (GSK3β) negatively regulates MT dynamics by the phosphorylation of several +TIPs [69, 75]. CLASP2 is phosphorylated by GSK3β at multiple sites required for EB1-independent MT plus-end tracking as well as for the interaction with EB1. GSK3β phosphorylation thus leads to CLASPs dissociation from MTs [75]. Similarly, GSK3β phosphorylation negatively regulates binding of APC to MTs [69].

+TIPs are often regulated by cell-cycle specific phosphorylations. Aurora kinases modulate MT plus-end dynamics in mitotic cells and they are required for normal spindle kinetics [76, 77]. Kinesin-8 motor protein, Kif18b, interacts with EB1 to bind to astral MTs, and forms the complex with MCAK to depolymerise MTs in mitosis. Aurora A and B kinases phosphorylate MCAK, which leads to Kif18b-MCAK complex disassembly and MT plus-end stability [76]. In yeast, EB1 is in the complex with Aurora B. During anaphase, Aurora B phosphorylates EB1 at multiple sites, which leads to dissociation of EB1 from MTs [77]. MT plus-end tracking by CLASP2 is in mitosis disrupted by the concerted action of cyclin-dependent kinase (Cdk) and GSK3 phosphorylation. These kinases phosphorylate CLASP2 at multiple sites close to SxIP motifs to abrogate CLASP2 interaction with EB1 [75, 78].

+TIPs are also regulated by Ca^{2+} signalling. Calcineurin, the Ca^{2+}-dependent phosphatase is involved in the dephosphorylation and stabilization of EB3 that can in turn promote MT

growth [79]. Calcineurin associates with its inhibitor calcineurin-binding protein 1 (Cabin 1). The hyperphosphorylation of Cabin 1 by Ca^{2+}-dependent protein kinase C (PKC) leads to the suppression of calcineurin signalling [80] and thus to the inhibition of MT growth [79]. Ca^{2+} can also regulate MT dynamics directly by its binding to MT plus-end-interacting protein BPAG1n4. Ca^{2+} inhibits binding of BPAG1n4 to EB1 and promotes the association of BPAG1n4 with the MT lattice [81].

I.2.3 Microtubule minus-end tracking proteins

Regulation of MT minus-ends in MTs not attached to MTOCs is much less understood than MT plus-end regulation. Minus-ends of MTs grow more slowly, catastrophes are less frequent, and remain relatively stable. Nevertheless, their dynamics contributes to MT turnover, organization of interphase MTs, and they are also important for controlling the architecture of the mitotic spindle during cell division [82]. The main factor that specifically binds to the MT minus-end is γ-tubulin ring complex (γTuRC). Beside γ-tubulin complexes, several other proteins that bind to the MT minus-end (-TIPs) were characterized.

Proteins from calmodulin-regulated spectrin-associated protein (CAMSAP)/ Patronin/Nezha family specifically recognize MT minus-ends and control their dynamics in different animal systems [82]. CAMSAPs stabilize growing minus-ends of non-centrosomal MTs that are not capped by γTuRCs or other factors [83, 84]. CAMSAP1 dynamically tracks growing MT minus-ends, whereas CAMSAP2 and CAMSAP3 stably decorate stretches of the MT minus-end lattice. CAMSAP2 and 3 thus stabilize minus-ends against the depolymerization and slow down the polymerization at these MT ends. Except the creation of stable non-centrosomal MTs, CAMSAP stretches at the MT can serve as “seeds” for non-centrosomal MT nucleation [83]. Another -TIPs are KAT8-associated nonspecific lethal (KANSL)1 and KANSL3 proteins. They are epigenetic regulators that associate with MT minus-ends to stabilize them in mitotic spindles [85].

I.3 Regulation of microtubule nucleation

The nucleation of new MTs is an essential, tightly regulated cellular process. Typically, MT nucleation is restricted to MTOC, which determines the specific position where MTs are nucleated. Beside canonical MTOCs such as spindle pole bodies and centrosomes,

non-centrosomal sites such as Golgi apparatus, nuclear envelope, chromatin, surface of pre-existing MTs, and plasma membrane-associated sites can nucleate MTs as well [32].

I.3.1 γ-Tubulin and γ-tubulin complexes

Centrosomal and non-centrosomal MTOCs consist from multi-subunit γ-tubulin complexes [32]. γ-Tubulins are minor members of the tubulin superfamily [86] and represent highly conserved proteins encoded by one to three genes in eukaryotic genomes [35]. In humans there are two γ-tubulins that are nucleation competent [87]. γ-Tubulin associates with γ-tubulin complex proteins (GCPs) into complexes that are essential for MT nucleation. GCPs have a low level of sequence identity, but share homologous regions. Short N-terminal GRIP1 and C-terminal GRIP2 regions are unique for GCPs [88]. γ-Tubulin complexes differ in their sizes. Basically, there are γ-tubulin small complexes (γTuSCs) and large γTuRCs [8].

γTuSCs (~300 kDa) have an Y-shaped structure, which consists of two molecules of γ-tubulin and one molecule each of GCP2 and GCP3 [89]. Several γTuSCs assemble with GCP4, GCP5, and GCP6 into the large complex of γTuRC (~2.2 MDa). γTuRC is named for its ring-shaped structure that mimics MT geometry and serves as a template for efficient MT nucleation [90, 91]. In γTuRC, γ-tubulin directly binds each of GCP2-GCP6, which leads to the generation of γTuSCs and γTuSCs-like structures (Fig. 4). Hybrid γTuSCs are created by the replacement of one of GCP2/GCP3 with one of GCP4-GCP6. Novel γTuSCs have both GCP2 and GCP3 changed for any combination from GCP4-GCP6 proteins, and half γTuSCs complexes can be composed from a single γ-tubulin and one molecule of GCP4, GCP5 or GCP6. Therefore, the composition of γTuRC might vary according to GCPs integrated into γTuSCs and γTuSCs-like structures. The precise stoichiometry of GCP4-GCP6 within γTuRC remains unknown [88].

The template-based nucleation model (Fig. 4) is an accepted model for MT nucleation that uses γTuRC as a platform for the assembly of the αβ-tubulin heterodimers. γTuRC contains 13 γ-tubulin molecules ordered into the ring shape, matching the structure of the MT [92, 93]. GCP2 and GCP3 are flexible proteins, generating either open or close form of γTuRC. The closed state of γ-tubulin complex is more active MT nucleator, which precisely matches the symmetry of MTs. The activity of γTuRC can be thus conformationally regulated [89, 94]. γTuRCs are efficient MT nucleators that associate with a number of targeting, activating and modulating proteins enabling MT nucleation from centrosomal and various non-centrosomal sites [32].

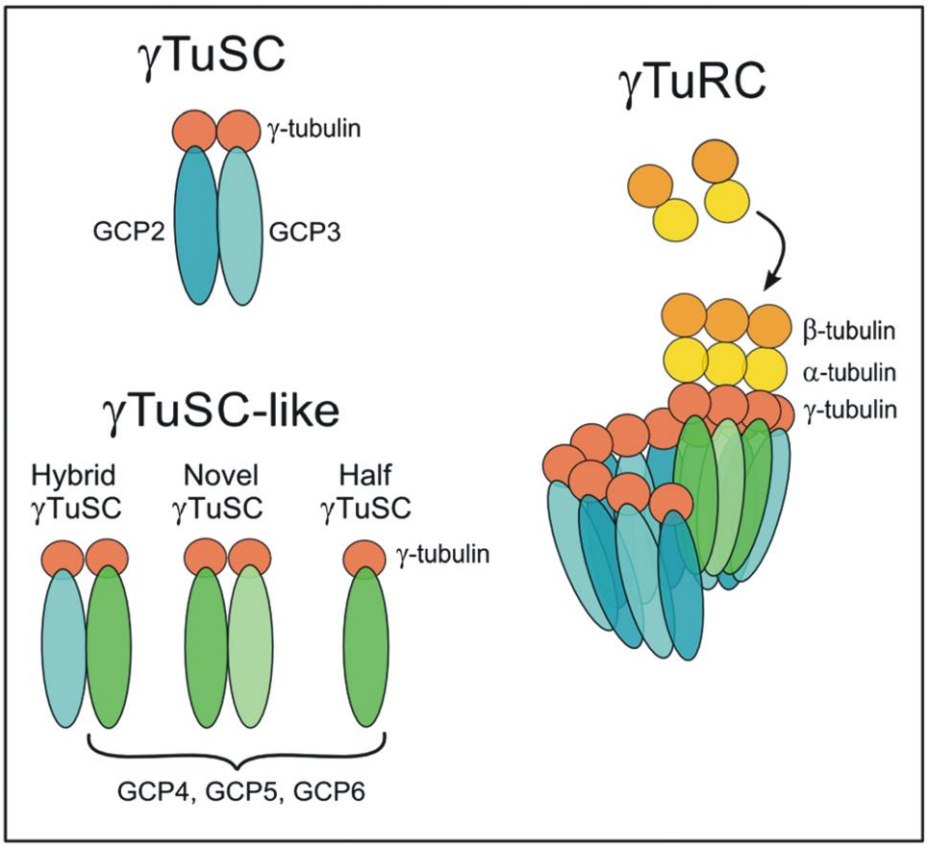

Figure 4. γ-Tubulin complexes and the template nucleation model. γTuSC is composed of two molecules of γ-tubulin and one molecule each of GCP2 and GCP3. γTuSCs-like structures have one or both of GCP2/3 replaced with GCP4, GCP5 or GCP6. γTuRC is generated by the association of γTuSCs and/or γTuSCs-like complexes. γ-Tubulins in γTuRC interact with the αβ-tubulin heterodimers and serve as a platform for the nucleating MT (the template nucleation model). Adapted from [95].

I.3.2 Centrosomal nucleation

In animal cells, MTs emanate to a large extent from the centrosome that serves as the main MTOC. The centrosome is composed from a pair of orthogonally oriented centrioles and a surrounding pericentriolar matrix (PCM). The older centriole is called mother and the newer one is termed daughter [8]. The PCM is a highly structured network with layers of proteins organized around the proximal end of the mother centriole [96]. In *Caenorhabditis elegans*, a PCM scaffolding protein SPD-5 assembles into the spherical condensates. These condensates in turn recruit a MT polymerase and MT-stabilizing protein, the two proteins that regulate MT nucleation. Together, these three proteins concentrate tubulin ~4-fold over the

background. Therefore, the PCM might organize MT arrays by the concentration of tubulin at local sites [97].

The recruitment of γTuRCs to the centrosome correlates with an increased MT nucleation and is regulated by a set of centrosomal proteins. Among them is a neural precursor cell expressed, developmentally down-regulated protein 1 (NEDD1/GCP-WD), which is responsible for γTuRC localization to the centrosome [98]. Mitotic spindle-organizing protein (Mozart)1/GCP9 and Mozart2/GCP8 are involved in γTuRC targeting to centrosomes in mitotic and interphase cells, respectively [99]. Several other proteins, such as A-kinase anchor protein 450 (AKAP450/CG-NAP) [100], pericentrin [100], ninein [101] and centrosomal protein 192 (Cep192) [102] have been identified to be involved in γTuRC localization, and also in its anchorage at the centrosome.

After the recruitment to the centrosome, γTuRC has to be activated for efficient MT nucleation. The precise molecular mechanism of γTuRC activation remains unknown, but may involve the conformation switch between the open and close form of γTuRC [94]. Two mostly studied γTuRC activators are cyclin-dependent kinase 5 regulatory subunit-associated protein 2 (CDK5RAP2) [103] and nucleoside-diphosphate kinase 7 (NME7) [104]. CDK5RAP2 increases the nucleation capacity by γTuRCs ~7-fold [103], whereas NME7 enhances MT nucleation by ~2.5 fold [104]. CDK5RAP2 contains several motifs among which γTuRC-mediated nucleation activator (γ-TuNA) associates with γTuRC to activate MT nucleation [103]. Besides that, myomegalin is recruited to the centrosome in an AKAP450-dependent manner to promote MT nucleation by γTuRC recruitment [105]. Efficient MT nucleation is achieved by MT plus-end regulators such as ch-TOG and its binding partner transforming acidic coiled-coil 3 (TACC3) [106], EB1 and CLASP [8].

MT nucleation is regulated by signalling proteins, such as protein kinase D3 (PDK3), Aurora A, Cdk1 and polo-like kinase 1 (Plk1) [106-108]. In mitosis, Aurora A phosphorylates TACC3 to target it to centrosomes [106], while Cdk1 and Plk1 phosphorylate NEDD1 to regulate γTuRC localization to the centrosome [108].

I.3.3 Non-centrosomal nucleation

While the centrosome is the main nucleation site in animals, non-centrosomal nucleation also plays an undisputable role in the creation and maintenance of MT architecture [32]. In this case, MTs emanate from MTOCs localised outside the centrosome. This type of

nucleation was first observed in higher plants that do not have centrosomes. Non-centrosomal MTOCs have been identified in different organisms and some of them have such nucleation only in specialized cell types [109, 110]. Well known are non-centrosomal nucleations from the Golgi apparatus, nuclear envelope, chromatin, surface of MTs and plasma membrane-associated sites [32]. Molecular mechanisms of MT nucleation from different cellular sites overlap. For example, factors implicated in chromatin-mediated MT nucleation regulate also the nucleation of branched MTs from pre-existing MTs in *Xenopus laevis* egg extracts [111]. The same factors also regulate non-centrosomal nucleation in neurons at the neurite tip and within the soma [112].

I.3.3.1 Nucleation from Golgi apparatus

The Golgi apparatus (Fig. 5a) serves as the MTOC in animal cells [113]. γTuRCs are recruited to the Golgi membrane by Golgin subfamily A member 2 protein (GM130) which recruits AKAP450 [114]. AKAP450 then interacts with CDK5RAP2 [115] or myomegalin [105]. CDK5RAP2 binds to pericentrin to attach γTuRCs to the Golgi apparatus [115]. Generated protein complex enables myomegalin and CDK5RAP2 to promote MT nucleation [105]. To make the nucleation from the Golgi kinetically favourable, +TIPs CLASPs and EB1s either stabilize newly nucleated short MTs [116] or associate with myomegalin to localize MTs [105]. In addition, tubulin-specific chaperone E (TBCE) increases the αβ-tubulin heterodimer concentration in the vicinity of Golgi-localized γTuRCs [117].

I.3.3.2 Nucleation from nuclear envelope

The nuclear envelope (Fig. 5b) has been identified as the MT nucleation site in several cell types, and among them skeletal muscles, together with higher plants are best characterised. Pavarotti kinesin-like protein (Pav) localizes Rac GTPase activating protein 50C (RacGap50C) to multiple foci at the nuclear envelope. RacGap50C then binds γ-tubulin complexes [118]. Pericentrin and ninein, MT anchorage-proteins, also associate with the nuclear membrane in animals [119]. In plants, GCP3-interacting protein 1 (GIP1) and GCP3-interacting protein 2 (GIP2), the Mozart homologous proteins, localize and stabilize γ-tubulin complexes in the nuclear periphery [120-122].

I.3.3.3 Chromatin-mediated nucleation

Chromatin-mediated MT nucleation (Fig. 5c) is cell cycle-dependent and occurs after the breakdown of the nuclear envelope. The regulator of chromosome condensation 1 (RCC1), the Ras-related nuclear protein guanine nucleotide exchange factor (RanGEF), associates with chromosomes to produce a gradient of RanGTP. RanGTP gradient then stimulates the dissociation of TPX2 from importins [123], TPX2 interaction with Aurora A, and Aurora A autophosphorylation [124]. Besides Aurora A, TPX2 associates with the receptor for hyaluronan-mediated motility (RHAMM), NEDD1, and γTuRCs [125]. The phosphorylation of NEDD1 by Aurora A is critical for MT nucleation in the vicinity of chromosomes [126]. TPX2 also stabilizes early nucleation intermediates and cooperates with the MT polymerase ch-TOG [127]. It was suggested that MT nucleation occurs also from kinetochores [128, 129]. However, it is more probable that MTs nucleated by chromatin-mediated MT nucleation are stabilized in the kinetochore area and amplified through MT nucleation from the pre-existing MTs [123].

I.3.3.4 Nucleation from pre-existing microtubules

Lateral surface of other MTs (Fig. 5d) nucleates non-centrosomal branched MTs. They are formed mainly during mitosis facilitating robust spindle assembly and proper completion of the cytokinesis [130]. They can be also found in post-mitotic cells such as interphase plant cells and neurons [131, 132]. This type of the nucleation is based on augmin [133] hetero-octameric protein complex containing an essential subunit Hice1 (HAUS8). Augmin forms complex with NEDD1 and its associated γTuRC [134]. NEDD1 is phosphorylated by Cdk1, which leads to its interaction with Plk1 kinase and subsequent Hice1 phosphorylation by Plk1. Activated Hice1 promotes binding of augmin with associated γTuRC to MTs [135]. MT stretches of -TIPs CAMSAPs can serve as “seeds” for non-centrosomal MT nucleation [83]. New MTs are nucleated as branches on the mother MT at angles from 0° to 30° in mitotic spindles. Alternatively, MTs are nucleated at angles ~40° or in parallel with the pre-existing MT in the plant cortical array [134].

I.3.3.5 Nucleation from plasma membrane-associated sites

In differentiated cells, PCM proteins that are redistributed to the cellular cortex and plasma membrane-associated sites can functionally replace centrosomes. In the apical plasma

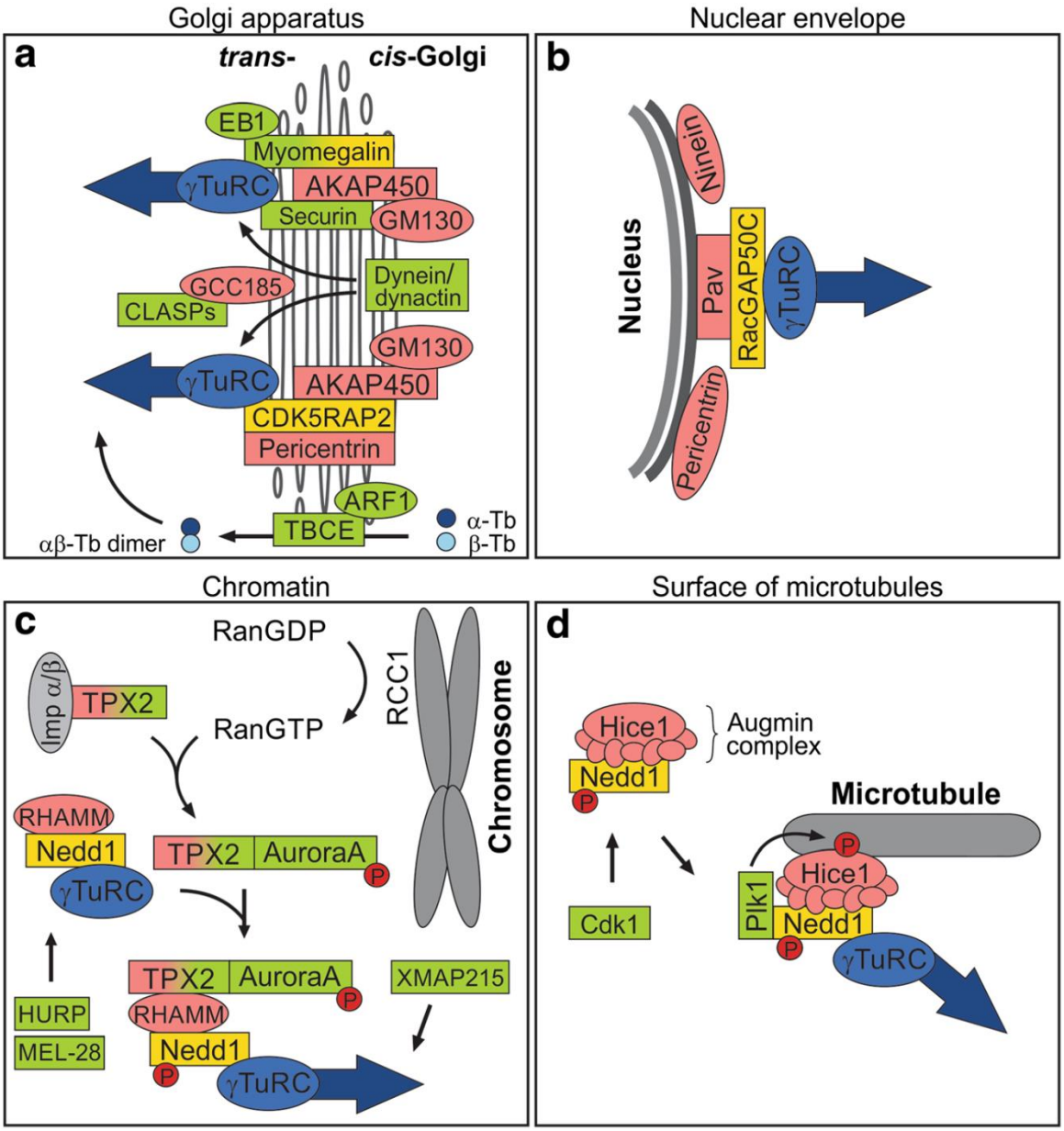

Figure 5. Models of non-centrosomal nucleation. The regulation of MT nucleation from the Golgi apparatus (**a**), nuclear envelope (**b**), chromatin (**c**), and surface of pre-existing MTs (**d**). Regulatory proteins are coloured to depict their roles: γTuRC targeting (*yellow*), anchoring (*red*) and modulating proteins (*green*). Adapted from [95].

membrane of polarized epithelial cells, γTuRC localization is regulated by keratin that directly binds to GCP6 [136]. The anchorage and stabilization of new MTs can be supported by -TIP CAMSAPs (mammals), patronin (invertebrates) [82], and ninein [137]. Ninein-related non-centrosomal array protein 1 (NOCA-1) contributes to non-centrosomal MT assembly in *Caenorhabditis elegans* [138]. Src family protein tyrosine kinases (e.g. Fyn)

and phosphatidylinositol-3-kinase (PI3K) can form complexes with γ-tubulin [139]. Hypothetically, Fyn can phosphorylate PI3K, which might then regulate γ-tubulin through its direct interaction with the regulatory subunit of PI3K. In plants, γ-TuSCs are localized at plasma membranes [120, 140] and newly formed crosswalls [141].

I.4 Mast cells

Mast cells play a crucial role in innate and adaptive immunity, and belong to the fastest immune responders. They are derived from bone marrow-derived hematopoietic stem cells which develop into multipotent progenitors (MPPs) and subsequently into mast cell myeloid progenitors (MCp). Immature MCp are less- or non-granulated cells that circulate in the blood stream [142]. Terminal differentiation of MCp is preceded by a migration to the sites of potential infection, such as the skin, pulmonary epithelia, and gastrointestinal tract [143, 144]. They are distributed as mucosal or connective tissue mast cells according to their localization, phenotypes, molecular compositions and function [145, 146]. Mast cells are long-lived cells capable to survive for months. Their differentiation and survival in the peripheral tissue is determined by a local tissue and cytokine environment [147]. Once activated, they modulate the surroundings either by the release of preformed mediators from cytoplasmic granules or by newly synthesized biologically active compounds (Fig. 6) [148]. Recent evidence suggests that mast cell activation is regulated by the balance of both positive and negative intracellular signals. Signalling pathways are complex and besides traditional kinases and phosphatases they contain multiple other signalling molecules [143, 149-151].

I.4.1 Mast cell activation

Mast cell activation is a key event in allergic inflammatory responses. It is mainly mediated by high-affinity receptors for immunoglobulin E (IgE), but other receptors also markedly influence mast cell functions. Various signalling pathways that are initiated in response to ligand binding cooperate to achieve a fine-tuned regulation of mast cell activation.

I.4.1.1 Mast cell receptors and associated kinases

Mast cell activation is initiated by ligand binding to one of various receptors expressed on the mast cell plasma membrane. The most investigated receptor has been a tetrameric immune

receptor for IgE (FcεRI). It consists of one α subunit (FcεRIα) that binds antibody, one β subunit (FcεRIβ) which stabilizes the receptor complex and amplifies the downstream signal, and two disulfide-linked γ chains (FcεRIγ) providing signalling ability of FcεRI. Cytoplasmic tails of each FcεRIβ and FcεRIγ contain immunoreceptor tyrosine-based activation motifs (ITAMs) [146, 149]. ITAMs are phosphorylated after antigen (Ag)-induced FcεRI aggregation, and phosphorylated tyrosines serve as docking sites for kinases containing Src homology (SH)2 domains. β and γ ITAMs are functionally distinct. While γ ITAM initiates downstream signals, β ITAM rather amplifies these signals [152].

Among kinases interacting with ITAMs are non-receptor protein tyrosine kinases of Src family (e.g. Lyn, Fyn). The most abundant is Lyn kinase that associates with β subunit of FcεRI and phosphorylates FcεRIβ and FcεRIγ chains. Lyn possesses the positive as well as negative regulatory role in mast cell signalling, but precise molecular mechanisms still remain controversial [149, 151]. Other important kinase is Syk from the non-receptor tyrosine kinase Syk/Zap-70 family, associating with FcεRIγ [152]. The tyrosine kinase network is tightly regulated by protein tyrosine phosphatases which help to balance downstream signalling pathways. Both Lyn and Fyn can phosphorylate SH2-domain-containing protein tyrosine phosphatase (SHP)-1, but at different tyrosine positions. While Lyn-dependent phosphorylation activates the phosphatase, the phosphorylation by Fyn inhibits SHP-1 activity [153].

Besides FcεRI-mediated events, signalling pathways in mast cells might be initiated by many different receptors such as KIT receptor, G protein-coupled receptors (GPCRs), receptors for complement factors, toll-like receptors, receptors for interleukins, and several others [154]. KIT is a receptor for stem cell factor (SCF) responsible for mast cell homing, development and homeostasis. On contrary to FcεRI, KIT possesses inherent tyrosine kinase activity [152]. Binding of SCF leads to receptor dimerization and auto/transphosphorylation at tyrosine residues. The downstream signalling pathway of KIT receptor has several similar features to FcεRI signalling [155]. GPCR is the receptor with 7 transmembrane regions that associates with Gα, Gβ, and Gγ subunits of G protein. Ligand binding results in heterotrimer activation and dissociation of Gα from the rest of the receptor. Free α subunit functions as an effector and mediates downstream signalling. In humans, GPCR superfamily consists of more than 800 different proteins varying in the sequence, ligand binding and function [156]. Mast cells express different classes of GPCRs. Receptors for prostaglandin E2 (PGE2), sphingosine 1-phosphate (S1P), complement components, chemokines, neuropeptide, antimicrobial

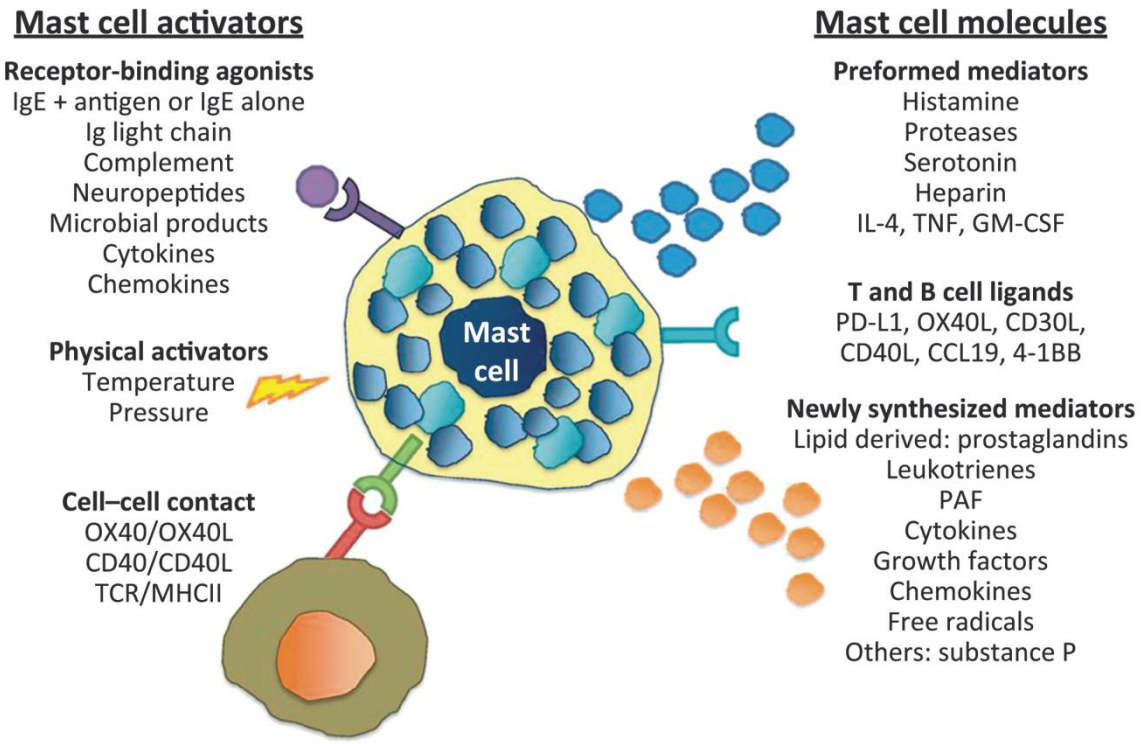

Figure 6. Mast cell activators and secreted mediators. Mast cells can be activated by ligand binding to its receptor, physical activation, and cell-cell contact. Upon activation, mast cells secrete various preformed molecules, *de novo* synthesized mediators, and ligands that mediate cell interactions with T and B cells. Abbreviations: CCL19 (C-C motif chemokine 19); CD30L (ligand for CD30 member of the TNF superfamily); CD40L (ligand for CD40 member of the TNF superfamily); GM-CSF (granulocyte-macrophage colony-stimulating factor); IgE (immunoglobulin E); IL-4 (interleukin 4); MHCII (major histocompatibility complex II); OX40L (ligand for OX40 member of the TNF superfamily); PAF (platelet-activating factor); PD-L1 (programmed cell death 1 ligand 1); TCR (T cell receptor); TNF (tumor necrosis factor); 4-1BB (type 2 transmembrane glycoprotein of the TNF superfamily). Adapted from [157].

peptides and adenosine are examples of GPCRs identified in mast cells [149]. GPCRs become the most common targets of pharmacotherapy [158, 159].

Various co-receptors fine-tune effector responses of mast cells leading to an intricate network of positive and negative signals. Inhibitory receptors are characterized by immunoreceptor tyrosine-based inhibitory motifs (ITIMs) [143]. The phosphorylation of ITIMs by Src kinases leads to the recruitment of tyrosine phosphatases such as SHP-1 and SHP-2, and to the decrease of mast cell activation [160]. Among the receptors containing ITIMs are IgG receptor FcγRIIB, CD200R, and other inhibitory receptors that can contribute to fine-tuning of mast cell activities [150].

I.4.1.2 Intracellular signalling pathways in mast cells

The main intracellular signalling pathway is through phosphorylation of transmembrane adaptor protein linker for activation of T-cells (LAT) and non-T-cells activation linker (NTAL) by Syk kinase. This creates binding sites for cytosolic adaptor proteins including growth factor receptor-bound protein 2 (GRB2), phospholipase (PLC)γ1, guanine nucleotide exchange factor VAV, SH2-domain-containing leukocyte protein of 76 kDa (SLP-76) and some others [151]. GRB2 brings to the plasma membrane GRB2-associated-binding protein 2 (GAB2) and PI3K. Activated PI3K phosphorylates phosphatidylinositol-4,5-bisphosphate ($PI(4,5)P_2$) to yield phosphatidylinositol-(3,4,5)-trisphosphate ($PI(3,4,5)P_3$), a binding site for PH-domain containing proteins such as Bruton's tyrosine kinase (Btk) and PLCγ. This step might be negatively regulated by SH2-containing inositol phosphatase 1 (SHIP-1) or phosphatase and tensin homolog (PTEN), that generate either $PI(3,4)P_2$ or $PI(4,5)P_2$. $PI(4,5)P_2$ is hydrolysed by PLCγ to a second messengers diacylglycerol (DAG) and inositol trisphosphate (IP_3) [149].

IP_3 interacts with the IP_3 receptor in the endoplasmic reticulum (ER) and induce the release of Ca^{2+} from the ER. The decrease of Ca^{2+} in the ER triggers clustering of stromal interaction molecule 1 (STIM1) in the ER and its translocation and interaction with transmembrane Ca^{2+} release-activated Ca^{2+} (CRAC) channel protein 1 (Orai1). Activated CRAC channel in the plasma membrane mediates the highly Ca^{2+} selective current (I_{CRAC}). This process is called the store-operated Ca^{2+} entry (SOCE). Ca^{2+} influx can be also mediated through transient receptor potential cation (TRPC) channels. Although they have been identified in mast cells [161, 162], TRPC channels do not contribute to FcεRI-mediated Ca^{2+} signalling in human mast cells [163]. Massive influx of Ca^{2+} activates cytosolic proteins such as Ca^{2+}-dependent cPKC or Ca^{2+}-dependent phosphatase calcineurin to regulate signalling pathways leading to changes in the cell morphology, adhesion to substrates, chemotaxis, degranulation and gene transcription [149]. Signalling pathways after FcεRI-crosslinking are shown in Fig. 7.

I.4.1.3 Unspecific activation of mast cells

Besides specific activations, mast cells can be also activated non-physiologically. Unspecific activators mimic the stimulatory effects of Ag and are thus often used to study mast cell signalling pathways under the laboratory conditions. Pervanadate is a potent protein

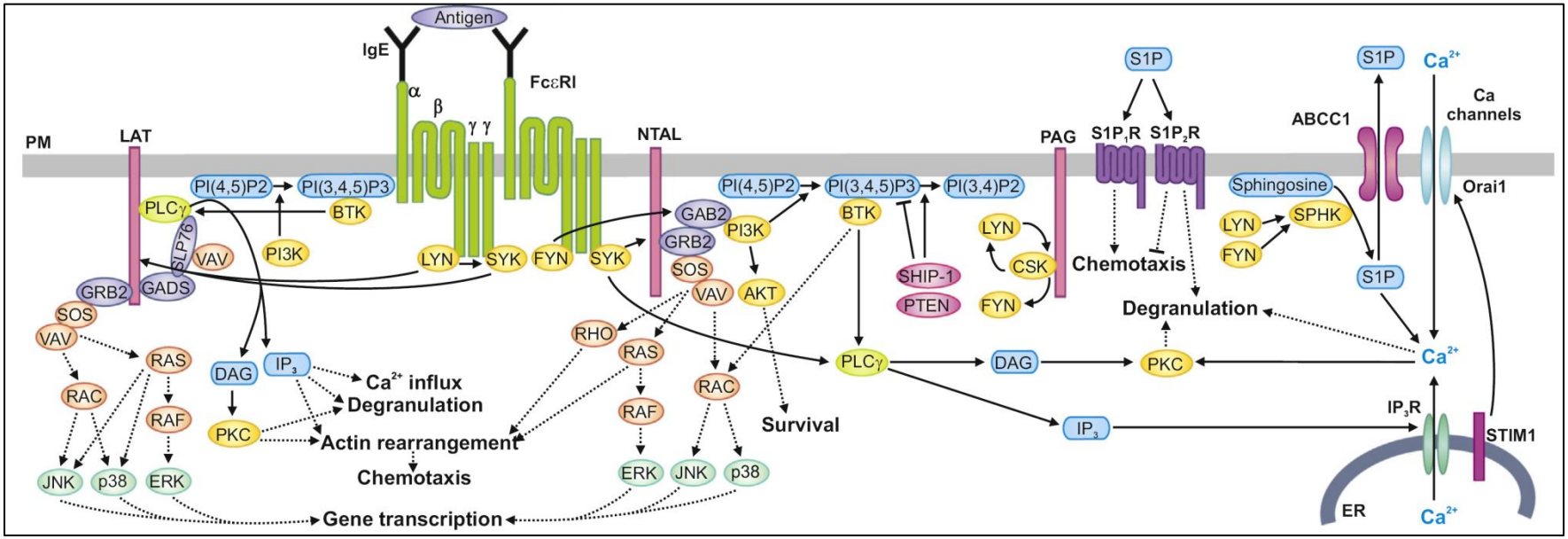

Figure 7. Signalling pathways after FcεRI signalling. FcεRIs with bound IgE are cross-linked with Ag. This triggers tyrosine phosphorylation of FcεRIβ and FcεRIγ by Lyn kinase, and binding and activation of Syk kinase. Kinases then phosphorylate their downstream targets to activate several signalling pathways. PLCγ generates IP_3 and DAG. Binding of IP_3 to its receptor on the ER triggers the release of Ca^{2+} from the ER. Subsequent opening of Ca^{2+} channels in the plasma membrane activates the influx of Ca^{2+} into the cytoplasm. Mast cells can be also activated by binding of S1P to its receptor. These and some other signalling molecules involved in the regulation of Ca^{2+} influx, degranulation, cytoskeleton rearrangement, chemotaxis, survival, and gene transcription are indicated. Main regulatory proteins are coloured according to their function: FcεRIs (*green*), adaptor linkers (*purple*), lipids and their products (*blue*), adaptor proteins (*violet*), kinases (without MAP kinases) (*magenta*), phosphatases (*pink*), phospholipases (*lime*), proteins of MAP kinase pathway (*orange and dark green*). Major signalling pathways are in detail described in the text. Adapted from [149].

tyrosine phosphatase inhibitor that causes massive protein phosphorylation [164] leading to histamine secretion, IP_3 formation and Ca^{2+} influx in mast cells [165]. Thapsigargin is another unspecific activator. It inhibits the ER Ca^{2+} ATPase and therefore blocks the ability of the cell to pump Ca^{2+} to the ER [166]. The depletion of Ca^{2+} in the ER activates SOCE and subsequent mast cell signalling pathways. A little less specific is the effect of Ca^{2+} ionophore. Ca^{2+} ionophore forms lipid-soluble complexes with divalent cations and carry them across the plasma membrane using diffusion [167].

I.4.2 Mast cell migration and chemotaxis

Migration of mast cells is essential for proper performance of their functions. MCp circulate in the bloodstream and upon the inflammation they migrate into peripheral tissues [142]. Following terminal maturation of mast cells is under the control of locally produced cytokines and growth factors. Chemoattractant-directed migration (chemotaxis) of MCp or mature cells belongs to one of the key mechanisms responsible for mast cell local accumulation under the physiological or pathological conditions [168]. Besides their own migration towards the chemoattractant, mast cells also stimulate chemotaxis in other immune cells, such as eosinophils and type 2 innate lymphocytes [147].

Mast cells express receptors for various ligands that have the ability to behave as chemoattractants and induce directed migration. The key signal inducing mast cell homing and recruitment into peripheral tissues is SCF that binds to the c-Kit receptor [169]. SCF-induced chemotaxis is regulated by Fyn kinase [170], which affects the activity of PI3K and Rac GTPases. These mediators are responsible for the reorganization of the cytoskeleton [170]. Proper signalling during migration towards SCF requires also phosphatases, such as protein tyrosine phosphatase (PTP)α and SHP-2 [149]. Directed migration can be also initiated by Ag binding to FcεRIs sensitized by IgE. In this case, Lyn and Syk kinases are important for flawless chemotaxis [171]. Among the other mast cell chemoattractants belong various chemokines (e.g. CC and CXC), cytokines (e.g. transforming growth factor β, TGFβ), bioactive lipids (e.g. S1P), eicosanoids (e.g. prostaglandins PGE_2 and PGD_2, and leukotrienes) and components of the complement (e.g. C1q, C3a, and C5a) [168]. It is well established that variable chemoattractants induce different signalling pathways.

Besides kinases and phosphatases, several other signalling proteins have been shown to be involved in the regulation of mast cell migration. In Ag-induced chemotaxis, adaptor protein NTAL [172] and phosphoprotein associated with glycosphingolipid-enriched

membrane microdomains (PAG) [173] are negative and positive regulators, respectively. Signal transduction must lead to the proper Ca^{2+} influx through CRAC channel, as STIM1 [174] and Orai1 [175] were shown to regulate mast cell chemotaxis.

I.4.3 Mast cell degranulation

As granulocytes, mast cells secrete various preformed and newly synthesized mediators from cytoplasmic granules (Fig. 6). The exocytosis is very complex process which is tightly controlled to ensure an appropriate biological response. Many proteins function in a coordinated manner to promote and control the rate and extent of mast cell degranulation [150]. Mast cells contain up to 1000 preformed granules with size of 300 - 1000 nm [176]. Within a second, mast cells release preformed mediators such as biogenic amines (histamine, serotonin, dopamine), proteoglycans (heparin), proteases (tryptase, chymase), lysosomal enzymes (β-hexosaminidase), cytokines and growth factors from their secretory granules [148]. These soluble preformed mediators are responsible for acute symptoms of the allergic reaction [147]. During mast cell activation, prostaglandins, leukotrienes and platelet activated factor (PAF) are generated from arachidonic acid and secreted in minutes. Later on, mast cells initiate *de novo* synthesis with the secretion occurring several hours after the stimulation. *De novo* synthesized products are pro-inflammatory cytokines (e.g. interleukins, ILs; tumour necrosis factor, TNF; interferons, IFNs; TGF-β; chemokines and vascular endothelial growth factor, VEGF) [177, 178].

The mediator release might be activated by various receptors, but it is mostly initiated through the aggregation of IgE-sensitized FcεRIs by Ag [176]. Fyn kinase plays a key role in mast cell degranulation by regulating the release through direct or indirect phosphorylation of Gab2 [179]. Syk kinase was also shown to modulate the degranulation as mutant form of Syk caused impaired exocytosis [180]. The importance of Lyn kinase has been broadly studied, but with no clear result. Several studies proved that the degranulation increases in mast cells from Lyn knockout mice [179, 181, 182], other showed no effect [183] or even slight degranulation decrease in mast cells from Lyn-deficient mice [184]. Besides kinases, also phosphatases (SHP-1, SHP-2 and SHIP1) were described to regulate mast cell degranulation at early stages of mast cell activation [176].

Critical for the degranulation are adaptor proteins Gab2, SLP-76 and LAT [150]. Both SLP-76 and LAT influence the exocytosis by Ca^{2+} mobilization, whereas Gab2 mediates it by the regulation of PI3K activity and PKC activation [176, 179]. Two distinct early signalling

pathways (Lyn-Syk-LAT-SLP-76-PLCγ and Fyn-Gab2-PI3K-PIP_3) cross-talk in later stages of the activation and appear to complement Ca^{2+} mobilization by DAG production and PKC activation, leading to mast cell degranulation [176].

Later signalling events control the translocation and fusion of granules. As the degranulation must occur within minutes, the process requires a more extensive crosstalk with the cytoskeleton. Therefore, the translocation of granules to the plasma membrane depends on MTs that serve as tracks for transporting vesicles [185]. Moreover, granules fuse in a granule-granule mode to obtain a maximal and fast release [177]. The translocation of granules to the plasma membrane and granule fusion requires the mobilization of Ca^{2+}, activation of PKC, active soluble NSF attachment protein receptor (SNARE) membrane fusion complex and remodelling of the actin cytoskeleton [148, 177]. Secretory vesicles are recruited to the MT molecular motor kinesin-1 by an adaptor protein Slp3 and small GTPase Rab27B proteins [186]. It was also shown that Rab27A limits the access of granules to the membrane by regulating the integrity of cortical actin [187]. The necessity of PKC in the late steps of exocytosis is well established. Upon cell activation, Ca^{2+} and PKCs act to reverse the inhibitory mechanisms of granule fusion and activate proteins and cellular events to promote the granule fusion [176].

I.4.4 Cytoskeleton in mast cells

The cytoskeleton of mast cells is significantly reorganized upon cell activation. It plays a pivotal role in the maintaining cell morphology, adhesion to various substrates, intracellular transport, migration and degranulation.

MTs dynamically reorganize in the reaction to mast cell activation. FcεRI aggregation as well as the activation by pervanadate or thapsigargin, results in enhanced formation of MTs and their accumulation in the cell periphery [155, 185, 188]. Attachment of mast cells to fibronectin that resembles physiological conditions of mast cell environment, results in the generation of Ca^{2+}-dependent protrusions that contain MTs. These protrusions are on the entire cell surface pointing to all directions [174]. It is well established that intact dynamic MTs are also essential for the movement of secretory granules [185, 189, 190]. Critical roles in MT-dependent mast cell degranulation play Fyn-Gab2-RhoA [179, 185] and Fyn-Gab2-PI3K-ADP-ribosylation factor (Arf)1 signalling pathways [191]. Moreover, atypical RacGEF DOCK5 associates with an adaptor protein Nck2 and Akt kinase to mediate

the phosphorylation and inactivation of GSK3β [192]. The inhibition of GSK3β then promotes MT assembly and the movement of secretory granules.

MFs are necessary for cell spreading, membrane ruffling, chemotactic responses and mediator release in mast cells [155]. Generally, the activation of mast cells is accompanied with an increase of polymeric F-actin. While cortical F-actin is reduced, its content increases in the cell interior after cell activation [193]. F-actin rearrangement during mast cell chemotaxis is regulated by Ca^{2+} influx [155, 185] and by Fyn-PI3K-Btk-Rac signalling pathway [170, 194, 195]. MFs play also a role in mast cell degranulation. Cortical F-actin forms a barrier that prevents the access of vesicles to the plasma membrane [155]. Thus, the disruption of MFs enhances FcεRI-mediated degranulation in mast cells [185]. Similarly as in chemotaxis, F-actin disassembly is regulated by Fyn, RhoA and Ca^{2+} signalling to promote the mediator release [185, 196, 197].

In mast cells, IFs are mostly represented by vimentin [198]. Vimentin filaments surround secretory granules in the cytoplasm. Cell activation induces their depolymerization which facilitates granule movement to the plasma membrane and exocytosis [155]. Disassembled, soluble vimentin interacts with MAP kinases to mediate the production of CCL2 chemokine upon FcεRI aggregation and CC chemokine receptor-mediated activation [199]. Moreover, vimentin binds Fyn kinase to negatively regulate mast cell degranulation and tyrosine phosphorylation of Fyn targets upon FcεRI stimulation [200].

I.4.5 Mast cell-derived diseases

Mast cells are protective cells that play an important role in various infections. Adaptive advantage of mast cells in the host defense is based on the evolutionary persistence of IgE isotype, committed network of receptors, and effector cell lineages [201]. Unfortunately, in the case of repeated or chronic stimuli, mast cell activation can lead to tissue damage and dysfunction. Mast cells are therefore involved in the pathophysiology of numerous diseases of all organs that are collectively called mast cell activation disorders [144]. The activation disorders are caused by the deregulation of mast cell functions and are classified into primary diseases associated with an abnormal production of mast cells carrying pathologic markers of clonal population (e.g. anaphylaxis, mastocytosis), secondary diseases where the normal mast cells are activated in a reaction to microenvironmental triggers (e.g. allergic disorders, urticarias) and to idiopathic diseases, which include cases without the evidence of any underlying disease (atherosclerosis, multiple sclerosis, atopic dermatitis, arthritis, tumours,

asthma, migraine, and others) [202, 203]. Drug treatment of mast cell-derived diseases is highly individualised according to the patient symptoms and complications. The therapy consists of the avoidance to triggers, antihistamines, mast cell membrane-stabilizing compounds, and drugs targeting individual symptoms [204].

New candidates for the treatment of mast cell-derived diseases have been investigated recently. Omalizumab is the humanized murine monoclonal antibody that specifically binds to free IgE in the blood and interstitial fluid. It was used as an adjunctive treatment in patients with mastocytosis and prevented recurrent refractory anaphylaxis in patients with mast cell activation syndrome [202, 205]. Currently, it is approved for the treatment of moderate-to-severe asthma and chronic idiopathic urticaria [206]. Besides omalizumab, various receptor antagonist and agonist [203], and inhibitors of tyrosine kinases [204] have been investigated to block early signalling events in mast cell-derived diseases.

Another promising drug is miltefosine (hexadecylphosphocholine), a derivative of plasmalogen phospholipids [207]. Miltefosine was shown to inhibit the activation in human mast cells [208] and reduces the disease progression in patients with mastocytosis [209], urticaria [210] and atopic dermatitis [211]. It was proposed that in mast cells, miltefosine acts as a lipid raft modulator through its interference with the structural organization of surface receptors in the plasma membrane [212]. As miltefosine is already used for the treatment of leishmaniasis [213] and free-living amebae infections [214], there have been many studies on its cellular effects. It was reported that miltefosine affects PI3K/Akt survival pathway [215], as well as activities of PLCβ [216], phospholipase D (PLD) [217] or PKC [218]. Despite this knowledge, the molecular mechanisms of miltefosine action in mast cells remain poorly understood.

I.5 Other model systems used in this study

In this thesis, the majority of experiments were performed on bone marrow-derived mast cells (BMMCs). Nevertheless in some cases, the human osteosarcoma cell line (U2OS) was used. U2OS cell line was developed from the human mesenchymal tumour cell line. It shows cytological atypia, chromosomal abnormalities, an epithelial-like pavement growth pattern and a potential for indefinite multiplication *in vitro*. U2OSs were developed to be the first cell line to provide the opportunity for comparing control and neoplastic human mesenchymal cells under the *in vitro* conditions [219]. Whereas mast cells are great model to study

signalling processes close to the pathology of allergies, the major advances of U2OSs are that they are adherent, quite large and can be easily transfected. Therefore, U2OSs enable better handling in more complex microscopic experiments, when studying MT organization, nucleation and dynamics.

To verify obtained finding we used also cells of different tissue origin such as human nontransformed retinal pigmented epithelium (hTERT-RPE1), human embryonic kidney (HEK-293), human glioblastoma (T98G) and rat basophilic leukemia (RBL) cell lines.

II. AIMS OF THE STUDY

The long-term goal of the Laboratory of biology of cytoskeleton is to understand the regulatory mechanisms of MT reorganization in activated mast cells. Mast cells are important immune cells, and the elucidation how they are regulated could help to improve the treatment of mast-cell driven diseases. We have shown previously that mast cell activation leads to the reorganization of MTs in Ca^{2+}-dependent manner (Hájková et al., 2011; see VII. Supplementary data). This study initiated several following projects running in the Laboratory, and so far obtained data are presented in this PhD thesis. We have focused on the reorganization, nucleation and dynamics of MTs in resting and activated cells. To do so, we aimed to develop new tools to monitor tubulin concentration, quantify MT nucleation and dynamics, and analyse chemotaxis in mast cells. Using these approaches we intended to characterize novel γ-tubulin interacting proteins and their role in MT nucleation. We also aimed to understand the function of Ca^{2+} signalling in the regulation of MTs. Finally, we intended to elucidate the role of miltefosine, a promising candidate for novel therapeutic strategies in mast-cell driven diseases, during mast cells activation.

Partial aims of this Ph.D. thesis were following:

1) Development of new tools for the quantification of tubulin concentration, MT nucleation, MT dynamics and cell chemotaxis in mast cells.

2) Analysis of MT nucleation in the course of mast cell activation.

3) Functional analysis of GIT1/βPIX signalling proteins and PAK1 kinase in MT nucleation.

4) Understanding the regulatory mechanisms of miltefosine action in mast cells.

III. COMMENTS ON PRESENTED PUBLICATIONS

III.1 Quantification of α-tubulin isotypes by sandwich ELISA with signal amplification through biotinyl-tyramide or immune-PCR

Dráberová E., Stegurová L., Sulimenko V., **Hájková Z.**, Dráber Pe., Dráber Pa. (2013). Quantification of α-tubulin isotypes by sandwich ELISA with signal amplification through biotinyl-tyramide or immune-PCR. Journal of Immunological Methods *395*, 63-70.

The equilibrium between soluble tubulin dimers and MTs, which is generated in every cell [21], can be changed by many proteins interacting with tubulin, as well as by TBAs [20]. Therefore, fast methods with high sensitivity and reproducibility are necessary to monitor tubulin changes in cytosolic pools.

In this work, we described two new assays for the quantification of α-tubulin. Both methods are based on a sandwich enzyme-linked immunosorbent assay (ELISA) with signal amplification by biotinyl-tyramide or immune-PCR. The key step in the sandwich ELISA is a matched pair of monoclonal antibodies that should recognize non-overlapping native epitopes on α-tubulin. We showed that antibodies TU-07 and DM1A provide required properties and recognize phylogenetically highly conserved epitopes that are localized outside the variable part of the C-terminal region of α-tubulin. TU-07 recognizes the epitope in the amino acid region 406-410 and DM1A antibody locates to the amino acid region 426-430 of α-tubulin. Both epitopes reacted with full length α-tubulin isolated from the porcine brain as well as with tubulins in mouse mast cells and other cell types of various species. The epitopes recognized by TU-07 and DM1A are evolutionary highly conserved and are preserved from human to plants. The matching antibody pair thus enables the quantification of α-tubulin isotypes in the phylogenetically distant species.

We demonstrated that reported methods with the amplification by biotinyl-tyramide or immune-PCR facilitate the detection of tubulin at very low concentrations. The biotinyl-tyramide amplification detects tubulin at concentration 2.5 ng/ml and immuno-PCR even at tubulin concentration 0.086 ng/ml. Immuno-PCR thus enables assessing tubulin concentration in lysates prepared from cells available only in limited amounts. In comparison

to the ELISA with the biotinyl-tyramide detection, the immuno-PCR detection provides enhanced sensitivity and wider dynamic range.

We also confirmed that presented techniques allow sensitive quantification of the tubulin in complex biological fluids. For the first time, we determined tubulin concentration in resting (2,331 ± 74.6 ng/ml) and taxol-treated (478 ± 14.1 ng/ml) mast cells. We proved that the taxol treatment leads to the depletion of soluble tubulin in mast cells. We also showed that activated mast cells release a small amount of cytosolic tubulin into the culture medium. This might be caused by the release of membrane-bound tubulin into the extracellular space during the degranulation or might originate from damaged exosomes.

Previously, it has been reported that patients with progressive multiple sclerosis have elevated tubulin concentration in the cerebrospinal fluid compared to healthy people [220]. Importantly, the assays reported here are much more sensitive than available commercial kit. The biotinyl-tyramide and immuno-PCR detections are up to 20x and 1,000x, respectively, more sensitive than the PathScan Total α-Tubulin Sandwich ELISA kit (Cell Signalling). Antibodies TU-07 and DM1A recognize phylogenetically highly conserved epitopes localized outside the C-terminal isotype-defining region of α-tubulin where multiple PTMs were identified [4]. Nevertheless, MAPs or the formation of tubulin dimers might mask TU-07 and DM1A epitopes. Therefore, these approaches should be used primarily for the relative monitoring of tubulin concentrations in control cells and cells treated with MT-stabilizing or MT-destabilizing agents. Reported methods might advance monitoring of changes in tubulin concentration during the diagnosis and treatment of neurological and oncological diseases.

In this work, I prepared samples of activated mast cells and cells treated with taxol, performed immunofluorescent experiments, and prepared respective figures. I participated in writing the manuscript and in responding to reviewer's comments.

III.2 Microscopy assays for evaluation of mast cell migration and chemotaxis

Bambousková M.*, **Hájková Z.***, Dráber Pa., Dráber Pe. (2014). Microscopy assays for evaluation of mast cell migration and chemotaxis. Methods in Molecular Biology *1192*, 161-176.

Mast cells are highly effective guarding cells that are localized close to sites of potential infection. Chemoattractant-directed migration of mast cells is one of the key mechanisms responsible for their local accumulation [143]. Insight into the molecular mechanisms that regulate mast cell migration and chemotaxis is thus essential for better understanding of mast cell functions. For imaging of individually migrating mast cells, it is necessary to apply new methodological approaches.

Various methods for studying migration and chemotaxis towards different chemoattractants have been developed. However, many of them are not suitable for non-adherent mast cells. Assays that are applicable for the quantification of chemotactic responses of mast cells do not allow the real-time imaging of individually moving cells and the analysis of cell trajectories. In this work, we described three newly developed approaches optimized for the real-time imaging of non-adherent mast cells, corresponding cell tracking and data analysis methods. Mast cells are either attached to fibronectin or kept in 3D collagen I gel. The chemoattractant gradient is created using μ-Slides from IBIDI [175, 221]. For non-adherent mast cells we used μ-Slide Chemotaxis^{3D} chambers that enable the creation of 3D gel from collagen I, stable chemoattractant gradients for long-term experiments, and simultaneous chemotaxis evaluation in three samples. Alternatively, gradients were generated by embedding the chemoattractant into porous materials such as an agarose gel [222]. Moving mast cells were imaged in the real-time by automated microscopy system equipped with the bright-field camera for recording the time-lapse video, motorized stage, and CO_2 and temperature regulated chamber. The MetaMorph program with parameters optimized for the tracking of mast cells imaged by the bright-field microscopy was used for the automatic cell tracking. Data analysis was performed using the free plugin "Chemotaxis and Migration Tool" working in the ImageJ program.

In this methodical article, we described used materials, step-by-step protocols for the sample preparation, tracking the cells and the data analysis for migration and chemotaxis of

mast cells. Moreover, protocols were supplied with notes highlighting alternative approaches and advices how to handle with the most essential or problematic steps. Data analysis provided parameters such as the directionality, distance or velocity, which could be presented in the numerical form or as various graphs. Described methods are regularly used in our laboratory.

In this work, I optimized the protocol for directed chemotaxis of non-adherent murine and human mast cells using μ-Slide Chemotaxis^{3D} chambers and performed corresponding experiments. I established protocols for the automatic cell tracking of the bright-field time-lapses in the MetaMorph and analysed obtained data. I participated in writing the manuscript and responding to reviewer's comments.

**B.M. and H.Z. contributed equally to this work. This declaration that had been stated in the manuscript was not, however, due to the overlooked typist's error, printed in the book.*

III.3 Synthesis and biological evaluation of structurally simplified noscapine analogues as microtubule binding agents

Ghaly P.E., Churchill C.D.M., Abou El-Magd R.M., **Hájková Z.**, Dráber P., West F.G., Tuszynski J.A. (2017). Synthesis and biological evaluation of structurally simplified noscapine analogues as microtubule binding agents. Canadian Journal of Chemistry *95(6)*, 649-655.

The demand for new and better anti-cancer drugs belongs to the long-term goal of the modern biomedicine. The accessible anti-cancer drugs are often chemotherapeutics targeted to MTs to inhibit their dynamics. This prevents the division of cancer cells. Unfortunately, these compounds have also therapy-limiting toxicities and recurrent cancers become resistant to used drugs [223]. In the recent decade, noscapine, an alkaloid that has long been used as a cough suppressant, was reported as a new anti-cancer drug [224]. It binds to the αβ-tubulin dimer and causes the conformational change of the protein resulting in MT disruption and the cell division arrest [225]. Contrary to other MT-interacting chemotherapeutics, noscapine and its analogues (noscapinoids) have lower toxicity and organisms are less resistant to the drug

treatment. Noscapine biosynthesis has been recently established [224], giving the advantage of large-scale biotechnological production of noscapinoids for the medicinal needs [223]. Therefore, noscapinoids provide promising, cost-effective and safe therapeutic drugs for the cancer chemotherapy. Current studies are directed to the preparation of new analogues with even better properties.

In this work, we report on the results of the chemical synthesis and biological assays performed on new noscapine analogues. We synthesized four analogues of noscapine and their corresponding enantiomers. Cytotoxic assays revealed that derivatives have the cytotoxic effect comparable to noscapine, with an IC50 of ~100 μM. The analogues also bound to the tubulin with the affinity comparable to that measured for noscapine. Biological activities of noscapine and its derivatives were tested on human osteosarcoma U2OS cells. For the evaluation of MT dynamics, it is essential to have a reliable automatic method for tracking growing MTs. For this purpose, MTs were labelled by the plus-end binding protein EB1 tagged with the green fluorescent protein (GFP). Life cell imaging of U2OS_EB1-GFP with subsequent analysis enabled to detect changes in dynamics parameters of MTs. The evaluation of MT distribution, nucleation and dynamics showed that new noscapine analogues did not significantly affect MTs in contrast to noscapine. Computational docking simulations revealed that noscapine derivatives bind to the colchicine and noscapine binding sites on the tubulin molecule. Slightly higher binding affinity was to colchicine site.

Newly prepared analogues therefore do not have better properties than noscapine in the terms of their efficacy against cancer cells and they do not offer a good alternative for noscapine in the cancer treatment. Nevertheless, it would be interesting to elucidate why small modifications have such a great effect on this class of compounds. As the affinity of noscapine analogues to both the noscapine and colchicine binding sites is almost comparable, these or similar compounds could work via a bimodal action depending on the concentration or buffer conditions. It was also reported that several noscapinoids bind strongly to γ-tubulin [226]. Therefore, future work might be directed to γ-tubulin to develop compounds, which bind preferentially to γ-tubulin than to αβ-tubulin.

In this work, I tested noscapine and its new analogues for their impact on MT dynamics. I participated in establishing of required method in the laboratory and performed experiments on human osteosarcoma U2OS cells stably expressing GFP-tagged EB1. I analysed the data and prepared respective documentation. I participated in writing the manuscript.

III.4 Microtubule nucleation in mouse bone marrow-derived mast cells is regulated by the concerted action of GIT1/βPIX proteins and calcium

Sulimenko V., **Hájková Z.**, Černohorská M., Sulimenko T., Sládková V., Dráberová L., Vinopal S., Dráberová E., Dráber P. (2015). Microtubule nucleation in mouse bone marrow-derived mast cells is regulated by the concerted action of GIT1/βPIX proteins and calcium. The Journal of Immunology *194*, 4099-4111.

The activation of mast cells by FcεRI aggregation initiates signalling events resulting in the Ca^{2+} influx through the plasma membrane, release of allergic mediators from cytoplasmic granules, and synthesis of cytokines and chemokines [143]. We have reported previously, that MTs are distinctly reorganized and their amount temporarily increases during BMMCs activation [155, 174]. This might be due to the modulation of MT nucleation or dynamics at MT plus-ends. The molecular mechanisms that control MT remodelling and organization in mast cells are largely unknown.

In this project, we concentrated on the nucleation of MTs in BMMCs. It is well known that the nucleation of MTs initiates from complexes that are formed by γ-tubulin and γ-tubulin complex proteins [8]. Previously, we and others showed that protein tyrosine kinases phosphorylate γ-tubulin or its associated proteins, which could lead to the modulation of γ-tubulin function(s) [188, 227, 228]. Here, we intended to identify substrates of tyrosine kinases that regulate γ-tubulin functions.

We showed that in BMMCs, γ-tubulin interacts with p21-activated kinase interacting exchange factor (βPIX) and G protein-coupled receptor kinase-interacting protein 1 (GIT1) proteins. Moreover, γ-tubulin forms complexes with tyrosine-phosphorylated GIT1 in BMMCs activated by pervanadate or Ag. Live-cell imaging with red fluorescent protein (RFP)-tagged γ-tubulin to mark centrosomes and GFP-tagged βPIX or GFP-tagged GIT1 revealed that both βPIX and GIT1 associate with centrosomes. We showed previously, that proteins phosphorylated on tyrosines concentrate in the centrosomal region during early stages of BMMC activation [188]. Moreover, tyrosines 246 and 293 on GIT1 were shown to be necessary for GIT1 intramolecular inhibition. The phosphorylation of these tyrosines releases the autoinhibition and helps to activate GIT1 [229]. Thus, tyrosine phosphorylation

of GIT1 might enhance its activation in stimulated mast cells in the centrosomal region. To reveal the importance of βPIX or GIT1 proteins for MT nucleation, we performed nocodazole-washout experiments on BMMCs with depleted levels of βPIX or GIT1. We found that βPIX is a negative regulator, and GIT1 positive regulator of MT nucleation in BMMCs. These results were confirmed by the phenotypic rescue experiments.

Further, we revealed by immunoprecipitation and pull-down experiments that an enhanced level of free cytosolic Ca^{2+} modulates γ-tubulin properties and stimulates the association of GIT1 and GCPs with γ-tubulin. We proved that Ca^{2+}-dependent changes in γ-tubulin are located in the C-terminal region of γ-tubulin (amino acids 423-451). Moreover, pull-down experiments revealed that GST-tagged C-terminal part of γ-tubulin associates with βPIX and GIT1 in the absence of Ca^{2+}. However, binding of βPIX to this γ-tubulin domain was inhibited in the presence of Ca^{2+}. Nocodazole-washout experiments performed in the absence of Ca^{2+} showed decreased MT nucleation. On the other hand, the nucleation increased when cells were activated by pervanadate that causes the influx of Ca^{2+} from the cultivation medium. These data suggest that Ca^{2+} is important for MT nucleation, presumably by its impact on the C-terminal region of γ-tubulin in mast cells.

We carried out additional experiments demonstrating that βPIX or GIT1 regulate Ag-directed migration and degranulation in BMMCs activated by FcεRI aggregation. The depletion of βPIX increased the degranulation, whereas the depletion of GIT1 reduced it. These results correlated with increased (βPIX) or decreased (GIT1) nucleation of MTs in BMMCs with depleted levels of βPIX or GIT1, respectively. In the case of chemotaxis, we showed that GIT1 is a negative and βPIX positive regulator of chemotaxis in activated mast cells. The observed opposite effects of βPIX and GIT1 in the degranulation and chemotaxis might be explained by different roles of MTs in these processes. While granule translocation to the plasma membrane was shown to be MT-dependent [185], it was suggested that cell motility might be restrained by MTs [230]. Moreover, data obtained from chemotactic experiments might also reflect changes in actin cytoskeleton, as GIT/PIX complex regulates actin-dependent cell migration [231].

Collectively taken, we showed for the first time that MT nucleation in mast cells is regulated by a novel signalling pathway where tyrosine kinases activate GIT1 and βPIX in concert with Ca^{2+} signalling. MT nucleation could be regulated by several mechanisms in activated BMMCs. We also showed that βPIX and GIT1 are involved in the regulation of mast cell migration and chemotaxis.

In this project, my major contribution was in the examination of the role of Ca^{2+}, cell activation, and βPIX and GIT1 proteins on the nucleation of MTs. I established nocodazole-washout assay on BMMCs and performed experiments on cells with depleted levels of βPIX and GIT1, as well as the phenotypic rescue experiments. The further assays included immunofluorescent imaging on fixed and living cells. I prepared the most of the immunofluorescent figures, participated in the designing the experiments, formulation of hypothesis, manuscript preparation and responding to reviewer's comments.

III.5 GIT1/βPIX signaling proteins and PAK1 kinase regulate microtubule nucleation

Černohorská M., Sulimenko V., **Hájková Z.**, Sulimenko T., Sládková V., Vinopal S., Dráberová E., Dráber P. (2016). GIT1/βPIX signaling proteins and PAK1 kinase regulate microtubule nucleation. BBA Molecular Cell Research *1863*, 1282-1297.

The nucleation of MTs is in mast cells modulated by GIT1 and βPIX signalling proteins that form complexes with γ-tubulin [232]. In this work, we intended to understand whether the same regulatory mechanism is involved in MT nucleation in other cell types. Moreover, we wanted to know whether p21 protein [Cdc42/Rac]-activated kinase 1 (PAK1) that associates with GIT1/βPIX, play role in this process.

We showed that GIT1, βPIX and PAK1 are in complexes with γ-tubulin in human and rat cells of different tissue origin (osteogenic sarcoma, U2OS; nontransformed retinal epithelium, RPE1; embryonic kidney, HEK; glioblastoma, T98G and rat basophilic leukemia cell line, RBL) as well as in BMMCs (primary cells and established cell lines; [232]). Immunofluorescence microscopy revealed that GIT1, βPIX and active PAK1 are localized on interphase and mitotic centrosomes. Centrosomal localization of GIT1, βPIX and PAK1 does not require intact MTs. Nocodazole-washout experiments confirmed that also in interphase, well-adherent U2OS cells, βPIX is the negative regulator, and GIT1 positive regulator of MT nucleation. Moreover, PAK1 kinase positively regulated MT nucleation. Data for GIT1 and βPIX were confirmed by counting of new MTs, marked by GFP-tagged EB1, emanating from centrosomes during MT re-growth. Effects of GIT1 and βPIX were also verified in the

phenotypic rescue experiments. The necessity of active PAK1 for MT nucleation was confirmed by the inhibition of its kinase activity with ATP-noncompetitive allosteric inhibitor IPA-3. The re-growth experiment on U2OS cells treated with IPA-3 showed the same results as in cells with depleted level of PAK1. Obtained findings on U2OSs thus confirmed our previous results on BMMCs [232], and propose that the modulation of MT nucleation by GIT1 and βPIX is not limited to BMMCs.

Importantly, we found that the increase or decrease of MT nucleation from centrosomes in cells with depleted levels of GIT1, βPIX or PAK1 correlated with the amount of γ-tubulin recruited to the centrosome. The increase of MT nucleation was accompanied with the higher amount of γ-tubulin at the centrosome and conversely, the decrease of MT nucleation correlated with the lower amount of γ-tubulin. Nevertheless, we did not observe changes in the amount of centrosomal pericentrin in cells with depleted level of GIT1, βPIX or PAK1. This indicates that the PCM integrity is not affected. Centrosomal localizations of GIT1, βPIX and PAK1 were also independent of γ-tubulin. Current studies in the Laboratory are directed to the identification of their interaction partner(s) in the centrosome.

Furthermore, we attempted to identify regions on GIT1 and βPIX that mediate interactions with γ-tubulin in U2OS cells. GIT1 is a multi-domain protein with known specific binding sites for several signalling molecules including βPIX, PAK1 and paxillin [233]. We have observed, using pull-down experiments, that γ-tubulin interacts with GIT1 directly. Its binding site is located on the N-terminal GTPase-activating protein (GAP) domain that also targets GIT1 to the centrosome [234]. βPIX is a multi-domain protein as well, and binds GIT1 and PAK1 [231]. We found that the binding site for γ-tubulin on βPIX is located in its C-terminal domain, and this binding is independent of PAK1 kinase. Finally, using *in vitro* kinase assay we confirmed that both GIT1 and βPIX were phosphorylated in U2OS cells by PAK1. In contrast, γ-tubulin was not a substrate for PAK1 kinase.

We proposed a model in which centrosomal βPIX negatively regulates MT nucleation by its interaction with centrosomal GIT1. This maintains GIT1 in its autoinhibitory folded conformation resulting in the lower nucleation of MTs. When PAK1 is activated, it phosphorylates GIT1 or interacting βPIX which leads to the change in GIT1 conformation and the release of βPIX. Activated GIT1 (the positive regulator of MT nucleation) then enables the accumulation of γ-tubulin/γTuRCs at the centrosome resulting in the increase of MT nucleation. At present, it is unclear whether PAK1 phosphorylates other centrosomal proteins important for MT nucleation.

Collectively, our data proposed a novel regulatory mechanism of MT formation in interphase cells, in which GIT1/βPIX signalling proteins phosphorylated by PAK1 kinase modulate MT nucleation by affecting the accumulation of γ-tubulin in the centrosome.

In this study, I performed nocodazole-washout experiments on U2OS cells with decreased levels of βPIX, GIT1 or PAK1, as well as after the phenotypic rescue of corresponding protein. I performed immunofluorescent experiments, imaging and analysis of obtained data. I prepared several publication figures, participated in the planning of experiments, formulation of hypothesis, writing the manuscript and responding to reviewer's comments.

III.6 Regulation of microtubule nucleation mediated by γ-tubulin complexes

Sulimenko V., **Hájková Z.**, Klebanovych A., Dráber P. (2017). Regulation of microtubule nucleation mediated by γ-tubulin complexes. Protoplasma *254*, 1187-1199.

New findings in the structure of γ-tubulin complexes and the characterization of γTuRCs-interacting factors have contributed to better understanding of MT nucleation. Nevertheless, the precise molecular mechanisms that regulate MT nucleation remain not fully understood.

In this requested review we summarized recent data about factors and regulatory mechanisms involved in centrosomal and non-centrosomal MT nucleation. We described in detail current view on the architecture of γ-tubulin complexes and critically reviewed MT nucleation from spindle pole bodies, centrosomes and non-centrosomal sites (the Golgi apparatus, nuclear envelope, plasma membrane-associated sites, chromatin and surface of pre-existing MTs). For each type of nucleation, we recapitulated known associated proteins and discussed their respective regulatory roles. For clarity, we summarized building components of γ-tubulin complexes in different model systems, as well as proteins regulating MT nucleation into tables, and proposed models of non-centrosomal nucleations. This review should help to integrate recent experimental results into already established theories and formulate new tasks.

Although a lot is known about the regulation of MT nucleation, there are still gaps that need to be filled. The conformational changes of γ-tubulin complexes in the course of MT nucleation should be precisely clarified. The initiation of nucleation from the specific sites in cells, as well as upstream signalling pathways needs further investigations. Answers to these and other tasks are essential for the comprehension of the regulation of MT nucleation to form an effective functional MT network in cells under the physiological and pathological conditions.

In this review, I summarized all recent data connected to non-centrosomal MT nucleation, prepared corresponding table and designed schematic models of non-centrosomal MT nucleation. I participated in writing the manuscript and responding to reviewer's comments.

III.7 Miltefosine modulates cell activation as well as microtubule organization and dynamics in murine mast cells

Hájková Z., Sulimenko V., Paulenda T., Dráber P. Miltefosine modulates cell activation as well as microtubule organization and dynamics in murine mast cells. Allergy (Submitted).

Mast cells are involved in the pathophysiology of numerous diseases of all human organs [144]. Because mast cell-derived disorders are hard-to-treat, the demand for new and better treatments increases. Recently, a promising candidate miltefosine (hexadecylphosphocholine) was shown to inhibit human mast cell activation and reduce the disease progression in patients with mastocytosis, urticaria and atopic dermatitis [212]. Moreover, miltefosine is used as the treatment of leishmaniasis [213] and free-living amebae infections [214]. The obvious advantages of miltefosine are thus known side effects, which are relatively safe, dose-dependent and reversible [235]. As miltefosine preferentially localizes in raft microdomains [236], it has been proposed that it acts as a lipid raft modulator through its interference with the structural organization of surface receptors in the cell membrane [212]. Besides that, it modulates various signalling pathways [215-218, 237]. Nevertheless, the molecular mechanisms of miltefosine action in mast cells remain poorly understood. In this project, we focused on better understanding of miltefosine function(s) in mast cells. For this

we applied previously established methods for the evaluation of chemotaxis (III.2) and MT dynamics (III.3).

We found that murine BMMCs are sensitive to miltefosine as β-hexosaminidase release was inhibited in miltefosine-treated cells after the activation induced by FcεRI aggregation or the treatment with thapsigargin, pervanadate or Ca^{2+} ionophore. To visualise the movement of secretory granules in living BMMCs we labelled cells with Alexa Fluor 555 tagged lectin, wheat germ agglutinin (WGA) [186]. Time-lapse imaging showed a decrease in WGA-stained granule movement after 15 min treatment with miltefosine. Previously, we demonstrated that the activation of BMMCs leads to the rapid cytoskeleton rearrangement and generation of protrusions containing MTs [174]. To determine whether miltefosine modulates MT reorganization in activated BMMCs, we evaluated miltefosine-treated BMMCs activated by FcεRI aggregation, thapsigargin, Ca^{2+} ionophore or pervanadate for the presence of MT protrusions. MT reorganization was suppressed by miltefosine in all tested activations. We also found that miltefosine inhibited chemotaxis in Ag-activated BMMCs. This was likely influenced by deregulated cell movement as the cell velocity and accumulated distance were decreased in miltefosine-treated BMMCs. These data showed that miltefosine acts in different cellular compartments and could affect various signalling pathways.

To study molecular mechanisms of miltefosine function in mast cells in more detail, we analysed the early stages of cell activation. It is known that the aggregation of FcεRIs expressed at the plasma membrane of mast cells leads to tyrosine phosphorylation of FcεRIs. This is followed by the release of Ca^{2+} from the ER and by subsequent activation of SOCE [143]. The influx of free Ca^{2+} then represents a second messenger for further signalling. We showed that the overall level of tyrosine phosphorylation, as well as tyrosine phosphorylation of FcεRIs in Ag-activated cells was attenuated in miltefosine-treated BMMCs. These data were confirmed by immunofluorescence staining showing that FcεRI aggregation was suppressed in BMMCs with miltefosine. To test the next step in mast cell activation, we checked SOCE in activated non-treated and miltefosine-treated cells. Unexpectedly, miltefosine did not affect the extracellular Ca^{2+} influx through CRAC channels in activated cells, as the level of Ca^{2+} remained unchanged or even slightly increased after the miltefosine treatment. These data revealed that miltefosine attenuates the aggregation and phosphorylation of FcεRIs on the plasma membrane in activated cells, but it does not inhibit Ca^{2+} influx in these cells. To rule out whether effects observed with miltefosine are only due to the disruption of lipid rafts, we used a typical lipid raft disrupting drug,

methyl-β-cyclodextrin [238], and measured the mediator release in activated BMMCs. While methyl-β-cyclodextrin treatment partially inhibited β-hexosaminidase release in Ag-treated cells, it had no impact on thapsigargin activation (unpublished results). This was in contrast to miltefosine-treated BMMCs in which the degranulation was inhibited even after thapsigargin activation.

This led us to hypothesize that miltefosine modulates signalling pathways not only by its incorporation into the plasma membrane [212], but also by its action inside the cell. To evaluate miltefosine localization, we documented that BODIPY-tagged miltefosine [239] accumulated in BMMCs to the plasma membrane, as well as to intracellular membraneous structures and cytosol. Miltefosine internalization to intracellular structures was rapid and occurred at low miltefosine concentrations. Structures were visible already after 1 min incubation with 15 μM BODIPY-miltefosine. In the case of 1 μM BODIPY-miltefosine, the staining was observed after 15 min and the intensity increased in a time-dependent manner. Similarly as untagged miltefosine, BODIPY-miltefosine inhibited the generation of MT protrusions in cells activated with thapsigargin. The results from these experiments suggested that miltefosine easily incorporates into intracellular membranes and could affect signalling pathways in the BMMC cytosol.

Proper MT functions are essential for the cytoskeletal organization, cell motility and mast cell degranulation [155]. All these processes were affected by miltefosine. For this reason, we analysed MT dynamics and found that cytosolic miltefosine affects MT plus-end dynamics in Ca^{2+}-dependent manner in BMMCs. The increase of MT growth speed was observed also in thapsigargin-activated BMMCs, as reported previously [174]. It was described earlier that MT dynamics is regulated by the phosphorylation and dephosphorylation of +TIPs [34]. Phosphorylated +TIPs usually dissociate from MTs, whereas the dephosphorylation promotes their binding and MT stabilization [79]. In our study, *in vitro* kinase assay showed that miltefosine attenuated the phosphorylation of plus-end binding protein EB1-interacting proteins. The lower phosphorylation of EB1-interacting proteins correlated with increased MT growth speed in miltefosine-treated BMMCs. The effect of miltefosine on MT dynamics was not limited to BMMCs, as in human hTERT-RPE1 cells miltefosine also increased MT growth speed in Ca^{2+}-dependent manner (unpublished results). Thus we propose that miltefosine actively modulates Ca^{2+}-dependent kinases or phosphatases that regulate MT plus-end proteins, and affects MT dynamics in BMMCs. Moreover, this process might be universal in different cell types. In the course of these experiments, we observed that also

activation of BMMCs by thapsigargin affected MT dynamics in Ca^{2+}-dependent manner, and that thapsigargin attenuated the phosphorylation of EB1-interacting proteins. This suggests that while thapsigargin stimulates and miltefosine inhibits BMMCs activation, they both affect MT dynamics in a similar way. Nevertheless, the corresponding signalling pathways to +TIPs in the resting and activated BMMCs could be different and reflect the intracellular Ca^{2+} concentration.

Hypothetically, Ca^{2+}-dependent cPKCs could be involved in miltefosine-affected signalling to +TIPs. Miltefosine was described to inhibit PKCs in various cell types [218] and we confirmed that miltefosine inhibits cPKCs in BMMCs (unpublished data). It was shown that cPKCs suppress calcineurin signalling through the phosphorylation of calcineurin-binding protein 1 (Cabin 1) [80]. Miltefosine could inhibit cPKCs which would lead to the activation of calcineurin, dephosphorylation of +TIPs and increase of MT growth speed. Deciphering the miltefosine function in the regulation of MT dynamics warrants further investigation.

Taken together, we demonstrated that miltefosine modulates physiology of murine BMMCs at different levels as it inhibited the degranulation, MT reorganization, MT dynamics, granule movement and chemotaxis. Our results indicate that miltefosine affects mast cells through modulation of lipid rafts at the cell surface and intracellular signalling pathway(s). We suppose that the effective treatment of mast cell-driven disorders might be based on miltefosine action at multiple sites in cells. The signalling pathway directed to MT plus-ends modulated by miltefosine is under the study in the Laboratory.

In this project, I performed activation of mast cells followed by the immunofluorescence with the statistical evaluation of cells with protrusions and analysis of FcεRI aggregation. I acquired live cell imaging of cells expressing EB1-GFP or BODIPY-miltefosine to quantify MT plus-end dynamics and the localization of the drug. I carried out migration and chemotaxis assays. I participated in the conceiving and designing of all experiments, formulating hypothesis and preparing most of the images for publication. I participated in writing the manuscript.

IV. CONCLUSIONS

1) We developed new techniques for the quantification of α-tubulin to allow sensitive analysis of tubulin concentration in complex biological fluids. These assays are based on the matched pair of monoclonal antibodies recognizing non-overlapping native epitopes of α-tubulin. To quantify MT nucleation in BMMCs, we developed a new method for measurement of α-tubulin and γ-tubulin fluorescent signals corresponding to MT nucleation efficiency of the cell. We optimized the assay for the quantification of MT plus-end dynamics in living BMMCs using semi-automatic tracking of GFP-tagged EB1 protein. To analyse cell migration and chemotaxis we worked out a new technique based on the real-time imaging of non-adherent BMMCs in 3D collagen I gel using special chambers for generating the chemoattractant gradient. These tools that are described in the presented publications were used in subsequent projects, and are routinely used in our laboratory.

2) We found that GIT1 and βPIX signalling proteins interact with γ-tubulin and associate with centrosomes in BMMCs. GIT1 represents the positive regulator, whereas βPIX is the negative regulator of MT nucleation. We showed that γ-tubulin properties and associations of GIT1 and GCPs with γ-tubulin are Ca^{2+}-dependent. Correspondingly, Ca^{2+} affects MT nucleation in mast cells. In activated BMMCs, tyrosine-phosphorylated GIT1 interacts with γ-tubulin. We propose that tyrosine kinases, GIT1/βPIX signalling proteins, and Ca^{2+} are involved in the propagation of signals leading to the regulation of MT nucleation in activated mast cells.

3) We showed that GIT1/βPIX signalling proteins and PAK1 kinase are in γ-tubulin complexes in different cell types. We determined direct interactions of γ-tubulin with GIT1 and βPIX, and localised GIT1, βPIX and PAK1 to centrosomes. PAK1 and GIT1 were proved to be positive regulators of MT nucleation and βPIX was confirmed as the negative regulator of MT nucleation in U2OS cells. The level of nucleation correlates with changes of γ-tubulin accumulation at the centrosome. PAK1 phosphorylates GIT1 and βPIX signalling proteins that directly interact with γ-tubulin. We propose that GIT1/βPIX signalling proteins with PAK1 kinase represent the novel regulatory mechanism of MT nucleation in interphase cells of different types.

4) We demonstrated for the first time that miltefosine, a novel candidate for the treatment of mast cell-driven diseases, modulates BMMCs at the plasma membrane as well as in the cytosol. Miltefosine regulates the degranulation, MT reorganization, MT dynamics, granule movement and chemotaxis in BMMCs. While the treatment with miltefosine suppresses the aggregation and tyrosine phosphorylation of FcεRIs in activated BMMCs, it does not affect Ca^{2+} influx. We showed that miltefosine modulates MT dynamics in Ca^{2+}-dependent manner and attenuates the phosphorylation of EB1-interacting proteins. This opens new directions in the study of signalling pathways to +TIPs. We propose that miltefosine regulates the physiology of murine BMMCs through the modulation of lipid rafts at the cell surface and through affecting intracellular signalling pathway(s). The effective treatment of mast-cell derived diseases by miltefosine could be based on its action at multiple sites in cells.

V. REFERENCES

1. Kühn, S. and Mannherz, H.G. (2017). Actin: structure, function, dynamics, and interactions with bacterial toxins. Curr Top Microbiol Immunol *399*, 1-34.
2. Lowery, J., Kuczmarski, E.R., Herrmann, H., and Goldman, R.D. (2015). Intermediate filaments play a pivotal role in regulating cell architecture and function. J Biol Chem *290*, 17145-53.
3. Alfaro-Aco, R. and Petry, S. (2015). Building the microtubule cytoskeleton piece by piece. J Biol Chem *290*, 17154-62.
4. Gadadhar, S., Bodakuntla, S., Natarajan, K., and Janke, C. (2017). The tubulin code at a glance. J Cell Sci *130*, 1347-1353.
5. Dyachuk, V., Bierkamp, C., and Merdes, A. (2016). Non-centrosomal microtubule organization in differentiated cells. The Microtubule Cytoskeleton: Organisation, Function and Role in Disease.
6. Sanchez, A.D. and Feldman, J.L. (2017). Microtubule-organizing centers: from the centrosome to non-centrosomal sites. Curr Opin Cell Biol *44*, 93-101.
7. Hamada, T. (2014). Microtubule organization and microtubule-associated proteins in plant cells. Int Rev Cell Mol Biol *312*, 1-52.
8. Wu, J. and Akhmanova, A. (2017). Microtubule-organizing centers. Annu Rev Cell Dev Biol.
9. Kobayashi, T. and Dynlacht, B.D. (2011). Regulating the transition from centriole to basal body. J Cell Biol *193*, 435-44.
10. Banterle, N. and Gönczy, P. (2017). Centriole biogenesis: From identifying the characters to understanding the plot. Annu Rev Cell Dev Biol.
11. Hirono, M. (2014). Cartwheel assembly. Philos Trans R Soc Lond B Biol Sci *369*.
12. Guichard, P., Hachet, V., Majubu, N., Neves, A., Demurtas, D., Olieric, N., et al. (2013). Native architecture of the centriole proximal region reveals features underlying its 9-fold radial symmetry. Curr Biol *23*, 1620-8.
13. Paintrand, M., Moudjou, M., Delacroix, H., and Bornens, M. (1992). Centrosome organization and centriole architecture: their sensitivity to divalent cations. J Struct Biol *108*, 107-28.
14. Zhu, X., Liu, Y., and Yang, P. (2017). Radial spokes-a snapshot of the motility regulation, assembly, and evolution of cilia and flagella. Cold Spring Harb Perspect Biol *9*.
15. Ichikawa, M., Liu, D., Kastritis, P.L., Basu, K., Hsu, T.C., Yang, S., et al. (2017). Subnanometre-resolution structure of the doublet microtubule reveals new classes of microtubule-associated proteins. Nat Commun *8*, 15035.
16. Prosser, S.L. and Pelletier, L. (2017). Mitotic spindle assembly in animal cells: a fine balancing act. Nat Rev Mol Cell Biol *18*, 187-201.
17. Meraldi, P. (2016). Centrosomes in spindle organization and chromosome segregation: a mechanistic view. Chromosome Res *24*, 19-34.
18. Borisy, G.G. and Taylor, E.W. (1967). The mechanism of action of colchicine. Colchicine binding to sea urchin eggs and the mitotic apparatus. J Cell Biol *34*, 535-48.
19. Ludueña, R.F. (2013). A hypothesis on the origin and evolution of tubulin. Int Rev Cell Mol Biol *302*, 41-185.
20. Katsetos, C.D. and Dráber, P. (2012). Tubulins as therapeutic targets in cancer: from bench to bedside. Curr Pharm Des *18*, 2778-92.
21. Bailey, M.E., Jiang, N., Dima, R.I., and Ross, J.L. (2016). Microtubule severing enzymes couple ATPase activity with tubulin GTPase spring loading. Biopolymers *105*, 547-56.

22. Nogales, E., Wolf, S.G., and Downing, K.H. (1998). Structure of the αβ tubulin dimer by electron crystallography. Nature *391*, 199-203.

23. Barbier, P., Dorléans, A., Devred, F., Sanz, L., Allegro, D., Alfonso, C., et al. (2010). Stathmin and interfacial microtubule inhibitors recognize a naturally curved conformation of tubulin dimers. J Biol Chem *285*, 31672-81.

24. Montecinos-Franjola, F., Schuck, P., and Sackett, D.L. (2016). Tubulin dimer reversible dissociation: affinity, kinetics, and demonstration of a stable monomer. J Biol Chem *291*, 9281-94.

25. Amos, L.A. and Schlieper, D. (2005). Microtubules and MAPs. Adv Protein Chem *71*, 257-98.

26. Mukhtar, E., Adhami, V.M., and Mukhtar, H. (2014). Targeting microtubules by natural agents for cancer therapy. Mol Cancer Ther *13*, 275-84.

27. Rohena, C.C. and Mooberry, S.L. (2014). Recent progress with microtubule stabilizers: new compounds, binding modes and cellular activities. Nat Prod Rep *31*, 335-55.

28. Bates, D. and Eastman, A. (2017). Microtubule destabilising agents: far more than just antimitotic anticancer drugs. Br J Clin Pharmacol *83*, 255-268.

29. Nogales, E. and Zhang, R. (2016). Visualizing microtubule structural transitions and interactions with associated proteins. Curr Opin Struct Biol *37*, 90-6.

30. Amos, L. and Klug, A. (1974). Arrangement of subunits in flagellar microtubules. J Cell Sci *14*, 523-49.

31. McIntosh, J.R., Morphew, M.K., Grissom, P.M., Gilbert, S.P., and Hoenger, A. (2009). Lattice structure of cytoplasmic microtubules in a cultured mammalian cell. J Mol Biol *394*, 177-82.

32. Petry, S. and Vale, R.D. (2015). Microtubule nucleation at the centrosome and beyond. Nat Cell Biol *17*, 1089-93.

33. Mitchison, T. and Kirschner, M. (1984). Dynamic instability of microtubule growth. Nature *312*, 237-42.

34. Akhmanova, A. and Steinmetz, M.O. (2015). Control of microtubule organization and dynamics: two ends in the limelight. Nat Rev Mol Cell Biol *16*, 711-26.

35. Findeisen, P., Mühlhausen, S., Dempewolf, S., Hertzog, J., Zietlow, A., Carlomagno, T., et al. (2014). Six subgroups and extensive recent duplications characterize the evolution of the eukaryotic tubulin protein family. Genome Biol Evol *6*, 2274-88.

36. Libusová, L. and Dráber, P. (2006). Multiple tubulin forms in ciliated protozoan Tetrahymena and Paramecium species. Protoplasma *227*, 65-76.

37. Ruiz, F., Dupuis-Williams, P., Klotz, C., Forquignon, F., Bergdoll, M., Beisson, J., et al. (2004). Genetic evidence for interaction between η- and β-tubulins. Eukaryot Cell *3*, 212-20.

38. Parker, A.L., Teo, W.S., McCarroll, J.A., and Kavallaris, M. (2017). An emerging role for tubulin isotypes in modulating cancer biology and chemotherapy resistance. Int J Mol Sci *18*.

39. Honda, Y., Tsuchiya, K., Sumiyoshi, E., Haruta, N., and Sugimoto, A. (2017). Tubulin isotype substitution revealed that isotype combination modulates microtubule dynamics in C. elegans embryos. J Cell Sci *130*, 1652-1661.

40. Pamula, M.C., Ti, S.C., and Kapoor, T.M. (2016). The structured core of human β tubulin confers isotype-specific polymerization properties. J Cell Biol *213*, 425-33.

41. Bhattacharya, R., Yang, H., and Cabral, F. (2011). Class V β-tubulin alters dynamic instability and stimulates microtubule detachment from centrosomes. Mol Biol Cell *22*, 1025-34.

42. Belvindrah, R., Natarajan, K., Shabajee, P., Bruel-Jungerman, E., Bernard, J., Goutierre, M., et al. (2017). Mutation of the α-tubulin Tuba1a leads to straighter microtubules and perturbs neuronal migration. J Cell Biol *216*, 2443-2461.

43. Chakraborti, S., Natarajan, K., Curiel, J., Janke, C., and Liu, J. (2016). The emerging role of the tubulin code: From the tubulin molecule to neuronal function and disease. Cytoskeleton (Hoboken) *73*, 521-550.

44. Fiore, M., Goulas, C., and Pillois, X. (2017). A new mutation in TUBB1 associated with thrombocytopenia confirms that C-terminal part of β1-tubulin plays a role in microtubule assembly. Clin Genet *91*, 924-926.

45. Tischfield, M.A., Baris, H.N., Wu, C., Rudolph, G., Van Maldergem, L., He, W., et al. (2010). Human TUBB3 mutations perturb microtubule dynamics, kinesin interactions, and axon guidance. Cell *140*, 74-87.

46. Feng, R., Sang, Q., Kuang, Y., Sun, X., Yan, Z., Zhang, S., et al. (2016). Mutations in TUBB8 and human oocyte meiotic arrest. N Engl J Med *374*, 223-32.

47. Janke, C. and Bulinski, J.C. (2011). Post-translational regulation of the microtubule cytoskeleton: mechanisms and functions. Nat Rev Mol Cell Biol *12*, 773-86.

48. Argaraña, C.E., Barra, H.S., and Caputto, R. (1978). Release of [14C]tyrosine from tubulinyl-[14C]tyrosine by brain extract. Separation of a carboxypeptidase from tubulin-tyrosine ligase. Mol Cell Biochem *19*, 17-21.

49. Paturle-Lafanechère, L., Eddé, B., Denoulet, P., Van Dorsselaer, A., Mazarguil, H., Le Caer, J.P., et al. (1991). Characterization of a major brain tubulin variant which cannot be tyrosinated. Biochemistry *30*, 10523-8.

50. Aillaud, C., Bosc, C., Saoudi, Y., Denarier, E., Peris, L., Sago, L., et al. (2016). Evidence for new C-terminally truncated variants of α- and β-tubulins. Mol Biol Cell *27*, 640-53.

51. Elie, A., Prezel, E., Guérin, C., Denarier, E., Ramirez-Rios, S., Serre, L., et al. (2015). Tau co-organizes dynamic microtubule and actin networks. Sci Rep *5*, 9964.

52. Kadavath, H., Hofele, R.V., Biernat, J., Kumar, S., Tepper, K., Urlaub, H., et al. (2015). Tau stabilizes microtubules by binding at the interface between tubulin heterodimers. Proc Natl Acad Sci U S A *112*, 7501-6.

53. Bosc, C., Andrieux, A., and Job, D. (2003). STOP proteins. Biochemistry *42*, 12125-32.

54. Gigant, B., Curmi, P.A., Martin-Barbey, C., Charbaut, E., Lachkar, S., Lebeau, L., et al. (2000). The 4 Å X-ray structure of a tubulin:stathmin-like domain complex. Cell *102*, 809-16.

55. Zehr, E., Szyk, A., Piszczek, G., Szczesna, E., Zuo, X., and Roll-Mecak, A. (2017). Katanin spiral and ring structures shed light on power stroke for microtubule severing. Nat Struct Mol Biol.

56. Goryunov, D. and Liem, R.K. (2016). Microtubule-actin cross-linking factor 1: domains, interaction partners, and tissue-specific functions. Methods Enzymol *569*, 331-53.

57. Barlan, K. and Gelfand, V.I. (2017). Microtubule-based transport and the distribution, tethering, and organization of organelles. Cold Spring Harb Perspect Biol *9*.

58. Laan, L., Pavin, N., Husson, J., Romet-Lemonne, G., van Duijn, M., López, M.P., et al. (2012). Cortical dynein controls microtubule dynamics to generate pulling forces that position microtubule asters. Cell *148*, 502-14.

59. Ferreira, J.G., Pereira, A.L., and Maiato, H. (2014). Microtubule plus-end tracking proteins and their roles in cell division. Int Rev Cell Mol Biol *309*, 59-140.

60. Akhmanova, A. and Steinmetz, M.O. (2008). Tracking the ends: a dynamic protein network controls the fate of microtubule tips. Nat Rev Mol Cell Biol *9*, 309-22.

61. Maurer, S.P., Bieling, P., Cope, J., Hoenger, A., and Surrey, T. (2011). GTPγS microtubules mimic the growing microtubule end structure recognized by end-binding proteins (EBs). Proc Natl Acad Sci U S A *108*, 3988-93.

62. Jain, I. and Tran, P.T. (2017). Multiple motifs compete for EB-dependent microtubule plus end binding. Structure *25*, 821-822.

63. Seetapun, D., Castle, B.T., McIntyre, A.J., Tran, P.T., and Odde, D.J. (2012). Estimating the microtubule GTP cap size in vivo. Curr Biol *22*, 1681-7.

64. Maurer, S.P., Cade, N.I., Bohner, G., Gustafsson, N., Boutant, E., and Surrey, T. (2014). EB1 accelerates two conformational transitions important for microtubule maturation and dynamics. Curr Biol *24*, 372-84.

65. Widlund, P.O., Stear, J.H., Pozniakovsky, A., Zanic, M., Reber, S., Brouhard, G.J., et al. (2011). XMAP215 polymerase activity is built by combining multiple tubulin-binding TOG domains and a basic lattice-binding region. Proc Natl Acad Sci U S A *108*, 2741-6.

66. Ayaz, P., Ye, X., Huddleston, P., Brautigam, C.A., and Rice, L.M. (2012). A TOG:αβ-tubulin complex structure reveals conformation-based mechanisms for a microtubule polymerase. Science *337*, 857-60.

67. Honnappa, S., Gouveia, S.M., Weisbrich, A., Damberger, F.F., Bhavesh, N.S., Jawhari, H., et al. (2009). An EB1-binding motif acts as a microtubule tip localization signal. Cell *138*, 366-76.

68. Al-Bassam, J., Kim, H., Brouhard, G., van Oijen, A., Harrison, S.C., and Chang, F. (2010). CLASP promotes microtubule rescue by recruiting tubulin dimers to the microtubule. Dev Cell *19*, 245-58.

69. Zumbrunn, J., Kinoshita, K., Hyman, A.A., and Näthke, I.S. (2001). Binding of the adenomatous polyposis coli protein to microtubules increases microtubule stability and is regulated by GSK3β phosphorylation. Curr Biol *11*, 44-9.

70. Kumar, A., Manatschal, C., Rai, A., Grigoriev, I., Degen, M.S., Jaussi, R., et al. (2017). Short linear sequence motif LxxPTPh targets diverse proteins to growing microtubule ends. Structure *25*, 924-932 e4.

71. van der Vaart, B., Manatschal, C., Grigoriev, I., Olieric, V., Gouveia, S.M., Bjelić, S., et al. (2011). SLAIN2 links microtubule plus end-tracking proteins and controls microtubule growth in interphase. J Cell Biol *193*, 1083-99.

72. van de Willige, D., Hoogenraad, C.C., and Akhmanova, A. (2016). Microtubule plus-end tracking proteins in neuronal development. Cell Mol Life Sci *73*, 2053-77.

73. Le Grand, M., Rovini, A., Bourgarel-Rey, V., Honore, S., Bastonero, S., Braguer, D., et al. (2014). ROS-mediated EB1 phosphorylation through Akt/GSK3β pathway: implication in cancer cell response to microtubule-targeting agents. Oncotarget *5*, 3408-23.

74. Ran, J., Luo, Y., Zhang, Y., Yang, Y., Chen, M., Liu, M., et al. (2017). Phosphorylation of EB1 regulates the recruitment of CLIP-170 and p150glued to the plus ends of astral microtubules. Oncotarget *8*, 9858-9867.

75. Kumar, P., Lyle, K.S., Gierke, S., Matov, A., Danuser, G., and Wittmann, T. (2009). GSK3β phosphorylation modulates CLASP-microtubule association and lamella microtubule attachment. J Cell Biol *184*, 895-908.

76. Tanenbaum, M.E., Macurek, L., van der Vaart, B., Galli, M., Akhmanova, A., and Medema, R.H. (2011). A complex of Kif18b and MCAK promotes microtubule depolymerization and is negatively regulated by Aurora kinases. Curr Biol *21*, 1356-65.

77. Zimniak, T., Stengl, K., Mechtler, K., and Westermann, S. (2009). Phosphoregulation of the budding yeast EB1 homologue Bim1p by Aurora/Ipl1p. J Cell Biol *186*, 379-91.

78. Kumar, P., Chimenti, M.S., Pemble, H., Schönichen, A., Thompson, O., Jacobson, M.P., et al. (2012). Multisite phosphorylation disrupts arginine-glutamate salt bridge networks required for binding of cytoplasmic linker-associated protein 2 (CLASP2) to end-binding protein 1 (EB1). J Biol Chem *287*, 17050-64.

79. Komarova, Y.A., Huang, F., Geyer, M., Daneshjou, N., Garcia, A., Idalino, L., et al. (2012). VE-cadherin signaling induces EB3 phosphorylation to suppress microtubule growth and assemble adherens junctions. Mol Cell *48*, 914-25.

80. Szíjgyárto, Z., Szucs, K., Kovács, I., Zákány, R., Sipka, S., and Gergely, P. (2007). The role of protein kinase C isoenzymes in the regulation of calcineurin activity in human peripheral blood mononuclear cells. Int J Mol Med *20*, 359-64.

81. Kapur, M., Wang, W., Maloney, M.T., Millan, I., Lundin, V.F., Tran, T.A., et al. (2012). Calcium tips the balance: a microtubule plus end to lattice binding switch operates in the carboxyl terminus of BPAG1n4. EMBO Rep *13*, 1021-9.

82. Akhmanova, A. and Hoogenraad, C.C. (2015). Microtubule minus-end-targeting proteins. Curr Biol *25*, R162-71.

83. Jiang, K., Hua, S., Mohan, R., Grigoriev, I., Yau, K.W., Liu, Q., et al. (2014). Microtubule minus-end stabilization by polymerization-driven CAMSAP deposition. Dev Cell *28*, 295-309.

84. Yau, K.W., van Beuningen, S.F., Cunha-Ferreira, I., Cloin, B.M., van Battum, E.Y., Will, L., et al. (2014). Microtubule minus-end binding protein CAMSAP2 controls axon specification and dendrite development. Neuron *82*, 1058-73.

85. Meunier, S., Shvedunova, M., Van Nguyen, N., Avila, L., Vernos, I., and Akhtar, A. (2015). An epigenetic regulator emerges as microtubule minus-end binding and stabilizing factor in mitosis. Nat Commun *6*, 7889.

86. Oakley, C.E. and Oakley, B.R. (1989). Identification of γ-tubulin, a new member of the tubulin superfamily encoded by mipA gene of Aspergillus nidulans. Nature *338*, 662-4.

87. Vinopal, S., Černohorská, M., Sulimenko, V., Sulimenko, T., Vosecká, V., Flemr, M., et al. (2012). γ-Tubulin 2 nucleates microtubules and is downregulated in mouse early embryogenesis. PLoS One *7*, e29919.

88. Kollman, J.M., Merdes, A., Mourey, L., and Agard, D.A. (2011). Microtubule nucleation by γ-tubulin complexes. Nat Rev Mol Cell Biol *12*, 709-21.

89. Kollman, J.M., Zelter, A., Muller, E.G., Fox, B., Rice, L.M., Davis, T.N., et al. (2008). The structure of the γ-tubulin small complex: implications of its architecture and flexibility for microtubule nucleation. Mol Biol Cell *19*, 207-15.

90. Zheng, Y., Wong, M.L., Alberts, B., and Mitchison, T. (1995). Nucleation of microtubule assembly by a γ-tubulin-containing ring complex. Nature *378*, 578-83.

91. Moritz, M., Braunfeld, M.B., Sedat, J.W., Alberts, B., and Agard, D.A. (1995). Microtubule nucleation by γ-tubulin-containing rings in the centrosome. Nature *378*, 638-40.

92. Moritz, M., Braunfeld, M.B., Guénebaut, V., Heuser, J., and Agard, D.A. (2000). Structure of the γ-tubulin ring complex: a template for microtubule nucleation. Nat Cell Biol *2*, 365-70.

93. Keating, T.J. and Borisy, G.G. (2000). Immunostructural evidence for the template mechanism of microtubule nucleation. Nat Cell Biol *2*, 352-7.

94. Kollman, J.M., Greenberg, C.H., Li, S., Moritz, M., Zelter, A., Fong, K.K., et al. (2015). Ring closure activates yeast γTuRC for species-specific microtubule nucleation. Nat Struct Mol Biol *22*, 132-7.

95. Sulimenko, V., Hájková, Z., Klebanovych, A., and Dráber, P. (2017). Regulation of microtubule nucleation mediated by γ-tubulin complexes. Protoplasma *254*, 1187-1199.

96. Lawo, S., Hasegan, M., Gupta, G.D., and Pelletier, L. (2012). Subdiffraction imaging of centrosomes reveals higher-order organizational features of pericentriolar material. Nat Cell Biol *14*, 1148-58.

97. Woodruff, J.B., Ferreira Gomes, B., Widlund, P.O., Mahamid, J., Honigmann, A., and Hyman, A.A. (2017). The centrosome is a selective condensate that nucleates microtubules by concentrating tubulin. Cell *169*, 1066-1077 e10.

98. Lüders, J., Patel, U.K., and Stearns, T. (2006). GCP-WD is a γ-tubulin targeting factor required for centrosomal and chromatin-mediated microtubule nucleation. Nat Cell Biol *8*, 137-47.

99. Teixidó-Travesa, N., Villén, J., Lacasa, C., Bertran, M.T., Archinti, M., Gygi, S.P., et al. (2010). The γTuRC revisited: a comparative analysis of interphase and mitotic human γTuRC redefines the set of core components and identifies the novel subunit GCP8. Mol Biol Cell *21*, 3963-72.

100. Takahashi, M., Yamagiwa, A., Nishimura, T., Mukai, H., and Ono, Y. (2002). Centrosomal proteins CG-NAP and kendrin provide microtubule nucleation sites by anchoring γ-tubulin ring complex. Mol Biol Cell *13*, 3235-45.

101. Delgehyr, N., Sillibourne, J., and Bornens, M. (2005). Microtubule nucleation and anchoring at the centrosome are independent processes linked by ninein function. J Cell Sci *118*, 1565-75.

102. Gomez-Ferreria, M.A., Rath, U., Buster, D.W., Chanda, S.K., Caldwell, J.S., Rines, D.R., et al. (2007). Human Cep192 is required for mitotic centrosome and spindle assembly. Curr Biol *17*, 1960-6.

103. Choi, Y.K., Liu, P., Sze, S.K., Dai, C., and Qi, R.Z. (2010). CDK5RAP2 stimulates microtubule nucleation by the γ-tubulin ring complex. J Cell Biol *191*, 1089-95.

104. Liu, P., Choi, Y.K., and Qi, R.Z. (2014). NME7 is a functional component of the γ-tubulin ring complex. Mol Biol Cell *25*, 2017-25.

105. Roubin, R., Acquaviva, C., Chevrier, V., Sedjai, F., Zyss, D., Birnbaum, D., et al. (2013). Myomegalin is necessary for the formation of centrosomal and Golgi-derived microtubules. Biol Open *2*, 238-50.

106. Kinoshita, K., Noetzel, T.L., Pelletier, L., Mechtler, K., Drechsel, D.N., Schwager, A., et al. (2005). Aurora A phosphorylation of TACC3/maskin is required for centrosome-dependent microtubule assembly in mitosis. J Cell Biol *170*, 1047-55.

107. Zhang, T., Braun, U., and Leitges, M. (2016). PKD3 deficiency causes alterations in microtubule dynamics during the cell cycle. Cell Cycle *15*, 1844-54.

108. Zhang, X., Chen, Q., Feng, J., Hou, J., Yang, F., Liu, J., et al. (2009). Sequential phosphorylation of Nedd1 by Cdk1 and Plk1 is required for targeting of the γTuRC to the centrosome. J Cell Sci *122*, 2240-51.

109. Lüders, J. and Stearns, T. (2007). Microtubule-organizing centres: a re-evaluation. Nat Rev Mol Cell Biol *8*, 161-7.

110. Bartolini, F. and Gundersen, G.G. (2006). Generation of noncentrosomal microtubule arrays. J Cell Sci *119*, 4155-63.

111. Petry, S., Groen, A.C., Ishihara, K., Mitchison, T.J., and Vale, R.D. (2013). Branching microtubule nucleation in Xenopus egg extracts mediated by augmin and TPX2. Cell *152*, 768-77.

112. Chen, W.S., Chen, Y.J., Huang, Y.A., Hsieh, B.Y., Chiu, H.C., Kao, P.Y., et al. (2017). Ran-dependent TPX2 activation promotes acentrosomal microtubule nucleation in neurons. Sci Rep *7*, 42297.

113. Sanders, A.A. and Kaverina, I. (2015). Nucleation and dynamics of Golgi-derived microtubules. Front Neurosci *9*, 431.

114. Rivero, S., Cardenas, J., Bornens, M., and Rios, R.M. (2009). Microtubule nucleation at the cis-side of the Golgi apparatus requires AKAP450 and GM130. EMBO J *28*, 1016-28.

115. Wang, Z., Wu, T., Shi, L., Zhang, L., Zheng, W., Qu, J.Y., et al. (2010). Conserved motif of CDK5RAP2 mediates its localization to centrosomes and the Golgi complex. J Biol Chem *285*, 22658-65.

116. Efimov, A., Kharitonov, A., Efimova, N., Loncarek, J., Miller, P.M., Andreyeva, N., et al. (2007). Asymmetric CLASP-dependent nucleation of noncentrosomal microtubules at the trans-Golgi network. Dev Cell *12*, 917-30.

117. Bellouze, S., Schäfer, M.K., Buttigieg, D., Baillat, G., Rabouille, C., and Haase, G. (2014). Golgi fragmentation in pmn mice is due to a defective ARF1/TBCE cross-talk that coordinates COPI vesicle formation and tubulin polymerization. Hum Mol Genet *23*, 5961-75.

118. Guerin, C.M. and Kramer, S.G. (2009). RacGAP50C directs perinuclear γ-tubulin localization to organize the uniform microtubule array required for Drosophila myotube extension. Development *136*, 1411-21.

119. Bugnard, E., Zaal, K.J., and Ralston, E. (2005). Reorganization of microtubule nucleation during muscle differentiation. Cell Motil Cytoskeleton *60*, 1-13.

120. Seltzer, V., Janski, N., Canaday, J., Herzog, E., Erhardt, M., Evrard, J.L., et al. (2007). Arabidopsis GCP2 and GCP3 are part of a soluble γ-tubulin complex and have nuclear envelope targeting domains. Plant J *52*, 322-31.

121. Janski, N., Masoud, K., Batzenschlager, M., Herzog, E., Evrard, J.L., Houlné, G., et al. (2012). The GCP3-interacting proteins GIP1 and GIP2 are required for γ-tubulin complex protein localization, spindle integrity, and chromosomal stability. Plant Cell *24*, 1171-87.

122. Batzenschlager, M., Masoud, K., Janski, N., Houlné, G., Herzog, E., Evrard, J.L., et al. (2013). The GIP gamma-tubulin complex-associated proteins are involved in nuclear architecture in Arabidopsis thaliana. Front Plant Sci *4*, 480.

123. Meunier, S. and Vernos, I. (2016). Acentrosomal microtubule assembly in mitosis: the where, when, and how. Trends Cell Biol *26*, 80-87.

124. Tsai, M.Y. and Zheng, Y. (2005). Aurora A kinase-coated beads function as microtubule-organizing centers and enhance RanGTP-induced spindle assembly. Curr Biol *15*, 2156-63.

125. Scrofani, J., Sardon, T., Meunier, S., and Vernos, I. (2015). Microtubule nucleation in mitosis by a RanGTP-dependent protein complex. Curr Biol *25*, 131-40.

126. Pinyol, R., Scrofani, J., and Vernos, I. (2013). The role of NEDD1 phosphorylation by Aurora A in chromosomal microtubule nucleation and spindle function. Curr Biol *23*, 143-9.

127. Roostalu, J., Cade, N.I., and Surrey, T. (2015). Complementary activities of TPX2 and chTOG constitute an efficient importin-regulated microtubule nucleation module. Nat Cell Biol *17*, 1422-34.

128. Mishra, R.K., Chakraborty, P., Arnaoutov, A., Fontoura, B.M., and Dasso, M. (2010). The Nup107-160 complex and γ-TuRC regulate microtubule polymerization at kinetochores. Nat Cell Biol *12*, 164-9.

129. Torosantucci, L., De Luca, M., Guarguaglini, G., Lavia, P., and Degrassi, F. (2008). Localized RanGTP accumulation promotes microtubule nucleation at kinetochores in somatic mammalian cells. Mol Biol Cell *19*, 1873-82.

130. Uehara, R., Kamasaki, T., Hiruma, S., Poser, I., Yoda, K., Yajima, J., et al. (2016). Augmin shapes the anaphase spindle for efficient cytokinetic furrow ingression and abscission. Mol Biol Cell *27*, 812-27.

131. Liu, T., Tian, J., Wang, G., Yu, Y., Wang, C., Ma, Y., et al. (2014). Augmin triggers microtubule-dependent microtubule nucleation in interphase plant cells. Curr Biol *24*, 2708-13.

132. Sánchez-Huertas, C., Freixo, F., Viais, R., Lacasa, C., Soriano, E., and Lüders, J. (2016). Non-centrosomal nucleation mediated by augmin organizes microtubules in post-mitotic neurons and controls axonal microtubule polarity. Nat Commun *7*, 12187.

133. Goshima, G., Mayer, M., Zhang, N., Stuurman, N., and Vale, R.D. (2008). Augmin: a protein complex required for centrosome-independent microtubule generation within the spindle. J Cell Biol *181*, 421-9.

134. Sánchez-Huertas, C. and Lüders, J. (2015). The augmin connection in the geometry of microtubule networks. Curr Biol *25*, R294-9.

135. Johmura, Y., Soung, N.K., Park, J.E., Yu, L.R., Zhou, M., Bang, J.K., et al. (2011). Regulation of microtubule-based microtubule nucleation by mammalian polo-like kinase 1. Proc Natl Acad Sci U S A *108*, 11446-51.

136. Oriolo, A.S., Wald, F.A., Canessa, G., and Salas, P.J. (2007). GCP6 binds to intermediate filaments: a novel function of keratins in the organization of microtubules in epithelial cells. Mol Biol Cell *18*, 781-94.

137. Mogensen, M.M., Malik, A., Piel, M., Bouckson-Castaing, V., and Bornens, M. (2000). Microtubule minus-end anchorage at centrosomal and non-centrosomal sites: the role of ninein. J Cell Sci *113 (Pt 17)*, 3013-23.

138. Wang, S., Wu, D., Quintin, S., Green, R.A., Cheerambathur, D.K., Ochoa, S.D., et al. (2015). NOCA-1 functions with γ-tubulin and in parallel to Patronin to assemble non-centrosomal microtubule arrays in C. elegans. Elife *4*, e08649.

139. Macurek, L., Dráberová, E., Richterová, V., Sulimenko, V., Sulimenko, T., Dráberová, L., et al. (2008). Regulation of microtubule nucleation from membranes by complexes of membrane-bound γ-tubulin with Fyn kinase and phosphoinositide 3-kinase. Biochem J *416*, 421-30.

140. Erhardt, M., Stoppin-Mellet, V., Campagne, S., Canaday, J., Mutterer, J., Fabian, T., et al. (2002). The plant Spc98p homologue colocalizes with γ-tubulin at microtubule nucleation sites and is required for microtubule nucleation. J Cell Sci *115*, 2423-31.

141. Ambrose, C. and Wasteneys, G.O. (2011). Cell edges accumulate gamma tubulin complex components and nucleate microtubules following cytokinesis in Arabidopsis thaliana. PLoS One *6*, e27423.

142. Dahlin, J.S. and Hallgren, J. (2015). Mast cell progenitors: origin, development and migration to tissues. Mol Immunol *63*, 9-17.

143. Bulfone-Paus, S., Nilsson, G., Draber, P., Blank, U., and Levi-Schaffer, F. (2017). Positive and negative signals in mast cell activation. Trends Immunol *38*, 657-667.

144. Arthur, G. and Bradding, P. (2016). New developments in mast cell biology: Clinical implications. Chest *150*, 680-93.

145. Irani, A.M., Bradford, T.R., Kepley, C.L., Schechter, N.M., and Schwartz, L.B. (1989). Detection of MCT and MCTC types of human mast cells by immunohistochemistry using new monoclonal anti-tryptase and anti-chymase antibodies. J Histochem Cytochem *37*, 1509-15.

146. Stone, K.D., Prussin, C., and Metcalfe, D.D. (2010). IgE, mast cells, basophils, and eosinophils. J Allergy Clin Immunol *125*, S73-80.

147. Modena, B.D., Dazy, K., and White, A.A. (2016). Emerging concepts: mast cell involvement in allergic diseases. Transl Res *174*, 98-121.

148. Vukman, K.V., Försönits, A., Oszvald, A., Tóth, E.A., and Buzás, E.I. (2017). Mast cell secretome: Soluble and vesicular components. Semin Cell Dev Biol *67*, 65-73.

149. Draber, P., Halova, I., Polakovicova, I., and Kawakami, T. (2016). Signal transduction and chemotaxis in mast cells. Eur J Pharmacol *778*, 11-23.

150. Rivera, J. and Gilfillan, A.M. (2006). Molecular regulation of mast cell activation. J Allergy Clin Immunol *117*, 1214-25; quiz 1226.

151. Gilfillan, A.M. and Tkaczyk, C. (2006). Integrated signalling pathways for mast-cell activation. Nat Rev Immunol *6*, 218-30.

152. Gilfillan, A.M. and Rivera, J. (2009). The tyrosine kinase network regulating mast cell activation. Immunol Rev *228*, 149-69.

153. Mkaddem, S.B., Murua, A., Flament, H., Titeca-Beauport, D., Bounaix, C., Danelli, L., et al. (2017). Lyn and Fyn function as molecular switches that control immunoreceptors to direct homeostasis or inflammation. Nat Commun *8*, 246.

154. Yu, Y., Blokhuis, B.R., Garssen, J., and Redegeld, F.A. (2016). Non-IgE mediated mast cell activation. Eur J Pharmacol *778*, 33-43.

155. Dráber, P., Sulimenko, V., and Dráberová, E. (2012). Cytoskeleton in mast cell signaling. Front Immunol *3*, 130.

156. Wacker, D., Stevens, R.C., and Roth, B.L. (2017). How ligands illuminate GPCR molecular pharmacology. Cell *170*, 414-427.

157. Silver, R. and Curley, J.P. (2013). Mast cells on the mind: new insights and opportunities. Trends Neurosci *36*, 513-21.

158. Okayama, Y., Saito, H., and Ra, C. (2008). Targeting human mast cells expressing G-protein-coupled receptors in allergic diseases. Allergol Int *57*, 197-203.

159. Subramanian, H., Gupta, K., and Ali, H. (2016). Roles of Mas-related G protein-coupled receptor X2 on mast cell-mediated host defense, pseudoallergic drug reactions, and chronic inflammatory diseases. J Allergy Clin Immunol *138*, 700-710.

160. Kraft, S. and Kinet, J.P. (2007). New developments in FcεRI regulation, function and inhibition. Nat Rev Immunol *7*, 365-78.

161. Ambudkar, I.S., de Souza, L.B., and Ong, H.L. (2017). TRPC1, Orai1, and STIM1 in SOCE: Friends in tight spaces. Cell Calcium *63*, 33-39.

162. Holowka, D., Wilkes, M., Stefan, C., and Baird, B. (2016). Roles for Ca2+ mobilization and its regulation in mast cell functions: recent progress. Biochem Soc Trans *44*, 505-9.

163. Wajdner, H.E., Farrington, J., Barnard, C., Peachell, P.T., Schnackenberg, C.G., Marino, J.P., Jr., et al. (2017). Orai and TRPC channel characterization in FcεRI-mediated calcium signaling and mediator secretion in human mast cells. Physiol Rep *5*.

164. Zick, Y. and Sagi-Eisenberg, R. (1990). A combination of H2O2 and vanadate concomitantly stimulates protein tyrosine phosphorylation and polyphosphoinositide breakdown in different cell lines. Biochemistry *29*, 10240-5.

165. Teshima, R., Ikebuchi, H., Nakanishi, M., and Sawada, J. (1994). Stimulatory effect of pervanadate on calcium signals and histamine secretion of RBL-2H3 cells. Biochem J *302 (Pt 3)*, 867-74.

166. Thastrup, O., Cullen, P.J., Drøbak, B.K., Hanley, M.R., and Dawson, A.P. (1990). Thapsigargin, a tumor promoter, discharges intracellular Ca2+ stores by specific inhibition of the endoplasmic reticulum Ca2(+)-ATPase. Proc Natl Acad Sci U S A *87*, 2466-70.

167. Pressman, B.C. (1976). Biological applications of ionophores. Annu Rev Biochem *45*, 501-30.

168. Halova, I., Draberova, L., and Draber, P. (2012). Mast cell chemotaxis - chemoattractants and signaling pathways. Front Immunol *3*, 119.

169. Meininger, C.J., Yano, H., Rottapel, R., Bernstein, A., Zsebo, K.M., and Zetter, B.R. (1992). The c-kit receptor ligand functions as a mast cell chemoattractant. Blood *79*, 958-63.

170. Samayawardhena, L.A., Kapur, R., and Craig, A.W. (2007). Involvement of Fyn kinase in Kit and integrin-mediated Rac activation, cytoskeletal reorganization, and chemotaxis of mast cells. Blood *109*, 3679-86.

171. Kitaura, J., Kinoshita, T., Matsumoto, M., Chung, S., Kawakami, Y., Leitges, M., et al. (2005). IgE- and IgE+Ag-mediated mast cell migration in an autocrine/paracrine fashion. Blood *105*, 3222-9.

172. Tůmová, M., Koffer, A., Šimíček, M., Dráberová, L., and Dráber, P. (2010). The transmembrane adaptor protein NTAL signals to mast cell cytoskeleton via the small GTPase Rho. Eur J Immunol *40*, 3235-45.

173. Draberova, L., Bugajev, V., Potuckova, L., Halova, I., Bambouskova, M., Polakovicova, I., et al. (2014). Transmembrane adaptor protein PAG/CBP is involved in both positive and negative regulation of mast cell signaling. Mol Cell Biol *34*, 4285-300.

174. Hájková, Z., Bugajev, V., Dráberová, E., Vinopal, S., Dráberová, L., Janáček, J., et al. (2011). STIM1-directed reorganization of microtubules in activated mast cells. J Immunol *186*, 913-23.

175. Lee, J., Veatch, S.L., Baird, B., and Holowka, D. (2012). Molecular mechanisms of spontaneous and directed mast cell motility. J Leukoc Biol *92*, 1029-41.

176. Blank, U. and Rivera, J. (2004). The ins and outs of IgE-dependent mast-cell exocytosis. Trends Immunol *25*, 266-73.

177. Blank, U., Madera-Salcedo, I.K., Danelli, L., Claver, J., Tiwari, N., Sánchez-Miranda, E., et al. (2014). Vesicular trafficking and signaling for cytokine and chemokine secretion in mast cells. Front Immunol *5*, 453.

178. Theoharides, T.C., Alysandratos, K.D., Angelidou, A., Delivanis, D.A., Sismanopoulos, N., Zhang, B., et al. (2012). Mast cells and inflammation. Biochim Biophys Acta *1822*, 21-33.

179. Parravicini, V., Gadina, M., Kovarova, M., Odom, S., Gonzalez-Espinosa, C., Furumoto, Y., et al. (2002). Fyn kinase initiates complementary signals required for IgE-dependent mast cell degranulation. Nat Immunol *3*, 741-8.

180. Schwartz, S.L., Cleyrat, C., Olah, M.J., Relich, P.K., Phillips, G.K., Hlavacek, W.S., et al. (2017). Differential mast cell outcomes are sensitive to FcεRI-Syk binding kinetics. Mol Biol Cell.

181. Hernandez-Hansen, V., Smith, A.J., Surviladze, Z., Chigaev, A., Mazel, T., Kalesnikoff, J., et al. (2004). Dysregulated FcεRI signaling and altered Fyn and SHIP activities in Lyn-deficient mast cells. J Immunol *173*, 100-12.

182. Odom, S., Gomez, G., Kovarova, M., Furumoto, Y., Ryan, J.J., Wright, H.V., et al. (2004). Negative regulation of immunoglobulin E-dependent allergic responses by Lyn kinase. J Exp Med *199*, 1491-502.

183. Nishizumi, H. and Yamamoto, T. (1997). Impaired tyrosine phosphorylation and Ca2+ mobilization, but not degranulation, in lyn-deficient bone marrow-derived mast cells. J Immunol *158*, 2350-5.

184. Kawakami, Y., Kitaura, J., Satterthwaite, A.B., Kato, R.M., Asai, K., Hartman, S.E., et al. (2000). Redundant and opposing functions of two tyrosine kinases, Btk and Lyn, in mast cell activation. J Immunol *165*, 1210-9.

185. Nishida, K., Yamasaki, S., Ito, Y., Kabu, K., Hattori, K., Tezuka, T., et al. (2005). FcεRI-mediated mast cell degranulation requires calcium-independent microtubule-dependent translocation of granules to the plasma membrane. J Cell Biol *170*, 115-26.

186. Munoz, I., Danelli, L., Claver, J., Goudin, N., Kurowska, M., Madera-Salcedo, I.K., et al. (2016). Kinesin-1 controls mast cell degranulation and anaphylaxis through PI3K-dependent recruitment to the granular Slp3/Rab27b complex. J Cell Biol *215*, 203-216.

187. Singh, R.K., Mizuno, K., Wasmeier, C., Wavre-Shapton, S.T., Recchi, C., Catz, S.D., et al. (2013). Distinct and opposing roles for Rab27a/Mlph/MyoVa and Rab27b/Munc13-4 in mast cell secretion. FEBS J *280*, 892-903.

188. Sulimenko, V., Dráberová, E., Sulimenko, T., Macůrek, L., Richterová, V., Dráber, P., et al. (2006). Regulation of microtubule formation in activated mast cells by complexes of γ-tubulin with Fyn and Syk kinases. J Immunol *176*, 7243-53.

189. Smith, A.J., Pfeiffer, J.R., Zhang, J., Martinez, A.M., Griffiths, G.M., and Wilson, B.S. (2003). Microtubule-dependent transport of secretory vesicles in RBL-2H3 cells. Traffic *4*, 302-12.

190. Martin-Verdeaux, S., Pombo, I., Iannascoli, B., Roa, M., Varin-Blank, N., Rivera, J., et al. (2003). Evidence of a role for Munc18-2 and microtubules in mast cell granule exocytosis. J Cell Sci *116*, 325-34.

191. Nishida, K., Yamasaki, S., Hasegawa, A., Iwamatsu, A., Koseki, H., and Hirano, T. (2011). Gab2, via PI-3K, regulates ARF1 in FcεRI-mediated granule translocation and mast cell degranulation. J Immunol *187*, 932-41.

192. Ogawa, K., Tanaka, Y., Uruno, T., Duan, X., Harada, Y., Sanematsu, F., et al. (2014). DOCK5 functions as a key signaling adaptor that links FcεRI signals to microtubule dynamics during mast cell degranulation. J Exp Med *211*, 1407-19.

193. Norman, J.C., Price, L.S., Ridley, A.J., Hall, A., and Koffer, A. (1994). Actin filament organization in activated mast cells is regulated by heterotrimeric and small GTP-binding proteins. J Cell Biol *126*, 1005-15.

194. Kuehn, H.S., Rådinger, M., Brown, J.M., Ali, K., Vanhaesebroeck, B., Beaven, M.A., et al. (2010). Btk-dependent Rac activation and actin rearrangement following FcεRI aggregation promotes enhanced chemotactic responses of mast cells. J Cell Sci *123*, 2576-85.

195. Ramírez-Valadez, K.A., Vázquez-Victorio, G., Macías-Silva, M., and González-Espinosa, C. (2017). Fyn kinase mediates cortical actin ring depolymerization required for mast cell migration in response to TGF-β in mice. Eur J Immunol *47*, 1305-1316.

196. Sullivan, R., Price, L.S., and Koffer, A. (1999). Rho controls cortical F-actin disassembly in addition to, but independently of, secretion in mast cells. J Biol Chem *274*, 38140-6.

197. Suzuki, R., Liu, X., Olivera, A., Aguiniga, L., Yamashita, Y., Blank, U., et al. (2010). Loss of TRPC1-mediated Ca2+ influx contributes to impaired degranulation in Fyn-deficient mouse bone marrow-derived mast cells. J Leukoc Biol *88*, 863-75.

198. Horny, H.P., Reimann, O., and Kaiserling, E. (1988). Immunoreactivity of normal and neoplastic human tissue mast cells. Am J Clin Pathol *89*, 335-40.

199. Toda, M., Kuo, C.H., Borman, S.K., Richardson, R.M., Inoko, A., Inagaki, M., et al. (2012). Evidence that formation of vimentin mitogen-activated protein kinase (MAPK) complex mediates mast cell activation following FcεRI/CC chemokine receptor 1 cross-talk. J Biol Chem *287*, 24516-24.

200. Nahm, D.H., Tkaczyk, C., Fukuishi, N., Colucci-Guyon, E., Gilfillan, A.M., and Metcalfe, D.D. (2003). Identification of Fyn-binding proteins in MC/9 mast cells using mass spectrometry. Biochem Biophys Res Commun *310*, 202-8.

201. Oettgen, H.C. (2016). Fifty years later: Emerging functions of IgE antibodies in host defense, immune regulation, and allergic diseases. J Allergy Clin Immunol *137*, 1631-1645.

202. Frieri, M. (2015). Mast cell activation syndrome. Clin Rev Allergy Immunol.

203. Singh, J., Shah, R., and Singh, D. (2016). Targeting mast cells: Uncovering prolific therapeutic role in myriad diseases. Int Immunopharmacol *40*, 362-384.

204. Molderings, G.J., Brettner, S., Homann, J., and Afrin, L.B. (2011). Mast cell activation disease: a concise practical guide for diagnostic workup and therapeutic options. J Hematol Oncol *4*, 10.

205. Sokol, K.C., Ghazi, A., Kelly, B.C., and Grant, J.A. (2014). Omalizumab as a desensitizing agent and treatment in mastocytosis: a review of the literature and case report. J Allergy Clin Immunol Pract *2*, 266-70.

206. Kawakami, T. and Blank, U. (2016). From IgE to Omalizumab. J Immunol *197*, 4187-4192.

207. Barratt, G., Saint-Pierre-Chazalet, M., and Loiseau, P.M. (2009). Cellular transport and lipid interactions of miltefosine. Curr Drug Metab *10*, 247-55.

208. Weller, K., Artuc, M., Jennings, G., Friedrichson, T., Guhl, S., dos Santos, R.V., et al. (2009). Miltefosine inhibits human mast cell activation and mediator release both in vitro and in vivo. J Invest Dermatol *129*, 496-8.

209. Hartmann, K., Siebenhaar, F., Belloni, B., Brockow, K., Eben, R., Hartmann, B., et al. (2010). Effects of topical treatment with the raft modulator miltefosine and clobetasol in cutaneous mastocytosis: a randomized, double-blind, placebo-controlled trial. Br J Dermatol *162*, 185-90.

210. Magerl, M., Rother, M., Bieber, T., Biedermann, T., Brasch, J., Dominicus, R., et al. (2013). Randomized, double-blind, placebo-controlled study of safety and efficacy of miltefosine in antihistamine-resistant chronic spontaneous urticaria. J Eur Acad Dermatol Venereol *27*, e363-9.

211. Dölle, S., Hoser, D., Rasche, C., Loddenkemper, C., Maurer, M., Zuberbier, T., et al. (2010). Long-term reduction in local inflammation by a lipid raft molecule in atopic dermatitis. Allergy *65*, 1158-65.

212. Maurer, M., Magerl, M., Metz, M., Weller, K., and Siebenhaar, F. (2013). Miltefosine: a novel treatment option for mast cell-mediated diseases. J Dermatolog Treat *24*, 244-9.

213. Monge-Maillo, B. and López-Vélez, R. (2015). Miltefosine for visceral and cutaneous leishmaniasis: drug characteristics and evidence-based treatment recommendations. Clin Infect Dis *60*, 1398-404.

214. Schuster, F.L., Guglielmo, B.J., and Visvesvara, G.S. (2006). In-vitro activity of miltefosine and voriconazole on clinical isolates of free-living amebas: Balamuthia mandrillaris, Acanthamoeba spp., and Naegleria fowleri. J Eukaryot Microbiol *53*, 121-6.

215. Ruiter, G.A., Zerp, S.F., Bartelink, H., van Blitterswijk, W.J., and Verheij, M. (2003). Anti-cancer alkyl-lysophospholipids inhibit the phosphatidylinositol 3-kinase-Akt/PKB survival pathway. Anticancer Drugs *14*, 167-73.

216. Ward, P.D., Ouyang, H., and Thakker, D.R. (2003). Role of phospholipase C-β in the modulation of epithelial tight junction permeability. J Pharmacol Exp Ther *304*, 689-98.

217. Lucas, L., Hernández-Alcoceba, R., Penalva, V., and Lacal, J.C. (2001). Modulation of phospholipase D by hexadecylphosphorylcholine: a putative novel mechanism for its antitumoral activity. Oncogene *20*, 1110-7.

218. Überall, F., Oberhuber, H., Maly, K., Zaknun, J., Demuth, L., and Grunicke, H.H. (1991). Hexadecylphosphocholine inhibits inositol phosphate formation and protein kinase C activity. Cancer Res *51*, 807-12.

219. Pontén, J. and Saksela, E. (1967). Two established in vitro cell lines from human mesenchymal tumours. Int J Cancer *2*, 434-47.

220. Madeddu, R., Farace, C., Tolu, P., Solinas, G., Asara, Y., Sotgiu, M.A., et al. (2013). Cytoskeletal proteins in the cerebrospinal fluid as biomarker of multiple sclerosis. Neurol Sci *34*, 181-6.

221. Zengel, P., Nguyen-Hoang, A., Schildhammer, C., Zantl, R., Kahl, V., and Horn, E. (2011). μ-Slide Chemotaxis: a new chamber for long-term chemotaxis studies. BMC Cell Biol *12*, 21.

222. Heit, B. and Kubes, P. (2003). Measuring chemotaxis and chemokinesis: the under-agarose cell migration assay. Sci STKE *2003*, PL5.

223. Tomar, V., Kukreti, S., Prakash, S., Madan, J., and Chandra, R. (2017). Noscapine and its analogs as chemotherapeutic agent: Current updates. Curr Top Med Chem *17*, 174-188.

224. Chen, X., Dang, T.T., and Facchini, P.J. (2015). Noscapine comes of age. Phytochemistry *111*, 7-13.

225. Ye, K., Ke, Y., Keshava, N., Shanks, J., Kapp, J.A., Tekmal, R.R., et al. (1998). Opium alkaloid noscapine is an antitumor agent that arrests metaphase and induces apoptosis in dividing cells. Proc Natl Acad Sci U S A *95*, 1601-6.

226. Suri, C. and Naik, P.K. (2015). Combined molecular dynamics and continuum solvent approaches (MM-PBSA/GBSA) to predict noscapinoid binding to γ-tubulin dimer. SAR QSAR Environ Res *26*, 507-19.

227. Vogel, J., Drapkin, B., Oomen, J., Beach, D., Bloom, K., and Snyder, M. (2001). Phosphorylation of γ-tubulin regulates microtubule organization in budding yeast. Dev Cell *1*, 621-31.

228. Keck, J.M., Jones, M.H., Wong, C.C., Binkley, J., Chen, D., Jaspersen, S.L., et al. (2011). A cell cycle phosphoproteome of the yeast centrosome. Science *332*, 1557-61.

229. Totaro, A., Astro, V., Tonoli, D., and de Curtis, I. (2014). Identification of two tyrosine residues required for the intramolecular mechanism implicated in GIT1 activation. PLoS One *9*, e93199.

230. Ganguly, A., Yang, H., Sharma, R., Patel, K.D., and Cabral, F. (2012). The role of microtubules and their dynamics in cell migration. J Biol Chem *287*, 43359-69.

231. Zhou, W., Li, X., and Premont, R.T. (2016). Expanding functions of GIT Arf GTPase-activating proteins, PIX Rho guanine nucleotide exchange factors and GIT-PIX complexes. J Cell Sci *129*, 1963-74.

232. Sulimenko, V., Hájková, Z., Černohorská, M., Sulimenko, T., Sládková, V., Dráberová, L., et al. (2015). Microtubule nucleation in mouse bone marrow-derived mast cells is regulated by the concerted action of GIT1/βPIX proteins and calcium. J Immunol *194*, 4099-111.

233. Webb, D.J., Mayhew, M.W., Kovalenko, M., Schroeder, M.J., Jeffery, E.D., Whitmore, L., et al. (2006). Identification of phosphorylation sites in GIT1. J Cell Sci *119*, 2847-50.

234. Zhao, Z.S., Lim, J.P., Ng, Y.W., Lim, L., and Manser, E. (2005). The GIT-associated kinase PAK targets to the centrosome and regulates Aurora-A. Mol Cell *20*, 237-49.

235. Verhaar, A.P., Wildenberg, M.E., Peppelenbosch, M.P., Hommes, D.W., and van den Brink, G.R. (2014). Repurposing miltefosine for the treatment of immune-mediated disease? J Pharmacol Exp Ther *350*, 189-95.

236. Ménez, C., Buyse, M., Farinotti, R., and Barratt, G. (2007). Inward translocation of the phospholipid analogue miltefosine across Caco-2 cell membranes exhibits characteristics of a carrier-mediated process. Lipids *42*, 229-40.

237. van Blitterswijk, W.J. and Verheij, M. (2008). Anticancer alkylphospholipids: mechanisms of action, cellular sensitivity and resistance, and clinical prospects. Curr Pharm Des *14*, 2061-74.

238. Zidovetzki, R. and Levitan, I. (2007). Use of cyclodextrins to manipulate plasma membrane cholesterol content: evidence, misconceptions and control strategies. Biochim Biophys Acta *1768*, 1311-24.

239. Hornillos, V., Carrillo, E., Rivas, L., Amat-Guerri, F., and Acuña, A.U. (2008). Synthesis of BODIPY-labeled alkylphosphocholines with leishmanicidal activity, as fluorescent analogues of miltefosine. Bioorg Med Chem Lett *18*, 6336-9.

VI. PRESENTED PUBLICATIONS

VI.1

Dráberová E., Stegurová L., Sulimenko V., **Hájková Z.**, Dráber Pe., Dráber Pa. (2013). Quantification of α-tubulin isotypes by sandwich ELISA with signal amplification through biotinyl-tyramide or immuno-PCR. Journal of Immunological Methods *395*, 63-70.

Journal of Immunological Methods 395 (2013) 63–70

Contents lists available at SciVerse ScienceDirect

Journal of Immunological Methods

journal homepage: www.elsevier.com/locate/jim

Research paper

Quantification of α-tubulin isotypes by sandwich ELISA with signal amplification through biotinyl-tyramide or immuno-PCR

Eduarda Dráberová [a,1], Lucie Stegurová [b,1], Vadym Sulimenko [a], Zuzana Hájková [a], Petr Dráber [b], Pavel Dráber [a,*]

[a] Laboratory of Biology of Cytoskeleton, Institute of Molecular Genetics, Academy of Sciences of the Czech Republic, CZ-142 20 Prague 4, Czech Republic
[b] Laboratory of Signal Transduction, Institute of Molecular Genetics, Academy of Sciences of the Czech Republic, CZ-142 20 Prague 4, Czech Republic

ARTICLE INFO

Article history:
Received 25 April 2013
Received in revised form 2 July 2013
Accepted 2 July 2013
Available online 10 July 2013

Keywords:
α-Tubulin isotypes
Biotinyl-tyramide
ELISA
Immuno-PCR
Mast cells

ABSTRACT

Microtubules formed by αβ-tubulin dimers represent cellular structures that are indispensable for the maintenance of cell morphology and for cell motility generation. Microtubules in intact cells are in highly regulated equilibrium with cellular pools of soluble tubulin dimers. Sensitive, reproducible and rapid assays are necessary to monitor tubulin changes in cytosolic pools after treatment with anti-mitotic drugs, during the cell cycle or activation and differentiation events. Here we describe new assays for α-tubulin quantification. The assays are based on sandwich ELISA, and the signal is amplified with biotinyl-tyramide or immuno-PCR. Matching monoclonal antibody pair recognizes phylogenetically highly conserved epitopes localized outside the C-terminal isotype-defining region. This makes it possible to detect α-tubulin isotypes in different cell types of various species. Biotinyl-tyramide amplification and immuno-PCR amplification enable detection of tubulin at concentrations 2.5 ng/ml and 0.086 ng/ml, respectively. Immuno-PCR detection shows enhanced sensitivity and wider dynamic range when compared to ELISA with biotinyl-tyramide detection. Our results on taxol-treated and activated bone marrow-derived mast cells demonstrate, that the assays allow sensitive quantification of tubulin in complex biological fluids.

1. Introduction

Microtubules are highly dynamic structures vital for numerous cellular processes, including cellular organization, intracellular trafficking, migration, and cell division. Microtubules can rapidly reorganize their arrangements depending on external signals. They usually consist of 13 laterally associated protofilaments made up of αβ-tubulin dimers. In vertebrates tubulins are encoded by multiple genes and their products, tubulin isotypes, differ mainly in their C-terminal regions. Certain isotypes are tissue specific, and the isotype composition affects microtubule properties (Ludueña and Banerjee, 2008). Multiple α- and β-tubulin isotypes can be present in the same cell, and tubulin heterogeneity is further enhanced by various posttranslational modifications (Linhartová et al., 1992). In intact cells a highly regulated equilibrium exists between microtubules and the pools of soluble tubulin dimers. Tubulin binds to tubulin-binding agents, small molecule inhibitors, such as anti-mitotic drugs (e.g. taxol, vinblastin, nocodazole, colchicine) that can change the ratio between polymeric and soluble tubulin pools (Katsetos and Dráber, 2012).

Abbreviations: BMMC, bone marrow-derived mast cell; BSA, bovine serum albumin; BSS, buffered saline solution; C_q, quantification cycle; ELISA, enzyme-linked immunosorbent assay; PCR, polymerase chain reaction; PBS, phosphate buffer solution; TBS, Tris buffer solution; TBST, TBS containing 0.05% Tween 20; TMB, 3,3′,5,5′-tetramethylbenzidine.

* Corresponding author at: Laboratory of Biology of Cytoskeleton, Institute of Molecular Genetics, Academy of Sciences of the Czech Republic, Vídeňská 1083, 142 20 Prague 4, Czech Republic. Tel.: +420 241 062 632; fax: +420 241 062 758.
E-mail address: paveldra@img.cas.cz (P. Dráber).

[1] E.D. and L.S. contributed equally to this work.

0022-1759/$ – see front matter © 2013 Elsevier B.V. All rights reserved.
http://dx.doi.org/10.1016/j.jim.2013.07.001

Sensitive, reproducible and rapid assays are needed for monitoring tubulin changes in cytosolic pools after treatment with anti-mitotic drugs, during the cell cycle, and activation or differentiation events. Several methods have been described for quantification of total tubulin in cells or tissue extracts, including colchicine binding (Pipeleers et al., 1977; Wilson, 1970) or radioimmunoassay (Bulinski et al., 1980; Das et al., 1989). However, both the colchicine binding assay and radioimmunoassay use radioactive compounds. Competitive enzyme-linked immunosorbent assay (ELISA) was alternatively elaborated for quantification of tubulin pools (Thrower et al., 1991) or β-tubulin isotypes (Dozier et al., 2003); the detection limit is around 1 μg/ml.

Mast cells play an essential role in innate immunity, allergy and inflammation. When activated they release mediators that are pivotal for initiation of inflammatory reactions associated with allergic disorders (Rivera et al., 2008). In the course of mouse bone marrow-derived mast cell (BMMC) activation, substantial changes in reorganization of microtubules take place (Hájková et al., 2011). However, it is not known whether or not activation-induced changes, degranulation and/or exosome release also lead to the release of tubulin into extracellular space. Such process has been documented for some other cellular components (Valadi et al., 2007).

Here we report on the development of new sensitive assays for tubulin quantification. The assays are based on sandwich ELISA, and the signal is amplified with biotinyl-tyramide or immuno-polymerase chain reaction (PCR). The key component of the system is a matching antibody pair recognizing phylogenetically highly conserved epitopes localized outside the C-terminal isotype-defining region. This makes it possible to detect α-tubulin isotypes in different cell types of various species. The results on taxol-treated and activated BMMCs confirm, that the techniques offer sensitive alternative of quantification of tubulin in complex biological fluids.

2. Material and methods

2.1. Tubulin preparation

Microtubule protein was purified from porcine brain by two temperature-dependent cycles of assembly and disassembly (Shelanski et al., 1973), followed by subsequent purification by phosphocellulose chromatography (Weingarten et al., 1975). The eluted tubulin in column buffer (100 mM PIPES pH 6.9, 1 mM EGTA, 1 mM $MgCl_2$, 1 mM DTT, 0.5 mM GTP) was supplemented with GTP to 1 mM and polymerized by sodium glutamate added to final concentration 1.0 M. Pelleted microtubules were resuspended in BRB80 buffer (80 mM PIPES pH 6.8, 1 mM EGTA, 1 mM $MgCl_2$) supplemented with 0.1 mM GTP (BRB80-GTP) and depolymerized by cold. Tubulin concentration in supernatant was checked by measuring the absorbance at 280 nm using an extinction coefficient at 280 nm of 115,000 M^{-1} cm^{-1}. Recycled tubulin was more than 98% pure as determined by SDS-PAGE, and it was stored in liquid nitrogen in aliquots at ~200 μM concentration. Alternatively, tubulin at concentration ~200 μM was freeze-dried in small aliquots in the presence of trehalose and stored at ambient temperature (Dráberová et al., 2010). Freeze-dried tubulin was rehydrated with cold Millipore water at 4 °C to the original aliquot volume and incubated on ice for 20 min. Concentrated tubulin samples were diluted in precooled BRB80-GTP to the concentration ~50 μM and centrifuged at 300,000 ×*g* for 5 min at 4 °C; to remove any aggregates. Tubulin concentration in supernatants was determined by absorbance at 280 nm.

2.2. Cells

Mouse cell line of BMMCs, which grow in the absence of stem cell factor, was provided by M. Hibbs (Ludwig Institute for Cancer Research, Melbourne, Australia) (Hibbs et al., 1995). The cells were incubated in suspension cultures in freshly prepared culture medium (RPMI 1640 supplemented with 20 mM HEPES, pH 7.5, 100 U/ml penicillin, 100 μg/ml streptomycin, 100 μM MEM nonessential amino acids, 1 mM sodium pyruvate) supplemented with 10% fetal calf serum (FCS) and 10% WEHI-3 cell supernatant as a source of interleukin 3. Mouse embryonal fibroblasts NIH 3T3 were obtained from the American Type Culture Collection. Cells were cultured in Dulbecco's modified Eagle's medium (DMEM) containing 10% FCS, penicillin (100 U/ml), and streptomycin (0.1 mg/ml). Cells were grown at 37 °C in 5% CO_2 in air and passaged every 2 days.

To compare tubulin concentration in extracts prepared from control and taxol-treated cells, BMMCs in culture media were incubated for 2.5 h in the absence or presence of taxol at final concentration 10 μM. Cells were pelleted by centrifugation (240 ×*g*, 5 min, 25 °C), washed in ice-cold HEPES buffer (50 mM HEPES adjusted to pH 7.6 with KOH, 75 mM KCl, 1 mM EGTA, 1 mM $MgCl_2$), pelleted and counted after resuspension. Samples of 10×10^6 cells were resuspended in 1 ml of ice-cold HEPES buffer supplemented with protease (Protease inhibitor cocktail tablets; Roche) and phosphatase (1 mM Na_3VO_4 and 1 mM NaF) inhibitors and 1% NP-40. After 10 min incubation at 4 °C, cell extracts were centrifuged (20,000 ×*g*, 15 min, 4 °C) and collected supernatants were used for determination of tubulin concentration.

To quantify the release of tubulin from thapsigargin-activated cells into the culture medium, BMMCs (44×10^6 cells) were resuspended in 1 ml of buffered saline solution (BSS; 20 mM HEPES, pH 7.4, 135 mM NaCl, 5 mM KCl, 1.8 mM $CaCl_2$, 5.6 mM glucose, 2 mM $MgCl_2$) supplemented with 0.1% BSA (Sigma-Aldrich, Cat. No. A7030) (BSS-BSA) and incubated for 20 min at 37 °C in the absence or presence of thapsigargin (Sigma-Aldrich; Cat. No. 79033) at final concentration 2 μM. Cells were pelleted by centrifugation (240 ×*g*, 5 min, 25 °C) and the collected supernatant was further centrifuged (200,000 ×*g*, 4 min, 4 °C) to remove any cellular debris. Collected supernatants were used for determination of tubulin concentration.

2.3. Antibodies

Purified mouse monoclonal antibody DM1A (IgG1) to α-tubulin (Blose et al., 1984) at 1 mg/ml concentration was bought from Abcam (Cat. No. ab7291). The antibody recognizes epitope located in the C-terminal region of α-tubulin (a.a. 426–451) of various species; amino acids within the positions 426 and 430 are particularly important for antibody reactivity (Breitling and Little, 1986). The mouse monoclonal antibody TU-07 (IgM) against α-tubulin of various species (Dráber et al., 1986), recognizes the epitope exposed on the surface

of polymerized microtubules (Dráber et al., 1990; Smertenko et al., 1997).

TU-07 was purified from ascitic fluid by ammonium sulfate precipitation followed by gel chromatography on the column of Sepharose 6B. Purity verified by SDS-PAGE exceeded 85% as TU-07 antibody was biotinylated using EZ-Link Sulfo-NHS-LC-biotin from Pierce according to manufacturer's recommendation. Conjugated antibody was dialyzed against phosphate buffer solution (PBS; 10 mM phosphate, 150 mM NaCl, pH 7.4) and stored in 50% glycerol at −20 °C (final antibody concentration = 0.6 mg/ml). The capability of biotinylated antibody to bind tubulin was verified by immunoblotting on total 3T3 lysate, by staining of microtubules in fixed 3T3 cells (Dráber et al., 1989) and by indirect ELISA on immobilized tubulin. The antibody reacted on immunoblots with protein band corresponding to tubulin, stained interphase and mitotic microtubules, and bound to purified tubulin in ELISA (not shown).

Mouse monoclonal antibody TUB 2.1 (IgG_1) to β-tubulin labeled with indocarbocyanate (Cy3) was from Sigma-Aldrich. Anti-mouse antibody conjugated with horseradish peroxidase was purchased from Promega Biotec.

2.4. Epitope mapping

Synthetic overlapping peptides (15-meric peptides with 5 amino acid overlaps) were prepared by SPOT synthesis (Jerini Peptide Technologies, Berlin, Germany). Each spot carried approximately 5-nmol peptide covalently bound to cellulose-β-alanine membrane. Peptide scans (45 peptides) covered the sequences 1–451 of porcine (*Sus scrofa*) α-tubulin 1A (TUBA1A, accession number P02550 in the UniProtKB/Swiss-Prot database). Epitope mapping was performed using horseradish-conjugated anti-mouse antibody and chemiluminescent detection of bound antibodies as described (Blume et al., 2010).

2.5. Gel electrophoresis and immunoblotting

SDS-PAGE on 12% polyacrylamide gel and immunoblotting were performed using standard protocols (Sulimenko et al., 2002). Protein quantifications in cell lysates were performed with bicinchoninic acid assay (Thermo Scientific, Cat. No. 23227). DM1A and purified TU-07 were diluted 1:5000 and 1:1000, respectively. Peroxidase-conjugated secondary anti-mouse antibody (Promega, Cat. No. W4028) was diluted 1:10,000. Bound antibodies were detected by Super-Signal WestPico Chemiluminescent reagents (Pierce).

2.6. Sandwich ELISA

The assay was routinely performed in high binding 96-well half-area polystyrene plates (Corning Inc.; Cat. No. 3690). Alternatively, polycarbonate TopYield Strips (Nunc; Cat. No. 248917) were used. Washings throughout the assay (200 μl/well, four times per washing step, if not specified otherwise) were carried out by means of automatic washing device HydroFlex Platform (TECAN) with Tris buffer solution (TBS; 10 mM Tris–Cl, pH 7.4, 150 mM NaCl) containing 0.05% Tween 20 (TBST). Anti-tubulin antibody DM1A was coated at a concentration of 5 μg/ml in PBS (30 μl/well) overnight (~16 h) at 4 °C. After washing, the plates were blocked by adding 2% BSA in TBS (BSA/TBS) (185 μl/well) for 6 h at room temperature. The plates were then washed and incubated overnight (~16 h) at 4 °C with tubulin standards or tested samples diluted in 1% BSA in PBS (30 μl/well). The sample diluent served as negative control. Washed plates were then incubated for 1 h at room temperature with biotinylated anti-tubulin antibody TU-07 at concentration 1 μg/ml in 1% bovine serum albumin (BSA) in TBST (BSA/TBST) (30 μl/well). Washed plates were incubated for 45 min at room temperature with extravidin-horseradish peroxidase (Sigma-Aldrich, Cat. No. E2886) diluted 1:5000 in BSA/TBST (30 μl/well). After repeated washing, the sensitivity of the assay was augmented by biotinyl-tyramide signal amplification using the ELAST ELISA Amplification System (PerkinElmer, Cat. No. NEP116001EA) according to the manufacturer's directions. Shortly, plates were incubated with biotinyl-tyramide, diluted 1:500 in amplification diluent (30 μl/well) for 15 min at room temperature in dark, washed (5 times) and incubated with streptavidin-peroxidase diluted 1:1000 in BSA/TBST (30 μl/well) for 30 min at room temperature in dark. The plates were washed (5 times) and incubated with 3,3′,5,5′-tetramethylbenzidine (TMB) Liquid Substrate (Sigma-Aldrich, Cat. No. T8665) (30 μl/well). Reaction was stopped after 13 min by adding Stop Reagent for TMB Substrate (Sigma-Aldrich) (30 μl/well). Absorption was determined at 450 nm on Sunrise plate Reader (TECAN). Background values of negative controls were subtracted from the readings.

For long-term storage, TopYield Strips were coated with DM1A antibody and blocked with BSA; excess blocking solution was removed before air-drying. Precoated strips were stored at 4 °C in the presence of desiccant. Wells were rehydrated by adding BSA/TBS for 30 min at room temperature. The strips were then washed and incubated with samples.

2.7. Immuno-PCR

The immuno-PCR was performed as described (Niemeyer et al., 2005; Potůčková et al., 2011) with some modifications. Twenty-five microliter aliquots of capture anti-tubulin antibody DM1A (5 μg/ml) in 100 mM borate buffer (pH 9.5) were dispensed into each well of TopYield strips. The wells were incubated for 2 h at 37 °C and washed four times with 200 μl of TBST. Free binding sites were blocked with BSA/TBS. After 2 h at 37 °C, the strips were washed again four times, followed by adding 25 μl of tubulin standards or tested samples diluted in 1% BSA in PBS. The strips were further incubated for 1 h at 37 °C and then overnight at 4 °C, followed by four washings. Subsequently, 25 μl aliquots of biotinylated anti-tubulin antibody TU-07 (1 μg/ml in TBS–1% BSA) were added and the samples were incubated for 1 h at 37 °C. After washing four times, the wells were filled with 25 μl aliquots of extravidin (0.1 μg/ml, Sigma-Aldrich, Cat. No. E2511) in TBS–1% BSA, incubated for 1 h at 37 °C and then washed as before. The next step consists in the addition of 25 μl of biotinylated DNA template (0.27 pg/ml). The template was prepared by amplification of a DNA fragment corresponding to nucleotides 989–1209 of human tyrosine-protein kinase ABL1 (GenBank accession no. M14752) with biotinylated primer 5B-HRM1-F, 5′-biotin-AAACTCATCACCACGCTCCATTA-3′, and HRM1-R, 5′-TCTTCCACCTCCATGGTGTC-3′ (Generi Biotech, Czech Republic). The strips were then incubated for 1 h at 37 °C followed by washing four times with TBST and twice

with MilliQ water. Template DNA immobilized on antigen in the wells was quantified by real-time PCR. An aliquot of 25 μl of master mix solution was added into each well containing 75 mM Tris–HCl (pH 8.8), 20 mM $(NH_4)_2SO_4$, 2.5 mM $MgCl_2$, 200 μM dATP, 200 μM dGTP, 200 μM dCTP, 200 μM dTTP, Taq DNA polymerase (25 U/ml; TopBio, Czech Republic), 2 μM SYTO-9 (Invitrogen) and primers (200 nM each); forward HRM1-F (5′-CTCATCACCACGCTCCATTA-3′) and reverse HRM1-R (see above). Finally, each well was overlaid with 5 μl of light mineral oil (TopBio) and sealed with Light cycler sealing foil (Roche). The cycling conditions were as follows: 2 min at 95 °C as an initial denaturation step and 40 cycles consisting of 15 s at 95 °C, 60 s at 60 °C, and elongation step for 60 s at 72 °C using Realplex^4 Mastercycler (Eppendorf, Hamburg, Germany). The C_q (quantification cycle) values were determined using the software of the cycler.

2.8. Degranulation assay

The degree of degranulation was quantified as the release of β-glucuronidase from control or thapsigargin-activated cells, using 4-methylumbelliferyl β-D-glucuronide as a substrate (Surviladze et al., 2001). The total content of the enzyme was evaluated in supernatants from cells lysed by 0.1% Triton X-100.

2.9. Microscopy and FACS

Immunofluorescence microscopy was performed on fixed cells as described (Dráberová and Dráber, 1993). Shortly, cells were rinsed with microtubule-stabilizing buffer (0.1 M MES, pH 6.9, 2 mM EGTA, 2 mM $MgCl_2$, 4% polyethylene glycol 6000), fixed for 20 min in 3% formaldehyde in microtubule-stabilizing buffer and extracted for 4 min with 0.5% Triton X-100 in microtubule-stabilizing buffer. TUB 2.1 mAb conjugated with Cy3 was diluted 1:600. The preparations were examined with Olympus A70 Provis microscope.

Data obtained with Accuri cytometer (BD Accuri Cytometers Inc.) were employed to compare the total numbers and the viability of cells before and after activation with thapsigargin.

2.10. Data analysis

Calibration curves were constructed after plotting the absorbance or C_q values against tubulin concentrations and using a four-parameter logistic regression model function (variable slope) within GrafPad Prism 5 (GraphPad Software). The limit of detection (LOD) was calculated as the mean of the sample diluent plus 3 standard deviations of the sample diluent. Statistical analysis made use of the Student's two-tailed unpaired *t*-test.

3. Results

3.1. Epitope mapping

Sandwich ELISA requires a matched pair of antibodies recognizing non-overlapping native epitopes on the same target. Previously we have shown that some monoclonal antibodies to C-terminal domain of α-tubulin, including the TU-07 antibody, recognize epitopes exposed on the surface of tubulin molecule (Dráber et al., 1989). Peptide scan of immobilized overlapping peptides covering porcine α-tubulin (a.a. 1–451; 45 linear 15-meric peptides with 5 amino acid overlaps) was used for a more accurate epitope location of TU-07. Results of immunostaining with antibody TU-07 and with another anti-α-tubulin antibody, DM1A, are shown in Fig. 1. Epitope mapping revealed the localization of TU-07 epitope to the a.a. region 406–410 (sequence HWYVG). The epitope recognized by DM1A antibody was located to the a.a. region 426–430 (sequence AALEK); this is in accordance with previous data inferred from reactivity of the antibody with tryptic and cyanogen bromide peptides of pig brain α-tubulin (Breitling and Little, 1986). Antibodies TU-07 and DM1A thus recognize non-overlapping epitopes on α-tubulin molecule. Immunoblotting analysis revealed that the two antibodies are capable of reacting with full length tubulin isolated from porcine brain as well as with full length tubulins in cells as demonstrated on 1% NP-40 lysates from mouse BMMCs (Fig. 2). Moreover, the antibodies react with α-tubulins of various species (human, rat, chicken, plant *Nicotiana tabacum*) and do not bind to β- or γ-tubulins (not shown).

3.2. ELISA with biotinyl-tyramide signal amplification

To set up sandwich ELISA for quantification of α-tubulin, we used 96-well half-area plates (Corning) or TopYield Strips (Nunc). Antibodies, tested samples and reagents amounted to a volume of 30 μl/well. DM1A antibody was used as the capture antibody and biotinylated TU-07 antibody was applied for detection of bound tubulin. Immobilized biotinylated antibody was detected by extravidin-horseradish peroxidase and the enzyme signal was augmented by biotinyl-tyramide amplification. TMB was used as chromogen. Reaction was stopped, and absorption determined at 450 nm. Highly purified polymerization-competent porcine brain tubulin stored either in liquid nitrogen or at room temperature after freeze-drying in the presence of trehalose (Dráberová et al., 2010) was used to generate calibration curves. Concentrated tubulin samples were prediluted to ~50 μM, and any aggregates originating from the thawing and/or rehydrating process were removed by centrifugation. Actual concentration of tubulin in supernatant was checked spectrophotometrically and tubulin was then diluted to the required concentration. A typical calibration curve obtained by sandwich ELISA with biotinyl-tyramide amplification is shown in Fig. 3. Absorbance at 450 nm was measured at different tubulin concentrations ranging from 0.5 to 250 ng/ml (Fig. 3A), the curve was linear in the range of 5 to 100 ng/ml (Fig. 3B). The LOD was found to be 2.5 ng/ml. No difference was

Fig. 1. Epitope mapping. Immunostaining of peptide scans covering porcine α-tubulin 1A sequence with monoclonal antibodies TU-07 and DM1A. Peptide scans were prepared by immobilization of 45 linear 15-meric peptides with 5 amino acid overlaps. Numbers at the left and right denote positions of peptide spots in the upper, middle and lower rows of the scan; 1, a.a. 1–15 from the N-terminal end.

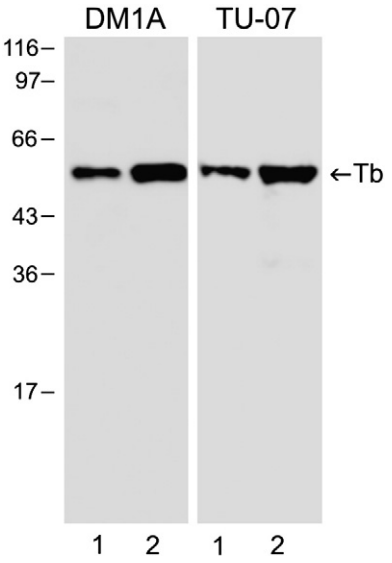

Fig. 2. Immunoblot analysis of BMMC cell extracts with monoclonal antibodies DM1A and TU-07. Porcine brain tubulin (lane 1) or 1% NP40 cell lysate from BMMCs (lane 2) was separated on 12% SDS-PAGE. Aliquots of tubulin (20 ng) were loaded in lane 1 and 4 μg of protein in lane 2. Bars on the left margin denote position of molecular weight markers in kilodaltons. Tb denotes position of tubulin.

observed when tubulin was stored in liquid nitrogen or in freeze-dried form. Very similar results were obtained when rehydrated strips, precoated with capture antibody and blocking BSA, were used after 6 months of storage at 4 °C. Usage of precoated strips can significantly save time of the assay.

3.3. Quantification of tubulin by immuno-PCR

The assay was carried out on polycarbonate TopYield strips fitting into the wells of the 96-well real-time PCR cyclers. Biotinylated TU-07 antibody was detected after incubation with extravidin followed by incubation with biotinylated DNA template. Template DNA immobilized on tubulin was quantified by real-time PCR. Compared to the widely used polypropylene PCR wells, wells of TopYield strips have a large diameter and possess a higher protein binding capacity. To prevent evaporation of PCR mixes from the wells during PCR cycling, it is essential to cover the surface of each well with light mineral oil before they are sealed (Potůčková et al., 2011). Detection of tubulin by sandwich ELISA with PCR amplification is shown in Fig. 4. Standard curves were produced with different concentrations of tubulin in the range of 0.01 to 1000 ng/ml (Fig. 4A), and the curve was linear from 0.1 to 1000 ng/ml of isolated tubulin (Fig. 4B). The LOD was found to be 0.086 ng/ml. Compared to biotinyl-tyramide signal amplification assay, the immuno-PCR amplification is characterized by broader range of detectable tubulin concentrations and higher sensitivity.

3.4. Tubulin detection in cell lysates and culture media

To prove the capability of the sandwich ELISA for monitoring the amount of tubulin, its concentrations were determined in BMMC extracts prepared from untreated and taxol-treated cells. Taxol treatment makes more tubulin in cell to polymerize

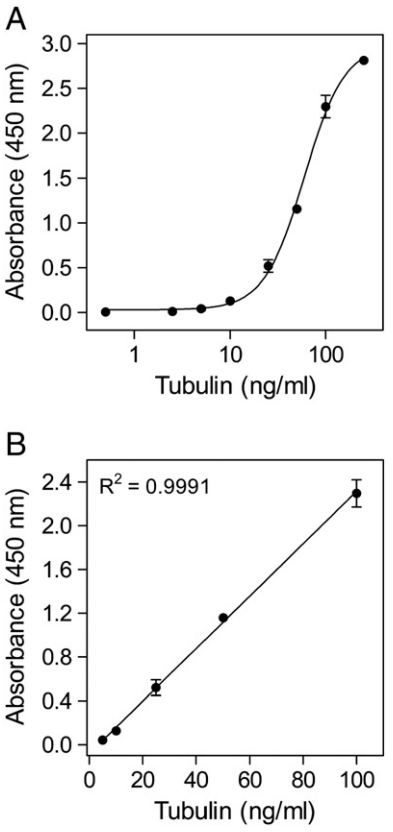

Fig. 3. Detection of tubulin at various concentrations by ELISA with biotinyl-tyramide amplification. (A) Tubulin concentration range from 0.5 to 250 ng/ml. (B) Tubulin concentration range from 5 to 100 ng/ml; R denotes correlation coefficient. Data represent mean ± SD (n = 2).

into microtubules that remain stable at 4 °C (Schiff and Horwitz, 1980). In taxol-treated BMMCs typical microtubule bundles are formed and can be detected by immunofluorescence microscopy (Fig. 5). BMMCs were solubilized in 1% NP-40 at 4 °C, and supernatants were analyzed after spinning-down the cell debris. Tubulin concentration in control cells, determined by sandwich ELISA with biotinyl-tyramide signal amplification, was 2331 ± 74.6 ng/ml (mean ± SEM, n = 3). However, preincubation of the cells for 2.5 h with 10 μM taxol reduced free tubulin concentrations to 478 ± 14.1 ng/ml (mean ± SEM, n = 3). These data document that exposure of cells to taxol leads to a substantial depletion of soluble tubulin (Fig. 6A).

Substantial changes in cell morphology and reorganization of microtubules occur during activation of BMMCs with thapsigargin (Hájková et al., 2011). Furthermore, the cells release granules containing various mediators (Dráberová et al., 2007). To find out whether thapsigargin-induced changes are accompanied by the release of tubulin into culture medium, tubulin concentrations were determined by immuno-PCR in media from resting and activated cells. While the tubulin concentration in resting cells medium was 5.3 ± 1.2 ng/ml (mean ± SEM, n = 3), it increased to 18.7 ± 5.5 ng/ml (mean ± SEM, n = 3) after thapsigargin-activation (Fig. 6B). To rule out that the increase is due to changes in cell viability, FACS measurements were performed in control and thapsigargin-activated BMMCs. The results revealed

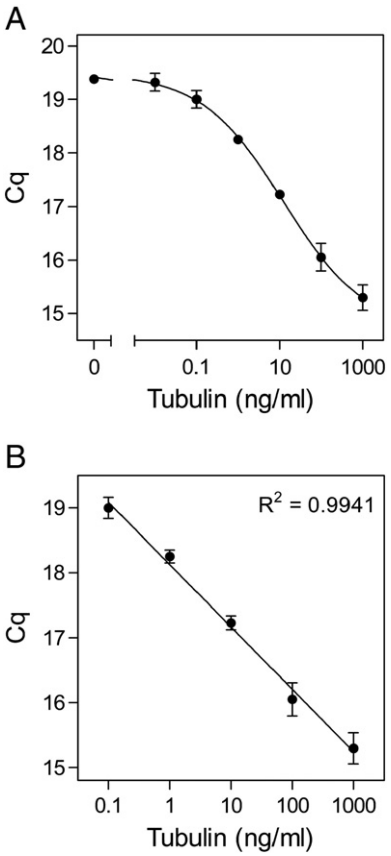

Fig. 4. Detection of various tubulin concentrations by immuno-PCR. (A) Tubulin concentration range from 0.01 to 1000 ng/ml. (B) Tubulin concentration range from 0.1 to 1000 ng/ml; R denotes correlation coefficient. Data represent mean ± SD (n = 2).

that the numbers of living cells were comparable in both samples (not shown). Activation of cells was confirmed by degranulation assay checking the level of β-glucuronidase. In control cells β-glucuronidase reached 1 ± 0.4% (mean ± SEM, n = 3) of total content of the enzyme, whereas in thapsigargin-activated cells it reached 58.4 ± 3.8% (mean ± SD, n = 3) of total enzyme content. The data thus confirm that activation of BMMCs is accompanied by release of cytosolic tubulin into medium.

4. Discussion

We have developed a new sensitive sandwich ELISA with biotinyl-tyramide or PCR signal amplification for quantification of α-tubulin isotypes in various cell types of different species. While biotinyl-tyramide amplification enhances the signal from an analyte-dependent reporter enzyme (horseradish peroxidase) (Bobrow et al., 1989), the PCR signal amplification uses analyte-dependent biotinylated DNA template for quantification by real-time PCR (Adler et al., 2003; Potůčková et al., 2011).

The components of critical importance in immunoassays are antibodies, since they can differ in their specificity, affinity to target antigen as well as non-specific binding to solid phase (Niemeyer et al., 2007). In search for biotinylated antibodies suitable for sandwich ELISA to quantify α-tubulin, we tested several commercially available conjugated antibodies as well as our own monoclonal antibodies of the TU-series (Dráber et al., 1989). Biotinylated mouse monoclonal antibody TU-07 showed the lowest nonspecific binding to "blocked" solid phase, and was therefore combined with mouse monoclonal antibody DM1A to form a matching antibody pair.

Compared to commercial PathScan Total α-Tubulin Sandwich ELISA kit (Cell Signaling), reported assays are more sensitive. Using the commercial kit, we were able to detect purified tubulin at the lowest concentration limit of 100 ng/ml (Dráberová, unpublished result), while the range of detectability was 5 to 100 ng/ml and 0.1 to 1000 ng/ml, respectively, for ELISA with biotinyl-tyramide signal amplification (Fig. 3B) and immuno-PCR (Fig. 4B). Immuno-PCR shows a >4 log dynamic range and femtomolar detection limit for tubulin dimer. The immuno-PCR thus enables to assess tubulin concentration in lysates prepared from cells, which are available only in limited amounts, e.g. cells in primary culture. Specifically in case of BMMCs, 200 cells are sufficient for determination of tubulin concentration (30 μl sample in triplicate). Performing the assays in half-area polystyrene plates or polycarbonate strips saves precious samples and reagents that are applied at volumes of only 25–30 μl. When precoated strips are used the whole assay can be performed during a single day.

Antibodies specific for α-tubulin, DM1A and TU-07, recognize amino acid sequences AALEK and HWYVG, respectively, that are evolutionarily highly conserved and are preserved from human to plants. The epitopes are located outside the C-terminal isotype-defining regions, beyond a.a. residue 430 (Khodiyar et al., 2007), and are identical in a great majority of

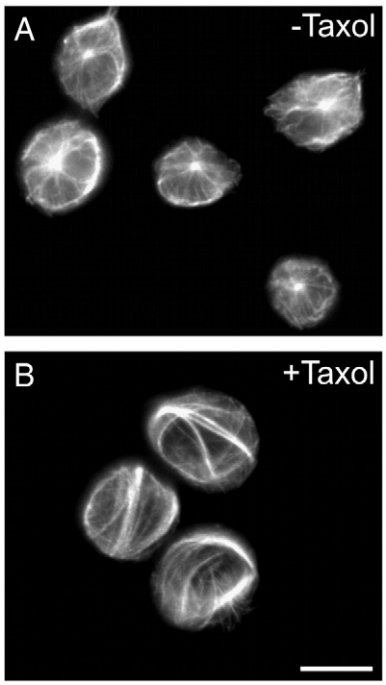

Fig. 5. Bundling of microtubules in BMMCs pretreated with anti-mitotic drug taxol. Immunofluorescence staining of control (A, −Taxol) and taxol-treated cells (B, +Taxol) with anti-tubulin antibody. Bar, 10 μm.

α-tubulin isotypes in human (*Homo sapiens* genes TUBA1A, TUBA1B, TUBA1C, TUBA3C, TUBA3D, TUBA3E, TUBA4A, TUBA8; nomenclature according to HGNC [HUGO Gene Nomenclature Committee]), mouse (*Mus musculus* genes Tuba1a, Tuba1b, Tuba1c, Tuba3a, Tuba3b, Tuba4a, Tuba8; nomenclature according to MGNC [Mouse Genomic Nomenclature Committee]) or mouse-ear cress (*Arabidopsis thaliana* genes TUA1, TUA2, TUA3, TUA4, TUA5, TUA6; nomenclature according to The Arabidopsis Information Resource [TAIR]). The matching antibody pair thus enables quantification of α-tubulin isotypes in phylogenetically distant species. Moreover, porcine brain tubulin, on which epitope mapping for antibodies DM1A and TU-07 was performed, can be utilized for the preparation of calibration curves, and controls using tubulins isolated from the same species are therefore unnecessary. Although the epitopes are located in the C-terminal region of tubulin molecule, that might potentially be cleaved off. Immunoblotting analysis revealed that antibodies recognize full-length tubulins and proteolytic fragments of tubulin were not generated during sample preparation (Fig. 2).

Epitopes recognized by DM1A and TU-07 antibodies are located outside the very C-terminal regions of α-tubulin molecules where multiple posttranslational modifications including polyglycylation and polyglutamylation were identified (Janke and Bulinski, 2011). Thus, binding of antibodies to target epitopes should not be affected by posttranslational modifications. On the other hand one cannot rule out that epitopes might in cells be masked by microtubule-associated proteins or by formation of tubulin oligomers (Mozziconacci et al., 2008). For these reasons, the assays described in this study are primarily intended for relative profiling of tubulin concentrations in lysates from different cell types and for monitoring tubulin changes after pretreatment of the cells with agents affecting equilibrium between polymeric and soluble tubulin pools. This is evident e.g. in the case of taxol that generates microtubule bundles (Fig. 5B) and depletes cytosolic tubulin from BMMCs (Fig. 6A). On the other hand, pretreatment of BMMCs with nocodazole at a concentration that depolymerizes microtubules (10 μM for 1 h) resulted in an increase of tubulin concentration in cytosolic pool (Dráberová, unpublished results).

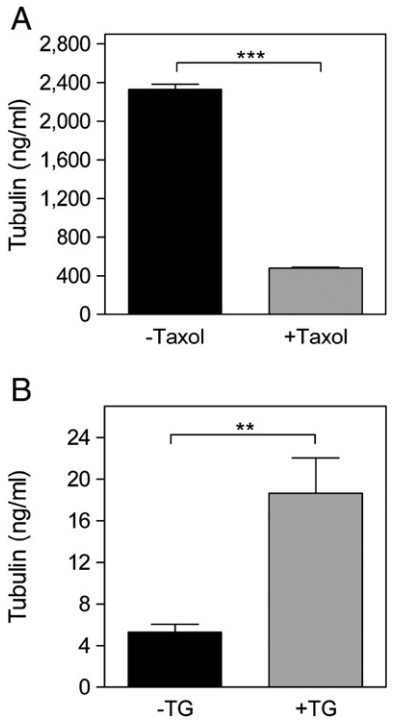

Fig. 6. Determination of tubulin concentration changes. (A) Concentration of cytosolic tubulin in untreated (−Taxol) or taxol-treated (+Taxol) BMMCs determined by ELISA with biotinyl-tyramide amplification. Bundling of microtubules by taxol leads to depletion of cytosolic tubulin. (B) Concentration of tubulin in BMMC culture media from untreated (−TG) or thapsigargin-treated (+TG) cells determined by immuno-PCR. Activation of BMMCs with thapsigargin leads to release of tubulin into media. Data are presented as the means ± SEM obtained from three independent experiments with duplicate samples. $^{**}p < 0.01$; $^{***}p < 0.001$.

Activation of mouse BMMCs, leading to the release of various mediators into extracellular space, is accompanied by dramatic changes in cell morphology and reorganization of microtubules (Dráber et al., 2012). Our data indicate, for the first time, that a small amount of tubulin during this process is also released into the culture medium (Fig. 6B). An association of tubulin with plasma membrane and detergent-resistant membranes was reported in various systems (Wolff, 2009; Macurek et al., 2008), and membrane-bound tubulin might be released into extracellular space during degranulation. Alternatively, tubulin could originate from damaged exosomes, secreted microvesicles, where tubulin subunits were also identified (Valadi et al., 2007).

It has been reported that patients with progressive multiple sclerosis, unlike healthy people, have increased tubulin concentration in cerebrospinal fluid (Semra et al., 2002; Madeddu et al., 2013). It has also been shown that evaluation of βIII-tubulin isotype levels in sera from patients with advanced gastric cancer, receiving paclitaxel treatment, is relevant prognostically for evaluation of clinical outcome (Yu et al., 2012). Due to high sensitivity of new sandwich ELISA-based assays we described here, changes in tubulin levels might be easier to detect in human body fluids.

In conclusion, sandwich ELISA assays for detection of α-tubulin isotypes make it possible to profile tubulin concentration in lysates of various cell types of different species, as well as monitor changes in tubulin concentration after treatment of cells with microtubule stabilizing or destabilizing agents. Immuno-PCR detection shows enhanced sensitivity and wider dynamic range than ELISA with biotinyl-tyramide detection. Detection of tubulin concentration at subnanogram levels might advance application of the new immunoassay for monitoring changes in tubulin concentration in body fluids during neurological or oncological diseases.

Acknowledgments

We thank T. Sulimenko for the help with epitope mapping and I. Mlchová for the excellent technical assistance. This work was supported in part by the Grant KAN200520701 from Academy of Sciences of the Czech Republic, Grants P302/12/1673, P302/11/P709, P302/10/1759, and 301/09/1826 from the Czech Science Foundation, Grants LD13015 and LD12073 from Ministry of Education, Youth and Sport of the Czech Republic to support COST Action BM1007 Mast Cells and Basophils — Targets for Innovative Therapies, and by the

Institutional Research Support (RVO 68378050). Z. Hájková and L. Stegurová were supported in part by the Faculty of Science, Charles University, Prague, Czech Republic.

References

Adler, M., Wacker, R., Niemeyer, C.M., 2003. A real-time immuno-PCR assay for routine ultrasensitive quantification of proteins. Biochem. Biophys. Res. Commun. 308, 240.

Blose, S.H., Meltzer, D.I., Feramisco, J.R., 1984. 10-nm filaments are induced to collapse in living cells microinjected with monoclonal and polyclonal antibodies against tubulin. J. Cell Biol. 98, 847.

Blume, Y., Yemets, A., Sheremet, Y., Nyporko, A., Sulimenko, V., Sulimenko, T., Dráber, P., 2010. Exposure of beta-tubulin regions defined by antibodies on an *Arabidopsis thaliana* microtubule protofilament model and in the cells. BMC Plant Biol. 10, 29.

Bobrow, M.N., Harris, T.D., Shaughnessy, K.J., Litt, G.J., 1989. Catalyzed reporter deposition, a novel method of signal amplification. Application to immunoassays. J. Immunol. Methods 125, 279.

Breitling, F., Little, M., 1986. Carboxyl-terminal regions on the surface of tubulin and microtubules. Epitope locations of YOL 1/34, DM1A and DM1B. J. Mol. Biol. 189, 367.

Bulinski, J.C., Morgan, J.L., Borisy, G.G., Spooner, B.S., 1980. Comparison of methods for tubulin quantitation in HeLa cell and brain tissue extracts. Anal. Biochem. 104, 432.

Das, S., Banerjee, S.K., Sil, M., Sarkar, P.K., 1989. An ELISA method for quantitation of tubulin using poly-1-lysine coated microtiter plates. Indian J. Exp. Biol. 27, 972.

Dozier, J.H., Hiser, L., Davis, J.A., Thomas, N.S., Tucci, M.A., Benghuzzi, H.A., Frankfurter, A., Correia, J.J., Lobert, S., 2003. β class II tubulin predominates in normal and tumor breast tissues. Breast Cancer Res. 5, R157.

Dráber, P., Dráberová, E., Zicconi, D., Sellito, C., Viklický, V., Cappuccinelli, P., 1986. Heterogeneity of microtubules recognized by monoclonal antibodies to alpha-tubulin. Eur. J. Cell Biol. 41, 82.

Dráber, P., Dráberová, E., Linhartová, I., Viklický, V., 1989. Differences in the exposure of C- and N-terminal tubulin domains in cytoplasmic microtubules detected with domain-specific monoclonal antibodies. J. Cell Sci. 92, 519.

Dráber, P., Vater, W., Böhm, K., Kuklová, E., Unger, E., 1990. Inhibition of microtubule assembly in vitro by anti-tubulin monoclonal antibodies. FEBS Lett. 262, 209.

Dráber, P., Sulimenko, V., Dráberová, E., 2012. Cytoskeleton in mast cell signaling. Front. Immunol. 3, 130.

Dráberová, E., Dráber, P., 1993. A microtubule-interacting protein involved in coalignment of vimentin intermediate filaments with microtubules. J. Cell Sci. 106, 1263.

Dráberová, L., Shaik, G.M., Volná, P., Heneberg, P., Tůmová, M., Lebduška, P., Korb, J., Dráber, P., 2007. Regulation of Ca^{2+} signaling in mast cells by tyrosine-phosphorylated and unphosphorylated non-T cell activation linker. J. Immunol. 179, 5169.

Dráberová, E., Sulimenko, V., Sulimenko, T., Böhm, K.J., Dráber, P., 2010. Recovery of tubulin functions after freeze-drying in the presence of trehalose. Anal. Biochem. 397, 67.

Hájková, Z., Bugajev, V., Dráberová, E., Vinopal, S., Dráberová, L., Janáček, J., Dráber, Pe, Dráber, P., 2011. STIM1-directed reorganization of microtubules in activated cells. J. Immunol. 186, 913.

Hibbs, M.L., Tarlinton, D.M., Armes, J., Grail, D., Hodgson, G., Maglitto, R., Stacker, S.A., Dunn, A.R.R., 1995. Multiple defects in the immune-system of Lyn-deficient mice, culminating in autoimmune-disease. Cell 83, 301.

Janke, C., Bulinski, J.C., 2011. Post-translational regulation of the microtubule cytoskeleton: mechanisms and functions. Nat. Rev. Mol. Cell Biol. 12, 773.

Katsetos, C.D., Dráber, P., 2012. Tubulins as therapeutic targets in cancer: from bench to bedside. Curr. Pharm. Des. 18, 2778.

Khodiyar, V.K., Maltais, L.J., Ruef, B.J., Sneddon, K.M., Smith, J.R., Shimoyama, M., Cabral, F., Dumontet, C., Dutcher, S.K., Harvey, R.J., Lafanechere, L., Murray, J.M., Nogales, E., Piquemal, D., Stanchi, F., Povey, S., Lovering, R.C., 2007. A revised nomenclature for the human and rodent α-tubulin gene family. Genomics 90, 285.

Linhartová, I., Dráber, P., Dráberová, E., Viklický, V., 1992. Immunological discrimination of β-tubulin isoforms in developing mouse brain. Posttranslational modification of non-class III β-tubulins. Biochem. J. 288, 919.

Ludueña, R.F., Banerjee, A., 2008. The isotypes of tubulin: distribution and functional significance. In: Fojo, T. (Ed.), The Role of Microtubules in Cell Biology, Neurobiology and Oncology. Humana Press, Totowa, NJ, p. 123.

Macurek, L., Dráberová, E., Richterová, V., Sulimenko, V., Sulimenko, T., Dráberová, L., Marková, V., Dráber, P., 2008. Regulation of microtubule nucleation in differentiating embryonal carcinoma cells by complexes of membrane-bound γ-tubulin with Fyn kinase and phosphoinositide 3-kinase. Biochem. J. 416, 421.

Madeddu, R., Farace, C., Tolu, P., Solinas, G., Asara, Y., Sotgiu, M.A., Delogu, L.G., Prados, J.C., Sotgiu, S., Montella, A., 2013. Cytoskeletal proteins in the cerebrospinal fluid as biomarker of multiple sclerosis. Neurol. Sci. 34, 181.

Mozziconacci, J., Sandblad, L., Wachsmuth, M., Brunner, D., Karsenti, E., 2008. Tubulin dimers oligomerize before their incorporation into microtubules. PLoS One 3, e3821.

Niemeyer, C.M., Adler, M., Wacker, R., 2005. Immuno-PCR: high sensitivity detection of proteins by nucleic acid amplification. Trends Biotechnol. 23, 208.

Niemeyer, C.M., Adler, M., Wacker, R., 2007. Detecting antigens by quantitative immuno-PCR. Nat. Protoc. 2, 1918.

Pipeleers, D.G., Pipeleers-Marichal, M.A., Sherline, P., Kipnis, D.M., 1977. A sensitive method for measuring polymerized and depolymerized forms of tubulin in tissues. J. Cell Biol. 74, 341.

Potůčková, L., Franko, F., Bambousková, M., Dráber, P., 2011. Rapid and sensitive detection of cytokines using functionalized gold nanoparticle-based immuno-PCR, comparison with immuno-PCR and ELISA. J. Immunol. Methods 371, 38.

Rivera, J., Fierro, N.A., Olivera, A., Suzuki, R., 2008. New insights on mast cell activation via the high affinity receptor for IgE. Adv. Immunol. 98, 85.

Schiff, P.B., Horwitz, S.B., 1980. Taxol stabilizes microtubules in mouse fibroblast cells. Proc. Natl. Acad. Sci. U. S. A. 77, 1561.

Semra, Y.K., Seidi, O.A., Sharief, M.K., 2002. Heightened intrathecal release of axonal cytoskeletal proteins in multiple sclerosis is associated with progressive disease and clinical disability. J. Neuroimmunol. 122, 132.

Shelanski, M.L., Gaskin, F., Cantor, C.R., 1973. Microtubule assembly in the absence of added nucleotides. Proc. Natl. Acad. Sci. U. S. A. 70, 765.

Smertenko, A., Blume, Y., Viklický, V., Dráber, P., 1997. Exposure of tubulin structural domains in *Nicotiana tabacum* microtubules probed by monoclonal antibodies. Eur. J. Cell Biol. 72, 104.

Sulimenko, V., Sulimenko, T., Poznanovic, S., Nechiporuk-Zloy, V., Böhm, J.K., Macůrek, L., Unger, E., Dráber, P., 2002. Association of brain γ-tubulins with αβ-tubulin dimers. Biochem. J. 365, 889.

Surviladze, Z., Dráberová, L., Kovářová, M., Boubelík, M., Dráber, P., 2001. Differential sensitivity to acute cholesterol lowering of activation mediated via the high-affinity IgE receptor and Thy-1 glycoprotein. Eur. J. Immunol. 31, 1.

Thrower, D., Jordan, M.A., Wilson, L., 1991. Quantitation of cellular tubulin in microtubules and tubulin pools by a competitive ELISA. J. Immunol. Methods 136, 45.

Valadi, H., Ekström, K., Bossios, A., Sjöstrand, M., Lee, J.J., Lötvall, J.O., 2007. Exosome-mediated transfer of mRNAs and microRNAs is a novel mechanism of genetic exchange between cells. Nat. Cell Biol. 9, 654.

Weingarten, M.D., Lockwood, A.H., Hwo, S.Y., Kirschner, M.W., 1975. A protein factor essential for microtubule assembly. Proc. Natl. Acad. Sci. U. S. A. 72, 1858.

Wilson, L., 1970. Properties of colchicine binding protein from chick embryo brain. Interactions with vinca alkaloids and podophyllotoxin. Biochemistry 9, 4999.

Wolff, J., 2009. Plasma membrane tubulin. Biochim. Biophys. Acta 1788, 1415.

Yu, J., Gao, J., Lu, Z., Li, Y., Shen, L., 2012. Serum levels of TUBB3 correlate with clinical outcome in Chinese patients with advanced gastric cancer receiving first-line paclitaxel plus capecitabine. Med. Oncol. 29, 3029.

VI.2

Bambousková M.*, **Hájková Z.***, Dráber Pa., Dráber Pe. (2014). Microscopy assays for evaluation of mast cell migration and chemotaxis. Methods in Molecular Biology *1192*, 161-176.

Chapter 12

Microscopy Assays for Evaluation of Mast Cell Migration and Chemotaxis

Monika Bambousková, Zuzana Hájková, Pavel Dráber, and Petr Dráber

Abstract

A better understanding of the molecular mechanisms leading to mast cell migration and chemotaxis is the long-term goal in mast cell research and is essential for comprehension of mast cell function in health and disease. Various techniques have been developed in recent decades for in vitro and in vivo assessment of mast cell motility and chemotaxis. In this chapter three microscopy assays facilitating real-time quantification of mast cell chemotaxis and migration are described, focusing on individual cell tracking and data analysis.

Key words Mast cells, Cell migration, Chemotaxis, Chemokine, Chemoattractant

1 Introduction

Mast cells are best known for their role in mediating allergic diseases [1]. Recent studies have highlighted their important functions in the innate immunity contributing to protection against bacterial infection, angiogenesis, and autoimmunity [2, 3]. Under pathological conditions, mast cells are involved in immediate hypersensitivity, chronic allergic reactions, asthma, and other inflammatory diseases [4]. As highly effective sentinel cells they are localized close to blood vessels in common sites of potential infection, such as skin, airways, and the gastrointestinal tract. Chemoattractant-directed migration of mature mast cells or their progenitors might be one of the key mechanisms responsible for local accumulation of these cells under physiological or pathological conditions [5]. Chemotactic mechanisms can be therefore potentially targeted by therapeutic interventions.

$CD13^+/CD34^+/CD117$ $(c\text{-}Kit)^+$ mast cell progenitors arise in bone marrow where they start their differentiation under the influence of chemokines and growth factors [6]. During this process they leave bone marrow and migrate into bloodstream to reach

Bernhard F. Gibbs and Franco H. Falcone (eds.), *Basophils and Mast Cells: Methods and Protocols*, Methods in Molecular Biology, vol. 1192, DOI 10.1007/978-1-4939-1173-8_12, © Springer Science+Business Media New York 2014

various body sites. The key signal for mast cell homing and recruitment into peripheral tissues is provided by interaction of the stem cell factor (SCF) with its receptor, the c-Kit [7]. In rodents another critical factor, interleukin-3 (IL-3), which binds to its surface receptor is involved [8]. In peripheral tissues mast cell progenitors mature and terminally differentiate under the influence of the local environment. Two predominant phenotypes of mature mast cells, the connective tissue and the mucosal mast cells, differ by the expression of various secretory granule proteins [9] (*see* Chapter 9). Migration of mast cell progenitors to the site of their residency is directed by various chemokines which bind to chemokine receptors [10]. The expression pattern of these molecules is different in progenitors and mature mast cells and differences are also observed between particular mast cell subtypes [11]. Several other chemotactic ligands affecting mast cell migration have been identified; these include sphingosine-1-phosphate [12], arachidonic acid metabolites as leukotriene B4 [13], and prostaglandin E_2 (PGE_2) [14, 15], as well as antigen, recognized by IgE anchored to the high-affinity IgE receptor (FcεRI) [16, 17]. In target tissues mast cells participate actively in immune responses against various pathogens by releasing a broad spectrum of mediators, either stored in secretory granules or rapidly synthesized after cell triggering. Mediators produced by mast cells include leukotrienes, prostaglandins, cytokines, and chemokines (*see* Chapter 10), which in turn can recruit other immune cells to sites of inflammation [18, 19]. Importantly, mature mast cells in sensitized individuals exposed to allergens produce mediators that attract mast cell-committed progenitors to the place of pathogen entry [13]. In healthy tissues the number of mast cells is stable and can be regulated by proliferation, migration, and mast cell survival. On the other hand, inflamed tissues show an increased number of mast cells, and their enhanced accumulation is characteristic for a number of pathological states [20, 21].

Numerous methods have been developed for studies on mast cell migration and chemotaxis towards various chemoattractants. Most of the in vitro studies utilized various modifications of Boyden's chamber system where cells migrate through pores (usually 5 or 8 μm) of polycarbonate membrane towards increasing concentrations of chemoattractants [22]. These techniques are well established for quantification of chemotactic responses [13, 15, 23]. However, they do not allow recording the movement of individual cells at selected time intervals and analyzing cell trajectories. Therefore, new methods have been developed for analysis of chemotaxis using real-time imaging. The gradient of chemoattractant is usually created by arranging special chambers in various settings [24]. Alternatively, a gradient is produced by embedding chemoattractants in porous materials such as agarose [25–27]. Using a microscope equipped with a camera and proper software,

the images are processed with image analysis software capable of obtaining coordinates of individual trajectories. They are then used for calculation of cell movement parameters (e.g., directionality, achieved distance, velocity) [24, 28, 29]. Since primary mast cells are non-adherent, the 2D or the 3D tracking of their movement encounters some difficulties. To overcome these problems, mast cells are attached to the surface with some natural adhesive compounds, such as fibronectin. Furthermore, cell attachment has to be preserved during the whole experiment to prevent any artificial movement of cells during analysis. These techniques resulted in the development of new methods for analysis of migration and chemotaxis of non-adherent mast cells. In this chapter we describe several experimental settings for real-time analysis of cell motility or directed chemotaxis optimized for non-adherent mast cells. The techniques utilize commercially available migration chambers or simple homemade devices.

2 Materials

2.1 Chemicals

1. Fibronectin from bovine plasma for cell cultures.
2. Recombinant murine IL-3.
3. Recombinant murine SCF: Stock solution containing 1 mg/mL of SCF in H_2O is aliquoted to avoid repeated freeze-thaw cycles.
4. Agarose.
5. Collagen I (3.1 mg/mL).
6. PGE_2 (1 mM stock solution is prepared in DMSO).

2.2 Buffers and Media

1. HEPES solution (1 M).
2. RPMI-1640.
3. Minimum essential medium (MEM) nonessential amino acids.
4. 10× concentrated MEM Eagle with Hanks' salts (H-MEM).
5. Migration medium (MM): RPMI-1640, 0.1 % BSA (w/v), 20 mM HEPES, pH 7.4.
6. StemPro-34® serum-free medium.

2.3 Mast Cells

1. Bone marrow from femurs and tibias of 6–10-week-old mice is used as a source of mast cell precursors. The cells are cultured in RPMI-1640 supplemented with 20 mM HEPES, pH 7.5, 100 U/mL penicillin, 100 µg/mL streptomycin, 100 µM MEM nonessential amino acids, 1 mM sodium pyruvate, 41 µM 2-mercaptoethanol, 10 % (v/v) fetal calf serum, IL-3 (20 ng/mL), and SCF (15 ng/mL). After 5–7 weeks, most of the cultured cells (up to 95 %) express FcεRI and c-Kit, markers of mast cells. Such bone marrow-derived mast cells (BMMCs)

have been extensively used in studies on cell signaling since they closely resemble normal mast cells in respect to their requirement of IL-3 and SCF for optimal growth and their ability to respond to various physiological stimuli, and particularly because they can be isolated from mouse strains deficient in genes which are possibly involved in a variety of signaling pathways.

2. A particular cell line derived from mouse BMMCs (BMMCL) has been isolated by Hibbs [30]. These cells are cultured in complete RPMI-1640 supplemented as described above but without SCF and with recombinant IL-3 replaced by 10 % (v/v) WEHI-3 cell supernatant. These cells can be recovered after freezing in 10 % (v/v) DMSO and storage at −70 °C or liquid nitrogen. BMMCL can be used instead of BMMCs for their easier culturing and fast growth. Further, they react in almost the same way as BMMCs to a variety of treatments [31].
3. The human mast cell line (LUVA) was originally obtained by growing $CD34^+$-enriched mononuclear cells derived from the peripheral blood of a human donor [32] (*see* Subheading 2.3 in Chapter 8). LUVA cells are maintained in StemPro-34 serum-free medium in the absence of any exogenously added cytokines. Although they have the morphology of mast cells, after several passages in vitro they lose surface expression of FcεRI (our own unpublished data).

2.4 Other Materials

1. Test tubes and 1.5 mL Eppendorf tubes.
2. 96-Well black optical bottom plates, suitable for microscopy.
3. Bevelled pipette tips for filling ports on μ-Slide.
4. Slant tweezers for plug handling.
5. Cell culture dishes 40 × 11 mm.
6. Glass beads (2 mm diameter).
7. μ-Slide Chemotaxis^{3D} chambers containing μ-Slide^{3D} for evaluation of cell chemotaxis in three samples, a cultivation lid, and 18 plugs (Ibidi).

2.5 Equipment

1. Laminar flow box.
2. CO_2 incubator.
3. Inverted microscope equipped with 10× bright-field objective, camera for time-lapse video recording, motorized stage, and CO_2- and temperature-regulated chamber.
4. Automated microscopy system equipped with 10× and 20× bright-field objectives, camera for recording time-lapse video, motorized stage, CO_2- and temperature-regulated chamber, and platform for 96-well plates.
5. Milli-Q water purification system or equivalent.

2.6 Software

1. MetaMorph Offline (Version 7.7.9.0; Molecular Devices).
2. ImageJ (Version 1.46; National Institutes of Health) with Chemotaxis and Migration Tool plug-in (Version 1.01; Ibidi).

3 Methods

For quantitative studies of mast cell migration and chemotaxis by microscopy, three assays are presented: simple motility assay, chemotaxis measured in μ-Slide chemotaxis chamber, and chemotaxis analyzed in homemade chamber with chemoattractants embedded in agarose cone.

3.1 Motility Assay

This technique is used to determine the general ability of mast cells to move. It is useful when cells of different properties are investigated or if activity of selected drugs on cell movement is tested. The method allows measurement in 96-well plate format. Mast cells are allowed to attach to fibronectin-coated surfaces and are treated with an activator such as PGE_2. The velocities of cell movement and/or the distances reached from the start point are automatically determined (*see* Fig. 1). However, no information on directionality of migration is provided.

All solutions intended for handling live cells and the microscope heating chamber should be pre-warmed to 37 °C.

1. Prepare fibronectin-coated 96-well optical bottom plate by adding 50 μL of fibronectin (50 μg/mL) in PBS into each well of the plate and incubate for 14–16 h at 4 °C (*see* **Note 1**).
2. Grow BMMCs at concentration 2×10^6/mL without SCF and IL-3 for 12–16 h before experiment (*see* **Note 2**).
3. Wash the cells twice with MM, resuspend in MM, and adjust the concentration to 5×10^5/mL.
4. Wash the fibronectin-coated surfaces briefly with PBS and pipet 100 μL of cell suspension into each well.
5. Allow the cells to attach for 30 min at 37 °C and then gently wash the wells once with warm MM (*see* **Note 3**).
6. Add carefully 100 μL of MM or activator (e.g., PGE_2) diluted in MM into each well (*see* **Note 4**).
7. Monitor the cell motility on automated microscopy system with 10× or 20× objective and define the number of examined sites per well and their XYZ positions. Take time-lapse images for 1–2 h at 1-min intervals (*see* **Note 5**).
8. Analyze the data using the procedure described in Subheading 3.4.

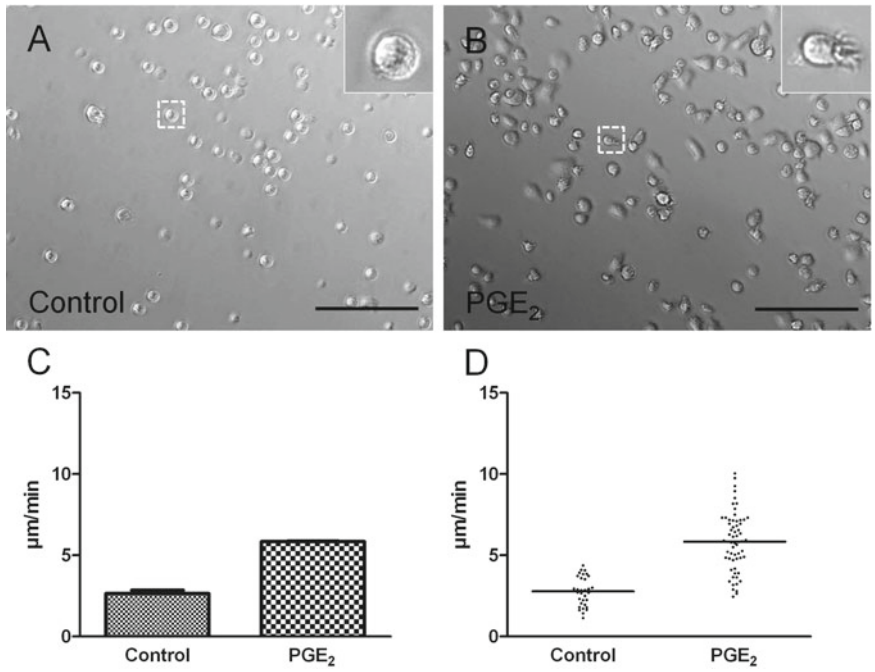

Fig. 1 Increased motility of BMMCs after PGE_2 activation. (**a**) Non-activated (control) or (**b**) activated (PGE_2) BMMCs, attached to fibronectin-coated surface, were monitored with automated microscopy system with 20× objective. Time-lapse images were taken for 60 min at a frequency of 1.27 min/frame. Representative cells are magnified and shown in *inserts* (**a**, **b**; *right upper corners*). (**c**) Individual trajectories of 30–50 cells were processed and the average velocity ± SD was calculated from duplicates in one representative experiment. (**d**) Distribution of velocities of individual cells is presented with vertical scatterplot; average values of all analyzed cells are also shown. Bars in (**a**) and (**b**) = 100 µm

3.2 Mast Cell Chemotaxis in µ-Slide Chemotaxis^{3D} Chambers

The µ-Slide Chemotaxis^{3D} chambers make it possible to study directed migration of non-adherent cells towards the chemoattractant. Each µ-Slide^{3D} contains three identical chambers for parallel monitoring of samples. Cells are kept in a chamber using 3D collagen I gel. The unique working arrangement of µ-Slide^{3D} enables to create the required chemoattractant gradient. Mast cell movement is monitored by time-lapse microscopy followed by data analysis (*see* Subheadings 3.4 and 3.5).

All procedures with µ-Slide Chemotaxis^{3D} chambers are performed in a laminar flow box to maintain sterility.

1. One day before the experiment, place the culture medium for BMMCs, BMMCL, or LUVA cells, sterile H_2O for tissue culture, and the µ-Slide^{3D} (*see* Fig. 2a) into incubator for gas equilibration. Aqueous solutions should be transferred into semi-closed test tubes, while the µ-Slide^{3D} should stay packaged to maintain sterility (*see* **Note 6**).
2. Prepare a mast cell suspension at a concentration of 9×10^6 cells/mL in proper equilibrated culture medium (*see* **Note 7**).

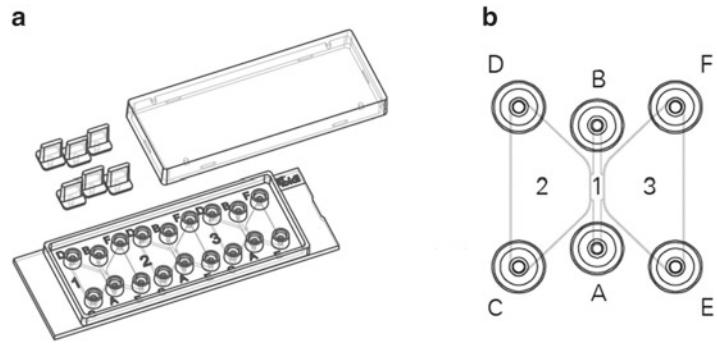

Fig. 2 Components of μ-Slide Chemotaxis^{3D} and configuration of a chamber for evaluation of cell motility in one tested sample. (**a**) μ-Slide Chemotaxis^{3D} contains a slide with chambers for simultaneous evaluation of three samples (areas *1–3*), six plugs, and a lid. (**b**) Chamber configuration. *1*, channel (observation area); *2*, left reservoir; *3*, right reservoir; *A–F*, filling ports

3. Mix 6 μL of 10× H-MEM, 21.9 μL of sterile H_2O for tissue culture, 2.1 μL of 7.5 % (w/v) $NaHCO_3$, and 15 μL of proper culture medium in a sterile Eppendorf tube (premix; total volume 45 μL). Pipet 30 μL of collagen I into a second Eppendorf tube (*see* **Note 8**).
4. Using tweezers close the filling ports C, D, E, and F (*see* Fig. 2b) with the plugs in the μ-Slide^{3D}. Prepare a humid chamber by placing moistened tissue into a sterile 10 cm Petri dish.
5. Pipet 45 μL of the premix into Eppendorf tube containing 30 μL of collagen I and immediately add 15 μL of cell suspension. Mix well, but carefully with a 100 μL pipette (*see* **Note 9**).
6. Apply 6 μL of the mixture to the top of filling port A (use bevelled pipette tip). Immediately after loading aspirate the air from the opposite port B to fill the channel (*see* #1 in Fig. 2b) homogenously with the mixture (*see* **Note 10**). Repeat this step in all three chambers.
7. Remove all plugs from the slide and close filling ports A and B with plugs (filling ports A and B will stay closed till the end of the experiment). Insert the slide into the humid chamber and put into CO_2 incubator for 30–40 min (*see* **Note 11**).
8. Meanwhile dilute chemoattractant (SCF or PGE_2) stocks 1:5,000 in proper culture medium to obtain 200 ng/mL SCF or 0.2 μM PGE_2, respectively. Prepare 40 μL of the chemoattractants for one chamber (*see* **Note 12**).
9. After collagen polymerization, fill the reservoirs (*see* #2 and #3 in Fig. 2b). First, close reservoir #2 with plugs (close filling ports C and D) and directly pipet 65 μL of chemoattractant-free medium through one of the two opened filling ports (E or F). Then remove plugs from filling ports C and D and

close filling ports E and F. Fill reservoir #2 with 65 μL of chemoattractant-free medium. Repeat this step twice to fill reservoirs in all three chambers.

10. To create the chemoattractant gradient, apply 15 μL of 2× concentrated chemoattractant (e.g., SCF or PGE_2) to the top of the filling port C and immediately aspirate 15 μL of the medium from the filling port D. This time press the pipette tip directly inside the port. Repeating this step again leads to filling of 30 μL of 2× concentrated chemoattractant into the reservoir. Close all filling ports. An equilibrium gradient of chemoattractant is created during 1–2 h (*see* **Note 13**).
11. Monitor cell chemotaxis with an inverted microscope immediately after chemoattractants are added. Define XYZ positions of channels (observation areas) of all three chambers. Take time-lapse images for 7–10 h at 2-min intervals with the intensity of 71 and exposure time 6 ms. Autofocus can be used during the time-lapse (*see* **Note 14**).
12. Analyze the data using the procedure described in Subheading 3.4.

Further information about this method is available online (*see* **Note 15**).

3.3 Chemotaxis in Homemade Chambers

This method allows characterizing directional movement of cells towards chemoattractant embedded in an agarose cone. After attachment of cells to a fibronectin-coated surface, chemoattractant embedded in an agarose cone is added. Movement of cells starts after an initial 15-min period of sensing the chemoattractant. As a relatively simple and cheap alternative to commercial systems this method can be used for observation of cell behavior and changes in morphology during chemotaxis.

1. Prepare a fibronectin-coated culture dish by adding 1 mL of fibronectin (50 μg/mL) in PBS and incubate it for 12–16 h at 4 °C (*see* **Note 1**).
2. Grow BMMCs at concentration 2×10^6/mL without SCF and IL-3 for 12–16 h (*see* **Note 2**).
3. For preparation of the agarose cone with embedded chemoattractant dissolve 1 % (w/v) agarose in PBS by short heating at 80 °C followed by slow chilling to approximately 40 °C. Keep the agarose solution at the same temperature and dilute PGE_2 in agarose solution to final 1 μM concentration. Dispense 15 μL aliquots of this solution to the bottom of 1.5 mL Eppendorf tubes (tubes should be pre-warmed to 40 °C). Immediately insert a glass bead into the agarose solution at the bottom of each tube (*see* Fig. 3a). The glass bead acts as a weight and will help stabilize the cone at the same position in culture dish during the test. Prepare control cones without chemoattractant in the same way. Let the agarose solidify in

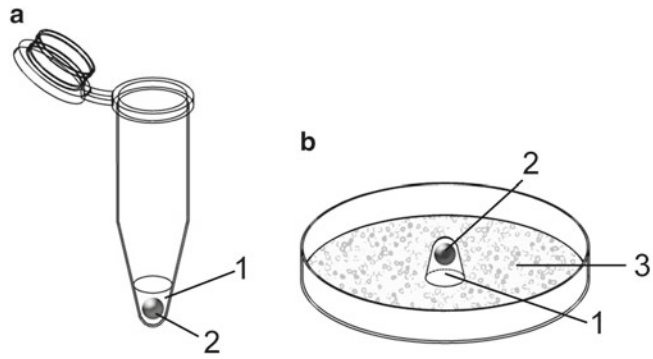

Fig. 3 Agarose cone with embedded chemoattractant. (**a**) Agarose cone with embedded chemoattractant and glass bead in Eppendorf tube; (**b**) position of agarose cone in a culture dish with cells and medium; *1*. Chemoattractant in 1 % agarose; *2*. glass bead; *3*. cell layer

the tubes at 4 °C for at least 15 min and keep it so until use (*see* **Note 16**).

4. Wash the cells with MM and adjust their concentration to 5×10^5/mL.
5. Wash the fibronectin-coated dish with 1 mL of PBS before attaching the cells.
6. Dispense 2 mL aliquots of cell suspension (1×10^6 cells) into each dish and incubate undisturbed for 30 min at 37 °C.
7. Gently wash the dish with 1 mL of MM and add 5 mL of new MM.
8. Fix the dish in a proper position in microscope. Carefully remove the agarose cone containing the glass bead from the Eppendorf tube using tweezers and place it slowly in the middle of the dish with the flat bottom facing down the cell layer (*see* Fig. 3b). Cover the dish with a lid.
9. Find the edge of the agarose cone in the field of view of the inverted microscope with a 10× objective (*see* Fig. 4a) and monitor the cells in time-lapse images for 2–3 h at 1-min intervals (*see* Fig. 4b).
10. Analyze the data as described in Subheading 3.4 (*see* Fig. 4c and d). Start the analysis at frame 60 and end with frames 120–180 (*see* **Note 17**).

3.4 Tracking Cells

Automatic tracking using a MetaMorph program with optimized parameters for mast cells is described in the following section. However, there are also other options to track cells in bright-field time-lapse movies (*see* **Note 18**).

[*Italic font style is used for buttons, option buttons, and headlines. Underlined text refers to dialog boxes.*]

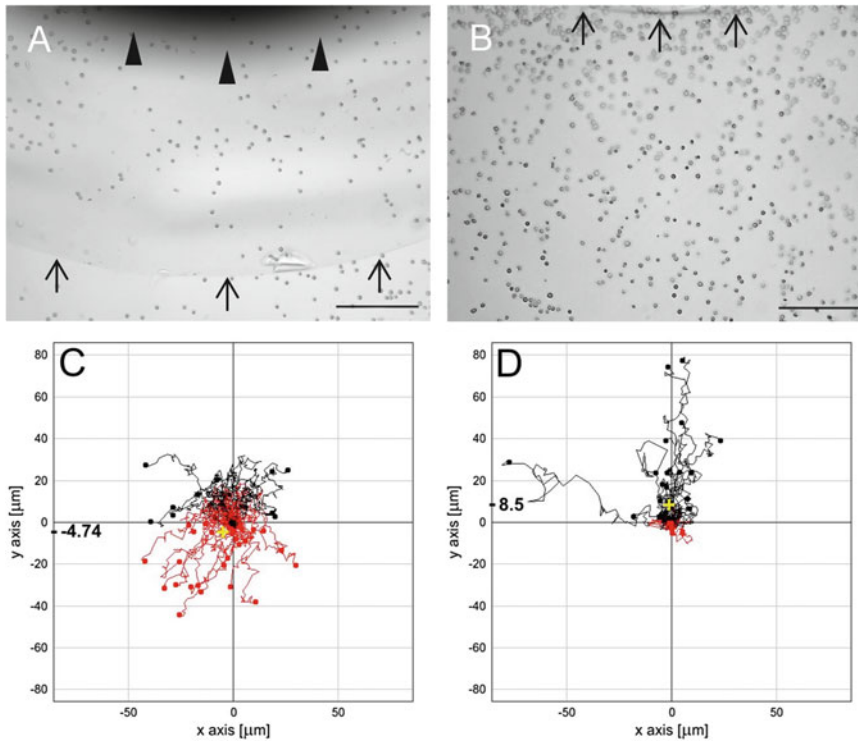

Fig. 4 Mast cell chemotaxis towards PGE_2 embedded in an agarose cone. (**a**) The edge of agarose cone is marked by *arrows* and the glass bead by *triangles*. (**b**) BMMCs were attached to fibronectin-coated surface, and the agarose cone with embedded PGE_2 was inserted into the dish containing the cells. The cone edge is indicated by *arrows*. The image was captured 15 min after insertion of the cone (when the first changes in cell morphology were observed in the vicinity of agarose cone). Images were taken with an inverted microscope equipped with a 10× objective. (**c**, **d**) Representative images from a single experiment showing migration trajectory graphs expressing directionality of BMMC movement. Chemotaxis towards PGE_2 is reflected by a shift of a center of cell mass in *x*-axis (*crosses*). Bars = 250 μm

1. Open time-lapse sequence in the MetaMorph program. Choose *Threshold* → *Threshold Image*. Mark off *Inclusive* and use the slider to adjust the threshold so that only the cells of interest are marked (*see* Fig. 5a) (*see* **Note 19**).
2. Select *Apps* → *Track Objects* and set the following parameters in Track Objects dialog box:
   (a) In *Source for images* mark off *Stack*.
   (b) Using *Search Options* button open Search Options dialog box and in *Algorithm* set *Threshold Results*. Then choose what the program should do in *If object not found* (e.g., *Select position*). Also set *Delay* (e.g., 0 s/object) and *Object size match requirement* (*as* %) (e.g., 35).
   (c) Set other parameters in Track Objects Interval Options, Track Overlay Options, and Origin Options dialog boxes by

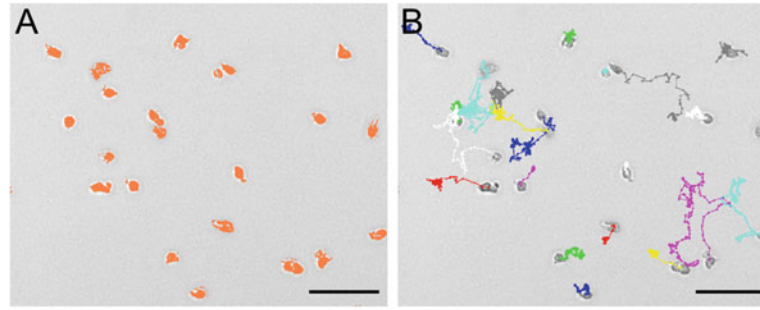

Fig. 5 Analysis of cell migration with MetaMorph. (**a**) Representative thresholded image of time-lapse sequence. (**b**) Trajectories of individual cells. Chemotaxis of BMMCs towards 100 μM PGE_2 loaded into the left reservoir of μ-Slide Chemotaxis^{3D} chamber. Images were taken with an inverted microscope with a 10× objective. Bars = 100 μm

choosing *Set Interval*, *Set Overlay*, and *Set Origin* buttons, respectively.

(d) Choose *Track* to select tracked cells.

3. Select Objects dialog box appears. To choose objects to be tracked hold down the [Ctrl] and click on each object using the left mouse button. Adjust the size of the search regions (*see* **Note 20**). Then choose *OK* and object tracking will proceed automatically.
4. It is recommended to follow tracking during whole analysis. In case MetaMorph tracks in a wrong way (e.g., skips to another cell) press [Esc] to stop tracking. The Tracking dialog box will open. If necessary press the *Step Back* to return the analysis to the last correctly tracked plane. Then do a correction by hand (move the search region to the correct position using left mouse button), and continue in the analysis by choosing *Update Position And Continue* in Tracking dialog box. In such cases it can be worth marking off *Continue one step and pause* in Tracking dialog box.
5. If MetaMorph loses an object during the tracking, it proceeds according to the previous selection in the *If object not found* options in Search Options dialog box. In case *Select position* is marked off, it is necessary to do the correction by hand as described in **step 4**.
6. After the tracking is finished, all trajectories of individually tracked cells are marked in the time-lapse movie (*see* Fig. 5b) and Track Objects dialog box appears again.

(a) Select *Open Log*, and define where the data should be saved and a blank Excel file opens. Thereafter choose *Log Data* to save all the data from tracking. Sometimes it is easier to track only several cells at one time and each time log newly tracked data to the same Excel document.

3.5 Presenting Chemotaxis Data

Chemotaxis is analyzed by means of Chemotaxis and Migration Tool. This is a free software for ImageJ that can be downloaded at http://ibidi.com/software/chemotaxis_and_migration_tool/.

[*Italic font style is used for buttons, check boxes, and headlines. Underlined text refers to bookmarks.*]

1. Download and open Chemotaxis and Migration Tool in the ImageJ. Import the data table from MetaMorph by choosing *Import Data* in Import dataset bookmark (*see* **Note 21**).
2. Choose which cell tracks from the data table will be analyzed by filling in the *Number of slices*. Only specified tracks with exact number or within entered range of slices will be used. Then choose *Add dataset*, and mark off *Selected Dataset* in the main panel (*see* **Note 22**).
3. Calibrate the software in Settings bookmark. XY coordinates from MetaMorph are in pixels; it is therefore necessary to define the size of one pixel in *X/Y Calibration*. Also fill in *Time interval* that was used during time-lapse monitoring. Afterwards choose *Apply settings* in the main panel.
4. To analyze only selected time intervals from imported time-lapse choose *Open restrictions* in the main panel, mark off *Split dataset* check box, and fill in required slices (*see* **Note 23**). Then choose *Apply settings* in the main panel.
5. Now the tool is prepared to plot graphs and diagrams and export various statistic values. One can plot Chemotaxis Plot in Plot feature bookmark → *Plot graph* (*see* Figs. 4c, d and 6a, b). Sector feature and Diagram feature bookmarks allow plotting other graphs (e.g., Rose diagram; *see* Fig. 6c, d). Statistic feature bookmark provides statistic values that can be used for further statistical analysis.

4 Notes

1. Alternatively, fibronectin-coated surface can be prepared by 1-h incubation at 37 °C.
2. Starvation of BMMCs for IL-3 should not exceed 14–16 h. In case of suboptimal results, overnight culturing with a small amount of IL-3 can be optionally tested.
3. Removal of fibronectin-unbound cells is an important step and should be carried out with maximal caution to avoid any washing out or damaging of fibronectin-attached cell layer.
4. Best results are achieved with PGE_2 concentrations between 50 and 100 nM.
5. The length of time intervals depends on the number of monitored sites. If many sites are being examined, it is advisable to

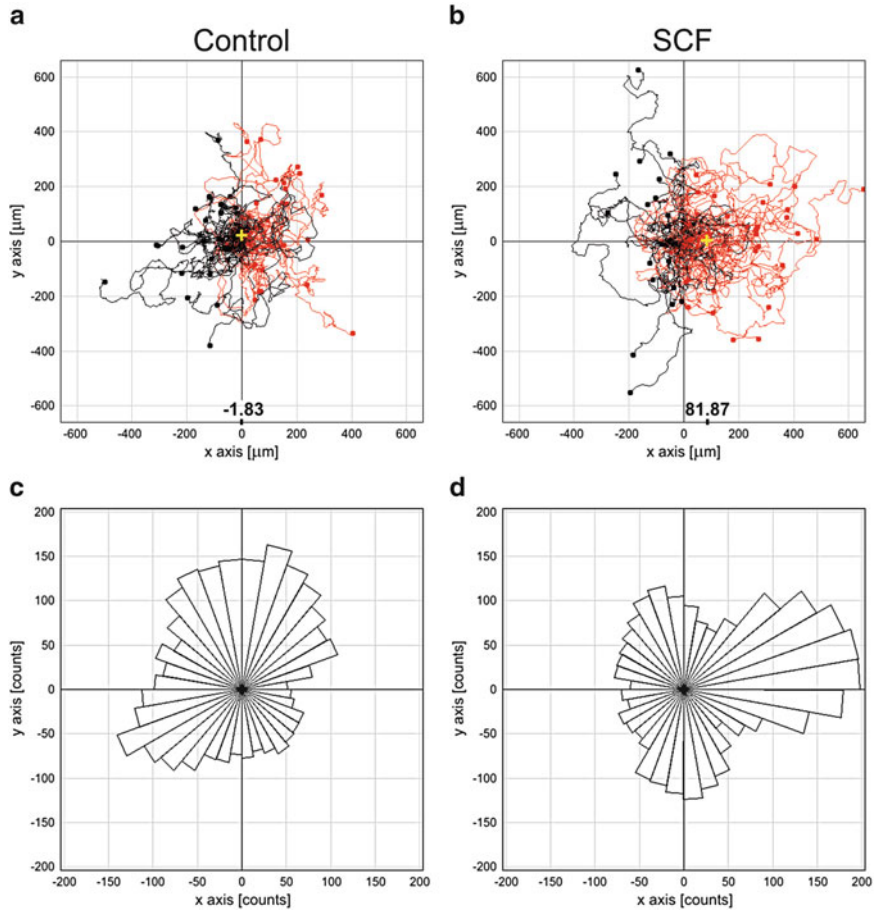

Fig. 6 Chemotaxis of LUVA cells. Representative images from a single experiment showing migration trajectory graphs (**a**, **b**) and rose diagrams expressing direction tendencies of LUVA cells (**c**, **d**). Cells without (**a**, **c**; control) and with 100 ng/mL SCF in the right reservoir (**b**, **d**; SCF). Chemotaxis of LUVA cells towards SCF is reflected by a shift of the center of cell mass in *x*-axis (*crosses* in **a**, **b**). LUVA cells in collagen I matrix were monitored for 10 h in an inverted microscope equipped with a 10× objective

choose as short time interval as possible. Cells become most active after the initial 15 min. An optimal time interval for subsequent analysis can be defined for individual experiments.

6. Equilibration prevents formation of air bubbles during loading of the µ-Slide^{3D}. Packaged µ-Slide^{3D} enables gas equilibration. Do not equilibrate collagen I.
7. Cell suspension will be consequently diluted into final concentration of 1.5×10^6 cells/mL. Cell concentration could vary according to individual experimental preferences—more cells for obtaining extensive statistic data, and less cells for easier cell tracking (cells are isolated and trajectories do not interfere).
8. This amount corresponds to collagen I concentration 1 mg/mL.

9. Mix well, but avoid generating bubbles. Polymerization starts approximately 5 min after mixing collagen I with premix.
10. Do not inject the mixture directly; rather maintain a small gap between the tip and the filling port A. Insert then the pipette tip directly into the filling port B and aspirate until the gel level reaches the pipette tip. Both ports should be filled but not overfilled.
11. Cell concentration and morphology should be checked with a microscope. The remaining gelation mixture in the Eppendorf tube helps determine the moment when the process of polymerization is completed.
12. To generate chemoattractant gradient, only half of the reservoir will be filled. Therefore, to achieve the desired final concentration, double the chemoattractant concentration.
13. Reservoirs must be filled, but not overfilled. This will prevent unwanted medium fluxes.
14. For later easier cell tracking it is better to contrast the cells against the background rather than perfectly focus the cells themselves.
15. Further information about working with μ-Slide Chemotaxis^{3D} chambers can be found on the Ibidi website, http://ibidi.com/applications/chemotaxis/u-slide-chemotaxis-3d/.
16. Manipulation with viscous agarose solution might be facilitated if pipette tips with cut off narrow ends are used. Low-melting-point agarose with gelling point around or below 40 °C is not recommended.
17. Do not include data obtained during the first 60 min into analysis because of possible irregularities caused by addition of agarose cone.
18. Cells can be also tracked with Manual Tracking plug-in for ImageJ, which is freely available. Furthermore, several commercially available platforms offer automated cell tracking online (e.g., Wimasis Image Analysis, http://www.wimasis.com/Products/chemotaxis-assay.html).
19. If the time-lapse displays dark borders or periphery, it is advisable to cut it off from the time-lapse sequence. The goal is to get as many marked cells as possible without marked background. Cells that are not properly marked are not tracked easily. On the other hand, too much background signal slows down the tracking process. It is possible to modify the threshold during automated tracking.
20. For this type of tracking it is best to use search regions of the size similar to that occupied by the cell.
21. Data loaded from MetaMorph must be in the same order and format as those from the Manual Tracking from ImageJ. It is therefore necessary to alter the .xlsx file from MetaMorph.

The first column should contain numbers of each tracked slice (from 1 to the very last line). The second column should indicate the number of tracks (Track no.). The third column should show the number of each slice in every track (Slice no.). Two other columns indicate X and Y coordinates. Save data table as .txt file.

22. This tool enables to work with more imported datasets at one time.
23. This option enables to analyze cell chemotaxis from the same time after adding the chemoattractant in every experiment.

Acknowledgements

This work was supported in part by Grants P302-14-09807S, P305-14-00703S, 301/09/1826, P302/10/1759, P302/12/G101, and P302/12/1673 from the Czech Science Foundation, project LD13015 and LD12073 from the Ministry of Education, Youth and Sport of the Czech Republic. We also acknowledge support of the COST Action BM1007 Mast Cells and Basophils—Targets for Innovative Therapies as well as Institutional support RVO 68378050. M.B. and Z.H. were supported in part by the Faculty of Science, Charles University, Prague.

References

1. Galli SJ, Tsai M, Piliponsky AM (2008) The development of allergic inflammation. Nature 454:445–454
2. Abraham SN, St. John AL (2010) Mast cell-orchestrated immunity to pathogens. Nat Rev Immunol 10:440–452
3. Maltby S, Khazaie K, McNagny KM (2009) Mast cells in tumor growth: angiogenesis, tissue remodelling and immune-modulation. Biochim Biophys Acta 1796:19–26
4. Galli SJ, Tsai M (2012) IgE and mast cells in allergic disease. Nat Med 18:693–704
5. Halova I, Draberova L, Draber P (2012) Mast cell chemotaxis - chemoattractants and signaling pathways. Front Immunol 3:119
6. Kirshenbaum AS, Metcalfe DD (2006) Growth of human mast cells from bone marrow and peripheral blood-derived CD34$^+$ pluripotent progenitor cells. Methods Mol Biol 315: 105–112
7. Ashman LK (1999) The biology of stem cell factor and its receptor c-Kit. Int J Biochem Cell Biol 31:1037–1051
8. Lantz CS, Boesiger J, Song CH, Mach N, Kobayashi T, Mulligan RC, Nawa Y, Dranoff G, Galli SJ (1998) Role for interleukin-3 in mast-cell and basophil development and in immunity to parasites. Nature 392:90–93
9. Welle M (1997) Development, significance, and heterogeneity of mast cells with particular regard to the mast cell-specific proteases chymase and tryptase. J Leukoc Biol 61:233–245
10. Taub D, Dastych J, Inamura N, Upton J, Kelvin D, Metcalfe D, Oppenheim J (1995) Bone marrow-derived murine mast cells migrate, but do not degranulate, in response to chemokines. J Immunol 154:2393–2402
11. Okayama Y, Kawakami T (2006) Development, migration, and survival of mast cells. Immunol Res 34:97–115
12. Jolly PS, Bektas M, Olivera A, Gonzalez-Espinosa C, Proia RL, Rivera J, Milstien S, Spiegel S (2004) Transactivation of sphingosine-1-phosphate receptors by FcεRI triggering is required for normal mast cell degranulation and chemotaxis. J Exp Med 199:959–970
13. Weller CL, Collington SJ, Brown JK, Miller HRP, Al-Kashi A, Clark P, Jose PJ, Hartnell A, Williams TJ (2005) Leukotriene B4, an activation product of mast cells, is a chemoattractant for their progenitors. J Exp Med 201: 1961–1971

14. Weller CL, Collington SJ, Hartnell A, Conroy DM, Kaise T, Barker JE, Wilson MS, Taylor GW, Jose PJ, Williams TJ (2007) Chemotactic action of prostaglandin E2 on mouse mast cells acting via the PGE_2 receptor 3. Proc Natl Acad Sci 104:11712–11717
15. Kuehn HS, Jung M-Y, Beaven MA, Metcalfe DD, Gilfillan AM (2011) Prostaglandin E2 activates and utilizes mTORC2 as a central signaling locus for the regulation of mast cell chemotaxis and mediator release. J Biol Chem 286:391–402
16. Ishizuka T, Okajima F, Ishiwara M, Iizuka K, Ichimonji I, Kawata T, Tsukagoshi H, Dobashi K, Nakazawa T, Mori M (2001) Sensitized mast cells migrate toward the antigen: a response regulated by p38 mitogen-activated protein kinase and Rho-associated coiled-coil-forming protein kinase. J Immunol 167:2298–2304
17. Kitaura J, Kinoshita T, Matsumoto M, Chung S, Kawakami Y, Leitges M, Wu D, Lowell CA, Kawakami T (2005) IgE- and IgE + Ag-mediated mast cell migration in an autocrine/paracrine fashion. Blood 105:3222–3229
18. Echtenacher B, Mannel DN, Hultner L (1996) Critical protective role of mast cells in a model of acute septic peritonitis. Nature 381:75–77
19. Malaviya R, Ikeda T, Ross E, Abraham SN (1996) Mast cell modulation of neutrophil influx and bacterial clearance at sites of infection through TNF-α. Nature 381:77–80
20. Brightling CE, Bradding P, Symon FA, Holgate ST, Wardlaw AJ, Pavord ID (2002) Mast-cell infiltration of airway smooth muscle in asthma. N Engl J Med 346:1699–1705
21. Quintás-Cardama A, Jain N, Verstovsek S (2011) Advances and controversies in the diagnosis, pathogenesis, and treatment of systemic mastocytosis. Cancer 117:5439–5449
22. Boyden S (1962) The chemotactic effect of mixtures of antibody and antigen on polymorphonuclear leucocytes. J Exp Med 115: 453–466
23. Hálová I, Dráberová L, Bambousková M, Machyna M, Stegurová L, Smrž D, Dráber P (2013) Crosstalk between tetraspanin CD9 and transmembrane adaptor protein non-T cell activation linker (NTAL) in mast cell activation and chemotaxis. J Biol Chem 288:9801–9814
24. Lee J, Veatch SL, Baird B, Holowka D (2012) Molecular mechanisms of spontaneous and directed mast cell motility. J Leukoc Biol 92: 1029–1041
25. Heit B, Kubes P (2003) Measuring chemotaxis and chemokinesis: the under-agarose cell migration assay. Sci STKE 2003:pl5
26. Wiggins HL, Rappoport JZ (2010) An agarose spot assay for chemotactic invasion. Biotechniques 48:121–124
27. Poole TJ, Zetter BR (1983) Stimulation of rat peritoneal mast cell migration by tumor-derived peptides. Cancer Res 43:5857–5861
28. Kuiper JWP, Sun C, Magalhães MA, Glogauer M (2011) Rac regulates PtdInsP3 signaling and the chemotactic compass through a redox-mediated feedback loop. Blood 118:6164–6171
29. Zengel P, Nguyen-Hoang A, Schildhammer C, Zantl R, Kahl V, Horn E (2011) μ-Slide chemotaxis: a new chamber for long-term chemotaxis studies. BMC Cell Biol 12:21
30. Hibbs ML, Tarlinton DM, Armes J, Grail D, Hodgson G, Maglitto R, Stacker SA, Dunn AR (1995) Multiple defects in the immune system of Lyn-deficient mice, culminating in autoimmune disease. Cell 83:301–311
31. Hájková Z, Bugajev V, Dráberová E, Vinopal S, Dráberová L, Janáček J, Dráber P, Dráber P (2011) STIM1-directed reorganization of microtubules in activated mast cells. J Immunol 186:913–923
32. Laidlaw TM, Steinke JW, Tinana AM, Feng C, Xing W, Lam BK, Paruchuri S, Boyce JA, Borish L (2011) Characterization of a novel human mast cell line that responds to stem cell factor and expresses functional FcεRI. J Allergy Clin Immunol 127:815–822

VI.3

Ghaly P.E., Churchill C.D.M., Abou El-Magd R.M., **Hájková Z.**, Dráber P., West F.G., Tuszynski J.A. (2017). Synthesis and biological evaluation of structurally simplified noscapine analogues as microtubule binding agents. Canadian Journal of Chemistry *95(6),* 649-655.

NRC Research Press

ARTICLE

Synthesis and biological evaluation of structurally simplified noscapine analogues as microtubule binding agents

Peter E. Ghaly, Cassandra D.M. Churchill, Rabab M. Abou El-Magd, Zuzana Hájková, Pavel Dráber, F.G. West, and Jack A. Tuszynski

Abstract: This paper reports on the results of chemical synthesis and biological assays performed on several new analogues of noscapine. We have successfully synthesized four noscapine analogues called **1a–4a**, as well as their four corresponding enantiomers called **1b–4b**. The chemical pathway consisted of three steps with yields in excess of 60% in each step. Subsequently, we have performed biological activity assays intended to reveal the mode of action of these compounds on microtubules in buffer and in cancer cell lines. We have assayed fluorescence quenching effects in microtubule polymerization experiments, cytotoxicity evaluation in breast cancer cell lines, as well as microtubule dynamicity assessments, for each of the synthesized compounds. Finally, we performed computational docking simulations to two binding sites on β-tubulin: (*a*) the colchicine binding site and (*b*) the noscapine binding site. Our results indicate that these compounds have relatively low cytotoxicity profile and less pronounced effects on microtubule dynamics compared with noscapine. Our computational results indicate that these compounds bind to both putative binding sites but have higher affinity for the colchicine site.

Key words: noscapine, microtubule, tubulin, cytotoxicity, microtubule dynamics, docking.

Résumé : Le présent article présente la synthèse chimique de plusieurs nouveaux analogues de la noscapine et les résultats d'essais biologiques réalisés sur ces composés. Nous avons effectué la synthèse de quatre analogues de la noscapine désignés par les structures **1a–4a** ainsi que leurs quatre énantiomères respectifs désignés par les structures **1b–4b**. La voie de synthèse consistait en trois étapes dont les rendements individuels dépassaient les 60 %. Par la suite, nous avons soumis ces composés à des essais d'activité biologique en vue de mettre en évidence leur mode d'action sur les microtubules dans un milieu tampon et dans des lignées de cellules cancéreuses. Nous avons évalué chacun des composés synthétisés pour déterminer leurs effets sur l'extinction de la fluorescence dans des expériences de polymérisation des microtubules ainsi que leur cytotoxicité dans des lignées de cellulaires de cancer du sein. Nous avons également étudié leurs effets sur la dynamique des microtubules. Enfin, nous avons modélisé leur amarrage sur deux sites de liaison de la β-tubuline : (*a*) le site de liaison de la colchicine et (*b*) le site de liaison de la noscapine. Nos résultats indiquent que ces composés présentent une toxicité relativement faible ainsi que des effets moins marqués sur la dynamique des microtubules comparativement à la noscapine. Nos résultats de modélisation indiquent par ailleurs que ces composés se lient aux deux sites de liaison présumés avec une plus grande affinité toutefois pour le site de liaison de la colchicine. [Traduit par la Rédaction]

Mots-clés : noscapine, microtubule, tubuline, cytotoxicité, dynamique des microtubules, amarrage.

Introduction

Noscapine (Fig. 1), a phthalideisoquinoline alkaloid isolated from the opium poppy as a byproduct, is an antitussive agent. However, at higher concentrations, noscapine has exhibited cytotoxic activity with a potential as an anticancer agent. Noscapine has shown encouraging preclinical results, inducing tumor regression in animal models[1] and having high oral bioavailability and low toxicity in normal tissues.[2] Noscapine derivatives have been developed with modifications at the C9′, C6′, C1, and C7 positions (Fig. 1).[3–14] 9′-Bromonoscapine and 9′-nitronoscapine have shown particular promise in preclinical studies.[4,6,7,15] Novel third-generation water-soluble noscapine analogues bearing a negatively charged sulfonato and a positively charged ammonium group have also been synthesized using noscapine, 9′-bromonoscapine, and 9′-aminonoscapine as scaffolds and have potential for future preclinical drug development.[16]

The anticancer activity of noscapine is a result of its binding to the αβ-tubulin dimer, which is a building block of microtubules, causing a conformational change in the protein, as determined by its quenching of tryptophan fluorescence.[18] This conformational change disrupts microtubules and prevents them from separating chromosomes in metaphase, thereby stopping cell division.[18] However, noscapine does not significantly promote or inhibit polymerization of microtubules,[19] making its mechanism of action

Received 16 December 2016. Accepted 15 February 2017.

P.E. Ghaly, C.D.M. Churchill, and F.G. West. Department of Chemistry, University of Alberta, E3-43 Gunning-Lemieux Chemistry Center, Edmonton, AB T6G 2G2, Canada.
R.M. Abou El-Magd. Department of Oncology, University of Alberta, Edmonton, AB T6G 1Z2, Canada; Genetic Engineering and Biotechnology Institute, City of Scientific Research and Technological Application, New Borg El-Arab City, Alexandria, 21934, Egypt.
Z. Hájková and P. Dráber. Laboratory of Biology of Cytoskeleton, Institute of Molecular Genetics, Academy of Sciences of the Czech Republic, CZ-142 20, Prague 4, Czech Republic.
J.A. Tuszynski. Department of Oncology, University of Alberta, Edmonton, AB T6G 1Z2, Canada; Department of Physics, University of Alberta, Edmonton, AB T6G 2E1, Canada.
Corresponding author: F.G. West (email: frederick.west@ualberta.ca).

Fig. 1. The chemical structure and numbering of (*a*) (*S*,*R*)-noscapine, with the "seed" structure proposed by Alisaraie and Tuszynski[17] highlighted in blue, (*b*) colchicine, and (*c*) the analogues studied in the present work. In the analogues, the piperidine ring of the tetrahydroisoquinoline has been replaced with a simple one-carbon linker substituted with various heteroatom groups. [Colour online.]

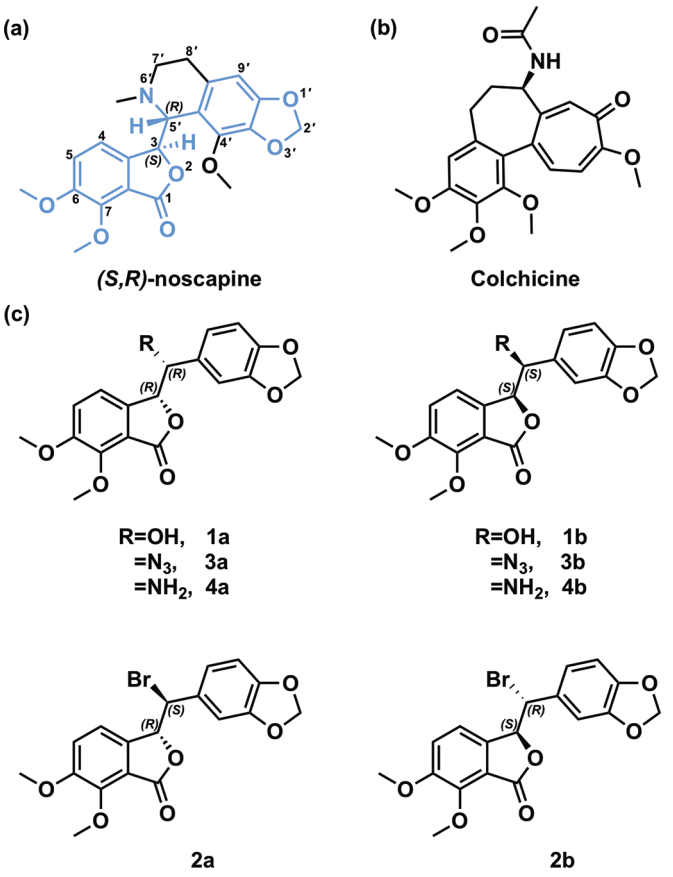

unique from that of other antimitotic agents, which are typically classified as microtubule polymerization promoters (e.g., taxanes) or polymerization inhibitors (e.g., vinca alkaloids, colchicine). Interestingly, different buffer conditions (pH of 6.8 vs. 7.0) cause noscapine to exhibit different behaviors in connection with microtubule assembly,[18] suggesting that the protonation of noscapine at the tertiary amine (reported pK_a values of 6.24[20] and 7.8[21]) may alter its mechanism of action. This indicates that the mode of action of noscapine, and possibly its derivatives, on microtubules is highly dependent on the structure and electric charge of the compound.

The identification of the noscapine binding site on tubulin has been challenging, because no structure of tubulin has yet been co-crystallized with noscapine and variable effects have been observed for different noscapine derivatives. The colchicine binding site, located at the intradimer interface between α-tubulin and β-tubulin,[22] generally binds agents that prevent polymerization of microtubules due to a conformational change they induce. Despite the structural similarity between colchicine and noscapine, no competition has been found between these two ligands and noscapine binding does not influence the fluorescence of colchicine–tubulin complexes.[18] In contrast, 9′-bromonoscapine competes with colchicine binding and affects colchicine–tubulin fluorescence,[23] which indicates that 9′-bromonoscapine binds at a site overlapping or near the colchicine site. Blind docking studies performed by Naik et al. indicated that noscapine and 9′-bromonoscapine have the greatest affinity for the colchicine site.[23]

Previous computational work in our group identified a site on the intradimer interface with high affinity for noscapine that is unique from the colchicine site.[17] Based on this newly identified site, Alisaraie and Tuszynski proposed novel noscapine analogues that contained the scaffold of a so-called "seed" compound that interacted most strongly in the proposed noscapine site.[17] This scaffold included the benzodioxole and isobenzofuranone moieties of the parent noscapine compound, joined by an amino-substituted linker (Fig. 1*a*) where the amino group is not constrained by a ring. The goal of the present work was to evaluate the activity of this seed structure, as well as compounds that could be relatively easily obtained using the same synthetic pathway. Therefore, we present the synthesis and an investigation of the activity of several new noscapine analogues (Fig. 1*b*).

Results

Chemical synthesis

Our synthesis (Scheme 1) began with the previously synthesized enantiomerically pure alcohol (**1a**),[24] which was converted, via an Appel reaction, to **2a** in 74% yield and >99% ee. Using NaN_3, the bromine in **2a** was displaced with an azide group to give compound **3a** in 62% yield and >99% ee. The azide in **3a** was finally reduced to give the amine **4a** in 60% yield and 85% ee. Compound **4a** represents the proposed seed structure.[17] To investigate the effect of stereochemistry on activity, we synthesized enantiomers of the above four analogues. The alcohol **1b** was synthesized using the same procedure for the synthesis of **1a**[24] but replacing AD mix-β for AD mix-α. Using the above-mentioned methodology, we were able to synthesize compounds **2b**, **3b**, and **4b** in comparable yields and ee.

Cytotoxicity assays

The MTT (3-(4,5-dimethylthiazol-2-yl)-2,5-diphenyltetrazolium bromide) colorimetric assay was used to evaluate the antiproliferative activity of our newly synthesized analogues, as well as the parent noscapine. For this cytotoxicity assay, the SKBR-3 human breast cancer cell line was used. Compounds **1a–4a** were first examined and compared with noscapine (Fig. 2*a*). Results from this assay indicate that the four analogues have a comparable cytotoxic effect with noscapine with an IC_{50} of ~100 μmol/L. Similar results were obtained with the four enantiomeric compounds **1b–4b** (Fig. 2*b*). These results indicate that varying the stereochemistry at the two chiral centers found in the analogues does not have a significant effect on the biological activity, as similar cytotoxic effects were observed for both the **1a–4a** and **1b–4b** analogues.

Fluorescence quenching assay

The presence of tryptophan moieties within the α and β subunits of tubulin renders the protein intrinsically fluorescent. The addition of small molecules that can act as fluorescence resonance acceptors (or compounds whose binding to tubulin affects the conformational state of the tryptophan residue's vicinity) will result in quenching the intrinsic tryptophan fluorescence. This provides a means of measuring the binding affinity of compounds to the tubulin protein. Because our cytotoxicity data showed similar antiproliferative effects for both the **1a–4a** and **1b–4b** analogues, only the **1a–4a** analogues were considered in this assay. The binding affinity of the **1a–4a** analogues was then compared with that of the parent noscapine. Results from the fluorescence quenching assay (Table 1) indicate that the analogues bind to tubulin with an affinity comparable with that of noscapine. These results indicate that changing the substituents in our analogues (OH, Br, N_3, and NH_2) has little effect on tubulin binding.

Microtubule distribution and nucleation

When U2OS cells were pre-treated with noscapine (concentrations, 50–250 μmol/L) for 24 h, both changes in the organization of

Scheme 1. Reagents and conditions: (*a*) PPh_3, CBr_4, DCM, rt, 1.0 h (74%); (*b*) NaN_3, DMF, 0 °C, 4 h (62%); (*c*) H_2, Pd/C, DMF, rt, 2 h (60%).

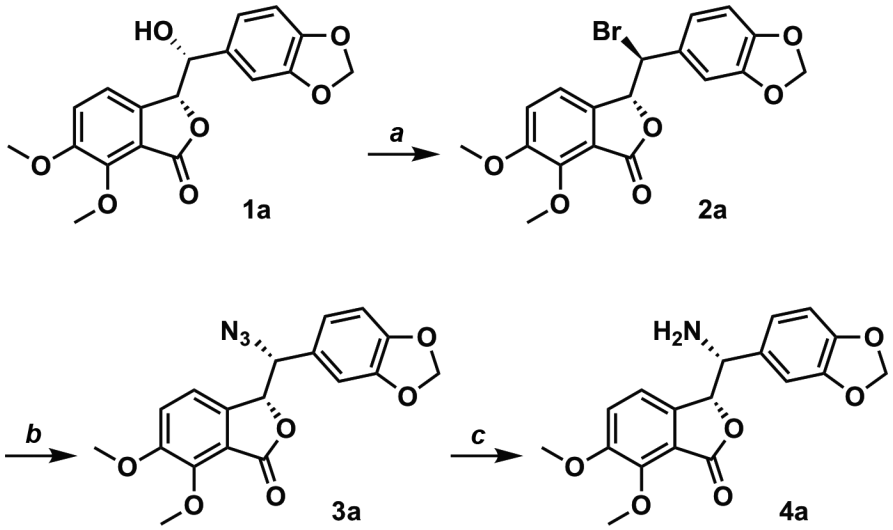

Fig. 2. Cytotoxicity (percent cell viability) of SKBR-3 human breast cancer cells in the presence of varying concentrations of the newly synthesized noscapine analogues and the parent compound, noscapine, determined using the colorimetric MTT assay. Panels *a* and *b* show the cytotoxic effect of compounds **1a–4a** and **1b–4b**, respectively, compared with noscapine. Results show no significant difference in cytotoxicity between the newly synthesized analogues and noscapine (p value > 0.05). [Colour online.]

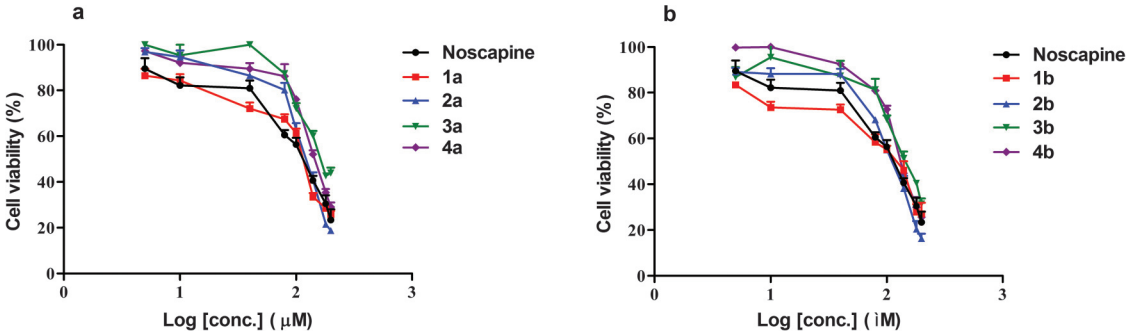

Table 1. Results of the fluorescence quenching assay involving tubulin and noscapine and its analogues.

Analogue	K_a value	K_d value (μmol/L)
Noscapine	3.77±0.02	265.25
1a	3.64±0.02	274.59
2a	4.66±0.02	214.59
3a	5.96±0.04	167.78
4a	3.16±0.02	315.46

microtubules and nuclei morphology were observed. No such effects were detected when cells were treated with noscapine analogues **1a–4a** and **1b–4b**. Typical examples are shown in Fig. 3. Cells in interphase that were pre-treated for 24 h with 100 μmol/L noscapine displayed atypical bundling of microtubules (Fig. 3*a*) and nuclei were often fragmented (Fig. 3*b*). In contrast, cells pre-treated for 24 h with 100 μmol/L of **1a** showed organization of microtubules (Fig. 3*d*) and morphology of the nuclei (Fig. 3*e*) similar to that of untreated cells (Figs. 3*g* and 3*h*).

To evaluate if the noscapine analogues could affect de novo microtubule formation from interphase centrosomes, nocodazole washout experiments were performed as previously described.[25,26] In control cells, a microtubule array was observed originating from the centrosomes, which appeared after 3 min (Fig. 4*a*), and a fully developed microtubule array was detected after 10 min. When 250 μmol/L noscapine was present during the regrowth, very small microtubule asters were formed after 3 min (Fig. 4*b*), and substantial inhibition of microtubule aster formation was also observed after 10 min. In contrast, under the same conditions, the noscapine analogues had no effect on microtubule formation, as illustrated for **1a** (Fig. 4*c*). These findings indicate that noscapine analogues are not significantly affecting microtubule distribution and nucleation.

Microtubule dynamics

Microtubule dynamicity measurements indicate the amount of dynamic instability occurring in the microtubule population assayed. Higher dynamicity reflects faster adjustment of microtubules to their surrounding microenvironment. To directly assess the effect of noscapine and noscapine analogues on microtubule dynamics, we have used U2OS stably expressing GFP-tagged end binding protein 1 (U2OS_EB1-GFP) that marks ends of growing microtubules. The EB1 comets were visualized using time-lapse microscopy in cells pre-treated with noscapine, **1a**, or **4a** at a concentration of 50 μmol/L for 1 h. Although noscapine substantially suppressed microtubule dynamics when compared with control cells containing DMSO carrier, the **1a** and **4a** noscapine analogues had no pronounced effect on microtubule dynamics (Table 2; Fig. 5).

Computational docking

Two receptor models were used to examine docking to the colchicine site and proposed noscapine site. The colchicine site was

Fig. 3. A comparison of microtubule organization in cells pre-treated with (*a*–*c*) noscapine and (*d*–*f*) **1a** and (*g*–*i*) in untreated cells. U2OS cells were pre-incubated for 24 h with 100 μmol/L of either noscapine or **1a**. Preparations were fixed and microtubules were immunostained with antibody to α-tubulin (*a*, *d*, and *g*) and indicated in green (*c*, *f*, and *i*); DNA was stained with DAPI (*b*, *e*, and *h*) and indicated with blue (*c*, *f*, and *i*). Scale bar, 20 μm. [Colour online.]

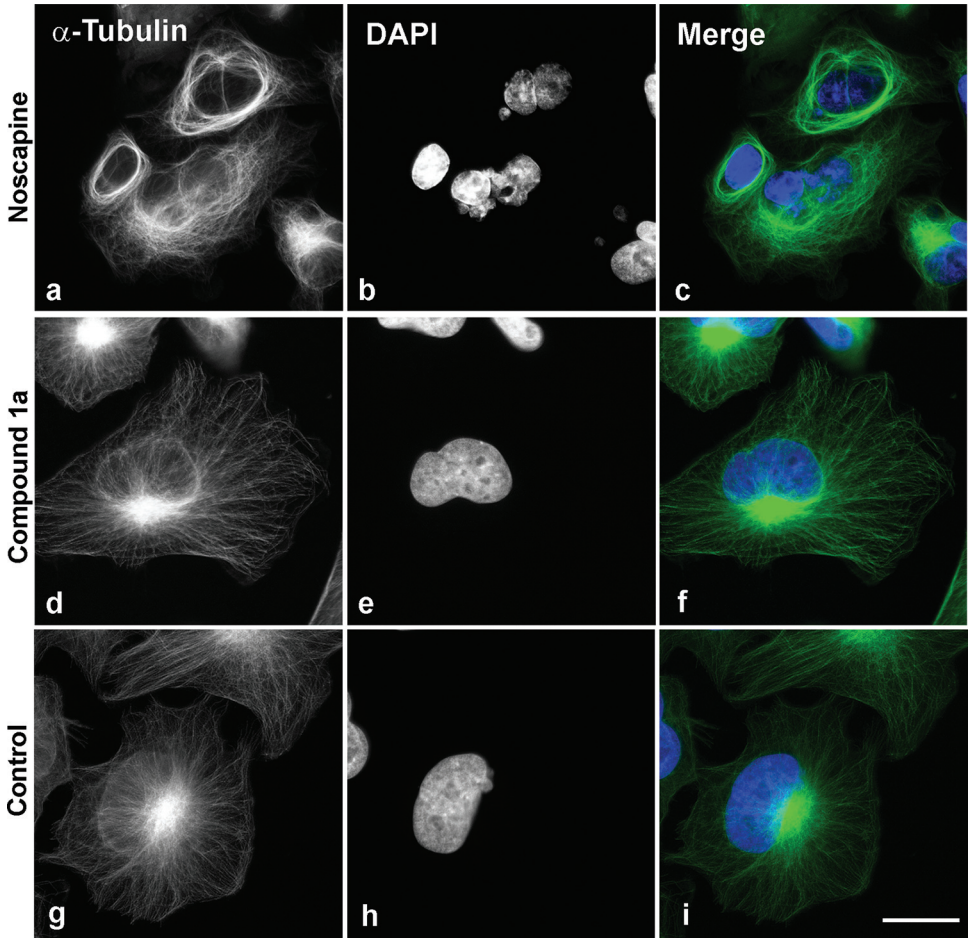

modeled using the colchicine–αβ-tubulin complex obtained from the 1SA0 crystal structure found in the Protein Data Bank (PDB).[22] The proposed noscapine site was modeled using the noscapine–αβ-tubulin complex from the study by Alisaraie and Tuszynski.[17] Both receptor structures were energy minimized prior to docking using Amber12:EHT in the Molecular Operating Environment (MOE) software package.[27] Ligand coordinates for noscapine and the analogues (Fig. 1*b*) were obtained following a B3LYP/6-31G(d,p) optimization with Gaussian 09.[28] Noscapine was modeled in both cationic (protonated, Nos^{+}) and neutral (Nos^{0}) states, with the lone pair or proton directed above (Nos^{R}) or below (Nos^{S}) the plane, for a total of four noscapine models (Nos^{+R}, Nos^{0R}, Nos^{+S}, and Nos^{0S}; Supplementary Fig. S1). Both **4a** and **4b** were also modeled in cationic (**4a**$^{+}$ and **4b**$^{+}$) and neutral (**4a**^{0} and **4b**^{0}) forms.

Docking calculations were performed with the MOE program using an induced fit protocol. The receptor was defined as the protein, nucleotide cofactors, and Mg^{2+} ions, and protein atoms within 4.5 Å from the binding site were allowed to move. During docking, duplicate poses were discarded. Poses were first scored with the London dG method, and the top 30 hits were rescored with the GBVI/WSA dG methods, where the top 10 hits were retained. Calculations at both the colchicine and proposed noscapine sites were performed in duplicate to enhance sampling, and the top-ranking pose for each receptor–ligand complex was analyzed (Table 3). Subsequently, this complex was energy minimized using the Amber12:EHT force field in MOE to analyze protein–ligand contacts. In our calculations, the top binding pose for colchicine in the colchicine site resembled that found in the 1SA0 crystal structure,[22] providing us with confidence in our docking protocols.

The compounds were docked to both the colchicine and proposed noscapine site in an attempt to determine the preferred site at which they bind to tubulin. Contrary to previous results, noscapine (all noscapine models) was found to prefer binding to the colchicine site rather than the noscapine site, with an estimated binding energy difference of up to 2.2 kcal mol^{-1}. In addition, the charge and isomer type of noscapine had little effect on its affinity (up to 0.2 kcal mol^{-1}) for either site. However, protonation did affect the top pose for the (*S*,*R*)-Nos^{+S} isomer (isoquinoline-containing moiety towards α-tubulin), which differs in its binding pose from the other three noscapine models (dimethoxybenzofuranone moiety towards α-tubulin; see (*S*,*R*)-Nos^{+R} in Fig. 6).

The docking scores indicate that the newly synthesized compounds also have a slight preference for the colchicine site (by 1.2–1.8 kcal mol^{-1}). In the case of the **4a** and **4b** compounds binding to the colchicine site, binding of the neutral compounds (**4a**^{0} and **4b**^{0}) is preferred over the binding of their protonated counterparts (**4a**$^{+}$ and **4b**$^{+}$) by 0.3–0.5 kcal mol^{-1}.

Discussion

In this paper, we have revisited earlier recommendations regarding the potential improvement in the activity of noscapine by its derivatization. We report here on the results of chemical

Fig. 4. Effect of noscapine and **1a** on microtubule regrowth. U2OS cells were treated with nocodazole to depolymerize microtubules, nocodazole was washed out, and microtubule regrowth was allowed in the absence or presence of tested agents. Immunofluorescence for α-tubulin in cells containing (*a*, control) DMSO carrier, (*b*) noscapine at concentration 250 μmol/L, or (*c*) **1a** at concentration 250 μmol/L at 3 min of microtubule regrowth. All images were collected and processed in exactly the same manner. Scale bar, 20 μm.

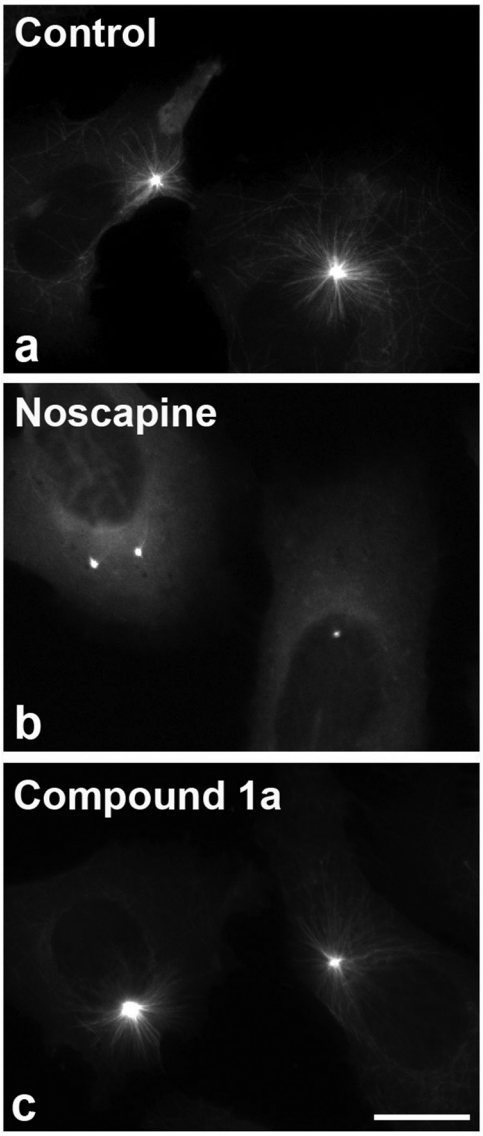

Table 2. Parameters of microtubule growth and dynamicity in control and drug-treated cells.

Cells	Growth speed (μm/min)	Growth length (μm)	Growth lifetime (sec)	Dynamicity (μm/min)
Control	15.39±0.85	2.32±0.11	8.28±0.13	8.30±0.46
Noscapine	9.39±0.15	1.03±0.03	7.24±0.34	5.80±1.58
1a	14.83±0.24	2.21±0.10	8.35±0.29	7.79±0.20
4a	15.63±0.55	2.32±0.20	8.22±0.43	8.21±0.52

Note: U2OS cells expressing EB1-GFP were pre-treated with 50 μmol/L noscapine or its analogues for 1 h. Control cells contained DMSO carrier. Three independent experiments were performed, each involving at least 27 cells. Data are mean ± standard deviation (control, $n = 112$; noscapine, $n = 83$; **1a**, $n = 100$; **4a**, $n = 98$).

Fig. 5. Effect of noscapine and selected analogues on microtubule dynamics. Proportions of microtubule subpopulations have been classified by growth speed and growth lifetime. U2OS cells expressing EB1-GFP were pre-treated with noscapine, **1a**, or **4a** (concentration of 50 μmol/L for 1 h). Control cells contained equivalent volumes of the DMSO carrier. Microtubule subpopulations were divided based on whether they were above or below the median of growth speed (15.6 μm/min) and median of growth lifetime (6 s) of EB1 tracks from control cells. The four subpopulations of microtubules (MT) are coded by colour. Numbers of evaluated cells (*n*) are shown on the right. [Colour online.]

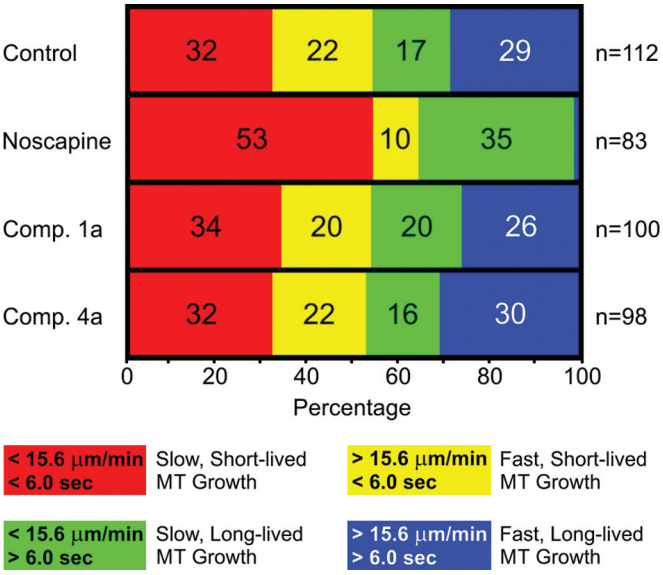

Table 3. The binding affinity (kcal mol^{-1}) of different compounds for the colchicine and proposed noscapine sites on αβ-tubulin, obtained from docking calculations.

Compound	Colchicine site	Noscapine site
Colchicine	–9.541	–7.182
(*S*,*R*)-Nos^{0R}	–8.933	–7.044
(*S*,*R*)-Nos^{+R}	–8.844	–6.911
(*S*,*R*)-Nos^{0S}	–8.916	–6.875
(*S*,*R*)-Nos^{+S}	–9.051	–6.836
1a	–7.884	–6.735
1b	–7.884	–6.751
2a	–7.831	–6.445
2b	–8.007	–6.362
3a	–8.371	–6.534
3b	–8.176	–6.572
4a^{+}	–7.638	–6.473
4a^{0}	–7.987	–6.224
4b^{+}	–7.499	–6.164
4b^{0}	–8.011	–6.284

synthesis and biological assays performed on eight new analogues of noscapine. Although previously reported analogues are usually synthesized directly from noscapine by functionalization of the parent compound, our analogues are simplified compounds that share some structure features with noscapine. The new analogues were designed from noscapine by the removal of the piperidine ring, as well as the 4′-methoxy group, and the introduction of different substituents (OH, Br, N_3, and NH_2) at the 5′ position (Fig. 1). Our analogues were synthesized in sequence where each analogue is obtained by a single transformation from the preced-

Fig. 6. The energy-minimized docking poses of select compounds in the colchicine (top row) and proposed noscapine (bottom row) binding sites. These binding sites are located at the intradimer interface between α-tubulin (grey) and β-tubulin (teal). GTP (blue) and Mg^{2+} (yellow) molecules are also shown. [Colour online.]

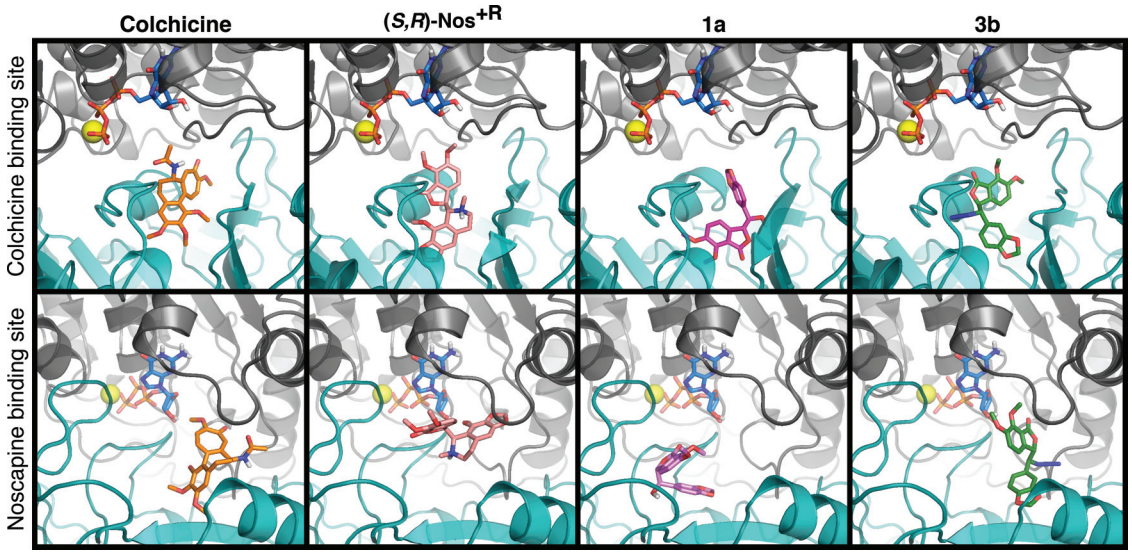

ing one, resulting in four analogues **1a–4a** (Scheme 1). Moreover, to investigate the influence of the stereochemistry on the binding affinity of the new analogues towards microtubules, as well as their cytotoxicity towards cancer cell lines, we synthesized the corresponding enantiomers **1b–4b** through the same pathway using a different chiral catalyst.

To understand the mode of action of these analogues on microtubules, we have performed several biological assays. Two different cancer cell lines were used in our studies: the human breast cancer cell line (SKBR-3) and the human osteosarcoma cell line (U2OS). Both cell lines have epithelial-like morphology, with microtubules reaching cell periphery in well adherent interphase cells. Both cell lines have also been previously used for evaluation of microtubule organization and dynamics after antimitotic drug treatments. For microscopic evaluation, we have selected U2OS, as a previously established U2OS cell line expressing EB1-GFP was successfully used in the analysis of microtubule dynamics.[29]

The antiproliferative effect of these analogues was evaluated using the colorimetric MTT assay and compared with noscapine. Our results show that the eight newly synthesized analogues have comparable cytotoxicity with each other, as well as to the parent noscapine (Fig. 2). These results indicate that neither the identity of the substituents considered in this work, nor the stereochemistry at the two of chiral centers have an effect on the activity. Previously synthesized noscapine analogues, including 9′-bromonoscapine,[7] as well as 7-hydroxynoscapine,[12] have shown improved cytotoxicity compared with noscapine using a different cancer cell line. On the other hand, our brominated analogues **2a** and **2b** failed to show cytotoxicity enhancement.

To assess the binding affinity of the analogues for tubulin, we have used fluorescence-quenching effects in microtubule polymerization experiments. Representative analogues **1a–4a** were used for this assay. It was found that both noscapine and the new analogues have similar binding affinity towards tubulin. Nocodazole washout experiments were then performed to evaluate the ability of the analogues to affect the de novo microtubule formation from interphase centrosomes. After 10 min, noscapine showed substantial inhibition of microtubule aster formation; however, no changes were observed when the cells were pretreated with the analogue **1a**. In microtubule dynamicity measurements, analogues **1a** and **4a** did not show pronounced effects on microtubule dynamics compared with noscapine, where microtubules stay longer in the slower phase of growth and shrinkage. These results indicate that, despite the binding of the noscapine analogues to tubulin, they do not significantly affect microtubule distribution, nucleation, or dynamics.

Finally, computational docking simulations were performed to identify if there was a preference for the analogues binding at the colchicine binding site or the noscapine binding sites, both located at the intradimer interface of an αβ-tubulin heterodimer. Colchicine has a preference of 2.4 kcal mol^{-1} for its binding site compared with the smaller preference of the noscapine analogues for the colchicine site (1.2–1.8 kcal mol^{-1}). However, these differences are very small, and it is difficult to make such conclusions based on binding affinity alone. Examining the poses associated with these compounds shows that colchicine commonly adopts the same pose within its binding site, which agrees with the 1SA0 crystal structure. Conversely, noscapine and its analogues can adopt a variety of poses in either binding site. This lack of consensus[30] in regard to the poses of noscapine and its analogues, as well as the calculated binding affinities, indicate that the binding of noscapine and the analogues studied here is somewhat indiscriminate. This suggests that these compounds may have an affinity for both sites, which is not surprising because it is known in the literature that small modifications to the noscapine structure (e.g., bromination[23]) or using different buffer conditions[18] can significantly affect its binding location and effect on microtubules. Additionally, the greater variations in binding poses observed in the proposed noscapine site over the colchicine site (Fig. 6) suggests that future studies modifying noscapine may find that large structural variations can be better accommodated in the noscapine site over the colchicine site, driving the binding specificity towards the noscapine site and increasing affinity by making additional drug–protein contacts.

In conclusion, although these analogues do not offer an alternative for noscapine in terms of their efficacy against cancer cells, their comparable affinity for both the noscapine and colchicine sites suggests that the possibility that these compounds, or similar compounds, could work via a bimodal action depending on concentration or pH. Evidence of such action is found in the varying ability of noscapine to affect microtubules under different buffer conditions[18] and has been observed in the binding of the antimitotic agent, paclitaxel, to tubulin, as it has both a well-characterized, high-affinity binding site and a lower affinity, in-

termediate binding site on tubulin.[31] Future work is necessary to further probe the binding location and mechanism of action of noscapine and its analogues to understand why small modifications have such a drastic effect on this class of compounds. Experimental techniques such as hydrogen–deuterium exchange mass spectrometry have been very successful in addressing such questions about the binding of other compounds to tubulin.[32] Given the unique behavior of noscapine analogues, comparisons with colchicine, as well as with noscapine, may be appropriate. Future work with these analogues may include studies towards γ-tubulin, as it was recently reported that amino- and bromo-noscapine derivatives can bind strongly to γ-tubulin,[33] which may provide an avenue for developing compounds that selectively bind to γ-tubulin over αβ-tubulin.

Supplementary data

Supplementary data are available with the article through the journal Web site at http://nrcresearchpress.com/doi/suppl/10.1139/cjc-2016-0649.

Acknowledgements

This research was partially funded by grants from NSERC (Canada) awarded to J.A.T and F.G.W and grant 15-22194S from the Grant Agency of the Czech Republic awarded to P.D. C.D.M.C thanks NSERC, Alberta Innovates-Technology Futures, the Killam Trust, the IODE War Memorial Scholarship, and the University of Alberta for funding.

References

(1) Jackson, T.; Chougule, M. B.; Ichite, N.; Patlolla, R. R.; Singh, M. *Cancer Chemother. Pharmacol.* **2008**, *63*, 117. doi:10.1007/s00280-008-0720-z.
(2) Aneja, R.; Dhiman, N.; Idnani, J.; Awasthi, A.; Arora, S. K.; Chandra, R.; Joshi, H. C. *Cancer Chemother. Pharmacol.* **2007**, *60*, 831. doi:10.1007/s00280-007-0430-y.
(3) Anderson, J. T.; Ting, A. E.; Boozer, S.; Brunden, K. R.; Crumrine, C.; Danzig, J.; Dent, T.; Faga, L.; Harrington, J. J.; Hodnick, W. F.; Murphy, S. M.; Pawlowski, G.; Perry, R.; Raber, A.; Rundlett, S. E.; Stricker-Krongrad, A.; Wang, J.; Bennani, Y. L. *J. Med. Chem.* **2005**, *48*, 7096. doi:10.1021/jm050674q.
(4) Aneja, R.; Miyagi, T.; Karna, P.; Ezell, T.; Shukla, D.; Vij Gupta, M.; Yates, C.; Chinni, S. R.; Zhau, H.; Chung, L. W. K.; Joshi, H. C. *Eur. J. Cancer* **2010**, *46*, 1668. doi:10.1016/j.ejca.2010.02.017.
(5) Aneja, R.; Vangapandu, S. N.; Joshi, H. C. *Bioorg. Med. Chem.* **2006**, *14*, 8352. doi:10.1016/j.bmc.2006.09.012.
(6) Aneja, R.; Vangapandu, S. N.; Lopus, M.; Chandra, R.; Panda, D.; Joshi, H. C. *Mol. Pharmacol.* **2006**, *69*, 1801. doi:10.1124/mol.105.021899.
(7) Aneja, R.; Vangapandu, S. N.; Lopus, M.; Viswesarappa, V. G.; Dhiman, N.; Verma, A.; Chandra, R.; Panda, D.; Joshi, H. C. *Biochem. Pharmacol.* **2006**, *72*, 415. doi:10.1016/j.bcp.2006.05.004.
(8) Debono, A. J.; Mistry, S. J.; Xie, J.; Muthiah, D.; Phillips, J.; Ventura, S.; Callaghan, R.; Pouton, C. W.; Capuano, B.; Scammells, P. J. *ChemMedChem* **2014**, *9*, 399. doi:10.1002/cmdc.201300395.
(9) DeBono, A.; Capuano, B.; Scammells, P. J. *J. Med. Chem.* **2015**, *58*, 5699. doi:10.1021/jm501180v.
(10) Manchukonda, N. K.; Sridhar, B.; Naik, P. K.; Joshi, H. C.; Kantevari, S. *Bioorg. Med. Chem. Lett.* **2012**, *22*, 2983. doi:10.1016/j.bmcl.2012.02.033.
(11) Manchukonda, N. K.; Naik, P. K.; Santoshi, S.; Lopus, M.; Joseph, S.; Sridhar, B.; Kantevari, S. *PLoS One* **2013**, *8* (10), e77970. doi:10.1371/journal.pone.0077970.
(12) Mishra, R. C.; Gundala, S. R.; Karna, P.; Lopus, M.; Gupta, K. K.; Nagaraju, M.; Hamelberg, D.; Tandon, V.; Panda, D.; Reid, M. D.; Aneja, R. *Bioorg. Med. Chem. Lett.* **2015**, *25*, 2133. doi:10.1016/j.bmcl.2015.03.076.
(13) Zhou, J.; Gupta, K.; Aggarwal, S.; Aneja, R.; Chandra, R.; Panda, D.; Joshi, H. C. *Mol. Pharmacol.* **2003**, *63*, 799. doi:10.1124/mol.63.4.799.
(14) Santoshi, S.; Manchukonda, N. K.; Suri, C.; Sharma, M.; Sridhar, B.; Joseph, S.; Lopus, M.; Kantevari, S.; Baitharu, I.; Naik, P. K. *J. Comput.-Aided Mol. Des.* **2015**, *29*, 249. doi:10.1007/s10822-014-9820-5.
(15) Rida, P. C. G.; LiVecche, D.; Ogden, A.; Zhou, J.; Aneja, R. *Med. Res. Rev.* **2015**, *35*, 1072. doi:10.1002/med.21357.
(16) Henary, M.; Narayana, L.; Ahad, S.; Gundala, S. R.; Mukkavilli, R.; Sharma, V.; Owens, E. A.; Yadav, Y.; Nagaraju, M.; Hamelberg, D.; Tandon, V.; Panda, D.; Aneja, R. *Biochem. Pharmacol.* **2014**, *92*, 192. doi:10.1016/j.bcp.2014.07.020.
(17) Alisaraie, L.; Tuszynski, J. A. *Chem. Biol. Drug Des.* **2011**, *78*, 535. doi:10.1111/j.1747-0285.2011.01189.x.
(18) Ye, K.; Ke, Y.; Keshava, N.; Shanks, J.; Kapp, J. A.; Tekmal, R. R.; Petros, J.; Joshi, H. C. *Proc. Natl. Acad. Sci.* **1998**, *95*, 1601. doi:10.1073/pnas.95.4.1601.
(19) Zhou, J.; Panda, D.; Landen, J. W.; Wilson, L.; Joshi, H. C. *J. Biol. Chem.* **2002**, *277*, 17200. doi:10.1074/jbc.M110369200.
(20) Thoma, K.; Zimmer, T. *Int. J. Pharm.* **1990**, *58*, 197. doi:10.1016/0378-5173(90)90195-A.
(21) Mukkavilli, R.; Gundala, S. R.; Yang, C.; Jadhav, G. R.; Vangala, S.; Reid, M. D.; Aneja, R. *Eur. J. Pharm. Sci.* **2015**, *77*, 90. doi:10.1016/j.ejps.2015.05.026.
(22) Ravelli, R. B. G.; Gigant, B.; Curmi, P. A.; Jourdain, I.; Lachkar, S.; Sobel, A.; Knossow, M. *Nature* **2004**, *428*, 198. doi:10.1038/nature02393.
(23) Naik, P. K.; Santoshi, S.; Rai, A.; Joshi, H. C. *J. Mol. Graphics Modell.* **2011**, *29*, 947. doi:10.1016/j.jmgm.2011.03.004.
(24) Ghaly, P. E.; Abou El-Magd, R. M.; Churchill, C. D.; Tuszynski, J. A.; West, F. G. *Oncotarget* **2016**, *7*, 40518. doi:10.18632/oncotarget.9642.
(25) Colello, D.; Reverte, C. G.; Ward, R.; Jones, C. W.; Magidson, V.; Khodjakov, A.; LaFlamme, S. E. *J. Cell Sci.* **2010**, *123*, 2094. doi:10.1242/jcs.057505.
(26) Sulimenko, V.; Hájková, Z.; Černohorská, M.; Sulimenko, T.; Sládková, V.; Dráberová, L.; Vinopal, S.; Dráberová, E.; Dráber, P. *J. Immunol.* **2015**, *194*, 4099. doi:10.4049/jimmunol.1402459.
(27) Molecular Operating Environment (MOE). 1010 Sherbooke St. West, Suite #910, Montreal, QC H3A 2R7, Canada: Chemical Computing Group Inc.; 2013.08.
(28) Frisch, M. J., Trucks, G. W., Schlegel, H. B., Scuseria, G. E., Robb, M. A., Cheeseman, J. R., Scalmani, G., et al. Gaussian 09, Revison A.02 ed. Gaussian 09, Revison A02 ed. Gaussian, Inc.: Wallingford, CT, 2009.
(29) Vinopal, S.; Černohorská, M.; Sulimenko, V.; Sulimenko, T.; Vosecká, V.; Flemr, M.; Dráberová, E.; Dráber, P. *PLoS One* **2012**, *7*, e29919. doi:10.1371/journal.pone.0029919.
(30) Houston, D. R.; Walkinshaw, M. D. *J. Chem. Inf. Model.* **2013**, *53*, 384. doi:10.1021/ci300399w.
(31) Freedman, H.; Huzil, J. T.; Luchko, T.; Ludueña, R. F.; Tuszynski, J. A. *J. Chem. Inf. Model.* **2009**, *49*, 424. doi:10.1021/ci8003336.
(32) Percy, A. J.; Rey, M.; Burns, K. M.; Schriemer, D. C. *Anal. Chim. Acta* **2012**, *721*, 7. doi:10.1016/j.aca.2012.01.037.
(33) Suri, C.; Naik, P. K. *SAR QSAR Environ. Res.* **2015**, *26*, 507. doi:10.1080/1062936X.2015.1070200.

VI.4

Sulimenko V., **Hájková Z.**, Černohorská M., Sulimenko T., Sládková V., Dráberová L., Vinopal S., Dráberová E., Dráber P. (2015). Microtubule nucleation in mouse bone marrow–derived mast cells is regulated by the concerted action of GIT1/βPIX proteins and calcium. The Journal of Immunology *194*, 4099-4111.

Microtubule Nucleation in Mouse Bone Marrow–Derived Mast Cells Is Regulated by the Concerted Action of GIT1/βPIX Proteins and Calcium

Vadym Sulimenko,* Zuzana Hájková,*,† Markéta Černohorská,*,† Tetyana Sulimenko,* Vladimíra Sládková,* Lubica Dráberová,‡ Stanislav Vinopal,* Eduarda Dráberová,* and Pavel Dráber*

Ag-mediated activation of mast cells initiates signaling events leading to Ca^{2+} response, release of allergic mediators from cytoplasmic granules, and synthesis of cytokines and chemokines. Although microtubule rearrangement during activation has been described, the molecular mechanisms that control their remodeling are largely unknown. Microtubule nucleation is mediated by complexes that are formed by γ-tubulin and γ-tubulin complex proteins. In this study, we report that, in bone marrow–derived mast cells (BMMCs), γ-tubulin interacts with p21-activated kinase interacting exchange factor β (βPIX) and G protein–coupled receptor kinase-interacting protein (GIT)1. Microtubule regrowth experiments showed that the depletion of βPIX in BMMCs stimulated microtubule nucleation, whereas depletion of GIT1 led to the inhibition of nucleation compared with control cells. Phenotypic rescue experiments confirmed that βPIX and GIT1 represent negative and positive regulators of microtubule nucleation in BMMCs, respectively. Live-cell imaging disclosed that both proteins are associated with centrosomes. Immunoprecipitation and pull-down experiments revealed that an enhanced level of free cytosolic Ca^{2+} affects γ-tubulin properties and stimulates the association of GIT1 and γ-tubulin complex proteins with γ-tubulin. Microtubule nucleation also was affected by Ca^{2+} level. Moreover, in activated BMMCs, γ-tubulin formed complexes with tyrosine-phosphorylated GIT1. Further experiments showed that GIT1 and βPIX are involved in the regulation of such important physiological processes as Ag-induced chemotaxis and degranulation. Our study provides for the first time, to our knowledge, a possible mechanism for the concerted action of tyrosine kinases, GIT1/βPIX proteins, and Ca^{2+} in the propagation of signals leading to the regulation of microtubule nucleation in activated mast cells. *The Journal of Immunology*, **2015, 194: 4099–4111.**

Mast cells play a crucial role in allergy, as well as in innate and adaptive immune responses. They express plasma membrane–associated high-affinity IgERs (FcεRIs), the aggregation of which triggers mast cell activation, resulting in degranulation, the release of proinflammatory mediators, and the production of various cytokines. The first step in FcεRI signaling is tyrosine phosphorylation of the FcεRI β- and γ-subunits by the Src family nonreceptor kinase Lyn. This is followed by enhanced activity of tyrosine kinase Syk and the phosphorylation of transmembrane adaptors, which organize and coordinate further signals, resulting in a Ca^{2+} efflux from the endoplasmic reticulum (ER). Depletion of Ca^{2+} from the ER lumen induces Ca^{2+} influx across the plasma membrane, leading to enhancement of the free cytoplasmic Ca^{2+} concentration, a step that is important in further signaling events (1).

Microtubules, built up from αβ-tubulin heterodimers, are important for mast cell degranulation, because the movement of secretory granules depends on intact microtubules (2, 3), and compounds inhibiting tubulin polymerization suppress degranulation (4). It was reported that FcεRI aggregation leads to reorganization of microtubules (3, 5) and that the influx of Ca^{2+} plays a decisive role in microtubule remodeling (6, 7). An important role in Ca^{2+} influx was reported for stromal-interacting protein 1 (STIM1), the Ca^{2+} sensor in ER that associates with the end binding protein 1 located on the tips of growing microtubules (8). Depletion of STIM1 resulted in the inhibition of microtubule reorganization in stimulated cells (6). Although these data point to the necessity of the microtubule network for mast cell degranulation, the molecular mechanisms responsible for microtubule reorganization in activated mast cells are still largely unknown. The role of Ca^{2+} in this process is also unclear.

In cells, microtubules are dominantly nucleated from centrosomes or the other microtubule-organizing centers. One of the key

*Department of Biology of Cytoskeleton, Institute of Molecular Genetics, Academy of Sciences of the Czech Republic, CZ-142 20 Prague 4, Czech Republic; †Department of Cell Biology, Faculty of Science, Charles University Prague, CZ-128 43 Prague 2, Czech Republic; and ‡Department of Signal Transduction, Institute of Molecular Genetics, Academy of Sciences of the Czech Republic, CZ-142 20 Prague 4, Czech Republic

Received for publication September 26, 2014. Accepted for publication February 27, 2015.

This work was supported in part by Grants P302/12/1673, P302/11/P709, P302/14/09807S, and 15-22194S from the Grant Agency of the Czech Republic, Grants LD13015 and LH12050 from the Ministry of Education, Youth, and Sports of the Czech Republic, Grant NT14467 from Ministry of Health of the Czech Republic, Grant GAUK 796913 from the Grant Agency of Charles University, and by Institutional Research Support (RVO 68378050). We also acknowledge support of the COST Action BM1007 Mast Cells and Basophils–Targets for Innovative Therapies.

Address correspondence and reprint requests to Dr. Pavel Dráber, Department of Biology of Cytoskeleton, Institute of Molecular Genetics, Academy of Sciences of the Czech Republic, Vídeňská 1083, 142 20 Prague 4, Czech Republic. E-mail address: paveldra@img.cas.cz

The online version of this article contains supplemental material.

Abbreviations used in this article: BMMC, bone marrow–derived mast cell; BMMCL, BMMC line; BMMCL-γTb, BMMCL stably expressing TagRFP-tagged mouse γ-tubulin; ER, endoplasmic reticulum; GCP, γ-tubulin complex protein; GIT, G protein–coupled receptor kinase-interacting protein; HEK, HEK 293-FT; hGIT1, human GIT1; hβPIX, human βPIX; mGIT1, mouse GIT1; mβPIX, mouse βPIX; MS, mass spectrometry; PAK, p21-activated kinase; βPIX, p21-activated kinase interacting exchange factor β; P-Tyr, phosphotyrosine; ROI, region of interest; shRNA, short hairpin RNA; STIM1, stromal-interacting protein 1; γTuRC, γ-tubulin ring complex; tv, transcript variant.

components for microtubule nucleation is γ-tubulin (9), a highly conserved member of the tubulin superfamily. In cytosol, γ-tubulin exists as a γ-tubulin ring complex (γTuRC; with size ~2.2 MDa) comprising γ-tubulin small complexes (~280 kDa), composed of two molecules of γ-tubulin, one molecule of γ-tubulin complex protein (GCP)2, one molecule of GCP3, and some other proteins (10). Cumulative data indicate that protein tyrosine kinases phosphorylate γ-tubulin or associated proteins and, in this way, modulate γ-tubulin functions (5, 11, 12). The significance of Src kinases for microtubule nucleation from centrosomes was ascertained by microtubule regrowth experiments (13). Identification of tyrosine kinase substrates that regulate γ-tubulin functions should help to elucidate the mechanisms involved in the regulation of microtubule nucleation.

In this study, we examined the hypothesis that phosphotyrosine (P-Tyr) proteins associated with γ-tubulin modulate microtubule nucleation in activated mast cells. We identified p21-activated kinase (PAK) interacting exchange factor β (βPIX) and G protein–coupled receptor kinase-interacting protein (GIT)1 as signaling proteins that interact with γ-tubulin and associate with centrosomes. GIT1 is phosphorylated on tyrosine in activated cells and interacts with γ-tubulin in a Ca^{2+}-dependent manner. Our data suggest a novel signaling pathway for microtubule rearrangement in mast cells, where tyrosine kinase–activated GIT1 and βPIX work in concert with Ca^{2+} signaling to regulate microtubule nucleation. Through this pathway, Ag-induced signaling pathways leading to chemotaxis and degranulation could be regulated.

Materials and Methods

Reagents

BAPTA-AM, fibronectin, nocodazole, puromycin, ionomycin, and Hygromycin B were from Sigma. IL-3 and stem cell factor were from PeproTech EC. Protein A immobilized on Trisacryl GF-2000 and SuperSignal West Pico Chemiluminescent reagents were bought from Pierce. Protease-inhibitor mixture tablets (Complete EDTA-free) were from Roche Molecular Biochemicals, GFP-trap_A was purchased from ChromoTek, and Ni-NTA-agarose was from QIAGEN. Restriction enzymes were from New England Biolabs, and Glutathione Sepharose 4 Fast Flow was from GE Healthcare Life Sciences. Oligonucleotides were synthesized by East Port.

Abs

The following anti-peptide Abs prepared to human γ-tubulin were used: mouse mAb TU-31 (IgG2b) and mAb TU-30 (IgG1) to the sequence 434–449 (14) and mAb GTU 88 (IgG1; Sigma, cat. no. T6657) to the sequence 38–53. α-Tubulin was detected with rabbit Ab from GeneTex (GTX15246). Rabbit Abs to βPIX (HPA004744), GFP (G1544), GAPDH (G9545), and actin (A2066) were from Sigma. Rabbit Ab to GIT1 (sc-13961) and mAb to GCP4 (IgG1; sc-271876) were from Santa Cruz. Rabbit mAb to GIT1 (ab156001) was from Abcam. Rabbit mAb D11B8 to GIT2 (8072) was from Cell Signaling, and rabbit Ab to tRFP (AB234) was from Evrogen. mAb 4G10 (IgG2b) to P-Tyr conjugated with HRP (16-184) was from Upstate Laboratories, and mAb to 6xHis was from BD Biosciences (San Jose, CA; IgG2b; 8916-1). mAb GCP2-02 (IgG1) to GCP2 protein was described previously (15). Rabbit Ab to nonmuscle myosin H chain (BT-561; Biomedical Technologies) and mAb NF-09 (IgG2a) to neurofilament NF-M protein (16) served as negative controls in the immunoprecipitation experiments. Rabbit Ab to GST was from Dr. Petr Dráber (Institute of Molecular Genetics). The DY488-conjugated anti-rabbit and the DY549-conjugated anti-mouse Abs were from Jackson ImmunoResearch. Secondary HRP-conjugated Abs were from Promega Biotech.

Cell cultures and transfection

Bone marrow–derived mast cells (BMMCs) were isolated from the femurs and tibias of 6–8-wk-old BALB/c mice. All mice were maintained and used in accordance with the Institute of Molecular Genetics guidelines (permit number 12135/2010-17210) and national guidelines (2048/2004-1020). The cells were differentiated in suspension cultures for 6–8 wk, as previously described (6).

Stable cell lines derived from mouse BMMCs and $Lyn^{-/-}$ BMMCs were donated by Dr. M. Hibbs (Ludwig Institute for Cancer Research, Melbourne, Australia) (17). In this article, the cells are denoted as BMMC lines (BMMCLs) or $Lyn^{-/-}$ BMMCLs. Both the Ca^{2+} response (18) and Ag-induced degranulation (L. Dráberová and P. Dráber, unpublished observations) were decreased in $Lyn^{-/-}$ BMMCLs compared with BMMCLs. Cells were cultured in freshly prepared culture medium (RPMI 1640 supplemented with 20 mM HEPES [pH 7.5], 100 U/ml penicillin, 100 mg/ml streptomycin, 100 mM MEM nonessential amino acids, 1 mM sodium pyruvate, 10% FCS, and 10% WEHI-3 cell supernatant as a source of IL-3). In some cases, cells were cultivated for 30 min in serum-free and Ca^{2+}-free medium to which Ca^{2+} was freshly added to a final concentration of 1.8 mM. Alternatively, cells were incubated with 1 μM ionomycin in the presence or absence of Ca^{2+}. Cells were grown at 37°C in 5% CO_2 in air and passaged every 2 d.

HEK 293-FT (HEK) cells (Promega Biotech) were grown at 37°C in 5% CO_2 in DMEM supplemented with 10% FCS and antibiotics. The cells used for lentivirus production were at passage 4–15. HEK cells were transfected with 17 μg DNA/9-cm tissue culture dish using 51 μg polyethylenimine (Polysciences) and serum-free DMEM. After 24 h, the transfection mixture was replaced with fresh medium supplemented with serum, and cells were incubated for an additional 24 h.

Cell activation

Cells were sensitized with DNP-specific IgE and activated with Ag (DNP-BSA conjugate, 30–40 mol DNP/mol BSA), as described (6). Alternatively, cells were activated by pervanadate. Pervanadate solution was freshly prepared by mixing sodium orthovanadate solution with H_2O_2 to get a 10 mM final concentration of both components. The pervanadate solution was incubated for 15 min at room temperature and then diluted 1:100 in buffered saline solution (6).

DNA constructs

To prepare N-terminally EGFP-tagged human γ-tubulin (*TUBG1*; RefSeq ID: NM_001070.4), pH3-16 plasmid containing the full-length cDNA of human γ-tubulin (19) was digested with EcoRI/BglII restriction enzymes, and the fragment was inserted into pEGFP-C1 (Clontech), resulting in the plasmid pEGFP-hTUBG1_1-451. To prepare truncated forms of EGFP-tagged γ-tubulin, fragments encoding aa regions 1–440, 1–422, and 1–382 were amplified by PCR from the pH3-16 using forward primer 5′-AGTCAAGCTTATGCCGAGGGAAATCATC-3′ and the following reverse primers: 5′-CTAAGATCTCTACCGTGTGGCCGCATG-3′ (aa 1–440); 5′-GTCAGATCTCTAGTCCATCTCATCAAAGTTGTCC-3′ (aa 1–422), and 5′-CAAAGATCTCTAGGTGTGGTTGGCCATCAT-3′ (aa 1–382), respectively. Sites recognized by restriction endonucleases are underlined. PCR products were digested with HindIII/BglII and inserted into pEGFP-C3 (Clontech), resulting in the plasmids pEGFP-hTUBG1_1-440, pEGFP-hTUBG1_1-422, and pEGFP-hTUBG1_1-382, respectively. The C-terminal part of γ-tubulin (aa 362–451) was amplified from pH3-16 using forward 5′-TCGGATCCAGGAAGTCTCCCTACCT-3′ and reverse 5′-TTCTCGAGTCACTGCTCCTGGGTG-3′ primers. The PCR product was digested with BamHI/XhoI and ligated into pGEX-6P-1 (Amersham Biosciences), resulting in the plasmid pGST-hTUBG1_362-451. The shorter C-terminal part of γ-tubulin (aa 378–451) was amplified from pGST-hTUBG1_362-451 using forward 5′-GAATTCGGCCAACCACACCAGC-3′ and reverse 5′-GGATCCTCACTGCTCCTGGGTGC-3′ primers. The C-terminal part of α-tubulin (aa 378–451) was amplified from pGST-hTUBA1B_364-451 (V. Sulimenko, manuscript in preparation) using forward 5′-GAATTCGAGCAACACCACAGCC-3′ and reverse 5′-GGATCCTTAGTATTCCTCTCCTTCTTCC-3′ primers. PCR products were ligated into pCR2.1 (Invitrogen) by TA cloning, and fragments were excised with EcoRI/BamHI and ligated into pEGFP-C1, resulting in the plasmids pEGFP-hTUBG1_378-451 and pEGFP-hTUBA1B_378-451. To prepare N-terminally 6xHis-tagged γ-tubulin, the coding sequence was amplified from pH3-16 using forward 5′-AAGCATGCCGAGGGAAATCATCAC-3′ and reverse 5′-CTAAGCTTTCACTGCTCCTGGGTGC-3′ primers. The PCR product was digested with SphI/HindIII and ligated to pQE-82L (QIAGEN), resulting in the plasmid 6xHis-hTUBG1_1-451. γ-Tubulin fragment (aa 1–225) was amplified from pH3-16 using forward 5′-AAGCATGCCGAGGGAAATCATCAC-3′ and reverse 5′-AATAAGCTTTCAGGAGAAGGATGGGTTC-3′ primers. The PCR product was digested with SphI/HindIII and ligated to pQE-82L (QIAGEN), resulting in the plasmid 6xHis-hTUBG1_1-225. γ-Tubulin fragment (aa 223–451) was amplified from pH3-16 using forward 5′-AATGGTACCTCCTTCTCCCAGATCAAC-3′ and reverse 5′-GATTAAGCTTTCACTGCTCCTGGGTGC-3′ primers. The PCR product was digested with KpnI/HindIII and ligated to pQE-80 (QIAGEN), resulting in the plasmid 6xHis-hTUBG1_223-451. A cassette encoding mouse γ-tubulin fused to TagRFP was digested out from the pmTubg1-TagRFP construct (20) by EcoRI/NotI and ligated to pCDH-CMV-MCS-EF1-puro vector (System Biosciences), resulting in the lentiviral construct pmTubg1-TagRFP-puro.

A cassette encoding mouse GIT1 (mGIT1; *Git1*; RefSeq ID: NM_001004144.1) fused to GFP was amplified from the TurboGFP-tagged *Git1* cDNA ORF clone (MG210556; OriGene Technologies) using forward 5′-GTCTAGAGAGGAGATCTGCCGCCG-3′ and reverse 5′-GCCGGGAATTCGTTTAAACTCTTTC-3′ primers. The PCR product was ligated into pCR 2.1 by TA cloning, and the fragment was excised with XbaI/EcoRI and ligated into pCDH-CMV-MCS-EF1-puro, resulting in the lentiviral construct pmGIT1-GFP-puro. The coding sequence of human GIT1 (hGIT1; *GIT1*, transcript variant [tv]1; RefSeq ID: NM_001085454.1) was excised from phGIT1(tv1)-neo (M. Černohorská, manuscript in preparation) with NheI/NotI and ligated into the pCDH-CMV-MCS-EF1-hygro vector (System Biosciences), resulting in the lentiviral construct phGIT1(tv1)-hygro.

A cassette encoding mouse βPIX (mβPIX; *Arhgef7*, tv3; RefSeq ID: NM_017402.4) fused to GFP was amplified from the TurboGFP-tagged *Arhgef7* cDNA ORF clone (MG223397; OriGene Technologies) using forward 5′-TATGCTAGCGTCGACTGGATCCGG-3′ and reverse 5′-GCCGGGAATTCGTTTAAACTCTTTC-3′ primers. The PCR product was ligated into pCR 2.1 by TA cloning, and the fragment was excised with NheI/EcoRI and ligated into pCDH-CMV-MCS-EF1-puro, resulting in the lentiviral construct pmβPIX(tv3)-GFP-puro. The coding sequence of human βPIX (hβPIX; *ARHGEF7*, tv1; RefSeq ID: NM_003899.3) was excised from GST-hβPIX(tv1) (21) with BamHI/NotI and ligated into the pCDH-CMV-MCS-EF1-hygro vector. For a phenotypic rescue experiment, two silent point mutations (a1620g, t1623g) were generated in this construct by site-directed mutagenesis using the QuikChange II XL Site-Directed Mutagenesis Kit (Stratagene), according to the manufacturer's protocol. The resulting lentiviral construct was named phβPIX(tv1)mut-hygro.

All constructs were verified by sequencing. Plasmid pFYSH2 encoding the GST-tagged SH2 domain of mouse Fyn kinase was described previously (5). The lentiviral vector pCT-Mito-GFP containing cytochrome oxidase c subunit VIII (COX8) tag for visualization of mitochondria was obtained from System Biosciences (CYTO102-PB-1).

Lentiviral infection

Lentiviral infections were done as described previously (6), using HEK packaging cells for virus preparation. The transfection mixture was replaced after 3 d with fresh complete medium containing 5 μg/ml puromycin. Stable selection was achieved by culturing cells for 1–2 wk in the presence of puromycin. In phenotypic rescue experiments, medium containing puromycin was supplemented with 1 mg/ml Hygromycin B, and stable selection was achieved by culturing cells for 1–2 wk. BMMCL stably expressing TagRFP-tagged mouse γ-tubulin (BMMCL-γTb) was prepared by lentiviral transduction with pmTubg1-TagRFP-puro. To follow the distribution of GIT1 or βPIX in living cells, BMMCL-γTb was transduced with pmGIT1-GFP-puro or pmβPIX(tv3)-GFP-puro. After 3 d, cells expressing fluorescently tagged proteins were flow sorted using the BD Influx cell sorter (BD Biosciences). GFP and TagRFP emission was triggered by 488- and 561-nm lasers; fluorescence was detected with 525/50 and 585/20 band-pass filters. Only double-positive cells were used for subsequent live-cell imaging.

RNA interference

A set of five mouse Arhgef7 (National Center for Biotechnology Information RefSeq: NM_001113517.1, NM_001113518.1, NM_017402.4) short hairpin RNA (shRNA) constructs cloned into the lentiviral pLKO.1 vector (TRCN0000110025, TRCN0000110026, TRCN0000110027, TRCN0000110028, and TRCN0000110029) were purchased from Open Biosystems. With the exception of TRCN0000110025, the vectors target all transcript variants of Arhgef7. A set of five murine GIT1 (National Center for Biotechnology Information RefSeq: NM_001004144.1) shRNA constructs cloned into the pLKO.1 vector (TRCN0000106120, TRCN0000106121, TRCN0000106122, TRCN0000106123, and TRCN0000106124) were also purchased from Open Biosystems. Immunoblotting experiments revealed that cells with the greatest reduction in βPIX protein were obtained with TRCN0000110026 (βPIX-KD1) and TRCN0000110027 (βPIX-KD2). Similarly, cells with the greatest reduction in GIT1 protein were obtained with TRCN0000106122 (GIT1-KD1) and TRCN0000106121 (GIT1-KD2). The stable selected cells with the greatest reduction in βPIX or GIT1 were used for additional experiments. Cells transduced with empty lentiviral pLKO.1 vector (Addgene) or pLKO.1 vector containing nontarget shRNA (Sigma) were used as negative controls.

Preparation of cell extracts

Whole-cell extracts for SDS-PAGE were prepared by washing the cells in cold HEPES buffer (50 mM HEPES [pH 7.6], 75 mM NaCl, 1 mM $MgCl_2$, and 1 mM EGTA), solubilizing them in hot SDS sample buffer without bromophenol blue, and boiling for 5 min. When preparing extracts for immunoprecipitation and GST pull-down assays, cells were rinsed twice in cold HEPES buffer and extracted at a concentration of 15×10^6 cells/ml for 10 min at 4°C with HEPES buffer supplemented with 1% Nonidet P-40 (extraction buffer), protease inhibitor mixture, and phosphatase inhibitors (1 mM Na_3VO_4, 1 mM NaF). The suspension was spun down (20,000 × g, 15 min, 4°C), and supernatant was collected. In some cases, cell lysates were supplemented with $CaCl_2$ at concentrations ranging from 50 μM to 1.0 mM or with 10 mM EGTA. Alternatively, lysates were supplemented with $MgCl_2$ or $ZnCl_2$ at a concentration of 0.8 mM. When preparing extracts for gel-filtration chromatography, cells were extracted at a concentration of 14×10^7 cells/ml. Protein quantification in lysates and SDS-PAGE samples was assessed with a bicinchoninic acid assay and a silver dot assay, respectively (22).

Gel-filtration chromatography

Gel filtration was performed using fast protein liquid chromatography (AKTA-FPLC system; Amersham) on a Superose 6 10/300 GL column (Amersham). Column equilibration and chromatography were performed in an extraction buffer. The column was eluted at 30 ml/h, and 0.5-ml aliquots were collected. Samples for SDS-PAGE were prepared by mixing with 5× concentrated SDS sample buffer. The following molecular mass standards were used: IgM (900 kDa), thyroglobulin (669 kDa), ferritin (440 kDa), catalase (232 kDa), and BSA (66 kDa).

Immunoprecipitation, GST pull-down assay, gel electrophoresis, and immunoblotting

Immunoprecipitation was performed as previously described (23). Cell extracts were incubated with Protein A beads (Pierce, Rockford, IL) saturated with mAb TU-31 (IgG2b) to γ-tubulin, rabbit Ab to GIT1, rabbit Ab to βPIX, rabbit Ab to RFP, rabbit Ab to nonmuscle myosin (negative control), mAb NF-09 (IgG2a; negative control), or immobilized protein A alone. Abs to βPIX, GIT1, and tRFP were used at Ig concentrations of 2, 2, and 5 μg/ml, respectively. Ab to myosin was used at a dilution of 1:100. mAb TU-31 and mAb NF-09, in the form of hybridoma supernatants, were diluted 1:2. GFP-tagged proteins were immunoprecipitated using GFP-trap_A, according to the manufacturer's directions.

For large-scale immunoprecipitation experiments, $Lyn^{-/-}$ BMMCLs (total 6×10^8 cells) were activated by pervanadate, as described (6), and resuspended in 15 ml cold extraction buffer supplemented with protease and phosphatase inhibitors. After 10 min of incubation at 4°C, the suspension was centrifuged at 28,000 × *g* for 15 min at 4°C. Supernatant was incubated with anti-peptide mAb TU-31 to γ-tubulin immobilized on 5 ml Protein A beads overnight at 4°C. After extensive washing in TBST (10 mM Tris-HCl [pH 7.4] 150 mM NaCl, 0.05% Tween 20), immobilized protein A with bound proteins was loaded into a 10-ml (7 × 1.5 cm) column, washed with 70 ml TBST, and eluted with peptide used for immunization (14) at a concentration of 200 μg/ml in TBST. From the 0.5-ml fractions collected, 1-μl aliquots were spotted onto nitrocellulose and probed with anti–P-Tyr mAb conjugated with HRP (dilution 1:30,000), followed by chemiluminescent detection of bound Ab. Fractions containing tyrosine-phosphorylated proteins were collected (total 2 ml) and loaded onto 50 μl pelleted glutathione-Sepharose with bound GST-tagged mouse Fyn-SH2 domain to concentrate the tyrosine-phosphorylated proteins capable of binding this domain. After 3 h of incubation at 4°C and extensive washing, the proteins associated with the domain were dissolved in 50 μl 2× SDS sample buffer and boiled for 5 min.

Preparation and purification of GST-tagged fusion proteins were described previously, as were pull-down assays with whole-cell extracts (23). For comparison of immunoprecipitation and pull-down assays in the presence or absence of Ca^{2+}, protein extracts were used at the same protein concentration. Gel electrophoresis and immunoblotting were performed using standard protocols. Preparation, purification, and immobilization of 6xHis-tagged proteins onto Ni-NTA agarose were performed according to the manufacturer's recommendations.

SDS-PAGE and immunoblotting were performed using standard protocols (24). For immunoblotting, mAbs to 6xHis, γ-tubulin (GTU-88), P-Tyr, and GCP4 were diluted 1:50,000, 1:10,000, 1:10,000, and 1:1,000, respectively. mAb to GCP2, in the form of spent culture supernatant, was diluted 1:10. Rabbit Abs to GAPDH, βPIX, GIT1, actin, and GIT2 were diluted 1:50,000, 1:4,000, 1:2,000, 1:2,000, and 1:500, respectively. Rabbit Abs to GST, GFP, and RFP were diluted 1:20,000, 1:5,000, and 1:5,000, respectively. Secondary anti-mouse and anti-rabbit Abs conjugated with HRP were diluted 1:10,000. Bound Abs were detected by SuperSignal West Pico Chemiluminescent reagents (Pierce).

Mass spectrometry

Following large-scale immunoprecipitation and concentration of peptide-eluted samples on the GST-Fyn-SH2 domain, proteins dissolved in SDS sample buffer were separated on preparative 7.5% SDS-PAGE using the

Multigel-Long electrophoretic system (Biometra). Gels were stained by Coomassie Brilliant Blue G-250. The bands of interest were excised from the gel, destained, and digested by trypsin. Extracted peptides were analyzed by a MALDI-FTICR mass spectrometer (APEX-Qe) equipped with a 9.4 tesla superconducting magnet (both from Bruker Daltonics, Billerica, MA) at the Core facility of the Institute of Microbiology, Academy of Sciences of the Czech Republic. The obtained data were processed by Data Analysis 4.0 software (Bruker Daltonics) and searched by the ProFound (PROWL) search engine against the nonredundant database of all known *Mus musculus* proteins.

Degranulation assay

The degree of degranulation was quantified as the release of β-glucuronidase from anti-TNP IgE-sensitized cells activated with Ag (TNP-BSA conjugate, 15–25 mol TNP/mol BSA), using 4-methylumbelliferyl β-D-glucuronide as substrate (25). The total content of the enzyme was evaluated in supernatants from cells lysed by 0.1% Triton X-100.

Chemotaxis assay

The chemotactic response of cells was examined using a 24-well Transwell system with 8-μm-diameter pore size polycarbonate filters (Corning), as described previously (26). TNP-BSA, at a concentration of 250 ng/ml in RPMI 1640, supplemented with 20 mM HEPES and 1% BSA (assay buffer), served as a chemoattractant.

Evaluation of cell proliferation and apoptosis

Cell proliferation was assessed by manual counting of stable cell lines with the greatest reduction in βPIX or GIT1. Cells transduced with empty lentiviral pLKO.1 vector or pLKO.1 vector containing nontarget shRNA (pLKO.1-NT) were used as negative controls. A total of 2×10^5 transfected cells was plated on a 6-cm-diameter petri dish. Cells were counted from 1 to 5 d. Samples were counted in doublets in a total of three independent experiments. Cell viability was evaluated by a trypan blue exclusion test.

One of the classic features of apoptosis is the cleavage of genomic DNA into oligonucleosomal fragments represented by multiples of 180–200 bp. Genomic DNA was isolated from BMMCLs by the QIAamp DNA Mini kit (QIAGEN), according to the manufacturer's directions, and prepared samples were incubated with RNase A (Fermentas) at a final concentration of 10 μg/ml for 1 h at 37°C. DNA integrity was evaluated by electrophoresis in 1.5% agarose gel in 40 mM Tris-acetate/1 mM EDTA buffer. For staining, we used GelRed Nucleic Acid Gel Stain (Biotium). GeneRuler 1 kb Plus DNA Ladder 75 to 20,000 bp (Thermo Scientific) was used for DNA sizing. Apoptosis was induced in control BMMCLs by treating cells with 10 μM 17-(allylamino)-17-demethoxygeldanamycin (Sigma) for 24 h.

Microtubule regrowth

Microtubule regrowth from centrosomes was followed in a nocodazole-washout experiment. BMMCLs in complete medium were overlaid on fibronectin-coated coverslips (6) and allowed to attach for 1 h at 37°C. Cells were then treated with nocodazole at a final concentration of 10 μM for 50 min at 37°C to depolymerize microtubules. Cells were washed with medium precooled to 4°C (3 × 5 min each) to remove the drug, and microtubule regrowth was allowed for 1–6 min at 26°C. To test the effect of pervanadate, cells treated with 10 μM nocodazole for 40 min at 37°C were transferred into medium containing 10 μM nocodazole and freshly prepared pervanadate. After 10 min of incubation at 37°C, cells were washed (2 × 2 min each) with precooled medium, and microtubule regrowth was allowed in the presence of pervanadate. Samples were fixed in cold methanol, air-dried, and washed in PBS before immunostaining (27). In some cases, nocodazole-washout experiments were performed in the absence of both extracellular and intracellular Ca^{2+}. Cells in complete medium were treated with nocodazole (10 μM, 40 min, at 37°C), transferred into Ca^{2+}- and serum-free medium supplemented with 5 μM BAPTA-AM and 10 μM nocodazole, and incubated for 10 min at 37°C to deplete intracellular Ca^{2+}. After washing in cold Ca^{2+}- and serum-free medium to remove the drug, microtubule regrowth was allowed for 1–6 min at 26°C in Ca^{2+}- and serum-free medium containing 5 μM BAPTA-AM. The nocodazole-washout experiment also was performed in the absence of extracellular Ca^{2+} only. In control experiments, Ca^{2+}- and serum-free medium was substituted for serum-free medium with 1.8 mM Ca^{2+}.

Immunofluorescence microscopy

Immunofluorescence staining was performed as described (27). To visualize centrosomes and microtubules in fixed cells, coverslips were incubated with mAb TU-30 (spent culture supernatant diluted 1:5) and rabbit Ab to α-tubulin (diluted 1:150). Anti-mouse DY549-conjugated Ab was diluted 1:800, and anti-rabbit DY488-conjugated Ab was diluted 1:300. The preparations were mounted in MOWIOL 4-88 (Calbiochem), supplemented with 4,6-diamidino-2-phenylindole (Sigma), and examined on an Olympus Scan^R system (Olympus) equipped with Acquisition Scan^R program and an oil-immersion objective 60×/1.4 NA. Huygens Deconvolution Software (Scientific Volume Imaging) was used for preparation of immunofluorescence figures.

Quantification of the microtubule regrowth assay was performed on a large number of cells that were selected automatically and compared with the quantification of cells selected manually to confirm the reliability of the automatic method. In the course of automatic quantification, 36 areas/sample were taken in both fluorescence channels, and optical z-sections were acquired at 0.3-μm steps. Maximum intensity projection of γ-tubulin staining was used to identify the position of centrosomes. The sum of α-tubulin immunofluorescence intensities was generated by Sum Slices projection in ImageJ software (National Institutes of Health). The α-tubulin fluorescent signal near the centrosome was measured in separate concentric circles centered at the centrosome with radii of 1, 1.5, and 2 μm (regions of interest; ROIs). Background fluorescence using circles of corresponding sizes was subtracted from each measurement. Measurements were made using ImageJ. In manually performed analyses, only images of cells with a homogenous background around the centrosomes were selected. The sum of α-tubulin immunofluorescence intensities was obtained from 11 consecutive frames (0.2-μm steps), with the middle frame chosen with respect to the highest γ-tubulin intensity. For statistical analysis, the two-tailed, unpaired Student *t* test was used to compare samples and to obtain *p* values.

Live-cell imaging

BMMCL-γTb expressing mGIT1-GFP, mβPIX-GFP, or GFP-COX8 tags were plated on 35-mm glass-bottom culture dishes (MatTek; P35G-1.5-14-C) precoated with fibronectin (6), and cells were allowed to attach for 1 h at 37°C. Cells were washed and subsequently incubated in medium for live-cell imaging (RPMI 1640 without phenol red, riboflavin, folic acid, pyridoxal, $Fe[NO_3]_3$) supplemented with 20 mM HEPES. Cells were imaged on the Delta Vision Core system (Applied Precision) equipped with a 60×/1.42 NA oil-immersion objective. Optical z-sections were acquired in 0.3-μm steps.

Results

Proteins βPIX and GIT1 interact with γ-tubulin and associate with centrosomes in BMMCLs

We showed previously that, in FcεRI- or pervanadate-activated BMMCLs or $Lyn^{-/-}$ BMMCLs, γ-tubulin interacts with a similar set of tyrosine-phosphorylated proteins (5). In an attempt to identify these proteins, we applied large-scale immunoprecipitation coupled with mass spectrometry (MS). Lysates from pervanadate-activated cells were immunoprecipitated with anti-peptide mAb to γ-tubulin, and the bound proteins were eluted with peptide used for immunization. Eluted proteins were concentrated on the immobilized GST-SH2 domain of Fyn kinase, which effectively binds tyrosine-phosphorylated proteins (23). Bound proteins were separated on SDS-PAGE and subjected to MALDI/MS fingerprint analysis. Because slightly higher recovery of tyrosine-phosphorylated proteins associated with γ-tubulin was observed from activated $Lyn^{-/-}$ BMMCLs (5), we used these cells for MALDI/MS fingerprint analysis. Of the three independent experiments, βPIX (also known as Rho guanine nucleotide exchange factor 7, Arhgef7, β-Pix, COOL-1; gene name *Arhgef7*; Swiss-Prot identifier Q9ES28) was identified three times. A typical example of MS identification is shown in Supplemental Table I.

In cells, βPIX forms complexes with GITs, which are GTPase-activating proteins for the ADP-ribosylation factor family of small GTP-binding proteins (28). Such complexes might serve as scaffolds to bring together signaling molecules affecting various cellular processes, including cytoskeletal organization (29). To ascertain whether βPIX or GIT1 associates with γ-tubulin in $Lyn^{-/-}$ BMMCL cells, immunoprecipitation experiments were performed with Abs to βPIX and GIT1. Immunoblot analysis revealed the coprecipitation of γ-tubulin with both βPIX (Fig. 1A, *lane 3*) and GIT1 (Fig. 1B, *lane 3*). In addition, reciprocal precipitation with Ab to γ-tubulin confirmed an interaction between both βPIX (Fig. 1F, *lane 3*)

and GIT1 (Fig. 1I, *lane 3*) with γ-tubulin. As expected, Ab to βPIX coprecipitated GIT1 (Fig. 1G, *lane 3*), and Ab to GIT1 coprecipitated βPIX (Fig. 1E, *lane 3*). Immunoblot analysis revealed that GIT2 also interacted with γ-tubulin (Supplemental Fig. 1A, *lane 3*). Negative-control mAb of IgG2b class or rabbit polyclonal Ab did not precipitate GIT1, βPIX, or γ-tubulin (Supplemental Fig. 1D). No association of γ-tubulin with βPIX and GIT1 was detected when precipitation with anti-peptide Ab to γ-tubulin was performed in the presence of immunizing peptide (data not shown). Immunoprecipitation experiments also confirmed interactions between γ-tubulin and βPIX, GIT1, or GIT2 in BMMCLs, proving that the association of γ-tubulin with these proteins is not restricted to cells with depleted Lyn kinase (data not shown). To independently confirm the interaction of γ-tubulin with βPIX and GIT1, immunoprecipitation experiments were performed with BMMCL-γTb. Precipitation with anti-RFP Ab revealed the coprecipitation of endogenous βPIX (Fig. 1J, *lane 3*) and GIT1 (Fig. 1K, *lane 3*). Precipitation of γ-tubulin–TagRFP is shown in Fig. 1L (*lane 3*). Immunoblot analysis also revealed that GIT2 was coprecipitated by anti-RFP Ab (Supplemental Fig. 1B, *lane 3*). Multiple phosphorylation sites were identified on hGIT1 (30). To determine whether GIT1 can be phosphorylated on tyrosine in activated BMMCLs or $Lyn^{-/-}$ BMMCLs, as well as whether tyrosine-phosphorylated GIT1 interacts with γ-tubulin, pervanadate-activated cells were precipitated with Abs to γ-tubulin and GIT1. Blots were probed with Abs to P-Tyr and GIT1. Both Abs precipitated P-Tyr proteins from both cell lines (Fig. 1M, *lanes 1, 2*), which were stained with Ab to GIT1 (Fig. 1N, *lanes 1, 2*). Negative-control Abs did not precipitate tyrosine-phosphorylated GIT1 from activated cells (data not shown). Thus, tyrosine-phosphorylated GIT1 from pervanadate-activated cells is capable of interacting with γ-tubulin. Similar, but less profound, results were obtained after activation of the cells by aggregation of FcεRI (data not shown). To decide whether γ-tubulin and βPIX or GIT1 protein appear in the form of complexes, BMMCL extracts were subjected to gel-filtration chromatography on the Superose 6 column. γ-Tubulin was distributed through a large zone in complexes of various sizes. Large complexes of ~2 MDa could represent γTuRCs. Importantly, βPIX and GIT1 also were present in the complexes, and their distribution partially overlapped with γ-tubulin. In contrast, control actin was only found in low molecular mass fractions (Supplemental Fig. 1C). Immunoprecipitation experiments with anti–γ-tubulin Ab from fractions containing GIT1 and PIX (fractions 24–26 in Supplemental Fig. 1C) revealed the formation of complexes between γ-tubulin and these proteins (data not shown). Isotype controls for immunoprecipitation experiments are shown in Supplemental Fig. 1D.

For the localization of centrosomes in live cells, BMMCL-γTb were used. The TagRFP-tagged γ-tubulin marked centrosomes and properly nucleated microtubules as documented by microtubule staining of mitotic cells (Fig. 2A–C). Because βPIX (tv3) is the most abundant variant in BMMCLs (V. Sládková, unpublished observations), GFP-tagged mβPIX (tv3) was expressed in BMMCL-γTb. Live-cell imaging revealed the association of βPIX with centrosomes of interphase BMMCLs. Moreover, diffuse staining of the cytoplasm was observed (Fig. 2D–F). Similarly, GFP-tagged GIT1 localized to centrosomes, and granular staining in cytoplasm was detected (Fig. 2G–I). Nocodazole treatment did not affect GIT1 localization on the centrosome, indicating no requirement for intact microtubules (data not shown). In control cells expressing GFP-tagged mitochondrial marker, no association of the expressed protein with the centrosome was detected (Fig. 2J–L). Collectively, the data suggest that βPIX and GITs form complexes with γ-tubulin and that βPIX and GIT1 associate with centrosomes in BMMCLs.

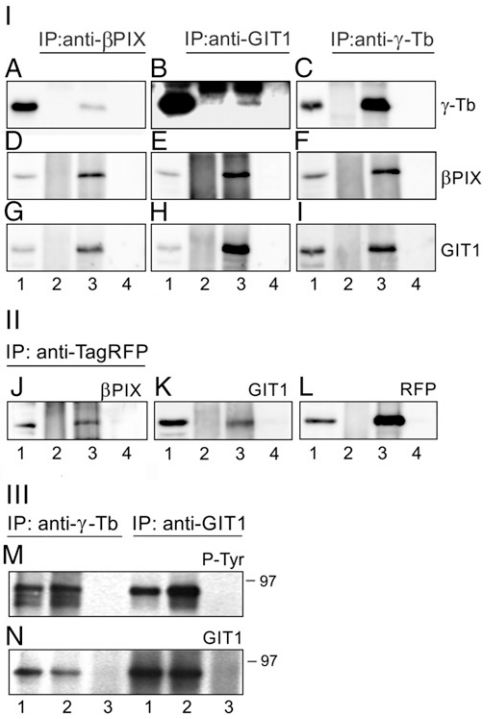

FIGURE 1. γ-Tubulin interacts with βPIX and GIT1 in mast cells. (**A–I**) γ-Tubulin coprecipitates with βPIX and GIT1 in $Lyn^{-/-}$ BMMCLs. Extracts were precipitated with Protein A–immobilized Abs specific to βPIX (A, D, and G), GIT1 (B, E, and H), or γ-tubulin (C, F, and I). Blots were probed with Abs to γ-tubulin (γ-Tb), βPIX, or GIT1. Load (*lane 1*), immobilized Abs not incubated with cell extract (*lane 2*), immunoprecipitated proteins (*lane 3*), and protein A without Abs, incubated with cell extracts (*lane 4*). (**J–L**) TagRFP-tagged γ-tubulin associates with βPIX and GIT1 in BMMCLs. Extracts from BMMCL-γTb were precipitated with Protein A–immobilized Abs specific to RFP (J–L). Blots were probed with Abs to βPIX (J), GIT1 (K), and RFP (L). Load (*lane 1*), immobilized Abs not incubated with cell extract (*lane 2*), immunoprecipitated proteins (*lane 3*), and protein A without Abs, incubated with cell extracts (*lane 4*). In (J), one quarter of the load was applied compared with (K) and (L). (**M** and **N**) GIT1 is a substrate for protein tyrosine kinases in activated $Lyn^{-/-}$ BMMCLs and BMMCLs. Extracts from pervanadate-activated $Lyn^{-/-}$ BMMCLs (*lane 1*) or BMMCLs (*lane 2*) were precipitated with Protein A–immobilized Abs specific to γ-tubulin or GIT1. Immobilized Abs not incubated with cell extracts (*lane 3*). Blots were probed with Abs to P-Tyr (M) and GIT1 (N). Lines on the *right* indicate the positions of molecular mass markers (in kDa).

Ca^{2+} level affects γ-tubulin properties and its interaction with GITs and GCPs in BMMCLs

During the immunoprecipitation experiments, we noticed that Ca^{2+} affects the association of γ-tubulin with GITs and GCPs. When BMMCLs were cultivated for 30 min in serum- and Ca^{2+}-free medium to which Ca^{2+} was freshly added to a final concentration of 1.8 mM, more GIT1 (Fig. 3A) or GIT2 (Fig. 3A) coprecipitated with γ-tubulin. Similarly, more GCP2 (Fig. 3A) or GCP4 (Fig. 3A) was associated with γ-tubulin in the presence of Ca^{2+}. No substantial changes in the amount of βPIX associated with γ-tubulin were observed in the presence or absence of Ca^{2+} (Fig. 3A, βPIX), and actin (negative control) did not coprecipitate with γ-tubulin (Fig. 3A, Actin). Interestingly, two protein bands with different electrophoretic mobilities were detected in γ-tubulin immunoprecipitates from extracts containing Ca^{2+}: an upper band with slow mobility and a lower band with fast mobility. Sometimes, three closely spaced γ-tubulin bands were detected in the presence of Ca^{2+}. This was an unexpected finding because no

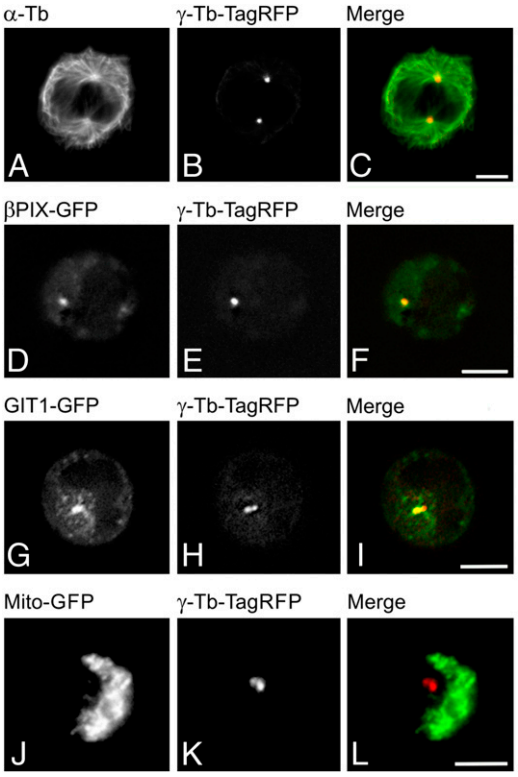

FIGURE 2. Subcellular localization of GFP-tagged βPIX and GIT1 in BMMCLs. Mitotic BMMCL-γTb stained for α-tubulin (**A**) to visualize localization of TagRFP-tagged γ-tubulin (**B**). (**C**) Superposition of images (α-tubulin, green; γ-tubulin, red), methanol-fixed cells. Localization of βPIX-GFP (**D**) and γ-tubulin–TagRFP (**E**) in live BMMCL-γTb cells. (**F**) Superposition of images (βPIX, green; γ-tubulin, red). Localization of GIT1-GFP (**G**) and γ-tubulin–TagRFP (**H**) in live BMMCL-γTb. (**I**) Superposition of images (GIT1, green; γ-tubulin, red). Localization of control mitochondrial Mito-GFP (**J**) and γ-tubulin-TagRFP (**K**) in live BMMCL-γTb. (**L**) Superposition of images (Mito-GFP, green; γ-tubulin, red). In (D)–(L), the best centrosomal plane is shown. Scale bars, 5 μm.

such split in γ-tubulin electrophoretic mobilities was observed in loads (Fig. 3A, γ-Tb). Comparable results from immunoprecipitation experiments were obtained when Ca^{2+} was added to cell extracts. Moreover, Ca^{2+} similarly affected the electrophoretic mobility of γ-tubulin immunoprecipitated from BMMCs (data not shown). Negative-control Abs did not precipitate βPIX, GIT1, GIT2, γ-Tb, GCP2, or GCP4 from lysates containing Ca^{2+} (data not shown).

Immunoprecipitation experiments with Ab to γ-tubulin also were performed with extracts obtained from cells incubated with ionomycin, an effective Ca^{2+} ionophore, in the presence or absence of Ca^{2+}. In the absence of Ca^{2+}, ionomycin did not affect the mobility of γ-tubulin and coprecipitation of GCP2 and GCP4 with γ-tubulin. However, in the presence of ionophore and Ca^{2+}, large amounts of GCP4 coprecipitated with γ-tubulin. Under such conditions the amount of coprecipitated GCP2 increased only slightly, and the amount of modified γ-tubulin was basically unchanged (Supplemental Fig. 1E).

When TagRFP–γ-tubulin was precipitated in the presence of Ca^{2+}, slow-migrating electrophoretic variants of tagged γ-tubulin were detected (Fig. 3B, *lane 3*). Together, these data suggest that Ca^{2+} modulates the interaction of γ-tubulin with GITs and GCPs in BMMCLs and that both endogenous and exogenous γ-tubulin concentrated by immunoprecipitation is affected by an increased concentration of Ca^{2+} in BMMCLs.

C-terminal region of γ-tubulin is essential for Ca^{2+}-dependent changes in γ-tubulin

To obtain deeper insight into the γ-tubulin region that is sensitive to Ca^{2+}, we performed experiments with truncated γ-tubulins. For this, we used human γ-tubulin 1, which shows 99% identity with mouse γ-tubulin 1 (20). First, we immobilized 6xHis-tagged whole-length γ-tubulin (aa 1–451) or its truncated constructs covering aa regions 1–225 and 223–451 on Ni-NTA agarose and incubated them with BMMCL extracts in the presence or absence of Ca^{2+}. The shift in electrophoretic mobility of γ-tubulin was observed in the C-terminal part of the molecule (Fig. 4A). When γ-tubulin was incubated with Ca^{2+} in the absence of extract, no mobility shift was observed (Fig. 4A, Control). Next, we prepared EGFP-tagged versions of γ-tubulin truncated from the C-terminal end of molecules containing α-helixes H11 (aa 385–400) and H12 (aa 419–437), which are exposed on the surface of the molecule (Protein Data Bank ID: 3CB2). A schematic diagram of the used constructs is depicted in Fig. 4B. The EGFP-tagged proteins covering γ-tubulin aa regions 1–382, 1–422, 1–440, and 1–451

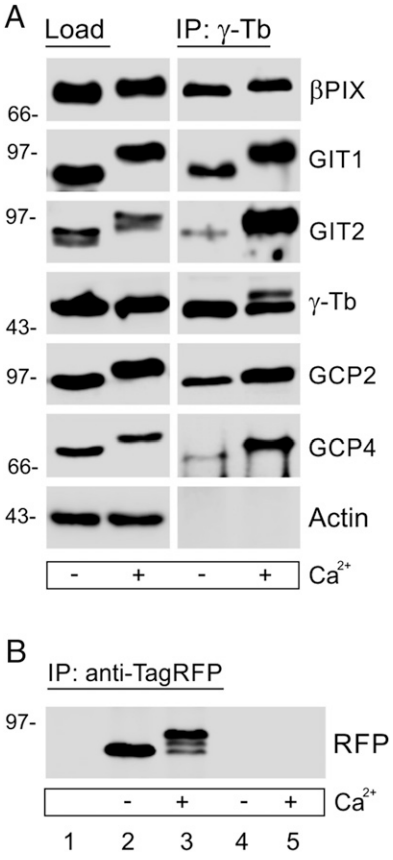

FIGURE 3. Effect of Ca^{2+} on coimmunoprecipitation of proteins with γ-tubulin. (**A**) Ca^{2+} stimulates coprecipitation of GITs and GCPs with γ-tubulin. BMMCLs were preincubated in the presence or absence of 1.8 mM Ca^{2+}, and extracts were precipitated with Ab to γ-tubulin immobilized on Protein A. Blots were probed with Abs to βPIX, GIT1, GIT2, γ-tubulin (γ-Tb), GCP2, GCP4, or actin. Note the change in electrophoretic mobility of precipitated γ-tubulin and the higher amount of coprecipitated GIT1, GIT2, GCP2, and GCP4 in the presence of Ca^{2+}. (**B**) Ca^{2+} affects the electrophoretic mobility of TagRFP-tagged γ-tubulin. Extracts from BMMCL-γTb were supplemented or not with 0.8 mM Ca^{2+} and precipitated with Ab to RFP immobilized on protein A. Blot was probed with Ab to RFP. Immobilized Ab not incubated with cell extract (*lane 1*), immunoprecipitated proteins (*lanes 2* and *3*), and protein A without Ab, incubated with cell extract (*lanes 4* and *5*). Lines on the *left* indicate the positions of the molecular mass markers (in kDa).

were precipitated from HEK-293 lysates using GFP-trap; after thorough washing, immobilized constructs were incubated with BMMCL extracts in the presence or absence of Ca^{2+}. Although electrophoretic mobilities were basically not affected in truncated γ-tubulins (aa 1–382 or 1–422), a Ca^{2+}-dependent shift in mobility was seen in whole-length γ-tubulin and in truncated γ-tubulin (aa 1–440) (Fig. 4C). When the EGFP-tagged γ-tubulin C-terminal region (aa 378–451) was used, a shift in electrophoretic mobility was detected, whereas the EGFP-tagged C-terminal region of α-tubulin (aa 378–451) was not affected (Fig. 4D). Mg^{2+} or Zn^{2+} ions were not capable of forming γ-tubulin variants; when EGTA was added to deplete Ca^{2+}, the generation of slow-migrating γ-tubulin forms was inhibited. Generation of γ-tubulin electrophoretic variants in the presence of Ca^{2+} also was observed when lysates from BMMCs were used in pull-down experiments (data not shown). Altogether, these findings indicate that the C-terminal region of γ-tubulin (aa 423–451) is essential for Ca^{2+}-dependent changes in γ-tubulin in the presence of BMMCL or BMMC extracts.

Ca^{2+} modulates the interaction of βPIX with the C-terminal region of γ-tubulin

In HEK cells expressing either GFP-tagged whole-length (aa 1–451) or truncated (aa 1–382) γ-tubulin, anti-βPIX and anti-GIT1 Abs coprecipitated GFP-tagged whole-length γ-tubulin. Coprecipitation of the truncated form of γ-tubulin was undetectable or it was substantially lower (Fig. 5A). This indicated that the C-terminal region of γ-tubulin is important for the interaction with βPIX and GIT1. Because Ca^{2+} affected the interactions of GIT1 with γ-tubulin and also generated changes in the C-terminal domain of γ-tubulin, we evaluated the possibility that Ca^{2+} might modulate the binding of GIT1 and βPIX to the γ-tubulin C-terminal region. The pull-down experiments were performed with the GST-tagged C-terminal part of γ-tubulin (aa 362–451) and BMMCL extracts in the presence or absence of Ca^{2+}. βPIX associated with the GST-tagged γ-tubulin domain, but its binding was inhibited in the presence of Ca^{2+}. In contrast, GIT1 bound to the GST-fusion protein both in the absence and presence of Ca^{2+}. Actin (negative control) did not bind to the GST-tagged γ-tubulin domain, and no binding of GIT1 or βPIX was observed when GST alone was used in the pull-down assay (Fig. 5B). These findings suggest that Ca^{2+} adversely affects the interaction of βPIX with the C-terminal region of the γ-tubulin molecule in BMMCLs.

Nucleation of microtubules in BMMCLs is affected by Ca^{2+} and cell activation

To evaluate the possibility that the Ca^{2+} level affects microtubule assembly from centrosomes, we performed the nocodazole-washout assay. Microtubules were depolymerized with nocodazole and allowed to grow in the absence of the drug. To perform microtubule regrowth in the absence of both intracellular and extracellular Ca^{2+}, cells were preincubated with BAPTA-AM, which depleted intracellular Ca^{2+}. Cells for analysis were selected either manually or automatically. The α-tubulin fluorescence of microtubule asters was measured in ROIs centered at centrosomes that were marked by staining for γ-tubulin immunofluorescence, as previously described (13). In control cells, a clearly visible microtubule array, originating from the centrosomes, appeared after 3 min (Fig. 6Aa), and a fully developed microtubule array was detected after 4 min. In the absence of both extracellular and intracellular Ca^{2+}, only small microtubule asters were formed after 3 min of microtubule regrowth (Fig. 6Ac), and a fully developed microtubule array was observed after 6 min. Statistical evaluation of α-tubulin fluorescence in ROIs with diameters of 1, 1.5, or 2 μm after manual selection documented clear differences between regrowth in control

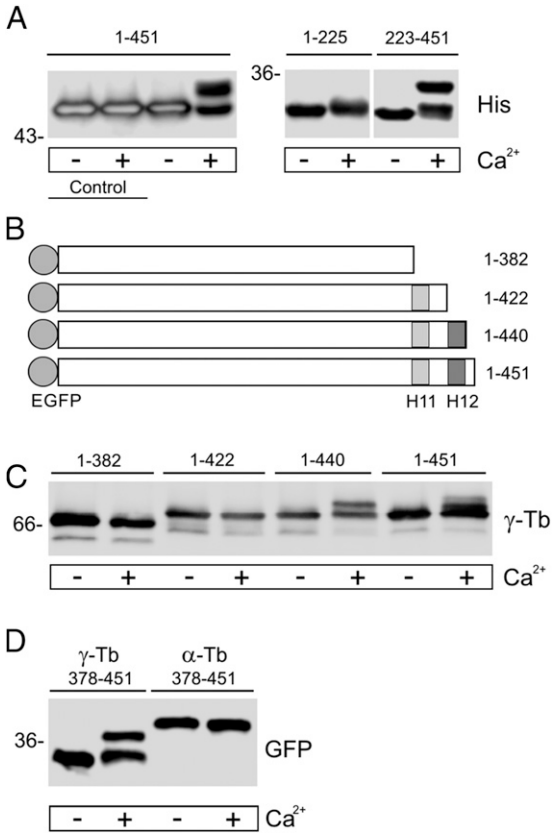

FIGURE 4. Ca^{2+}-dependent changes in electrophoretic mobility of γ-tubulin C-terminal domain. Immobilized tagged human γ-tubulin fragments were incubated with BMMCL extracts in the presence or absence of 0.8 mM Ca^{2+} for 30 min at 37°C before immunoblotting. (**A**) 6xHis-tagged human whole-length γ-tubulin or its fragments encoding aa regions 1–225 and 223–451 immobilized on Ni-NTA agarose and immunoblotted with Ab to 6xHis. Extracts were not added in the Control. (**B**) Schematic diagram of the constructs used. Positions of helixes H11 (gray) and H12 (dark gray) are highlighted. (**C**) EGFP-tagged truncated forms of human γ-tubulin encoding aa regions 1–382, 1–422, 1–440, and full-length γ-tubulin (1–451) immobilized on GFP-trap and immunoblotted with Ab to γ-tubulin (γ-Tb). (**D**) EGFP-tagged human γ-tubulin or α-tubulin fragments encoding aa regions 378–451 immobilized on GFP-trap and immunoblotted with Ab to GFP. Lines on the *left* indicate the positions of molecular mass markers (in kDa).

and Ca^{2+}-depleted cells (Fig. 6B). Similar results were obtained when analysis was performed on a large number of cells selected automatically (data not shown). When Ca^{2+} was absent only in the medium, a delay in microtubule regrowth was also observed (data not shown). When cells were activated by pervanadate, a potent protein tyrosine phosphatase inhibitor that mimics, in part, the stimulatory effect of Ag (31), microtubule regrowth was increased (Fig. 6C). The extent of microtubule regrowth could be modulated by mechanisms regulating either microtubule nucleation or microtubule dynamics. It was reported previously that microtubule dynamics is regulated at the cell periphery (32) and that a delay in microtubule regrowth is associated with defects in microtubule nucleation (13, 33). Together, these data suggest that both Ca^{2+} level and cell activation affect microtubule nucleation in BMMCLs.

Opposite regulatory roles of βPIX and GIT1 in nucleation of microtubules in BMMCLs

Because βPIX and GIT1 interact with γ-tubulin, we compared microtubule regrowth from centrosomes in BMMCLs with a re-

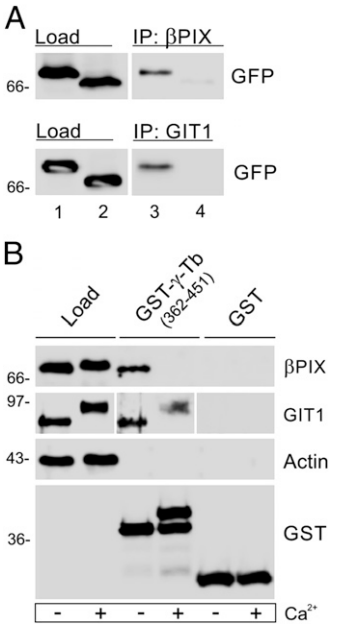

FIGURE 5. Effect of Ca^{2+} on βPIX and GIT1 binding to the C-terminal domain of γ-tubulin. (**A**) βPIX and GIT1 interact with whole-length γ-tubulin but not with its truncated form lacking a C-terminal region. Extracts from HEK cells expressing either GFP-tagged whole-length (aa 1–451; *lanes 1* and *3*) or truncated (aa 1–382; *lanes 2* and *4*) γ-tubulin were precipitated with Protein A–immobilized Abs specific to βPIX or GIT1. Blots were probed with Ab to GFP. Loads (*lanes 1* and *2*), immunoprecipitated proteins (*lanes 3* and *4*). (**B**) Binding of βPIX to the C-terminal region of γ-tubulin is affected by Ca^{2+}. Extracts from BMMCLs (Load) were incubated in the presence or absence of 0.8 mM Ca^{2+} with the GST-tagged C-terminal region of γ-tubulin (aa 362–451) or GST alone immobilized on glutathione-Sepharose beads. Blots of bound proteins were probed with Abs to βPIX, GIT1, actin, or GST. Lines on the *left* indicate the positions of molecular mass markers (in kDa).

duced level of βPIX or GIT1 in nocodazole-washout experiments. The βPIX- and GIT1-deficient cells were produced using lentiviral vectors. A typical result of immunoblotting experiments after depletion of βPIX or GIT1 is shown in Fig. 7A and Fig. 7B, respectively. At the best silencing, the amount of βPIX in βPIX-KD1 cells reached 14.7 ± 2.9% and the amount of GIT1 in GIT1-KD1 cells was 10.7 ± 2.8% (mean ± SD; $n = 5$) compared with the expression level in control cells with an empty pLKO.1 vector. Three independent experiments were performed with selected stable cells with reduced levels of βPIX, GIT1, and corresponding control cells. α-Tubulin immunofluorescence was measured at 1.5 min after washout in a 1.0-μm ROI. Control experiments revealed similar nucleation of microtubules when empty pLKO.1 vector or pLKO.1 vector with nontarget shRNA (pLKO.1-NT) was used (Supplemental Fig. 2H). Results of regrowth experiments are presented after analysis of a large number of cells selected automatically, but similar results were obtained after the analysis of a limited number of cells selected manually.

βPIX depletion resulted in an increase in microtubule regrowth (Fig. 7C). Typical staining of α-tubulin in control cells and βPIX-depleted cells is shown in Supplemental Fig. 2Ab and 2Ac, respectively. The increase in microtubule regrowth also was observed in cells with a lower level of βPIX depletion, denoted βPIX-KD2 (Supplemental Fig. 2B). For phenotypic rescue experiments, two silent point mutations were introduced into hβPIX to prevent its depletion by the shRNA. Rescue experiments revealed that the introduction of hβPIX to BMMCLs with depleted mβPIX levels led to restoration of nucleation capacity, as in control cells (Fig. 7D). Microtubule regrowth after control βPIX depletion in rescue experiments is shown in Supplemental Fig. 2C, and an immunoblot from the rescue experiment is shown in Supplemental Fig. 2D.

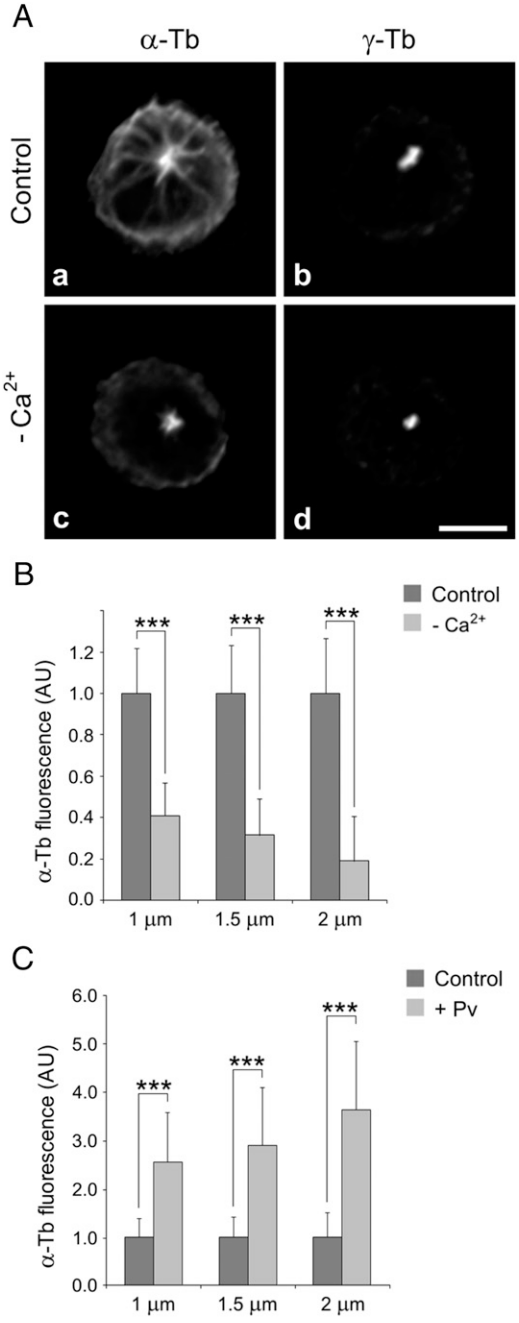

FIGURE 6. Effect of Ca^{2+} depletion and cell activation on microtubule regrowth. (**A**) Double-labeling of α-tubulin (**a** and **c**) and γ-tubulin (**b** and **d**) in a microtubule regrowth experiment in the presence or absence of Ca^{2+}. Both extracellular and intracellular Ca^{2+} were depleted, and cells were fixed at 3 min of microtubule regrowth. Scale bar, 5 μm. (**B**) Statistical analysis of α-tubulin fluorescence intensity in 1-, 1.5-, and 2-μm ROIs of BMMCLs nucleated in the absence of Ca^{2+} relative to BMMCLs nucleated in the presence of Ca^{2+}. Four independent experiments were performed, each involving 30 control cells and 30 Ca^{2+}-depleted cells (- Ca^{2+}). Data are mean ± SD ($n = 120$). (**C**) Statistical analysis of α-tubulin fluorescence intensity in 1-, 1.5-, and 2-μm ROIs of pervanadate-activated BMMCLs relative to unstimulated BMMCLs. Cells were fixed at 2.5 min of microtubule regrowth. Three independent experiments were performed, each involving 40 control cells and 40 pervanadate-activated cells (+ Pv). Data are mean ± SD ($n = 120$). ***$p < 0.001$.

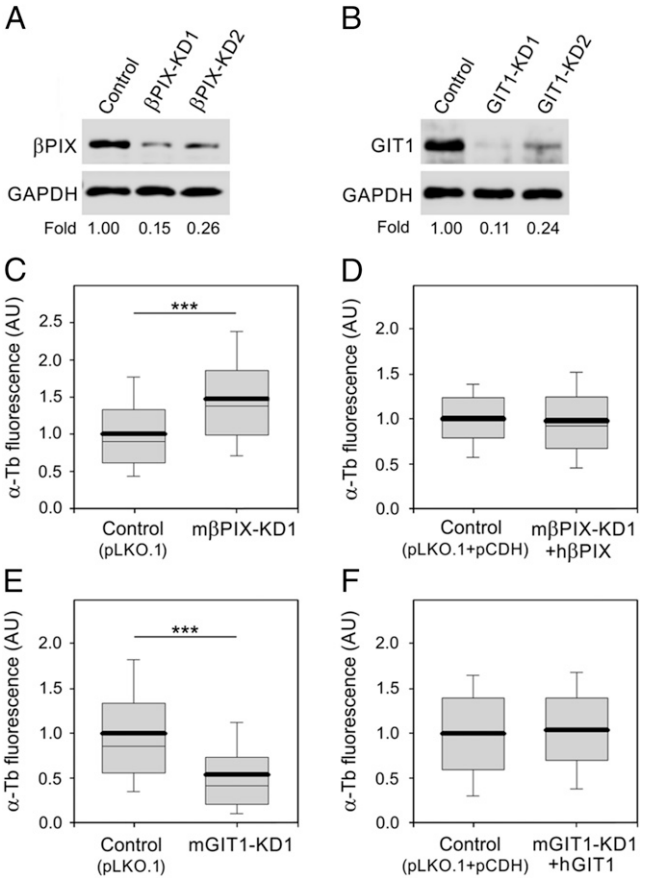

FIGURE 7. βPIX and GIT1 depletion affects microtubule regrowth. (**A**) Immunoblot analysis of cells with reduced levels of βPIX. Whole-cell lysates from cells infected with empty pLKO.1 vector (Control) or from cells selected after the knockdown of βPIX by shRNA1 (βPIX-KD1) or shRNA2 (βPIX-KD2). (**B**) Immunoblot analysis of cells with reduced levels of GIT1. Whole-cell lysates from cells infected with empty pLKO.1 vector (Control) or from cells selected after knockdown of GIT1 by shRNA1 (GIT1-KD1) or by shRNA2 (GIT1-KD2). Numbers under the blots indicate the relative amounts of βPIX (A) or GIT1 (B) normalized to control cells and to the amount of GAPDH in individual samples (Fold). (**C**–**F**) Distribution of α-tubulin fluorescence intensities (arbitrary units [AU]) in 1-μm ROI at 1.5 min of microtubule regrowth are shown as box plots (three independent experiments, >700 cells counted for each experimental condition). (C) Box plot of βPIX-depleted cells (mβPIX-KD1; $n = 4501$) relative to control cells (Control, pLKO.1; $n = 2788$). (D) Box plot of βPIX-depleted cells rescued by hβPIX (mβPIX-KD1 + hβPIX; $n = 2269$) relative to control cells (Control, pLKO.1 + pCDH; $n = 2645$). (E) Box plot of GIT1-depleted cells (mGIT1-KD1; $n = 3641$) relative to control cells (Control, pLKO.1, $n = 2938$). (F) Box plot of mGIT1-depleted cells rescued by hGIT1 (mGIT1-KD1 + hGIT1; $n = 4503$) relative to control cells (Control, pLKO.1 + pCDH; $n = 2,688$). In (C)–(F), bold and thin lines within the box represent the mean and median (the 50th percentile), respectively. The bottom and top of the box represent the 25th and 75th percentiles. Whiskers below and above the box indicate the 10th and 90th percentiles. $***p < 1 \times 10^{-15}$.

The data obtained suggest that βPIX represents a negative regulator of microtubule nucleation from the centrosomes in BMMCLs.

In contrast, GIT1 depletion resulted in a decrease in microtubule regrowth (Fig. 7E). Typical staining of α-tubulin in GIT1-depleted cells is shown in Supplemental Fig. 2Ad. The decrease in microtubule nucleation also was observed in cells with a lower level of GIT1 depletion, denoted GIT1-KD2 (Supplemental Fig. 2E). Rescue experiments confirmed that the introduction of hGIT1 into BMMCLs with a reduced level of mGIT1 restored nucleation capacity to that observed in control cells (Fig. 7F). Microtubule regrowth after control GIT1 depletion in rescue experiments is shown in Supplemental Fig. 2F, and an immunoblot from the rescue experiment is shown in Supplemental Fig. 2G. These experiments indicate that GIT1 represents a positive regulator of microtubule nucleation from the centrosomes in BMMCLs. Altogether, the results of these experiments suggest that βPIX and GIT1 differentially regulate microtubule nucleation.

Differential effect of βPIX and GIT1 depletion on degranulation and cell motility

We performed immunoprecipitation experiments to evaluate how the depletion of mβPIX affects the interaction of GIT1 with γ-tubulin, as well as how the depletion of GIT1 affects the interaction of βPIX with γ-tubulin. Although decreased levels of βPIX had no effect on the interaction between mGIT1 and γ-tubulin (Fig. 8A, *lanes 4, 5*, GIT1), depletion of GIT1 led to the increased association of βPIX with γ-tubulin (Fig. 8B, *lanes 4, 5*, βPIX). These results indicate that GIT1 modulates the formation of γ-tubulin/βPIX complexes.

Because microtubules are important for cell proliferation and survival, we assessed how depletion of βPIX or GIT1 affects these processes. Proliferation of βPIX-depleted cells was comparable to negative-control cells (pLKO.1 and pLKO.1-NT). In contrast, depletion of GIT1 resulted in partial inhibition of proliferation (Supplemental Fig. 3A). The viability of cells in the evaluated time interval was >99, >99, >98, and >95% for pLKO.1, pLKO.1-NT, βPIX-depleted cells, and GIT1-depleted cells, respectively. No differences between control cells (pLKO.1 and pLKO.1-NT) and βPIX- or GIT1-depleted cells were detected when genomic DNAs were analyzed for the presence of oligonucleosomal fragments characteristic of apoptotic cells (Supplemental Fig. 3B).

Finally, we measured the role of GIT1 and βPIX in Ag-induced chemotaxis and degranulation. Data in Fig. 9A show that cells with reduced GIT1 exhibited a significantly stronger Ag-mediated chemotactic response than did the control cells. In contrast, βPIX-depleted cells showed a less efficient chemotactic response. Interestingly, the general migration of GIT1-deficient cells also was enhanced, as indicated by the greater migration of cells in the absence of Ag (Fig. 9A, Control). Rescue experiments confirmed that the introduction of hGIT1 into BMMCLs with a reduced level of mGIT1 restored the chemotactic response to that observed in control cells. Similarly, the chemotactic response was rescued after the introduction of hβPIX into BMMCLs with a reduced level of mβPIX (Fig. 9A, Ag). In contrast to chemotaxis, cells with depleted GIT1 exhibited reduced degranulation, whereas βPIX-deficient cells showed significantly higher degranulation compared with control cells (Fig. 9B). Similar results were obtained when pLKO.1 or pLKO.1-NT were used as negative controls (Supplemental Fig. 3C). Two cell lines with reduced GIT1 (GIT1-KD1, GIT1-KD2) gave comparable results in the degranulation assay. Similarly, no statistically significant differences were detected in degranulation between two cell lines with reduced βPIX (βPIX-KD1, βPIX-KD2) (Supplemental Fig. 3C). Rescue experiments confirmed that introduction of hGIT1 into BMMCLs with reduced levels of mGIT1 restored degranulation to that observed in control cells. Degranulation also was recovered after the introduction of hβPIX into BMMCLs with a reduced level of mβPIX (Fig. 9B). Altogether, the results suggest that βPIX and GIT1 differentially regulate Ag-induced chemotaxis and degranulation in BMMCs.

Discussion

Ag-induced activation of mast cells leads to rapid cytoskeleton rearrangements and degranulation. Accumulating data point to the

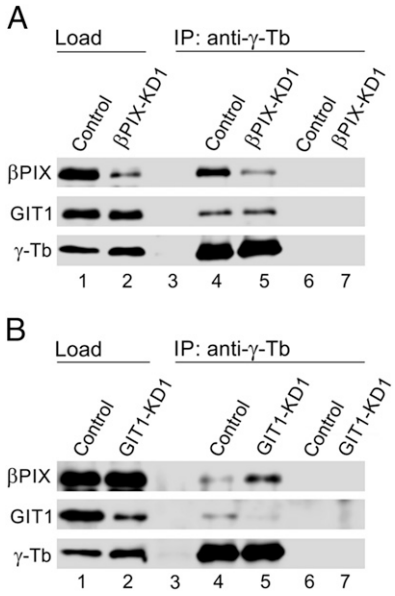

FIGURE 8. Depletion of GIT1 promotes interaction of βPIX with γ-tubulin. (**A**) Extracts from BMMCLs infected with empty pLKO.1 vector (Control) or BMMCLs with reduced levels of βPIX (βPIX-KD1) were precipitated with Protein A–immobilized Ab to γ-tubulin. Blots were probed with Abs to βPIX, GIT1, and γ-tubulin (γ-Tb). Load of control cells (*lane 1*), load of βPIX-KD1 cells (*lane 2*), immobilized Ab not incubated with cell extract (*lane 3*), precipitated proteins from control cells (*lane 4*), precipitated proteins from βPIX-KD1 cells (*lane 5*), Protein A without Ab, incubated with extract from control cells (*lane 6*), and Protein A without Ab, incubated with extract from βPIX-KD1 cells (*lane 7*). (**B**) Extracts from BMMCLs infected with empty pLKO.1 vector (Control) or BMMCLs with reduced levels of GIT1 (GIT1-KD1) were precipitated with Protein A–immobilized Ab to γ-tubulin. Blots were probed with Abs to βPIX, GIT1, and γ-tubulin (γ-Tb). Load of control cells (*lane 1*), load of GIT1-KD1 cells (*lane 2*), immobilized Ab not incubated with cell extract (*lane 3*), precipitated proteins from control cells (*lane 4*), precipitated proteins from GIT1-KD1 cells (*lane 5*), Protein A without Ab, incubated with extract from control cells (*lane 6*), and Protein A without Ab, incubated with extract from GIT1-KD1 cells (*lane 7*).

importance of microtubules in this process (3, 4, 7, 34). We showed previously that the stimulation of mast cells or basophils through FcεRI aggregation or by pervanadate exposure triggers the generation of complexes containing γ-tubulin, tyrosine-phosphorylated proteins, and tyrosine kinases (5, 35) and the reorganization of microtubules (5, 6). In this article, we report on GIT1 and βPIX as signaling proteins interacting with γ-tubulin in a Ca^{2+}-dependent manner, associating with centrosomes, and modulating microtubule nucleation from the centrosomes of BMMCLs. βPIX and GIT1 represent negative and positive regulators of microtubule nucleation, respectively. Our study provides a possible mechanism for the concerted action of tyrosine kinases, GIT1 and βPIX proteins, and Ca^{2+} in the propagation of signals leading to microtubule nucleation in activated mast cells.

Several lines of evidence indicate that the association of βPIX and GIT1 with γ-tubulin is specific. First, βPIX was repeatedly identified by MALDI/MS fingerprint analysis after immunoprecipitation of activated $Lyn^{-/-}$ BMMCLs with an anti-peptide mAb to γ-tubulin, elution of bound proteins with peptide, and concentration of tyrosine-phosphorylated proteins on an immobilized SH2 domain. Second, reciprocal precipitation experiments confirmed an interaction between βPIX or GIT1 and γ-tubulin. Third, TagRFP- or GFP-tagged γ-tubulins interacted with GIT1 and βPIX. Fourth, βPIX and GIT1 were associated with the GST-tagged C-terminal region of γ-tubulin. Finally, live-cell imaging revealed the localization of βPIX and GIT1 to centrosomes, where γ-tubulin is accumulated. Because the identification of βPIX in γ-tubulin complexes was carried out in lysates from $Lyn^{-/-}$ BMMCLs, we also analyzed GITs/βPIX–γ-tubulin complexes in BMMCLs. Although the differential expression of GIT1 and GIT2 was described in mouse tissues (36), our data document the expression of both proteins in BMMCLs and $Lyn^{-/-}$ BMMCLs. The results also demonstrate that the deletion of Lyn kinase does not affect the formation of complexes containing γ-tubulin, βPIX, and GITs.

GITs are multidomain proteins, and several signaling molecules, including βPIX, PAK, focal adhesion kinase, phospholipase Cγ, MAPK 1, and the synaptic protein Piccolo, associate with GIT1 through its Spa2 homology domain (30). Our data demonstrate that GIT1 is substrate for tyrosine kinases in pervanadate or FcεRI aggregation-activated BMMCLs. Moreover, tyrosine-phosphorylated GIT1 forms complexes with γ-tubulin. GIT1 was shown to be phosphorylated in cells in a Src kinase–dependent manner (37), and different studies pointed to the relevance of tyrosine phosphorylation in the regulation of GIT1 functions. It was shown that tyrosine phosphorylation of GIT1 is required for intramolecular

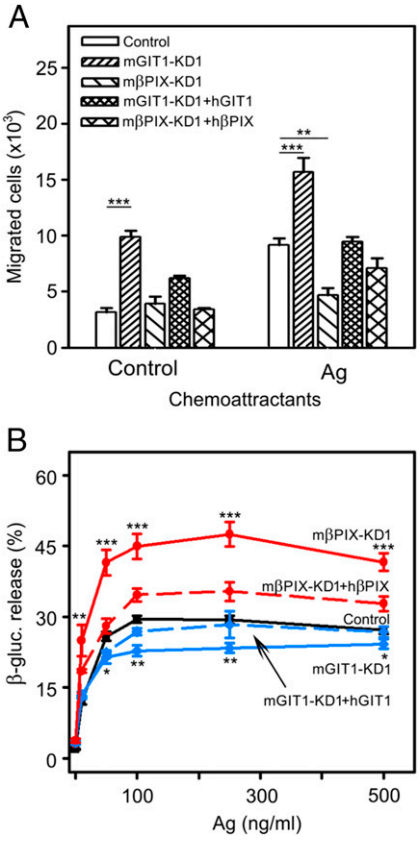

FIGURE 9. Differential effect of βPIX and GIT1 depletion on Ag-induced chemotaxis and degranulation. IgE-sensitized control cells or cells deficient in GIT1 (mGIT1-KD1) or βPIX (mβPIX-KD1) were used. hGIT1 or hβPIX was applied in rescue experiments. (**A**) The cells were analyzed in chemotactic assays with chemotaxis medium alone (Control) or supplemented with Ag (TNP-BSA, 250 ng/ml). The numbers of cells migrating into lower wells were determined after 8 h. Mean ± SE was calculated from three independent experiments performed in duplicates or triplicates. (**B**) IgE-sensitized cells were stimulated with various concentrations of Ag, and the amount of β-glucuronidase released from the cells was determined after 30 min. Mean ± SE was calculated from three independent experiments performed in duplicates or triplicates. The statistical significance of differences between control cells and βPIX-deficient cells is shown in the upper part, whereas those between control and GIT1-deficient cells are shown in the lower part. $*p < 0.05$, $**p < 0.01$, $***p < 0.001$.

conformational changes in GIT1 and release its autoinhibitory interaction (38). Phosphorylation of GIT1 by Src family kinases is required for its association with focal adhesion kinase (39), as well as for phospholipase Cγ activation (40). In contrast, tyrosine phosphorylation of βPIX, in a Src-dependent manner, weakens its ability to bind GIT1 (41). Association of Src family kinases with γ-tubulin complexes was reported in activated RBL-2H3 (35), activated BMMCLs (5), and in differentiating P19 embryonic carcinoma cells (23, 42). Thus, tyrosine phosphorylation of GIT1 in stimulated mast cells might lead to its activation.

There are reports suggesting an important role for tyrosine kinases in the regulation of microtubule nucleation from centrosomes. Fyn kinase was found on centrosomes in myelocytic leukemia cells HL-60 (43) and in human T lymphocytes (44). Androgen and Src signaling modulated microtubule nucleation during interphase by promoting the centrosomal localization of γ-tubulin (13) via activation of the MAPK/Erk signaling pathway (45). It also was shown that Syk is catalytically active at the centrosome (46). Previous studies showed that early stages of BMMCL activation, when microtubule formation is stimulated, are characterized by the concentration of tyrosine-phosphorylated proteins in the centrosomal region (5).

Although the FcεRI proximal signaling pathways involved in mast cell activation are well defined (1), the signaling events downstream of Ca^{2+} influx are less well studied. Ca^{2+}-dependent kinases or phosphatases might participate in microtubule stability in activated mast cells (47). It was reported that STIM1-regulated Ca^{2+} influx is essential for reorganization of microtubules in activated mast cells (6). In this study, we show that the depletion of Ca^{2+} substantially delays microtubule regrowth. In contrast, elevated levels of Ca^{2+} are accompanied by increased amounts of GCP2, GCP4, and GITs in complexes with γ-tubulin. Interestingly, Ca^{2+} inhibits binding of βPIX to the C-terminal region of γ-tubulin. Direct Ca^{2+}-dependent interaction between βPIX and calmodulin was reported recently (48). Live-cell imaging with EGFP-calmodulin chimeras revealed the association of calmodulin with centrosomes after activation of RBL-2H3 (49). A truncated splice variant of the FcεRIβ binding calmodulin, Gab2, and Fyn kinase was found to accumulate in the centrosome–Golgi region and stimulate microtubule formation and degranulation in human LAD-2 mast cells. It was suggested that the truncated splice variant may act to propagate Ca^{2+} signals for microtubule nucleation (7). It also was reported that the Fyn kinase/Gab2/PI3K pathway is critical for the formation of microtubules (3, 50). Our data support the importance of Ca^{2+} for microtubule nucleation in BMMCLs.

Interestingly, elevated levels of Ca^{2+} affected γ-tubulin properties manifested by changes in the electrophoretic mobility of γ-tubulin in BMMCLs. This conclusion is supported by several findings. First, both endogenous and exogenous γ-tubulins were modified. Second, 6xHis-tagged whole-length γ-tubulin or its C-terminal part (aa 223–451) was affected. Third, EGFP-tagged whole-length γ-tubulin or its C-terminal region (aa 378–451) was modified. Fourth, experiments with EGFP-tagged C-terminal regions of γ-tubulin or α-tubulin revealed that the mobility shift is specific for γ-tubulin. Finally, the presence of EGTA inhibited the mobility shift of γ-tubulin, and elevated concentrations of Mg^{2+} or Zn^{2+} did not demonstrate this effect. It was shown that Ca^{2+} has high-affinity binding sites on the C-terminal regions of αβ-tubulin dimers (51). However, it is unlikely that only the direct binding of Ca^{2+} to the C-terminal region of γ-tubulin causes observed changes, because no mobility shift was detected when Ca^{2+} alone was added to 6xHis-tagged γ-tubulin (Fig. 4A, Control). Unique changes in γ-tubulin properties in BMMCLs warrant further investigation. Ca^{2+}-dependent modifications in the C-terminal region of γ-tubulin could affect γ-tubulin binding characteristics and, thus, modulate the nucleation of microtubules in activated cells.

Our data from live-cell imaging revealed that GIT1 and βPIX are located on centrosomes in BMMCLs, which could reflect their regulatory roles in microtubule nucleation. Although GIT1/βPIX complexes are usually connected with cell migration, the centrosomal function of the complexes has only been reported in fibroblasts. GIT1 targeting to the centrosome served as a scaffold for βPIX. Associated PAK, activated via a process not requiring Rho GTPases, phosphorylated Aurora A in mitosis (52). Our data demonstrate that GIT1 and βPIX regulate interphase microtubules of mast cells. Although GIT1 and βPIX are both associated with centrosomes in BMMCLs, they play opposite regulatory roles in microtubule nucleation from centrosomes. Depletion of βPIX led to increased nucleation, whereas depletion of GIT1 resulted in decreased nucleation. The obtained data were confirmed by rescue experiments. GIT1/βPIX could regulate the nucleation of microtubules via several mechanisms. They may directly promote the assembly of γTuRCs and/or the recruitment of γTuRCs to the centrosome. Thus, kinases associated with GIT1/βPIX may phosphorylate components of γTuRC to promote the assembly of the complex, or they may regulate the association or activity of NEDD1/GCP-WD, the attachment factor that lies most proximal to γTuRC and is required for the centrosomal recruitment of γTuRC (53). Alternatively, GIT1/βPIX may indirectly affect this process by regulating the assembly of the pericentriolar matrix or the activity of a centrosomal protein(s) required for the anchorage of γTuRCs (54).

It is generally thought that the GIT1/βPIX complex serves as a signaling cassette that elicits changes in cell shape and migration (29). Our data indicate that depletion of βPIX enhances degranulation in Ag-activated cells. This could reflect increased microtubule nucleation. In contrast, depletion of GIT1 resulted in reduced degranulation, which could be related to decreased levels of microtubule nucleation in such cells. Both proteins are also involved in chemotaxis toward Ag, where they play opposite regulatory roles: GIT1 is a negative regulator, whereas βPIX serves as a positive regulator of chemotaxis. The negative regulatory role of GIT2 in cell motility was reported in other cell types (55). In contrast, it was shown that fMLP-induced fibronectin-mediated chemotaxis was unaffected after depletion of GIT2 and was inhibited after depletion of GIT1 (56). The difference in the results presented in this study and those of another study (56) may be attributed to the different experimental cell models, different chemoattractants used, and the presence or absence of fibronectin during the chemotactic assays. Although microtubules have long been implicated in cell motility, their role in this process varies with cell types. The mechanism of their involvement in cell motility is poorly understood. It was suggested that microtubules normally act to restrain cell motility (57). This could explain the observed opposite effects in degranulation and chemotaxis after the depletion of GIT1 and βPIX proteins. Because the GIT/PIX complex affects actin-dependent processes, including cell motility (29), the observed changes in chemotaxis could reflect changes in the microtubules, as well as in the actin cytoskeleton.

In conclusion, our data suggest a novel signaling pathway for microtubule rearrangement in mast cells; tyrosine kinase–activated GIT1 and βPIX, in concert with Ca^{2+} signaling, regulate microtubule nucleation. Enhanced levels of Ca^{2+} affect γ-tubulin properties, resulting in greater binding of GCPs to γ-tubulin. Presumably, through this action, GIT1 and βPIX are involved in the regulation of such important processes in mast cells physiology as is Ag-induced degranulation and chemotaxis. Interference with the microtubular network via specific regulators of microtubule nucleation in mast

cells could open up rational new approaches to the treatment of inflammatory and allergic diseases.

Acknowledgments

We thank Dr. M. Hibbs for the BMMCLs, Dr. P.L. Hordijk (Sanquin Research and Landsteiner Laboratory, University of Amsterdam, Amsterdam, the Netherlands) for the GST-tagged βPIX construct, and Dr. Petr Dráber for providing BMMCs and the Ab to GST, as well as for critical reading of the manuscript.

Disclosures

The authors have no financial conflicts of interest.

References

1. Gilfillan, A. M., and J. Rivera. 2009. The tyrosine kinase network regulating mast cell activation. *Immunol. Rev.* 228: 149–169.
2. Smith, A. J., J. R. Pfeiffer, J. Zhang, A. M. Martinez, G. M. Griffiths, and B. S. Wilson. 2003. Microtubule-dependent transport of secretory vesicles in RBL-2H3 cells. *Traffic* 4: 302–312.
3. Nishida, K., S. Yamasaki, Y. Ito, K. Kabu, K. Hattori, T. Tezuka, H. Nishizumi, D. Kitamura, R. Goitsuka, R. S. Geha, et al. 2005. FcεRI-mediated mast cell degranulation requires calcium-independent microtubule-dependent translocation of granules to the plasma membrane. *J. Cell Biol.* 170: 115–126.
4. Martin-Verdeaux, S., I. Pombo, B. Iannascoli, M. Roa, N. Varin-Blank, J. Rivera, and U. Blank. 2003. Evidence of a role for Munc18-2 and microtubules in mast cell granule exocytosis. *J. Cell Sci.* 116: 325–334.
5. Sulimenko, V., E. Dráberová, T. Sulimenko, L. Macůrek, V. Richterová, P. Dráber, and P. Dráber. 2006. Regulation of microtubule formation in activated mast cells by complexes of γ-tubulin with Fyn and Syk kinases. *J. Immunol.* 176: 7243–7253.
6. Hájková, Z., V. Bugajev, E. Dráberová, S. Vinopal, L. Dráberová, J. Janáček, P. Dráber, and P. Dráber. 2011. STIM1-directed reorganization of microtubules in activated mast cells. *J. Immunol.* 186: 913–923.
7. Cruse, G., M. A. Beaven, I. Ashmole, P. Bradding, A. M. Gilfillan, and D. D. Metcalfe. 2013. A truncated splice-variant of the FcεRIβ receptor subunit is critical for microtubule formation and degranulation in mast cells. *Immunity* 38: 906–917.
8. Grigoriev, I., S. M. Gouveia, B. van der Vaart, J. Demmers, J. T. Smyth, S. Honnappa, D. Splinter, M. O. Steinmetz, J. W. Putney, Jr., C. C. Hoogenraad, and A. Akhmanova. 2008. STIM1 is a MT-plus-end-tracking protein involved in remodeling of the ER. *Curr. Biol.* 18: 177–182.
9. Oakley, C. E., and B. R. Oakley. 1989. Identification of γ-tubulin, a new member of the tubulin superfamily encoded by mipA gene of *Aspergillus nidulans. Nature* 338: 662–664.
10. Oegema, K., C. Wiese, O. C. Martin, R. A. Milligan, A. Iwamatsu, T. J. Mitchison, and Y. Zheng. 1999. Characterization of two related *Drosophila* γ-tubulin complexes that differ in their ability to nucleate microtubules. *J. Cell Biol.* 144: 721–733.
11. Vogel, J., B. Drapkin, J. Oomen, D. Beach, K. Bloom, and M. Snyder. 2001. Phosphorylation of γ-tubulin regulates microtubule organization in budding yeast. *Dev. Cell* 1: 621–631.
12. Keck, J. M., M. H. Jones, C. C. Wong, J. Binkley, D. Chen, S. L. Jaspersen, E. P. Holinger, T. Xu, M. Niepel, M. P. Rout, et al. 2011. A cell cycle phosphoproteome of the yeast centrosome. *Science* 332: 1557–1561.
13. Colello, D., C. G. Reverte, R. Ward, C. W. Jones, V. Magidson, A. Khodjakov, and S. E. LaFlamme. 2010. Androgen and Src signaling regulate centrosome activity. *J. Cell Sci.* 123: 2094–2102.
14. Nováková, M., E. Dráberová, W. Schürmann, G. Czihak, V. Viklický, and P. Dráber. 1996. γ-Tubulin redistribution in taxol-treated mitotic cells probed by monoclonal antibodies. *Cell Motil. Cytoskeleton* 33: 38–51.
15. Hořejší, B., S. Vinopal, V. Sládková, E. Dráberová, V. Sulimenko, T. Sulimenko, V. Vosecká, A. Philimonenko, P. Hozák, C. D. Katsetos, and P. Dráber. 2012. Nuclear γ-tubulin associates with nucleoli and interacts with tumor suppressor protein C53. *J. Cell. Physiol.* 227: 367–382.
16. Dráberová, E., V. Sulimenko, V. Kukharskyy, and P. Dráber. 1999. Monoclonal antibody NF-09 specific for neurofilament protein NF-M. *Folia Biol. (Praha)* 45: 163–165.
17. Hibbs, M. L., D. M. Tarlinton, J. Armes, D. Grail, G. Hodgson, R. Maglitto, S. A. Stacker, and A. R. R. Dunn. 1995. Multiple defects in the immune system of Lyn-deficient mice, culminating in autoimmune disease. *Cell* 83: 301–311.
18. Kovářová, M., P. Tolar, R. Arudchandran, L. Dráberová, J. Rivera, and P. Dráber. 2001. Structure-function analysis of Lyn kinase association with lipid rafts and initiation of early signaling events after Fcε receptor I aggregation. *Mol. Cell. Biol.* 21: 8318–8328.
19. Zheng, Y., M. K. Jung, and B. R. Oakley. 1991. γ-Tubulin is present in *Drosophila melanogaster* and *Homo sapiens* and is associated with the centrosome. *Cell* 65: 817–823.
20. Vinopal, S., M. Černohorská, V. Sulimenko, T. Sulimenko, V. Vosecká, M. Flemr, E. Dráberová, and P. Dráber. 2012. γ-Tubulin 2 nucleates microtubules and is downregulated in mouse early embryogenesis. *PLoS ONE* 7: e29919.
21. ten Klooster, J. P., Z. M. Jaffer, J. Chernoff, and P. L. Hordijk. 2006. Targeting and activation of Rac1 are mediated by the exchange factor β-Pix. *J. Cell Biol.* 172: 759–769.
22. Dráber, P. 1991. Quantification of proteins in sample buffer for sodium dodecyl sulfate-polyacrylamide gel electrophoresis using colloidal silver. *Electrophoresis* 12: 453–456.
23. Kukharskyy, V., V. Sulimenko, L. Macůrek, T. Sulimenko, E. Dráberová, and P. Dráber. 2004. Complexes of γ-tubulin with nonreceptor protein tyrosine kinases Src and Fyn in differentiating P19 embryonal carcinoma cells. *Exp. Cell Res.* 298: 218–228.
24. Dráber, P., L. A. Lagunowich, E. Dráberová, V. Viklický, and I. Damjanov. 1988. Heterogeneity of tubulin epitopes in mouse fetal tissues. *Histochemistry* 89: 485–492.
25. Surviladze, Z., L. Dráberová, M. Kovářová, M. Boubelík, and P. Dráber. 2001. Differential sensitivity to acute cholesterol lowering of activation mediated via the high-affinity IgE receptor and Thy-1 glycoprotein. *Eur. J. Immunol.* 31: 1–10.
26. Polakovicova, I., L. Draberova, M. Simicek, and P. Draber. 2014. Multiple regulatory roles of the mouse transmembrane adaptor protein NTAL in gene transcription and mast cell physiology. *PLoS ONE* 9: e105539.
27. Dráberová, E., and P. Dráber. 1993. A microtubule-interacting protein involved in coalignment of vimentin intermediate filaments with microtubules. *J. Cell Sci.* 106: 1263–1273.
28. Hoefen, R. J., and B. C. Berk. 2006. The multifunctional GIT family of proteins. *J. Cell Sci.* 119: 1469–1475.
29. Frank, S. R., and S. H. Hansen. 2008. The PIX-GIT complex: a G protein signaling cassette in control of cell shape. *Semin. Cell Dev. Biol.* 19: 234–244.
30. Webb, D. J., M. W. Mayhew, M. Kovalenko, M. J. Schroeder, E. D. Jeffery, L. Whitmore, J. Shabanowitz, D. F. Hunt, and A. F. Horwitz. 2006. Identification of phosphorylation sites in GIT1. *J. Cell Sci.* 119: 2847–2850.
31. Teshima, R., H. Ikebuchi, M. Nakanishi, and J. Sawada. 1994. Stimulatory effect of pervanadate on calcium signals and histamine secretion of RBL-2H3 cells. *Biochem. J.* 302: 867–874.
32. Komarova, Y. A., I. A. Vorobjev, and G. G. Borisy. 2002. Life cycle of MTs: persistent growth in the cell interior, asymmetric transition frequencies and effects of the cell boundary. *J. Cell Sci.* 115: 3527–3539.
33. Delgehyr, N., J. Sillibourne, and M. Bornens. 2005. Microtubule nucleation and anchoring at the centrosome are independent processes linked by ninein function. *J. Cell Sci.* 118: 1565–1575.
34. Tasaka, K., M. Mio, K. Fujisawa, and I. Aoki. 1991. Role of microtubules on Ca^{2+} release from the endoplasmic reticulum and associated histamine release from rat peritoneal mast cells. *Biochem. Pharmacol.* 41: 1031–1037.
35. Dráberová, L., E. Dráberová, Z. Surviladze, P. Dráber, and P. Dráber. 1999. Protein tyrosine kinase p53/p56(lyn) forms complexes with γ-tubulin in rat basophilic leukemia cells. *Int. Immunol.* 11: 1829–1839.
36. Schmalzigaug, R., H. Phee, C. E. Davidson, A. Weiss, and R. T. Premont. 2007. Differential expression of the ARF GAP genes GIT1 and GIT2 in mouse tissues. *J. Histochem. Cytochem.* 55: 1039–1048.
37. Bagrodia, S., D. Bailey, Z. Lenard, M. Hart, J. L. Guan, R. T. Premont, S. J. Taylor, and R. A. Cerione. 1999. A tyrosine-phosphorylated protein that binds to an important regulatory region on the cool family of p21-activated kinase-binding proteins. *J. Biol. Chem.* 274: 22393–22400.
38. Totaro, A., V. Astro, D. Tonoli, and I. de Curtis. 2014. Identification of two tyrosine residues required for the intramolecular mechanism implicated in GIT1 activation. *PLoS ONE* 9: e93199.
39. Ren, Y., L. Yu, J. Fan, Z. Rui, Z. Hua, Z. Zhang, N. Zhang, and G. Yin. 2012. Phosphorylation of GIT1 tyrosine 321 is required for association with FAK at focal adhesions and for PDGF-activated migration of osteoblasts. *Mol. Cell. Biochem.* 365: 109–118.
40. Wang, J., G. Yin, P. Menon, J. Pang, E. M. Smolock, C. Yan, and B. C. Berk. 2010. Phosphorylation of G protein-coupled receptor kinase 2-interacting protein 1 tyrosine 392 is required for phospholipase C-γ activation and podosome formation in vascular smooth muscle cells. *Arterioscler. Thromb. Vasc. Biol.* 30: 1976–1982.
41. Feng, Q., D. Baird, S. Yoo, M. Antonyak, and R. A. Cerione. 2010. Phosphorylation of the cool-1/β-Pix protein serves as a regulatory signal for the migration and invasive activity of Src-transformed cells. *J. Biol. Chem.* 285: 18806–18816.
42. Macurek, L., E. Dráberová, V. Richterová, V. Sulimenko, T. Sulimenko, L. Dráberová, V. Marková, and P. Dráber. 2008. Regulation of microtubule nucleation from membranes by complexes of membrane-bound γ-tubulin with Fyn kinase and phosphoinositide 3-kinase. *Biochem. J.* 416: 421–430.
43. Katagiri, K., T. Katagiri, K. Kajiyama, T. Yamamoto, and T. Yoshida. 1993. Tyrosine-phosphorylation of tubulin during monocytic differentiation of HL-60 cells. *J. Immunol.* 150: 585–593.
44. Ley, S. C., M. Marsh, C. R. Bebbington, K. Proudfoot, and P. Jordan. 1994. Distinct intracellular localization of Lck and Fyn protein tyrosine kinases in human T lymphocytes. *J. Cell Biol.* 125: 639–649.
45. Colello, D., S. Mathew, R. Ward, K. Pumiglia, and S. E. LaFlamme. 2012. Integrins regulate microtubule nucleating activity of centrosome through mitogen-activated protein kinase/extracellular signal-regulated kinase kinase/extracellular signal-regulated kinase (MEK/ERK) signaling. *J. Biol. Chem.* 287: 2520–2530.
46. Fargier, G., C. Favard, A. Parmeggiani, A. Sahuquet, F. Mérezègue, A. Morel, M. Denis, N. Molinari, P. H. Mangeat, P. J. Coopman, and P. Montcourrier. 2013. Centrosomal targeting of Syk kinase is controlled by its catalytic activity and depends on microtubules and the dynein motor. *FASEB J.* 27: 109–122.
47. Dráber, P., V. Sulimenko, and E. Dráberová. 2012. Cytoskeleton in mast cell signaling. *Front. Immunol.* 3: 130.

48. Singh, V. K., K. Munro, and Z. Jia. 2012. A novel calmodulin-β-PIX interaction and its implication in receptor tyrosine kinase regulation. *Cell. Signal.* 24: 1790–1796.
49. Psatha, M. I., M. Razi, A. Koffer, S. E. Moss, D. B. Sacks, and S. R. Bolsover. 2007. Targeting of calcium:calmodulin signals to the cytoskeleton by IQGAP1. *Cell Calcium* 41: 593–605.
50. Sibilano, R., B. Frossi, R. Suzuki, F. D'Incà, G. Gri, S. Piconese, M. P. Colombo, J. Rivera, and C. E. Pucillo. 2012. Modulation of FcεRI-dependent mast cell response by OX40L via Fyn, PI3K, and RhoA. *J. Allergy Clin. Immunol.* 130: 751–760, e2.
51. Lefèvre, J., K. G. Chernov, V. Joshi, S. Delga, F. Toma, D. Pastré, P. A. Curmi, and P. Savarin. 2011. The C terminus of tubulin, a versatile partner for cationic molecules: binding of Tau, polyamines, and calcium. *J. Biol. Chem.* 286: 3065–3078.
52. Zhao, Z. S., J. P. Lim, Y. W. Ng, L. Lim, and E. Manser. 2005. The GIT-associated kinase PAK targets to the centrosome and regulates Aurora-A. *Mol. Cell* 20: 237–249.
53. Lüders, J., U. K. Patel, and T. Stearns. 2006. GCP-WD is a γ-tubulin targeting factor required for centrosomal and chromatin-mediated microtubule nucleation. *Nat. Cell Biol.* 8: 137–147.
54. Teixidó-Travesa, N., J. Roig, and J. Lüders. 2012. The where, when and how of microtubule nucleation - one ring to rule them all. *J. Cell Sci.* 125: 4445–4456.
55. Frank, S. R., M. R. Adelstein, and S. H. Hansen. 2006. GIT2 represses Crk- and Rac1-regulated cell spreading and Cdc42-mediated focal adhesion turnover. *EMBO J.* 25: 1848–1859.
56. Gavina, M., L. Za, R. Molteni, R. Pardi, and I. de Curtis. 2010. The GIT-PIX complexes regulate the chemotactic response of rat basophilic leukaemia cells. *Biol. Cell* 102: 231–244.
57. Ganguly, A., H. Yang, R. Sharma, K. D. Patel, and F. Cabral. 2012. The role of microtubules and their dynamics in cell migration. *J. Biol. Chem.* 287: 43359–43369.

Supplemental Table 1

Mass spectrometry identification of the mouse Rho guanine nucleotide exchange factor 7 (mβPIX)

Measured mass	Theoretical mass	Error (ppm)	Peptide sequence	Peptide position
1225.586	1225.588	-1	TGWFPSNYVR	209 - 218
1368.632	1368.634	-1	NAFEISGSM(ox)IER	522 - 534
1452.817	1452.818	-1	ELELQILTEPIR	435 - 446
1595.837	1595.840	-2	KESAPQVLLPEEEK	774 - 787
1612.701	1612.701	0	VEEGGWWEGTHNGR	195 – 208
1832.820	1832.821	0	FNFQQTNEDELSFSK	172 - 186
1977.041	1977.041	0	SLVDTVYALKDEVQELR	805 - 821
2077.104	2077.104	0	ELQSVLSTYLRPLQTSDK	268 - 285

```
  1 MNSAEQTVTW LITLGVLESP KKTISDPEVF LQASLKDGVV LCRLLERLLP GTIEKVYPEP
 61 RNESECLSNI REFLRACGAS LRLETFDAND LYQGQNFNKV LSSLVTLNKV TADIGLGSDS
121 VCARPSSHRI KSFDSLGSQS SHSRTSKLLQ SQYRSLDMTD NTNSQLVVRA KFNFQQTNED
181 ELSFSKGDVI HVTRVEEGGW WEGTHNGRTG WFPSNYVREI KPSEKPVSPK SGTLKSPPKG
241 FDTTAINKSY YNVVLQNILE TEHEYSKELQ SVLSTYLRPL QTSDKLSSAN TSYLMGNLEE
301 ISSFQQVLVQ SLEECTKSPE AQQRVGGCFL SLMPQMRTLY LAYCANHPSA VSVLTEHSED
361 LGEFMETKGA SSPGILVLTT GLSKPFMRLD KYPTLLKELE RHMEDYHPDR QDIQKSMTAF
421 KNLSAQCQEV RKRKELELQI LTEPIRSWEG DDIKTLGSVT YMSQVTIQCA GSEEKNERYL
481 LLFPNLLLML SASPRMSGFI YQGKLPTTGM TITKLEDSEN HRNAFEISGS MIERILVSCT
541 SQQDLHEWVE HLQKQTKVTS VSNPTIKPHS VPSHTLPSHP LTPSSKHADS KPVALTPAYH
601 TLPHPSHHGT PHTTISWGPL EPPKTPKPWS LSCLRPAPPL RPSAALCYKE DLSKSPKTMK
661 KLLPKRKPER KPSDEEFAVR KSTAALEEDA QILKVIEAYC TSAKTRQTLN STWQGTDLMH
721 NHVLADDDQS SLDSLGRRSS LSRLEPSDLS EDSEYDSIWT AHSYRMGSAS RSRKESAPQV
781 LLPEEEKIIV EETKSNGQTV IEEKSLVDTV YALKDEVQEL RQDNKKMKKS LEEEQRARKD
841 LEKLVRKVLK NMNDPAWDET NL
```

Amino acids of the identified peptides in the mouse Rho guanine nucleotide exchange factor 7 (Arhgef7, canonical sequence of isoform B; UniProtKB/Swiss-Prot Q9ES28-1) are indicated in bold and underlined (bottom part of the table). The matched peptides cover 12.99 % of the protein sequence.

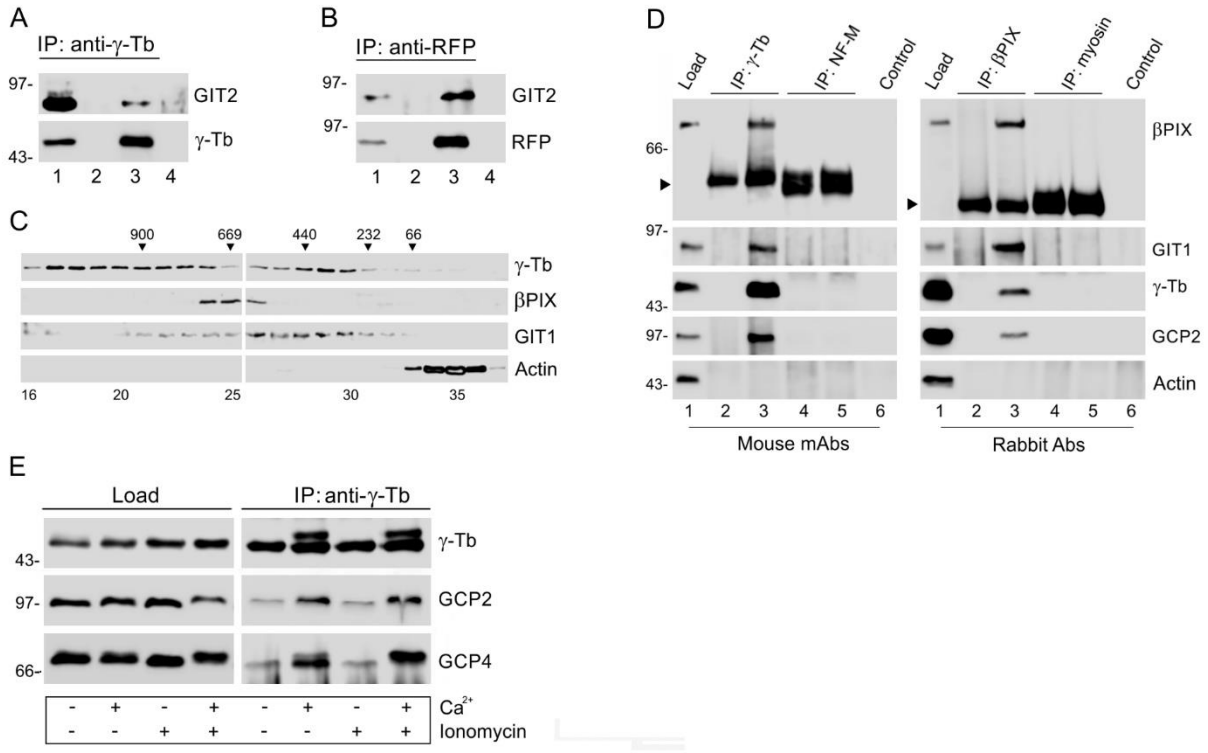

FIGURE S1. γ-Tubulin interacts with GIT2, co-distributes with βPIX and GIT1 during size fractionation of cytosolic extract of mast cells, and its interaction with GCPs is Ca^{2+}-dependent. *A*, Extract from $Lyn^{-/-}$ BMMCL was precipitated with protein A immobilized Ab to γ-tubulin. Blots were probed with Abs to GIT2 and γ-tubulin (γ-Tb). *B*, Extract from BMMCL-γTb expressing TagRFP-tagged γ-tubulin was precipitated with protein A immobilized Ab to RFP. Blots were probed with Abs to GIT2 and RFP. In *A-B*: load (*lane 1*), immobilized Ab not incubated with cell extract (*lane 2*), immunoprecipitated protein (*lane 3*), and protein A without Ab, incubated with cell extract (*lane 4*). Lines on the left indicate positions of molecular mass markers in kDa. *C*, Size fractionation of cytosolic extract. Proteins extracted from BMMCL were fractionated on Superose 6B and blots of collected fractions were probed with Abs to γ-tubulin, βPIX, GIT1 and actin. Calibration standards (in kDa) are indicated on the top. Numbers at the bottom denote individual fractions. *D*, Isotype controls for immunoprecipitation experiments. Extracts from $Lyn^{-/-}$ BMMCL were precipitated with protein A immobilized mouse mAb to γ-tubulin (IgG2b), mouse mAb to NF-M (IgG2a, control), rabbit Ab to βPIX or rabbit Ab to myosin (control). Blots were probed with Abs to βPIX, GIT1, γ-tubulin (γ-Tb), GCP2 and actin. Load (*lane 1*), immobilized Abs not incubated with cell extracts (*lanes 2 and 4*), immunoprecipitated proteins (*lanes 3 and 5*), and protein A without Ab, incubated with cell extract (*lane 6*). Lines on the left indicate positions of molecular mass markers in kDa. Arrowheads indicate position of Ab heavy chains. *E*, Effect of Ca^{2+} and ionomycin on co-immunoprecipitation of proteins with γ-tubulin. BMMCL were pre-incubated in the presence or absence of 1.8 mM Ca^{2+} and extracts were precipitated with Ab to γ-tubulin immobilized on protein A. Blots were probed with Abs to γ-tubulin (γ-Tb), GCP2 and GCP4. Note the change in electrophoretic mobility of precipitated γ-tubulin and the higher amount of co-precipitated GCP2 and GCP4 in the presence of Ca^{2+}. Lines on the left indicate positions of molecular mass markers in kDa.

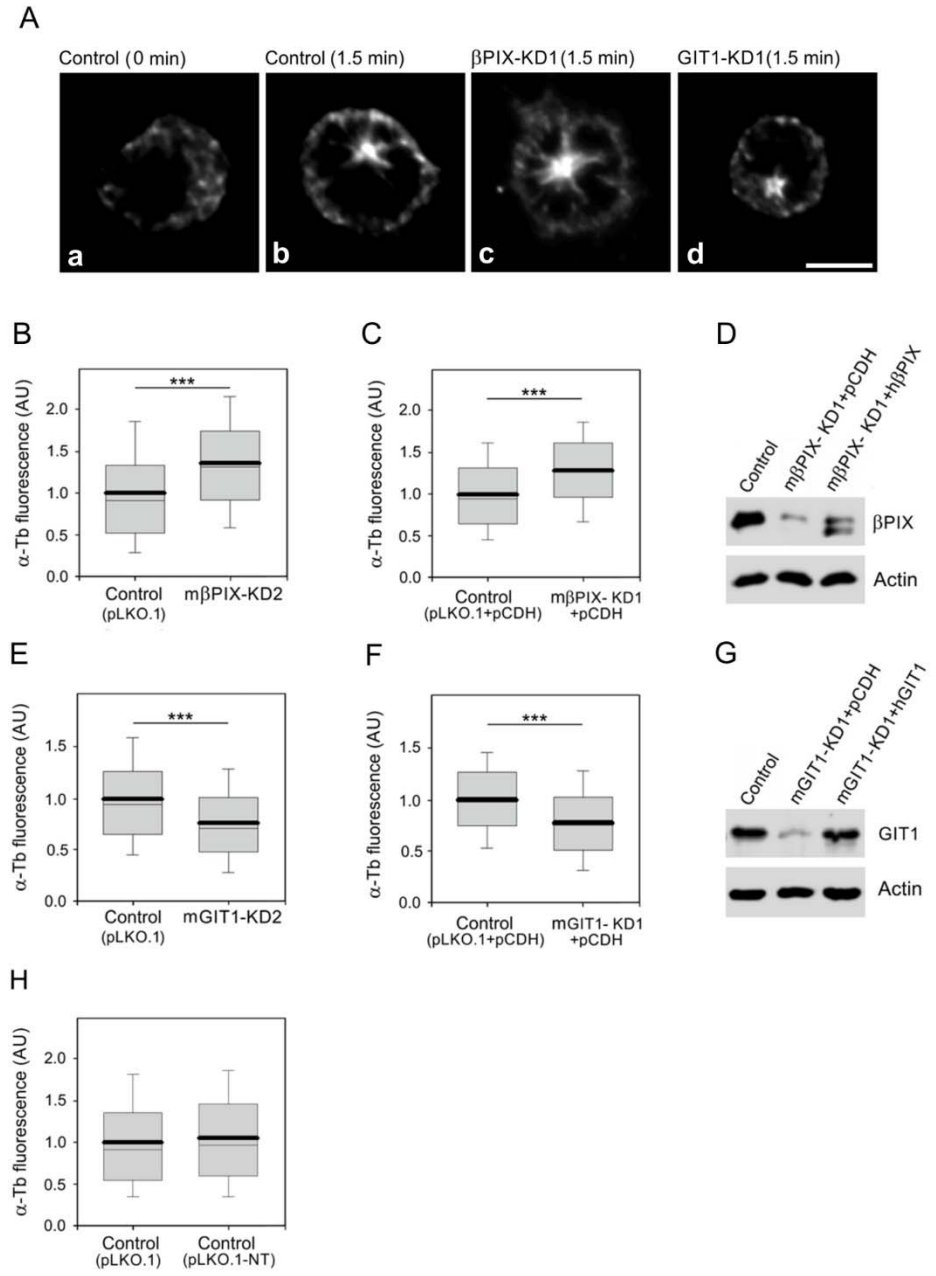

FIGURE S2. Effect of βPIX and GIT1 depletion on microtubule regrowth in BMMCL. *A*, Labeling of α-tubulin in microtubule regrowth experiment in control cells infected with empty pLKO.1 vector (*a*-*b*) and after depletion of βPIX (*c*; βPIX-KD1) or GIT1 (*d*; GIT1-KD1). Cells were fixed at 1.5 min of microtubule regrowth. Scale bar, 5 μm. (*B-C, E-F*) The distributions of α-tubulin fluorescence intensities (arbitrary units, AU) in 1 μm ROI at 1.5 min of microtubule regrowth are shown as box plot diagrams (three independent experiments, more than 400 cells counted for each experimental condition). *B*, Box plot of cells with a lower level of βPIX depletion (mβPIX-KD2; n = 1,894) relative to negative control cells (Control, pLKO.1; n = 1,254). *C*, Box plot of βPIX-depleted cells (mβPIX-KD1 + pCDH; n = 2,688)

relative to negative control cells (Control, pLKO.1 + pCDH; n = 1,938) in rescue experiment. *D*, Immunoblot analysis of cells in βPIX rescue experiment. Whole cell lysate from cells infected with empty pLKO.1 and pCDH vectors (Control), cells with depleted level of mβPIX containing empty pCDH vector (mβPIX-KD1 + pCDH); cells with depleted level of mβPIX rescued by hβPIX (mβPIX-KD1 + hβPIX). *E*, Box plot of cells with a lower level of GIT1 depletion (mGIT1-KD2; n = 1,590) relative to negative control cells (Control, pLKO.1; n = 1,966). *F*, Box plot of mGIT1-depleted cells (mGIT1-KD1 + pCDH; n = 2,475) relative to negative control cells (Control, pLKO.1 + pCDH; n =2,402) in rescue experiment. *G*, Immunoblot analysis of cells in the GIT1 rescue experiment. Whole cell lysate from cells infected with empty pLKO.1 and pCDH vectors (Control); cells with depleted level of mGIT1 containing empty pCDH vector (mGIT1-KD1 + pCDH); cells with depleted level of mGIT1 rescued by hGIT1 (mGIT1-KD1 + hGIT1). *H*, Box plot of cells containing non-target shRNA (pLKO.1-NT; n = 625) relative to negative control cells (pLKO.1; n = 413). In (*B-C, E-F* and *H*) bold and thin lines within the box represent mean and median (the 50th percentile), respectively. The bottom and top of the box represent the 25th and 75th percentiles. Whiskers below and above the box indicate the 10th and 90th percentiles. ***, $p < 1 \times 10^{-15}$.

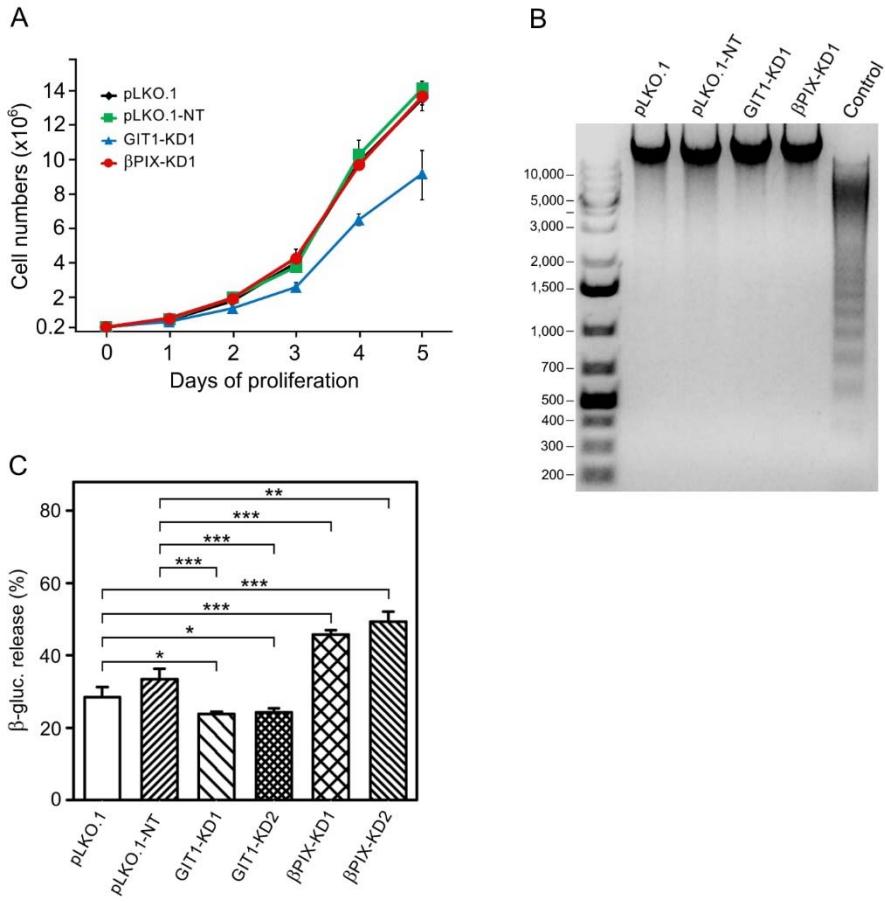

FIGURE S3. Effect of βPIX and GIT1 depletion on cell proliferation, apoptosis and degranulation in BMMCL. *A*, Growth curves of negative control cells (pLKO.1, pLKO.1-NT) and cells with depleted levels of βPIX (βPIX-KD1) or GIT1 (GIT1-KD1). A total of 2 x 10^5 cells were plated both in controls and βPIX- or GIT1-depleted cells. Values indicate mean ± SD; n = 3. *B*, Electrophoretic detection of apoptotic cells. DNA size marker (bp) and genomic DNA isolated from negative controls (pLKO.1, pLKO.1-NT), βPIX- (βPIX-KD1) or GIT1- (GIT1-KD1) depleted cells, and apoptotic cells (positive control) separated on 1.5 % agarose gel. *C*, Different effect of βPIX and GIT1 depletion on Ag-induced degranulation. IgE sensitized control cells (pLKO.1, pLKO.1-NT) and cells with depleted levels of βPIX (βPIX-KD1, βPIX-KD2) or GIT1 (GIT1-KD1, GIT1-KD2) were stimulated with 100 ng/ml of Ag and amount of β-glucuronidase released from the cells was determined after 30 min. Means ± SE were calculated from 3 independent experiments performed in duplicates or triplicates.

VI.5

Černohorská M., Sulimenko V., **Hájková Z.**, Sulimenko T., Sládková V., Vinopal S., Dráberová E., Dráber P. (2016). GIT1/βPIX signaling proteins and PAK1 kinase regulate microtubule nucleation. BBA Molecular Cell Research *1863*, 1282-1297.

Biochimica et Biophysica Acta 1863 (2016) 1282–1297

Contents lists available at ScienceDirect

Biochimica et Biophysica Acta

journal homepage: www.elsevier.com/locate/bbamcr

GIT1/βPIX signaling proteins and PAK1 kinase regulate microtubule nucleation

Markéta Černohorská, Vadym Sulimenko, Zuzana Hájková, Tetyana Sulimenko, Vladimíra Sládková, Stanislav Vinopal, Eduarda Dráberová, Pavel Dráber *

Department of Biology of Cytoskeleton, Institute of Molecular Genetics, Academy of Sciences of the Czech Republic, CZ-142 20 Prague 4, Czech Republic

ARTICLE INFO

Article history:
Received 21 September 2015
Received in revised form 14 March 2016
Accepted 18 March 2016
Available online 22 March 2016

Keywords:
Centrosome
Microtubule nucleation
γ-tubulin
GIT1/βPIX signaling proteins
PAK1 kinase

ABSTRACT

Microtubule nucleation from γ-tubulin complexes, located at the centrosome, is an essential step in the formation of the microtubule cytoskeleton. However, the signaling mechanisms that regulate microtubule nucleation in interphase cells are largely unknown. In this study, we report that γ-tubulin is in complexes containing G protein-coupled receptor kinase-interacting protein 1 (GIT1), p21-activated kinase interacting exchange factor (βPIX), and p21 protein (Cdc42/Rac)-activated kinase 1 (PAK1) in various cell lines. Immunofluorescence microscopy revealed association of GIT1, βPIX and activated PAK1 with centrosomes. Microtubule regrowth experiments showed that depletion of βPIX stimulated microtubule nucleation, while depletion of GIT1 or PAK1 resulted in decreased nucleation in the interphase cells. These data were confirmed for GIT1 and βPIX by phenotypic rescue experiments, and counting of new microtubules emanating from centrosomes during the microtubule regrowth. The importance of PAK1 for microtubule nucleation was corroborated by the inhibition of its kinase activity with IPA-3 inhibitor. GIT1 with PAK1 thus represent positive regulators, and βPIX is a negative regulator of microtubule nucleation from the interphase centrosomes. The regulatory roles of GIT1, βPIX and PAK1 in microtubule nucleation correlated with recruitment of γ-tubulin to the centrosome. Furthermore, *in vitro* kinase assays showed that GIT1 and βPIX, but not γ-tubulin, serve as substrates for PAK1. Finally, direct interaction of γ-tubulin with the C-terminal domain of βPIX and the N-terminal domain of GIT1, which targets this protein to the centrosome, was determined by pull-down experiments. We propose that GIT1/βPIX signaling proteins with PAK1 kinase represent a novel regulatory mechanism of microtubule nucleation in interphase cells.

1. Introduction

During interphase, microtubules built up from αβ-tubulin heterodimers determine the subcellular localization of organelles, promote intracellular transport and direct cell migration. The centrosome is a major site for microtubule organization in animal cells. It comprises a central pair of centrioles surrounded by pericentriolar matrix [1,2]. The assembly of the microtubules is a highly regulated process initiated by nucleation. Newly nucleated microtubules become anchored at the centrosome and exhibit growth, shrinkage, and stabilization in response to external and internal signals.

One of the key components of microtubule nucleation is γ-tubulin [3], a highly conserved member of the tubulin superfamily. It associates with other γ-tubulin complex proteins (GCPs) in the cytoplasm to form γ-tubulin ring complexes (γTuRCs) comprising a γ-tubulin small complexes (γTuSCs, composed of two molecules of γ-tubulin, one molecule of GCP2, and one molecule of GCP3) and some other proteins [4]. γ-TuRCs accumulate at the centrosome to serve as templates for microtubule nucleation [1]. NEDD1 and several other γTuRCs-associated proteins have been implicated in γTuRCs regulation, by mediating subcellular targeting of the complexes to centrosomes [5]. It is known that recruitment of γTuRCs to the centrosome correlates with increased microtubule nucleation at the onset of mitosis [6,7], and kinases Plk1 and Cdk1 promote enhanced centrosomal localization of γ-tubulin at mitosis [8,9]. It was reported that Src signaling, which leads to activation of the MEK/ERK pathway, regulates microtubule nucleation by promoting accumulation of the γ-tubulin at interphase centrosome [10,11]. We have recently reported that tyrosine-activated G-protein-coupled receptor kinase-interacting protein (GIT)1 and p21-activated kinase interacting exchange factor β (βPIX) interact with γ-tubulin and differentially modulate nucleation of microtubules in mouse bone marrow-

Abbreviations: Ab, Antibody; EB1, end-binding protein 1; GIT1, G protein-coupled receptor kinase-interacting protein 1; PAK1, p21 protein (Cdc42/Rac)-activated kinase 1; βPIX, p21-activated kinase interacting exchange factor; ROI, region of interest; γTuRC, γ-tubulin ring complex; tv, transcript variant.

* Corresponding author at: Department of Biology of Cytoskeleton, Institute of Molecular Genetics, Academy of Sciences of the Czech Republic, Vídeňská 1083, 142 20 Prague 4, Czech Republic.
E-mail address: paveldra@img.cas.cz (P. Dráber).

http://dx.doi.org/10.1016/j.bbamcr.2016.03.016
0167-4889/

derived mast cells during interphase [12]. Thus, microtubule nucleation is dynamically regulated throughout the cell cycle.

GIT1 and βPIX are multi-domain signaling proteins that associate to provide a platform for the formation of macromolecular assemblies [13]. The GIT1/βPIX1 complex serves as a signaling cassette that regulates membrane ruffling, focal adhesion turnover, polarity in motile cells, and consequently cell spreading as well as directional migration [14]. While involvement of GIT1/βPIX complexes in the regulation of actin cytoskeleton is well established, their role in the regulation of microtubules is much less understood. The GIT1/βPIX complex was found in the centrosome with associated p21 protein (Cdc42/Rac)-activated kinase 1 (PAK1) which was activated by centrosome targeting. Once activated, PAK1 dissociated from GIT1/βPIX and phosphorylated Aurora A in mitosis [15].

In this study, we identified GIT1/βPIX signaling proteins and PAK1 kinase as important regulators of microtubule nucleation. GIT1 with PAK1 represent positive regulators and βPIX negative regulator of this process. The regulation is due to changes in γ-tubulin accumulation at the interphase centrosome. GIT1/βPIX signaling proteins are phosphorylated by PAK1 and directly interact with γ-tubulin. The binding site for γ-tubulin on GIT1 is located in its N-terminal domain targeting GIT1 to the centrosome. Our data suggest a novel regulatory mechanism of microtubule nucleation.

2. Material and methods

2.1. Reagents

Nocodazole, puromycin, geneticin (G418) and GST-tagged active PAK1 were from Sigma. Protein A immobilized on Trisacryl GF-2000 and SuperSignal WestPico Chemiluminescent reagents were purchased from Pierce. Protease-inhibitor mixture tablets (Complete EDTA-free) were from Roche Molecular Biochemicals. PAK1 inhibitor IPA-3 was bought from Merck-Millipore and 20 mM stock was prepared in DMSO. Purified C-terminally FLAG-tagged GIT1, βPIX and nucleophosmin were from Origene. Restriction enzymes were from New England Biolabs and Glutathione Sepharose 4 Fast Flow from GE Healthcare Life Sciences. Oligonucleotides were synthesized by Sigma.

2.2. Antibodies

The following anti-peptide Abs prepared to human γ-tubulin were used: mouse monoclonal Ab (mAb) TU-30 (IgG1), TU-31 (IgG2b) and mAb TU-32 (IgG1) to the sequence 434–449 [16], and mAb GTU 88 (IgG1; Sigma, Catalog No.T6657) to the sequence 38–53. α-Tubulin was detected with rabbit Ab from Genetex (GTX15246). Rabbit Abs to βPIX (HPA004744), PAK1 (HPA03565), GAPDH (G9545), FLAG (F7425) and actin (A2066) as well as mAb to Hsp70 (H5147) were from Sigma. Rabbit Abs to phosphorylated S144 of PAK1 (ab4079) and pericentrin (ab4448) were from Abcam. Rabbit Abs to GIT1 (sc-13961), PAK1 (sc-882) and phosphorylated T423 of PAK1 (sc-21903) were from Santa Cruz. Rabbit Ab to tRFP (AB234) was from Evrogen and mAb to paxillin (612405) was from BD Transduction Laboratories. Rabbit Ab to non-muscle myosin heavy chain (BT-561; Biomed Tech. Inc.) and mAb NF-09 (IgG2a) to neurofilament NF-M protein [17] served as negative controls in the immunoprecipitation experiments. Rabbit Ab to GST was from Dr. Pe. Dráber (Institute of Molecular Genetics, Prague, Czech Republic). DY648-, DY549- and DY488-conjugated anti-mouse Abs as well as Cy3- and DY488-conjugated anti-rabbit Abs were from Jackson Immunoresearch Laboratories. Secondary HRP-conjugated antibodies were from Promega Biotech.

2.3. Cell cultures and transfection

Human osteogenic sarcoma cell line U-2 OS (U2OS) (Catalog No. ATCC-HTB-96) and human neuroblastoma cells SH-SY5Y (Catalog No. ATCC-CRL-2266) were obtained from the American Type Culture Collection. Immortalized human retinal pigment epithelial cells stably expressing telomerase reverse transcriptase hTERT-RPE1 (RPE1) were obtained from Dr. M. Bonhivers (Université Bordeaux, Bordeaux, France). HEK 293-FT (HEK) cells were from Promega Biotec. U2OS cells stably expressing EB1-GFP (U2OS-EB1) were described previously [18]. Cells were cultured in Dulbecco's modified Eagle's medium (DMEM) containing 10% FCS, penicillin (100 units/ml), and streptomycin (0.1 mg/ml). Cells were grown at 37 °C in 5% CO_2 in air and passaged every 2 d. In some cases, cells were cultivated with 10 μM nocodazole for 1 h to depolymerize microtubules. Alternatively, cells were incubated with 5 or 20 μM IPA-3 for 3 h.

HEK cells were transfected with 17 μg DNA per 9-cm tissue culture dish using 51 μg polyethylenimine (Polysciences) and serum-free DMEM. After 12 h, the transfection mixture was replaced with fresh medium supplemented with serum, and cells were incubated for an additional 24 h. The HEK cells for lentivirus production were at passages 4–15.

To prepare U2OS cells stably expressing TagRFP-tagged proteins, cells were transfected with 2.5 μg DNA (phGIT1-TagRFP, phβPIX-TagRFP or phPAK1-TagRFP) per 3-cm tissue culture dish using Lipofectamine LTX (Invitrogen) according to the manufacturer's instructions. After 12 h, the transfection mixture was replaced with fresh complete medium and cells were incubated for 48 h. Cells were thereafter incubated in fresh complete medium containing G418 at concentration 1.2 mg/ml for 7 days. Cells expressing fluorescently-tagged protein were flow-sorted using the BD Influx cell sorter (BD Bioscience, USA). TagRFP emission was triggered by 561 nm lasers; fluorescence was detected with 585/20 band-pass filter. Lentiviral transduction of U2OS with phTUBG1-TagRFP-puro vector followed by selection in 2.0 μg/ml puromycin was used to prepare a stable cell line expressing γ-tubulin-TagRFP. Lentiviral transduction of U2OS with phGIT1(tv1)-neo vector followed by selection in 800 μg/ml G418 was used to prepare a stable cell line expressing hGIT1 (U2OS_hGIT1-neo). Cells transduced with vector pCDH-CMV-MCS-EF1-Neo (System Biosciences) were used as a negative control (U2OS_pCDH-neo).

2.4. DNA constructs

Total cellular RNA was isolated from SH-SY5Y cells using RNeasy Mini kit (QIAGEN), according to the manufacturer's directions. The quality of RNA was checked in 2100 Bioanalyzer (Agilent Technologies). Reverse transcription was performed with oligo(dT) primers and SuperScript III Reverse Transcriptase kit (Invitrogen). The full-length human GIT1 (hGIT1, gene *GIT1*) was amplified by PCR using forward 5′-GCTGAGGATGTCCCGAAAGGG-3′ and reverse 5′-TGGCAGCACTAA GGGCACTTG-3'primers and SH-SY5Y cDNA as template. The PCR product was ligated into pCR2.1 vector (Invitrogen) by the TA-cloning method resulting in plasmid pCR-hGIT1 corresponding to transcript variant 1 (tv1; Refseq ID: NM_001085454.1). To prepare C-terminally TagRFP-tagged human GIT1, the coding sequence without stop codon was amplified from the pCR-hGIT1(tv1) using forward 5′-TCCAGAATTCAGGA TGTCCCGAAAG-3′ and reverse 5′-AGTGTCGACCTGCTTCTTCTCTCG-3′ primers. Sites recognized by restriction endonucleases are underlined. The PCR product was digested with *EcoRI*/*SalI* and ligated to pCI-TagRFP [18] resulting in the plasmid phGIT1(tv1)-TagRFP. To prepare N-terminally GST-tagged human GIT1(tv1), the coding sequence with stop codon was amplified from the pCR-hGIT1(tv1) using forward 5′-TCCAGAATTCAGGATGTCCCGAAAG-3′ and reverse 5′-AGTGTCG ACTCACTGCTTCTTCTCTCG-3′ primers. The PCR product was digested with *EcoRI*/*SalI* and ligated to pGEX-6P-1 (Amersham Biosciences) resulting in plasmid pGST-hGIT1_1–770. The N-terminal parts of GIT1 (aa 1–124), (aa 1–253) and (aa 1–376) were amplified from pCR-hGIT1(tv1) using forward primer 5′-TCCAGAATTCAGGATGTCCCGA AAG-3′ and the following reverse primers: 5′-ATTGTCGACTTAGAAGT TGGCCTGGGC-3′ (aa 1–124), 5′-ATTGTCGACTTAGTCAGCCATCTGTGG

GAT-3′ (aa 1–253) and 5′-ATTGTCGACTTAGAGGTTGTCTGTGG-3′ (aa 1–376), respectively. The PCR products were digested with *EcoRI*/*SalI* and ligated into pGEX-6P-1, resulting in plasmids pGST-hGIT1_1–124, pGST-hGIT1_1–253 and pGST-hGIT1_1–376, respectively. The C-terminal part of GIT1 (aa 377–770) was amplified from pCR-hGIT1(tv1) using forward 5′-TCCAGAATTCGAGCTGTCTCTGCGGAG-3′ and reverse 5′-AGTGTCGACTCACTGCTTCTTCTCTCG-3′ primers. The PCR product was digested with *EcoRI*/*SalI* and ligated into pGEX-6P-1, resulting in plasmid pGST-hGIT1_377–770. The N-terminal part of GIT1 (aa 1–124) was excised from pGST-hGIT1_1–124 with *EcoRI*/*SalI* and ligated to pEGFP-C2 vector (Clontech), resulting in plasmid pEGFP-hGIT1_1–124. The coding sequence of human GIT1(tv1), transcript variant 1 (NM_001085454.1) was excised from pGST-hGIT1(tv1) with *EcoRI*/*NotI* and ligated into the pCDH-CMV-MCS-EF1-neo vector (System Biosciences), resulting in lentiviral construct phGIT1(tv1)-neo.

To prepare C-terminally TagRFP-tagged human βPIX (hβPIX; gene *ARHGEF7*; RefSeq ID: NM_003899.3), the coding sequence without stop codon was amplified from N-terminally GST-tagged hβPIX(tv1), kindly provided by Dr. P.J. Hordijk [19,20] and in this paper denoted as pGST-hβPIX(tv1)_1–646, using forward 5′-AGCGCTAGCGACATGACCG ATAATAGC-3′ and reverse 5′-TCAGTCGACTAGATTGGTCTCATCCCA-3′ primers. The PCR product was digested with *NheI*/*SalI* and ligated to pCI-TagRFP [18] resulting in plasmid phβPIX(tv1)-TagRFP. For a phenotypic rescue experiment, three silent point mutations (a332c, a335c, c338t) were generated in this construct by site-directed mutagenesis using the QuikChange II XL Site-Directed Mutagenesis Kit (Stratagene), according to the manufacturer's protocol. The resulting construct was named phβPIX(tv1)mut-TagRFP. The N-terminal part of hβPIX(tv1) (aa 1–292) was amplified from the pGST-hβPIX(tv1)_1–646 using forward 5′-GCCAGAATTCATGACCGATAATAGCAAC-3′ and reverse 5′-AGTGTCGACTTACTCCCAGTTCCGGAT-3′ primers. The PCR product was digested with *EcoRI*/*SalI* and ligated to pGEX-6P-1, resulting in plasmid pGST-hβPIX_1–292. The C-terminal part of hβPIX(tv1) (aa 293–646) was amplified from the pGST-hβPIX(tv1)_1–646 using forward 5′-TCCAGAATTCGGCGATGACATTAAAACTC-3′ and reverse 5′-AGTGTCG ACTTATAGATTGGTCTCATCCCAG-3′ primers. The PCR product was digested with *EcoRI*/*SalI* and ligated into pGEX-6P-1, resulting in plasmid pGST-hβPIX_293–646. The fragment of hβPIX(tv1) (aa 293–485) was amplified from the pGST-hβPIX(tv1)_1–646 using forward 5′-TCCAGAATTCGGCGATGACATTAAAACTC-3′ and reverse 5′-CGAGTCG ACTTAGGGCCGGAGGGGA-3′ primers. The PCR product was digested with *EcoRI*/*SalI* and ligated to pGEX-6P-1, resulting in plasmid pGST-hβPIX_293–485. The fragment of hβPIX(tv1) (aa 486–646) was amplified from the pGST-hβPIX(tv1)_1–646 using forward 5′-GCCAGAAT TCTCAGCTGCTCTCTGCTA-3′ and reverse 5′-AGTGTCGACTTATAGATTGGT CTCATCCCAG-3′ primers. The PCR product was digested with *EcoRI*/*SalI* and ligated to pGEX-6P-1, resulting in plasmid pGST-hβPIX_486–646.

To prepare C-terminally TagRFP-tagged human PAK1 (hPAK1; gene *PAK1*; RefSeq ID: NM_001128620.1), the coding sequence without stop codon was amplified from the C-terminally Myc-DDK-tagged PAK1(tv1) (Origene, Catalog No. RC225947) using forward 5′-TAAGCTA GCCATGTCAAATAACGGCCTAGA-3′ and reverse 5′-ACAGTCGACACTGCA GCAATCAGTGGAGTG-3′ primers. The PCR product was digested with *NheI*/*SalI* and ligated to pCI-TagRFP [18] resulting in plasmid phPAK1(tv1)-TagRFP.

To prepare C-terminally TagRFP-tagged human γ-tubulin, the coding sequence without stop codon was digested from phTUBG1-FLAG [21] *by EcoRI*/*SalI* and ligated into pCI-TagRFP [18] resulting in plasmid phTUBG1-TagRFP. Subsequently, the cassette encoding γ-tubulin-TagRFP was digested from the phTUBG1-TagRFP by *Eco*RI/*Not*I and ligated into pCDH-CMV-MCS-EF1-puro vector (System Biosciences), resulting in lentiviral construct phTUBG1-TagRFP-puro.

All constructs were verified by sequencing. The construct for C-terminally FLAG-tagged human nucleophosmin was obtained from Origene (RC203344). Constructs phTUBG1-FLAG for FLAG-tagged human γ-tubulin [21] and pGST-hTUBG1 for GST-tagged human γ-tubulin [22] were described previously. Plasmid pFYSH2 encoding the GST-tagged SH2 domain of Fyn kinase was described [23].

2.5. RNA interference

U2OS cells in 6-well plates were transfected with short interfering RNAs (siRNAs) at final concentration 5 nM using LipofectamineRNAi MAX (Invitrogen) according to the manufacturer's instruction. Cells were harvested 72 h after transfection. The siRNAs that target the regions present in human GIT1 (*GIT1*, NCBI RefSeq: NM_001085454.1, NM_014030.3) were purchased from Ambion and Dharmacon. The siRNAs that target the regions present in human βPIX (*ARHGEF7*, NCBI RefSeq: NM_003899.3, NM_145735.2, NM_001113511.1, NM_001113512.1, NM_001113513.1) were purchased from Ambion. The siRNAs that target the regions present in human PAK1 (*PAK1*, NCBI RefSeq: NM_001128620.1, NM_002576.4) were purchased from Ambion. Immunoblotting analysis revealed that the highest reduction of GIT1 was obtained with siRNA #s26306 (Ambion); 5′-CCTTGATCAT CGACATTCT-3′ (GIT1-KD1) and siRNA #J-020565-07 (Dharmacon); 5′-CGAGCTGCTTGTAGTGTAT-3′ (GIT1-KD2). The highest reduction of βPIX was obtained with siRNA #s16948; 5′-CAACGACAGGAATGAC AAT-3′ (βPIX-KD1) and siRNA #s16950; 5′-GGATATTAGTGTCGTG CAA-3′ (βPIX-KD2). The highest reduction of PAK1 was obtained with siRNA #143703; 5′-CCGATTTTACCGATCCATT-3′ (PAK1-KD1) and siRNA #143705; 5′-CCACTTCCTGTCACTCCAA-3′ (PAK1-KD2). The selected siRNAs targeted all transcript variants of GIT1, ARHGEF7, or PAK1, respectively.

To deplete human γ-tubulin 1 (*TUBG1*, NCBI RefSeq: NM_001070.4), siRNA s120194 (Ambion); 5′-CGCATCTCTTTCTCATATA-3′ was used [18]. Silencer GAPDH positive control siRNA (AM4624) and Silencer Negative Control #1 siRNA were from Ambion (siRNA).

Short hairpin RNAs (shRNAs), cloned into the lentiviral pLKO.1 vectors, were used for depletion of human GIT1, βPIX and PAK1 in phenotypic rescue experiments. A sets of five human GIT1 shRNA constructs, a set of five human βPIX shRNA constructs and a set of four human PAK1 shRNA constructs were purchased from Open Biosystems. Immunoblotting experiments revealed that cells with the highest reduction of GIT1 protein were obtained with vector TRCN0000008401 (GIT1-KD). Similarly, cells with the highest reduction of ARHGEF7 protein were obtained with vector TRCN0000047596 (βPIX-KD), and cells with the highest reduction of PAK1 protein were obtained with vector TRCN0000002227 (PAK1-KD). The selected vectors targeted all transcript variants of GIT1, ARHGEF7, or PAK1, respectively. The stable selected cells with reduced GIT1, βPIX or PAK1 were used for additional experiments. Cells transduced with pLKO.1 vector containing non-target shRNA (Sigma) were used as negative controls.

2.6. Lentiviral infection

Lentiviral infections were done as described previously [24] using HEK 293FT packaging cells for virus preparation. Virus particles were added to the cells and replaced after 3 d with fresh complete medium containing 2.5 μg/ml puromycin. Stable selection was achieved by culturing cells for 1–2 wk in the presence of puromycin. In phenotypic rescue experiments, selected cells with depleted GIT1, βPIX or PAK1 levels were transfected with phGIT1(tv1)-TagRFP, phβPIX(tv1)mut-TagRFP or phPAK1(tv1)-TagRFP, respectively, using Lipofectamine LTX (Invitrogen) according to the manufacturer's protocol and analyzed 72 h after transfection.

2.7. Preparation of cell extracts

Whole-cell extracts for SDS–PAGE were prepared by washing the cells in cold HEPES buffer (50 mM HEPES pH 7.6, 75 mM NaCl, 1 mM $MgCl_2$ and 1 mM EGTA), solubilizing them in hot SDS-sample buffer

without bromophenol blue and boiling for 5 min. When preparing extracts for immunoprecipitation, cells were rinsed twice in cold HEPES buffer and incubated for 10 min at 4 °C with HEPES buffer supplemented with 1% NP-40 (extraction buffer), protease inhibitor mixture and phosphatase inhibitors (1 mM Na_3VO_4, 1 mM NaF). For GST pull-down assays, cells were extracted in RIPA buffer (50 mM Tris pH 8.0, 150 mM NaCl, 1% NP-40, 0.5% sodium deoxycholate, 0.1% SDS) supplemented with protease and phosphatase inhibitors. The suspensions were then spun down (20,000 ×*g*, 15 min, 4 °C) and supernatants were collected. Protein quantification in 1% NP-40 lysates and SDS–PAGE samples was assessed with a bicinchoninic acid assay kit (Pierce) and a silver dot assay, respectively [25].

2.8. Immunoprecipitation, GST pull-down assay, kinase assay, gel electrophoresis, and immunoblotting

Immunoprecipitation was performed as previously described [26]. Cell extracts were incubated with beads of protein A saturated with: (i) mAb TU-31 (IgG2b) to γ-tubulin, (ii) rabbit Ab to GIT1, (iii) rabbit Ab to βPIX, (iv) rabbit Ab to PAK1 (sc-882), (v) rabbit Ab to non-muscle myosin (negative control), (vi) mAb NF-09 (IgG2a; negative control), or with (vii) immobilized protein A alone. Abs to GIT1, βPIX and PAK1 were used at Ig concentrations of 2 μg/ml. Ab to myosin was used at a dilution of 1:100. mAb TU-31 and mAb NF-09, in the form of hybridoma supernatants, were diluted 1:2. Alternatively, beads with immunoprecipitated material were used for the *in vitro* kinase assay as described previously [23]. The ^{32}P-labeled-immunocomplexes were separated by gel electrophoresis, blotted to membranes, and ^{32}P-labeled proteins were detected by autoradiography.

Large-scale immunoprecipitation experiments with anti-peptide monoclonal antibody to γ-tubulin TU-31 from HEK cells pretreated with pervanadate to enrich population of phosphotyrosine proteins as well as preparation of samples for MALDI/MS fingerprint analysis were performed as described previously [12]. Total 50 ml of 1% NP-40 extract at concentration 1 mg/ml was used for large-scale immunoprecipitation.

Preparation and purification of GST-tagged fusion proteins was described previously, as were pull-down assays with whole-cell extracts [27]. Alternatively, sedimented beads with immobilized GST-γ-tubulin were incubated with FLAG-tagged GIT1, βPIX or nucleophosmin at a concentration of 0.5 μg/ml in TBS (Tris-buffered saline; 10 mM Tris pH 7.4 and 150 mM NaCl). Sedimented beads with immobilized GST-GIT1 or GST-βPIX fragments were also incubated with purified FLAG-tagged γ-tubulin. The FLAG-tagged γ-tubulin was purified on Anti-FLAG M2 Affinity gel (Sigma) according to the manufacturer's protocol. In some experiments, 0.1 μg PAK1 kinase (specific activity 63–85 nmole/min/mg) was added to the beads with immobilized GST-fusion proteins and subjected to a kinase assay. For comparison of immunoprecipitation and pull-down assays, protein extracts were used at the same protein concentration.

Gel electrophoresis and immunoblotting were performed using standard protocols [28]. For immunoblotting, mAb to γ-tubulin (GTU-88) was diluted 1:10,000 and mAb to γ-tubulin (TU-32), in the form of spent culture supernatant, was diluted 1:10. Rabbit Abs to GAPDH, PAK1 (HPA03565), βPIX, actin, FLAG and GIT1 were diluted 1:50,000, 1:5000, 1:3000, 1:3000, 1:2000 and 1:1000, respectively. MAbs to paxillin and Hsp70 were diluted 1:30,000 and 1:2000, respectively. Rabbit Abs to GST and tRFP were diluted 1:50,000 and 1:1000, respectively. Secondary anti-mouse and anti-rabbit Abs conjugated with HRP were diluted 1:10,000. Bound Abs were detected by SuperSignal WestPico Chemiluminescent reagents.

2.9. Mass spectrometry

Following large-scale immunoprecipitation and concentration of peptide-eluted samples on the GST-Fyn-SH2 domain, proteins dissolved in SDS sample buffer were separated on preparative 7.5% SDS–PAGE using the Multigel-Long electrophoretic system (Biometra). Gels were stained by Coomassie Brilliant Blue G-250. The bands of interest were excised from the gel, destained, and digested by trypsin. Extracted peptides were analyzed by a MALDI-FTICR mass spectrometer (APEX-Qe) equipped with a 9.4 T superconducting magnet (both from Bruker Daltonics) at the Core Facility of the Institute of Microbiology, Academy of Sciences of the Czech Republic. The instrument was externally calibrated by using the PepMix II standard (Bruker Daltonics). The data were processed by Data Analysis 4.0 software (Bruker Daltonics) and searched by the Mascot search engine against the SwissProt 2015 database of all known *Homo sapiens* proteins.

2.10. Microtubule regrowth

Microtubule regrowth from centrosomes was followed in a nocodazole washout experiment. Cells growing on coverslips were treated with nocodazole at a final concentration of 10 μM for 1 h at 37 °C to depolymerize microtubules. Cells were then washed with medium precooled to 4 °C (4 times 5 min each) to remove the drug, transferred to new medium tempered to 26 °C, and microtubule regrowth was allowed for 1–3 min at 26 °C. After that, samples were fixed in formaldehyde/Triton X-100 [29] and postfixed in cold methanol (F/Tx/M).

2.11. Immunofluorescence microscopy

Immunofluorescence staining was performed as described [29]. Shortly, cells on coverslips were extracted with 0.1% Triton X-100 in microtubule-stabilizing buffer (MSB), fixed in 3% formaldehyde in MSB and post-fixed in methanol (Tx/F/M). Alternatively, cells were fixed with cold methanol for 20 min. In microtubule regrowth experiments, microtubules were stained with rabbit Ab to α-tubulin diluted 1:200. To visualize centrosomes, samples were incubated with mAb TU-30 (hybridoma spent culture supernatant) diluted 1:30. Rabbit Abs to pericentrin, PAK1(pS144) and PAK1(pT423) were diluted 1:500, 1:200 and 1:100, respectively. The DY549-, DY-648- and DY488-conjugated anti-mouse Abs were diluted 1:800, 1:500 and 1:200, respectively. The Cy3- and DY488-conjugated anti-rabbit Abs were diluted 1:1000 and 1:200, respectively. The preparations were mounted in MOWIOL 4-88 (Calbiochem) or in MOWIOL 4-88 supplemented with 4,6-diamidino-2-phenylindole (DAPI; Sigma) and examined in an Olympus AX-70 Provis microscope (Olympus) equipped with 60×/1.0 NA water objective. The preparations from microtubule regrowth assay were examined on the Delta Vision Core system (AppliedPrecision) equipped with 40×/0.75 NA dry objective.

Quantification of the microtubule regrowth assay was performed in a large number of cells that after staining for α- and γ-tubulin were analyzed automatically and compared with manual analysis of a smaller number of cells to confirm the reliability of the automatic method. In the course of automatic analysis, twenty different areas per sample were taken in both fluorescence channels, and 12 optical z-sections were acquired at 0.45 μm steps. Maximum intensity projection of γ-tubulin staining was used to identify the position of centrosomes. The sum of α-tubulin immunofluorescence intensities was generated by Sum Slices projection in ImageJ software (NIH). The α-tubulin fluorescent signal near the centrosome was measured in two separate concentric circles centered at the centrosome with radii of 1.0 and 1.5 μm (regions of interest; ROIs). Background fluorescence using circles of corresponding sizes was subtracted from each measurement. Measurements were made using ImageJ. In manually performed analysis, only images of cells with a homogenous background around the centrosomes were selected. The sum of α-tubulin immunofluorescence intensities was obtained from nine-consecutive frames (0.2 μm steps) with the middle frame chosen with respect to the highest γ-tubulin intensity. For statistical analysis, two-tailed, unpaired Student's t-test was used to compare samples and to obtain P values.

2.12. Microtubule nucleation visualized by time-lapse imaging

For time-lapse imaging, U2OS cells expressing EB1-GFP were grown in glass-bottom dishes (InVitroScientific, D35–14-1.5-N) and transfected with different siRNAs, as specified in the Results section. Cells were treated with nocodazole at a final concentration of 10 μM for 1 h at 37 °C to depolymerize microtubules. Cells were then 5 times quickly rinsed with medium for live-cell imaging (DMEM without phenol red, riboflavin, folic acid, pyridoxal, $Fe[NO_3]_3$) tempered to 30 °C to remove the drug. Time-lapse sequences were immediately collected for 2 min at 1 s interval in Delta Vision Core system (Applied Precision) equipped with 60×/1.42 NA oil-immersion objective and heated chamber (30 °C). Time-lapse sequences were deconvolved by Hyugens Professional software (SVI). Newly nucleated microtubules were detected by tracking EB1 comets emanating from the centrosomes.

3. Results

3.1. GIT1, βPIX and PAK1 associate with γ-tubulin and locate to centrosomes

We have previously identified βPIX as a protein interacting with γ-tubulin in mouse bone marrow-derived mast cell line pretreated with pervanadate, a potent protein tyrosine phosphatase inhibitor [30]. For that we used immunoprecipitation with anti-peptide monoclonal antibody to γ-tubulin, elution of bound proteins with the peptide, and concentration of eluted tyrosine-phosphorylated proteins on the Fyn-SH2 domain. Proteins were then separated on SDS–PAGE and subjected to MALDI/MS fingerprint analysis. Immunoprecipitation experiments confirmed association of γ-tubulin with βPIX and its interaction protein GIT1 [12]. To evaluate whether GIT1/βPIX proteins form complexes with γ-tubulin in the other cell type, we applied the same experimental setup in HEK cells. MALDI/MS fingerprint analysis revealed that of the two independent experiments, GIT1 (also known as G protein-coupled receptor kinase-interacting protein 1, ARF GTPase-activating protein GIT1, Cool-associated and tyrosine-phosphorylated Protein, CAT1; gene name *GIT1*; Swiss-Prot identifier Q9Y2X7) was identified in the γ-tubulin complex two times. A typical example of MS identification is shown in Supplementary data, Table S1.

In cells, the GIT1/βPIX proteins can form scaffold to bring together signaling molecules affecting various cellular processes, including cytoskeletal organization [14]. It is well established that p21 protein (Cdc42/Rac)-activated kinase 1 (PAK1) associates with βPIX [31]. To ascertain whether GIT1 and βPIX associate with γ-tubulin in well-adherent U2OS cells and whether PAK1 is part of such complexes, immunoprecipitation experiments were performed with Abs to βPIX, GIT1 and PAK1. Immunoblot analysis revealed the co-precipitation of γ-tubulin with GIT1 (Fig. 1A, lane 3), βPIX (Fig. 1B, lane 3) and PAK1 (Fig. 1C, lane 3) in U2OS cells. In addition, reciprocal precipitation with Ab to γ-tubulin confirmed an interaction of GIT1 (Fig. 1H, lane 3), βPIX (Fig. 1L, lane 3) and PAK1 (Fig. 1P, lane 3) with γ-tubulin. As expected, Ab to GIT1 co-precipitated βPIX (Fig. 1I, lane 3) and PAK1 (Fig. 1M, lane 3), Ab to βPIX co-precipitated GIT1 (Fig. 1F, lane 3) and PAK1 (Fig. 1N, lane 3), and finally Ab to PAK1 co-precipitated GIT1 (Fig. 1G, lane 3) and βPIX (Fig. 1K, lane 3). Immunoprecipitation experiments also confirmed interactions between γ-tubulin and GIT1, βPIX and PAK1 in non-transformed immortalized human retinal pigment epithelial cells RPE1, proving that the association of γ-tubulin with these proteins is not restricted to transformed cells (Supplementary data, Fig. S1A–P). To independently confirm the interaction of γ-tubulin with GIT1, βPIX and PAK1, immunoprecipitation experiments were performed from HEK cells expressing C-terminally FLAG-tagged γ-tubulin or nucleophosmin. Antibodies to GIT1, βPIX and PAK1 co-immunoprecipitated exogenous γ-tubulin (Supplementary data, Fig. S1Q–S, lane 4) but not nucleophosmin, as documented in immunoprecipitation with anti-PAK1 Ab (Supplementary data, Fig. S1T, lane 5). Isotype controls for immunoprecipitation experiments are shown in Supplementary data, Fig. S2.

The hGIT1, hβPIX, and hPAK1 possess two, five, and two transcription variants (tv), respectively. Transcription variants hGIT1(tv1), hβPIX (tv1) and hPAK1(tv1) were detected in U2OS cells using cDNA and specific primers (not shown). We prepared cell lines stably expressing phGIT1(tv1)-TagRFP, phβPIX(tv1)-TagRFP or phPAK1(tv1)-TagRFP to evaluate localization of these proteins in U2OS cells. In interphase cells, both GIT1-TagRFP (Fig. 2, a–c) and βPIX-TagRFP (Fig. 2, d–f) were associated with centrosomes. Both GIT1-TagRFP (Supplementary data, Fig. S3-I, a–d) and βPIX-TagRFP (Supplementary data, Fig. S3-I, e–h) were also present on mitotic spindle poles. Similar results were obtained in live cells where, however, association of GIT1-TagRFP and βPIX-TagRFP with centrosomes was less obvious due to diffuse staining of the cytosol. On the other hand, PAK-TagRFP failed to show centrosome enrichment in interphase (Fig. 2, g–i) and mitotic cells (not shown). This also indicates that the centrosomal localizations of GIT1-TagRFP and βPIX-TagRFP are not artifacts due to protein overexpression. When different tested commercial Abs were used for immunofluorescence detection of GIT1 and βPIX, centrosomal staining was highly dependent on the used antibody batches, and some of them did not decorate centrosomes at all. For this reason, TagRFP-tagged GIT1 and TagRFP-tagged βPIX were used for subsequent localization experiments.

To detect centrosomal PAK1 we used Abs. It is well established that increased PAK1 activity is associated with autophosphorylation of

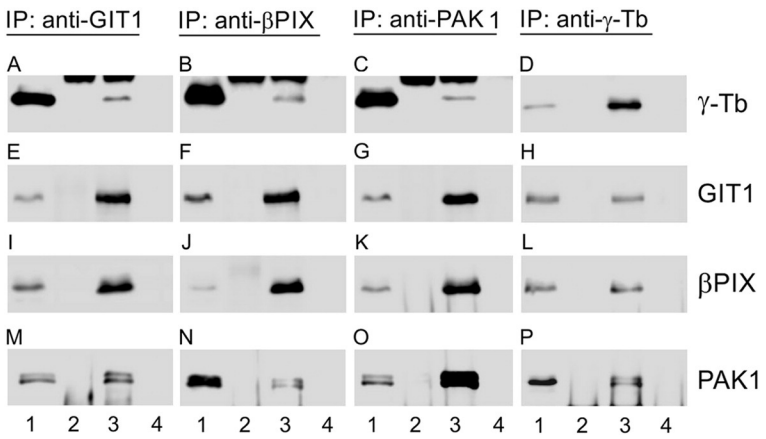

Fig. 1. GIT1, βPIX and PAK1 interact with γ-tubulin in U2OS cells. Extracts from U2OS cells were precipitated with Protein A-immobilized Abs specific to GIT1 (A, E, I and M), βPIX (B, F, J and N), PAK1 (C, G, K and O) or γ-tubulin (D, H, L and P). Blots were probed with Abs to γ-tubulin (γ-Tb), GIT1, βPIX and PAK1. Load (*lane 1*), immobilized Abs not incubated with cell extracts (*lane 2*), immunoprecipitated proteins (*lane 3*), and protein A without Abs, incubated with cell extracts (*lane 4*).

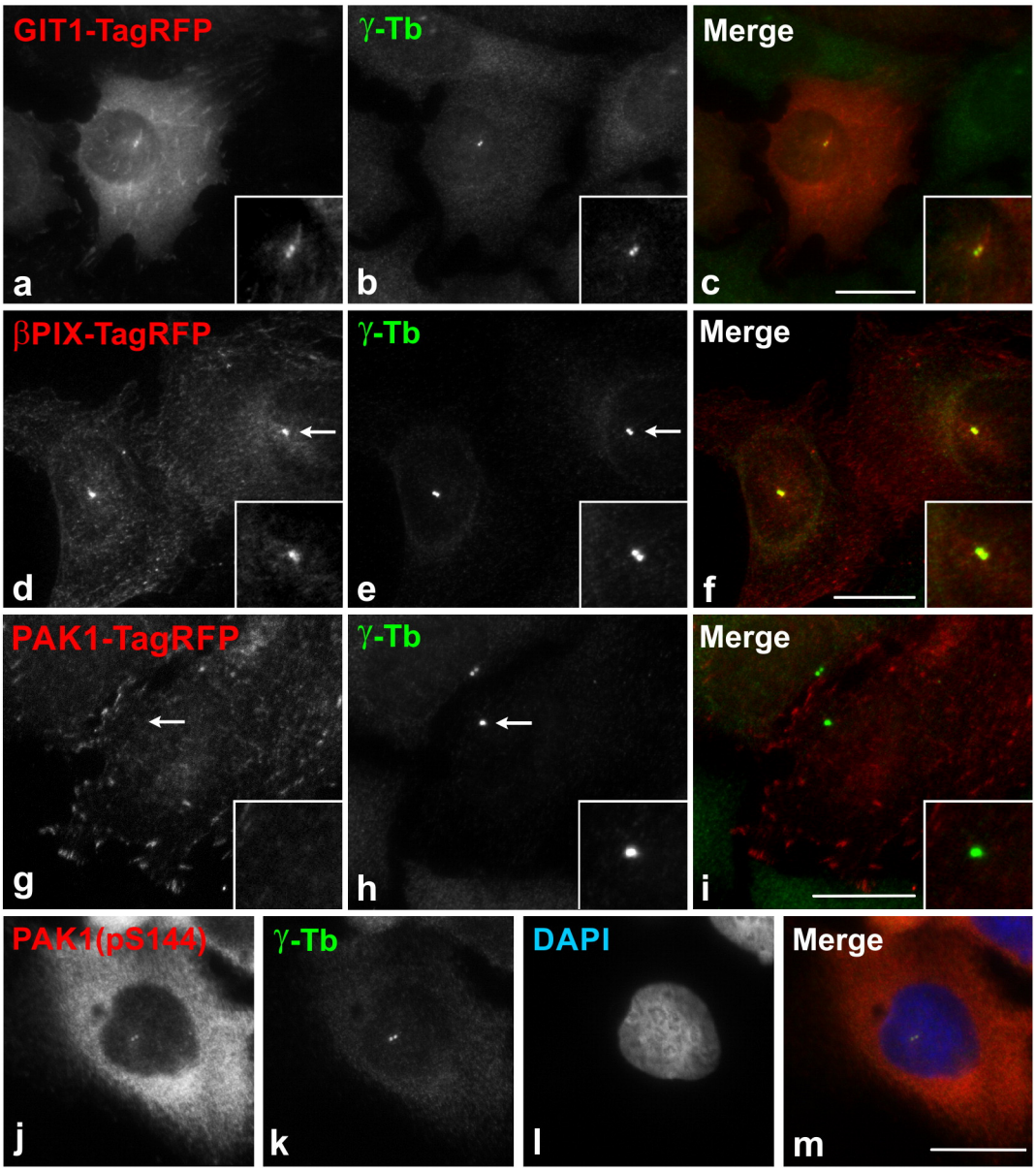

Fig. 2. Subcellular localization of GIT1, βPIX and PAK1 in interphase cells. (a–i) U2OS cells expressing TagRFP-tagged proteins were fixed and stained for γ-tubulin. (a–c) Localization of GIT1-TagRFP (a) and γ-tubulin (b). Superposition of images (c, GIT1-TagRFP, red; γ-tubulin, green). (d–f) Localization of βPIX-TagRFP (d) and γ-tubulin (e). Superposition of images (f, βPIX, red; γ-tubulin, green). (g–i) Localization of PAK1-TagRFP (g) and γ-tubulin (h). Superposition of images (i, PAK1-TagRFP, red; γ-tubulin, green). In (a–i), the best centrosomal plane is shown. Centrosomal regions are enlarged in the inserts. Arrows in (d, e, g, h) point to blown-up regions. Fixation Tx/F/M. (j–m) U2OS cells were fixed and stained for PAK1(pS144) (j), γ-tubulin (k) and DAPI (l). Superposition of images (m, PAK1(pS144), red; γ-tubulin, green; DAPI, blue). Fixation by methanol. Bars, 20 μm.

specific sites, including S144 and S199 [32]. Using Ab recognizing phospho-PAK1(pS144), clear association of autophosphorylated PAK1 with centrosomes both in interphase and mitotic cells was observed. While the immunostaining was weak in the interphase (Fig. 2, j–m), more intensive signal was detected in prophase (Supplementary data, Fig. S3-II, a–d) and metaphase (Supplementary data, Fig. S3-II, e–h), as assessed from DNA staining with DAPI. When the cells were stained with Ab to phospho-PAK1(pT423), which marks activated PAK1 [33], interphase and mitotic centrosomes were labeled (Supplementary data, Fig. S3-II, i–l). Antibody to PAK1(pS144) was used in subsequent quantification experiments, as it provided robust staining of interphase centrosomes. Centrosome localization of GIT1, βPIX and PAK1 was not affected when cells were treated with nocodazole at a final concentration of 10 μM for 60 min at 37 °C to depolymerize microtubules. This indicates no requirement for intact microtubules (not shown).

Taken collectively, the presented data suggest that GIT1, βPIX and PAK1 form complexes with γ-tubulin in various cell types, and that GIT1, βPIX and active PAK1 associate with interphase and mitotic centrosomes in U2OS cells.

3.2. GIT1, βPIX and PAK1 do not regulate microtubule nucleation in the same way

Because GIT1, βPIX and PAK1 interact with γ-tubulin, we compared microtubule regrowth from interphase centrosomes in U2OS cells with a reduced level of GIT1, βPIX or PAK1 in nocodazole-washout experiments as previously described [10,12]. To verify the method we compared microtubule regrowth in the cells where the levels of GAPDH (negative control) or γ-tubulin were depleted by siRNAs (Supplementary data, Fig. S4A). While in control cells (siControl), as well as in

GAPDH-depleted cells (data not shown), a clearly visible microtubule arrays were detected, cells with depleted γ-tubulin displayed only small microtubule asters (Supplementary data, Fig. S4G, a–b). This was supported by statistical analysis (Supplementary data, Fig. S4B–C). The extent of microtubule regrowth could be modulated by mechanisms regulating either microtubule nucleation or microtubule dynamics. It was previously reported that microtubule dynamics is regulated at the cell periphery [34] and that a delay in microtubule regrowth is associated with defects in microtubule nucleation [10,12,35].

Typical results of immunoblotting experiments after depletion of GIT1, βPIX or PAK1 proteins are shown in Fig. 3A, C and E, respectively. At the best silencing, the amount of GIT1 in GIT1-KD1 cells reached 13.4 ± 2.4%, the amount of βPIX in βPIX-KD1 cells 14.3 ± 3.1% and the amount of PAK1 in PAK1-KD1 cells 19.3 ± 3.9% (means ± SD; n = 3), compared with the expression level in control cells containing scrambled siRNA. Three independent experiments were performed with cells displaying reduced levels of GIT1, βPIX, PAK1 and corresponding control cells. α-Tubulin immunofluorescence was measured 1.5 min after washout in a 1.0 μm ROI. The results of regrowth experiments are presented after analysis of large numbers of cells analyzed automatically, but similar results were also obtained after manual analysis of limited numbers of cells. The GIT1 depletion in both GIT1-KD1 and GIT1-KD2 cells resulted in a decrease of microtubule regrowth (Fig. 3B). On the other, hand βPIX depletion led to an increase of microtubule regrowth in both βPIX-KD1 and βPIX-KD2 cells (Fig. 3D). Finally, PAK depletion resulted in a decrease of regrowth in PAK1-KD1 and PAK1-KD2 cells (Fig. 3F). Typical staining of α-tubulin in control and GIT1-depleted, βPIX-depleted or PAK1-depleted cells is shown in Fig. 3G. Immunofluorescence experiments confirmed that silencing of GIT1 (Supplementary data, Fig. S5A, a–d) or βPIX (Supplementary data, Fig. S5A, e–h) led to depletion of TagRFP-tagged proteins at centrosomes. Similarly, depletion of PAK1 resulted in centrosomal depletion of PAK1(pS144) (Supplementary data, Fig. S5A, i–l). The level of depletion of the corresponding proteins is shown in immunoblots (Supplementary data, Fig. S5B).

For phenotypic rescue experiments we prepared GIT1-, βPIX- or PAK1-deficient cells using lentiviral vectors. At the best silencing, the amount of GIT1 in GIT1-deficient cells reached 11.8 ± 1.9%, the amount of βPIX in βPIX-deficient cells 16.3 ± 2.3%, and the amount of PAK1 in PAK1-deficient cells 36.8 ± 3.9% (means ± SD; n = 3), compared with the expression level in control cells with nontarget shRNA (pLKO.1-NT). Depletion of PAK1 in PAK1-deficient cells was thus much less efficient when compared with siRNA. To rescue microtubule regrowth, TagRFP-tagged GIT1 or βPIX were expressed in GIT1- or βPIX-deficient cell lines, respectively. As the used lentiviral vector targeted 3′ UTR of mRNA for GIT1, we could rescue the knockdown phenotype with a vector producing GIT1-TagRFP. A typical result of immunoblotting experiment is shown in Fig. 4A. GIT1 depletion by shRNA resulted in a decrease in microtubule regrowth. Introduction of GIT1-TagRFP into cells with a reduced level of GIT1 restored microtubule regrowth to that in control cells (Fig. 4B). Two silent point mutations were introduced into βPIX-TagRFP to prevent its depletion by shRNA. A typical result of immunoblotting experiment is shown in Fig. 4D. βPIX depletion by shRNA led to an increase in microtubule regrowth. Introduction of βPIX-TagRFP then restored the nucleation capacity to that observed in control cells (Fig. 4E).

As a second approach, we counted the numbers of new microtubules emanating from centrosomes during microtubule regrowth using the microtubule end-binding protein 1 (EB1) to label plus ends of the growing microtubules [36]. The number of EB1 comets leaving the centrosomes per unit time (nucleation rate) was used to measure the nucleation events in real time [7,10]. To verify the method, we compared nucleation rates in control cells and cells with a depleted level of γ-tubulin (Supplementary data, Fig. S4D). While control cells had the nucleation rate 33.6 ± 2.1 comets/min (mean ± SD; n = 43), cells with the depleted level of γ-tubulin displayed 26.2 ± 1.4 comets/min (mean ± SD; n = 48). After depletion of GIT1, the nucleation rate decreased when compared to control cells (Fig. 4C). On the other hand, depletion of βPIX resulted in an increase of the nucleation rate when compared to control cells (Fig. 4F). These data support the results obtained by measuring of α-tubulin signal.

As GIT1 positively regulated microtubule nucleation, we compared microtubule regrowth in cells with an increased level of GIT1 (U2OS_GIT1-neo) and in negative control cells (U2OS_pCDH-neo). Only a minor increase in nucleation was detected in interphase U2OS_GIT-neo when compared to control cells (Z. Hájková, unpublished data). This suggests that the capacity of centrosome to harbor GIT1 or the capacity of proteins essential for activation of GIT1 to promote nucleation might be limited in interphase cells.

It has been reported that βPIX requires GIT1 for centrosome localization [15]. To investigate whether this also holds true in the U2OS cells, GIT1 was depleted by siRNA in cells expressing TagRFP-tagged βPIX and red fluorescence was quantified in GIT1-depleted and control cells. A decrease of Tag-RFP-tagged βPIX was detected in the centrosomal region (Supplementary data, Fig. S6A). However, when βPIX was depleted in cells expressing TagRFP-tagged GIT1, an increase of centrosomal GIT1-TagRFP was detected, suggesting that βPIX might also somehow modulate GIT1 localization to the centrosome (Supplementary data, Fig. S6B).

Taken collectively, these data indicate that GIT1 and PAK1 represent positive regulators and βPIX negative regulator of microtubule nucleation from the interphase centrosomes in U2OS cells.

3.3. GIT1, βPIX and PAK1 regulate the centrosome requirement for γ-tubulin

As GIT1, βPIX and PAK1 affect microtubule nucleation differently, we evaluated the possibility that the regulatory role of these proteins in microtubule nucleation is due to different accumulation of γ-tubulin at the centrosome. Firstly we quantified the immunofluorescence intensity of γ-tubulin in a control regrowth experiment, and secondly in the cells with depleted levels of GIT1, βPIX and PAK1. Both in control cells (siControl) and in GAPDH-depleted cells (negative control; data not shown) we confirmed no changes in γ-tubulin signal at the centrosomes, while depletion of γ-tubulin (positive control) resulted, as expected, in a decrease of γ-tubulin signal (Supplementary data, Fig. S4G, c–d). Statistical evaluation of γ-tubulin fluorescence documented clear differences between GAPDH-depleted (Supplementary data, Fig. S4E) and γ-tubulin-depleted (Supplementary data, Fig. S4F) cells.

After depletion of GIT1 (Fig. 5A) and PAK1 (Fig. 5C), the amount of γ-tubulin decreased, while after depletion of βPIX, the amount of γ-tubulin increased (Fig. 5B). On the other hand, the amount of pericentrin, pericentriolar marker, was not affected by depletion of GIT1, βPIX and PAK1 (Fig. 5D–F). Typical co-staining of γ-tubulin and pericentrin in control and GIT1-, βPIX- or PAK1-depleted cells is shown in Fig. 5G. The α-tubulin signals measured in these experiments were similar to those documented in Fig. 3, and correlated with the signals for γ-tubulin. Altogether, these data suggest that the regulatory roles of GIT1, βPIX and PAK1 proteins in microtubule nucleation from centrosomes are conveyed by the amount of γ-tubulin nucleation complexes (γTuRCs) at the centrosomes.

3.4. Centrosomal localization of GIT1, βPIX and PAK1 is independent of γ-tubulin

Since microtubule nucleation in GIT1-, βPIX- and PAK1-depleted cells correlated with the amount of the γ-tubulin in centrosome, we wanted to know whether the centrosomal localization of GIT1, βPIX and PAK1 in interphase cells is dependent on the presence of γ-tubulin. γ-Tubulin was depleted in U2OS cells or U2OS cells expressing GIT1-TagRFP or βPIX-TagRFP, and fluorescence of TagRFP-tagged proteins or immunofluorescence signal after staining with Ab to PAK1(pS144) was quantified in the centrosomal region.

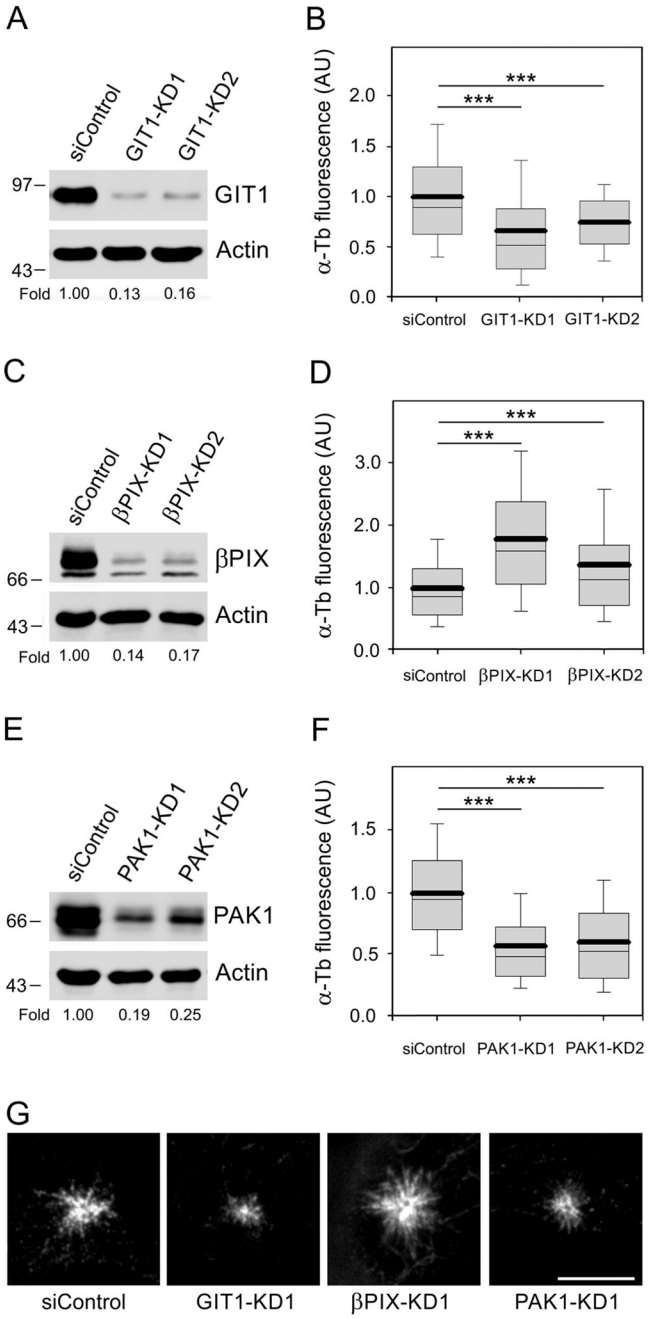

Fig. 3. GIT1, βPIX and PAK1 differently modify microtubule regrowth. (A, C, E) Immunoblot analysis of cells with reduced levels of GIT1 (A), βPIX (C) or PAK1(E). Whole-cell lysates from cells transfected with scrambled siRNA (siControl), GIT1 (A) or βPIX (C) or PAK1 (E) siRNAs. Numbers under the blots indicate the relative amount of GIT1 (A), βPIX (C) or PAK1 (E) normalized to control cells and to the amount of actin in individual samples (Fold). (B, D, F) Statistical analysis of α-tubulin fluorescence intensity in cells with depletion of GIT1 (B), βPIX (D) or PAK1 (F) relative to the control cells. Distribution of α-tubulin fluorescence intensities (arbitrary units [AU]) in 1.0-μm ROI at 1.5 min of regrowth is shown as box plots (three independent experiments, >96 cells counted for each experimental condition). (B) Box plot of GIT1-depleted cells (GIT-KD1, n = 1116; GIT-KD2, n = 631) relative to control cells (siControl, n = 942). (D) Box plot of βPIX-depleted cells (βPIX-KD1, n = 993; βPIX-KD2, n = 1228) relative to control cells (siControl, n = 1052). (F) Box plot of PAK1-depleted cells (PAK1-KD1, n = 304; PAK1-KD2, n = 288) relative to control cells (siControl, n = 313). In (B, D, F), bold and thin lines within the box represent mean and median (the 50th percentile), respectively. The bottom and top of the box represent the 25th and 75th percentiles. Whiskers below and above the box indicate the 10th and 90th percentiles. ***, $p < 1 \times 10^{-5}$. (G) Labeling of α-tubulin in microtubule regrowth experiment in control cells (siControl) and after depletion of GIT1 (GIT1-KD1), βPIX (βPIX-KD1) or PAK1 (PAK1-KD1). Cells were fixed with F/Tx/M at 1.5 min of regrowth. Images were collected and processed in exactly the same manner. Scale bar, 5 μm.

Immunoblotting experiments revealed that the amount of γ-tubulin in depleted cells reached ~15% compared to the expression level in control cells containing scrambled siRNA (not shown). Statistical evaluation revealed that depletion of γ-tubulin did not affect the amount of GIT1-TagRFP (Fig. 6A), βPIX-TagRFP (Fig. 6B) or PAK(pS144) (Fig. 6C) associated with the centrosome. Typical co-staining of the studied proteins with γ-tubulin in control and γ-tubulin-depleted cells is shown in Fig. 6D.

Taking these findings together, it is likely that the centrosomal localizations of GIT1, βPIX and PAK1 are γ-tubulin independent, and thus resemble the other proteins of pericentriolar matrix.

3.5. Identification of γ-tubulin binding sites on GIT1 and βPIX

Because γ-tubulin associated with GIT1 and βPIX in U2OS cells, we attempted to identify the regions on GIT1 and βPIX molecules responsible

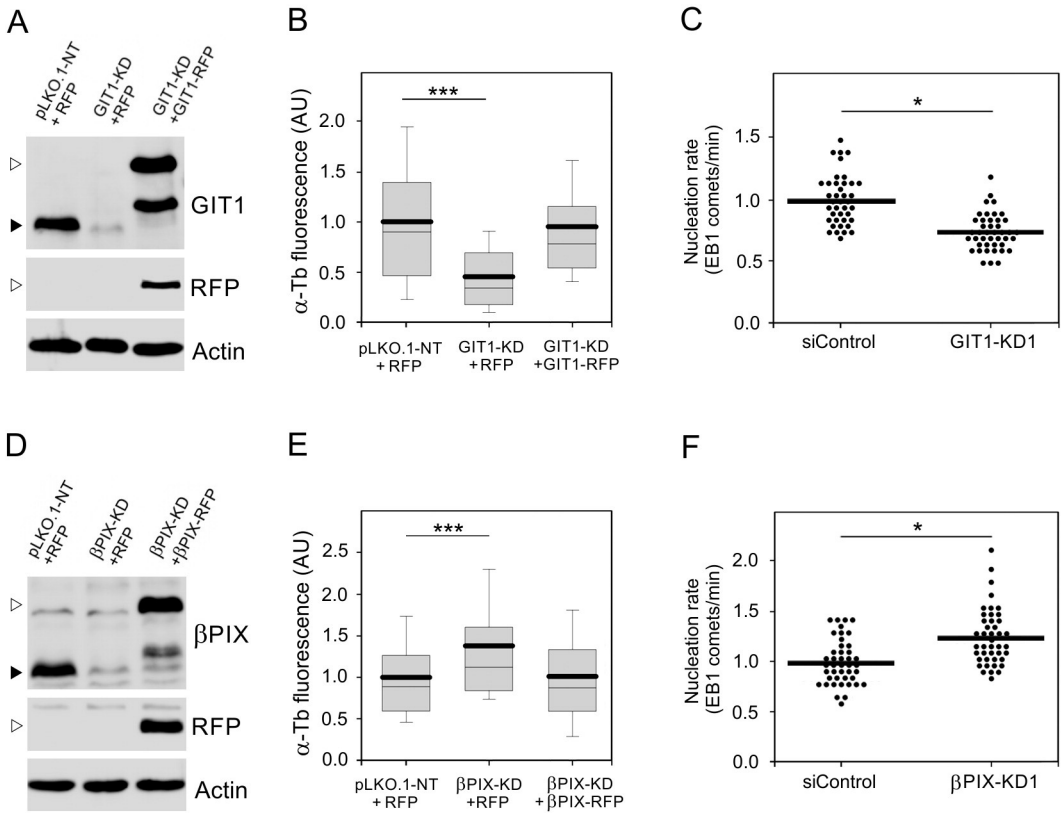

Fig. 4. Rescue of microtubule regrowth, and nucleation rate in cells with depleted levels of GIT1 or βPIX. (A, D) Immunoblot analysis of whole-cell lysates in GIT1 (A) or βPIX (D) phenotypic rescue experiments. (B, E) Microtubule regrowth in GIT1 (B) or βPIX (E) phenotypic rescue experiments. Distribution of α-tubulin fluorescence intensities (arbitrary units [AU]) in 1.0-μm ROI at 1.5 min of regrowth is shown as box plots (three independent experiments, >53 cells counted for each experimental condition). (C, F) Statistical analysis of nucleation rate in cells with a depleted level of GIT1 (C) or βPIX (F). Time-lapse imaging was used to track newly nucleated microtubules in cells stably expressing EB1-GFP. The rate of nucleated microtubules (EB1 comets/min) calculated from three independent experiments, >14 cells counted for each experimental condition. (A) Cells infected with non-target shRNA (pLKO.1-NT) containing pCI-TagRFP vector (pLKO.1-NT + RFP), cells selected after depletion of GIT1 by shRNA containing pCI-TagRFP vector (GIT1-KD + RFP), cells with depleted level of GIT1 rescued by pGIT1-TagRFP (GIT1-KD + GIT1-RFP). Blots probed with Abs to GIT1, RFP and actin. Black and white arrowheads point to GIT1 or GIT1-TagRFP, respectively. Lower band in the 3rd lane of blot stained by Ab to GIT1 represents the proteolytic fragment of GIT1-TagRFP. (B) Box plot of GIT1-depleted cells (GIT1-KD + RFP; n = 171) and GIT1-depleted cells rescued by GIT1-TagRFP (GIT1-KD + GIT1-RFP; n = 190) relative to control cells (pLKO.1-NT + RFP; n = 160). (C) Nucleation rate in cells after depletion of GIT1 by siRNA (GIT1-KD1) relative to control cells (siControl). (D) Cells infected with non-target shRNA (pLKO.1-NT) containing pCI-TagRFP vector (pLKO.1-NT + RFP), cells selected after depletion of βPIX by shRNA containing pCI-TagRFP vector (βPIX-KD + RFP), cells with depleted level of βPIX rescued by βPIXmut-TagRFP (βPIX-KD + βPIX-RFP). Blots probed with Abs to βPIX, RFP and actin. Black and white arrowheads point to βPIX or βPIXmut-TagRFP, respectively. Lower band in the 3rd lane of blot stained by Ab to βPIX represents the proteolytic fragment of βPIX-TagRFP. (E) Box plot of βPIX-depleted cells (βPIX-KD + RFP; n = 160) and βPIX-depleted cells rescued by βPIXmut-TagRFP (βPIX-KD + βPIX-RFP; n = 203) relative to control cells (pLKO.1-NT + RFP; n = 190). (F) Nucleation rate in cells after depletion of βPIX by siRNA (βPIX-KD1) relative to control cells (siControl). In (B, E), bold and thin lines within the box represent mean and median (the 50th percentile), respectively. The bottom and top of the box represent the 25th and 75th percentiles. Whiskers below and above the box indicate the 10th and 90th percentiles. ***, $p < 1 \times 10^{-5}$. In (C, F) bold line represents mean. *, $p < 0.05$.

for the interaction with γ-tubulin. GIT1 is a multi-domain protein with specific binding sites for βPIX and paxillin [37], as schematically illustrated in Fig. 7A. GST-tagged whole-length GIT1, its truncated versions (Fig. 7B), and GST alone were used in pull-down experiments. γ-Tubulin associated with the full-length molecule and all the fusion proteins containing the C-terminal GAP domain (aa 1–376, 1–253 and 1–124). No interaction was observed with the fusion protein covering the C-terminal half of the molecule (aa 377–770) or GST alone (Fig. 7C, γ-Tb). βPIX interacted with the full-length protein and 1–376 fragment containing the Spa2 homology domain (SHD) that is responsible for the binding of βPIX to GIT1 (Fig. 7C, βPIX). We observed almost no binding of endogenous paxillin to the full-length GIT1 protein, while paxillin interacted with the truncated GIT1 (aa 377–770) containing paxillin binding domain PBD (Fig. 7C, Paxillin). Very poor binding of endogenous paxillin to the full-length inactivated GIT1 has been reported previously [38]. As expected, PAK1, which associates with βPIX, interacted with the aa region 1–376 (not shown). The staining with Ab to GST was used to detect the amount of immobilized GST fusion proteins (Fig. 7C, GST). These results indicate that association of γ-tubulin with GST-GIT1 is independent of paxillin. When lysates prepared from wild-type, βPIX- or PAK1-depleted cells were used in the pull-down experiment with the 1–376 fragment, the amounts of bound of γ-tubulin were comparable in all three samples (not shown). The γ-tubulin-binding region on GIT1 is thus the most probably located in the GAP (aa 1–124) domain of GIT1. GAP domain of GIT1 associates with centrosome as documented in fixed U2OS cells expressing EGFP-tagged GAP domain (Fig. 7D, a) and stained for γ-tubulin (Fig. 7D, b).

βPIX is also a multi-domain protein with binding sites for GIT1 and PAK1 [39], as schematically illustrated in Fig. 7E. When the pull-down assay was performed with GST-tagged whole-length βPIX or N-terminal and C-terminal parts of the βPIX molecule (Fig. 7F), γ-tubulin associated with the full-length molecule and C-terminal aa region 293–646. No interaction was observed with the fusion protein covering the N-terminal half of the molecule (aa 1–292) or GST alone (Fig. 7G, γ-Tb). As expected, GIT1 interacted with the 293–646 fragment, as it contains the GIT1 binding domain (GBD) (Fig. 7G, GIT1). PAK1 interacted with βPIX *via* SH3 domain located in the aa region 1–292 (Fig. 7G, PAK1). The amounts of immobilized GST fusion proteins were similar, as evidenced by staining with Ab to GST (Fig. 7G, GST). These results indicate that the association of γ-tubulin with βPIX is independent of PAK1. When lysates prepared from wild-type or GIT1-depleted cells were used in the pull-down experiment with 293–646 fragment, the amount of bound γ-tubulin was comparable (not shown). This suggests that γ-tubulin could bind to βPIX not only *via* GIT1.

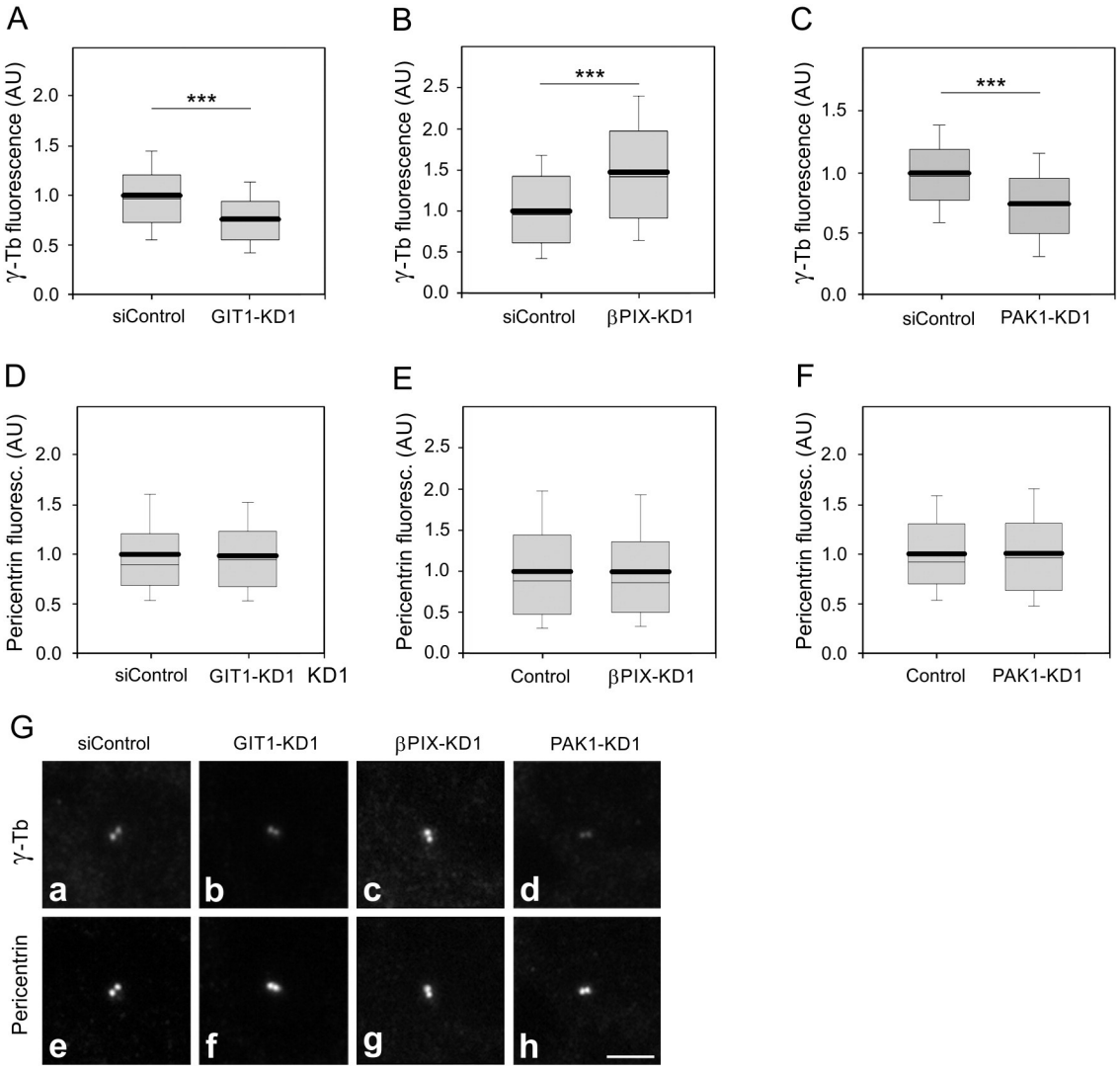

Fig. 5. GIT1, βPIX and PAK1 differently affect accumulation of γ-tubulin but not pericentrin in the centrosome. Statistical analysis of γ-tubulin (A–C) or pericentrin (D-F) fluorescence intensities in U2OS cells with a depleted level of GIT1 (A, D), βPIX (B, E) or PAK1 (C, F) relative to control cells. Distribution of γ-tubulin fluorescence intensities (arbitrary units [AU]) in 1-μm ROI at 1.5 min of regrowth is shown as box plots (three independent experiments, >75 cells counted for each experimental condition. (A) Box plot of GIT1-depleted cells (GIT-KD1, n = 612) relative to control cells (siControl, n = 816). (B) Box plot of βPIX-depleted cells (βPIX-KD1, n = 452) relative to control cells (siControl, n = 672). (C) Box plot of PAK1-depleted cells (PAK1-KD1, n = 225) relative to control cells (siControl, n = 240). (D) Box plot of GIT1-depleted cells (GIT-KD1, n = 277) relative to control cells (siControl, n = 418). (E) Box plot of βPIX-depleted cells (βPIX-KD1, n = 660) relative to control cells (siControl, n = 865). (F) Box plot of PAK1-depleted cells (PAK1-KD1, n = 326) relative to control cells (siControl, n = 355). Bold and thin lines within the box represent mean and median (the 50th percentile), respectively. The bottom and top of the box represent the 25th and 75th percentiles. Whiskers below and above the box indicate the 10th and 90th percentiles. ***, $p < 1 \times 10^{-5}$. (G) Labeling of γ-tubulin (a–d) and pericentrin (e-h) in microtubule regrowth experiment in control cells (siControl) and after depletion of GIT1 (GIT1-KD1), βPIX (βPIX-KD1) or PAK1 (PAK1-KD1). Cells were fixed with F/Tx/M at 1.5 min of regrowth. Images (a–d) or (e–h) were collected and processed in exactly same manner. Scale bar, 5 μm.

To decide whether γ-tubulin interacts with GIT1 and βPIX directly, the GST pull-down assay was performed with GST-γ-tubulin and purified FLAG-tagged GIT1, βPIX or nucleophosmin (NPM1, negative control). Although both GIT1 and βPIX did bind to GST-γ-tubulin, they failed to bind to GST alone. To γ-tubulin bound substantially more GIT1 than βPIX. FLAG-tagged nucleophosmin did not bind either to GST-γ-tubulin or GST (Fig. 7H). The amounts of immobilized GST fusion proteins present in each pull-down were similar (not shown). These data indicate direct binding of GIT1 and βPIX to γ-tubulin. This conclusion was supported by the pull-down assay with GST fusion domains from GIT1 or βPIX and purified FLAG-tagged γ-tubulin. The assay revealed direct binding of γ-tubulin to GIT1 (aa 1–124) (Supplementary data, Fig. S7A), as well as direct binding of γ-tubulin to βPIX (aa 486–646) (Supplementary data, Fig. S7B). FLAG-tagged nucleophosmin did not bind to GST fusion domains (not shown).

3.6. PAK1 phosphorylates GIT1 and βPIX, and inhibition of its enzymatic activity attenuates microtubule regrowth

As PAK1 can be in complex with γ-tubulin, we asked whether γ-tubulin could be phosphorylated by PAK1. The kinase assay with GST-tagged γ-tubulin, GIT1 or βPIX and purified active recombinant PAK1 revealed that while GIT1 and βPIX were phosphorylated, phosphorylation of γ-tubulin was not detected. Autophosphorylation of PAK1 was also found out (Fig. 8A). The kinase assay with GST-tagged GIT1 fragments showed that PAK1 phosphorylates multiple sites in GIT1 molecule (aa 1–376, aa 377–770), but not in the N-terminal region containing GAP (aa 1–124) and ANK domains (aa 1–253). This indicates that PAK1 phosphorylates GIT1 in the aa region 254–376 (Fig. 8B). The amounts of immobilized GST fusion proteins were similar as in Fig. 7C.

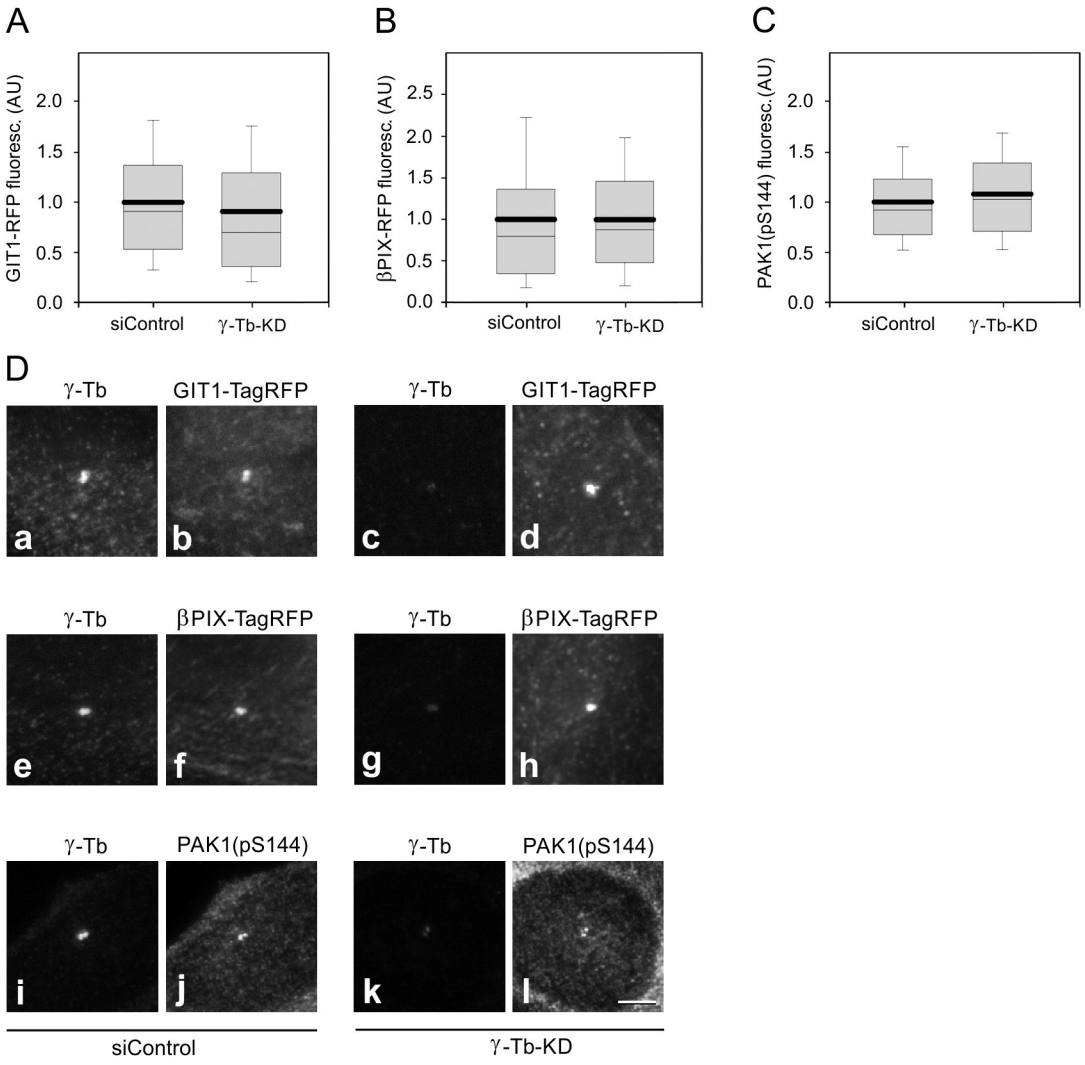

Fig. 6. Centrosomal localization of GIT1, βPIX and PAK1 is not dependent on γ tubulin. (A-C) Statistical analysis of GIT1-TagRFP (A), βPIX-TagRFP (B) or PAK1(pS144) (C) localization at centrosomes in U2OS cells with depletion of γ-tubulin relative to the control cells. Distribution of fluorescence intensities (arbitrary units [AU]) is shown as box plots (three independent experiments, >57 cells counted for each experimental condition). (A) Box plot of γ-tubulin-depleted cells (γ-Tb-KD, n = 171) relative to control cells (siControl, n = 189). (B) Box plot of γ-tubulin-depleted cells (n = 347) relative to control cells (n = 205). (C) Box plot of γ-tubulin-depleted cells (n = 197) relative to control cells (n = 212). In (A, B, C) bold and thin lines within the box represent mean and median (the 50th percentile), respectively. The bottom and top of the box represent the 25th and 75th percentiles. Whiskers below and above the box indicate the 10th and 90th percentiles. (D) Centrosomal localization of GIT1, βPIX and PAK1(pS144) in control cells and after depletion of γ-tubulin. Cells expressing GIT1-TagRFP or βPIX-TagRFP were transfected with scrambled siRNA (siControl; a–b, e–f) or γ-tubulin siRNA (c–d, g–h), fixed with Tx/F/M and stained for γ-tubulin. Alternatively, U2OS cells were transfected with scrambled siRNA (siControl; i–j) or γ-tubulin siRNA (k-l), fixed with methanol and stained for PAK1(pS144) and γ-tubulin. Pairs of images (a, c), (b, d), (e, g), (f, h), (i, k) and (j, l) were collected and processed in exactly same the manner. Bar, 5 μm.

PAK1 contains a regulatory domain that suppresses the catalytic activity of its kinase domain. IPA-3, an ATP-noncompetitive allosteric inhibitor, binds to the PAK1 regulatory domain and prevents binding to its upstream activator Rac/Cdc42. IPA-3 is a highly specific inhibitor of PAK1 [40]. Pretreatment of U2OS cells with 20 μM IPA-3 for 3 h followed by immunoprecipitation with Ab to GIT1 and *in vitro* kinase assay confirmed that both GIT1 and co-precipitated βPIX were phosphorylated by PAK1 as their phosphorylation was inhibited by IPA-3 (Fig. 8C). Phosphorylation of γ-tubulin by PAK1 kinase was not observed (not shown).

We next determined whether inhibition of PAK1 would affect nucleation and targeting of γ-tubulin to the centrosome. U2OS cells were pre-incubated in the presence of 5 μM IPA-3 or DMSO carrier (Control) for 3 h before microtubule regrowth assay. Inhibition of PAK1 activity resulted in a decrease of immunofluorescence signal for both α-tubulin (Fig. 9A) and γ-tubulin (Fig. 9B). Typical co-staining of α-tubulin and γ-tubulin or α-tubulin and pericentrin in control and IPA-3-treated cells is shown in Fig. 9C.

Altogether, these results document that GIT1 and βPIX, but not γ-tubulin, are substrates for PAK1 and that enzymatically active PAK1 modulates nucleation of microtubules in U2OS cells.

4. Discussion

The assembly of functional microtubules in interphase cells is a fundamental process involving microtubule nucleation, anchorage, and growth from centrosomes. In this study, we identified GIT1/βPIX signaling proteins and PAK1 kinase as important modulators of microtubule nucleation. GIT1 with PAK1 represent positive regulators and βPIX negative regulator of this process. We also demonstrated that the regulation is due to the changes in γ-tubulin accumulation at the interphase centrosome.

Several lines of evidence indicate that the association of GIT1, βPIX and PAK1 with γ-tubulin is specific. First, GIT1 was repeatedly identified by MALDI/MS fingerprint analysis after immunoprecipitation of

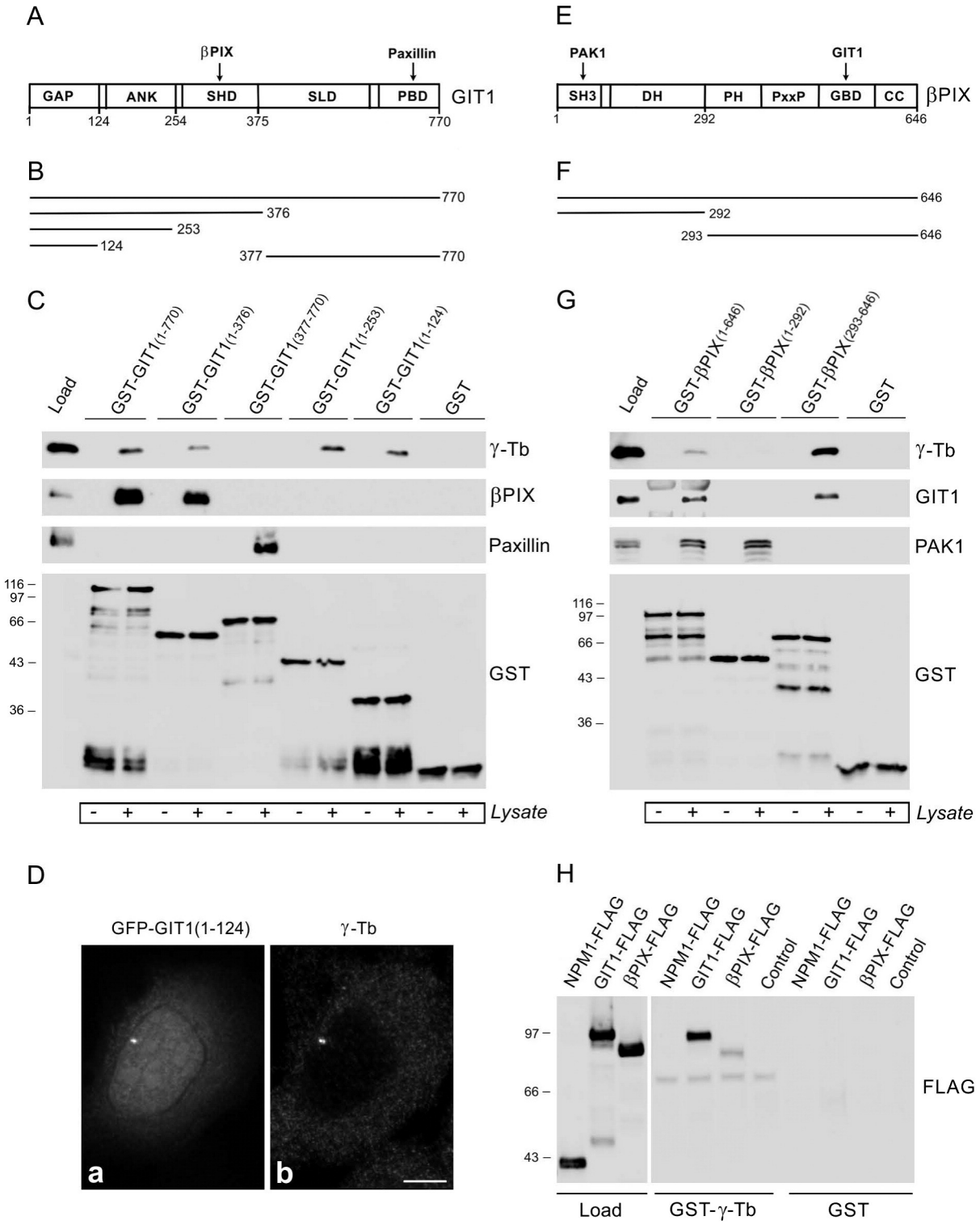

Fig. 7. Interaction of γ-tubulin with GIT1 and βPIX. (A) Schematic illustration of GIT1 (isoform 3) with domains. GIT1 contains the ARF-GAP domain (GAP), ankyrin repeats (ANK), Spa2 homology domain (SHD), synaptic localization domain (SLD) and paxillin-binding domain (PBD). βPIX and paxillin associate with GIT1 through the SHD and PBD domain, respectively. (B) Truncated forms of GIT1 used in pull-down assay. (C) GST pull-down assay with truncated GIT1. Whole-cell lysates (Load) were incubated with GST-fusion proteins or GST alone immobilized on Glutathione-Sepharose beads. Immunoblots of bound proteins were probed with Abs to γ-tubulin (γ-Tb), βPIX, paxillin and GST. (D) GAP domain of GIT1 localizes to centrosome. U2OS cells expressing EGFP-tagged amino-terminal GAP domain (aa 1–124) of GIT1 (a) were fixed and stained for γ-tubulin (b). Fixation Tx/F/M. Bar, 10 μm. (E) Schematic illustration of βPIX (isoform 1) with domains. βPIX contains the SH3 homology 3 domain (SH3), Dbl homology domain containing the Rho GEF activity (DH), pleckstrin homology domain (PH), prolin-rich region (PxxP), GIT binding domain (GBD) and coiled-coil region (CC). PAK1 and GIT1 associate with βPIX through the SH3 and GBD domain, respectively. (F) Truncated forms of βPIX used in pull-down assay. (G) GST pull-down assay with truncated βPIX. Whole-cell lysates (Load) were incubated with GST-fusion proteins or GST alone immobilized on Glutathione-Sepharose beads. Immunoblots of bound proteins were probed with Abs to γ-tubulin (γ-Tb), GIT1, PAK1 and GST. (H) GST pull-down assay with γ-tubulin. Purified FLAG-tagged GIT1, βPIX or nucleophosmin (NMP1; negative control) were incubated with immobilized GST-γ-tubulin (GST-γ-Tb) or GST alone. Controls were incubated without FLAG-tagged proteins. Immunoblots of bound proteins were probed with Ab to FLAG. Molecular-mass markers (in kDa) in C, G and H are indicated on the left.

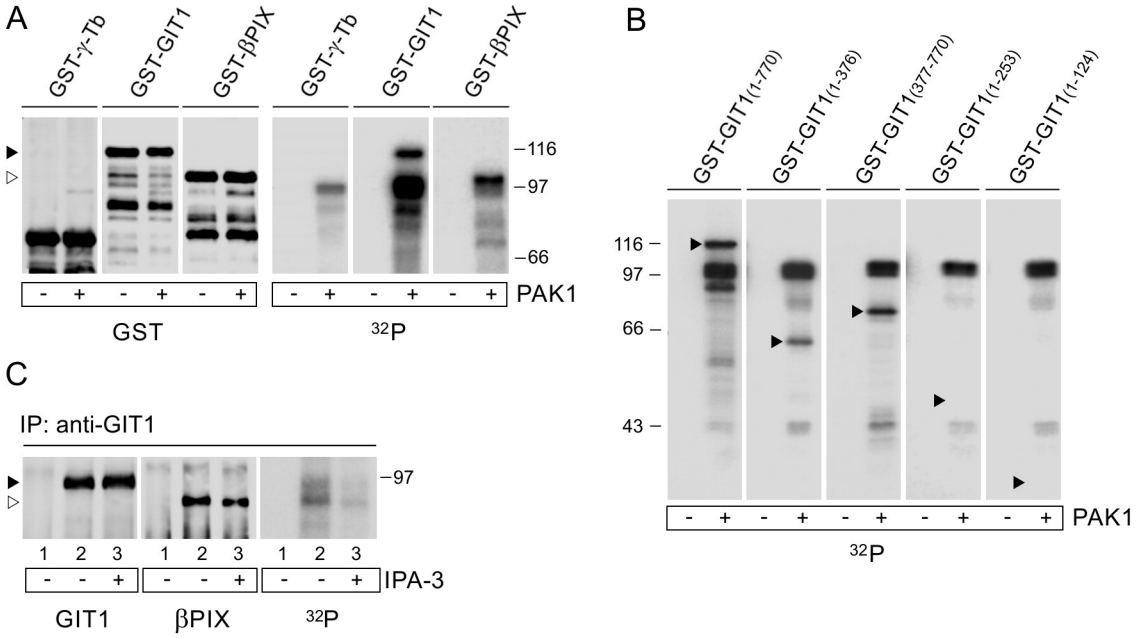

Fig. 8. PAK1 phosphorylates GIT1 and βPIX. (A) PAK1 phosphorylates GIT1 and βPIX, but not γ-tubulin, *in vitro*. GST-fusion proteins were immobilized on Glutathione-Sepharose beads and subjected to kinase assay with active PAK1. Blots were probed with Ab to GST and phosphorylated proteins were detected by autoradiography (^{32}P). Black and white arrowheads point to GIT1-GST and βPIX-GST, respectively. (B) PAK1 phosphorylates multiple sites on GIT1 *in vitro*. GST-tagged whole-length GIT1 and its truncated versions were immobilized on Glutathione-Sepharose beads and subjected to kinase assay with active PAK1. Phosphorylated proteins were detected by autoradiography (^{32}P). Black arrowheads point to position of GST-tagged proteins. Molecular-mass markers (in kDa) are indicated on the left. (C) PAK1 phosphorylates GIT1 and βPIX in U2OS cells. Cells pretreated for 3 h with 20 μM IPA-3, inhibitor of PAK1 kinase activity, or DMSO carrier alone were precipitated with Ab to GIT1, and immunocomplexes were subjected to *in vitro* kinase assay. Blots were probed with Abs to GIT1 or βPIX and phosphorylated proteins were detected by autoradiography (^{32}P). Immobilized Ab not incubated with cell extract (*lane 1*), immunoprecipitated proteins (*lanes 2–3*). Black and white arrowheads point to GIT1-GST and βPIX-GST, respectively.

pervanadate-pretreated cells with an anti-peptide mAb to γ-tubulin, elution of bound proteins with the peptide and concentration of tyrosine-phosphorylated proteins on an immobilized SH2 domain. Second, reciprocal precipitation experiments confirmed an interaction between γ-tubulin and GIT1, βPIX or PAK1. Third, FLAG-tagged γ-tubulin interacted with GIT1, βPIX and PAK1. Fourth, purified GIT1 and βPIX interacted with γ-tubulin. Finally, fluorescence microscopy with GIT1-TagRFP and βPIX-TagRFP as well as Abs to phosphorylated PAK1 revealed the localization of GIT1, βPIX and activated PAK1 on centrosomes, where γ-tubulin is accumulated, both in interphase and mitotic cells.

Interaction of γ-tubulin with GIT1, βPIX and PAK1 was observed in human cells of different tissue origin (U2OS, osteogenic sarcoma; HEK, embryonic kidney; T98G, glioblastoma; RPE1, nontransformed retinal epithelium) as well as in primary culture of mouse bone-marrow mast cells (BMMCs), established BMMC lines, and rat basophilic leukemia cell line RBL [12] (V. Sulimenko unpublished data). Formation of complexes containing γ-tubulin and these signaling molecules is, therefore, not limited to one cell type or transformed cells. Coimmunoprecipitation of PAK1 with anti-γ-tubulin Ab has been described previously [41].

GIT1 is a multi-domain protein, and several signaling molecules, including βPIX, PAK1, focal adhesion kinase (FAK), phospholipase Cγ (PLCγ) and mitogen-activated protein kinase 1 (MEK1), associate with GIT1 through its Spa2 homology domain (SHD). Paxillin binds to the paxillin-binding domain (PBD) located in the C-terminal region of GIT1 [37]. Our results from pull-down assays indicate that γ-tubulin can directly interact with GIT1 and its binding site is in the N-terminal ARF GTPase-activating protein (ARF-GAP) domain (aa 1–124). Expression of EGFP-tagged GAP domain in U2OS cells led to its concentration in centrosome. It was reported that centrosome targeting of GIT1 resides in the aa region 1–119 [15]. ADP ribosylation factors (ARFs) are small GTP-binding proteins that have several important functions, including recruitment of coat proteins that promote sorting of cargo into vesicles, recruitment and activation of enzymes such as phosphoinositide kinases, and interaction with cytoskeletal factors [42]. Previously, we have shown interaction of membrane-bound γ-tubulin with the regulatory subunit of phosphoinositide 3-kinase [22]. It has also been shown that γ-TuRC components are associated with recycling endosomes [43]. As GIT1 interacts with endosomes [44], it is possible that association of γ-tubulin with GIT1 is not limited to centrosomes.

βPIX is also a multi-domain protein, which interacts with GIT1 through GBD and with PAK1 kinase through the SH3 domain located in the N-terminal end of the molecule [31]. Our pull-down experiments revealed direct binding of γ-tubulin to the C-terminal part of molecule (aa 486–646), outside the SH3 domain. This might indicate that interaction of γ-tubulin with PAK1 is indirect. In mouse bone-marrow mast cells expressing either GFP-tagged full-length (aa 1–451) or truncated (aa 1–382) γ-tubulin, Abs to βPIX or GIT1 coprecipitated only full-length γ-tubulin. This suggests that the C-terminal region of γ-tubulin is important for the interaction with GIT1 and βPIX [12].

The phosphorylation map of GIT1 revealed multiple phosphorylation sites [37], but the corresponding kinases that phosphorylate these sites are largely unknown. Phosphorylation of GIT1 by PAK1 on serine 709, which is located within PBD of GIT1, increased its binding to paxillin and regulated protrusion activity in the cells [45]. Another PAK1-specific phosphorylation site on GIT1 was identified on serine 517, and phosphorylated PAK1 was found at centrosomes in both mitotic and interphase cells [15]. Additionally, our data showed that PAK1 can phosphorylate GIT1 in the aa region 254–376. PAK1 also phosphorylates βPIX with major phosphorylation sites on serine 525 and threonine 526 [46]. *In vitro* kinase experiments with PAK1 kinase and GST-tagged γ-tubulin, GIT1 or βPIX revealed that both GIT1 and βPIX, but not γ-tubulin, serve as substrates for PAK1. The same results were obtained when the *in vitro* kinase assay was performed after immunoprecipitation with Ab to GIT1.

Localization of GIT1, βPIX and PAK1 proteins on centrosomes in U2OS cells is independent of microtubule integrity, ruling out passive centrosomal accumulation through the microtubule transport. Their

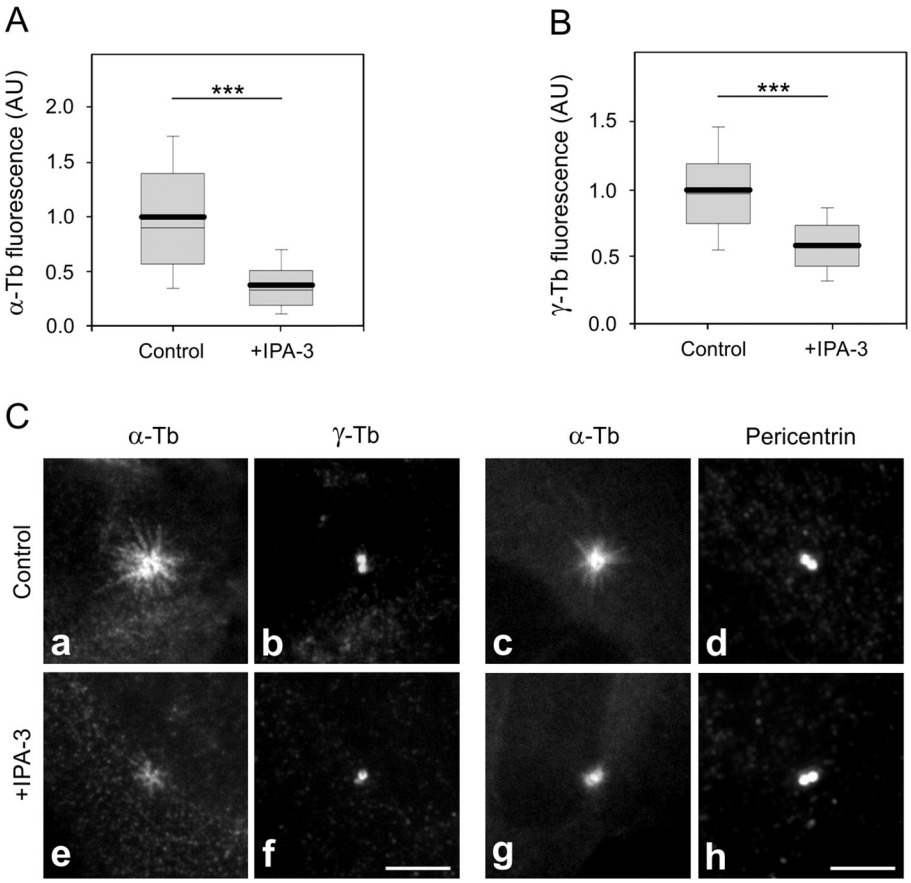

Fig. 9. Inhibition of PAK1 enzymatic activity attenuates microtubule nucleation. (A-B) U2OS cells were preincubated in the presence of 5 μM IPA-3 or DMSO carrier (Control) for 3 h before microtubule regrowth assay. Distribution of α-tubulin or γ-tubulin fluorescence intensities (arbitrary units [AU]) in 1-μm ROI at 1.5 min of regrowth is shown as box plots (three independent experiments, >133 cells counted for each experimental condition). (A) Box plot of α-tubulin fluorescence intensities in IPA-3 preincubated cells (+IPA-3, n = 418) relative to control cells (Control, n = 400). (B) Box plot of γ-tubulin fluorescence intensities in IPA-3 preincubated cells (+IPA-3, n = 418) relative to control cells (Control, n = 400). Bold and thin lines within the box represent mean and median (the 50th percentile), respectively. The bottom and top of the box represent the 25th and 75th percentiles. Whiskers below and above the box indicate the 10th and 90th percentiles. ***, $p < 1 \times 10^{-5}$. (C) Labeling of α-tubulin and γ-tubulin in microtubule regrowth experiment in control cells with DMSO carrier (Control; a–d) and cells pretreated with 5 μM IPA-3 for 3 h (+IPA-3; e–h). Cells were fixed with F/Tx/M at 1.5 min of regrowth. Pairs of images (a, e), (b, f), (c, g), (d, h) were collected and processed in exactly the same manner. Bar, 5 μm.

centrosomal localization is also independent of γ-tubulin, as revealed by experiments with depletion of γ-tubulin. In this respect GIT1, βPIX and PAK1 resemble the other proteins of pericentriolar matrix. Association of active PAK1 with the centrosome was confirmed by immunofluorescence using Abs to phosphorylated PAK1, PAK1(pS144) and PAK1(pT423). The GIT1/βPIX complex has been most widely studied in the context of integrin-mediated cell spreading and cell motility [14]. The centrosomal function of the complexes in fibroblasts has so far been reported only once. GIT1 targeting to the centrosome served as a scaffold for βPIX, and associated PAK1, activated via a process not requiring Rho GTPases, phosphorylated Aurora A in mitosis [15]. Our data demonstrate that GIT1, βPIX, as well as PAK1, regulate nucleation of interphase microtubules. Although GIT1, βPIX, and phosphorylated PAK1 are associated with centrosomes in U2OS cells, they play different regulatory roles in microtubule nucleation. Depletion of βPIX led to increased nucleation, while depletion of GIT1 or PAK1 resulted in decreased nucleation evaluated by α-tubulin signal in close proximity of the centrosome. These data were confirmed in the case of GIT1 and βPIX by rescue experiments and by counting of new microtubules emanating from the centrosomes during microtubule regrowth using the EB1 to label the plus end of the growing microtubules. The importance of PAK1 for microtubule nucleation was confirmed by inhibition of its kinase activity with ATP-noncompetitive allosteric inhibitor IPA-3. These findings, in the case of GIT1 and βPIX, confirmed our previous results obtained in mast cells [12]. Modulation of microtubule nucleation by GIT1 and βPIX is thus not limited to specialized mast cells containing secretory granules.

Microtubule nucleation at the centrosome occurs from γ-TuRCs located in the pericentriolar material [5]. We therefore asked whether GIT1/βPIX signaling proteins and PAK1 kinase regulate microtubule nucleation by affecting the centrosomal γ-tubulin levels. Our data from measuring γ-tubulin signal in regrowth experiments suggest that while GIT1 and PAK1 promote accumulation of γ-tubulin at the centrosome, βPIX inhibits such accumulation. On the other hand, no changes in the amount of pericentrin were detected. Although only GIT1 and βPIX, but not γ-tubulin, can be directly phosphorylated by PAK1, enzymatically active PAK1 modulates recruitment of γ-tubulin to centrosome and nucleation of microtubules. It has been reported that βPIX requires GIT1 for centrosome localization [15]. Our data support this finding, but additionally we surprisingly found that βPIX depletion led to centrosomal accumulation of GIT1. We surmise that it might reflect negative regulatory role of βPIX in targeting of GIT1 to centrosome. It has been reported that androgen and Src signaling, which leads to activation of the MEK/ERK pathway, regulate microtubule nucleation by promoting the accumulation of γ-tubulin at the centrosome [10,11]. It was shown that GIT1 is phosphorylated in a Src kinase-dependent manner [20] and that phosphorylation of GIT1 at Y248 and Y293 is required to release its autoinhibitory interaction [38]. In contrast, tyrosine phosphorylation of βPIX weakens its ability to bind GIT1 [47]. PAK1 might play a similar regulatory role by phosphorylation of GIT1 or βPIX.

Based on published data and findings in this report, we suggest the following hypothetical model explaining how GIT1, βPIX and PAK1 could regulate γ-tubulin and microtubule nucleation from the interphase centrosome. When PAK1 kinase is not activated, centrosomal GIT1 is maintained in its autoinhibitory folded conformation by interaction with βPIX (negative regulator of microtubule nucleation), and both GIT1 and βPIX interact with γ-tubulin. Activated PAK1 phosphorylates GIT1 or βPIX, which results in a release of βPIX and change of GIT1 conformation. Activated GIT1 (positive regulator of nucleation) enables accumulation of γ-tubulin/γ-TuRCs, leading to increased microtubule nucleation. Alternatively, activated GIT1 stimulates so far uncharacterized protein(s) to bind more γ-tubulin/γTuRCs. Our data show that general pericentriolar matrix integrity, detected by pericentrin staining, is not affected by GIT1/βPIX/PAK1. However, other proteins directly interacting with γTuRCs [48,49] could be modulated by activated GIT1. At present it is unclear whether PAK1 kinase phosphorylates, besides GIT1 and βPIX, other centrosomal protein(s) important for microtubule nucleation. This issue warrants further investigation.

In conclusion, our data suggest a novel regulatory mechanism of microtubule formation in interphase cells, in which GIT1 and βPIX signaling proteins, phosphorylated by PAK1 kinase, modulate microtubule nucleation by regulating the amount of γ-tubulin in the centrosome.

Transparency document

The Transparency document associated with this article can be found, in online version.

Acknowledgments

We thank Dr. P.L. Hordijk (Sanquin Research and Landsteiner Laboratory, University of Amsterdam, Amsterdam, Netherlands) for the GST-tagged βPIX construct, Dr. M. Bonhivers (Université Bordeaux, Bordeaux, France) for the gift of RPE1 cells, Dr. Pe. Dráber (Institute of Molecular Genetics, Prague Czech Republic) for providing Ab to GST and Karel Beránek for the help with the preparation of samples for MALDI/MS fingerprint analysis. This study was supported by the grants from the Agency of the Czech Republic (grant nos. P302/12/1673, 15-22194S and 16-23705S); the Ministry of Education, Youth and Sports of the Czech Republic (grant no LH12050); the Ministry of Health of the Czech Republic (grant no NT14467); the Agency of Charles University (GAUK 888713) and Institutional Research Support (grant no RVO 68378050).

Appendix A. Supplementary data

Supplementary data to this article can be found online at http://dx.doi.org/10.1016/j.bbamcr.2016.03.016.

References

[1] J. Lüders, T. Stearns, Microtubule-organizing centres: a re-evaluation, Nat. Rev. Mol. Cell Biol. 8 (2007) 161–167 (PMID: 17245416).
[2] M. Bornens, The centrosome in cells and organisms, Science 335 (2012) 422–426 (PMID: 22282802).
[3] C.E. Oakley, B.R. Oakley, Identification of γ-tubulin, a new member of the tubulin superfamily encoded by mipA gene of *Aspergillus nidulans*, Nature 338 (1989) 662–664 (PMID: 2649796).
[4] K. Oegema, C. Wiese, O.C. Martin, R.A. Milligan, A. Iwamatsu, T.J. Mitchison, Y. Zheng, Characterization of two related *Drosophila* γ-tubulin complexes that differ in their ability to nucleate microtubules, J. Cell Biol. 144 (1999) 721–733 (PMID: 10037793).
[5] N. Teixidó-Travesa, J. Roig, J. Lüders, The where, when and how of microtubule nucleation — one ring to rule them all, J. Cell Sci. 125 (2012) 4445–4456 (PMID: 23132930).
[6] A. Khodjakov, C.L. Rieder, The sudden recruitment of γ-tubulin to the centrosome at the onset of mitosis and its dynamic exchange throughout the cell cycle, do not require microtubules, J. Cell Biol. 146 (1999) 585–596 (PMID: 10444067).
[7] M. Piehl, U.S. Tulu, P. Wadsworth, L. Cassimeris, Centrosome maturation: measurement of microtubule nucleation throughout the cell cycle by using GFP-tagged EB1, Proc. Natl. Acad. Sci. U. S. A. 101 (2004) 1584–1588 (PMID: 14747658).
[8] L. Haren, M.H. Remy, I. Bazin, I. Callebaut, M. Wright, A. Merdes, NEDD1-dependent recruitment of the γ-tubulin ring complex to the centrosome is necessary for centriole duplication and spindle assembly, J. Cell Biol. 172 (2006) 505–515 (PMID: 16461362).
[9] X. Zhang, Q. Chen, J. Feng, J. Hou, F. Yang, J. Liu, Q. Jiang, C. Zhang, Sequential phosphorylation of Nedd1 by Cdk1 and Plk1 is required for targeting of the γTuRC to the centrosome, J. Cell Sci. 122 (2009) 2240–2251 (PMID: 19509060).
[10] D. Colello, C.G. Reverte, R. Ward, C.W. Jones, V. Magidson, A. Khodjakov, S.E. LaFlamme, Androgen and Src signaling regulate centrosome activity, J. Cell Sci. 123 (2010) 2094–2102 (PMID: 20501699).
[11] D. Colello, S. Mathew, R. Ward, K. Pumiglia, S.E. LaFlamme, Integrins regulate microtubule nucleating activity of centrosome through mitogen-activated protein kinase/extracellular signal-regulated kinase kinase/extracellular signal-regulated kinase (MEK/ERK) signaling, J. Biol. Chem. 287 (2012) 2520–2530 (PMID: 22117069).
[12] V. Sulimenko, Z. Hájková, M. Černohorská, T. Sulimenko, V. Sládková, L. Dráberová, S. Vinopal, E. Dráberová, P. Dráber, Microtubule nucleation in mouse bone marrow-derived mast cells is regulated by the concerted action of GIT1/βPIX proteins and calcium, J. Immunol. 194 (2015) 4099–4111 (PMID: 25821222).
[13] O. Schlenker, K. Rittinger, Structures of dimeric GIT1 and trimeric β-PIX and implications for GIT-PIX complex assembly, J. Mol. Biol. 386 (2009) 280–289 (PMID: 19136011).
[14] S.R. Frank, S.H. Hansen, The PIX-GIT complex: a G protein signaling cassette in control of cell shape, Semin. Cell Dev. Biol. 19 (2008) 234–244 (PMID: 18299239).
[15] Z.S. Zhao, J.P. Lim, Y.W. Ng, L. Lim, E. Manser, The GIT-associated kinase PAK targets to the centrosome and regulates Aurora-A, Mol. Cell 20 (2005) 237–249 (PMID: 16246726).
[16] M. Nováková, E. Dráberová, W. Schürmann, G. Czihak, V. Viklický, P. Dráber, γ-Tubulin redistribution in taxol-treated mitotic cells probed by monoclonal antibodies, Cell Motil. Cytoskel. 33 (1996) 38–51 (PMID: 8824733).
[17] E. Dráberová, V. Sulimenko, V. Kukharskyy, P. Dráber, Monoclonal antibody NF-09 specific for neurofilament protein NF-M, Folia Biol. (Prague) 45 (1999) 163–165 (PMID: 10732731).
[18] S. Vinopal, M. Černohorská, V. Sulimenko, T. Sulimenko, V. Vosecká, M. Flemr, E. Dráberová, P. Dráber, γ-Tubulin 2 nucleates microtubules and is downregulated in mouse early embryogenesis, PLoS ONE 7 (2012) e29919 (PMID: 22235350).
[19] J.P. ten Klooster, Z.M. Jaffer, J. Chernoff, P.L. Hordijk, Targeting and activation of Rac1 are mediated by the exchange factor β-Pix, J. Cell Biol. 172 (2006) 759–769 (PMID: 16492808).
[20] S. Bagrodia, D. Bailey, Z. Lenard, M. Hart, J.L. Guan, R.T. Premont, S.J. Taylor, R.A. Cerione, A tyrosine-phosphorylated protein that binds to an important regulatory region on the cool family of p21-activated kinase-binding proteins, J. Biol. Chem. 274 (1999) 22393–22400 (PMID: 10428811).
[21] B. Hořejší, S. Vinopal, V. Sládková, E. Dráberová, V. Sulimenko, T. Sulimenko, V. Vosecká, A. Philimonenko, P. Hozák, C.D. Katsetos, P. Dráber, Nuclear γ-tubulin associates with nucleoli and interacts with tumor suppressor protein C53, J. Cell. Physiol. 227 (2012) 367–382 (PMID: 2146547).
[22] L. Macurek, E. Dráberová, V. Richterová, V. Sulimenko, T. Sulimenko, L. Dráberová, V. Marková, P. Dráber, Regulation of microtubule nucleation from membranes by complexes of membrane-bound γ-tubulin with Fyn kinase and phosphoinositide 3-kinase, Biochem. J. 416 (2008) 421–430 (PMID: 18636972).
[23] V. Sulimenko, E. Dráberová, T. Sulimenko, L. Macurek, V. Richterová, Pe. Dráber, P. Dráber, Regulation of microtubule formation in activated mast cells by complexes of γ-tubulin with Fyn and Syk kinases, J. Immunol. 176 (2006) 7243–7253 (PMID: 16751367).
[24] Z. Hájková, V. Bugajev, E. Dráberová, S. Vinopal, L. Dráberová, J. Janáček, Pe. Dráber, P. Dráber, STIM1-directed reorganization of microtubules in activated cells, J. Immunol. 186 (2011) 913–923 (PMID: 21160048).
[25] P. Dráber, Quantitation of proteins in sample buffer for sodium dodecyl sulfate–polyacrylamide gel electrophoresis using colloidal silver, Electrophoresis 12 (1991) 453–456 (PMID: 1716200).
[26] V. Sulimenko, T. Sulimenko, S. Poznanovic, V. Nechiporuk-Zloy, J.K. Böhm, L. Macurek, E. Unger, P. Dráber, Association of brain γ-tubulins with αβ-tubulin dimers, Biochem. J. 365 (2002) 889–895 (PMID: 11939909).
[27] V. Kukharskyy, V. Sulimenko, L. Macurek, T. Sulimenko, E. Dráberová, P. Dráber, Complexes of γ-tubulin with non-receptor protein tyrosine kinases Src and Fyn in differentiating P19 embryonal carcinoma cells, Exp. Cell Res. 298 (2004) 218–228 (PMID: 15242776).
[28] P. Dráber, L.A. Lagunowich, E. Dráberová, V. Viklický, I. Damjanov, Heterogeneity of tubulin epitopes in mouse fetal tissues, Histochemistry 89 (1988) 485–492 (PMID: 2459085).
[29] E. Dráberová, P. Dráber, A microtubule-interacting protein involved in coalignment of vimentin intermediate filaments with microtubules, J. Cell Sci. 106 (1993) 1263–1273 (PMID: 7907338).
[30] Y. Zick, R. Sagi-Eisenberg, A combination of H_2O_2 and vanadate concomitantly stimulates protein tyrosine phosphorylation and polyphosphoinositide breakdown in different cell lines, Biochemistry 29 (1990) 10240–10245 (PMID: 2176864).
[31] E. Manser, T.H. Loo, C.G. Koh, Z.S. Zhao, X.Q. Chen, L. Tan, I. Tan, T. Leung, L. Lim, PAK kinases are directly coupled to the PIX family of nucleotide exchange factors, Mol. Cell 1 (1998) 183–192 (PMID: 9659915).
[32] C. Chong, L. Tan, L. Lim, E. Manser, The mechanism of PAK activation. autophosphorylation events in both regulatory and kinase domains control activity, J. Biol. Chem. 276 (2001) 17347–17353 (PMID: 11278486).
[33] A. Gatti, Z. Huang, P.T. Tuazon, J.A. Traugh, Multisite autophosphorylation of p21-activated protein kinase γ-PAK as a function of activation, J. Biol. Chem. 274 (1999) 8022–8028 (PMID: 10075701).

[34] Y.A. Komarova, I.A. Vorobjev, G.G. Borisy, Life cycle of MTs: persistent growth in the cell interior, asymmetric transition frequencies and effects of the cell boundary, J. Cell Sci. 115 (2002) 3527–3539 (PMID: 12154083).
[35] N. Delgehyr, J. Sillibourne, M. Bornens, Microtubule nucleation and anchoring at the centrosome are independent processes linked by ninein function, J. Cell Sci. 118 (2005) 1565–1575 (PMID: 15784680).
[36] A. Akhmanova, M.O. Steinmetz, Tracking the ends: a dynamic protein network controls the fate of microtubule tips, Nat. Rev. Mol. Cell Biol. 9 (2008) 309–322 (PMID: 18322465).
[37] D.J. Webb, M.W. Mayhew, M. Kovalenko, M.J. Schroeder, E.D. Jeffery, L. Whitmore, J. Shabanowitz, D.F. Hunt, A.F. Horwitz, Identification of phosphorylation sites in GIT1, J. Cell Sci. 119 (2006) 2847–2850 (PMID: 16825424).
[38] A. Totaro, V. Astro, D. Tonoli, I. de Curtis, Identification of two tyrosine residues required for the intramolecular mechanism implicated in GIT1 activation, PLoS ONE 9 (2014) e93199 (PMID: 24699139).
[39] M.W. Mayhew, E.D. Jeffery, N.E. Sherman, K. Nelson, J.M. Polefrone, S.J. Pratt, J. Shabanowitz, J.T. Parsons, J.W. Fox, D.F. Hunt, A.F. Horwitz, Identification of phosphorylation sites in βPIX and PAK1, J. Cell Sci. 120 (2007) 3911–3918 (PMID: 17989089).
[40] S.W. Deacon, A. Beeser, J.A. Fukui, U.E. Rennefahrt, C. Myers, J. Chernoff, J.R. Peterson, An isoform-selective, small-molecule inhibitor targets the autoregulatory mechanism of p21-activated kinase, Chem. Biol. 15 (2008) 322–331 (PMID: 18420139).
[41] S.B. Pakala, V.S. Nair, S.D. Reddy, R. Kumar, Signaling-dependent phosphorylation of mitotic centromere-associated kinesin regulates microtubule depolymerization and its centrosomal localization, J. Biol. Chem. 287 (2012) 40560–40569 (PMID: 23055517).
[42] J.G. Donaldson, C.L. Jackson, ARF family G proteins and their regulators: roles in membrane transport, development and disease, Nat. Rev. Mol. Cell Biol. 12 (2011) 362–375 (PMID: 21587297).
[43] H. Hehnly, S. Doxsey, Rab11 endosomes contribute to mitotic spindle organization and orientation, Dev. Cell 28 (2014) 497–507 (PMID: 24561039).
[44] R.J. Hoefen, B.C. Berk, The multifunctional GIT family of proteins, J. Cell Sci. 119 (2006) 1469–1475 (PMID: 16598076).
[45] D.J. Webb, M. Kovalenko, L. Whitmore, A.F. Horwitz, Phosphorylation of serine 709 in GIT1 regulates protrusive activity in cells, Biochem. Biophys. Res. Commun. 346 (2006) 1284–1288 (PMID: 16797488).
[46] C.G. Koh, E. Manser, Z.S. Zhao, C.P. Ng, L. Lim, β1PIX, the PAK-interacting exchange factor, requires localization via a coiled-coil region to promote microvillus-like structures and membrane ruffles, J. Cell Sci. 114 (2001) 4239–4251 (PMID: 11739656).
[47] Q. Feng, D. Baird, S. Yoo, M. Antonyak, R.A. Cerione, Phosphorylation of the cool-1/β-Pix protein serves as a regulatory signal for the migration and invasive activity of Src-transformed cells, J. Biol. Chem. 285 (2010) 18806–18816 (PMID: 20375009).
[48] J. Lüders, U.K. Patel, T. Stearns, GCP-WD is a γ-tubulin targeting factor required for centrosomal and chromatin-mediated microtubule nucleation, Nat. Cell Biol. 8 (2006) 137–147 (PMID: 16378099).
[49] S. Petry, R.D. Vale, Microtubule nucleation at the centrosome and beyond, Nat. Cell Biol. 17 (2015) 1089–1093 (PMID: 26316453).

Supplementary data

Supplementary Table S1. Mass spectrometry identification of GIT1

Measured mass	Theoretical mass	Error (ppm)	Peptide sequence	Peptide position
1589.6760	1589.6749	1	GVLVCDECCSVHR	27 - 39
1151.5788	1151.5797	-1	YQM(ox)LAFVHK	111 - 119
834.4239	834.4236	0	TPIDYAR	202 - 208
1424.6600	1424.6606	0	LVECQYELTDR	219 - 229
998.5009	998.5008	0	LAFYLCGR	230 - 237
1842.8362	1842.8346	1	LFEELAMDVYDEVDR	275 - 289
1858.8282	1858.8295	-1	LFEELAM(ox)DVYDEVDR	275 - 289
2183.0625	2183.0607	1	ENDAVWLATQNHSTLVTER	291 - 309
1746.8940	1746.8941	0	SAVPFLPVNPEYSATR	310 - 325
1530.7884	1530.7889	0	SLSSPTDNLELSLR	359 - 372
1083.6030	1083.6036	-1	LQAENLQLR	464 - 472
1463.6573	1463.6576	0	AEHTPM(ox)APGGSTHR	488 - 501
884.5082	884.5079	0	NIQELLR	655 - 661

```
  1 MSRKGPRAEV CADCSAPDPG WASISRGVLV CDECCSVHRS LGRHISIVKH LRHSAWPPTL
 61 LQMVHTLASN GANSIWEHSL LDPAQVQSGR RKANPQDKVH PIKSEFIRAK YQMLAFVHKL
121 PCRDDDGVTA KDLSKQLHSS VRTGNLETCL RLLSLGAQAN FFHPEKGTTP LHVAAKAGQT
181 LQAELLVVYG ADPGSPDVNG RTPIDYARQA GHHELAERLV ECQYELTDRL AFYLCGRKPD
241 HKNGHYIIPQ MADSLDLSEL AKAAKKKLQA LSNRLFEELA MDVYDEVDRR ENDAVWLATQ
301 NHSTLVTERS AVPFLPVNPE YSATRNQGRQ KLARFNAREF ATLIIDILSE AKRRQQGKSL
361 SSPTDNLELS LRSQSDLDDQ HDYDSVASDE DTDQEPLRST GATRSNRARS MDSSDLSDGA
421 VTLQEYLELK KALATSEAKV QQLMKVNSSL SDELRRLQRE IHKLQAENLQ LRQPPGPVPT
481 PPLPSERAEH TPMAPGGSTH RRDRQAFSMY EPGSALKPFG GPPGDELTTR LQPFHSTELE
541 DDAIYSVHVP AGLYRIRKGV SASAVPFTPS SPLLSCSQEG SRHTSKLSRH GSGADSDYEN
601 TQSGDPLLGL EGKRFLELGK EEDFHPELES LDGDLDPGLP STEDVILKTE QVTKNIQELL
661 RAAQEFKHDS FVPCSEKIHL AVTEMASLFP KRPALEPVRS SLRLLNASAY RLQSECRKTV
721 PPEPGAPVDF QLLTQQVIQC AYDIAKAAKQ LVTITTREKK Q
```

Amino acids of the identified peptides in the human G protein-coupled receptor kinase-interacting protein (GIT)1 (canonical sequence of isoform 1; UniProtKB/Swiss-Prot Q9Y2X7-1) are indicated in bold and underlined (bottom part of the table). The matched peptides cover 18.7 % of the protein sequence.

Figure S1

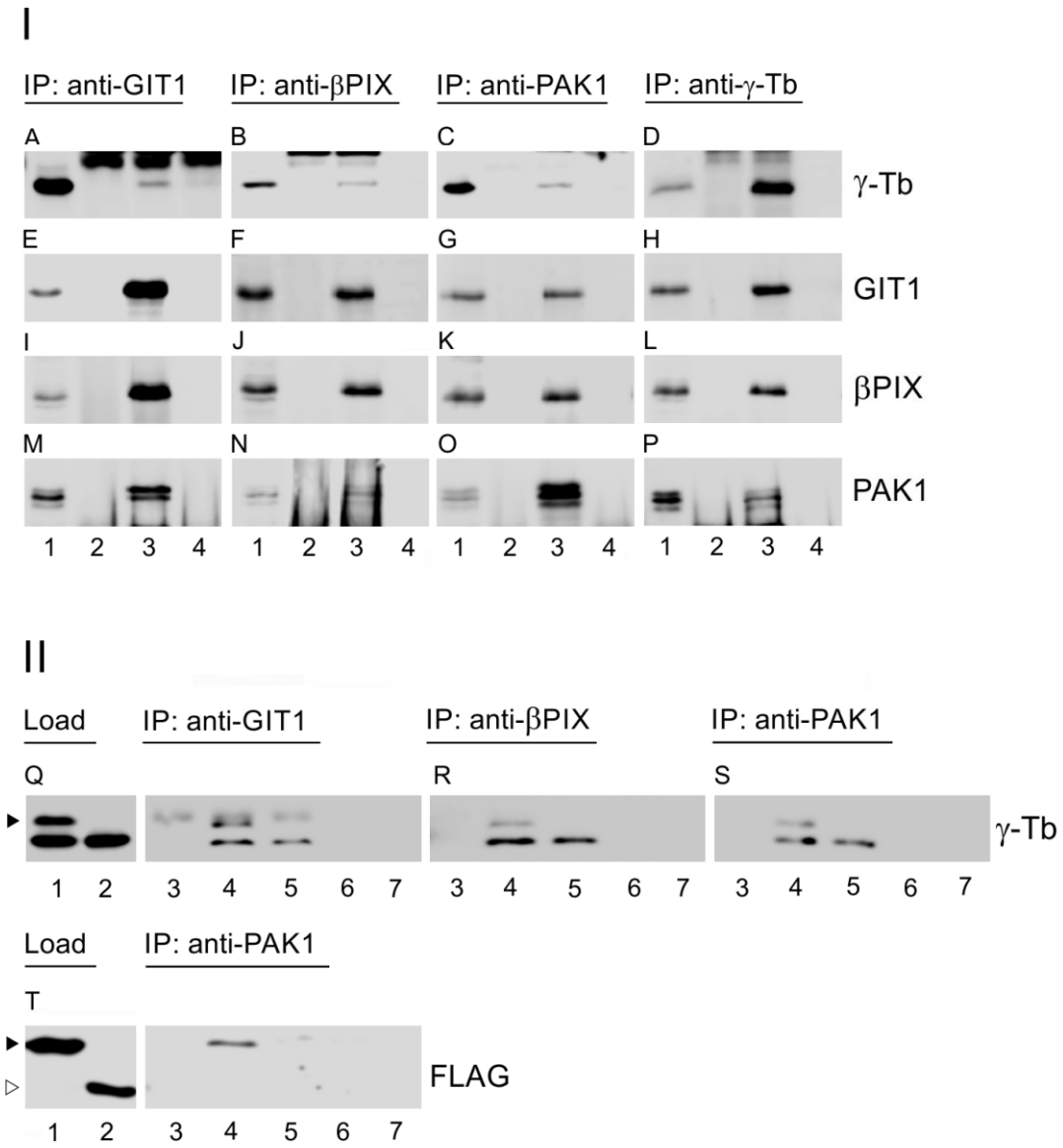

Fig. S1. GIT1, βPIX and PAK1 interact with γ-tubulin in nontransformed RPE1 cells and with exogenous γ-tubulin. (*I*) Extracts from RPE1 cells were precipitated with Protein A-immobilized Abs specific to GIT1 (A, E, I and M), βPIX (B, F, J and N), PAK1 (C, G, K and O), or γ-tubulin (D, H, L and P). Blots were probed with Abs to γ-tubulin (γ-Tb), GIT1, βPIX and PAK1. Load (*lane 1*), immobilized Abs not incubated with cell extracts (*lane 2*), immunoprecipitated proteins (*lane 3*), and protein A without Abs, incubated with cell extracts (*lane 4*). (*II*) Extracts from HEK cells expressing FLAG-tagged γ-tubulin or FLAG-tagged nucleophosmin were precipitated with Protein A-immobilized Abs specific to GIT1 (Q), βPIX (R) or PAK1 (S, T). Blots were probed with Abs to γ-tubulin (γ-Tb) or FLAG. Load with γ-tubulin-FLAG (*lane 1*), load with nucleophosmin-FLAG (*lane 2*), immobilized Abs not incubated with cell extract (*lane 3*), immunoprecipitated proteins from extract containing γ-tubulin-FLAG (*lane 4*), immunoprecipitated proteins from extract containing nucleophosmin-FLAG (*lane 5*), protein A without Abs, incubated with cell extract containing γ-tubulin-FLAG (*lane 6*) and protein A without Abs, incubated with cell extract containing nucleophosmin-FLAG (*lane 7*). Black arrowheads and white arrowhead point to γ-tubulin-FLAG or nucleophosmin-FLAG, respectively.

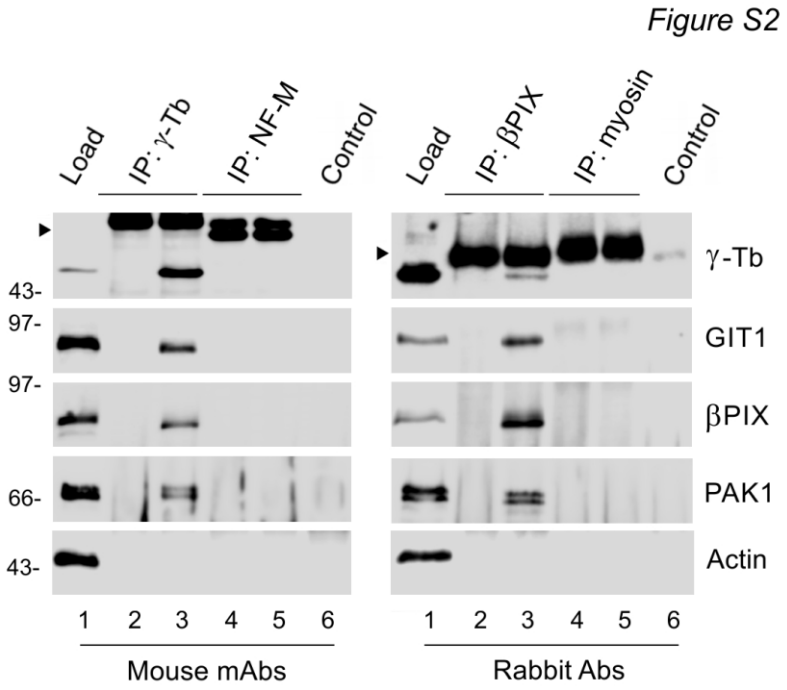

Fig. S2. Isotype controls for immunoprecipitation experiments. Extracts from U2OS cells were precipitated with Protein A-immobilized mAb to γ-tubulin (IgG2b), mAb to NF-M (IgG2a), rabbit Ab to βPIX, or rabbit Ab to myosin. Blots were probed with Abs to γ-tubulin (γ-Tb), GIT1, βPIX, PAK1 and actin. Load (*lane 1*), immobilized Abs not incubated with cell extracts (*lanes 2 and 4*), immunoprecipitated proteins (*lanes 3 and 5*), and Protein A without Ab, incubated with cell extract (*lane 6*, Control). Molecular-mass markers (in kDa) are indicated on the left. Black arrowheads indicate positions of Ab heavy chains.

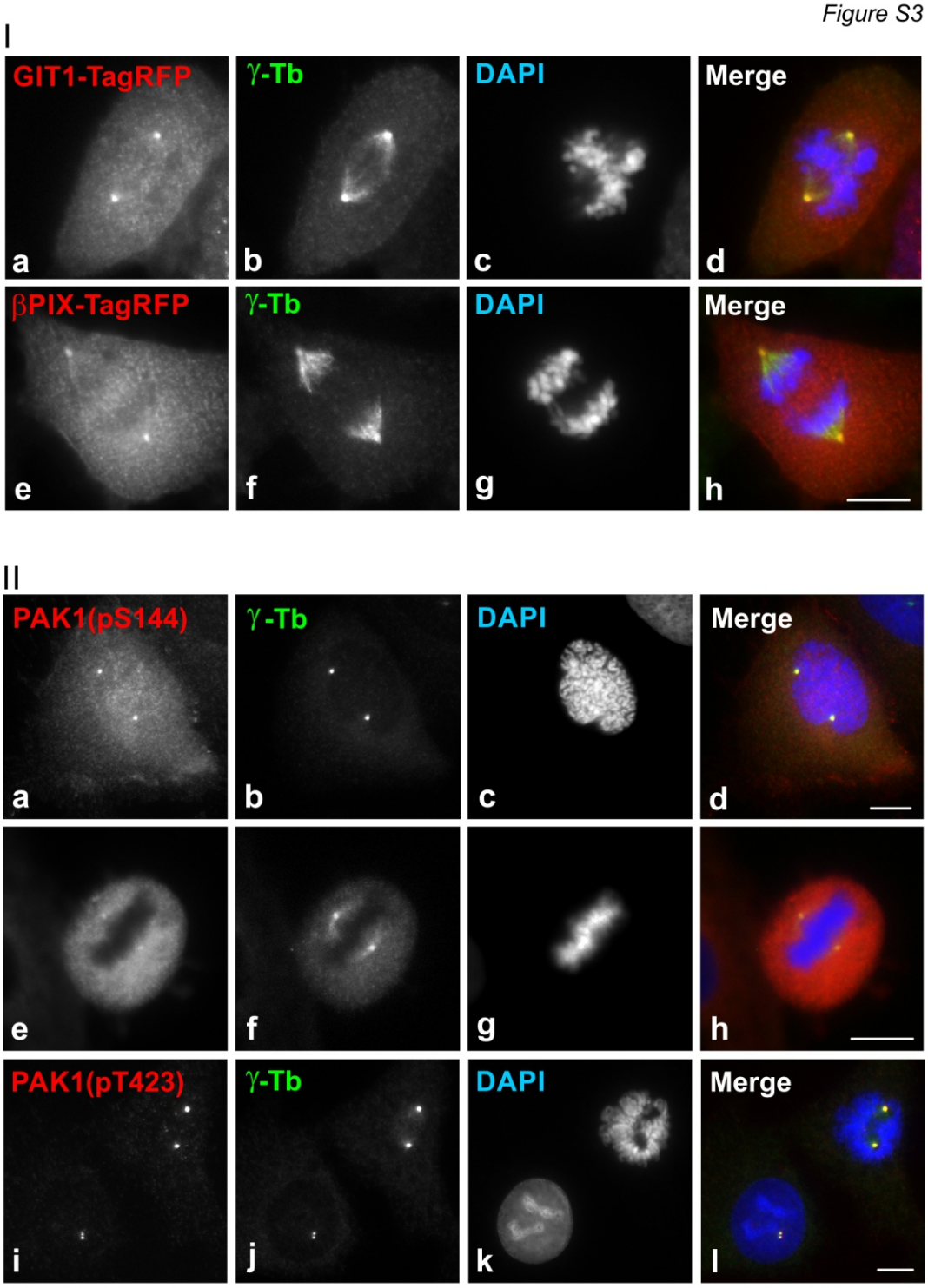

Fig. S3. Subcellular localization of GIT1, βPIX and PAK1 in mitotic U2OS cells. *(I)* Cells expressing TagRFP-tagged GIT1 or βPIX were fixed and stained for γ-tubulin. (a-d) Localization of GIT1-TagRFP (a), γ-tubulin (b) and DAPI (c). Superposition of images (d, GIT1-TagRFP, red; γ-tubulin, green; DAPI, blue). (e-h) Localization of βPIX-TagRFP (e), γ-tubulin (f) and DAPI (g). Superposition of images (h, βPIX-TagRFP, red; γ-tubulin, green; DAPI, blue). Fixation Tx/F/M. Bar, 10 μm. *(II)* Cells were fixed and stained for PAK1(pS144) (a, e; red) and γ-tubulin (b, f; green). DAPI (c, g; blue). Superposition of images (a-c) and (e-g) is shown in (d) and (h), respectively. Cells double-label stained for PAK1(pT423) (i; red) and γ-tubulin (j; green). DAPI (k; blue). Superposition of images (i-k) is shown in (l). Fixation with methanol. Bars, 10 μm.

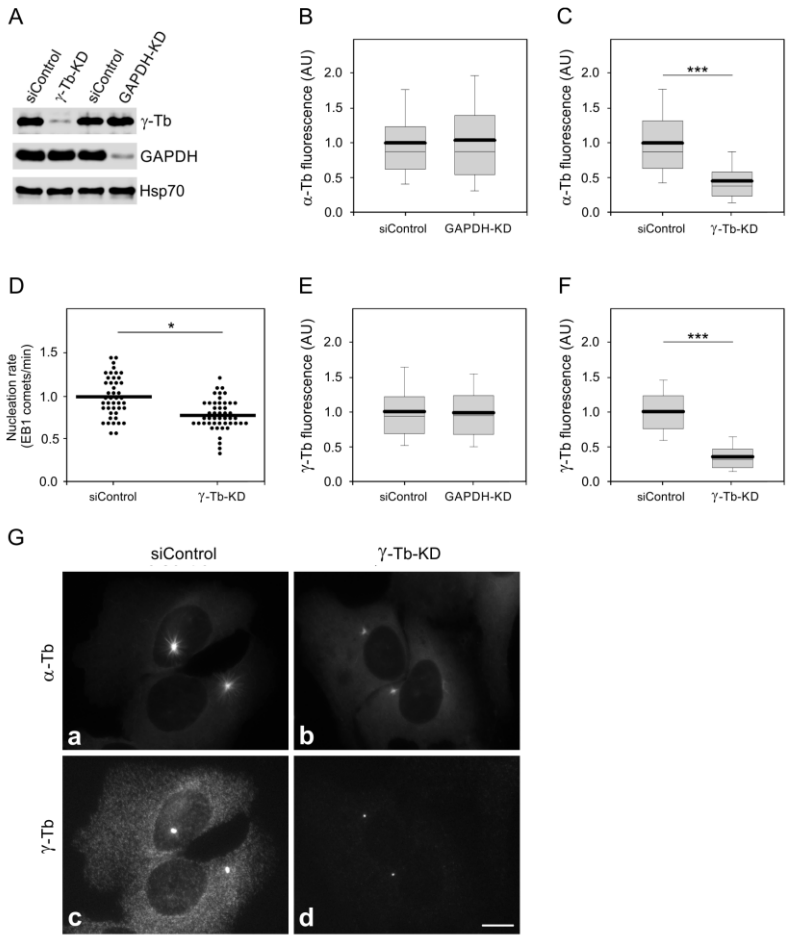

Fig. S4. Depletion of γ-tubulin affects microtubule regrowth. (A) Immunoblot analysis of cells with reduced levels of γ-tubulin and GAPDH. Whole-cell lysates from cells transfected with scrambled siRNA (siControl), γ-tubulin (γ-Tb-KD) or GAPDH (GAPDH-KD) siRNAs. Blots were probed with Abs to γ-tubulin (γ-Tb), GAPDH or Hsp70 (loading control). (B-C) Statistical analysis of α-tubulin fluorescence intensity in cells with depleted GAPDH (B) or γ-tubulin (C) relative to control cells. Distribution of α-tubulin fluorescence intensities (arbitrary units [AU]) in 1.0-μm ROI at 1.5 min of regrowth is shown as box plots (three independent experiments, >115 cells counted for each experimental condition). (B) Box plot of GAPDH-depleted cells (GAPDH-KD; n = 846) relative to control cells (siControl; n = 775). (C) Box plot of γ-tubulin-depleted cells (γ-Tb-KD; n = 347) relative to control cells (siControl; n = 446). (D) Statistical analysis of nucleation rate in cells with depleted γ-tubulin (γ-Tb-KD) relative to control cells (siControl). Time-lapse imaging was used to track newly nucleated microtubules during microtubule regrowth in cells stably expressing EB1-GFP. The rate of nucleated microtubules (EB1 comets/min) calculated from three independent experiments, >14 cells counted for each experimental condition. Bold line represents mean. *, $p < 0.05$. (E-F) Statistical analysis of γ-tubulin fluorescence intensity in cells with depleted GAPDH or γ-tubulin relative to control cells. Distribution of γ-tubulin fluorescence intensities (arbitrary units [AU]) in 1.0-μm ROI at 1.5 min of regrowth is shown as box plots (three independent experiments, > 110 cells counted for each experimental condition). (E) Box plot of GAPDH-depleted cells (GAPDH-KD; n = 641) relative to control cells (siControl; n = 607). (F) Box plot of γ-tubulin-depleted cells (γ-Tb-KD; n = 331) relative to control cells (siControl; n = 469). In (B-C) and (E-F) bold and thin lines within the box represent mean and median (the 50th percentile), respectively. The bottom and top of the box represent the 25th and 75th percentiles. Whiskers below and above the box indicate the 10th and 90th percentiles. ***, $p < 1 \times 10^{-5}$. (G) Double-label staining for α-tubulin (a-b) and γ-tubulin (c-d) in control (siControl) and γ-tubulin-depleted (γ-Tb-KD) cells at 1.5 min of microtubule regrowth. Fixation Tx/F/M. Images (a-b) and (c-d) were collected and processed in exactly the same manner. Bar, 10 μm.

Figure S5

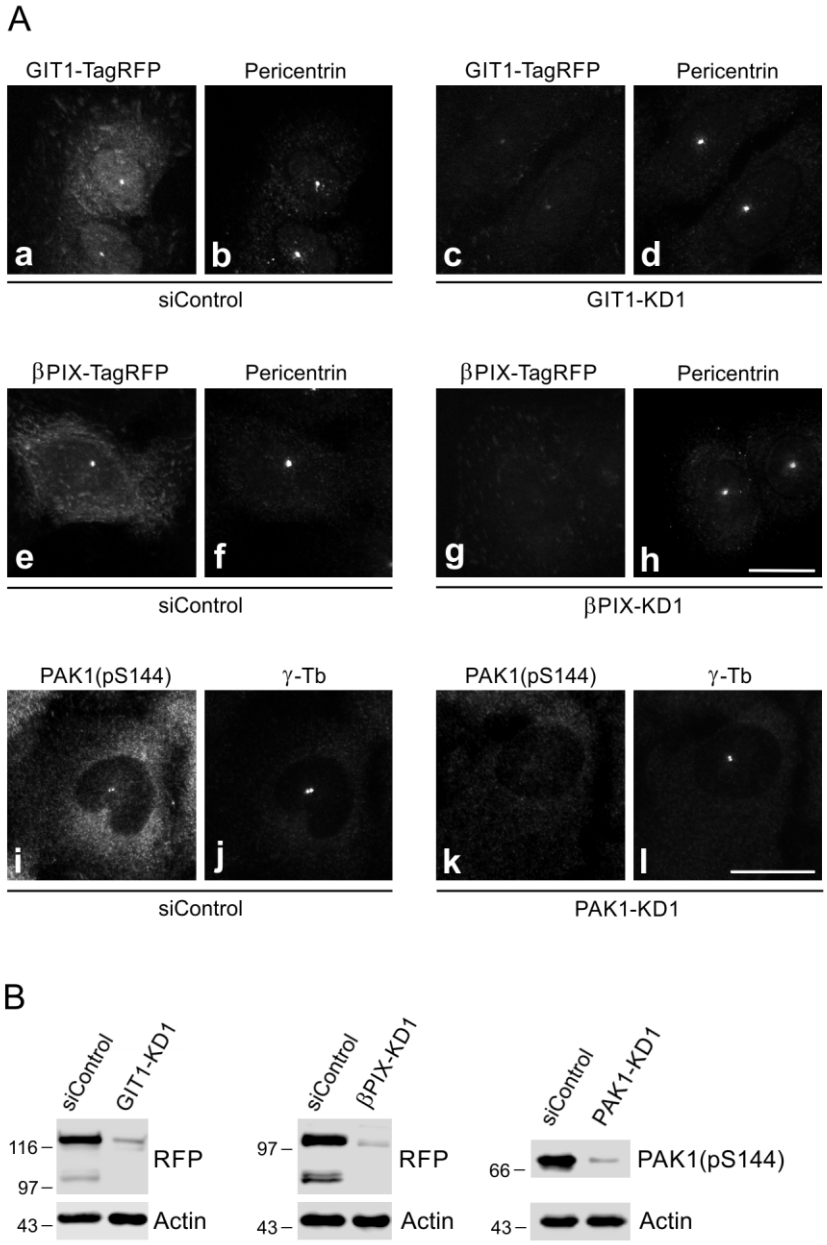

Fig. S5. Depletion of GIT1, βPIX and PAK1 inhibits their accumulation in the centrosome. (A) U2OS cells expressing TagRFP-tagged GIT1 or βPIX were transfected with scrambled siRNA (siControl; a-b, e-f), GIT1 siRNA (c-d) or βPIX siRNA (g-h), fixed with Tx/F/M and stained for pericentrin. Alternatively, U2OS cells were transfected with scrambled siRNA (siControl; i-j) or PAK1 siRNA (k-l) fixed with methanol and stained for PAK1(pS144) and γ-tubulin. Pairs of images (a, c), (b, d) (e, g) (f, h), (i, k) and (j, l) were collected and processed in exactly the same manner. Bars for (a-h) and (i-l), 20 μm. (B) Immunoblot analysis of cells with reduced levels of GIT1-TagRFP, βPIX-TagRFP or PAK1(pS144).

Figure S6

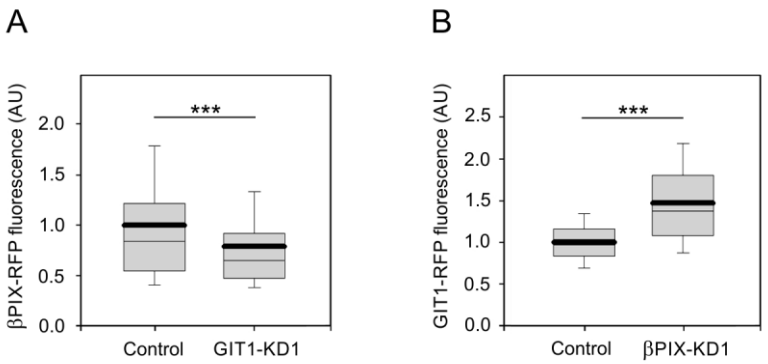

Fig. S6. Depletion of GIT1 can affect βPIX localization at centrosomes. (A) Statistical analysis of βPIX-TagRFP localization at centrosomes in cells with depletion of GIT1 relative to the control cells. (B) Statistical analysis of GIT1-TagRFP localization at centrosomes in cells with depletion of βPIX relative to the control cells. Distribution of fluorescence intensities (arbitrary units [AU]) at 1.5 min of regrowth is shown as box plots (three independent experiments, > 80 cells counted for each experimental condition). (A) Box plot of GIT1-depleted cells (GIT1-KD, n = 435) relative to control cells (siControl, n = 356). (B) Box plot of βPIX-depleted cells (βPIX-KD, n = 328) relative to control cells (n = 247). Bold and thin lines within the box represent mean and median (the 50th percentile), respectively. The bottom and top of the box represent the 25th and 75th percentiles. Whiskers below and above the box indicate the 10th and 90th percentiles. ***, $p < 1 \times 10^{-5}$.

Figure S7

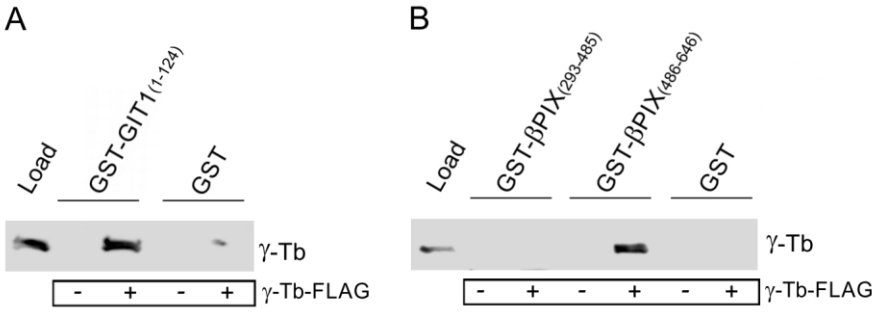

Fig. S7. Direct interaction of γ-tubulin with fragments of GIT1 and βPIX. (A) Purified FLAG-tagged γ-tubulin was incubated with immobilized GST-GIT1 fragments or GST alone. (B) Purified FLAG-tagged γ-tubulin was incubated with immobilized GST-βPIX fragments or GST alone. Immunoblots of bound proteins were probed with Ab to γ-tubulin (γ-Tb).

VI.6

Sulimenko V., **Hájková Z.**, Klebanovych A., Dráber P. (2017). Regulation of microtubule nucleation mediated by γ-tubulin complexes. Protoplasma *254*, 1187-1199.

Protoplasma (2017) 254:1187–1199
DOI 10.1007/s00709-016-1070-z

REVIEW ARTICLE

Regulation of microtubule nucleation mediated by γ-tubulin complexes

Vadym Sulimenko[1] · **Zuzana Hájková**[1] · **Anastasiya Klebanovych**[1] · **Pavel Dráber**[1]

Received: 14 October 2016 / Accepted: 22 December 2016 / Published online: 10 January 2017

Abstract The microtubule cytoskeleton is critically important for spatio-temporal organization of eukaryotic cells. The nucleation of new microtubules is typically restricted to microtubule organizing centers (MTOCs) and requires γ-tubulin that assembles into multisubunit complexes of various sizes. γ-Tubulin ring complexes (TuRCs) are efficient microtubule nucleators and are associated with large number of targeting, activating and modulating proteins. γ-Tubulin-dependent nucleation of microtubules occurs both from canonical MTOCs, such as spindle pole bodies and centrosomes, and additional sites such as Golgi apparatus, nuclear envelope, plasma membrane-associated sites, chromatin and surface of pre-existing microtubules. Despite many advances in structure of γ-tubulin complexes and characterization of γTuRC interacting factors, regulatory mechanisms of microtubule nucleation are not fully understood. Here, we review recent work on the factors and regulatory mechanisms that are involved in centrosomal and non-centrosomal microtubule nucleation.

Keywords Centrosomes · Microtubule nucleation · Microtubule-organizing centers · Non-centrosomal nucleation sites · Spindle pole bodies · γ-Tubulin complexes

Handling Editor: Reimer Stick

✉ Pavel Dráber
paveldra@img.cas.cz

[1] Department of Biology of Cytoskeleton, Institute of Molecular Genetics, Academy of Sciences of the Czech Republic, Vídeňská 1083, 142 20 Prague 4, Czech Republic

Abbreviations

AKAP450	A-kinase anchor protein 450
Cdk1	Cyclin-dependent kinase 1
CDK5RAP2	Cyclin-dependent kinase 5 regulatory subunit-associated protein 2
CLASP	Cytoplasmic linker associated protein
CM1	Centrosomin (Cnn) motif 1
EBs	End-binding proteins
γTuRC	γ-Tubulin ring complex
γTuSC	γ-Tubulin small complex
GCPs	γ-Tubulin complex proteins
GIPs	γ-Tubulin complex protein 3-interacting proteins
GM130	Golgin subfamily A member 2 protein
GRIPs	γ-Tubulin ring proteins
Mozart	Mitotic spindle-organizing protein
MTOC	Microtubule-organizing center
NEDD1	Neural precursor cell expressed, developmentally down-regulated protein 1
NME7	Nucleoside-diphosphate kinase 7
PCM	Pericentriolar material
Plk1	Polo-like kinase 1
Ran	Ras-related nuclear protein
SAFs	Spindle assembly factors
SPB	Spindle pole body
+TIPs	Microtubule plus-end tracking proteins
TPX2	Targeting protein for Xklp2

Introduction

Microtubules, 25-nm cylindrical cytoskeletal polymers, play an essential role in many vital cellular activities as maintenance of cell shape and polarity, division, migration and positioning of cellular organelles. They also serve as roads for ordered motor-

driven cargo transport and signal transduction. Microtubules can be organized into microtubule-based organelles with a specialized function, including the radial cytoplasmic network, axonemes, centrioles, midbodies and the mitotic/meiotic spindles. Singlet microtubules are the most ubiquitous forms of the polymer; however, microtubules can also form doublets (in cilia) or triplets (in centrioles and basal bodies) (Verhey and Gaertig 2007). Microtubules are assembled from globular α-tubulin–β-tubulin (αβ-tubulin) heterodimers in a GTP-dependent manner. Both α- and β-tubulins are encoded by multiple phylogenetically conserved genes (Ludueña and Banerjee 2008). Tubulins are arranged in a head-to-tail fashion to form protofilaments. A left-handed helical microtubule wall typically comprises 13 protofilaments. Microtubules are thus inherently polar and contain two structurally distinct ends: a slow-growing minus end, exposing α-tubulin subunits, and a fast-growing plus end, exposing β-tubulin subunits (Nogales and Wang 2006). In cells, microtubules are typically anchored by their minus end in microtubule organizing centers (MTOCs), whereas the plus ends are highly dynamic and switch between phases of growth and shrinkage. Microtubule dynamics helps remodel the microtubular network during the cell cycle. Microtubules can be adapted to highly divergent tasks by mechanisms that are not yet fully understood. Incorporation of alternative tubulin isotypes and post-translational modification of tubulin subunits can regulate microtubule properties. Intracellular microtubule organization is further controlled by the activity of microtubule-regulatory proteins and distribution of nucleation sites (Dráber and Dráberová 2012).

Nucleation, a de novo formation of microtubule polymer from αβ-tubulin dimers, plays the key role in microtubule organization. Microtubule assembly occurs spontaneously in vitro when the concentration of pure αβ-tubulin dimers exceeds a critical concentration. Besides that, the concentration of αβ-tubulin dimers in cells is subcritical and therefore requires a nucleating factor(s) to initiate polymerization. The canonical MTOCs are laminar spindle pole bodies (SPBs) in yeast and centrosomes in higher eukaryotes. Mitotic SPBs are embedded in the nuclear envelope with geometrically separated nuclear and cytoplasmic microtubule sites. In mammalian cells, microtubules are nucleated from centrosomes (Fig. 1), composed of two barrel-shaped orthogonally arranged centrioles wrapped in a multicomponent protein matrix called pericentriolar material (PCM). However, microtubule nucleation also takes place in other cellular locations. During interphase, microtubules are nucleated at the Golgi apparatus, the nuclear envelope, the plasma membrane-associated sites and pre-existing microtubules. During cell division, microtubules originate from spindle microtubules and the vicinity of chromatin. These non-centrosomal sites play an important role in the cell architecture (Lin et al. 2015; Petry and Vale 2015). The essential microtubule nucleation components are protein complexes formed by γ-tubulin and γ-tubulin complex proteins (GCPs) or γ-tubulin ring proteins (GRIPs).

This review will focus on the latest research and emerging questions concerning the microtubule nucleation by γ-tubulin complexes and their activating, docking and modulating factors. Specific attention will be given to centrosomal and non-centrosomal nucleation.

γ-Tubulin complexes

Microtubule nucleation is mediated in vivo by γ-tubulin protein complexes, which allow spatio-temporal control of new microtubule growth. γ-Tubulin is a highly conserved but minor member of the tubulin superfamily that is not incorporated into the microtubule polymer (Oakley and Oakley 1989). In contrast to α- and β-tubulins, there are only one to three γ-tubulin genes in eukaryotic genomes (Findeisen et al. 2014). Two human γ-tubulins are nucleation competent (Vinopal et al. 2012). γ-Tubulin is capable to form oligomers (Sulimenko et al. 2002), but it usually forms two distinct well characterized complexes. γ-Tubulin small complex (γTuSC) and the larger γ-tubulin ring complex (γTuRC), named for its characteristic ring-shaped structure. Multiple γTuSCs

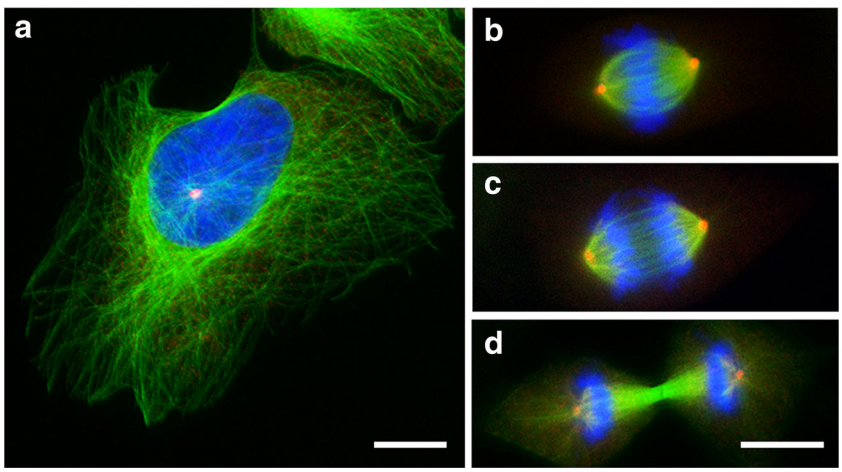

Fig. 1 Centrosomal nucleation of microtubules during the cell cycle. Human osteosarcoma U2OS cells in interphase (**a**), metaphase (**b**), anaphase (**c**) and telophase (**d**) were fixed and stained for microtubules with polyclonal antibody to α-tubulin (*green*) and for centrosomes with monoclonal antibody TU-30 (Nováková et al. 1996) to γ-tubulin (*red*). DNA is stained by DAPI (*blue*). *Bars*, 10 μm

assemble with GCP4, GCP5 and GCP6 into the conical oligomer γTuRC that is recruited to various MTOCs and serves as a template by presenting a γ-tubulin ring that mimics microtubule geometry (Kollman et al. 2011). The GCPs share regions of homology, although with very low levels of sequence identity. Two short homologous regions, N-terminal GRIP1 and C-terminal GRIP2, are unique for the GCPs (Gunawardane et al. 2000). Designations for γ-tubulins and GCPs in various organisms in which they have been studied extensively, such as *Homo sapiens*, *Xenopus laevis*, *Drosophila melanogaster*, *Arabidopsis thaliana*, *Aspergillus nidulans*, *Schizosaccharomyces pombe* and *Sacharomyces cerevisiae*, are shown in Table 1.

In budding yeast *S. cerevisiae*, which lacks the γTuRC-specific GCPs (Table 1), microtubules are nucleated from γTuSC oligomers. The γTuSC, a 300-kDa V-shaped structure, consists of two molecules of γ-tubulin molecules and one molecule each of GCP2 and GCP3. The GCPs 2 and 3 constitute elongated arms of the V shape, interacting laterally via their N-terminal domains. The C-terminal domains are located at the two tips of the V, each binding one molecule of γ-tubulin. The complex is flexible, with a hinge-like motion near the center of the GCP3 arm. The movement about this hinge alters position of γ-tubulin molecules (Kollman et al. 2008). In budding yeast, γTuSCs are driven to form γTuSC ring structure after binding to anchoraging coiled-coil protein Spc110 concentrated at SPB. In such γTuSC ring structure, resembling γTuRC, the γ-tubulin molecules are almost in the correct position to directly contact the base of the microtubule (Kollman et al. 2010). γTuRC assembly is critically dependent on the oligomerization state of Spc110, with higher-order oligomers dramatically enhancing the stability of assembled γTuRC (Lyon et al. 2016). When a hinge region in GCP3 is moved, the γ-tubulin ring precisely matches microtubule symmetry and the nucleating ability of the γTuSC ring structure is greatly enhanced. Conformation of GCP3 could therefore regulate the ability of the γTuRC to nucleate microtubules (Kollman et al. 2015). Further studies are necessary to elucidate what controls the rotation of GCP3 around its hinge.

In contrast, less is known about the architecture of a large ~2.1 MDa γTuRC. Based on the crystal structure of GCP4 and sequence similarity between GCPs, all members of GCPs were predicted to have the same elongated shape. It was confirmed that GCP4 interacts with γ-tubulin via its C-terminal domain (Guillet et al. 2011). According to the current model, GCP2-GCP6 each bind directly to γ-tubulin, and γTuSC-like structures can be formed. Replacement of one of GCP2/GCP3 with GCP4, GCP5 or GCP6 generates hybrid γTuSC. A novel γTuSC can be composed by two molecules of γ-tubulin and any combination of two molecules from GCP4-GCP6 proteins. Half complexes can be composed of a single molecule of GCP4, GCP5 or GCP6 interacting with γ-tubulin. The precise stoichiometry of GCP4–GCP6 within γTuRC remains unknown. γTuRC could be formed by five γTuSC and one molecule each of GCP4–GCP6 bound to γ-tubulin. The γTuRC then contains 13 γ-tubulin molecules, the arrangement of which matches microtubule symmetry. The flexibility of the GCP3 hinge is essential to close the γTuRC in a

Table 1 Building components of γ-tubulin complexes in different model systems

Homo sapiens	*Xenopus laevis*	*Drosophila melanogaster*	*Arabidopsis thaliana*	*Aspergillus nidulans*	*Schizosaccharomyces pombe*	*Saccharomyces cerevisiae*
TUBG1 γ-tubulin 1 *TUBG2* γ-tubulin 2	*tubg1* γ-tubulin	*gammaTub23C* γ-tubulin 1 *gammaTub37C* γ-tubulin 2	*TUBG1* γ-tubulin 1 *TUBG2* γ-tubulin 2	*mipA* γ-tubulin	*tug1* γ-tubulin	*TUB4* γ-tubulin
TUBGCP2 GCP2	*tubgcp2* Xgrip110	*Grip84* Dgrip84	*GCP2* AtGCP2	*gcpB* GCPB	*alp4* Alp4	*SPC97* Spc97
TUBGCP3 GCP3	*tubgcp3* Xgrip109	*Grip91* Dgrip91	*GCP3* AtGCP3	*gcpC* GCPC	*alp6* Alp6	*SPC98* Spc98
TUBGCP4 GCP4	*tubgcp4* Xgrip75	*Grip75* Dgrip75	*GCP4* AtGCP4	*gcpD* GCPD	*gfh1* Gfh1	
TUBGCP5 GCP5	*tubgcp5* Xgrip113	*Grip128* Dgrip128	*At1g80260* AtGCP5	*gcpE* GCPE	*mod21* Mod21	
TUBGCP6 GCP6	*tubgcp6* Xgrip210	*Grip163* Dgrip163	*At3g43610* AtGCP6	*gcpF* GCPF	*alp16* Alp16	

Gene identifiers (in italics) and protein names are shown for *Homo sapiens*, *Xenopus laevis*, *Drosophila melanogaster*, *Arabidopsis thaliana*, *Aspergillus nidulans*, *Schizosaccharomyces pombe and Saccharomyces cerevisiae*. Adapted from Teixidó-Travesa et al. (2012) and Oakley et al. (2015)

conformation compatible with the geometry of the microtubule, increasing its nucleation capacity. In this template-based nucleation model, γTuRC provides platform for the assembly of αβ-tubulin heterodimers (Kollman et al. 2011; Moritz et al. 2000). It was proposed that GCP4, GCP5 and GCP6 position together at the ends of the helix, which would allow them either to initiate or terminate the self-assembly of γTuSCs and/or to stabilize the structure by bridging the two ends (Farache et al. 2016). Although GCP4-6-dependent γTuRC assembly is not essential for spindle formation in *S. pombe*, *A. nidulans* and *D. melanogaster*, it may be important for the targeting of γTuRCs to specific cellular structures. In contrast, in human cells, γTuRCs are required for mitotic spindle formation (Lin et al. 2015). As GCPs are phosphorylated (Teixidó-Travesa et al. 2010), phosphorylation can regulate conformational changes that might be required for γTuRC activation (Kollman et al. 2011). Organization of proteins in γ-tubulin complexes is depicted in Fig. 2.

Nucleation from templates is itself a kinetically unfavourable process that is limited by the formation of a plus end capable of persistent growth. Anti-catastrophe factor targeting protein for Xklp2 (TPX2) and microtubule polymerase xenopus microtubule-associated protein 215 kDa (XMAP215), that belongs to microtubule plus end tracking proteins (+TIPs), help to transform nascent microtubule with a blunt end into microtubule with an actively growing plus end, which is splayed and outwardly curved. On the other hand, GTP hydrolysis inhibits microtubule nucleation by destabilizing the nascent plus ends (Wieczorek et al. 2015).

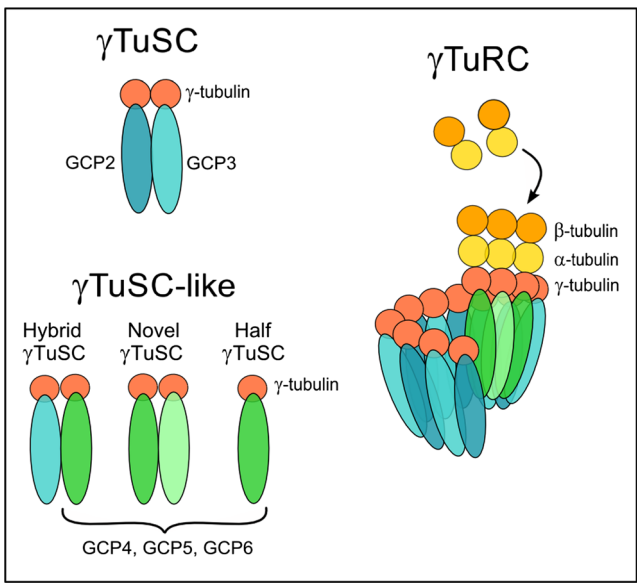

Fig. 2 Composition of γ-tubulin complexes and model of γTuRC assembly. γTuSC are composed of GCP2 and GCP3 and two molecules of γ-tubulin. Different γTuSC-like structures (hybrid γTuSC, novel γTuSC, half γTuSC) can be formed by replacement of GCP2 or GCP3 with GCP4, GCP5 or GCP6. All complexes participate in the formation of the γTuRC ring structure. Nucleation of microtubule polymerization involves longitudinal interactions of αβ-tubulin heterodimers with γ-tubulin in the γTuRC (template nucleation model)

In cells, γ-tubulin complexes are soluble in the cytoplasm. However, their nucleating activity seems to be limited to specific locations in the cell. Various associated proteins are involved in regulation of γ-tubulin complexes. These proteins are not essential for assembly of γTuSCs or TuRCs but target them to specific sites or activate their nucleation activity. An important role in microtubule nucleation at specific sites is also played by anchoring proteins that can affect recruitment of complexes as well as modulating proteins that have a less obvious role. Microtubule nucleation can be roughly categorized into three groups, from SPBs, centrosomes and from additional sites.

Nucleation from SPB

The SPB in budding yeast *S. cerevisiae* represents the simplest microtubule nucleation system of any model. The nuclear side of SPB nucleates microtubules for spindle formation, while the cytoplasmic side nucleates microtubules for proper nucleus and spindle positioning. Two targeting factors, Spc110 and Spc72, recruit γTuSCs to the nuclear and cytoplasmic side of the SPB, respectively (Kilmartin and Goh 1996; Soues and Adams 1998). The Spc110 directly interacts with Spc98/GCP3 and recruits γTuSCs to the nuclear side of SPB (Knop and Schiebel 1997). Spc110 contains two conserved elements, centrosomin [Cnn] motif 1 (CM1) and Spc110-Pcp1 motif (SPM), that are essential for γTuSC oligomerization and microtubule nucleation (Lin et al. 2014). Phosphorylation of Spc110 plays an important role in the regulation of its activity and γTuSC oligomerization. While phosphorylation of Spc110 by S-phase Cdk1-Clb5 kinase and Mps1 kinase promotes γTuSC oligomerization, subsequent phosphorylation by mitotic Cdk1-Clb2 kinase counteracts the activity of S-phase phosphorylation (Lin et al. 2015). Concerning microtubule nucleation on the cytoplasmic side of SPB, the targeting factor Spc72 possesses the CM1 element but lacks the SPM, suggesting a different form of interaction with γTuSC. Interestingly, Spc72 acts together with TOG domain Stu2 to anchor microtubules at the cytoplasmic side of SPB (Usui et al. 2003).

Protein Pcp1 is a homolog of Spc110 in fission yeast *S. pombe*. It contains both CM1 and SPM elements and targets γTuRCs and polo-like kinase (Plo1) to the nuclear side of SPBs and supports spindle formation (Fong et al. 2010). Mto1, containing the CM1 element, is the *S. cerevisiae* Spc72 ortholog and enables γTuRC binding on the cytoplasmic side of SPB during mitosis (Samejima et al. 2008). Targeting of γTuRCs to SPB is also supported by Mzt1/Tam4 that directly interacts with Alp6/GCP3 (Dhani et al. 2013). In addition to SPBs, *S. cerevisiae* employs additional

nucleation sites, termed interphase MTOCs (Sawin and Tran 2006), and both Mto1 with Mto2 and Mzt1/Tam4 are required for the non-SPB-derived microtubules. Mto1 and Mto2 cooperate to efficiently interact with γ-tubulin complexes (Samejima et al. 2008). Nucleation of microtubules from both SPB and additional nucleation sites has also been well described in *A. nidulans* (Lin et al. 2015).

Centrosomal nucleation

The relationship between the PCM and the microtubule nucleation capacity is well established and is observed during the cell cycle, whereby the centrosome recruits large amounts of γ-tubulin during mitosis concomitant with an increase in microtubule nucleation (Khodjakov and Rieder 1999). In contrast to the conventional view of the PCM as an amorphous protein network, advances in superresolution microscopy have revealed that it is highly structured with consecutive layers of proteins responsible for microtubule nucleation and γTuRC anchorage (Lawo et al. 2012).

In vertebrates centrosomal proteins neural precursor cell expressed, developmentally down-regulated protein 1 (NEDD1/GCP-WD) (Lüders et al. 2006), Mozart1 (mitotic spindle-organizing protein 1/Mzt1/GCP9), Mozart2 (mitotic spindle-organizing protein 2/Mzt2/GCP8) (Teixidó-Travesa et al. 2010) and CDK5RAP2 (cyclin-dependent kinase 5 regulatory subunit-associated protein 2/Cep215/centrosomin) (Choi et al. 2010) are implicated in γTuRCs targeting. NEDD1 is the attachment factor that lies most proximal to the γTuRC and is important for centrosomal localization of γTuRC in interphase and mitotic cells. Differential phosphorylation of NEDD1 controls the sites to which NEDD1 recruits γTuRCs (Pinyol et al. 2013). Mozart1 seems to be involved in γTuRC recruitment to centrosomes in mitotic cells, while Mozart2 plays this role in interphase cells (Teixidó-Travesa et al. 2010). Additional proteins AKAP450 (A-kinase anchor protein 450/AKAP9/CG-NAP) (Takahashi et al. 2002), pericentrin (PCNT/kendrin) (Zimmerman et al. 2004), ninein (GSK3B-interacting protein) (Delgehyr et al. 2005) and Cep192 (Centrosomal protein 192) (Gomez-Ferreria et al. 2007) are also important for localization of γTuRC to centrosomes. However, as these proteins are incorporated in PCM, they can also indirectly affect γTuRC anchoraging.

The best-characterized activator for γTuRC is CDK5RAP2 that contains activating ~5.5 kDa γ-tubulin complex binding domain (γ-TuNA; γTuRC-mediated nucleation activator 1/centrosomin motif 1/CM1). CDK5RAP2 contains also a centrosome-targeting domain (centrosomin motif 2/CM2). In vitro CDK5RAP2 activates γTuRC-mediated nucleation by ~7-fold (Choi et al. 2010; Wang et al. 2010). It is currently unclear how γ-TuNA activates γTuRCs. Another nucleation activator is nucleoside-diphosphate kinase 7 (NME7) that increases the nucleation capacity of γTuRC by ~2.5-fold (Choi et al. 2010; Liu et al. 2014). The association of NME7 with γTuRCs promotes centrosomal nucleation in kinase-dependent manner, but a corresponding target for NME7 was not identified. The molecular basis of γTuRC activation is currently unknown but may involve a conformation switch described for activation of γTuSC.

It is currently unclear whether multiple γTuRC recruitment factors interact with γTuRC simultaneously or whether the various factors function independently of each other. Recently, two functionally distinct γ-TuRC pools were identified in keratinocytes. CDK5RAP2-γTuRCs are potent nucleators, while NEDD1-γTuRCs do not nucleate microtubules but are required for microtubule anchoring (Muroyama et al. 2016). Future studies are necessary to find out if γ-TuRC heterogeneity is more widespread both in terms of γTuRC composition and generation of different microtubule arrays.

Several proteins are implicated in modulation of centrosomal microtubule nucleation, but the precise mechanism of their action remains to be defined. Protein lectin galactoside-binding soluble 3 binding protein (LGALS3BP) plays an essential role in centriolar integrity and biogenesis. In addition, LGALS3BP levels are critical for overall centrosome structure and function, as the increase or decrease of its protein level leads to PCM dispersion with enhanced γ-tubulin recruitment and defective microtubule aster formation, respectively (Fogeron et al. 2013). Nucleolin (C23), a nucleolar phosphoprotein involved in the synthesis and maturation of ribosomes, is associated with centrosomes, and its absence leads to defects in microtubule nucleation. It was suggested that nucleolin might act as an activator of microtubule nucleation when bound to centrosomal γTuRC (Gaume et al. 2015). Interestingly, several centrosomal proteins including γ-tubulin (Hořejší et al. 2012) and GCP2/GCP3 (Dráberová et al. 2015) have been observed in the nucleoli. On the other hand, nucleolar protein HCA66 (U3 small nucleolar RNA-associated protein 6 homolog) has been detected in the centrosome and it was proposed to play a role in stabilizing components of γTuSC (Fant et al. 2009). A molecular communication between the two cellular compartments may be essential to coordinate nucleolar and centrosomal functions (Gaume et al. 2015). In addition, it was reported that protein transforming acidic coiled-coil containing protein 3 (TACC3) is involved in the regulation of the centrosomal microtubule nucleation through the stabilization of the γTuRC assembly from γTuSCs (Singh et al. 2014). Centrobin (centriole duplication and spindle assembly protein), daughter centriole-specific protein participating in duplication and elongation of the centriole, regulates also microtubule nucleation from the centrosome. Centrobin depletion results in the increased recruitment of pericentriolar matrix proteins to the centrosome, including γ-tubulin, AKAP450 and pericentrin. It was proposed that centrobin might regulate

microtubule nucleation and organization by controlling the amount of pericentriolar matrix (Jeffery et al. 2013).

The regulatory role in centrosomal microtubule nucleation can also be played by signalling proteins. It was described recently that protein kinase D3 (PKD3) modulates microtubule nucleation, but a corresponding substrate in PCM is unknown (Zhang et al. 2016). Several other signalling proteins, such as G protein-coupled receptor kinase-interacting protein 1 (GIT1), p21-activated kinase interacting exchange factor (βPIX) and p21 protein [Cdc42/Rac]-activated kinase 1 (PAK1) were identified as regulators of microtubule nucleation. It was reported that GIT1 with PAK1 act as positive regulators, and βPIX is a negative regulator of microtubule nucleation from the interphase centrosomes. The regulatory roles of GIT1, βPIX and PAK1 correlated with recruitment of γ-tubulin to the centrosome (Černohorská et al. 2016; Sulimenko et al. 2015). It was shown that Aurora A phosphorylation of TACC3 is required for γ-tubulin accumulation and centrosome-dependent microtubule assembly in mitosis (Kinoshita et al. 2005) and that sequential phosphorylation of NEDD1 by Cyclin-dependent kinase 1 (Cdk1, Cdc2) and Polo-like kinase 1 (Plk1) is required for targeting of the γTuRC to the centrosome (Zhang et al. 2009).

Non-centrosomal nucleation

The majority of work on microtubule nucleation was performed on SPBs and centrosomes. However, non-centrosomal microtubule nucleation plays also a very important role in creation and maintenance of cellular architecture (Petry and Vale 2015). It can operate next to centrosomal nucleation or function independently. Non-centrosomal MTOCs were first described in higher plants that do not contain centrosome-like microtubule organizer at all (Lüders and Stearns 2007). Since then, many more non-centrosomal MTOCs have been described in different organisms and some of them appear to be functional only in specialized cell types. In differentiated animal cells, like polarized epithelial cells, myotubes or matured neurons, a substantial number of microtubules is not attached to centrosomes but forms parallel arrays with free plus and minus ends (Bartolini and Gundersen 2006). Non-centrosomal microtubules could be formed by nucleation and release from the centrosome, by assembly in the cytoplasm or by nucleation from non-centrosomal MTOC (Lüders and Stearns 2007).

Golgi apparatus

Golgi apparatus works as an MTOC and nucleates a subset of microtubules. To date, Golgi-derived microtubules have been characterized only in animal cells. Generally, there are three steps of microtubule formation: recruitment of γTuRC to the Golgi membrane, template-based nucleation and stabilization of Golgi-derived microtubules (Sanders and Kaverina 2015). It was proposed that Golgi apparatus shares the same anchoring and microtubule-nucleating components with centrosomes (Rivero et al. 2009).

The γTuRCs are recruited to the Golgi membrane by proteins possessing γTuRC-scaffolding capacity (Sanders and Kaverina 2015). Current model proposes that cis-Golgi protein GM130 (Golgin subfamily A member 2 protein) recruits AKAP450 (Rivero et al. 2009), which in turn binds CDK5RAP2 (Wang et al. 2010) or myomegalin (MMG/phosphodiesterase 4D interacting protein/PDE4DIP) isoform CM-MMG (centrosomin motif-myomegalin), that associates also with centrosome (Roubin et al. 2013). CDK5RAP2 can also bind to pericentrin to attach γTuRCs to Golgi apparatus (Wang et al. 2010). Both myomegalin and CDK5RAP2 promote microtubule nucleation at the cis-Golgi using GM130-AKAP450-CDK5RAP2/myomegalin-γTuRC axis, and they might play a redundant or complementary role in the microtubule nucleation (Roubin et al. 2013). Securin (pituitary tumour-transforming gene 1 (PTTG1)) was also reported to form a complex with GM130, AKAP450 and γ-tubulin at the cis face of the Golgi and its depletion results in a delay in microtubule nucleation (Moreno-Mateos et al. 2011). Moreover, it was shown that dynein/dynactin complexes retain microtubule seeds at the Golgi apparatus and function as other scaffolding proteins (Rivero et al. 2009).

Microtubule nucleation from Golgi membrane needs some additional factors to make the template nucleation kinetically favourable (Sanders and Kaverina 2015). Among them belong +TIP proteins cytoplasmic linker associated proteins (CLASPs; CLASP1 and CLASP2) that are recruited to and associate specifically with the trans-Golgi scaffold protein GCC185 (GRIP and coiled-coil domain-containing protein 2) at the Golgi periphery. It was suggested that newly nucleated Golgi-derived short microtubules are coated and stabilized with CLASPs, which were relocalized from the Golgi membrane (Efimov et al. 2007). However, CLASPs are also known to directly modify polymerizing microtubules (Grimaldi et al. 2014) and could therefore modulate the initial polymerization steps of Golgi-derived microtubules rather than simply stabilize already assembled polymers (Sanders and Kaverina 2015). Moreover, +TIP protein EB1 can associate with myomegalin isoform EB1-myomegalin (EB-MMG) and this affects EB1 loading on microtubules and microtubule growth (Roubin et al. 2013). Because of low γTuRC abundance at the Golgi, nucleation of microtubules from these γTuRCs templates requires high local concentration of functional tubulin dimers. This could be achieved by tubulin chaperone tubulin-specific chaperone E (TBCE) concentrating at the Golgi membrane in an ADP ribosylation factor 1 (Arf1) manner (Bellouze et al. 2014) and reviving tubulin in the vicinity of nucleation sites.

Nuclear envelope

Nuclear membrane serves as a microtubule nucleation site in several cell types among which skeletal muscle belongs to the well-characterized ones. During skeletal muscle differentiation, undifferentiated myoblasts fuse into multinucleated myotubes. It was reported that nuclei of undifferentiated cells have a dormant potential to bind centrosome proteins which becomes activated during the myoblast differentiation (Fant et al. 2009). Moreover, early after the fusion, the microtubule network is completely reorganized from radial array into parallel fibres which also involves redistribution of proteins of pericentriolar material from centrosome to the nuclear membrane (Dyachuk et al. 2016). During myogenesis in *D. melanogaster*, Rac GTPase activating protein 50C (RacGap50C) is necessary for binding γ-tubulin to various foci associated with the nuclear periphery. It was found that proper localization of RacGAP50C in nuclear periphery depends on Pavarotti kinesin-like protein (Pav) (Guerin and Kramer 2009). In mouse, muscle cells γ-tubulin as well as pericentrin and ninein are associated with nuclear membrane and γ-tubulin-dependent nucleation takes place along the nuclear membrane of myotubes (Bugnard et al. 2005).

Nuclear surface of higher plant cells also functions as a microtubule-nucleating site and proteins involved in this process are localized at the nuclear periphery. Besides the γ-tubulin (Binarová et al. 2000) and GCP3 (Erhardt et al. 2002), the whole γTuSCs were identified in the nuclear periphery of plant cells (Seltzer et al. 2007). Moreover, proteins GCP3-interacting protein 1 (GIP1) and GCP3-interacting protein 2 (GIP2), which are homologous to vertebrate Mozart1, localize at the nuclear periphery with γ-tubulin, GCP3 and/or GCP4 and stabilize γ-tubulin complexes (Janski et al. 2012). GIPs may have a dual function, both as components of microtubule nucleation complexes and as adaptors or modulators of nuclear envelope associated proteins (Batzenschlager et al. 2013). It was shown that the activity and positioning of the plant nuclear MTOC can influence cortical microtubule orientation and polarity along the long axis of the cell (Ambrose and Wasteneys 2014).

Chromatin and kinetochores

Chromatin-mediated microtubule nucleation occurs after the breakdown of nuclear envelope. The key player in the molecular mechanism is the small GTPase Ran (Ras-related nuclear protein). The association of Ran-guanine nucleotide exchange factor (GEF) regulator of chromosome condensation 1 (RCC1) with chromosomes produces a gradient of RanGTP which promotes dissociation of spindle assembly factors (SAFs) from importins. The released SAFs promote microtubule nucleation, stabilization and organization around the chromosomes (Meunier and Vernos 2016). SAFs also localize to microtubules, and this interaction leads to feedback based on spatial localization (Oh et al. 2016b). The most studied SAF is a nuclear protein TPX2. Interaction of TPX2 with Aurora A leads to Aurora A activation by its autophosphorylation in a RanGTP-dependent manner (Tsai and Zheng 2005). TPX2 also form complexes with γTuRC and microtubule-associated protein receptor for hyaluronan-mediated motility (RHAMM) (Groen et al. 2004). The TPX2-Aurora A complex associates with specific complex containing RHAMM-NEDD1-γTuRC (Scrofani et al. 2015). In this macro-complex, the activated Aurora A phosphorylates NEDD1 that is an essential prerequisite for microtubule nucleation in the proximity of chromosomes (Pinyol et al. 2013). The association of γ-tubulin with the mitotic spindle requires another specific NEDD1 phosphorylation (Lüders et al. 2006). The precise roles of NEDD1 phosphorylations are not known. Besides the regulation of the chromatin-mediated microtubule nucleation and γTuRCs scaffolding, TPX2 also promotes microtubule nucleation by stabilizing early nucleation intermediates. For faster and more efficient microtubule nucleation, TPX2 cooperates with microtubule polymerase XMAP215 (chTOG), which has only weak nucleation activity on its own (Roostalu et al. 2015). Moreover, other proteins are involved in RanGTP-dependent, chromatin-mediated nucleation. Hepatoma upregulated protein (HURP) was found to drive RanGTP-dependent, chromatin-induced microtubule assembly in a TPX2-independent manner and may be also involved in other steps of RanGTP-mediated microtubule nucleation (Casanova et al. 2008). Maternal effect lethal-28 protein (MEL-28) promotes RanGTP-dependent recruitment of γTuRC and microtubule nucleation (Yokoyama et al. 2014). In general, the RanGTP pathway was described in animal and plant cells and seems to be highly conserved. Nevertheless, its key player TPX2 is not highly conserved in organisms such as *D. melanogaster* and *Caenorhabditis elegans.* Although related proteins were described in both systems, they are fairly distant in terms of sequence and function (Meunier and Vernos 2016).

RanGTP gradient on mitotic chromatin favours microtubule nucleation in the vicinity of the chromosome rather than from γTuRCs localized at kinetochores as suggested previously (Mishra et al. 2010). However, kinetochores provide an environment for microtubule stabilization. The major role in microtubule stabilization is played by the kinetochore-associated chromosomal passenger complex (CPC) that localizes to centromeres (Meunier and Vernos 2016). Observation of γTuRC components at the kinetochores in microtubule regrowth experiments in plants (Binarová et al. 1998) may result from the presence of short microtubules connected to the kinetochores by their plus ends. It was suggested that after chromosomal RanGTP-dependent microtubule nucleation, microtubules are stabilized in the kinetochore area and amplified through microtubule nucleation by the augmin-dependent pathway (Meunier and Vernos 2016).

Surface of other microtubules

One of the possible mechanisms of non-centrosomal nucleation is the formation of new microtubules from the lateral surface of pre-existing "mother" microtubules. This γ-tubulin-dependent branching was initially observed in higher plant interphase cells (Murata et al. 2005). The essential role in this process is played by a hetero-octameric protein complex termed augmin. Augmin functions by recruiting NEDD1 and its associated γTuRC to preexisting microtubules (Goshima et al. 2008). Augmin-dependent nucleation of microtubules is phylogenetically conserved as it was described in plants (Hotta et al. 2012), *D. melanogaster* (Goshima et al. 2008), *X. laevis* (Petry et al. 2013) and human cells (Uehara et al. 2009). It is usually connected with formation of branching microtubules in bipolar metaphase spindle, but it also promotes central spindle assembly in anaphase and cytokinesis (Uehara et al. 2016). The augmin-γTuRC module organizes microtubules in post-mitotic neurons and controls axonal microtubule polarity (Sánchez-Huertas et al. 2016). In plants, augmin complex plays an important role not only in the formation of the acentrosomal spindle and microtubule-rich phragmoplast (Hotta et al. 2012) but also in triggering microtubule nucleation at the plant cortex (Liu et al. 2014). In *A. thaliana*, mutation of the augmin six subunit disturbs both mitotic and meiotic divisions due to malformation of the microtubular network (Oh et al. 2016a). Within the cortical array, microtubules are nucleated either along the mother microtubules as branches at angles ranging from 20° (= 20° angle) to 60° (~40° on average) or in parallel mode (0° angle). Microtubule-dependent microtubule nucleation thus provides an effective mean of quick amplification of microtubules with the same polarity (Sánchez-Huertas and Lüders 2015). An augmin-like protein complex was identified in *A. nidulans.* Although its subunits have significant homology to animal and plant proteins, it seems that the *A. nidulans* augmin

Table 2 Proteins regulating microtubule nucleation from centrosomal and non-centrosomal sites in animals

Location	Protein	Role	Reference
Centrosome	NEDD1[1], Mozart1[2], Mozart2[2], CDK5RAP2[3]	γTuRC targeting	[1] Lüders et al. 2006; [2] Teixidó-Travesa et al. 2010; [3] Choi et al. 2010; [4] Liu et al. 2014;
	CDK5RAP2[3], NME7[4]	γTuRC activation	[3] Choi et al. 2010; [4] Liu et al. 2014;
	AKAP450[5], Pericentrin[6], Ninein[7], Cep192[8]	Anchoring	[5] Takahashi et al. 2002; [6] Zimmerman et al. 2004; [7] Delgehyr et al. 2005; [8] Gomez-Ferreria et al. 2007;
	PDK3[9], Nucleolin[10], TACC3[11], Centrobin[12], LGALS3BP[13], GIT1[14,15], βPIX[14,15], PAK1[15], Aurora A[16], PLK1[17], myomegalin CM-MMG[18]	Modulating	[9] Zhang et al. 2016; [10] Gaume et al. 2015; [11] Singh et al. 2014; [12] Jeffery et al. 2013; [13] Fogeron et al. 2013; [14] Sulimenko et al. 2015; [15] Černohorská et al. 2016; [16] Kinoshita et al. 2005; [17] Zhang et al. 2009; [18] Roubin et al. 2013;
Golgi apparatus	myomegalin CM-MMG[18], CDK5RAP2[19]	γ-TuRC targeting	[18] Roubin et al. 2013; [19] Wang et al. 2010;
	Pericentrin[19], GM130[20], AKAP450[19], GCC185[21]	Anchoring	[19] Wang et al. 2010; [20] Chabin-Brion et al. 2001; [21] Efimov et al. 2007;
	Myomegalin EB-MMG[18], dynein/dynactin[22], CLASP1–2[23,24], Securin[25] , TBCE[26], Arf[26]	Modulating	[18] Roubin et al. 2013; [22] Rivero et al. 2009; [23] Efimov et al. 2007; [24] Grimaldi et al. 2014; [25] Moreno-Mateos et al. 2011; [26] Bellouze et al. 2014;
Nuclear envelope	RacGAP50C[27], GIP1–2[28,29]	γ-TuRC targeting	[27] Guerin and Kramer 2009; [28] Janski et al. 2012; [29] Batzenschlager et al. 2013;
	Pav[27], pericentrin[30], ninein[30]	Anchoring	[27] Guerin and Kramer 2009; [30] Bugnard et al. 2005;
Chromatin	NEDD1[31]	γ-TuRC targeting	[31] Pinyol et al. 2013;
	TPX2[32], RHAMM[33]	Anchoring	[32] Tsai and Zheng 2005; [33] Groen et al. 2004;
	TPX2[32], Aurora A[32], RCC1[33], Ran GTPase[34], HURP[35], XMAP215[36], MEL-28[37]	Modulating	[32] Tsai and Zheng 2005; [33] Carazo-Salas et al. 1999; [34] Kalab et al. 2006; [35] Casanova et al. 2008; [36] Roostalu et al. 2015; [37] Yokoyama et al. 2014;
Pre-existing microtubules	NEDD1[38]	γ-TuRC targeting	[38] Johmura et al. 2011;
	Augmin complex[39]	Anchoring	[39] Goshima et al. 2008;
	Plk1[38], Cdk1[38]	Modulating	[38] Johmura et al. 2011;
Plasma membrane	Ninein[40], keratin[41], NOCA-1[42]	Anchoring	[40] Mogensen et al. 2000; [41] Oriolo et al. 2007; [42] Wang et al. 2015;
	Fyn[43], PI3K[43,44]	Modulating	[43] Macurek et al. 2008; [44] Inukai et al. 2000.

complex is dispensable for spindle formation in fungi. Interestingly, Aug6-like genes were identified in several other fungal species but not in yeast (Edzuka et al. 2014).

Reconstitution of human augmin revealed that it is a Y-shaped complex that can adopt multiple conformations. Augmin subunit HAUS8 (Hice1) is responsible for binding of the complex to microtubules, but the whole complex binds to microtubules with more than 10-fold higher affinity than Hice1 alone (Hsia et al. 2014). The binding of augmin to microtubules is promoted by phosphorylation of the Hice1 by Plk1. This phosphorylation depends on Plk1-NEDD1 interaction that is induced by Cdk1 phosphorylation of NEDD1 (Johmura et al. 2011). In plant cells, microtubule branching is regulated by protein phosphatase 2A (PP2A). The PP2A signalling pathway plays an important role in the organization of interphase microtubule arrays through regulating nucleation geometry (Kirik et al. 2012).

Plasma membrane-associated sites

In differentiated cells of many tissues, PCM proteins lose their association with the centrosome and can redistribute to cellular cortex. Plasma membrane-associated sites can thus functionally replace the centrosomal MTOCs (Dyachuk et al. 2016). In polarized epithelial cells, microtubules are anchored in a region underlying the apical plasma membrane where ninein is concentrated. It was proposed that initial microtubule nucleation at the centrosome is followed by release, translocation and anchorage of microtubule minus ends to the apical membrane by ninein (Mogensen et al. 2000). The maintenance of such microtubule network may be further supported by minus end-targeting proteins (−TIPs), such as calmodulin-regulated spectrin-associated proteins 1–3 (CAMSAPs 1–3) in mammals or patronin in invertebrates (Akhmanova and Steinmetz 2015). It was reported that a ninein-related protein in the nematode *C. elegans*, non-centrosomal array protein 1 (NOCA-1) regulates together with γ-tubulin the assembly of non-centrosomal microtubules. Moreover, in epidermal cells, NOCA-1 has functional redundancy with patronin. This indicates that the functional roles of ninein and patronin families overlap (Wang et al. 2015). It has also been shown that keratin binds directly to GCP6 and mediates γTuRC localization to the apical domain of epithelial cells. Interaction with GCP6 was disrupted by Cdk1 phosphorylation of GCP6 phosphorylation (Oriolo et al. 2007).

Interestingly, in animal cells, protein tyrosine kinases of Src family, which are associated with cell surface receptors, form complexes with γ-tubulin and phosphorylates γ-tubulin associated proteins (Dráberová et al. 1999; Sulimenko et al. 2006). A direct interaction of γ-tubulin with regulatory subunit of

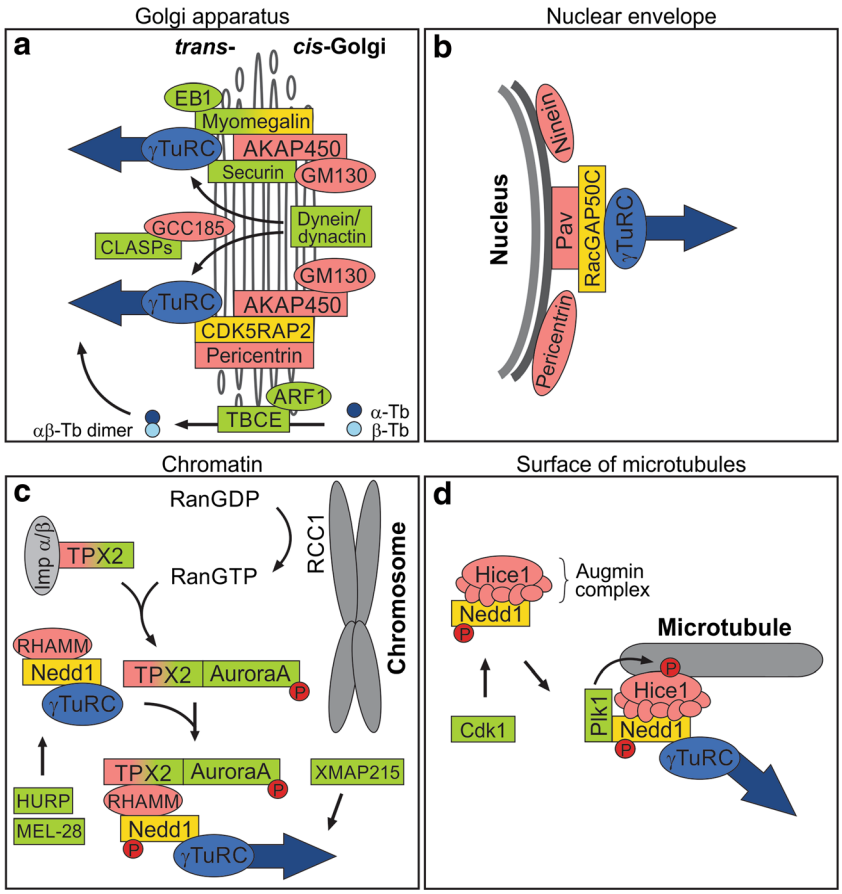

Fig. 3 Models of non-centrosomal microtubule nucleation. Schematic representation of microtubule nucleation from Golgi apparatus (**a**), nuclear envelope (**b**) chromatin (**c**) and surface of pre-existing microtubule (**d**). Regulatory proteins are distinguished according to their role in the nucleation: γTuRC targeting (*yellow*), anchoring (*red*) and modulating proteins (*green*). γTuRCs with nucleated microtubules are in *blue*. Not all regulatory proteins are depicted. Proteins are not in scale

phosphoinositide 3-kinase (PI3K) was also reported (Inukai et al. 2000). It was shown that microtubules are nucleated from detergent-resistant membranes containing γ-tubulin, and nucleation from membranes is dependent on the activity of tyrosine kinase Fyn (p59-FYN) and PI3K (Macurek et al. 2008). Fyn phosphorylates its substrate PI3K, which might then regulate γ-tubulin through direct interaction. The precise mechanism of kinase actions remains to be defined.

In higher plants, the nucleation activity of membrane-bound large γ-tubulin complexes has been shown in vitro (Dryková et al. 2003). Moreover, γ-tubulin, GCP2 and GCP3 were found at the plasma membrane in plants (Erhardt et al. 2002; Seltzer et al. 2007). γ-TuSC proteins are also enriched in post-cytokinetic, newly formed crosswalls of *A. thaliana,* where they nucleate microtubules (Ambrose and Wasteneys 2011). An important role in the formation of nucleation of microtubules at the plant cell cortex is played by augmin (see above) (Liu et al. 2014).

Proteins involved in the regulation of microtubule nucleation in animal cells are summarized in Table 2. Models of non-centrosomal nucleation from the Golgi apparatus, nuclear envelope, chromatin and surface of microtubules are depicted in Fig. 3.

Conclusions and future directions

Two decades of research on γ-tubulin complexes led to the conclusion that they are almost universally involved in microtubule nucleation. γ-Tubulin complexes have been shown to form microtubule templates that nucleate microtubules through longitudinal contacts with αβ-tubulin dimers. However, different mechanisms ensuring proper spatio-temporal regulation of microtubule nucleation are applied at specific locations in the cell. It seems that the γTuRC attachment to both centrosomal and non-centrosomal sites is correlated with an increase in its nucleating activity.

The recent structural studies on γTuSC have been highly illustrative, but a high-resolution structure of the γTuRC both before and after nucleation will be necessary to understand how GCP4, GCP5 and GCP6 are located in the complex and what are the specific interactions they make with each other and with the γTuSC. The transition from an open to a closed state of γTuSC provides an allosteric mechanism for modulating γTuSC activity. It remains to be determined what factors are involved in promoting this transition. Elucidation of precise mechanism of γTuRC activation also remains a pressing question in understanding γTuRC regulation. Many proteins interacting with γTuRCs, highlighted in this review, have been implicated in activation, targeting and modulation of γTuRCs. However, little is known about the upstream signalling pathways ensuring that these proteins initiate microtubule nucleation at the correct location and time. The importance of kinases and phosphatases in regulation of nucleation is emerging, but the details are only partially understood. Future studies are also necessary to find out if distinct γTuRCs may be independently used by different tissues to generate cell type-specific non-centrosomal microtubule arrays. Further studies are needed to assess microtubule branch angles during cell cycle stages and in different cell types. Finally, a thorough understanding of microtubule nucleation should clarify the relevance of γTuRC dysregulation in cancer cells and neurodevelopmental diseases.

Together, these studies will help us comprehend how microtubule nucleation is initiated and regulated in vivo to create microtubule arrays essential to various cell activities.

Acknowledgements We thank Dr. Eduarda Dráberová and Tetyana Sulimenko for help with figure preparation. This work was supported by the grant LD13015 for COST action (BM1007 Mast Cells and Basophils-Targets for Innovative Therapies) from the Ministry of Education Youth and Sport and by Institutional Research Support (RVO 68378050).

Compliance with ethical standards

Conflict of interest The authors declare that they have no conflict of interest.

References

Akhmanova A, Steinmetz MO (2015) Control of microtubule organization and dynamics: two ends in the limelight. Nat Rev Mol Cell Biol 16:711–726

Ambrose C, Wasteneys GO (2011) Cell edges accumulate gamma tubulin complex components and nucleate microtubules following cytokinesis in *Arabidopsis thaliana*. PLoS One 6:e27423

Ambrose C, Wasteneys GO (2014) Microtubule initiation from the nuclear surface controls cortical microtubule growth polarity and orientation in *Arabidopsis thaliana*. Plant Cell Physiol 55:1636–1645

Bartolini F, Gundersen GG (2006) Generation of noncentrosomal microtubule arrays. J Cell Sci 119:4155–4163

Batzenschlager M, Masoud K, Janski N, Houlné G, Herzog E, Evrard JL, Baumberger N, Erhardt M, Nominé Y, Kieffer B, Schmit AC, Chabouté ME (2013) The GIP γ-tubulin complex-associated proteins are involved in nuclear architecture in *Arabidopsis thaliana*. Front Plant Sci 4:480

Bellouze S, Schäfer MK, Buttigieg D, Baillat G, Rabouille C, Haase G (2014) Golgi fragmentation in pmn mice is due to a defective ARF1/TBCE cross-talk that coordinates COPI vesicle formation and tubulin polymerization. Hum Mol Genet 23:5961–5975

Binarová P, Doležel J, Dráber P, Heberle-Bors E, Strnad M, Bögre L (1998) Treatment of *Vicia faba* root tip cells with specific inhibitors to cyclin-dependent kinases leads to abnormal spindle formation. Plant J 16:697–707

Binarová P, Cenklová V, Hause B, Kubátová E, Lysák M, Doležel J, Bögre L, Dráber P (2000) Nuclear γ-tubulin during acentriolar plant mitosis. Plant Cell 12:433–442

Bugnard E, Zaal KJ, Ralston E (2005) Reorganization of microtubule nucleation during muscle differentiation. Cell Motil Cytoskeleton 60:1–13

Carazo-Salas RE, Guarguaglini G, Gruss OJ, Segref A, Karsenti E, Mattaj IW (1999) Generation of GTP-bound ran by RCC1 is required for chromatin-induced mitotic spindle formation. Nature 400:178–181

Casanova CM, Rybina S, Yokoyama H, Karsenti E, Mattaj IW (2008) Hepatoma up-regulated protein is required for chromatin-induced microtubule assembly independently of TPX2. Mol Biol Cell 19: 4900–4908

Černohorská M, Sulimenko V, Hájková Z, Sulimenko T, Sládková V, Vinopal S, Dráberová E, Dráber P (2016) GIT1/βPIX signaling proteins and PAK1 kinase regulate microtubule nucleation. BBA Mol Cell Res 1863:1282–1297

Chabin-Brion K, Marceiller J, Perez F, Settegrana C, Drechou A, Durand G, Poüs C (2001) The Golgi complex is a microtubule-organizing organelle. Mol Biol Cell 12:2047–2060

Choi YK, Liu P, Sze SK, Dai C, Qi RZ (2010) CDK5RAP2 stimulates microtubule nucleation by the γ-tubulin ring complex. J Cell Biol 191:1089–1095

Delgehyr N, Sillibourne J, Bornens M (2005) Microtubule nucleation and anchoring at the centrosome are independent processes linked by ninein function. J Cell Sci 118:1565–1575

Dhani DK, Goult BT, George GM, Rogerson DT, Bitton DA, Miller CJ, Schwabe JW, Tanaka K (2013) Mzt1/Tam4, a fission yeast MOZART1 homologue, is an essential component of the γ-tubulin complex and directly interacts with GCP3(Alp6). Mol Biol Cell 24: 3337–3349

Dráber P, Dráberová E (2012) Microtubules. In: Kavallaris M (ed) Cytoskeleton and human disease. Humana Press, New York, pp 29–55

Dráberová L, Dráberová E, Surviladze Z, Dráber P, Dráber P (1999) Protein tyrosine kinase p53/p56(lyn) forms complexes with γ-tubulin in rat basophilic leukemia cells. Int Immunol 11:1829–1839

Dráberová E, D'Agostino L, Caracciolo V, Sládková V, Sulimenko T, Sulimenko V, Sobol M, Maounis NF, Tzelepis E, Mahera E, Křen L, Legido A, Giordano A, Mörk S, Hozák P, Dráber P, Katsetos CD (2015) Overexpression and nucleolar localization of γ-tubulin small complex proteins GCP2 and GCP3 in glioblastoma. J Neuropathol Exp Neurol 74:723–742

Dryková D, Cenklová V, Sulimenko V, Volc J, Dráber P, Binarová P (2003) Plant gamma-tubulin interacts with alphabeta-tubulin dimers and forms membrane-associated complexes. Plant Cell 15:465–480

Dyachuk V, Bierkamp C, Merdes A (2016) Non-centrosomal microtubule organization in differentiated cells. In: Lüders J (ed) The microtubule cytoskeleton. Springer-Verlag, Wien, pp 27–42

Edzuka T, Yamada L, Kanamaru K, Sawada H, Goshima G (2014) Identification of the augmin complex in the filamentous fungus *Aspergillus nidulans*. PLoS One 9:e101471

Efimov A, Kharitonov A, Efimova N, Loncarek J, Miller PM, Andreyeva N, Gleeson P, Galjart N, Maia AR, McLeod IX, Yates JR 3rd, Maiato H, Khodjakov A, Akhmanova A, Kaverina I (2007) Asymmetric CLASP-dependent nucleation of noncentrosomal microtubules at the trans-Golgi network. Dev Cell 12:917–930

Erhardt M, Stoppin-Mellet V, Campagne S, Canaday J, Mutterer J, Fabian T, Sauter M, Muller T, Peter C, Lambert AM, Schmit AC (2002) The plant Spc98p homologue colocalizes with γ-tubulin at microtubule nucleation sites and is required for microtubule nucleation. J Cell Sci 115:2423–2431

Fant X, Gnadt N, Haren L, Merdes A (2009) Stability of the small γ-tubulin complex requires HCA66, a protein of the centrosome and the nucleolus. J Cell Sci 122:1134–1144

Farache D, Jauneau A, Chemin C, Chartrain M, Rémy MH, Merdes A, Haren L (2016) Functional analysis of γ-tubulin complex proteins indicates specific lateral association via their N-terminal domains. J Biol Chem 291:23112–23125

Findeisen P, Mühlhausen S, Dempewolf S, Hertzog J, Zietlow A, Carlomagno T, Kollmar M (2014) Six subgroups and extensive recent duplications characterize the evolution of the eukaryotic tubulin protein family. Genome Biol Evol 6:2274–2288

Fogeron ML, Müller H, Schade S, Dreher F, Lehmann V, Kühnel A, Scholz AK, Kashofer K, Zerck A, Fauler B, Lurz R, Herwig R, Zatloukal K, Lehrach H, Gobom J, Nordhoff E, Lange BM (2013) LGALS3BP regulates centriole biogenesis and centrosome hypertrophy in cancer cells. Nat Commun 4:1531

Fong CS, Sato M, Toda T (2010) Fission yeast Pcp1 links polo kinase-mediated mitotic entry to γ-tubulin-dependent spindle formation. EMBO J 29:120–130

Gaume X, Tassin AM, Ugrinova I, Mongelard F, Monier K, Bouvet P (2015) Centrosomal nucleolin is required for microtubule network organization. Cell Cycle 14:902–919

Gomez-Ferreria MA, Rath U, Buster DW, Chanda SK, Caldwell JS, Rines DR, Sharp DJ (2007) Human Cep192 is required for mitotic centrosome and spindle assembly. Curr Biol 17:1960–1966

Goshima G, Mayer M, Zhang N, Stuurman N, Vale RD (2008) Augmin: a protein complex required for centrosome-independent microtubule generation within the spindle. J Cell Biol 181:421–429

Grimaldi AD, Maki T, Fitton BP, Roth D, Yampolsky D, Davidson MW, Svitkina T, Straube A, Hayashi I, Kaverina I (2014) CLASPs are required for proper microtubule localization of end-binding proteins. Dev Cell 30:343–352

Groen AC, Cameron LA, Coughlin M, Miyamoto DT, Mitchison TJ, Ohi R (2004) XRHAMM functions in ran-dependent microtubule nucleation and pole formation during anastral spindle assembly. Curr Biol 14:1801–1811

Guerin CM, Kramer SG (2009) RacGAP50C directs perinuclear Akhmanova A and Steinmetz MO (2015) Control of microtubule organization and dynamics: two ends in the limelight. Nat Rev Mol Cell Biol 16:711–726

Guillet V, Knibiehler M, Gregory-Pauron L, Remy MH, Chemin C, Raynaud-Messina B, Bon C, Kollman JM, Agard DA, Merdes A, Mourey L (2011) Crystal structure of γ-tubulin complex protein GCP4 provides insight into microtubule nucleation. Nat Struct Mol Biol 18:915–919

Gunawardane RN, Lizarraga SB, Wiese C, Wilde A, Zheng Y (2000) γ-Tubulin complexes and their role in microtubule nucleation. Curr Top Dev Biol 49:55–73

Hořejší B, Vinopal S, Sládková V, Dráberová E, Sulimenko V, Sulimenko T, Vosecká V, Philimonenko A, Hozák P, Katsetos CD, Dráber P (2012) Nuclear γ-tubulin associates with nucleoli and interacts with tumor suppressor protein C53. J Cell Physiol 227:367–382

Hotta T, Kong Z, Ho CM, Zeng CJ, Horio T, Fong S, Vuong T, Lee YR, Liu B (2012) Characterization of the *Arabidopsis* augmin complex uncovers its critical function in the assembly of the acentrosomal spindle and phragmoplast microtubule arrays. Plant Cell 24:1494–1509

Hsia KC, Wilson-Kubalek EM, Dottore A, Hao Q, Tsai KL, Forth S, Shimamoto Y, Milligan RA, Kapoor TM (2014) Reconstitution of the augmin complex provides insights into its architecture and function. Nat Cell Biol 16:852–863

Inukai K, Funaki M, Nawano M, Katagiri H, Ogihara T, Anai M, Onishi Y, Sakoda H, Ono H, Fukushima Y, Kikuchi M, Oka Y, Asano T (2000) The N-terminal 34 residues of the 55 kDa regulatory subunits of phosphoinositide 3-kinase interact with tubulin. Biochem J 346(Pt 2):483–489

Janski N, Masoud K, Batzenschlager M, Herzog E, Evrard JL, Houlné G, Bourge M, Chabouté ME, Schmit AC (2012) The GCP3-interacting proteins GIP1 and GIP2 are required for γ-tubulin complex protein

localization, spindle integrity, and chromosomal stability. Plant Cell 24:1171–1187

Jeffery JM, Grigoriev I, Poser I, van der Horst A, Hamilton N, Waterhouse N, Bleier J, Subramaniam VN, Maly IV, Akhmanova A, Khanna KK (2013) Centrobin regulates centrosome function in interphase cells by limiting pericentriolar matrix recruitment. Cell Cycle 12:899–906

Johmura Y, Soung NK, Park JE, Yu LR, Zhou M, Bang JK, Kim BY, Veenstra TD, Erikson RL, Lee KS (2011) Regulation of microtubule-based microtubule nucleation by mammalian polo-like kinase 1. Proc Natl Acad Sci U S A 108:11446–11451

Kalab P, Pralle A, Isacoff EY, Heald R, Weis K (2006) Analysis of a RanGTP-regulated gradient in mitotic somatic cells. Nature 440: 697–701

Khodjakov A, Rieder CL (1999) The sudden recruitment of γ-tubulin to the centrosome at the onset of mitosis and its dynamic exchange throughout the cell cycle, do not require microtubules. J Cell Biol 146:585–596

Kilmartin JV, Goh PY (1996) Spc110p: assembly properties and role in the connection of nuclear microtubules to the yeast spindle pole body. EMBO J 15:4592–4602

Kinoshita K, Noetzel TL, Pelletier L, Mechtler K, Drechsel DN, Schwager A, Lee M, Raff JW, Hyman AA (2005) Aurora A phosphorylation of TACC3/maskin is required for centrosome-dependent microtubule assembly in mitosis. J Cell Biol 170:1047–1055

Kirik A, Ehrhardt DW, Kirik V (2012) TONNEAU2/FASS regulates the geometry of microtubule nucleation and cortical array organization in interphase *Arabidopsis* cells. Plant Cell 24:1158–1170

Knop M, Schiebel E (1997) Spc98p and Spc97p of the yeast γ-tubulin complex mediate binding to the spindle pole body via their interaction with Spc110p. EMBO J 16:6985–6995

Kollman JM, Zelter A, Muller EG, Fox B, Rice LM, Davis TN, Agard DA (2008) The structure of the γ-tubulin small complex: implications of its architecture and flexibility for microtubule nucleation. Mol Biol Cell 19:207–215

Kollman JM, Polka JK, Zelter A, Davis TN, Agard DA (2010) Microtubule nucleating γ-TuSC assembles structures with 13-fold microtubule-like symmetry. Nature 466:879–882

Kollman JM, Merdes A, Mourey L, Agard DA (2011) Microtubule nucleation by γ-tubulin complexes. Nat Rev Mol Cell Biol 12:709–721

Kollman JM, Greenberg CH, Li S, Moritz M, Zelter A, Fong KK, Fernandez JJ, Sali A, Kilmartin J, Davis TN, Agard DA (2015) Ring closure activates yeast γ-TuRC for species-specific microtubule nucleation. Nat Struct Mol Biol 22:132–137

Lawo S, Hasegan M, Gupta GD, Pelletier L (2012) Subdiffraction imaging of centrosomes reveals higher-order organizational features of pericentriolar material. Nat Cell Biol 14:1148–1158

Lin TC, Neuner A, Schlosser YT, Scharf AN, Weber L, Schiebel E (2014) Cell-cycle dependent phosphorylation of yeast pericentrin regulates γ-TuSC-mediated microtubule nucleation. Elife 3:e02208

Lin TC, Neuner A, Schiebel E (2015) Targeting of γ-tubulin complexes to microtubule organizing centers: conservation and divergence. Trends Cell Biol 25:296–307

Liu T, Tian J, Wang G, Yu Y, Wang C, Ma Y, Zhang X, Xia G, Liu B, Kong Z (2014) Augmin triggers microtubule-dependent microtubule nucleation in interphase plant cells. Curr Biol 24:2708–2713

Lüders J, Stearns T (2007) Microtubule-organizing centres: a re-evaluation. Nat Rev Mol Cell Biol 8:161–167

Lüders J, Patel UK, Stearns T (2006) GCP-WD is a γ-tubulin targeting factor required for centrosomal and chromatin-mediated microtubule nucleation. Nat Cell Biol 8:137–147

Ludueña RF, Banerjee A (2008) The isotypes of tubulin: distribution and functional significance. In: Fojo T (ed) The role of microtubules in cell biology, neurobiology and oncology. Humana Press, Totowa, pp 123–175

Lyon AS, Morin G, Moritz M, Yabut KC, Vojnar T, Zelter A, Muller E, Davis TN, Agard DA (2016) Higher-order oligomerization of Spc110p drives γ-tubulin ring complex assembly. Mol Biol Cell 27:2245–2258

Macurek L, Dráberová E, Richterová V, Sulimenko V, Sulimenko T, Dráberová L, Marková V, Dráber P (2008) Regulation of microtubule nucleation from membranes by complexes of membrane-bound γ-tubulin with Fyn kinase and phosphoinositide 3-kinase. Biochem J 416:421–430

Meunier S, Vernos I (2016) Acentrosomal microtubule assembly in mitosis: the where, when, and how. Trends Cell Biol 26:80–87

Mishra RK, Chakraborty P, Arnaoutov A, Fontoura BM, Dasso M (2010) The Nup107-160 complex and γ-TuRC regulate microtubule polymerization at kinetochores. Nat Cell Biol 12:164–169

Mogensen MM, Malik A, Piel M, Bouckson-Castaing V, Bornens M (2000) Microtubule minus-end anchorage at centrosomal and non-centrosomal sites: the role of ninein. J Cell Sci 113(Pt 17):3013–3023

Moreno-Mateos MA, Espina AG, Torres B, Gámez del Estal MM, Romero-Franco A, Ríos RM, Pintor-Toro JA (2011) PTTG1/securin modulates microtubule nucleation and cell migration. Mol Biol Cell 22:4302–4311

Moritz M, Braunfeld MB, Guénebaut V, Heuser J, Agard DA (2000) Structure of the γ-tubulin ring complex: a template for microtubule nucleation. Nat Cell Biol 2:365–370

Murata T, Sonobe S, Baskin TI, Hyodo S, Hasezawa S, Nagata T, Horio T, Hasebe M (2005) Microtubule-dependent microtubule nucleation based on recruitment of γ-tubulin in higher plants. Nat Cell Biol 7: 961–968

Muroyama A, Seldin L, Lechler T (2016) Divergent regulation of functionally distinct γ-tubulin complexes during differentiation. J Cell Biol 213:679–692

Nogales E, Wang HW (2006) Structural intermediates in microtubule assembly and disassembly: how and why? Curr Opin Cell Biol 18: 179–184

Nováková M, Dráberová E, Schürmann W, Czihak G, Viklický V, Dráber P (1996) γ-tubulin redistribution in taxol-treated mitotic cells probed by monoclonal antibodies. Cell Motil Cytoskeleton 33:38–51

Oakley CE, Oakley BR (1989) Identification of γ-tubulin, a new member of the tubulin superfamily encoded by mipA gene of *Aspergillus nidulans*. Nature 338:662–664

Oakley BR, Paolillo V, Zheng Y (2015) γ-Tubulin complexes in microtubule nucleation and beyond. Mol Biol Cell 26:2957–2962

Oh SA, Jeon J, Park HJ, Grini PE, Twell D, Park SK (2016a) Analysis of gemini pollen 3 mutant suggests a broad function of AUGMIN in microtubule organization during sexual reproduction in *Arabidopsis*. Plant J 87:188–201

Oh D, Yu CH, Needleman DJ (2016b) Spatial organization of the Ran pathway by microtubules in mitosis. Proc Natl Acad Sci U S A 113: 8729–8734

Oriolo AS, Wald FA, Canessa G, Salas PJ (2007) GCP6 binds to intermediate filaments: a novel function of keratins in the organization of microtubules in epithelial cells. Mol Biol Cell 18:781–794

Petry S, Vale RD (2015) Microtubule nucleation at the centrosome and beyond. Nat Cell Biol 17:1089–1093

Petry S, Groen AC, Ishihara K, Mitchison TJ, Vale RD (2013) Branching microtubule nucleation in *Xenopus* egg extracts mediated by augmin and TPX2. Cell 152:768–777

Pinyol R, Scrofani J, Vernos I (2013) The role of NEDD1 phosphorylation by aurora a in chromosomal microtubule nucleation and spindle function. Curr Biol 23:143–149

Rivero S, Cardenas J, Bornens M, Rios RM (2009) Microtubule nucleation at the cis-side of the Golgi apparatus requires AKAP450 and GM130. EMBO J 28:1016–1028

Roostalu J, Cade NI, Surrey T (2015) Complementary activities of TPX2 and chTOG constitute an efficient importin-regulated microtubule nucleation module. Nat Cell Biol 17:1422–1434

Roubin R, Acquaviva C, Chevrier V, Sedjaï F, Zyss D, Birnbaum D, Rosnet O (2013) Myomegalin is necessary for the formation of centrosomal and Golgi-derived microtubules. Biol Open 2:238–250

Samejima I, Miller VJ, Groocock LM, Sawin KE (2008) Two distinct regions of Mto1 are required for normal microtubule nucleation and efficient association with the γ-tubulin complex *in vivo*. J Cell Sci 121:3971–3980

Sánchez-Huertas C, Lüders J (2015) The augmin connection in the geometry of microtubule networks. Curr Biol 25:R294–R299

Sánchez-Huertas C, Freixo F, Viais R, Lacasa C, Soriano E, Lüders J (2016) Non-centrosomal nucleation mediated by augmin organizes microtubules in post-mitotic neurons and controls axonal microtubule polarity. Nat Commun 7:12187

Sanders AA, Kaverina I (2015) Nucleation and dynamics of Golgi-derived microtubules. Front Neurosci 9:431

Sawin KE, Tran PT (2006) Cytoplasmic microtubule organization in fission yeast. Yeast 23:1001–1014

Scrofani J, Sardon T, Meunier S, Vernos I (2015) Microtubule nucleation in mitosis by a RanGTP-dependent protein complex. Curr Biol 25: 131–140

Seltzer V, Janski N, Canaday J, Herzog E, Erhardt M, Evrard JL, Schmit AC (2007) *Arabidopsis* GCP2 and GCP3 are part of a soluble γ-tubulin complex and have nuclear envelope targeting domains. Plant J 52:322–331

Singh P, Thomas GE, Gireesh KK, Manna TK (2014) TACC3 protein regulates microtubule nucleation by affecting γ-tubulin ring complexes. J Biol Chem 289:31719–31735

Soues S, Adams IR (1998) SPC72: a spindle pole component required for spindle orientation in the yeast *Saccharomyces cerevisiae*. J Cell Sci 111:2809–2818

Sulimenko V, Sulimenko T, Poznanovic S, Nechiporuk-Zloy V, Böhm KJ, Macurek L, Unger E, Dráber P (2002) Association of brain γ-tubulins with αβ-tubulin dimers. Biochem J 365:889–895

Sulimenko V, Dráberová E, Sulimenko T, Macurek L, Richterová V, Dráber P, Dráber P (2006) Regulation of microtubule formation in activated mast cells by complexes of γ-tubulin with Fyn and Syk kinases. J Immunol 176:7243–7253

Sulimenko V, Hájková Z, Černohorská M, Sulimenko T, Sládková V, Dráberová L, Vinopal S, Dráberová E, Dráber P (2015) Microtubule nucleation in mouse bone marrow-derived mast cells is regulated by the concerted action of GIT1/βPIX proteins and calcium. J Immunol 194:4099–4111

Takahashi M, Yamagiwa A, Nishimura T, Mukai H, Ono Y (2002) Centrosomal proteins CG-NAP and kendrin provide microtubule nucleation sites by anchoring γ-tubulin ring complex. Mol Biol Cell 13:3235–3245

Teixidó-Travesa N, Villén J, Lacasa C, Bertran MT, Archinti M, Gygi SP, Caelles C, Roig J, Lüders J (2010) The γ-TuRC revisited: a comparative analysis of interphase and mitotic human γ-TuRC redefines the set of core components and identifies the novel subunit GCP8. Mol Biol Cell 21:3963–3972

Teixidó-Travesa N, Roig J, Lüders J (2012) The where, when and how of microtubule nucleation - one ring to rule them all. J Cell Sci 125: 4445–4456

Tsai MY, Zheng Y (2005) Aurora a kinase-coated beads function as microtubule-organizing centers and enhance RanGTP-induced spindle assembly. Curr Biol 15:2156–2163

Uehara R, Nozawa RS, Tomioka A, Petry S, Vale RD, Obuse C, Goshima G (2009) The augmin complex plays a critical role in spindle microtubule generation for mitotic progression and cytokinesis in human cells. Proc Natl Acad Sci U S A 106:6998–7003

Uehara R, Kamasaki T, Hiruma S, Poser I, Yoda K, Yajima J, Gerlich DW, Goshima G (2016) Augmin shapes the anaphase spindle for efficient cytokinetic furrow ingression and abscission. Mol Biol Cell 27:812–827

Usui T, Maekawa H, Pereira G, Schiebel E (2003) The XMAP215 homologue Stu2 at yeast spindle pole bodies regulates microtubule dynamics and anchorage. EMBO J 22:4779–4793

Verhey KJ, Gaertig J (2007) The tubulin code. Cell Cycle 6:2152–2160

Vinopal S, Černohorská M, Sulimenko V, Sulimenko T, Vosecká V, Flemr M, Dráberová E, Dráber P (2012) γ-Tubulin 2 nucleates microtubules and is downregulated in mouse early embryogenesis. PLoS One 7:e29919

Wang Z, Wu T, Shi L, Zhang L, Zheng W, Qu JY, Niu R, Qi RZ (2010) Conserved motif of CDK5RAP2 mediates its localization to centrosomes and the Golgi complex. J Biol Chem 285:22658–22665

Wang S, Wu D, Quintin S, Green RA, Cheerambathur DK, Ochoa SD, Desai A, Oegema K (2015) NOCA-1 functions with γ-tubulin and in parallel to Patronin to assemble non-centrosomal microtubule arrays in *C. elegans*. Elife 4:e08649

Wieczorek M, Bechstedt S, Chaaban S, Brouhard GJ (2015) Microtubule-associated proteins control the kinetics of microtubule nucleation. Nat Cell Biol 17:907–916

Yokoyama H, Koch B, Walczak R, Ciray-Duygu F, González-Sánchez JC, Devos DP, Mattaj IW, Gruss OJ (2014) The nucleoporin MEL-28 promotes RanGTP-dependent γ-tubulin recruitment and microtubule nucleation in mitotic spindle formation. Nat Commun 5:3270

Zhang X, Chen Q, Feng J, Hou J, Yang F, Liu J, Jiang Q, Zhang C (2009) Sequential phosphorylation of Nedd1 by Cdk1 and Plk1 is required for targeting of the γ-TuRC to the centrosome. J Cell Sci 122:2240–2251

Zhang T, Braun U, Leitges M (2016) PKD3 deficiency causes alterations in microtubule dynamics during the cell cycle. Cell Cycle 15:1844–1854

Zimmerman WC, Sillibourne J, Rosa J, Doxsey SJ (2004) Mitosis-specific anchoring of γ-tubulin complexes by pericentrin controls spindle organization and mitotic entry. Mol Biol Cell 15:3642–3657

VI.7

Hájková Z., Sulimenko V., Paulenda T., Dráber P. Miltefosine modulates cell activation as well as microtubule organization and dynamics in murine mast cells. Allergy (Submitted).

Miltefosine modulates cell activation as well as microtubule organization and dynamics in murine mast cells

Zuzana Hájková[1], Vadym Sulimenko[1], Tomáš Paulenda[2] and Pavel Dráber[1]

[1]Department of Biology of Cytoskeleton and [2]Department of Signal Transduction, Institute of Molecular Genetics, Academy of Sciences of the Czech Republic, CZ-142 20 Prague 4, Czech Republic

Running title: Miltefosine modulates microtubules in mast cells

Correspondence

Dr. Pavel Dráber, Department of Biology of Cytoskeleton, Institute of Molecular Genetics, Academy of Sciences of the Czech Republic, Vídeňská 1083, 142 20 Prague 4, Czech Republic. Tel.: (420) 241 062 632, Fax: (420) 241 062 758, E-mail: paveldra@img.cas.cz

Abstract

Background: Mast cells play an effector role in innate immunity, allergy, and inflammation. Their activation initiates signalling events leading to Ca^{2+} response, release of allergic mediators from cytoplasmic granules, and synthesis of cytokines and chemokines. Diseases associated with deregulated mast cell functions are hard-to-treat and the demand for new treatments increases. Miltefosine (hexadecylphosphocholine) appears to be a new candidate for therapeutic strategies as it inhibits mast cell degranulation and reduces progression in patients with mast cell-driven diseases. Because molecular mechanisms of its action remain poorly understood, we analysed the effects of miltefosine on mast cell activation events and on the microtubule organization and dynamics.

Methods: Degranulation and Ca^{2+} influx in mouse bone marrow-derived mast cells (BMMCs) were evaluated by β-hexosaminidase release and Fura-2-AM calcium reporter, respectively. Microscopic techniques were used for analysis of microtubule organization, miltefosine localization and chemotaxis. Microtubule dynamics was followed by time-lapse imaging of tagged microtubule plus-end-tracking protein EB1. The phosphorylation level was evaluated by an *in vitro* kinase assay.

Results: Miltefosine inhibited degranulation, reorganization of microtubules and antigen-induced chemotaxis. While aggregation and tyrosine phosphorylation of high-affinity IgE receptors were suppressed in activated BMMCs pre-treated with miltefosine, Ca^{2+} influx was not inhibited. BODIPY-labelled miltefosine localized to the plasma membrane, cytosol and intracellular membranes. Moreover, cytosolic miltefosine affected microtubule plus-end dynamics in a Ca^{2+}-dependent manner and attenuated phosphorylation of EB1 interacting proteins.

Conclusions: Collectively, our data suggest that miltefosine affects mast cells through both modulation of cell surface and intracellular signalling pathway(s) directed to microtubules, degranulation and chemotaxis.

Keywords

bone marrow-derived mast cells, cell activation, microtubule dynamics, miltefosine

Abbreviations

Ab(s), antibody(ies)

Ag, antigen

BMMC, bone marrow-derived mast cell

BSA, bovine serum albumin

DNP, dinitrophenyl

EB1, end-binding protein 1

FcεRI, high-affinity IgE receptor

Fura-2-AM, Fura-2-acetoxymethyl ester

GFP, green fluorescent protein

HRP, horseradish peroxidase

ITAM, immunoreceptor tyrosine-based activation motif

mAb, monoclonal antibody

4-NAG, 4-nitrophenyl N-acetyl-β-D-glucosaminide

PKC, protein kinase C

SOCE, store-operated Ca^{2+} entry

+TIPs, plus-end-tracking proteins

TIRF, total internal reflection fluorescence

Introduction

Mast cells play a pivotal role in innate immunity, allergy, and inflammation. Diseases associated with deregulated mast cell functions are hard-to-treat, and so the demand for new and better treatments targeting mast cell activation pathways increases. Mast cells express on their surfaces receptors with a high affinity for IgE (FcεRIs). Aggregation of FcεRIs by multivalent antigen (Ag)-IgE complexes leads to activation of signalling pathways resulting in the release of Ca^{2+} from the endoplasmic reticulum (ER) and subsequent activation of store-operated Ca^{2+} entry (SOCE). The influx of free Ca^{2+} is important for replenishment of Ca^{2+} in ER, but also works as a second messenger for further signalling. Activation events result in the release of preformed granule mediators and *de novo* synthesis and secretion of bioactive compounds, including lipid mediators, cytokines and chemokines (1, 2). Besides that, mast cell activation by FcεRIs aggregation is accompanied with changes in cell morphology, enhanced adhesion and migration. It was reported that activation of mast cells induces increased formation of microtubules (3, 4) and their reorganization into protrusions containing microtubules (microtubule protrusions) (5, 6). Independently of FcεRI aggregation, the activation events can be mimicked by non-specific activators such as protein tyrosine phosphatases inhibitor pervanadate and inhibitor of ER Ca^{2+}-ATPase pumps thapsigargin (5) or by calcium ionophore A23187 (7).

A promising candidate for novel therapeutic strategies in mast-cell driven diseases is miltefosine (hexadecylphosphocholine), as it inhibits activation in human mast cells (8) and reduces disease progression in patients with mast cell-derived mastocytosis (9), urticaria (10) and atopic dermatitis (11). Moreover, miltefosine is used as a treatment of leishmaniasis (12) and free-living amebae infections (13).

Miltefosine is a derivative of plasmalogen phospholipids (14), which is taken up by cells in a raft-dependent manner (15). It has been proposed that miltefosine acts as a lipid raft modulator through its interference with the structural organization of surface receptors in the cell membrane (16). Besides that, it modulates different signalling pathways. It has been reported that miltefosine affects phosphatidylcholine synthesis and stress-activated protein kinase/Jun N-terminal kinase apoptotic pathway (17), phosphatidylinositol 3-kinase/Akt survival pathway (18), as well as the activity of phospholipase Cβ (19), phospholipase D (20) and protein kinase C

(PKC) (21). Despite this knowledge, the molecular mechanisms of miltefosine action in mast cells remain poorly understood.

To get deeper insight into the function(s) of miltefosine in mast cells we evaluated early stages of cell activation after crosslinking of FcεRIs, such as Ca^{2+} influx, degranulation, microtubule reorganization and Ag-induced chemotaxis in miltefosine-treated BMMCs. Moreover, we characterized localization of miltefosine in BMMCs and its effect on microtubule dynamics. Our results indicate that miltefosine does not regulate mast cells only through lipid raft modulation, but also by affecting cytosolic signalling pathways that regulate microtubules, degranulation and chemotaxis in mast cells.

Materials and Methods

Reagents

Calcium ionophore A23187, dinitrophenyl-albumin (DNP-albumin), fibronectin, miltefosine, probenecid, puromycin, thapsigargin and 4-nitrophenyl N-acetyl-β-D-glucosaminide (4-NAG) were from Sigma-Aldrich (St. Louis, MO). Fura-2-acetoxymetyl ester (Fura-2-AM) was purchased from Invitrogen (Carlsbad, CA). Collagen I was from Advanced BioMatrix (San Diego, CA). Protein A Sepharose^{TM} CL-4B was from GE Healthcare Life Sciences (Chicago, IL). SuperSignal WestPico Chemiluminescent reagents were purchased from Pierce (Rockford, IL).

Antibodies

Mouse mAb TUB 2.1 (IgG1) to β-tubulin conjugated with indocarbocyanate (Cy3) and mouse mAb SPE-7 (IgE) specific for DNP were from Sigma-Aldrich (St. Louis, MO). α-Tubulin was detected with rabbit Ab (GTX15246) from Genetex (Irvine, CA). Rabbit polyclonal Ab to end-binding protein 1 (EB1) was from Santa Cruz Biotechnology (Dallas, TX). Rabbit polyclonal Ab to mouse IgE was described previously (22). Mouse mAb 4G10 (IgG2b) to phosphotyrosine conjugated with horseradish peroxidase (HRP) was from Upstate Laboratories (Syracuse, NY). Mouse mAb TU-32 (IgG1) to γ-tubulin was described previously (23). Anti-mouse and anti-rabbit Abs conjugated with HRP were from Promega Biotec (Madison, WI). Anti-mouse Ab conjugated with DyLight549 was from Jackson ImmunoResearch Laboratories (West Grove, PA).

Cell cultures and activation

Primary culture of bone marrow-derived mast cells from BALB/c and cells of mouse bone marrow-derived mast cell line (BMMC) (24) were prepared and cultured as previously described (5). For immunofluorescence experiments, cells were overlaid on fibronectin-coated coverslips (5). Cells were sensitized with DNP-specific IgE (mouse mAb SPE-7; 1 μg/ml) for 4 h in culture medium without 10% WEHI-3 cell supernatant and activated with Ag (DNP-albumin conjugate, 30-40 mol DNP/mol albumin) for 3 min in culture medium without 10% FCS and 10% WEHI-3 cell supernatant (activation medium). If not specified otherwise, Ag was used at concentration

1 μg/ml (5). Alternatively, sensitized cells were activated by crosslinking of bound IgE with anti-mouse Ab conjugated with DyLight549 (1.5 μg/ml) for 20 min at 37°C as described (25). Cells were also activated for 15 min at 37°C in activation medium containing 2 μM thapsigargin or pervanadate (5) or 0.5 μM ionophore A23187.

Cells were pre-treated with miltefosine at final concentration 5-25 μM for 15 min at 37°C prior to activation. In some cases, cells were incubated with 1-15 μM BODIPY-labelled miltefosine (MT-11c-6EtBDPY) (26) for 1-60 min at 37°C. If not specified otherwise, miltefosine or BODIPY-miltefosine were used at final concentration 15 μM for 15 min and were also present in the course of activation.

Constructs and cell transduction

The coding sequence of green fluorescent protein (GFP) was cut out from pEB1-GFP vector (27) by NheI/EcoRI and ligated into pCDH-CMV-MCS-EF1-puro lentiviral vector (System Biosciences, Palo Alto, CA), resulting in pGFP-puro vector. The coding sequence of mouse EB1 was cut out from pEB1-GFP vector by NheI/NheI and ligated into prepared pGFP-puro vector, resulting in lentiviral vector pmEB1-GFP-puro. Lentiviral packaging and infections were done as described previously (5), using selection in 5 μg/ml of puromycin. Stable cell line BMMC_mEB1-GFP was established after 14 d selection.

Determination of intracellular Ca^{2+} concentrations

Changes in the level of free intracellular Ca^{2+} were measured using Fura-2-AM as a cell permeant calcium reporter following the protocol for sample handling as described in (5). Intracellular free Ca^{2+} was measured in microplate reader Infinite M200 (Tecan, Männedorf, Switzerland) as a ratio of Fura emissions at 510 nm after excitation with 340 nm and 380 nm (340/380) lasers at the indicated time points. After measurement of the Ca^{2+} basic level, activation was triggered by addition of Ag, thapsigargin or ionophore A231287. Measurement continued up to 300 s.

Degranulation assay

The degree of degranulation was quantified as the release of β-hexosaminidase from Ag-, thapsigargin- or pervanadate-activated cells, using 4-NAG as substrate (3). The extent of

degranulation was calculated as follows: absorbance of culture supernatant × 100/absorbance of total cell lysate, and normalized to control cells.

Immunoprecipitations, kinase assay and immunoblotting

For immunoprecipitation experiments, BMMCs (1×10^7 cells per reaction) were activated with Ag or thapsigargin. Immunoprecipitation was performed as previously described (28). Cell extracts were incubated with Protein A beads saturated with i) rabbit Ab to IgE; ii) rabbit Ab to EB1 or iii) immobilized protein A alone. *In vitro* kinase assay was essentially performed as described and the ^{32}P-labelled proteins were detected by autoradiography (4). Whole cell extract preparation, gel electrophoresis and immunoblotting were described elsewhere (5). Abs to γ-tubulin (in the form of spent culture supernatant) and EB1 were diluted 1:2 and 1:1,000, respectively. Phosphotyrosine was detected by anti-phosphotyrosine Ab conjugated with HRP (dilution 1:2,000). Bound primary antibodies were detected after incubation of the blots with HRP-conjugated secondary Abs diluted 1:10,000. HRP signal was detected with chemiluminiscence reagents and quantified using the LAS 3000 imaging system (Fujifilm, Tokyo, Japan).

Chemotaxis and cell migration assay

Chemotaxis and cell migration assays were performed in μ-Slide Chemotaxis^{3D} chambers according to the protocols described elsewhere (29). In the case of chemotaxis assay, BMMCs were sensitized prior to seeding and one reservoir of each chamber was supplied with Ag at concentration 100 ng/ml. In miltefosine-treated cells, the drug was added to collagen I gel and to reservoirs and was present during the gel polymerization and imaging.

Immunofluorescence microscopy

Immunofluorescence microscopy was performed with cells attached to fibronectin-coated coverslips fixed as described (30). TUB 2.1 mAb conjugated with Cy3 was diluted 1:600. DyLight549-conjugated anti-mouse Ab was diluted 1:500. To visualize FcεRI aggregation, cells were fixed without Triton X-100 extraction to preserve intact cell membranes. The preparations were examined with an Olympus A70 Provis microscope (Olympus, Hamburg, Germany) or in the Delta Vision Core system (Applied Precision, Issaquah, WA). The conjugated secondary Ab

did not give any detectable staining. Live cell imaging of BMMCs treated with BODIPY-miltefosine was performed in the Delta Vision Core system. Images were deconvolved by integrated deconvolution software. Determination of the number of cells that responded to activation events by generation of microtubule protrusions was done as described previously. Three experiments were performed, and in each experiment 300-500 cells were examined (5). Statistical comparison of data was conducted by Student's *t* test.

Time-lapse imaging

For measurement of microtubule dynamics by total internal reflection fluorescence (TIRF) microscopy, cells were overlaid on a glass-bottom dish (Cellvis, Mountain View, CA, Catalog No. D35-14-1.5-N) pre-coated with fibronectin as described (5). Before imaging, cells were washed and incubated in medium for live-cell imaging (5) supplemented with thapsigargin (2 μM) or miltefosine (15 μM). Controls contained an equivalent volume of DMSO carrier. In some experiments, $[Ca^{2+}]$-free medium for live cell imaging was used for miltefosine pre-treatment and imaging. Cells were scanned for 20 min with a Leica AM TIRF MC (Leica Microsystems, Wetzlar, Germany) at 37°C, starting 3 min after replacement of medium with the medium for live-cell imaging containing thapsigargin or miltefosine. Time-lapse sequences of EB1-GFP were acquired as described (5). For chemotaxis and cell migration assay, cells were imaged with a Leica DMI6000 inverted MC at 37°C and 5% CO_2. Time-lapse sequences of bright-field images were taken for 7 h (chemotaxis) or 3 h (cell migration), at 1 min intervals with the intensity of 71 and exposure time 6 ms.

Image analysis

Microtubule growth dynamics was analysed from EB1 time-lapse movies using plusTipTracker software, version 1.1.4 (31, 32) based on Matlab (MathWorks, Natick, MA). The following parameter set for all movies in the dataset was used: maximum gap length, 3 frames; minimum track length, 3 frames; search radius range, 2-9 pixels; maximum forward angle, 30°; maximum backward angle, 10°; maximum shrinkage factor, 1.5; fluctuation radius, 1 pixel. For statistical analyses and categorizing EB1 tracks, the "Group analysis" and "Quadrant Scatter Plot" were applied, respectively. Generated percentage graphs divide microtubules into subpopulations

based on whether they are above or below the median growth speed and median growth lifetime of EB1 tracks from all control cells analysed in each experiment.

Chemotactic response and cell migration were analysed from time-lapse movies as described previously (29). Cells were tracked in the MetaMorph (Molecular Devices, Sunnyvale, CA) using the Track Object application. The data were proceeded by Chemotaxis and Migration Tool in ImageJ (NIH, Bethesda, MA). Analysis was performed for 7 h and 3 h imaging.

Results

Degranulation in activated BMMCs is inhibited by miltefosine.

Miltefosine is known to inhibit mediator release in human mast cells (8). To test whether the same holds true for mouse BMMCs, the degree of degranulation in miltefosine pre-treated and activated BMMCs was determined. Cells were incubated with different concentrations of miltefosine in the range of 5-25 μM for 15 min. The release of β-hexosaminidase was measured in cells activated by FcεRI aggregation using either low (Fig. 1*A*; Antigen, 25 ng/ml) or high (Fig. 1*B*; Antigen 1000 ng/ml) concentration of Ag. The β-hexosaminidase release decreased in a miltefosine dose-dependent manner at both Ag concentrations. The maximal inhibitory effect (more than 60 %) was observed at miltefosine concentration 25 μM. Alternatively, BMMCs were activated by thapsigargin. Miltefosine decreased the level of degranulation in a dose-dependent manner as well (Fig. 1*C*), and at miltefosine concentration 25 μM, ~ 50% inhibition was detected. A less prominent inhibitory effect was observed after stimulation of BMMCs by pervanadate. At miltefosine concentration 25 μM, ~ 35 % inhibition was detected (Fig. 1*D*). The least inhibitory effect (~ 21 % inhibition at miltefosine concentration 25 μM) was detected when the cells were activated by calcium ionophore A23187 (data not shown). Taken collectively, miltefosine inhibits degranulation in mouse BMMCs activated either specifically by FcεRI aggregation, or unspecifically by thapsigargin, pervanadate or calcium ionophore.

Miltefosine modulates microtubule organization and cell migration in BMMCs.

Generation of protrusions containing microtubules (microtubule protrusions) is a characteristic feature of activated BMMCs attached to fibronectin (5). To evaluate the effect of miltefosine on generation of such protrusions, cells were pre-treated for 15 min with 15 μM miltefosine and thereafter activated by Ag, thapsigargin, calcium ionophore or pervanadate in the presence of miltefosine. Control cells activated by FcεRI aggregation (Fig. 2*A*; *a*; + Antigen), thapsigargin (Fig. 2*A*; *c*), calcium ionophore (Fig. 2*A*; *e*) or pervanadate (data not shown) formed typical microtubule protrusions. On the other hand, cells activated in the presence of miltefosine by FcεRI aggregation (Fig. 2*A*; *b*; + Antigen), thapsigargin (Fig. 2*A*; *d*), calcium ionophore (Fig. 2*A*; *f*) or pervanadate were not capable to form microtubule protrusions. Statistical evaluation revealed a dose-dependent inhibitory effect of miltefosine on the formation of microtubule

protrusions (Fig. 2*B*). Activation of cells with Ag, thapsigargin, calcium ionophore or pervanadate showed a similar response to miltefosine treatment. Higher concentrations of miltefosine resulted in changes of cell morphology; cells were more spherical. The activation with Ag, thapsigargin or pervanadate was also performed in primary culture of BMMCs from BALB/c mice. Similarly as in BMMC cell line, miltefosine inhibited generation of microtubule protrusions in these cells (data not shown). These data document that miltefosine substantially affects microtubule organization under physiological as well as non-physiological activation conditions both in BMMCs in primary culture and in the cultured cell line.

Ag-induced chemotactic response is essential for mast cell local accumulation in the body, where they might perform their physiological roles. To study the effect of miltefosine on the migration of BMMCs to Ag, chemotaxis assays were performed. As shown in a representative experiment, miltefosine inhibited chemotaxis towards Ag. Moreover, tracks in miltefosine-treated cells were substantially shorter when compared to control cells (Fig. 2*C*). The cell migration assay without chemoattractant revealed that both mean cell velocity (Fig. 2*D*, left panel) and mean accumulated distance (Fig. 2*D,* right panel) of all moving cells decreased in miltefosine-treated cells. These data suggest that inhibition of Ag-induced chemotaxis by miltefosine is due to suppression of cell motility.

Miltefosine affects tyrosine phosphorylation and aggregation of FcεRI receptors in activated BMMCs.

It has been reported that miltefosine, as a lipid raft modulator, could interfere with the structural organization of FcεRI receptors in activated mast cells and thus inhibit downstream signalling events (16). Because protein tyrosine phosphorylation plays an essential role in propagation of signals in BMMCs activated by FcεRI aggregation, we evaluated the overall protein tyrosine phosphorylation level (P-Tyr) in control and miltefosine pre-treated cells activated by Ag-mediated FcεRI aggregation. While the P-Tyr level increased in Ag-activated cells when compared to non-activated cell controls (Fig 3*A*, lane 3), it decreased in cells treated with miltefosine (Fig. 3*A*, lane 4). It is well established that BMMC activation by Ag proceeds through tyrosine phosphorylation of immunoreceptor tyrosine-based activation motifs (ITAMs) located on the cytoplasmic tails of FcεRI β and γ subunits (33). We found that BMMCs activated with

Ag showed a significantly increased level of P-Tyr on FcεRIs (Fig. 3*B*, lane 8) when compared with non-activated cells (Fig. 3*B*, lanes 6-7). Phosphorylation of FcεRIs in activated cells clearly decreased in the presence of miltefosine (Fig. 3*B*, lane 9). These findings were corroborated by immunofluorescence staining of IgE bound to FcεRI receptors. BMMCs sensitized with IgE and activated with Ag showed clear aggregation of the bound IgE (Fig. 3*C, a).* The same result was obtained when the bound IgE was aggregated with anti-Ig Ab (Fig. 3*C, c*). However, when the cells were pre-treated with miltefosine, aggregation with either Ag (Fig 3*C, b*) or anti-Ig Ab (Fig. 3*C, d*) was substantially suppressed. These data directly demonstrate that miltefosine inhibits aggregation and tyrosine phosphorylation of FcεRI receptors at the plasma membrane in activated BMMCs.

Miltefosine does not inhibit Ca^{2+} influx in activated BMMCs but localizes to the cellular membranes and cytosol.

We have reported that reorganization of microtubules in later stages of BMMC activation depends on Ca^{2+} influx (5). To test whether miltefosine affects the Ca^{2+} influx, we measured the level of intracellular Ca^{2+} after BMMC activation in control and miltefosine-treated cells (Fig. 4*A*). Unexpectedly, 15 μM miltefosine did not inhibit the influx of extracellular Ca^{2+} in cells activated with FcεRI aggregation (Fig. 4*A*, Antigen). Miltefosine slightly increased the Ca^{2+} influx in thapsigargin-activated cells (Fig. 4*A*, Thapsigargin), and this trend was also observed in cells activated by calcium ionophore (Fig 4*A*, Calcium ionophore).

To evaluate the distribution of miltefosine in BMMCs we applied BODIPY-labelled miltefosine (26). Using this tool we localized it on the plasma membrane, intracellular membranous structures, as well as in the cytosol (Fig. 4*B*). Internalization of BODIPY-miltefosine was rapid, as intracellular structures were decorated already after 1 min incubation with 15 μM BODIPY-miltefosine. When the cells were incubated with 1 μM BODIPY-miltefosine for 15-60 min, the intensity of staining increased in a time-dependent manner.

BODIPY-miltefosine worked in the same way as the untagged miltefosine, as BODIPY-miltefosine inhibited generation of microtubule protrusions in cells activated with thapsigargin (Fig. 4*C, c-d*; BODIPY-miltefosine), in contrast to control cells not treated with BODIPY-miltefosine (Fig. 4*C, a-b*; Control). These data show that although miltefosine inhibits

aggregation and phosphorylation of FcεRI on the plasma membrane in activated cells, it does not inhibit Ca^{2+} influx in activated cells. Moreover, miltefosine could affect signalling pathways in the cytosol as it localizes into the cell interior of BMMCs.

Effect of miltefosine on microtubule dynamics in mast cells.

The cytoskeletal organization and cell motility of activated BMMCs depends on proper microtubule functions (34). The dynamics of microtubule plus ends is modulated by plus-end-tracking proteins (+TIPs) such as EB1, which associates with growing microtubules (35). To determine whether cytosolic miltefosine affects microtubule plus-end dynamics, we followed the growing microtubule ends, marked by EB1 tagged with GFP, in control and miltefosine-treated cells. Activation of BMMCs by thapsigargin resulted in an increase of microtubule growth speed (Fig. 5*A*; Thapsigargin), as reported previously (5). The same was true for cells treated with miltefosine (Fig. 5*A*; Miltefosine + Ca^{2+}) or by ionophore A23187 (data not shown). However, when the cells were treated with miltefosine and imaged in the medium for live-cell imaging without [Ca^{2+}], the microtubule growth speed decreased when compared to control (Fig. 5*A*; Miltefosine - Ca^{2+}). Quadrant scatter plots that divide microtubules according to their growth speed and growth lifetime showed that thapsigargin and miltefosine treatments led to higher amounts of fast, short-lived microtubules (Fig. 5*B;* Thapsigargin, Miltefosine + Ca^{2+}). On the other hand, miltefosine-treated cells in [Ca^{2+}]-free medium showed slower, long-lived microtubules at the expense of fast, short-lived microtubules (Fig. 5*B;* Thapsigargin, Miltefosine - Ca^{2+}). Representative 30-frames projection, coloured microtubule track subpopulations and percentage graphs are shown for control (Fig. 5*C*, *a-c*; Control) and miltefosine-treated cells (Fig. 5*C*; *d-f*; + Miltefosine). Collectively, these data document that miltefosine affects microtubule dynamics in BMMCs in a Ca^{2+}-dependent manner.

Miltefosine affects phosphorylation of proteins interacting with +TIP protein EB1.

Association of +TIPs with growing ends of microtubules is regulated by phosphorylation (36). To evaluate whether miltefosine could affect the phosphorylation level of proteins associated with EB1 in BMMCs, we performed *in vitro* kinase assays after immunoprecipitation with Ab to EB1. Autoradiography (^{32}P) revealed that anti-EB1 Ab co-precipitated kinases that phosphorylated

associated proteins (Fig 6, lane 1). Activation of cells with thapsigargin resulted in a decreased level of phosphorylation (Fig 6, lane 2). The same effect was observed for pre-treatment of cells with miltefosine (Fig 6, lane 3). On the other hand, no significant level of phosphorylation was detected in the controls (Fig 6, lanes 4-5). Staining of the immunoblot after autoradiography revealed comparable levels of precipitated EB1. The lower level of protein phosphorylation in the case of activated cells and miltefosine-treated cells correlates with increased microtubule growth speed (Fig 5*A*). These data suggest that miltefosine could regulate microtubule dynamics by modulating signalling pathway(s) affecting the phosphorylation level of +TIP proteins.

Discussion

Mast cell activation by crosslinking of FcεRIs triggers the signalling pathways resulting in Ca^{2+} influx, degranulation and synthesis of new mediators. Pharmaceutical agents that modulate integrity of the membrane environment or affect mast cell signalling events might be potentially used as treatments for mast cell-driven diseases. A promising candidate is the lipid raft modulator miltefosine (16). The obvious advantages of miltefosine are known side effects, which are relatively safe, dose-dependent and reversible (37). Although miltefosine was approved for the treatment of various diseases, the general mechanism of its action is still poorly understood (38).

It has been suggested that miltefosine affects organization of FcεRIs in the plasma membrane of human mast cells, which then leads to modulation of subsequent activation steps (8, 16). Our results demonstrate that mouse BMMCs are also sensitive to miltefosine. Degranulation was attenuated in miltefosine-treated cells in a dose-dependent manner after cell activation by FcεRI aggregation, thapsigargin, pervanadate or ionophore A23187. We have previously shown that activation of BMMCs leads to rapid cytoskeleton rearrangement and generation of microtubule protrusions (5). Here we demonstrate that in activated cells, miltefosine suppresses formation of these protrusions. Moreover, it also inhibits chemotaxis to Ag and cell motility, which points to a limited capability of miltefosine-treated cells to accumulate in the site of disease manifestation. These data indicate that miltefosine could modulate physiology of mast cells at different levels.

To get deeper insight into the effect(s) of miltefosine in mast cells, we evaluated early steps of cell activation after aggregation of FcεRIs by Ag. Miltefosine inhibited both the overall tyrosine phosphorylation level and the aggregation and tyrosine phosphorylation of FcεRIs. Diminished FcεRIs phosphorylation could be due to the changes in plasma membrane properties that inhibit formation of large FcεRIs aggregates. Protein tyrosine kinase Lyn can, therefore, only partially phosphorylate ITAMs (33) or tyrosine kinase Syk. This leads to lower phosphorylation of downstream signalling substrates. Hypothetically, the low level of phosphorylation could also be caused by the miltefosine's inhibitory effect on Lyn or other kinase, or stimulatory effect on protein tyrosine phosphatases. Our data thus support the previous suggestion that miltefosine attenuates FcεRI-mediated signalling events at the plasma membrane (8, 16).

The decreased level of aggregation and FcεRI phosphorylation in activated miltefosine-treated cells did not result in inhibition of the extracellular Ca^{2+} influx. This indicates that the low

level of FcεRIs phosphorylation observed after cell activation in the presence of miltefosine is sufficient to activate the subsequent signalling cascades. It was reported previously that the formation of large FcεRI aggregates is not necessary for triggering the signalling responses, and that Ag-activated mast cells propagate signals from small signalling domains formed around dimerized FcεRIs (39). Moreover, it is well established that cholesterol-dependent ordered lipids regulate the Ca^{2+} channel (Orai1), and polyunsaturated fatty acids with phosphoinositides regulate coupling of Orai1 to ER Ca^{2+} sensor (STIM1) in SOCE (40). Our results suggest that although miltefosine affects the membrane composition and aggregation of FcεRI receptors, this is not reflected in the Ca^{2+} influx level through SOCE.

Calcium mobilization has a critical impact on activation of many signal-transducing proteins, that are involved in the regulation of mast cell degranulation. We observed differential miltefosine inhibitory effects on degranulation in BMMCs activated by antigen, thapsigargin, pervanadate or ionophore A23187. This probably reflects the specificity and site(s) of action of the used activators. The finding that miltefosine does not inhibit Ca^{2+} influx but attenuates BMMC degranulation indicates that it might affect the cytosolic signalling pathway(s) after SOCE.

In BMMCs, miltefosine localized to the plasma membrane, cytosol and intracellular membranous structures including granules. Staining of intracellular structures with BODIPY-miltefosine was previously shown in *Leishmania donovani* at 7 μM concentration for 4 h (26). Here, we report that internalization of BODIPY-miltefosine in BMMCs is fast and even at 1 μM concentration it incorporates to intracellular membranous structures in the course of 15 min. It was showed that the granules can be visualized by negative contrast imaging in cells expressing cytosolic GFP (41). Alternatively, secretory granules in living mast cells can be labelled with tagged lectin, wheat germ agglutinin (WGA) (6). Time-lapse imaging of BMMCs pre-treated with Alexa Fluor 555-conjugated WGA showed attenuation of the granule movement during 15 min in the presence of 15 μM miltefosine (data not shown). Our results suggest that miltefosine easily enters cytosol, incorporates to cellular membranes, and might modulate movement of the secretory granules in BMMCs.

We have shown previously that activation of BMMCs with Ag or thapsigargin increases the number of growing microtubules in the cell periphery (5). In this study, more complex evaluation of microtubule plus end dynamics showed an increase in the population of fast, short-lived

microtubules. Moreover, increase in the growth speed after thapsigargin activation was Ca^{2+}-dependent (data not shown). It is known that microtubule dynamics is regulated by phosphorylation and dephosphorylation of +TIPs (35). Phosphorylated +TIPs disassociate from microtubules, whereas dephosphorylation promotes their binding and microtubule stabilization. Our data showed that pre-treatment of unstimulated cells with miltefosine also resulted in an increase in the population of fast, short-lived microtubules. Similarly to thapsigargin, the increase in the growth speed was Ca^{2+}-dependent. We hypothesize that in resting BMMCs, cytosolic miltefosine modulates the signalling pathway(s) regulating plus end microtubule dynamics. *In vitro* kinase assays revealed that EB1 interacting proteins were less phosphorylated in miltefosine- and thapsigargin-treated BMMCs. This suggests that while thapsigargin stimulates and miltefosine inhibits BMMC activation, they both affect microtubule dynamics in a similar way through modulating the phosphorylation state of +TIPs. Nevertheless, the corresponding signalling pathways to +TIPs in resting or activated BMMCs could be different and reflect intracellular Ca^{2+} concentration.

The affected signalling pathway to +TIPs could involve Ca^{2+}-dependent PKCs, as miltefosine was described to inhibit PKCs in different cell types (21) and our results from unpublished experiments revealed that it inhibits Ca^{2+}-dependent cPKCs in BMMCs. The cPKCs phosphorylate calcineurin-binding protein 1 (Cabin 1) associating with calcineurin (Ca^{2+}-dependent serine-threonine phosphatase). Phosphorylation of Cabin 1 leads to suppression of calcineurin signalling (42). One may speculate that inhibition of PKCs with miltefosine could activate calcineurin that dephosphorylates microtubule +TIPs. The involvement of calcineurin in dephosphorylation of EB3 and stabilization of growing microtubules was reported previously (43). Further studies are needed to decipher whether miltefosine modulates this or other Ca^{2+}-dependent pathways in BMMCs.

Based on the published data and findings in this report, we suggest that miltefosine might affect mast cell activation by different mechanisms. First, incorporation of miltefosine into the plasma membrane influences its properties. This results in morphological changes, inhibition of FcεRI aggregation by Ag, chemotaxis, and generation of microtubule protrusions in the course of specific (antigen) or unspecific (thapsigargin, pervanadate, ionophore A23187) activation. Second, as miltefosine did not inhibit Ca^{2+} response and rapidly entered into the cytosol, it is able to modulate the intracellular signalling pathways important for degranulation and microtubule

dynamics. Upon cell activation, Ca^{2+} and PKCs act to reverse the inhibitory mechanisms of granule fusion and activate proteins and cellular events to promote the granule fusion (44). Because miltefosine inhibits Ca^{2+}-dependent cPKCs, it could interfere with this pathway. Third, miltefosine attenuates movements of intracellular granules. It could therefore affect the function of microtubule motors that are important for transport of secretory granules in mast cells (6). Nevertheless, as miltefosine modulates different signalling pathways in various cell types (17), it might affect some other pathways in mast cells as well.

In conclusion, our data indicate that miltefosine modulates BMMCs both at the plasma membrane and in the cytosol. This leads to substantial morphological changes, inhibition of chemotaxis, degranulation and granule movement. It also affects microtubule plus end dynamics in a Ca^{2+}-dependent manner. Effective treatment of mast cell-derived diseases by miltefosine could be based on its action at multiple sites in the cells.

Acknowledgements

We thank I. Mlchová for the excellent technical assistance. We also thank Dr. A. U. Acuña (Instituto de Química-Física, CSIC, Madrid, Spain) for BODIPY-labelled miltefosine (MT-11c-6EtBDPY), Dr. Petr Dráber (IMG CAS, Prague) for rabbit polyclonal Ab to mouse IgE, Dr. M. Hibbs (Ludwig Institute for Cancer Research, Melbourne, Australia) for BMMC cells and Dr. Y. Mimori-Kiyosue (RIKEN Center for Life Science Technologies, Kobe, Japan) for EB1-GFP construct.

Funding

This work was supported in part by grant LD13015 for COST actions BM1007 from the Ministry of Education, Youth and Sports of the Czech Republic, grants 15-22194S, 16-25159S, 16-23702S, and 17-20915S from the Grant Agency of the Czech Republic and by Institutional Research Support (RVO 68378050).

Authors' contribution

ZH designed, performed and analysed microscopic experiments and prepared the manuscript, VS performed immunoprecipitation and kinase assays, TP performed intracellular Ca^{2+} measurements and PD planned the experiments, helped with result interpretation and revised the manuscript. All authors approved the final version of the manuscript.

Conflict of interest

The authors declare that they have no conflicts of interest.

References

1. Galli SJ, Tsai M, Piliponsky AM. The development of allergic inflammation. *Nature* 2008;**454**:445-454.
2. Metcalfe DD, Baram D, Mekori YA. Mast cells. *Physiol Rev* 1997;**77**:1033-1079.
3. Nishida K, Yamasaki S, Ito Y, Kabu K, Hattori K, Tezuka T, et al. FcεRI-mediated mast cell degranulation requires calcium-independent microtubule-dependent translocation of granules to the plasma membrane. *J Cell Biol* 2005;**170**:115-126.
4. Sulimenko V, Dráberová E, Sulimenko T, Macurek L, Richterová V, Dráber P, et al. Regulation of microtubule formation in activated mast cells by complexes of γ-tubulin with Fyn and Syk kinases. *J Immunol* 2006;**176**:7243-7253.
5. Hájková Z, Bugajev V, Dráberová E, Vinopal S, Dráberová L, Janáček J, et al. STIM1-directed reorganization of microtubules in activated mast cells. *J Immunol* 2011;**186**:913-923.
6. Munoz I, Danelli L, Claver J, Goudin N, Kurowska M, Madera-Salcedo IK, et al. Kinesin-1 controls mast cell degranulation and anaphylaxis through PI3K-dependent recruitment to the granular Slp3/Rab27b complex. *J Cell Biol* 2016;**215**:203-216.
7. Pressman BC. Biological applications of ionophores. *Annu Rev Biochem* 1976;**45**:501-530.
8. Weller K, Artuc M, Jennings G, Friedrichson T, Guhl S, dos Santos RV, et al. Miltefosine inhibits human mast cell activation and mediator release both in vitro and in vivo. *J Invest Dermatol* 2009;**129**:496-498.
9. Hartmann K, Siebenhaar F, Belloni B, Brockow K, Eben R, Hartmann B, et al. Effects of topical treatment with the raft modulator miltefosine and clobetasol in cutaneous mastocytosis: a randomized, double-blind, placebo-controlled trial. *Br J Dermatol* 2010;**162**:185-190.
10. Magerl M, Rother M, Bieber T, Biedermann T, Brasch J, Dominicus R, et al. Randomized, double-blind, placebo-controlled study of safety and efficacy of miltefosine in antihistamine-resistant chronic spontaneous urticaria. *J Eur Acad Dermatol Venereol* 2013;**27**:e363-369.
11. Dolle S, Hoser D, Rasche C, Loddenkemper C, Maurer M, Zuberbier T, et al. Long-term reduction in local inflammation by a lipid raft molecule in atopic dermatitis. *Allergy* 2010;**65**:1158-1165.
12. Monge-Maillo B, Lopez-Velez R. Miltefosine for visceral and cutaneous leishmaniasis: drug characteristics and evidence-based treatment recommendations. *Clin Infect Dis* 2015;**60**:1398-1404.
13. Schuster FL, Guglielmo BJ, Visvesvara GS. In-vitro activity of miltefosine and voriconazole on clinical isolates of free-living amebas: Balamuthia mandrillaris, Acanthamoeba spp., and Naegleria fowleri. *J Eukaryot Microbiol* 2006;**53**:121-126.
14. Barratt G, Saint-Pierre-Chazalet M, Loiseau PM. Cellular transport and lipid interactions of miltefosine. *Curr Drug Metab* 2009;**10**:247-255.
15. van der Luit AH, Vink SR, Klarenbeek JB, Perrissoud D, Solary E, Verheij M, et al. A new class of anticancer alkylphospholipids uses lipid rafts as membrane gateways to induce apoptosis in lymphoma cells. *Mol Cancer Ther* 2007;**6**:2337-2345.
16. Maurer M, Magerl M, Metz M, Weller K, Siebenhaar F. Miltefosine: a novel treatment option for mast cell-mediated diseases. *J Dermatolog Treat* 2013;**24**:244-249.

17. van Blitterswijk WJ, Verheij M. Anticancer alkylphospholipids: mechanisms of action, cellular sensitivity and resistance, and clinical prospects. *Curr Pharm Des* 2008;**14**:2061-2074.
18. Ruiter GA, Zerp SF, Bartelink H, van Blitterswijk WJ, Verheij M. Anti-cancer alkyl-lysophospholipids inhibit the phosphatidylinositol 3-kinase-Akt/PKB survival pathway. *Anticancer Drugs* 2003;**14**:167-173.
19. Ward PD, Ouyang H, Thakker DR. Role of phospholipase C-beta in the modulation of epithelial tight junction permeability. *J Pharmacol Exp Ther* 2003;**304**:689-698.
20. Lucas L, Hernandez-Alcoceba R, Penalva V, Lacal JC. Modulation of phospholipase D by hexadecylphosphorylcholine: a putative novel mechanism for its antitumoral activity. *Oncogene* 2001;**20**:1110-1117.
21. Überall F, Oberhuber H, Maly K, Zaknun J, Demuth L, Grunicke HH. Hexadecylphosphocholine inhibits inositol phosphate formation and protein kinase C activity. *Cancer Res* 1991;**51**:807-812.
22. Kovářová M, Tolar P, Arudchandran R, Dráberová L, Rivera J, Dráber P. Structure-function analysis of Lyn kinase association with lipid rafts and initiation of early signaling events after Fcε receptor I aggregation. *Mol Cell Biol* 2001;**21**:8318-8328.
23. Nováková M, Dráberová E, Schürmann W, Czihak G, Viklický V, Dráber P. γ-Tubulin redistribution in taxol-treated mitotic cells probed by monoclonal antibodies. *Cell Motil Cytoskeleton* 1996;**33**:38-51.
24. Hibbs ML, Tarlinton DM, Armes J, Grail D, Hodgson G, Maglitto R, et al. Multiple defects in the immune system of Lyn-deficient mice, culminating in autoimmune disease. *Cell* 1995;**83**:301-311.
25. Heneberg P, Lebduska P, Dráberová L, Korb J, Dráber P. Topography of plasma membrane microdomains and its consequences for mast cell signaling. *Eur J Immunol* 2006;**36**:2795-2806.
26. Hornillos V, Carrillo E, Rivas L, Amat-Guerri F, Acuña AU. Synthesis of BODIPY-labeled alkylphosphocholines with leishmanicidal activity, as fluorescent analogues of miltefosine. *Bioorg Med Chem Lett* 2008;**18**:6336-6339.
27. Mimori-Kiyosue Y, Shiina N, Tsukita S. The dynamic behavior of the APC-binding protein EB1 on the distal ends of microtubules. *Curr Biol* 2000;**10**:865-868.
28. Sulimenko V, Sulimenko T, Poznanovic S, Nechiporuk-Zloy V, Böhm KJ, Macurek L, et al. Association of brain γ-tubulins with αβ-tubulin dimers. *Biochem J* 2002;**365**:889-895.
29. Bambousková M, Hájková Z, Dráber P, Dráber P. Microscopy assays for evaluation of mast cell migration and chemotaxis. *Methods Mol Biol* 2014;**1192**:161-176.
30. Dráberová E, Dráber P. A microtubule-interacting protein involved in coalignment of vimentin intermediate filaments with microtubules. *J Cell Sci* 1993;**106**:1263-1273.
31. Applegate KT, Besson S, Matov A, Bagonis MH, Jaqaman K, Danuser G. plusTipTracker: Quantitative image analysis software for the measurement of microtubule dynamics. *J Struct Biol* 2011;**176**:168-184.
32. Matov A, Applegate K, Kumar P, Thoma C, Krek W, Danuser G, et al. Analysis of microtubule dynamic instability using a plus-end growth marker. *Nat Methods* 2010;**7**:761-768.
33. Kinet JP. The high-affinity IgE receptor (FcεRI): from physiology to pathology. *Annu Rev Immunol* 1999;**17**:931-972.

34. Dráber P, Sulimenko V, Dráberová E. Cytoskeleton in mast cell signaling. *Front Immunol* 2012;**3**:130.
35. Akhmanova A, Steinmetz MO. Control of microtubule organization and dynamics: two ends in the limelight. *Nat Rev Mol Cell Biol* 2015;**16**:711-726.
36. Bearce EA, Erdogan B, Lowery LA. TIPsy tour guides: how microtubule plus-end tracking proteins (+TIPs) facilitate axon guidance. *Front Cell Neurosci* 2015;**9**:241.
37. Verhaar AP, Wildenberg ME, Peppelenbosch MP, Hommes DW, van den Brink GR. Repurposing miltefosine for the treatment of immune-mediated disease? *J Pharmacol Exp Ther* 2014;**350**:189-195.
38. Pachioni Jde A, Magalhães JG, Lima EJ, Bueno Lde M, Barbosa JF, de Sá MM, et al. Alkylphospholipids - a promising class of chemotherapeutic agents with a broad pharmacological spectrum. *J Pharm Pharm Sci* 2013;**16**:742-759.
39. Dráberová L, Lebduška P, Hálová I, Tolar P, Štokrová J, Tolarová H, et al. Signaling assemblies formed in mast cells activated via Fcε receptor I dimers. *Eur J Immunol* 2004;**34**:2209-2219.
40. Holowka D, Baird B. Roles for lipid heterogeneity in immunoreceptor signaling. *Biochim Biophys Acta* 2016;**1861**:830-836.
41. Tanaka S, Takakuwa Y. A method for detailed analysis of the structure of mast cell secretory granules by negative contrast imaging. *Sci Rep* 2016;**6**:23369.
42. Szíjgyártó Z, Szucs K, Kovács I, Zákány R, Sipka S, Gergely P. The role of protein kinase C isoenzymes in the regulation of calcineurin activity in human peripheral blood mononuclear cells. *Int J Mol Med* 2007;**20**:359-364.
43. Komarova YA, Huang F, Geyer M, Daneshjou N, Garcia A, Idalino L, et al. VE-cadherin signaling induces EB3 phosphorylation to suppress microtubule growth and assemble adherens junctions. *Mol Cell* 2012;**48**:914-925.
44. Blank U, Rivera J. The ins and outs of IgE-dependent mast-cell exocytosis. *Trends Immunol* 2004;**25**:266-273.

Figure legends

Figure 1 Miltefosine inhibits degranulation in activated BMMCs. BMMCs pre-incubated with different concentrations of miltefosine (5-25 μM) were activated and degranulation was measured by β-hexosaminidase release in the presence or absence of miltefosine. ***(A, B)*** IgE-sensitized cells were activated by FcεRI aggregation using 25 ng/ml ***(A)*** or 1000 ng/ml ***(B)*** antigen. ***(C)*** Cells activated with thapsigargin. ***(D)*** Cells activated with pervanadate. Values represent means ± SD (n=3); **p* < 0.05; ***p* < 0.01; ****p* < 0.001.

Figure 2 Microtubule organization in activated BMMCs and Ag-induced chemotaxis are affected by miltefosine. ***(A)*** Microtubule organization. BMMCs incubated in the absence (*a, c, e*) or presence (*b*, *d, f*) of miltefosine were activated by FcεRI aggregation (*a*-*b*; + Antigen), thapsigargin (*c*-*d*) or calcium ionophore A23187 (*e*-*f*). Cells were fixed and stained for β-tubulin. Scale bars 10 μm (*a*-*b*), (*c*-*d*), *(e*-*f*). ***(B)*** Quantitative analysis of the frequency of microtubule protrusions. BMMCs incubated with various concentrations of miltefosine (5-15 μM) and BMMC controls were activated by FcεRI aggregation (+Antigen), thapsigargin or calcium ionophore. Values indicate means ± SD (n=3); ***p* < 0.01; ****p* < 0.001. ***(C)*** Chemotaxis assay. Migration tracks in control cells and cells treated with miltefosine. Tracks from a representative experiment were aligned with their starting points at the coordinate position [0, 0]. Black tracks indicate individual cells with net migration toward the left chamber that contained Ag (100 ng/ml), red tracks indicate cells migrating in the opposite direction. Yellow crosses represent the average of endpoints. ***(D)*** Cell migration. Migration velocities and accumulated distances of miltefosine-treated cells relative to the control cells. Data are means ± SD (n=5); **p* < 0.05.

Figure 3 Miltefosine affects tyrosine phosphorylation and aggregation of FcεRI receptors in activated BMMCs. ***(A)*** Comparison of protein tyrosine phosphorylation level (P-Tyr) in control cells and cells activated by FcεRI aggregation (+Ag) in the absence (lanes 1 and 3) or presence (lanes 2 and 4) of miltefosine. γ-Tubulin served as a loading control (γ-Tb). ***(B)*** Comparison of FcεRI receptor phosphorylation (P-Tyr) in the absence (lanes 1, 3, 5-6, 8 and 10) or presence (lanes 2, 4, 7 and 9) of miltefosine. Cells sensitized with mouse IgE to Ag were incubated with or

without miltefosine, activated by Ag, and extracts were precipitated with anti-IgE Ab immobilized on protein A beads. In the control, protein A without Ab was incubated with the cell extract (lane 10, Con.). Note the difference in signal intensities in the positions of co-precipitated FcεRI receptors when cells were incubated without (lane 8) or with (lane 9) miltefosine. (***A-B***) Bars on the left indicate positions of molecular weight markers in kDa. (***C***) Comparison of FcεRI aggregation in the absence or presence of miltefosine. Cells sensitized with mouse IgE to Ag were incubated without (*a, c*) or with (*b, d*) miltefosine and activated by crosslinking of bound IgE with Ag (*a-b;* Aggregation by Ag) or with anti-mouse Ig Ab conjugated with DY549 (*c-d;* Aggregation by anti-Ig Ab). Cells were fixed with formaldehyde, and in the case of Ag-activated cells (*a-b*), stained with anti-mouse Ab conjugated with DY549. Images *(a-b*) and (*c-d*) were collected and processed under identical conditions. Scale bar, 10 μm (*a-b*); 5 μm (*c-d*).

Figure 4 Miltefosine does not inhibit Ca^{2+} influx in activated BMMCs and localizes to cellular membranes and cytosol. ***(A)*** Effect of miltefosine on intracellular Ca^{2+} level during cell activation. Sensitized cells were loaded with Fura-2-AM, pre-treated with or without (Control) miltefosine and activated by Ag, thapsigargin or ionophore A23187. Arrows indicate addition of Ag, thapsigargin or ionophore A23187. Data represents means ± SE (n=2 for Ag; n=3 for thapsigargin or ionophore A23187) of independent experiments performed in duplicates. ***(B)*** BODIPY-miltefosine localizes to the cellular membranes and cytosol. Live-cell imaging of cells incubated with BODIPY-miltefosine. Scale bar, 10 μm. ***(C)*** BODIPY-miltefosine inhibits microtubule reorganization in activated cells. Controls or cells treated with BODIPY-miltefosine were activated by thapsigargin, fixed and stained for α-tubulin (*a, c*) or BODIPY (*b, d*). Images (*b, d*) were collected and processed under identical conditions. Scale bar, 5 μm (*a-d*).

Figure 5 Microtubule dynamics is affected by miltefosine. ***(A)*** Cell activation and miltefosine increase microtubule growth speed. BMMC_EB1-GFP were activated by thapsigargin, treated with miltefosine or treated with miltefosine in medium without Ca^{2+}. Data are means ± SD (n=3); $*p < 0.05$; $**p < 0.01$; $***p < 0.001$. ***(B)*** Cell activation and miltefosine affect microtubule subpopulations classified by growth speed and growth lifetime. Microtubule subpopulations were divided based on whether they were above or below the median of growth speed (18.4 μm/min) and median of growth lifetime (4.3 sec) of EB1 tracks from control cells. The four

subpopulations of microtubules are coded by colour: slow and short-lived (red), fast and short-lived (yellow), slow and long-lived (green) and fast and long-lived (blue). Numbers of evaluated cells (n) are shown on the right. ***(C)*** Representative time-lapse imaging of resting (*a, b;* Control) and miltefosine treated (*d, e;* + Miltefosine) BMMC_EB1-GFP. Maximum intensity projections of 30 consecutive frames (*a, d*) and coloured subpopulations of tracks were overlaid in images (*b, e*). Microtubule subpopulations are coloured as described in 5*B*, and the relative proportions of the subpopulations are shown on the right (*c, f*). Scale bar, 5 μm.

Figure 6 The kinase activity in EB1 immunocomplexes is inhibited by miltefosine. BMMC lysates were precipitated with anti-EB1 Ab bound to protein A carrier. Immunocomplexes were subjected to *in vitro* kinase assay, electrophoretically separated, and detected by autoradiography (^{32}P). The presence of EB1 in immunocomplexes was confirmed by immunoblotting with anti-EB1 Ab (EB1). Precipitation from resting cells (lane 1), cells activated with thapsigargin (lane 2) and cells pre-treated with miltefosine (lane 3). Controls contained protein A with Ab (lane 4) and protein A without Ab incubated with the cell extract (lane 5). Bars on the left indicate positions of molecular weight markers in kDa.

Figures

Figure 1

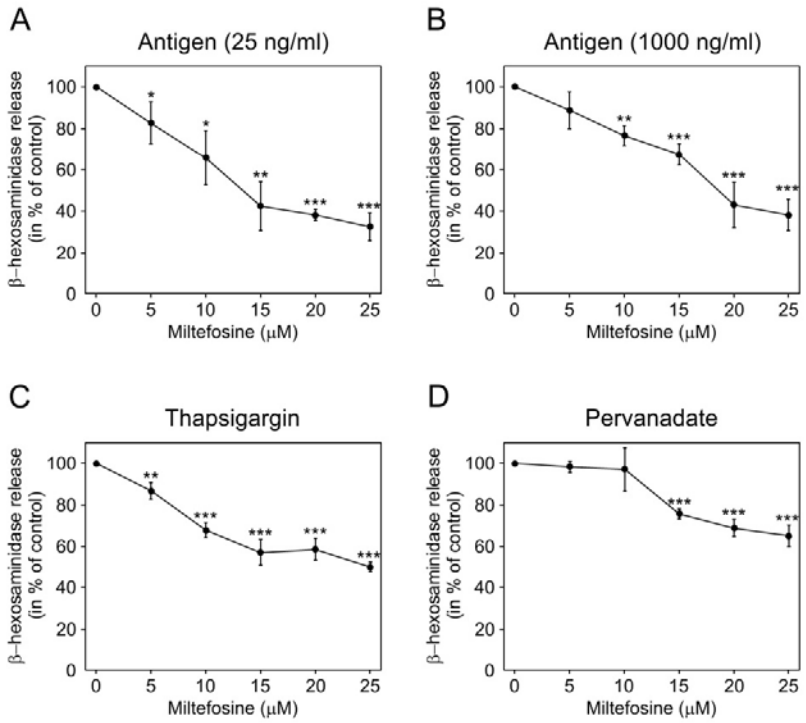

Figure 2

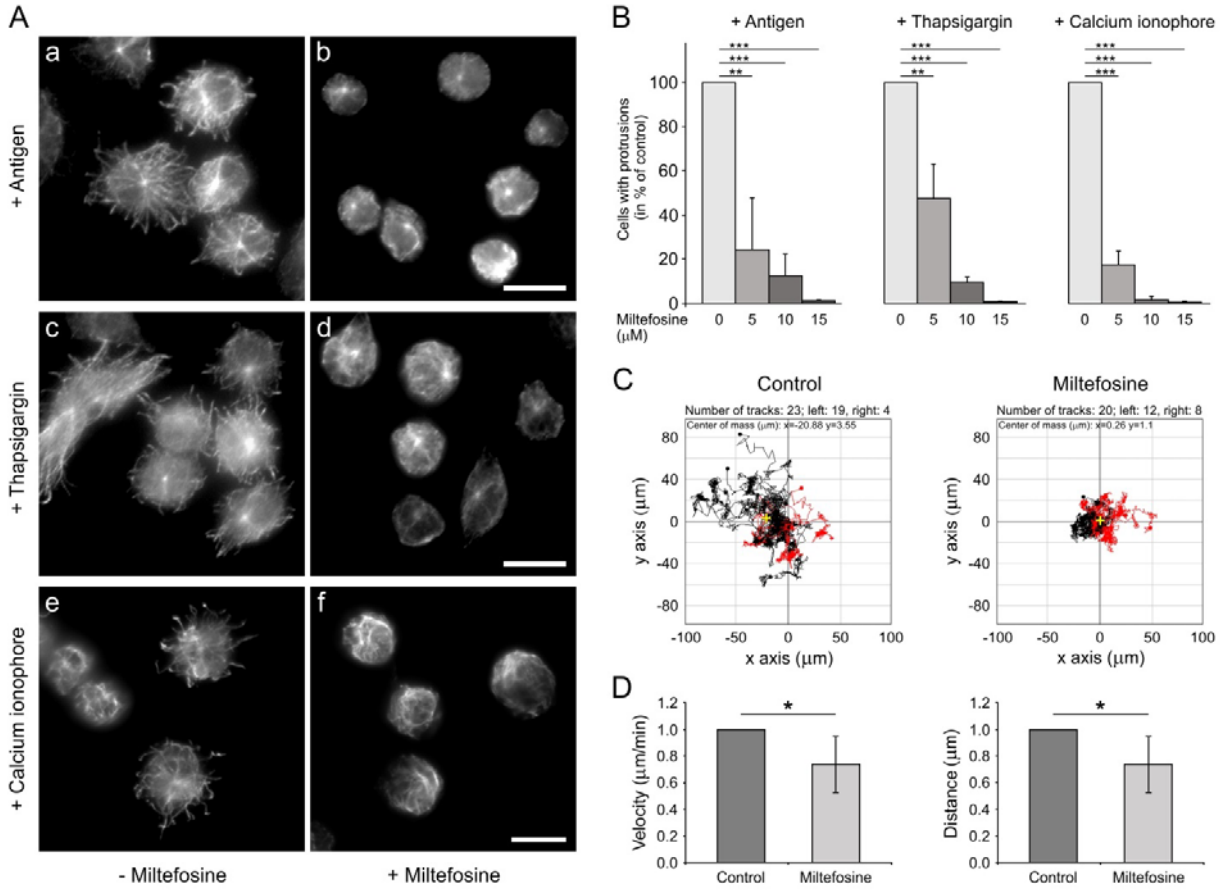
A
a
b
c
d
e
f
+ Antigen
+ Thapsigargin
+ Calcium ionophore
- Miltefosine
+ Miltefosine
B
+ Antigen
+ Thapsigargin
+ Calcium ionophore
Cells with protrusions (in % of control)
Miltefosine (µM)
0 5 10 15
C
Control
Miltefosine
Number of tracks: 23; left: 19, right: 4
Number of tracks: 20; left: 12, right: 8
y axis (µm)
x axis (µm)
D
Velocity (µm/min)
Distance (µm)
Control
Miltefosine

Figure 3

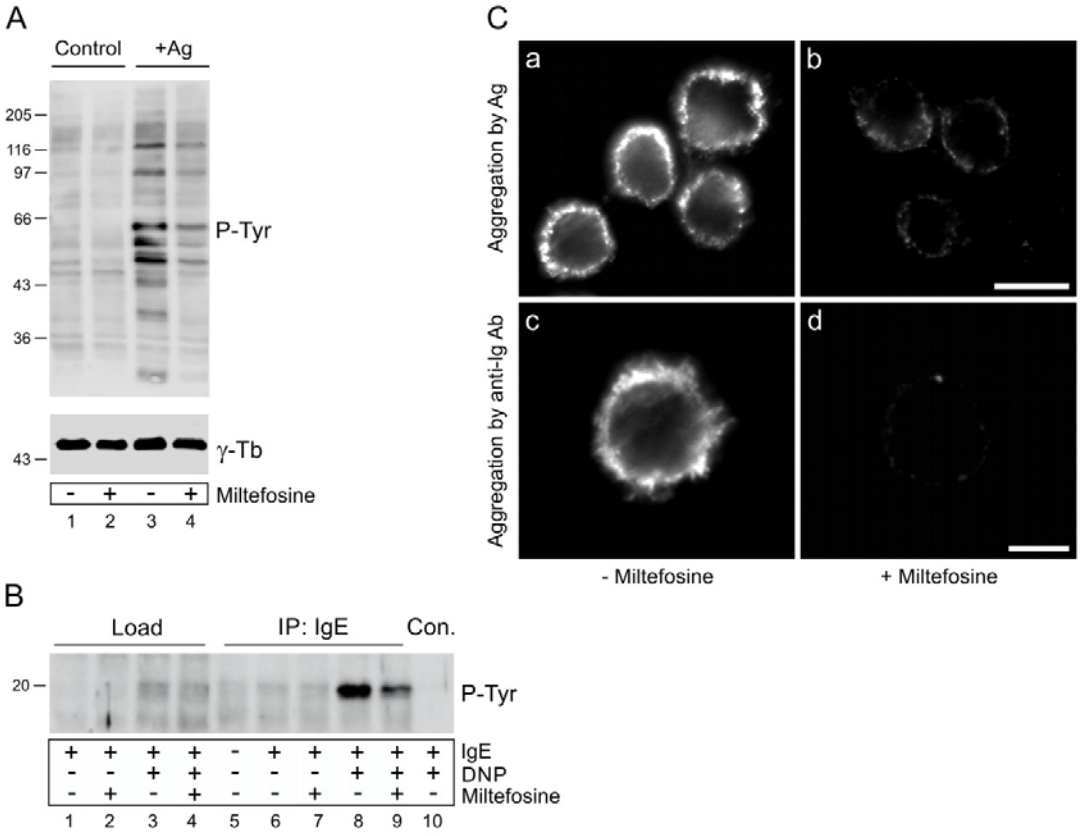
A
Control
+Ag
205
116
97
66
43
36
P-Tyr
43
γ-Tb
- + - +
Miltefosine
1 2 3 4
B
Load
IP: IgE
Con.
20
P-Tyr
+ + + + - + + + + +
- - + + - - - + + +
- + - + - - + - + -
IgE
DNP
Miltefosine
1 2 3 4 5 6 7 8 9 10
C
Aggregation by Ag
Aggregation by anti-Ig Ab
a
b
c
d
- Miltefosine
+ Miltefosine

Figure 4

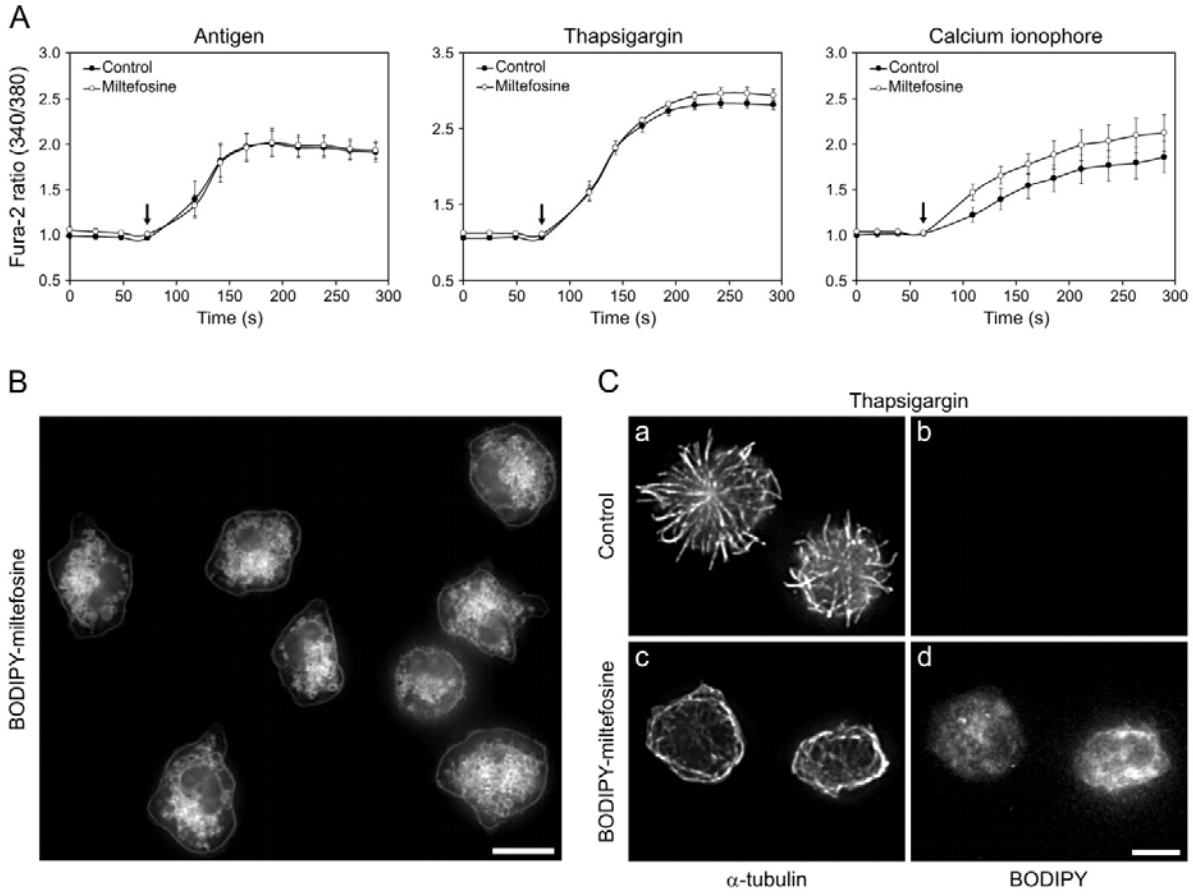
A
Antigen
Thapsigargin
Calcium ionophore
Control
Miltefosine
Fura-2 ratio (340/380)
Time (s)
B
BODIPY-miltefosine
C
Thapsigargin
a
b
c
d
Control
BODIPY-miltefosine
α-tubulin
BODIPY

Figure 5

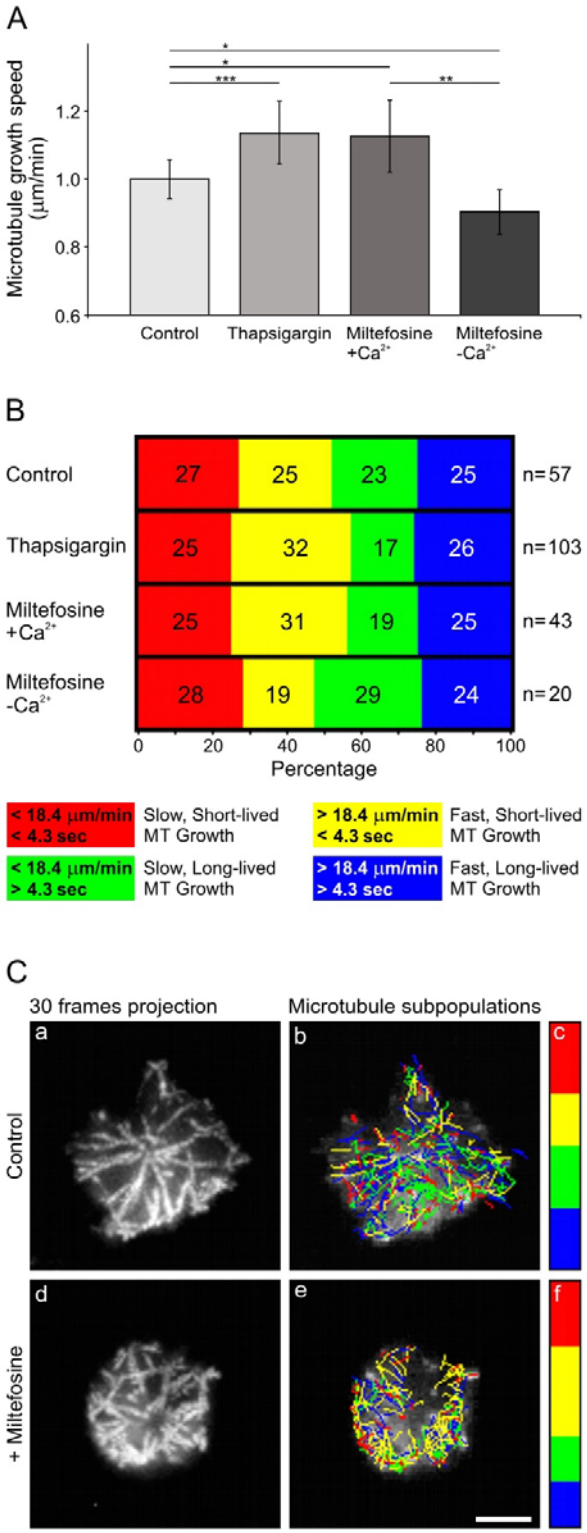
A
Microtubule growth speed (µm/min)
1.2
1.0
0.8
0.6
*
*
***
**
Control
Thapsigargin
Miltefosine +Ca2+
Miltefosine -Ca2+
B
Control
Thapsigargin
Miltefosine +Ca2+
Miltefosine -Ca2+
27
25
23
25
n=57
25
32
17
26
n=103
25
31
19
25
n=43
28
19
29
24
n=20
0
20
40
60
80
100
Percentage
< 18.4 µm/min < 4.3 sec Slow, Short-lived MT Growth
> 18.4 µm/min < 4.3 sec Fast, Short-lived MT Growth
< 18.4 µm/min > 4.3 sec Slow, Long-lived MT Growth
> 18.4 µm/min > 4.3 sec Fast, Long-lived MT Growth
C
30 frames projection
Microtubule subpopulations
a
b
c
Control
d
e
f
+ Miltefosine

Figure 6

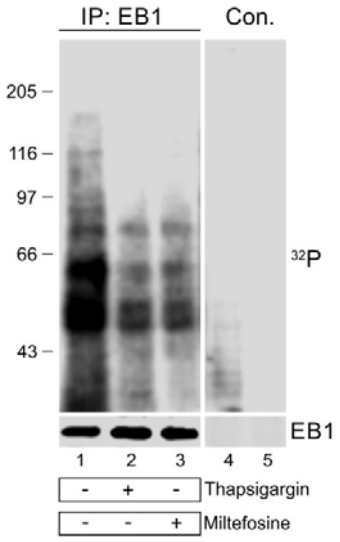
IP: EB1
Con.
205
116
97
66
43
32P
EB1
1 2 3 4 5
- + - Thapsigargin
- - + Miltefosine

VII. SUPPLEMENTARY DATA

VII.1

Hájková Z.*, Bugajev V.*, Dráberová E., Vinopal S., Dráberová L., Janáček J., Dráber Pe., Dráber Pa. (2011). STIM1-directed reorganization of microtubules in activated mast cells. The Journal of Immunology *186(2)*, 913-23.

STIM1-Directed Reorganization of Microtubules in Activated Mast Cells

Zuzana Hájková,*[,1] Viktor Bugajev,[†,1] Eduarda Dráberová,* Stanislav Vinopal,* Lubica Dráberová,[†] Jiří Janáček,[‡] Petr Dráber,[†] and Pavel Dráber*

Activation of mast cells by aggregation of the high-affinity IgE receptors (FcεRI) initiates signaling events leading to the release of inflammatory and allergic mediators stored in cytoplasmic granules. A key role in this process play changes in concentrations of intracellular Ca^{2+} controlled by store-operated Ca^{2+} entry (SOCE). Although microtubules are also involved in the process leading to degranulation, the molecular mechanisms that control microtubule rearrangement during activation are largely unknown. In this study, we report that activation of bone marrow-derived mast cells (BMMCs) induced by FcεRI aggregation or treatment with pervanadate or thapsigargin results in generation of protrusions containing microtubules (microtubule protrusions). Formation of these protrusions depended on the influx of extracellular Ca^{2+}. Changes in cytosolic Ca^{2+}concentration also affected microtubule plus-end dynamics detected by microtubule plus-end tracking protein EB1. Experiments with knockdown or reexpression of STIM1, the key regulator of SOCE, confirmed the important role of STIM1 in the formation of microtubule protrusions. Although STIM1 in activated cells formed puncta associated with microtubules in protrusions, relocation of STIM1 to a close proximity of cell membrane was independent of growing microtubules. In accordance with the inhibition of Ag-induced Ca^{2+} response and decreased formation of microtubule protrusions in BMMCs with reduced STIM1, the cells also exhibited impaired chemotactic response to Ag. We propose that rearrangement of microtubules in activated mast cells depends on STIM1-induced SOCE, and that Ca^{2+} plays an important role in the formation of microtubule protrusions in BMMCs. ***The Journal of Immunology*****, 2011, 186: 913–923.**

Mast cells play a pivotal role in innate immunity, allergy, and inflammation; they express plasma membrane-associated FcεRIs, the aggregation of which by multivalent Ag–IgE complexes triggers mast cell activation resulting in the degranulation and release of inflammatory mediators such as histamine, proteases, lipid mediators, and cytokines. The first defined step in FcεRI signaling is tyrosine phosphorylation of the FcεRI β and γ subunits by Src family kinase Lyn. This step is followed by enhanced activity of Syk kinase and phosphorylation of transmembrane adaptor linker for activation of T cells. Phosphorylated linker for activation of T cells is an anchor site for phospholipase Cγ. After membrane anchoring and activation, phospholipase Cγ produces inositol 1,4,5,-triphosphate that binds to its receptors in the endoplasmic reticulum (ER). This results in Ca^{2+} efflux from the ER (1). Subsequently, depletion of Ca^{2+} from ER lumen induces Ca^{2+} influx across the plasma membrane through store-operated Ca^{2+} channels (SOCs). The influx leads to enhancement of free cytoplasmic Ca^{2+} concentration, a step that is substantial in further signaling events. The store-operated Ca^{2+} entry (SOCE) is also important for the replenishment of intracellular stores by means of sarcoendoplasmatic reticulum Ca^{2+}-ATPase (SERCA) pumps located in the ER membrane (2, 3).

The stromal interacting molecule 1 (STIM1) is a pivotal component of the SOCE pathway (4, 5). It represents the Ca^{2+} sensor responsible for communicating the depleted state of intracellular Ca^{2+} compartments to SOCs. In quiescent cells with ER filled with Ca^{2+}, STIM1 is distributed homogenously throughout the ER (6), but relocates upon release of Ca^{2+} from ER stores to distinct puncta on the ER in close proximity to the plasma membrane (5). Aggregated STIM1 activates members of the Orai family of SOCs, resulting in the opening of the plasma membrane Ca^{2+} channels and Ca^{2+} influx into the cell (7); in this way STIM1 serves as a major regulator of SOCE.

STIM1 is a microtubule-tracking protein (8, 9) and interacts with the end-binding protein 1 (EB1) that associates with the tips of growing microtubules (10, 11). Although microtubules are necessary for positioning of membrane-enclosed organelles in-

*Department of Biology of Cytoskeleton, Institute of Molecular Genetics, Academy of Sciences of the Czech Republic, 142 20 Prague, Czech Republic; [†]Department of Signal Transduction, Institute of Molecular Genetics, Academy of Sciences of the Czech Republic, 142 20 Prague, Czech Republic; and [‡]Department of Biomathematics, Institute of Physiology, Academy of Sciences of the Czech Republic, 142 20 Prague, Czech Republic

[1]Z.H. and V.B. contributed equally to this work

Received for publication June 25, 2010. Accepted for publication November 13, 2010.

This work was supported in part by Grants 204/09/H084, 204/09/1777, 301/09/1826, and P302/10/1759 from the Grant Agency of the Czech Republic, Grants LC545, LC06063, and 1M6837805001 from the Ministry of Education, Youth and Sports of the Czech Republic, Grants KAN200520701 and M200520901 from the Grant Agency of the Czech Academy of Sciences, Grant 11109 from the Grant Agency of Charles University, and by the Institutional Research Supports (AVOZ 50520514 and 50110509). S.V. was supported in part by the Department of Cell Biology, Faculty of Science, Charles University, Prague, Czech Republic.

Address correspondence and reprint requests to Dr. Pavel Dráber or Dr. Petr Dráber, Department of Biology of Cytoskeleton, Institute of Molecular Genetics, AS CR v.v.i., Vídeňská 1083, 142 20 Prague, Czech Republic (Pavel Dráber), or Department of Signal Transduction, Institute of Molecular Genetics, AS CR v.v.i., Vídeňská 1083, 142 20 Prague, Czech Republic (Petr Dráber). E-mail addresses: paveldra@img.cas.cz (Pavel Dráber) and draberpe@img.cas.cz (Petr Dráber)

The online version of this article contains supplemental material.

Abbreviations used in this article: BMMC, bone marrow-derived mast cell; BMMCL, BMMC line; BSS, buffered saline solution; $[Ca^{2+}]_i$, concentration of free intracellular calcium; EB1, end-binding protein 1; ER, endoplasmic reticulum; KD, knockdown; SCF, stem cell factor; SERCA, sarcoendoplasmatic reticulum Ca^{2+}-ATPase; shRNA, short hairpin RNA; SOC, store-operated Ca^{2+} channels; SOCE, store-operated Ca^{2+} entry; STIM1, stromal interacting molecule 1; Tg, thapsigargin; TIRF, total internal reflection fluorescence; TIRFM, total internal reflection fluorescence microscopy; YFP, yellow fluorescent protein.

cluding ER (12), the role of microtubules in regulating SOCE is not fully understood. Whereas inhibition of microtubule dynamics by taxol, a microtubule stabilizer, or by knockdown (KD) of EB1 had no significant effect on SOCE (11), Ca^{2+} influx in different cell types was inhibited by microtubule depolymerizing drug nocodazole (13, 14). It has been suggested that microtubules play a facilitative role in SOCE signaling pathway by optimizing the localization of STIM1 (15).

Microtubules are involved in mast cell degranulation, because the movement of secretory granules depends on intact microtubules (16, 17). This finding is supported by demonstrations that agents inhibiting tubulin polymerization also suppress degranulation (18–20). Importantly, FcεRI aggregation triggers reorganization of microtubules and their concentration in cell periphery (17, 21). It has also been reported that translocation of granules along microtubules to plasma membranes occurred independently of Ca^{2+}, whereas the release of mediators and granule-plasma membrane fusion were dependent on Ca^{2+} (17). Although these data confirm that a microtubule network is required for mast cell degranulation, our understanding of the mechanisms responsible for microtubule formation in bone marrow-derived mast cells (BMMCs) during activation events is still limited.

In this study, we investigated the interplay between Ca^{2+} signaling and changes in microtubule distribution in the course of BMMC activation. Our results indicate that microtubules in activated cells are in protrusions that depend on STIM1 activity and Ca^{2+} influx. Whereas microtubules are not necessary for the relocation of STIM1 to puncta in close proximity to the plasma membrane in activated cells, changes in the concentration of cytoplasmic Ca^2 affect microtubule plus-end dynamics and result in dramatic modifications in cell physiology documented by chemotactic response. The results support the concept of a tight crosstalk between microtubular network and Ca^{2+} signaling machinery in the course of mast cell activation.

Materials and Methods

Reagents

Fibronectin, nocodazole, thapsigargin, probenecid, DNP-albumin, and DNP-lysine were acquired from Sigma-Aldrich (St. Louis, MO). Src-family selective tyrosine kinase inhibitor PP2 and the negative control, PP3, were obtained from Calbiochem (Darmstadt, Germany). Fluo 3-AM, Fura Red-AM, 4-methylumbelliferyl β-D-glucuronide, and Lipofectamine 2000 were purchased from Invitrogen (Carlsbad, CA), and puromycin was acquired from InvivoGen (San Diego, CA). IL-3 and stem cell factor (SCF) were from PeproTech (Rocky Hill, NJ). Restriction enzymes were bought from New England Biolabs (Ipswich, MA). SuperSignal WestPico Chemiluminescent reagents were bought from Pierce (Rockford, IL).

Abs

Mouse mAb PY-20 (IgG_{2b}) labeled with HRP and anti-STIM1(GOK) mAb (IgG_{2a}) were acquired from BD Biosciences (San Jose, CA). Rabbit Ab to α-tubulin was acquired from GeneTex (Irvine, CA). Rabbit Ab to actin, mAb TUB 2.1 (IgG_1) to β-tubulin labeled with indocarbocyanate (Cy3) and mAb SPE-7 (IgE) specific for DNP were acquired from Sigma-Aldrich. Anti-mouse and anti-rabbit Abs conjugated with HRP were purchased from Promega Biotec (Madison, WI), Alexa Fluor 488-conjugated anti-rabbit IgG Ab was acquired from Invitrogen (Carlsbad, CA), and FITC-conjugated anti-mouse IgG cross-reacting with mouse IgE were acquired from Jackson ImmunoResearch Laboratories (West Grove, PA).

To prepare mouse mAb specific for STIM1, 29-aa oligopeptide DNGSIGEETDSSPGRKKFPLKIFKKPLKK corresponding to the mouse STIM1 sequence 657-685 from the C-terminal end of the molecule (22) was synthesized by Clonestar Peptide Service (Brno, Czech Republic). A cysteine had been added to the N terminus of the peptide to allow oriented covalent coupling to the carrier proteins, maleimide-activated keyhole limpet hemocyanin, or BSA (Imject Activated Immunogen Conjugation Kit, Pierce, Rockford, IL), according to the manufacturer's directions. BALB/c mice were immunized with the peptide-keyhole limpet hemocyanin conjugate, and sera were monitored for Ab activity by ELISA on peptide-BSA conjugate as described (23). Fusion of splenocytes with mouse myeloma cells Sp2/0, screening by ELISA, cloning and production of ascitic fluids in BALB/c mice have been described previously (24). The subclasses of mAbs were identified by ISO1 isotyping kit (Sigma-Aldrich). The selected hybridoma cell line ST-01 produced Ab of the IgG_1 class.

Cell cultures and transfection

Bone marrow cells were isolated from the femurs and tibias of 6–8-wk-old BALB/c mice. All mice were maintained and used in accordance with the Institute of Molecular Genetics guidelines. The cells were differentiated in suspension cultures in freshly prepared culture medium (IMDM supplemented with antibiotics [100 U/ml penicillin, 100 μg/ml streptomycin] 10% FCS, 35 μM 2-ME, IL-3 [36 ng/ml] and SCF [36 ng/ml]). Cells were grown at 37˚C in 10% CO_2 in air and passaged every 2–3 d. After 6–8 wk, ~99% of cells were identified as mast cells, expressing FcεRI and c-Kit as detected by flow cytometry. BMMCs isolated from at least three mice were used for each experiment.

Mouse BMMC line (BMMCL) was by M. Hibbs (Ludwig Institute for Cancer Research, Melbourne, Australia). In this study, the cells are denoted as BMMCL and were cultured in freshly prepared culture medium (RPMI 1640 supplemented with 20 mM HEPES, pH 7.5, 100 U/ml penicillin, 100 μg/ml streptomycin, 100 μM MEM nonessential amino acids, 1 mM sodium pyruvate, 10% FCS, and 10% WEHI-3 cell supernatant as a source of IL-3). Cells were grown at 37˚C in 5% CO_2 in air and passaged every 2 d.

HEK 293FT packaging cells (Invitrogen) were grown at 37˚C in 5% CO_2 in DMEM supplemented with 10% FCS and antibiotics. The cells used for lentivirus production were at passage 4–15.

BMMCL cells were transfected with DNA constructs by nucleofection using Mouse Macrophage Kit and program Y-001 on Amaxa Nucleofector II (Lonza Cologne AG, Cologne, Germany) according to the manufacturer's instructions. After nucleofection, cells were transferred into culture media supplemented with IL-3 and cultured for 24–48 h before analysis.

DNA constructs

Full-length human STIM1 cloned into pDS_XB-YFP vector (pYFP-hSTIM1) was provided by Dr. T. Meyer (5). The signal-peptide region (22), sequence 1–23 aa, of STIM1 was recloned from this vector into pmCherry_N1 from Clontech Laboratories (Mountain View, CA) upstream of mCherry, using *Eco*RI and AgeI restriction sites. The remaining part of STIM1 was recloned downstream of mCherry into the BsrGI site. The construct was verified by DNA sequencing. Expression plasmid coding mouse EB1 fused with GFP (pEB1-GFP) was obtained from Dr. Y. Mimori-Kiyosue (25). Expression plasmid coding human EB3 fused with mRFP1 (26) was obtained from Dr. A. Akhmanova (11).

Lentivirus short hairpin RNAs and virus transduction

A set of five murine STIM1 (GenBank accession number: NM_ 009287) short hairpin RNA (shRNA) constructs cloned into the pLKO.1 vector (TRCN0000175139, TRCN0000175008, TRCN0000193877, TRCN0000193400, and TRCN0000173765) were purchased from Open Biosystems (Huntsville, AL). Aliquots of 1.4 ml Opti-MEM medium (Invitrogen) were mixed with 21 μl ViraPower Lentiviral Packaging Mix (Invitrogen), 14 μg STIM1 shRNA constructs, and 82 μl Lipofectamine 2000. The mixture was incubated for 20 min at room temperature before it was added to semiconfluent HEK-293FT packaging cells in a 150-cm^2 tissue-culture flask. After 3 d, viruses in culture supernatants were concentrated by centrifugation at 25,000 rpm for 2 h using a JA-25.50 rotor (Beckman Coulter, Palo Alto, CA). The pellets were resuspended in 1 ml of culture medium and added to 29 ml of medium, supplemented with 5 μg/ml puromycin containing 5×10^7 BMMCs or BMMCL cells. Stable selection was achieved by culturing cells for 1 wk in the presence of puromycin. Cells were pooled and analyzed for STIM1 expression by immunoblotting. Cells with the highest reduction of STIM1 protein, obtained with TRCN0000175008 (KD1) and TRCN0000193400 (KD2), were selected for additional experiments. Cells transfected with empty pLKO.1 vector were used as negative controls.

Cell activation

Cells at a concentration of 6×10^6 cells/ml were sensitized for 2 h at 37˚C in IL-3– and SCF-free culture medium supplemented with DNP-specific IgE mAb (SPE-7; 1 μg/ml). The cells were then washed in buffered saline solution (BSS; 20 mM HEPES, pH 7.4, 135 mM NaCl, 5 mM KCl, 1.8 mM $CaCl_2$, 5.6 mM glucose, 2 mM $MgCl_2$), supplemented with 0.1% BSA (BSS-BSA), and challenged with various concentrations of Ag (DNP-albumin; 30–40 mol of DNP per mole of albumin) or thapsigargin.

For immunofluorescence experiments, cells at a concentration of 6×10^6 cells/ml were sensitized in suspension for 1 h at 37˚C with DNP-specific

IgE (1 μg/ml) and diluted to a concentration of 1.5×10^6 cells/ml. The suspension (1 ml) was then overlaid on fibronectin-coated coverslips (immersed for 1 h at 37°C in 50 μg/ml fibronectin in 50 mM $NaHCO_3$ and rinsed in PBS) placed in a 3.5-cm tissue culture dish. Cells were allowed to attach for 1 h at 37°C, washed in BSS-BSA, and challenged for 3–5 min with Ag (DNP-albumin) at a final concentration of 100 ng/ml. To determine the time course of activation, cells were challenged with Ag for 1–10 min. For dose response curve construction, the concentration of Ag ranged from 10 to 1000 ng/ml.

Alternatively, cells were activated by pervanadate or thapsigargin, in which case the sensitization step was omitted. Pervanadate solution was prepared fresh by mixing sodium orthovanadate solution with hydrogen peroxide to get a final concentration (10 mM) of both components. The pervanadate solution was incubated for 15 min at room temperature and then diluted 1:100 in BSS-BSA. Attached cells were incubated with pervanadate solution for 15 min at 37°C. Cells were also incubated for 20 min with BSS-BSA containing 2 μM thapsigargin. To determine the time course of activation, cells were activated with thapsigargin for 5–20 min. Dose response measurements were done at thapsigargin concentrations ranging from 0.01 to 2 μM. In some experiments, $[Ca^{2+}]$-free BSS was used. Trypan blue exclusion test was used to evaluate the effect of pervanadate and thapsigargin on viability of cells.

To depolymerize microtubules, cells were treated for 1 h at 37°C with 10 μM nocodazole and activated with pervanadate or thapsigargin in the presence of nocodazole. To inhibit the activity of Src family kinases, IgE-sensitized cells were pretreated for 60 min with Src family selective tyrosine kinase inhibitor PP2 at a concentration of 10 μM before incubation with DNP-albumin. Cells treated for 60 min with 10 μM PP3 were used as controls.

Flow cytometry analysis of FcεRI

To determine the surface FcεRI expression, cells (5×10^5/ml) were exposed for 30 min on ice to 1 μg/ml anti-DNP IgE followed by 30 min incubation with FITC-conjugated anti-mouse Ab (cross-reacting with mouse IgE). After incubation the cells were washed in ice-cold BSS-BSA. Mean fluorescence intensities were determined in the FL1 channel of FACSCalibur (BD Biosciences, Mountain View, CA).

Degranulation assay

The degree of degranulation was quantified as the release of β-glucuronidase from anti-DNP IgE-sensitized and DNP-albumin or thapsigargin-activated cells, using 4-methylumbelliferyl β-D-glucuronide as a substrate (27). The total content of the enzyme was evaluated in supernatants from cells lysed by 0.1% Triton X-100.

Determination of intracellular Ca^{2+} concentrations and $^{45}Ca^{2+}$ uptake

Concentrations of free intracellular calcium ($[Ca^{2+}]_i$) were determined using Fluo3 as a reporter. Cells were sensitized with anti-DNP IgE (1 μg/ml) at 37°C in culture medium supplemented with 10% FCS, but devoid of SCF and IL-3. After 4 h, the cells were washed and resuspended at a concentration of 1×10^7 cells/ml in the same medium supplemented with Fluo3 and probenecid at final concentrations of 1 μg/ml and 2.5 mM, respectively. After 30 min, the cells were washed in BSS-BSA supplemented with probenecid and put on ice for 10 min. Before measurement, the cells (5×10^5) were briefly centrifuged, resuspended in 200 μl BSS-BSA, and preincubated for 4 min at 37°C. Cells were activated by adding 100 ng/ml DNP-albumin or 2 μM thapsigargin. Calcium mobilization was determined in the FL1 channel of a FACSCalibur Flow Cytometer (BD Biosciences, San Jose, CA) using FlowJo software (Ashland, OR). In the yellow fluorescent protein (YFP)-hSTIM1 rescue experiments, calcium responses were measured 48 h after nucleofection. STIM1 KD cells nucleofected with pYFP alone (Clontech Laboratories, Mountain View, CA) were used as a mock control. The experimental procedure was similar to that described above with some differences. Cells were loaded with the calcium reporter Fura Red (5 μg/ml), and changes in fluorescence intensity were monitored on an LSRII flow cytometer (BD Biosciences). Populations of live cells were selected based on forward and side scatters. In live nucleofected cells, YFP-positive cells were gated based on fluorescence in the FL1 channel. Fura Red was excited with 406- and 488-nm lasers, and data were collected separately using 675/45 BP and 675/20 BP filters, respectively.

Uptake of extracellular calcium was determined as described previously (28). Cells were sensitized with anti-DNP IgE (1 μg/ml) and activated for various time intervals with 100 ng/ml DNP-albumin or 2 μM thapsigargin in the presence of extracellular $^{45}Ca^{2+}$ (1 mM). Cell-bound radioactivity was measured in 10 ml scintillation liquid (EcoLite; ICN Biomedicals, Costa Mesa, CA) using a QuantaSmart TM counter.

Chemotaxis assay

Chemotactic responses of BMMCs were examined using 96-well chemotaxis plates (ChemoTx system; Neuro Probe, Gaithersburg, MD) with 8-μm pore size polycarbonate filters. Chemoatractant (DNP-BSA) at concentrations of 50–250 ng/ml in RPMI 1640 supplemented with 20 mM HEPES and 1% BSA (assay buffer), or assay buffer alone was added in 305 μl to the lower wells, and IgE-sensitized BMMCs (0.15×10^6) in 60-μl assay buffer were added on top of the membrane above each well. After 8 h incubation at 37°C and 5% CO_2 in humidified air, cells on the upper membrane surface were removed with suction, and the plates with membrane frames were centrifuged ($156 \times g$, 4 min). After centrifugation, 200 μl media above the cells was removed and 100 μl of water containing 0.1% Triton X-100 and 10 μM SYTOX Green nucleic acid stain (Invitrogen) was added to the well. Fluorescence was determined at 485-nm excitation and 530-nm emission, using TECAN Infinite M200 fluorescence microplate reader (Grödig, Austria). A linear standard curve with serial dilutions of the cells (400–50,000 cells) was included in each experiment to equate fluorescence intensity with cell number. Four independent experiments were run in triplicates.

Gel electrophoresis and immunoblotting

Whole-cell extracts were prepared by washing the cells in cold PBS, solubilizing them in hot SDS-sample buffer (29), and boiling for 5 min. SDS-PAGE on 7.5% gels, electrophoretic transfer of separated proteins onto nitrocellulose, and details of the immunostaining procedure have been described elsewhere (30). Abs against STIM1 and actin were diluted 1:2000 and 1:3000, respectively. Bound primary Abs were detected after incubation of the blots with HRP-conjugated secondary Ab diluted 1:10,000. Phosphotyrosine was detected by PY-20–HRP conjugate (dilution 1:2000). HRP signal was detected with chemiluminescence reagents in accordance with the manufacturer's directions and quantified using LAS 3000 imaging system (Fujifilm, Tokyo, Japan).

Immunofluorescence microscopy

Immunofluorescence microscopy was performed on fixed cells as described previously (31). Cells attached to fibronectin-coated coverslips were rinsed with microtubule-stabilizing buffer (0.1 M MES, pH 6.9, 2 mM EGTA, 2 mM $MgCl_2$, 4% polyethylene glycol 6000), fixed for 20 min in 3% formaldehyde in microtubule-stabilizing buffer, and extracted for 4 min with 0.5% Triton X-100 in microtubule-stabilizing buffer. TUB 2.1 mAb conjugated with Cy3 and polyclonal Ab to α-tubulin were diluted 1:600 and 1:200, respectively. AlexaFluor 488-conjugated anti-rabbit Ab was diluted 1:300. The preparations were mounted in MOWIOL 4-88 (Merck, Darmstadt, Germany), supplemented with DAPI to label nuclei, and examined with an Olympus A70 Provis microscope equipped with ×60 water-immersion or ×100 oil-immersion objectives. Images were recorded with a SensiCam cooled CCD camera (PCO IMAGING, Kelheim, Germany). Conjugated secondary Ab did not give any detectable staining.

Alternatively, samples were examined with a confocal laser scanning microscope Leica TCS SP5 equipped with an ×63/1.4.N.A. oil-immersion objective. Excitation and emission wavelengths were 561 nm and 566 to 633 nm for Cy3 (diode pumped solid-state laser). Optical sections were acquired in 125-nm steps, and z-series were made from 70 sections. Deconvolution and rotation was performed using Huygens Deconvolution Software (Scientific Volume Imaging, Hilversum, The Netherlands).

To estimate the number of cells that responded to activation events by generation of microtubule protrusions, three independent immunofluorescence experiments were performed. In each experiment usually 500 cells were examined, and cells with five and more microtubule protrusions after activation were counted up. These protrusions were not discernible in nonactivated cells. Statistical comparison of data was conducted with Student *t* test.

Time-lapse imaging by total internal reflection fluorescence microscopy

Control BMMCL cells, BMMCL cells with empty pLKO.1 vector, or cells with STIM1 KD were nucleofected with pEB1-GFP. Alternatively, BMMCL cells were nucleofected with YFP-hSTIM1 or simultaneously with YFP-hSTIM1 and EB3-mRFP1. Twenty-four hours later, 100 μl of cell suspension at concentration 1.5×10^6 cells/ml was overlaid on 35-mm glass-bottom culture dishes (MatTek, Ashland, MA; Cat. No. P35G-1.5-14-C) precoated with fibronectin (see above), and cells were allowed to attach for 1 h at 37°C. Perfusion insert for the 35-mm culture dish was

inserted (Warner Instruments, Hamden, CT; model RC-37F), and cells were washed and subsequently incubated in RPMI medium for live cell imaging (RPMI 1640 without phenol red, riboflavin, folic acid, pyridoxal, $Fe[NO_3]_3$) supplemented with 20 mM HEPES. Cells were imaged on the Leica AM total internal reflection fluorescence (TIRF) MC (Leica Microsystems) at 37˚C. Time-lapse sequences of EB1-GFP or YFP-hSTIM1 were acquired in TIRF mode (GFP cube, laser line 488 nm; Ex, 470/40; Em, 525/50; penetration depth, 150 nm) using HCX PL APO ×100/1.46 NA oil-immersion TIRF objective. Images were taken for 3 min at 1-s intervals with 30–40% laser power and exposure times ranging from 500–800 ms. Time-lapse sequences of EB3-mRFP1 in combination with YFP-hSTIM1 were acquired in TIRF mode (laser lines 561 nm or 488 nm, Em: 640/40 or 530/30, respectively; the same penetration depth 150 nm for both channels) using the same objective as above. Individual channels were imaged sequentially. Images were taken for 3 min at 2-s intervals with 50–80% (561 nm) or 30–40% (488 nm) laser power and exposure times ranging from 500–800 ms. Cells were scanned before, during, and after thapsigargin or nocodazole addition to final concentrations of 2 μM and 10 μM, respectively.

Time-lapse sequences were adjusted and analyzed with a particle tracking plug-in written in house. The images were smoothed to remove noise (σ 80 nm). The particles were then enhanced by subtracting the images obtained by Gaussian smoothing (σ 300 nm). The coordinates of particles were detected as centers of mass of maxima of the image intensity found by morphologic reconstruction (32). Regions of pixels with distance less than 3 μm from cell boundary were detected by thresholding the Euclidean distance transform (33) of the cell binary image. Only the particles in the selected region were evaluated. The corresponding particles in subsequent images were detected by pairing the closest particles, and the particle trajectories were constructed by continuation. The speed of the particles was calculated as the ratio of particle trajectory length and trajectory duration. The histogram of the particles speed was calculated from the trajectory speed weighted by the trajectory duration. The algorithms were implemented as plug-in modules of the Ellipse program, version 2.07 (ViDiTo, Systems, Košice Slovakia). Statistical analysis was done in Microsoft Excel.

Results

Reorganization of microtubules during activation of BMMCs

To compare microtubule organization in resting and activated mast cells, BMMCs were attached to fibronectin-coated coverslips and then activated by various means before fixation and immunofluorescence labeling for β-tubulin. Data showed a clear difference between resting and activated cells in microtubule distribution. Quiescent cells were characterized by rounded morphology and microtubules in cell periphery running predominantly alongside the plasma membrane (Fig. 1*A*, *a*, *b*; −Ag). When activated by FcεRI aggregation, many cells had multiple protrusions containing microtubules, in the following text denoted as microtubule protrusions (Fig. 1*A*, *c*, *d*; +Ag). Similarly, activation by pervanadate, a potent protein tyrosine phosphatase inhibitor (34) that mimics in part the stimulatory effect of Ag (35), gave rise to multiple microtubule protrusions (Fig. 1*A*, *e*, *f*; +Pv). Surprisingly, generation of robust microtubule protrusions was also found in cells treated with thapsigargin, a compound that discharges intracellular Ca^{2+} stores by inhibition of the SERCA (36) (Fig. 1*A*, *g*, *h*; +thapsigargin [Tg]). Microtubule protrusions do not reflect only the spreading of cells during activation events, because they are also found on the dorsal side of cells as clearly documented on deconvoluted three-dimensional images from laser scanning confocal microscopy. Although no protrusions were found in resting cells (Fig. 2*A*, 2*B*, –Ag), they were clearly discernible in cells activated by Ag-mediated FcεRI aggregation (Fig. 2*C*, 2*D*, +Ag), pervnadate (Fig. 2*E*, 2*F*, +Pv) or thapsigargin (Fig. 2*G*, 2*H*, +Tg). To determine whether the number of cells with protrusions depends on the mode of activation, BMMCs were evaluated for the presence of protrusions in three independent experiments (each included 500 cells). Activation of the cells with Ag, pervanadate, or thapsigargin resulted in 37 ± 9, 59 ± 8, and 94 ± 3% (mean ± SD; n = 3), respectively, of cells with microtubule protrusions (Fig. 1*B*). To prove that the generation of microtubule protrusion is not restricted only to cells of primary cultures, activations were repeated with an established cell line, BMMCL. In that case the rates of activation with Ag, pervanadate, or thapsigargin were 55 ± 10, 64 ± 3, and 80 ± 5% (mean ± SD; n = 3), respectively. The microtubule protrusions in cells activated by FcεRI aggregation were most prominent ~5 min after crosslinking. In contrast, cells stimulated by pervanadate or thapsigargin reached the maximum after 15 and 20 min, respectively.

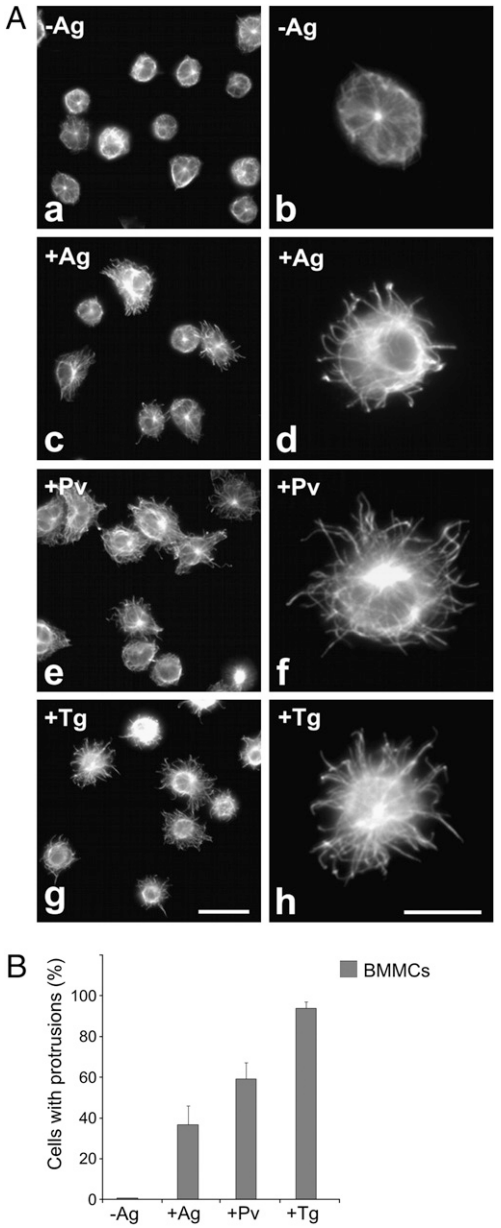

FIGURE 1. Organization of microtubules in resting and activated mast cells. *A*, Resting BMMCs (*a*, *b*; −Ag), the cells activated by FcεRI aggregation (*c*, *d*; +Ag), pervanadate (*e*, *f*; +Pv), or thapsigargin (*g*, *h*; +Tg) were fixed and stained for β-tubulin. The preparations were imaged by fluorescence microscopy. Scale bars, 20 μm (*g*) and 10 μm (*h*). Comparable magnifications are in (*a*, *c*, *e*, *g*) and in (*b*, *d*, *f*, *h*). *B*, Quantitative analysis of the frequency of microtubule protrusions in BMMCs. Resting cells (−Ag), cells activated by FcεRI aggregation (+Ag), pervanadate (+Pv) or thapsigargin (+Tg). Three independent experiments were performed, each involving 500 BMMCs examined for the presence of microtubule protrusions. Values indicate means ± SD (n = 3).

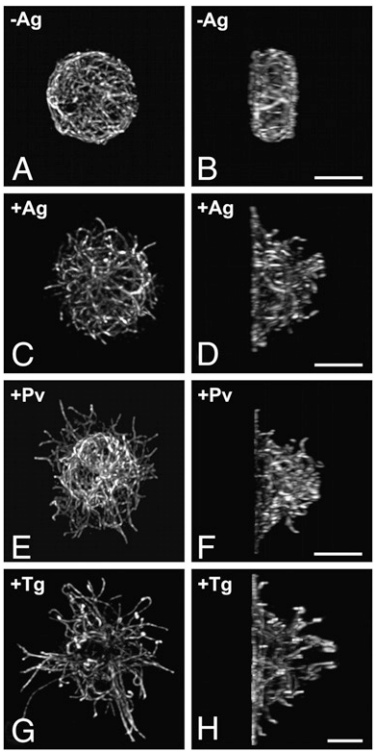

FIGURE 2. Changes in the spatial distribution of microtubules in resting and activated BMMCs. Resting cells (*A*, *B*; −Ag), cells activated by FcεRI aggregation (*C*, *D*; +Ag), pervanadate (*E*, *F*; +Pv), or thapsigargin (*G*, *H*; +Tg) were fixed and stained for β-tubulin. The preparations were imaged by laser scanning confocal microscopy. The stacks of confocal sections were deconvoluted and subjected to three-dimensional reconstruction. Resulting three-dimensional images viewed from top of the cells (*A*, *C*, *E*, *G*) and from the plane perpendicular to the plane of cell adhesion (*B*, *D*, *F*, *H*). Each pair (*A–B*, *C–D*, *E–F*, and *G–H*) represents the same cells. Scale bars, 5 μm.

Dose response curves demonstrating the relations between the formation of microtubule protrusions and the degree of degranulation, quantified as the release of β-glucuronidase, in BMMCL activated by FcεRI aggregation for 5 min and by thapsigargin for 20 min are shown in Supplemental Fig. 1A and 1B, respectively. There were dose response correlations between formation of microtubule protrusions and degranulation. Correlations between the time course of microtubule protrusion formation and the degree of degranulation after activation by FcεRI aggregation at Ag concentration 100 ng/ml and by thapsigargin at concentration 2 μM are shown in Supplemental Fig. 1C and 1D, respectively. Although there was a correlation between morphologic changes and degranulation in case of thapsigargin activation, cells activated by Ag reached the maximum of microtubule protrusions at 5 min, whereas the increase in β-glucuronidase release persisted to 10 min. Activation by either pervanadate or thapsigargin had no effect on viability of the cells (not shown). When the cells were pretreated with microtubule inhibitor nocodazole and activated in its presence, protrusions were not formed (not shown). This implies that microtubules are essential in this process.

Formation of microtubule protrusions in FcεRI-activated cells was substantially reduced if a monovalent hapten causing receptor disengagement (50 μM DNP-lysine) (37) was added together with or 1 min after Ag (not shown). Inhibition of protrusion formations was also observed in IgE-sensitized cells pretreated for 60 min with Src family inhibitor PP2 (10 μM) and then activated by Ag. Pretreatment with PP3 (negative control for PP2) failed to affect protrusion formation (not shown). This finding suggests that the activity of Src family protein tyrosine kinases is essential for this process. Interestingly, when the cells were activated by FcεRI aggregation, pervanadate, or thapsigargin in Ca^{2+}-free media, microtubule protrusions were basically not detectable. A typical example of the effect of extracellular Ca^{2+} on generation of microtubule protrusions in cells after their activation by FcεRI aggregation is shown in Fig. 3*A*. Statistical evaluation of these and other experiments is documented by histogram (Fig. 3*B*). Collectively, these data suggest that dramatic changes in microtubule arrangement during activation of BMMCs by FcεRI aggregation depend on the activity of Src family kinases and are modulated by Ca^{2+} influx.

Changes of microtubule dynamics in activated cells

Microtubule plus-end dynamics in BMMCL cells expressing EB1-GFP was monitored by means of time-lapse imaging using TIRF microscopy (TIRFM). Cells were activated or not by thapsigargin, and the distribution of growing microtubules in cell periphery was evaluated after collecting 180 frames in 1-s intervals for 3 min total time. In activated cells, time-lapse imaging started 13 min after thapsigargin addition. Data from a typical experiment are shown in Fig. 4*A*. A comparison of single-frame or 20-frame projections obtained either from control (Fig. 4*A*, *a*, *b*; –Tg) or thapsigargin-activated (Fig 4A, *c*, *d*; + Tg) cell indicated more growing microtubules in cell periphery of the latter. This finding was confirmed by statistical data evaluation and documented with

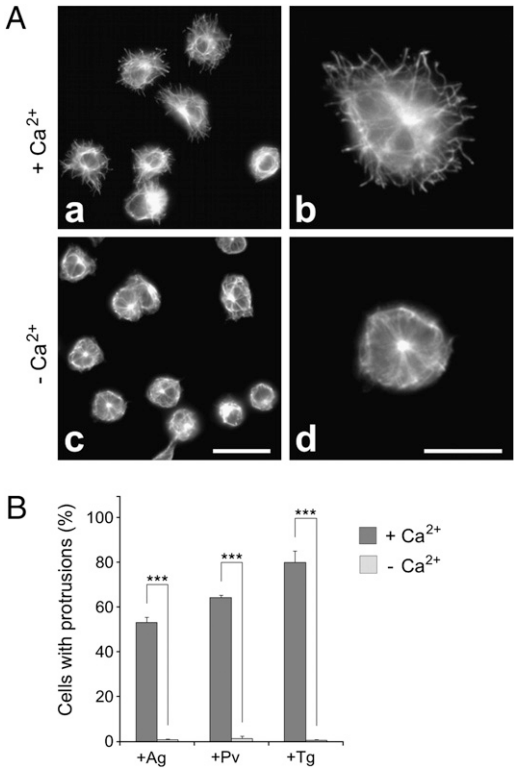

FIGURE 3. Effect of extracellular Ca^{2+} on generation of microtubule protrusions. *A*, BMMCL cells activated by FcεRI aggregation in the presence (*a*, *b*; $+Ca^{2+}$) or absence (*c*, *d*; $–Ca^{2+}$) of extracellular Ca^{2+} (1.8 mM) were fixed and stained for β-tubulin. Scale bars, 20 μm (*c*) and 10 μm (*d*). Comparable magnifications are in (*a*, *c*) and in (*b*, *d*). *B*, Statistical analysis of the frequency of microtubule protrusions in BMMCL cells. Cells activated by FcεRI aggregation (+Ag), pervanadate (+Pv), or thapsigargin (+Tg) in the presence ($+Ca^{2+}$) or absence ($-Ca^{2+}$) of extracellular Ca^{2+}. Three independent experiments were performed, each involving 500 cells, and examined for the presence of microtubule protrusions. Values indicate means ± SD, $n = 3$; $^{***}p < 0.001$.

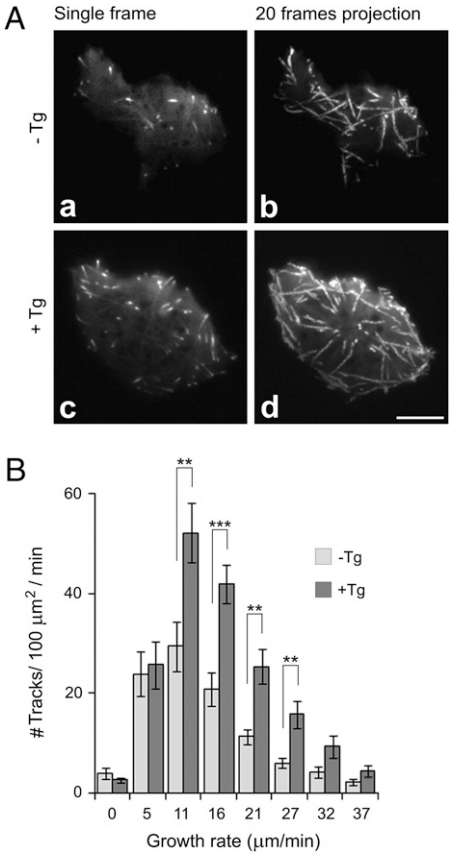

FIGURE 4. Activation of mast cells increases the number of growing microtubules in cell periphery as determined by TIRFM time-lapse imaging. *A*, Time-lapse imaging of resting (*a*, *b*) and thapsigargin-activated (*c*, *d*) BMMCL cells expressing EB1-GFP. Still images of EB1 (*a*, *c*) and tracks of EB1 comets over 20 s created by maximum intensity projection of the 20 consecutive frames (*b*, *d*). Scale bar, 5 μm. *B*, Histogram of microtubule growth rates in cell periphery of resting (−Tg) and thapsigargin-activated (+Tg) cells. A total of 15 different cells were tracked in five independent experiments. Values indicate mean ± SE, $n = 15$; $^{**}p < 0.01$; $^{***}p < 0.001$.

a histogram of the microtubule growth rates (Fig. 4*B*). Typical time-lapse imaging of control (Supplemental Video 1) and activated (Supplemental Video 2) cells are shown in the supplemental material. These data suggest that activation increases the number of growing microtubules in the cell periphery where microtubule protrusions are formed. More growing microtubules at cell periphery, compared with nonactivated cells, were also observed after activation of cells by FcεRI aggregation (Supplemental Fig. 2).

Reduced degranulation, Ca^{2+} influx, and free cytoplasmic Ca^{2+} concentration in cells with reduced level of STIM1

STIM1 represents the key regulator in the SOCE pathway leading to an influx of extracellular Ca^{2+}. To discover whether STIM1 is involved in the generation of microtubule protrusion, we first isolated cells with reduced levels of STIM1 and characterized their properties. STIM1-deficient cells were produced in both BMMCs and BMMCL cells using lentiviral vectors. At the best silencing, the amount of STIM1 in BMMCs and BMMCL cells reached 20 ± 12% and 10 ± 9% (means ± SD; n = 5-8), respectively, when compared with the expression level in control cells with an empty pLKO.1 vector. A typical immunoblotting experiment is shown in Fig. 5*A*, and evaluation of all data obtained is shown in Fig. 5*B*. Cells with the highest STIM1 reduction (denoted KD2) were selected for further experiments. As detected by flow cytometry, the

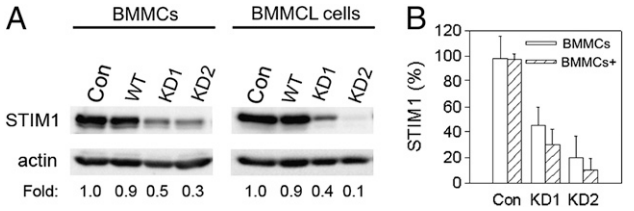

FIGURE 5. Characterization of mast cells with reduced level of STIM1. *A*, Immunoblots of whole cell lysates from BMMCs or BMMCL cells probed with anti-STIM1 and anti-actin (loading control) Abs. Control cells infected with empty pLKO.1 vector (Con), noninfected wild-type cells (WT), cells selected after KD of STIM1 by shRNA1 (KD1), or shRNA2 (KD2). Numbers under the blots indicate relative amounts of STIM1 normalized to control cells (Con) and to the amount of actin in individual samples (Fold). *B*, Comparison of STIM1 expression levels in control and STIM1 KD BMMCs or BMMCL cells. Values indicate means ± SD from independent experiments (n = 6 for controls; n = 3 for KD1; n = 5 for KD2).

expression levels of surface FcεRI were similar in cells with normal and reduced amount of STIM1 (not shown). No substantial changes in the profile of total tyrosine-phosphorylated proteins were detected in STIM1 KD2 cells (not shown).

It is well established that an increase in $[Ca^{2+}]_i$ is a prerequisite for mast cell degranulation (1). To confirm the functional relevance of STIM1 KD, we determined the degree of degranulation by measuring the release of β-glucuronidase in cells activated by FcεRI aggregation or by thapsigargin. As expected, a substantial decrease in degranulation was observed in BMMCs with STIM1 KD compared with control cells. The inhibition of degranulation was observed in cells activated by both FcεRI aggregation (Supplemental Fig. 3*A*) and by thapsigargin (Supplemental Fig. 3*B*). The uptake of $^{45}Ca^{2+}$ after activation by FcεRI aggregation (Supplemental Fig. 3*C*) or by thapsigargin (Supplemental Fig. 3*D*) was also inhibited in STIM1 KD cells. Finally, a substantially lower concentration of free intracellular calcium $[Ca^{2+}]_i$ was detected in STIM1 KD cells, after activation by both FcεRI aggregation (Supplemental Fig. 3*E*) and thapsigargin (Supplemental Fig. 3*F*; thapsigargin). Similar results were obtained with BMMCL cells (not shown). Collectively, these data clearly demonstrate that STIM1 is essential for Ca^{2+} mobilization and degranulation in cells used in this study.

Generation of microtubule protrusions is dependent on STIM1

When BMMCs carrying empty pLKO.1 vector were activated with thapsigargin, the formation of microtubule protrusions was prominent (Fig. 6*A*, *a*, *c*; control + Tg) and essentially the same as in BMMCs without vector (not shown). Alternatively, thapsigargin-induced activation in BMMCs with STIM1 KD failed to generate microtubule protrusions, and the cell shape was spherical (Fig. 6*A*, *b*, *d*; STIM1 KD + Tg). Significant inhibition of protrusion formations in STIM1 KD cells was also found after stimulation with pervanadate or Ag in both BMMCs and BMMCL cells (Fig. 6*B*). No obvious change in microtubule dynamics was detected by time-lapse imaging in BMMCL cells with STIM1 KD after activation by thapsigargin. Data from a typical experiment of time-lapse imaging are shown in Fig. 7*A*. Comparison of still images (single frame or 20 frames projections) from nonactivated (Fig. 7*A*, *a*, *b*; STIM1 KD – Tg) or activated (Fig 7A, *c*, *d*; STIM1 KD + Tg) cells disproved the notion that more microtubules grow in the cell periphery of activated cells. This finding was confirmed by the histogram comparing microtubule growth rates (Fig 7*B*). Although thapsigargin-activated cells exhibited some increase in the number of growing microtubules in the cell periphery, it was insignificant except for the fast-growing group (27 μm/min). In control

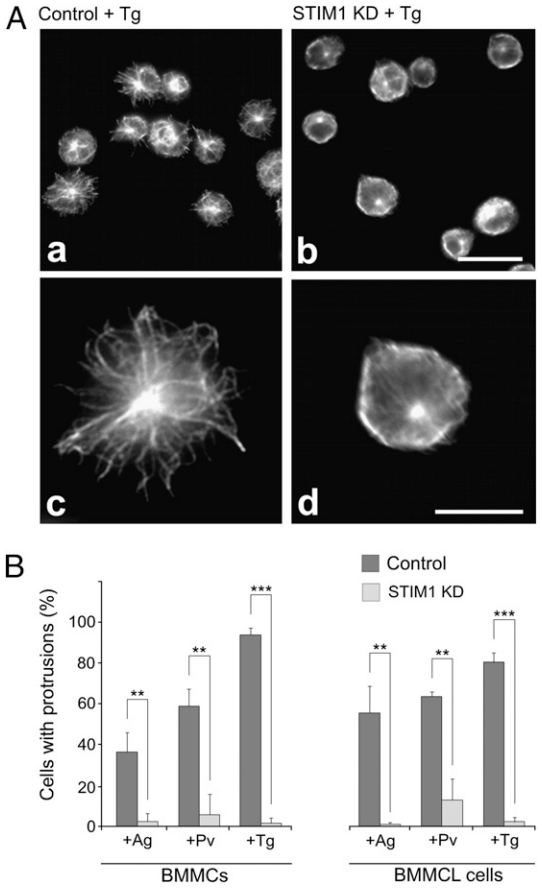

FIGURE 6. Decreased expression of STIM1 inhibits the generation of microtubule protrusions in activated cells. *A*, Control BMMCs, carrying empty pLKO.1 vector (*a*, *c*) or STIM1 KD2 cells (*b*, *d*) were activated by thapsigargin, fixed, and stained for β-tubulin. Scale bars, 20 μm (*a*, *b*) and 10 μm (*c*, *d*). *B*, Statistical analysis of the frequency of microtubule protrusions in control cells (carrying empty pLKO.1 vector) and STIM1 KD2 cells activated by FcεRI aggregation (+Ag), pervanadate (+Pv), or thapsigargin (+Tg). Three independent experiments were performed, each involving 500 BMMCs or BMMCL cells, and examined for the presence of microtubule protrusions. Values indicate means ± SD, $n = 3$; $^{**}p < 0.01$; $^{***}p < 0.001$.

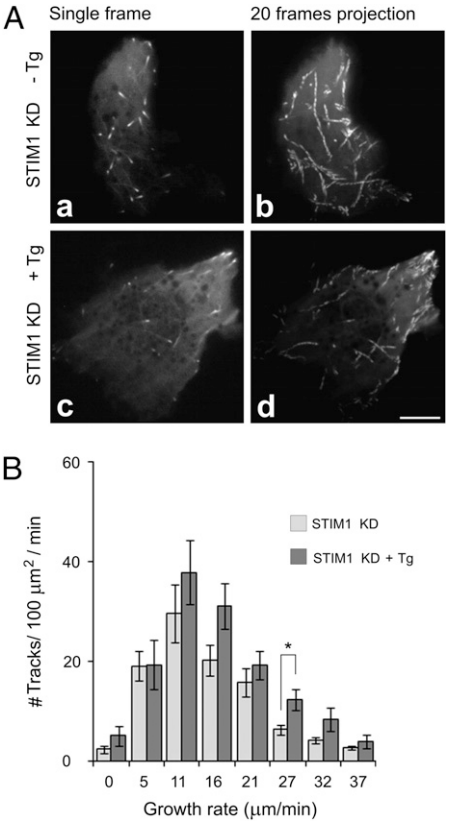

FIGURE 7. KD of STIM1 prevents changes in microtubule dynamics in activated cells as determined by TIRFM time-lapse imaging. STIM1 KD2 cells were nucleofected with EB1-GFP and used for time-lapse imaging. *A*, Resting (*a*, *b*) and thapsigargin-activated (*c*, *d*) STIM1 KD2 cells. Still images of EB1 (*a*, *c*) and tracks of EB1 comets over 20 s created by a maximum intensity projection of 20 consecutive frames (*b*, *d*). Scale bar, 5 μm. *B*, Histogram of microtubule growth rates in the cell periphery of resting (STIM1 KD) and thapsigargin-activated (STIM1 KD +Tg) cells. A total of nine different cells were tracked in three independent experiments. Values indicate means ± SE, $n = 9$; $^{*}p < 0.05$.

BMMCL cells carrying empty pLKO.1 vector, the distribution of growing microtubules in resting and thapsigargin-treated cells was similar as in BMMCL cells (Fig. 4).

To strengthen the evidence of STIM1-dependent formation of microtubule protrusions during activation, a rescue experiment was performed with construct-encoding mCherry-tagged human STIM1. Proper localization of mCherry-hSTIM1 was demonstrated in cells expressing EB1-GFP. It has been shown previously that STIM1 associates with the plus ends of growing microtubules (11); in addition, the mCherry-hSTIM1 localized in quiescent cells both in the ER and in the growing ends of microtubules labeled with EB1 (Fig. 8*A*, *a–c*). When BMMCL cells with STIM1 KD were nucleofected with mCherry-hSTIM1 and activated by thapsigargin, the formation of typical microtubule protrusions was recovered (Fig. 8*B*, *a–c*). Alternatively, no protrusions were generated after activation of cells nucleofected with empty mCherry vector (Fig. 8*B*, *d–f*). Control experiments revealed that no microtubule protrusions were evident in nonactivated BMMCL cells nucleofected either with mCherry-hSTIM1 or mCherry vector alone (not shown). The formation of microtubule protrusions was also recovered when YFP-hSTIM1 was used in rescue experiments as documented by quantitative data (Fig. 8*C*). Nucleofection of YFP-hSTIM1 into STIM1 KD2 cells also restored calcium mobilization upon triggering with thapsigargin (Fig. 8*D*) or aggregation of the FcεRI (not shown). Collectively, these data strongly suggest that STIM1 is essential for the generation of microtubule protrusions during activation of BMMCs.

Microtubules are not essential for STIM1 puncta formation

To address the question of whether microtubules in BMMCs have a role in activating SOCE, we investigated the effect of nocodazole, a microtubule-depolymerizing drug, on the distribution of STIM1 in the absence or presence of thapsigargin. In control cells, a typical comet-like movement was observed in quiescent BMMCs expressing YFP-hSTIM1 (Supplemental Video 3). After activation by thapsigargin, STIM1 formed puncta (Supplemental Video 4) similar to those previously described in other cells (5, 15). The addition of 10 μM nocodazole led to the rapid disappearance of comet-like movement of YFP-hSTIM1 as well as EB3-mRFP1, used as marker of growing microtubules. YFP-hSTIM1 was located only on the ER. When the nocodazole-treated cells were then activated with thapsigargin, YFP- hSTIM1 formed robust puncta (Supplemental Video 5). Staining of parallel samples for tubulin confirmed that most microtubules were disassembled (not shown). This finding suggests that initial STIM1 aggregation does not require intact microtubules. Interestingly, the disruption of microtubules only moderately inhibited the $^{45}Ca^{2+}$ uptake in

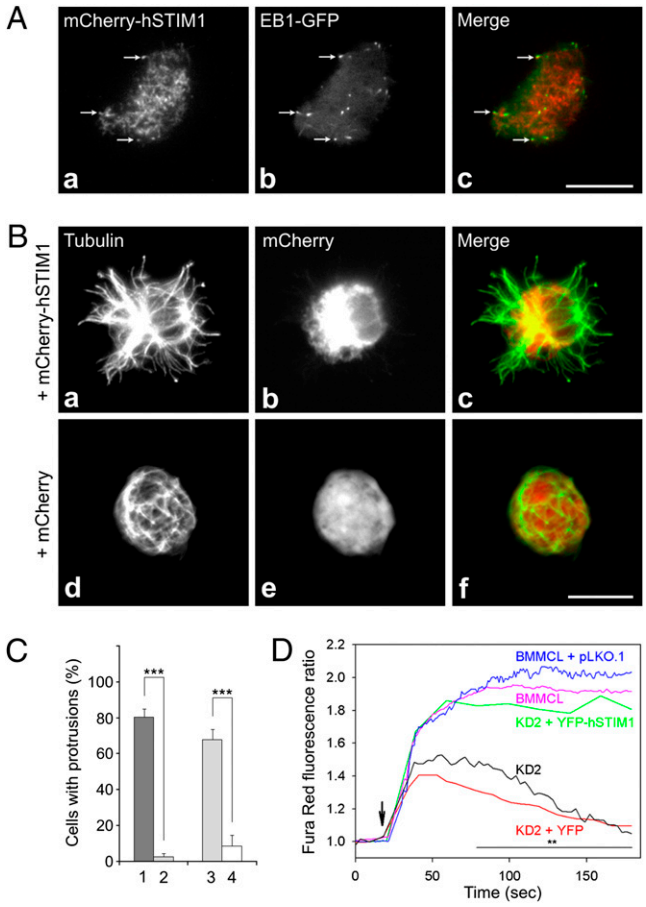

FIGURE 8. Phenotype rescue of STIM1 KD2 BMMCL cells after introduction of human STIM1. *A*, Localization of mCherry-tagged human STIM1 during TIRFM time-lapse imaging of resting cells expressing EB1-GFP. Still images of mCherry-hSTIM1 (*a*) EB1-GFP (*b*) and superposition of images (*c*; mCherry, red; GFP, green). Arrows indicate the same positions. Scale bar, 10 μm. *B*, STIM1 KD2 cells were nucleofected with mCherry-hSTIM1 (*a–c*) or mCherry vector alone (*d–f*; control) and activated by thapsigargin. Microtubules in fixed cells stained with anti-α-tubulin Ab (*a*, *d*). Fluorescence of nucleofected mCherry vectors (*b*, *e*). Superposition of images (*c*, *f*; tubulin, green; mCherry, red). The preparations were imaged by fluorescence microscopy; *a–c* and *d–f* represent the same cells. Scale bar, 10 μm. *C*, Statistical analysis of the frequency of microtubule protrusions in thapsigargin-activated control cells (1), STIM1 KD2 cells (2), STIM1 KD2 cells nucleofected with pYFP-hSTIM1 (3) and STIM1 KD2 cells nucleofected with pYFP empty vector (4). Three independent experiments were performed, each involving 500 (1, 2) or 100 (3, 4) cells examined for the presence of microtubule protrusions. Values indicate means ± SD, $n = 3$; $***p < 0.001$. *D*, Changes in intracellular Ca^{2+} mobilization. KD2 cells were nucleofected with pYFP-hSTIM1 (green line) or with pYFP empty vector (red line). Nontransfected cells (pink line), cells transfected with pLKO.1 (blue line) and STIM1 KD2 cells (black line) served as controls. The arrow indicates activation by 2 μM thapsigargin. The extent of activation is expressed as a ratio of Fura Red fluorescence intensity induced with 406- and 488-nm lasers. Representative curves are plotted against time. The line below the asterisks indicates the time interval of significant differences between STIM1 KD2 cell transfected with pYFP-hSTIM1 or with pYFP empty vector; $**p < 0.01$; $n = 3$.

thapsigargin-activated cells (Fig. 9*A*), but degranulation was substantially reduced (Fig. 9*B*).

STIM1 associates with microtubule protrusions and plays a role in chemotactic response

The movement of YFP-hSTIM1, not associated with growing tips of microtubules, was observable at later stages of activation when microtubule protrusions started to form. Association of YFP-hSTIM1 with microtubule protrusions was evident in thapsigargin-activated BMMCs and was detectable by confocal microscopy on cells stained for β-tubulin (Fig. 10*A*, *a–c*). Similarly, FcεRI aggregation led to partial association of YFP-hSTIM1 with microtubule protrusions (not shown).

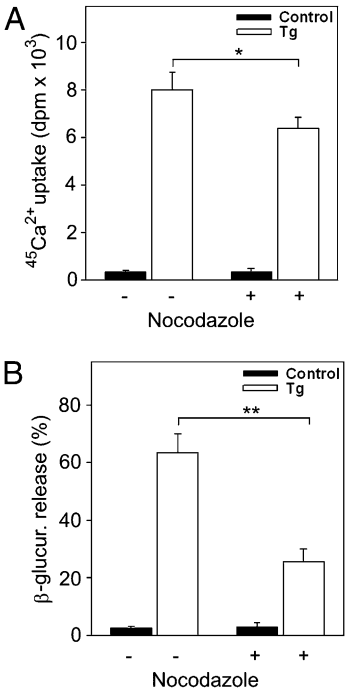

FIGURE 9. Effect of microtubule depolymerization on Ca^{2+} uptake and degranulation. *A*, Effect of nocodazole on Ca^{2+} uptake. BMMCs were treated or not with nocodazole (10 μM) for 30 min and then exposed to thapsigargin (2 μM; Tg) or BSS-BSA alone (Control) for 15 min in the presence of extracellular $^{45}Ca^{2+}$ (1 mM) and nocodazole (10 μM). *B*, Effect of nocodazole on degranulation. BMMCs were treated with nocodazole and exposed to thapsigargin as in *A*, and the release of β-glucuronidase was determined. Data in *A* and *B* represent means ± SD, $n = 6–8$; $*p < 0.05$; $**p < 0.01$.

The observed formation of STIM1-dependent microtubule protrusions could be related to enhanced movement of the activated cells. Therefore, in additional experiments, we investigated the chemotactic response of STIM1-deficient BMMCs. The data presented in Fig. 10*B* indicate that at low concentrations of Ag (25–100 ng/ml), the chemotactic response is contingent on STIM1 in a dose-dependent manner. At a higher concentration (250 ng/ml), the difference disappears mainly because of the high-dose–mediated inhibition of chemotaxis in control cells. This finding demonstrates that STIM1-dependent Ca^{2+} influx promotes chemotaxis.

Discussion

FcεRI stimulation of mast cells leads to rapid cytoskeleton rearrangement that is important for cell activation and degranulation. Accumulating recent data point to an important role of microtubules in these processes (38). Previous studies focused primarily on the role of microtubules in granular transport (13, 16, 17, 20) or on the initial stages of SOCE signaling pathway (13, 15, 39). In this study, we show that microtubule network rearrangement in activated BMMCs and formation of microtubule protrusions is dependent on the activity of Ca^{2+} sensor STIM1. This conclusion is supported by several lines of evidence. First, microtubule protrusions were found in cells stimulated by three types of activators that induced depletion of Ca^{2+} from internal stores (FcεRI aggregation, pervanadate, or thapsigargin treatment). Second, the generation of protrusions was impaired when multivalent Ag-

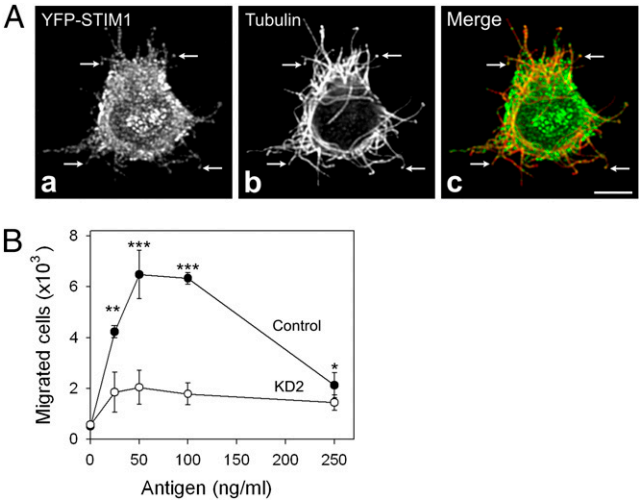

FIGURE 10. STIM1 associates with microtubule protrusions in activated cells and is essential for chemotactic response. *A*, Laser scanning confocal microscopy of BMMCL cells expressing YFP-hSTIM1 after activation by thapsigargin. Cells were fixed and immunostained for β-tubulin, and both STIM1 (*a*) and tubulin (*b*) were visualized in a single confocal section. Superposition of STIM1 and tubulin staining is shown in *c*. Association of YFP-hSTIM1 with microtubule protrusions is depicted (arrows). Scale bar, 5 μm. *B*, Chemotactic response in activated cells. Various concentrations of DNP-BSA (chemoattractant) were added to the lower wells of ChemoTx system plate, and IgE-sensitized BMMCs infected with empty pLKO.1 vector (Control) or STIM1 KD2 cells (KD2) were added on top of the membrane above each well. The numbers of cells migrated to the lower well were determined as described in *Materials and Methods*. Values indicate mean ± SD, $n = 12$; $*p < 0.05$; $**p < 0.01$; $***p < 0.001$.

induced FcεRI aggregation and signaling were inhibited either by monovalent hapten or by Src family specific inhibitor; this implies that early, physiologically relevant signaling events leading to STIM1 aggregation are important for microtubule rearrangement. Third, the formation of protrusions was also inhibited in cells with a decreased level of STIM1 and with correspondingly diminished influx of extracellular Ca^{2+}. Fourth, microtubule protrusions were restored in STIM1 KD cells after the introduction of hSTIM1. Finally, microtubule protrusions were not observed in cells activated in Ca^{2+}-free media. Thus, STIM1-regulated Ca^{2+} influx plays a crucial role in the generation of microtubule protrusions.

We have shown previously that, compared with resting cells, FcεRI- or pervanadate-induced activation of BMMCs attached to poly-L-lysine-coated coverslips resulted in more intense staining of microtubules. However, no obvious microtubule protrusions were detected (21). Similarly, activation and fixation of BMMCs in suspension followed by attachment to glass slides by cytospin intensified the tubulin immunostaining, but microtubule protrusions were not reported (17). In this study, the cells were attached to fibronectin before activation, resembling more closely the natural conditions in connective tissue where mast cells are congregated (40). Although the attachment of BMMCs to fibronectin alone did not generate microtubule protrusions, they were observable after cell triggering. It is known that engagement of integrins by their ligands activates some signaling pathways that modulate signals originating from other receptors (41). It has been reported that, when mast cells were activated simultaneously via both FcεRI and integrins, phosphorylation events were prolonged and intensified (42). Thus, generation of microtubule protrusions could reflect such integrated signals in activated cells.

To discover whether the generation of microtubule protrusions is limited to BMMCs, several other cell types were tested. However, thapsigargin treatment failed to induce formation of protrusions in any other cell type examined, including mouse embryonal fibroblasts 3T3, human osteosarcoma cell line U2OS or human glioblastoma T98G (Z. Hájková, unpublished data). By contrast, in BMMCL cells, which are grown for many years in the absence of SCF, the formation of protrusions was observed after triggering with cell activators (Ag, pervanadate, thapsigargin). The reduction of STIM1 expression both in BMMCs and BMMCL cells had a detrimental impact on the formation of microtubule protrusions. This finding indicates that protrusion formation could be a typical feature of mast cells that are characterized by immediate response to outer stimuli. However, we cannot rule out at present that the generation of microtubule protrusions can also be observable in the other cell types.

Colocalization of ER-embedded STIM1 with microtubules has been described for several cell types, including rat basophilic leukemia RBL-2H3 (8, 9, 15, 43), and comet-like movement of STIM1 was also reported (11). Furthermore, STIM1 contains a short sequence (SxIP) responsible for direct binding to EB1 (44). Thus, STIM1 can associate with growing microtubules, a mechanism that might facilitate the transport of STIM1 to plasma membrane. Using TIRFM we have confirmed the comet-like movement of STIM1 and its association with EB1 in resting BMMCL cells. This movement was substantially reduced after the addition of thapsigargin, which is in agreement with the impaired association of STIM1 with microtubules in Ag-activated RBL-2H3 cells (43). Recent data on FRET imaging of EB1 and STIM1 in HEK293 cells showed that, upon store depletion of Ca^{2+}, STIM1 dissociated from EB1 and associated with SERCA. This process was reversible, because the replenishment of intracellular Ca^{2+} stores also restored the STIM1–EB1 interactions (45). Moreover, no effect on SOCE was observed in HeLa cells with depleted EB1 (11). Taking these findings together, it is likely that the interaction of STIM1 with EB1 on growing microtubules is not essential for the transport of STIM1 to plasma membrane during mast cell activation.

After depletion of intracellular Ca^{2+} stores, STIM1 accumulates into puncta, discrete subregions of ER located in a close proximity (10–25 nm) to the plasma membrane (46). STIM1 puncta are formed several seconds before the opening of calcium channels (47), and one could expect that microtubules are involved in this process. However, our data demonstrate that although microtubule disruption by nocodazole abolished the comet-like movement of STIM1, it had no effect on puncta formation in activated cells. This finding is in line with our observation that the uptake of extracellular Ca^{2+} was only partially inhibited in nocodazole-pretreated and thapsigargin-activated BMMCs. This suggests that STIM1 aggregation beneath the plasma membrane and subsequent opening of Ca^{2+} release-activated Ca^{2+} channels does not require intact microtubules in activated mast cells. Previous studies often reported discordant effects of nocodazole treatment on SOCE or I_{CRAC}, the current most frequently associated with SOCE, in various cell types. Whereas there was no effect of nocodazole treatment observed in NIH 3T3 (48), RBL-1 (15, 39), and DT40 cells (8), an inhibitory effect was demonstrated for other cell types, such as RBL-2H3 cells, BMMCs (13), and HEK 293 (15). It appears that different factors, including cell type, treatment protocol and the way of Ca^{2+} depletion might modify the results of the experiments. It is also possible that microtubules play a supporting role in SOCE signaling by optimizing the location of ER containing STIM1 before cell activation (15).

Nocodazole treatment, in contrast, effectively suppressed degranulation in BMMCs, suggesting that microtubules have a key role in the intracellular transport of granules. This finding is in accordance with previously published data demonstrating

microtubule-dependent movement of secretory vesicles during exocytotic response (16, 17, 20) and studies documenting a dramatic decrease in degranulation, but not in Ca^{2+} response in nocodazole treated cells (49). Our observation that STIM1 puncta are associated with microtubules in protrusions (Fig. 10*A*) indicates that microtubules might be important for translocation of clustered STIM1 as well. This process could possibly be dependent on the movement of ER components to protrusions via microtubule motor proteins; an important role of kinesin and dynein in the distribution of ER has already been reported (14).

Compared with quiescent cells or cells with decreased expression of STIM1, the number of growing microtubules at the periphery of activated BMMCL cells is substantially increased. This finding suggests the stabilization of microtubule plus ends. It is known that an important role in stabilization of growing microtubules is to be assigned to the plus end-tracking proteins whose interactions with microtubules are regulated by phosphorylation (10). Ca^{2+}-dependent kinases (e.g., conventional protein kinases C, calcium-calmodulin–dependent kinases) or phosphatases (e.g., PP2B) might participate in the regulation of microtubule stability in activated BMMCs. It has been reported that calcium-dependent activation of Rac (from the RhoA family of small GTPases) depends on the activity of conventional protein kinase C (50). FcεRI stimulation induced in BMMCs the activation of RhoA (17), which participates in the stabilization of microtubule plus ends through its target mDia (51). It remains to be determined whether stimulated kinases, small GTPases, or both have a stabilizing role in thapsigargin-treated BMMCs.

Nishida et al. (17) reported that FcεRI stimulation of BMMCs triggered the formation of microtubules and the translocation of granules in a manner independent of Ca^{2+}. Alternatively, our results demonstrate Ca^{2+}-dependent formation of microtubule protrusions. This discrepancy could be explained by differences in cell activation (the absence or presence of integrin engagement) and unlike methods of preparation of samples for microscopic evaluation, as discussed above. However, it is also possible that the initial stages of microtubule formation and transport of granules along microtubules are independent of Ca^{2+}, but later stages of activation and formation of microtubule protrusions depend on sustained influx of Ca^{2+}. The presence of aggregated STIM1 in protrusion could help to organize Ca^{2+} release-activated Ca^{2+} channels (46) and open locally these channels to cause SOCE. These interactions could be modulated by Ca^{2+} channel regulators, such as calmodulin (52) and the recently discovered CRACR2A (53). Our finding that STIM1-deficient BMMCs exhibited defective chemotaxis toward Ag is in line with these interpretations, and it supports previous data on the role of Ca^{2+} in chemotaxis (54, 55). We propose that microtubule protrusions might be involved in sensing external chemotactic gradients of Ag or other signals reaching mast cells at inflammatory sites.

In conclusion, our data indicate that the activation of mast cells leads to microtubule rearrangements and formation of microtubule protrusions. This process is dependent on STIM1-induced SOCE and enhanced levels of free cytoplasmic Ca^{2+} concentration, which have an important role in the regulation of microtubule dynamics, degranulation, and chemotactic response. Interference with the microtubular network via STIM1 or other Ca^{2+} regulators could potentially open new rational approaches to the treatment of inflammatory and allergic diseases.

Acknowledgments

We thank Dr. M. Hibbs (Ludwig Institute for Cancer Research, Melbourne, Australia) for BMMCL cells, Dr. T. Meyer (Department of Molecular Pharmacology, Stanford University Medical School, Stanford, CA) for YFP–hSTIM1 construct, Dr. Y. Mimori-Kiyosue (KAN Research Institute, Kyoto, Japan) for EB1-GFP construct, and Dr. A. Akhmanova (Department of Cell Biology, Erasmus Medical Center, Rotterdam, The Netherlands) for EB3-mRFP1.

Disclosures

The authors have no financial conflicts of interest.

References

1. Rivera, J., N. A. Fierro, A. Olivera, and R. Suzuki. 2008. New insights on mast cell activation via the high affinity receptor for IgE. *Adv. Immunol.* 98: 85–120.
2. Parekh, A. B., and J. W. Putney, Jr. 2005. Store-operated calcium channels. *Physiol. Rev.* 85: 757–810.
3. Smyth, J. T., W. I. Dehaven, B. F. Jones, J. C. Mercer, M. Trebak, G. Vazquez, and J. W. Putney, Jr. 2006. Emerging perspectives in store-operated Ca^{2+} entry: roles of Orai, Stim and TRP. *Biochim. Biophys. Acta* 1763: 1147–1160.
4. Roos, J., P. J. DiGregorio, A. V. Yeromin, K. Ohlsen, M. Lioudyno, S. Zhang, O. Safrina, J. A. Kozak, S. L. Wagner, M. D. Cahalan, et al. 2005. STIM1, an essential and conserved component of store-operated Ca^{2+} channel function. *J. Cell Biol.* 169: 435–445.
5. Liou, J., M. L. Kim, W. D. Heo, J. T. Jones, J. W. Myers, J. E. Ferrell, Jr., and T. Meyer. 2005. STIM is a Ca^{2+} sensor essential for Ca^{2+}-store-depletion-triggered Ca^{2+} influx. *Curr. Biol.* 15: 1235–1241.
6. Dziadek, M. A., and L. S. Johnstone. 2007. Biochemical properties and cellular localisation of STIM proteins. *Cell Calcium* 42: 123–132.
7. Prakriya, M., S. Feske, Y. Gwack, S. Srikanth, A. Rao, and P. G. Hogan. 2006. Orai1 is an essential pore subunit of the CRAC channel. *Nature* 443: 230–233.
8. Baba, Y., K. Hayashi, Y. Fujii, A. Mizushima, H. Watarai, M. Wakamori, T. Numaga, Y. Mori, M. Iino, M. Hikida, and T. Kurosaki. 2006. Coupling of STIM1 to store-operated Ca^{2+} entry through its constitutive and inducible movement in the endoplasmic reticulum. *Proc. Natl. Acad. Sci. USA* 103: 16704–16709.
9. Mercer, J. C., W. I. Dehaven, J. T. Smyth, B. Wedel, R. R. Boyles, G. S. Bird, and J. W. Putney, Jr. 2006. Large store-operated calcium selective currents due to co-expression of Orai1 or Orai2 with the intracellular calcium sensor, Stim1. *J. Biol. Chem.* 281: 24979–24990.
10. Akhmanova, A., and M. O. Steinmetz. 2008. Tracking the ends: a dynamic protein network controls the fate of microtubule tips. *Nat. Rev. Mol. Cell Biol.* 9: 309–322.
11. Grigoriev, I., S. M. Gouveia, B. van der Vaart, J. Demmers, J. T. Smyth, S. Honnappa, D. Splinter, M. O. Steinmetz, J. W. Putney, Jr., C. C. Hoogenraad, and A. Akhmanova. 2008. STIM1 is a MT-plus-end-tracking protein involved in remodeling of the ER. *Curr. Biol.* 18: 177–182.
12. Terasaki, M., L. B. Chen, and K. Fujiwara. 1986. Microtubules and the endoplasmic reticulum are highly interdependent structures. *J. Cell Biol.* 103: 1557–1568.
13. Oka, T., M. Hori, and H. Ozaki. 2005. Microtubule disruption suppresses allergic response through the inhibition of calcium influx in the mast cell degranulation pathway. *J. Immunol.* 174: 4584–4589.
14. Wu, S., H. Chen, M. F. Alexeyev, J. A. King, T. M. Moore, T. Stevens, and R. D. Balczon. 2007. Microtubule motors regulate ISOC activation necessary to increase endothelial cell permeability. *J. Biol. Chem.* 282: 34801–34808.
15. Smyth, J. T., W. I. DeHaven, G. S. Bird, and J. W. Putney, Jr. 2007. Role of the microtubule cytoskeleton in the function of the store-operated Ca^{2+} channel activator STIM1. *J. Cell Sci.* 120: 3762–3771.
16. Smith, A. J., J. R. Pfeiffer, J. Zhang, A. M. Martinez, G. M. Griffiths, and B. S. Wilson. 2003. Microtubule-dependent transport of secretory vesicles in RBL-2H3 cells. *Traffic* 4: 302–312.
17. Nishida, K., S. Yamasaki, Y. Ito, K. Kabu, K. Hattori, T. Tezuka, H. Nishizumi, D. Kitamura, R. Goitsuka, R. S. Geha, et al. 2005. FcεRI-mediated mast cell degranulation requires calcium-independent microtubule-dependent translocation of granules to the plasma membrane. *J. Cell Biol.* 170: 115–126.
18. Urata, C., and R. P. Siraganian. 1985. Pharmacologic modulation of the IgE or Ca^{2+} Ionophore A23187 mediated Ca^{2+} influx, phospholipase activation, and histamine release in rat basophilic leukemia cells. *Int. Arch. Allergy Immunol.* 78: 92–100.
19. Tasaka, K., M. Mio, K. Fujisawa, and I. Aoki. 1991. Role of microtubules on Ca^{2+} release from the endoplasmic reticulum and associated histamine release from rat peritoneal mast cells. *Biochem. Pharmacol.* 41: 1031–1037.
20. Martin-Verdeaux, S., I. Pombo, B. Iannascoli, M. Roa, N. Varin-Blank, J. Rivera, and U. Blank. 2003. Evidence of a role for Munc18-2 and microtubules in mast cell granule exocytosis. *J. Cell Sci.* 116: 325–334.
21. Sulimenko, V., E. Dráberová, T. Sulimenko, L. Macurek, V. Richterová, P. Dráber, and P. Dráber. 2006. Regulation of microtubule formation in activated mast cells by complexes of γ-tubulin with Fyn and Syk kinases. *J. Immunol.* 176: 7243–7253.
22. Oritani, K., and P. W. Kincade. 1996. Identification of stromal cell products that interact with pre-B cells. *J. Cell Biol.* 134: 771–782.
23. Nováková, M., E. Dráberová, W. Schürmann, G. Czihak, V. Viklický, and P. Dráber. 1996. γ-Tubulin redistribution in taxol-treated mitotic cells probed by monoclonal antibodies. *Cell Motil. Cytoskeleton* 33: 38–51.
24. Dráber, P., J. Zikán, and M. Vojtíšková. 1980. Establishment and characterization of permanent murine hybridomas secreting monoclonal anti-thy-1 antibodies. *J. Immunogenet.* 7: 455–474.

25. Mimori-Kiyosue, Y., N. Shiina, and S. Tsukita. 2000. The dynamic behavior of the APC-binding protein EB1 on the distal ends of microtubules. *Curr. Biol.* 10: 865–868.
26. Campbell, R. E., O. Tour, A. E. Palmer, P. A. Steinbach, G. S. Baird, D. A. Zacharias, and R. Y. Tsien. 2002. A monomeric red fluorescent protein. *Proc. Natl. Acad. Sci. USA* 99: 7877–7882.
27. Surviladze, Z., L. Dráberová, M. Kovářová, M. Boubelík, and P. Dráber. 2001. Differential sensitivity to acute cholesterol lowering of activation mediated via the high-affinity IgE receptor and Thy-1 glycoprotein. *Eur. J. Immunol.* 31: 1–10.
28. Dráberová, L. 1990. Cyclosporin A inhibits rat mast cell activation. *Eur. J. Immunol.* 20: 1469–1473.
29. Laemmli, U. K. 1970. Cleavage of structural proteins during the assembly of the head of bacteriophage T_4. *Nature* 227: 680–685.
30. Dráber, P., L. A. Lagunowich, E. Dráberová, V. Viklický, and I. Damjanov. 1988. Heterogeneity of tubulin epitopes in mouse fetal tissues. *Histochemistry* 89: 485–492.
31. Dráberová, E., and P. Dráber. 1993. A microtubule-interacting protein involved in coalignment of vimentin intermediate filaments with microtubules. *J. Cell Sci.* 106: 1263–1273.
32. Soile, P. 2003. *Morphological Image Analysis – Principles and Applications.* Springer Verlag, Berlin.
33. Breu, H., D. Kirkpatrick, and M. Werman. 1995. Linear time euclidean distance transform algorithms. *IEEE Trans. Pattern Anal. Mach. Intell.* 17: 529–533.
34. Zick, Y., and R. Sagi-Eisenberg. 1990. A combination of H_2O_2 and vanadate concomitantly stimulates protein tyrosine phosphorylation and polyphosphoinositide breakdown in different cell lines. *Biochemistry* 29: 10240–10245.
35. Teshima, R., H. Ikebuchi, M. Nakanishi, and J. Sawada. 1994. Stimulatory effect of pervanadate on calcium signals and histamine secretion of RBL-2H3 cells. *Biochem. J.* 302: 867–874.
36. Thastrup, O., P. J. Cullen, B. K. Drøbak, M. R. Hanley, and A. P. Dawson. 1990. Thapsigargin, a tumor promoter, discharges intracellular Ca^{2+} stores by specific inhibition of the endoplasmic reticulum Ca^{2+}-ATPase. *Proc. Natl. Acad. Sci. USA* 87: 2466–2470.
37. Paolini, R., M. H. Jouvin, and J. P. Kinet. 1991. Phosphorylation and dephosphorylation of the high-affinity receptor for immunoglobulin E immediately after receptor engagement and disengagement. *Nature* 353: 855–858.
38. Gilfillan, A. M., and J. Rivera. 2009. The tyrosine kinase network regulating mast cell activation. *Immunol. Rev.* 228: 149–169.
39. Bakowski, D., M. D. Glitsch, and A. B. Parekh. 2001. An examination of the secretion-like coupling model for the activation of the Ca^{2+} release-activated Ca^{2+} current I_{CRAC} in RBL-1 cells. *J. Physiol.* 532: 55–71.
40. Galli, S. J., M. Tsai, and A. M. Piliponsky. 2008. The development of allergic inflammation. *Nature* 454: 445–454.
41. Schwartz, M. A., M. D. Schaller, and M. H. Ginsberg. 1995. Integrins: emerging paradigms of signal transduction. *Annu. Rev. Cell Dev. Biol.* 11: 549–599.
42. Lam, V., J. Kalesnikoff, C. W. Lee, V. Hernandez-Hansen, B. S. Wilson, J. M. Oliver, and G. Krystal. 2003. IgE alone stimulates mast cell adhesion to fibronectin via pathways similar to those used by IgE + antigen but distinct from those used by Steel factor. *Blood* 102: 1405–1413.
43. Calloway, N., M. Vig, J. P. Kinet, D. Holowka, and B. Baird. 2009. Molecular clustering of STIM1 with Orai1/CRACM1 at the plasma membrane depends dynamically on depletion of Ca^{2+} stores and on electrostatic interactions. *Mol. Biol. Cell* 20: 389–399.
44. Honnappa, S., S. M. Gouveia, A. Weisbrich, F. F. Damberger, N. S. Bhavesh, H. Jawhari, I. Grigoriev, F. J. van Rijssel, R. M. Buey, A. Lawera, et al. 2009. An EB1-binding motif acts as a microtubule tip localization signal. *Cell* 138: 366–376.
45. Sampieri, A., A. Zepeda, A. Asanov, and L. Vaca. 2009. Visualizing the store-operated channel complex assembly in real time: identification of SERCA2 as a new member. *Cell Calcium* 45: 439–446.
46. Cahalan, M. D. 2009. STIMulating store-operated Ca^{2+} entry. *Nat. Cell Biol.* 11: 669–677.
47. Wu, M. M., J. Buchanan, R. M. Luik, and R. S. Lewis. 2006. Ca^{2+} store depletion causes STIM1 to accumulate in ER regions closely associated with the plasma membrane. *J. Cell Biol.* 174: 803–813.
48. Ribeiro, C. M., J. Reece, and J. W. Putney, Jr. 1997. Role of the cytoskeleton in calcium signaling in NIH 3T3 cells. An intact cytoskeleton is required for agonist-induced $[Ca^{2+}]$i signaling, but not for capacitative calcium entry. *J. Biol. Chem.* 272: 26555–26561.
49. Hesketh, T. R., M. A. Beaven, J. Rogers, B. Burke, and G. B. Warren. 1984. Stimulated release of histamine by a rat mast cell line is inhibited during mitosis. *J. Cell Biol.* 98: 2250–2254.
50. Price, L. S., M. Langeslag, J. P. ten Klooster, P. L. Hordijk, K. Jalink, and J. G. Collard. 2003. Calcium signaling regulates translocation and activation of Rac. *J. Biol. Chem.* 278: 39413–39421.
51. Palazzo, A. F., T. A. Cook, A. S. Alberts, and G. G. Gundersen. 2001. mDia mediates Rho-regulated formation and orientation of stable microtubules. *Nat. Cell Biol.* 3: 723–729.
52. Mullins, F. M., C. Y. Park, R. E. Dolmetsch, and R. S. Lewis. 2009. STIM1 and calmodulin interact with Orai1 to induce Ca^{2+}-dependent inactivation of CRAC channels. *Proc. Natl. Acad. Sci. USA* 106: 15495–15500.
53. Srikanth, S., H. J. Jung, K. D. Kim, P. Souda, J. Whitelegge, and Y. Gwack. 2010. A novel EF-hand protein, CRACR2A, is a cytosolic Ca^{2+} sensor that stabilizes CRAC channels in T cells. *Nat. Cell Biol.* 12: 436–446.
54. Hartmann, K., B. M. Henz, S. Krüger-Krasagakes, J. Köhl, R. Burger, S. Guhl, I. Haase, U. Lippert, and T. Zuberbier. 1997. C3a and C5a stimulate chemotaxis of human mast cells. *Blood* 89: 2863–2870.
55. Hofstra, C. L., P. J. Desai, R. L. Thurmond, and W. P. Fung-Leung. 2003. Histamine H4 receptor mediates chemotaxis and calcium mobilization of mast cells. *J. Pharmacol. Exp. Ther.* 305: 1212–1221.

Fig. S1

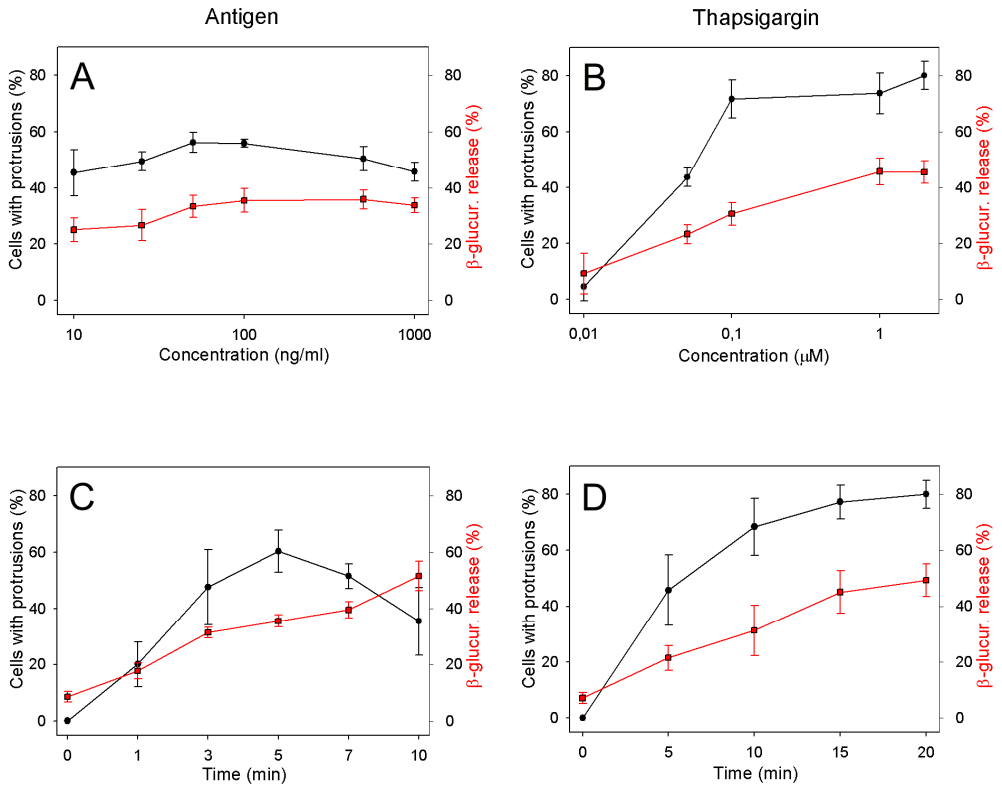

FIGURE S1. Correlation between formation of microtubule protrusions and degranulation in activated mast cells. Control or activated BMMCL cells were either fixed and stained for β-tubulin or used for determination of β-glucuronidase release. (A) IgE-sensitized (1 μg/ml) cells activated with different concentrations of Ag for 5 min. (B) Cells activated with different concentration of thapsigargin for 20 min. (C) IgE-sensitized cells activated with Ag (100 ng/ml) for various time intervals. (D) Cells activated with thapsigargin (2 μM) for various time. Three independent experiments were performed, each involving 500 cells and examined for the presence of microtubule protrusions. Values indicate means ± SD (n=3). Data for β-glucuronidase release represent means ± SD (n=3).

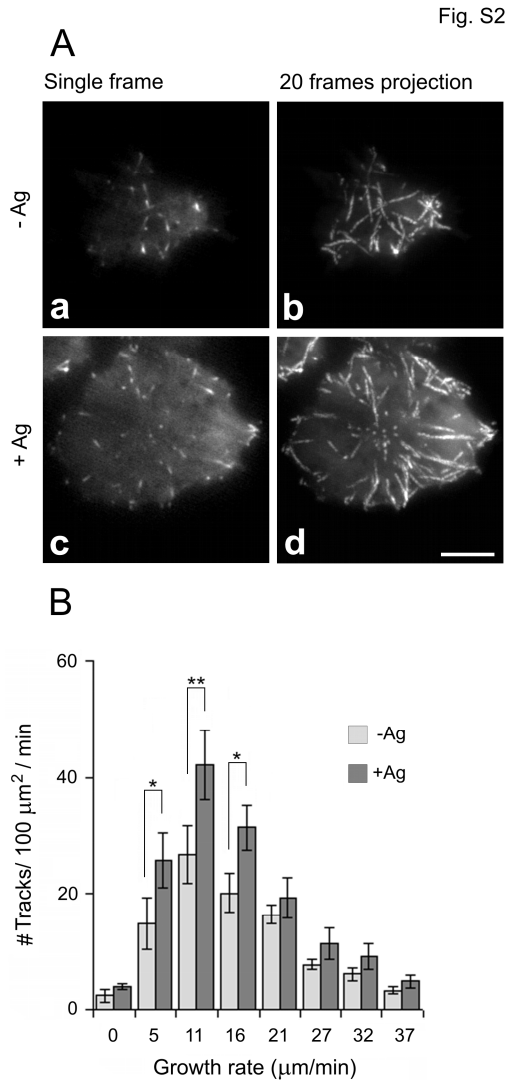

FIGURE S2. Activation of mast cells with Ag increases the number of growing microtubules in cell periphery as determined by TIRFM time-lapse imaging. (A) Time-lapse imaging of resting (a-b) and FcεRI aggregation-activated (c-d) BMMCL cells expressing EB1-GFP. Still images of EB1 (a, c) and tracks of EB1 comets over 20 sec created by maximum intensity projection of the 20 consecutive frames (b, d). Scale bar, 5 µm. (B) Histogram of microtubule growth rates in cell periphery of resting (-Ag) and Ag-activated (+Ag) cells. Total 10 different cells were tracked in 3 independent experiments. Values indicate mean ± SE, n=10 (*, $p<0.05$;**, $p<0.01$).

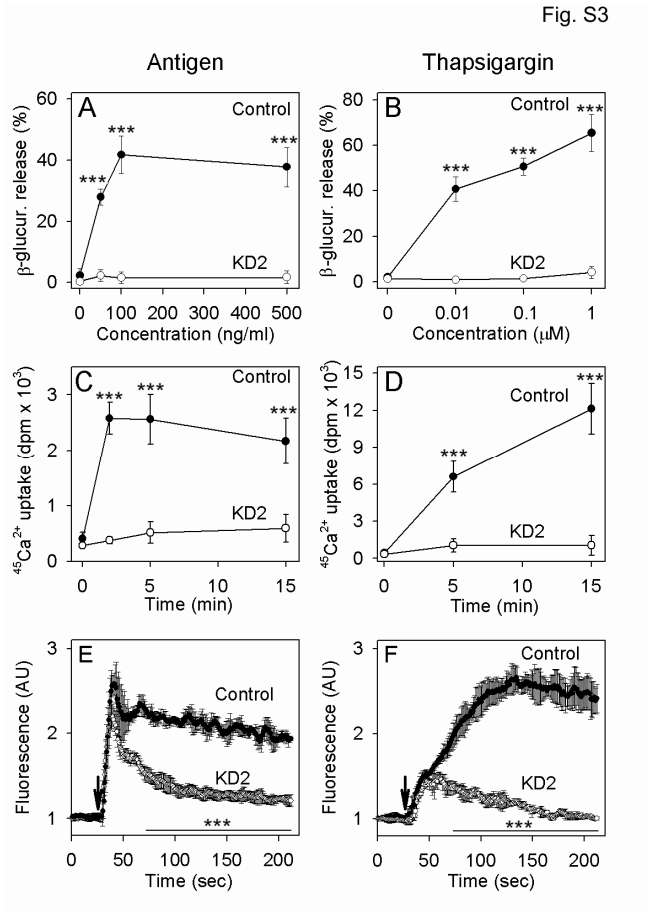

FIGURE S3. Degranulation and Ca^{2+} responses in cells with reduced STIM1 levels. (A-B) Changes in the degree of degranulation quantified as β-glucuronidase release. IgE-sensitized (1 μg/ml) cells infected with empty pLKO.1 vector (Control) or cells with reduced STIM1 after infection with shRNA2 (KD2) were activated with different concentrations of DNP-albumin for 30 min (A) or thapsigargin for 20 min (B) and the release of β-glucuronidase was determined. Data in (A) and (B) represent means ± SD (n=3, both for controls and KD2). (C-D) Changes in $^{45}Ca^{2+}$ uptake. IgE-sensitized (1 μg/ml) control cells (empty pLKO.1vector) or STIM1 KD2 cells were activated for various time intervals with 100 ng/ml DNP-albumin (C) or 2 μM thapsigargin (D) in the presence of extracellular $^{45}Ca^{2+}$ (1 mM). Data in (C) and (D) represent means ± SD (n=6, both for controls and KD2). (E-F) Changes in intracellular Ca^{2+} mobilization. IgE-sensitized (1 μg/ml) control cells (empty pLKO.1vector) or STIM1 KD2 cells loaded with Fluo 3-AM were activated (arrows) by 100 ng/ml DNP-albumin (E) or 2 μM thapsigargin (F). Data in (E) and (F) represent means ± SD (n=3, both for controls and KD2). (***, $p<0.001$; in E and F the line under asterisks indicate time interval of significant differences).

Movie S1. Time-lapse imaging of EB1-GFP in quiescent cells. BMMCL cells were imaged, with 0.5 s exposure time and 1 s interval between frames, for 3 min in TIRFM.
(http://www.jimmunol.org/content/suppl/2010/12/15/jimmunol.1002074.DC1/1.mov)

Movie S2. Time-lapse imaging of EB1-GFP in thapsigargin activated cells. BMMCL cells were imaged, with 0.5s exposure time and 1 s interval between frames, for 3 min in TIRFM. Imaging started 13 min after addition of thapsigargin at final concentration 2 μM.
(http://www.jimmunol.org/content/suppl/2010/12/15/jimmunol.1002074.DC1/2.mov)

Movie S3. Time-lapse imaging of YFP-hSTIM1 in quiescent cells. BMMCL cells were imaged, with 0.5s exposure time and 1 s interval between frames, for 3 min in TIRFM.
(http://www.jimmunol.org/content/suppl/2010/12/15/jimmunol.1002074.DC1/3.mov)

Movie S4. Time-lapse imaging of YFP-hSTIM1 in the course of thapsigargin activation of cells. BMMCL cells were imaged, with 0.5s exposure time and 1 s interval between frames, for 3 min in TIRFM. Thapsigargin was added 30s after starting the movie.
http://www.jimmunol.org/content/suppl/2010/12/15/jimmunol.1002074.DC1/4.mov)

Movie S5. Time-lapse imaging of YFP-hSTIM1 and EB3-mRFP1 in the course of nocodazole treatment of cells, folowed by thapsigargin activation. BMMCL cells were imaged, with exposure time ranging from 0.5-0.8s and 2 s interval between frames, for 3 min in TIRFM. Nocodazole and thapsigargin were added to the final concentration of 10 μM and 2 μM, respectively. Elapsed time in minutes and seconds is depicted in the upper right.
(http://www.jimmunol.org/content/suppl/2010/12/15/jimmunol.1002074.DC1/5.mov)